ROCK SLOPE INSTABILITY IN ALPINE GEOMORPHIC SYSTEMS, SWITZERLAND

DISSERTATION

zur

Erlangung des Doktorgrades (Dr. rer. nat.)

der

Mathematisch-Naturwissenschaftlichen Fakultät

der

Rheinischen Friedrich-Wilhelms-Universität Bonn

vorgelegt von

KAROLINE CHRISTINE MESSENZEHL

aus Aschaffenburg

Bonn, 2017

Angefertigt mit Genehmigung der Mathematisch-Naturwissenschaftlichen Fakultät der Rheinischen Friedrich-Wilhelms-Universität Bonn

1. Gutachter: Prof. Dr. Richard Dikau
2. Gutachter: Prof. Dr. Michael Krautblatter

Tag der Promotion: 09.02.2018

Erscheinungsjahr: 2018

There are more things in Heaven and Earth, Horatio,
Than are dreamt of in your philosophy.
(Hamlet, I, v)

To my grandma Christine Meßenzehl

my personal power-woman, who did so much for me
and inspired me with her courage and curosity

ACKNOWLEDGMENTS

Anyone who has walked through mountainaous terrain knows that such a walk can be exciting, breathtakingly beautiful and can make you feel like a discoverer, and at the same time, it can be tiring and takes effort. Looking back to my very exciting, incredibly rewarding and also sometimes tiring journey of this dissertation, I would like to thank several special persons along this journey:

First, for financially supporting this research, the fieldwork summer campaigns, my attendances at conference meetings and workshops and finally my research stay at the University of Oxford I am deeply grateful for scholarships, grants and awards from the European Geoscience Union (EGU), the American Geophysical Union (AGU), the AK Geomorphologie, the British Society for Geomorphology (BSG), the Gesellschaft für Erdkunde zu Berlin, the International Permafrost Association (IPA), the International Association of Geomorphologists (IAG), the German Exchange Service (DAAD) and the Studienstiftung des Deutschen Volkes.

Starting with my first teacher of rock slope instability, I would like to thank Michael Krautblatter, who always supported me since my master studies (not least with Schoki and warm clothes on cold field trips) and inspired me with his huge enthusiasm for research and teaching. I also thank Thomas Hoffmann for fruitful discussions and for introducing me to the exciting R-world with all its fancy boxplots. This thesis has furthmore benefited greatly from databases and previous studies of the Research Training Group 437 at the University of Bonn. In particular, I thank Michael Nyenhuis and Jan Otto. I am also grateful to Hanna Meyer (University of Marburg) for the opportunity to work with her in the machine-learning-world. My deep thanks go also to Rita Müller-Geiger, who managed not only all administrative issues, but was always caring about us. I also thank Norbert Grötsch and the cartography team and at the same time, I apologise for some last-minute poster printing actions and nerve-jangling afternoons for Gerd Storbeck.

My deep thanks go also to Familie Berckum whose warm welcoming every year in Oberems and famous cheese raclette evenings made the Turtmann Valley a bit of a second home. I must also thank several exceptional field assistants, who shared my love for Swiss cheese (and for Metzger-Meyer Würstchen) and supported me a lot: Many thanks to my 'strong guys' Andreas Ewald and Arne Brandschwede, the best teachers in talus slope surfing and the strongest SRT sluggers; Nikola Schulte-Kellinghaus and Luise Martin, the most caring talus mapping assistants I could have wished for; Katharina Eibisch, Kathrin Hoffmann and Sebastian Unger for carrying the heavy equipment within record time 1000 m uphill (while still looking awesome!). And thanks to Nele Meyer and Jana Eichel for leaving the glacier forefield and bringing a bit of biogeomorphology flavour to my rocky world. And don't forget: 'We worked *hardly*, but efficiently!'

For the last one and a half years of my PhD I was fortune enough to be visiting PhD student at the Rock Breakdown Laboratory of the University of Oxford and to become a part of a great working group: Many thanks to Martin Coombes, Vanessa Winchester, Scott Orr and the 'lab mums' Mona Edwards and Hong Zhang for providing such a supportive, caring and stimulating atmosphere and for finally conquering my wayward rocks. My special thanks go to ma petite Lucie Fusade and Martin Michette, with whom I shared a wonderful (PhD) life in Oxford with a lot of lab fun, road trips (with rocks in the car boot), many cycles in the rain, typical Oxford Harry Potter dinners and (punting) boat actions. And finally, to come to a special mentor in the final phase of my PhD, I am extremely grateful to Heather Viles. Many thanks, Heather, for your enormous support, all our discussions about small- and big-scale (research) topics, for inspiring me not just with your enthusiasm for research, for your encouraging 'mental box', your 'champagne glass' and for showing me that there is always a solution to any kind of problem (…also for our little basalt friends).

Many thanks to Martin, Carina, Scott and Katharina for their patent proofreading of several sections of this thesis! Furthermore, I must mention and thank my friends Anna Irrgang, Christina Fichtner and Elena Witzeck, always caring about me and refreshing me with non-geomorphic topics, as well as my Geomorph (…and Soil) Chicks. It could not have been better to start to my PhD with Jana Eichel and Nele Meyer and to grow up with them as scientists …or old chicks. Thank you, Jana, for being not just the best office mate, but for becoming a friend during a time with many sushi comas (with Nele) and hipster city-(conference)-food-trips. A special word of gratitude goes to my other chicks Carina Schmitz, Hannah Berger and Katharina Eibisch, with whom I shared, despite so many kilometres of distance, all my worries and difficult moments, but also the most wonderful times of delight and excitement for things alongside the PhD (… Elmo!). 'Meine Lieben', I can honestly say, all your encouraging 10 min-voice messages, your urgently needed Harzer Käse supply to the UK, all our conversations about life, and your deep love did immeasurably enrich more than just my PhD.

To come finally to my supervisor of this dissertation and mentor, my deep gratitude goes to Richard Dikau. His passion for the big questions far beyond gravitational mass movements and complex system behaviour guided me throughout my whole master studies and finally this PhD. I am so aware of the generous, intellectual and caring support as well as the big freedom I was given by him to perform my research, without publication pressure or scientific constraints, and to develop myself as scientist and person. I sincerely thank you, Richard, for all our stimulating several-hour meetings and our Bonn-Oxford phone calls, which all encouraged me, sharpened my eyes to *observe* things I didn't know before, made me think critically, systemically and 'big!' and moreover, led me think out of the geomorphic box. I am so proud to be one of your PhD students and extremely thankful for the incredible amount I learned from you, both scientifically and personally.

My final words and deep gratitude go to my father, and most particularly to my mum. Liebe Mama, despite, but therefore because of knowing little about geomorphology, your greatest and invaluable support was and is your belief in me, your unconditional love and that you never asked me to be more or less than I am!

CONTENT

PART A

PART B

PART C

SUMMARY

Rock slope instability is a complex condition that varies in magnitude and over time. In steep alpine areas, instability of rock slopes is of major significance for long-term erosion rates, landform evolution, sediment production and the overall efficiency of catchment sediment fluxes. When humans and infrastructures are affected, rockfalls released from unstable rock slopes represent one of the most prominent natural hazards. During recent decades an increased number of rockfalls of different magnitudes has been recorded both in the Swiss Alps and worldwide in mountain areas. However, the complex interplay of topoclimatic, cryospheric and rock mechanical controls is still little understood, particularly in valleys affected by glacier retreat. As a consequence, limited information exists explaining the short- and long-term effects of rock slope instability for the magnitude, intensity and timing of rockfall-dominated sediment cascades. Faced with these knowledge gaps, this thesis aims to improve our system and process understanding of rock slope instability in alpine systems at different spatial and temporal scales. A new methodological multi-scale approach is developed that accounts for the scale-dependency and emergence of rock slope systems. Five research studies are conducted in the Turtmann Valley (Valais Alps) and Swiss National Park spanning from the regional valley scale to the scale of individual rockwalls and intact rock.

At the valley scale, the thesis explores key controls on spatiotemporal activity of rock slope instability in alpine valleys undergoing glacier retreat since the Last Glacial Maximum. For the first time, a decision-tree-based random forest algorithm is applied in rockfall research in combination with a principal component logistic regression model. Both models indicate that permafrost degradation after glacier retreat is a key paraglacial rockfall control. Using ergodic reasoning, three scenarios of paraglacial adjustment are proposed accounting for different non-linear tectonic and structural conditioning of permafrost rockwalls. Additionally, quantitative and qualitative evidence is provided for geomorphic consequences of rock slope instability on cascading sediment fluxes in alpine catchments. A GIS-based connectivity model is combined with geomorphic field mapping to assess sediment pathways from unstable rockwalls to the fluvial system. Field and modelling observations emphasise that small- to mid-magnitude rock failures are of major significance for the long- and short-term efficiency of sediment cascades. Yet, it is also shown that one third of the deposited rockfall material is currently disconnected from the catchment flux system due to glacial topographic effects.

At the scale of individual rock slopes, the thesis investigates the cause-effect linkage between rock weathering, rock slope instability and rockfall supply onto talus slopes in three glaciated hanging valleys. A new holistic approach is presented that integrates abductive surveys of talus slopes with deductive geotechnical studies, 2-years rock temperature monitoring and numerical frost cracking modelling of associated source rockwalls. The rockwall-talus approach demonstrates that the complex interplay of joint spacing, kinematic failure conditions and depth-varying frost cracking controls the annual to decadal rockfall frequency-magnitude pattern and dictates, in combination with permafrost degradation, the long-term paraglacial variability in sediment production, rockfall size and deposition.

At the scale of intact rock, the thesis explores the individual and synergistic weathering efficiency of sun-induced thermal cycling and diurnal ice crystallisation in low-porosity mica schist. A novel two-phase weathering simulation is performed in the laboratory. Evidence is provided for cleavage-controlled, micro-sale rock fatigue after exposure to long-term repetition of frost events, particularly if rocks were thermally pre-stressed. The laboratory measurements indicate both positive and negative feedback effects during changing rock properties. The findings have implications for current research debates about the role of subcritical rock weathering agents for the near-surface bedrock instability.

This thesis highlights the need to pay more attention in geomorphic research to source rockwalls and to its inherent system properties, rather than solely on external topoclimatic factors. Moreover, this research emphasises that rock slope instability is a matter of scale. As spatial and temporal scales change, new causation and explanation on key controls, spatiotemporal activity and geomorphic effects for sediment cascades emerge. To deal with this scale-dependency and non-linearity of rock slope systems, this thesis proposes practical and philosophical solutions for future research.

ZUSAMMENFASSUNG

Die Instabilität von Felswänden ist ein komplexes Phänomen das in Zeit und Magnitude variiert. Vor allem in Hochgebirgsregionen sind Felsinstabilitäten von großer Relevanz für die langzeitliche Relieferosion und Landschaftsentwicklung, sowie für die Sedimentproduktion und Effizienz von alpinen Sedimentflüssen. Die damit verbundene Disposition von Sturzereignissen stellt zudem ein ernstzunehmendes Naturgefahrenpotenzial für Mensch und Infrastruktur dar. Untersuchungen zeigen weltweit, und speziell für die Schweizer Alpen, eine Zunahme von Felsinstabilitäten unterschiedlicher Magnituden in den letzten Jahrzehnten. Das komplexe Zusammenspiel von topoklimatischen, kryosphärischen und felsmechanischen Kontrollfaktoren, insbesondere in von Gletscherrückzug betroffenen alpinen Tälern, ist jedoch noch unzureichend verstanden. Folglich stehen nur begrenzt Informationen über die kurz- und langzeitlichen Konsequenzen von Felsinstabilitäten bezüglich Magnituden, Intensitäten und Frequenzen von Sturzprozessen in alpinen Kaskadensystem zur Verfügung. Angesichts dieser Wissenslücken hat diese Doktorarbeit zum Ziel unser System- und Prozessverständnis von alpinen Felsinstabilitäten auf unterschiedlichen Zeit- und Raumskalen zu vertiefen. Ein neuer multiskaliger methodologischer Ansatz wird entwickelt, welcher erlaubt die Skalenabhängigkeit und Emergenz von Felssystemen zu adressieren. Die Arbeit umfasst fünf empirische Studien auf unterschiedlichen räumlichen und zeitlichen Skalen mit Untersuchungsgebieten im Turtmanntal (Schweizer Waliser Alpen) und Schweizer National Park.

Auf der größten und längsten Skale untersucht diese Arbeit Hauptkontrollfaktoren für die raumzeitliche Aktivität von Felsinstabilitäten in alpinen Tälern seit dem letzten Glazialen Maximum. Zum ersten Mal in der Sturzprozessforschung wird ein Random Forest Klassifikationsalgorithmus angewandt und durch die Kombination mit einem Hauptkomponenten-basierten, logistischen Regressionsmodell weiter entwickelt. Die Modellkombination zeigt auf, dass Permafrostdegradation im Laufe des Gletscherrückzugs einer der wichtigsten Kontrollfaktoren für die Instabilität entgletscherter Felswände darstellt. Mit Hilfe eines ergodischen Ansatzes werden drei Szenarien paraglazialer Felsanpassung entwickelt, welches nichtlineare tektonische und strukturelle Konditionierungen von Permafrostwänden berücksichtigt. Die Arbeit liefert zudem quantitative und qualitative Beweise für die geomorphologische Signifikanz von Felsinstabilitäten für Sedimentkaskaden in alpinen Einzugsgebieten. Die Kombination aus einem GIS-basierten Konnektivitätsmodell und einer detaillierten geomorphologischen Feldkartierung ermöglicht es Sedimentflüsse von instabilen Felswänden zum fluvialen System zu identifiziert und im Hinblick auf ihre Effizienz zu bewerten. Die feld- und modellierungsbasierten Beobachtungen zeigen eine Dominanz von Sturzprozesse kleiner bis mittlerer Magnitude. Allerdings wird deutlich, dass aktuell ein Drittel des gespeicherten Sturzmaterials aufgrund der glazialen Talmorphometrie vom Hauptkaskadensystem entkoppelt ist.

Auf der Skale individueller Felswände analysiert diese Arbeit die Ursache-Wirkung Beziehung zwischen Felsverwitterung, Felsinstabilität sowie Materialspeicherung auf Schutthalden in drei vergletscherten Hängetälern. Ein neuer holistischer Ansatz wird vorgestellt, welcher abduktive Schutthaldenuntersuchungen mit deduktiven geotechnischen Kartierungen an Felswänden, einem zweijährigen Felstemperaturmonitoring und numerischer Frostverwitterungsmodellierung integriert. Dieser integrative Ansatz zeigt auf, dass die Komplexität aus Kluftabstand, der vorgegebenen Kinematik aus Haupttrennflächen sowie der tiefenvariierenden Intensität saisonaler Eissegregation wesentlich das jährlich-dekadische Frequenz-Magnituden Spektrum von Sturzprozessen steuert sowie, in Kombination mit Permafrostdegradation, die langzeitliche Variabilität von Sedimentproduktion und Formeigenschaften von Schutthalden kontrolliert.

Auf der Skale des intakten Fels widmet sich diese Arbeit der Frage nach der individuellen und synergetischen Verwitterungseffizienz hochfrequenter thermaler Zyklen und täglicher Eiskristallisation in Glimmerschiefer geringer Porosität. Ein neuartiges zweiphasiges Laborexperiment liefert Evidenzen für mikroskalige, strukturabhängige Felsermüdung in Folge wiederholter Frostzyklen, insbesondere in Felsproben, welche zuvor einer Phase thermalen Stresses ausgesetzt waren. Die Langzeitmessungen zeigen sowohl positive als auch negative Feedbackeffekte im Laufe verändernder mechanischer Felseigenschaften. Diese Beobachtungen haben Implikationen für aktuelle Forschungsdebatte über die Rolle subkrtitischer Verwitterungsmechanismen für oberflächennahe Felsinstabilitäten.

Diese Arbeit hebt hervor, dass geomorphologische Forschung dringend mehr Aufmerksamkeit auf die Quellgebiete in alpinen Systemen, also Felswände und ihre inhärenten Systemeigenschaften, richten muss. Zudem zeigen die Befunde dieser Arbeit auf, dass die Instabilität von Felswänden eine Skalenfrage ist. Jede räumliche und zeitliche Skale ist mit unterschiedlichen Kausalzusammenhängen und Erklärungen verbunden hinsichtlich Hauptkontrollfaktoren, raumzeitlicher Sturzprozessaktivität und geomorphologischen Effekten für Sedimentkaskaden. Um diese Skalenabhängigkeit und Nichtlinearität von Felssystemen zu adressieren, liefert diese Arbeit verschiedene praktische und philosophische Lösungsansätze für zukünftige Forschung.

LIST OF PUBLICATIONS

1. Messenzehl, K., Meyer, H., Otto, J.-C., Hoffmann, T., Dikau, R. (2017): Regional-scale controls on the spatial activity of rockfalls (Turtmann valley, Swiss Alps) - A multivariate modelling approach. In: Geomorphology 287: 29-45. DOI: 10.1016/j.geomorph.2016.01.008. **(Chapter 4)**
2. Messenzehl, K., Hoffmann, T., Dikau, R. (2014): Sediment connectivity in the high-alpine valley of Val Müschauns, Swiss National Park - linking geomorphic field mapping with geomorphometric modelling. In: Geomorphology 221: 215-229. DOI: 10.1016/j.geomorph.2014.05.033. **(Chapter 5)**
3. Messenzehl, K., Viles, H., Otto, J.-C., Ewald, A., Dikau, R. (minor revisions): Linking rock weathering, rockwall instability and rockfall sediment cascades in partially glaciated hanging valleys (Swiss Alps). Submitted to Permafrost and Periglacial Processes. **(Chapter 6)**
4. Messenzehl, K., Dikau, R. (2017): Structural and thermal controls of rockfall frequency and magnitude within rockwall–talus systems (Swiss Alps). In: Earth Surface Processes and Landforms. DOI: 10.1002/esp.4155. **(Chapter 7)**

LIST OF FIGURES

LIST OF TABLES

PART A

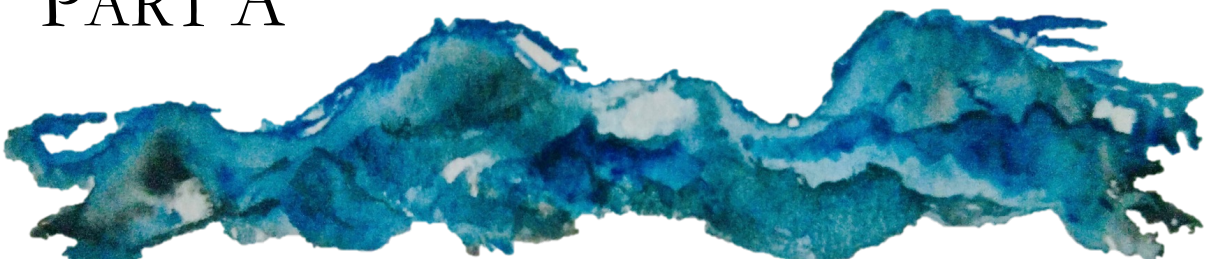

W-facings mountains of the Pipji Valley (Swiss Alps)

Chapter 1
INTRODUCTION

1.1 Questions and challenges to address

The instability of bare rock slopes is a complex phenomenon that can occur worldwide in different geologic, topographic and climatic environments. Rock slopes can become unstable and fail virtually anywhere with enough local relief to generate gravitational stresses (Terzaghi, 1962; Brunsden and Prior, 1984; Dikau et al., 1996a; Wyllie and Mah, 2004). However, rock slope instabilities are most common in alpine systems (Korup, 2012).

As mountains cover a total of 24% of the Earth terrestrial land area with about a quarter of humanity living in and around them (Price et al., 2013), rock slope instability is of global importance. Destabilisation of rock slopes is the key geomorphic driver for bedrock erosion and long-term mountain-scale relief evolution (Gilbert, 1877; Hewitt et al., 2008; Hales and Roering, 2009; Korup et al., 2010). Unstable rock slopes are also of vital significance for alpine sediment cascades (Chorley et al., 1984; Caine, 1986), as they are the prime producers of sediments and major controls of the overall sediment amount available to be delivered to fluvial systems (Jäckli, 1957; Rapp, 1960a, b; Caine, 1986; Burt and Allison, 2010). Furthermore, when humans and infrastructure are affected, rock slope instability constitutes one of the most damaging and deadly of natural hazards (Glade and Crozier, 2005; Petley, 2012). This is particularly true in alpine valleys under hydraulic and seismic conditions, as has become evident in Vajont in 1963 (Petley and Petley, 2005) or, more recently, in China after the 2008 earthquake (Yin et al., 2009). Due to the complexity of controls and high mobility, even the smallest rock failure can pose a serious threat to public safety and infrastructure entailing potentionally high economic costs (OECD, 2007).

During recent decades, an increased number of catastrophic and even many more small-sized rock slope failures have been recorded worldwide in mountain areas (Fischer et al., 2013; Ravanel and Deline, 2015). Current global warming is assumed to be the major driver (IPCC, 2014). The European Alps have undergone a temperature increase of around +2 °C between the late 19th and early 21st century (EEA, 2009), coupled with exceptional heat waves such as in summer 2003 and, more recently, in 2015 (Schär et al., 2004; Ravanel et al., 2017). It has been shown that, in particular, glacier retreat, warming and thawing of rock permafrost and increasing rock weathering activity in response to atmospheric warming (Haeberli and Beniston, 1998; Harris et al., 2009) significantly reduce stability of rock slopes (Gruber and Haeberli, 2007; Ravanel and Deline, 2011; Huggel et al., 2012; Krautblatter et al., 2013; Krautblatter and Leith, 2015). Until the mid of the 21st century, about 0.25 °C warming per decade is expected under the A1B emission scenario, and an accelerated 0.36 °C warming per decade in the second half of the century (Gobiet et al., 2014). At the same time, global population in and close to mountain areas also continues to increase (Price et al., 2013). Accordingly, with on-going climate change, alpine rock slope instability will probably become a more serious issue in the coming years (McGuire, 2010).

It is therefore more important than ever to ask: Why do rock slopes become unstable? How often do specific magnitudes of rock failure occur? How do rock slopes adjust to past and current deglaciation? What

consequences are to be expected further downslope? Research aimed at addressing those questions has increased in recent years including theoretical approaches, numerical or statistical modelling, field observations and small-scale laboratory experiments. Nevertheless, our system and process understanding of alpine rock slope instabilities is still incomplete (cf. Krautblatter and Leith, 2015).

One of the remaining scientific challenges is to understand the complicated interplay of different external and internal promoting, triggering and preconditioning controls of rock slope instability. For example, rock instability is not solely a function of unfavourable valley- and slope-scale topography in combination with large-scale and local climate influences (Barsch and Caine, 1984; Guzzetti et al., 2003). In addition rock slopes are rather made of discontinuous and anisotropic materials with non-linear properties (Krautblatter and Moore, 2014). Large-scale geological and tectonic genesis, long-term erosional and stress history of multiple glaciation cycles and millions of years of small-scale mechanical, thermal, hydrological and chemical processes have created distinct discontinuity patterns (Selby, 1993; Coe and Harp, 2007; Loye et al., 2012; Leith et al., 2014a). At the same time, in response to synergistic rock weathering agents (Hall et al., 2002; Matsuoka and Murton, 2008; Viles, 2013b), paraglacial stress release and permafrost degradation, new joints and planes of weaknesses generate - often delayed long after rock mass deglaciation (Hencher et al., 2011; McColl, 2012; Grämiger et al., 2017). However, within previous attempts to decipher this complex interplay between topoclimatic, cryospheric, paraglacial and pre-existing mechanical properties, the scale-dependency and non-linear complexity (Harrison, 2001; Phillips, 2003b) of alpine geomorphic systems is often neglected.

A further scientific challenge is still the spatial and temporal variability of rock slope instability. Rock slope instability highly varies in time and space and can take place through many types of mass movements (Varnes, 1978; Crozier and Glade, 1999). In high-elevated steep alpine terrain, the rapid release of rockfalls is among the predominating processes as reflected by the widespread occurrence of talus slope landforms at the foot of alpine rock slopes (Matsuoka and Sakai, 1999; Hales and Roering, 2005; Sass, 2010). Rockfalls can occur seasonally in form of small pebbles (Rapp, 1960b; André, 1997), annually to multi-annually as debris falls and boulder falls (Whalley, 1984; Cruden and Hu, 1994) or episodically in form of e.g. large Bergsturz events (Heim, 1932; Erismann and Abele, 2001). Thus, each rockfall event has its own magnitude and frequency pattern, driven by the balance between the rock mass resistance and the intensity of the applied stresses (Terzaghi, 1962; Selby 1994). Interestingly, major scientific focus lies on large-scale and deep-seated catastrophic rock failures, whilst comparatively little research takes place on small-sized events. Consequently, information on the frequency-magnitude pattern of rockfalls particularly at the lower magnitude spectrum is still scarce. This knowledge gap also accounts for long-time rockfall activity such as after the last glacial maximum. Although there is common agreement on inital rockfall peaks immediately after glacier retreat, it remains debated whether subsequent paraglacial rock slope adjustment towards nonglacial strength equilibrium follows an exhaustion, linearly decreasing or constant steady state path (Abele, 1972; Cruden and Hu, 1993; Ballantyne, 2002b; McColl, 2012; Ballantyne and Stone, 2013; Ballantyne et al., 2014).

Today, the issue of rock slope instability is addressed by multiple disciplines such as rock mechanics, geoengineering, hydrogeology, geophysics as well as geomorphology (Selby, 1980; Hoek and Bray, 1981; Dikau et al., 1996a; Wyllie and Mah, 2004; Jaeger et al., 2007). During recent decades, each discipline has significantly

contributed to this issue, but it seems, often with different scientific purposes and from different perspectives. In geomorphology, the growing multidisciplinarity since the 1970s and the availability of new technologies from other disciplines have encouraged alpine geomorphologists to pay greater attention to rock mass properties. Nevertheless, geomorphic research on unstable rock slopes still distinctly lags behind those studies that concentrate on sediment dynamics and their budgets. So, what has geomorphology to offer the current challenges and questions concerning rock slope instability in alpine environments? Are the increasingly process-based and reductiontic approaches adequate to unravel non-linear and emergent rock slope behaviour? Is the current 'sediment-dominated' perspective on sediment storages and budgets sufficient to tackle current problems in alpine systems adjusting to glacier retreat and atmospheric warming?

1.2 Aims and major objectives

The discussion above shows that major questions, systemic knowledge gaps and methodological shortcomings in our understanding of alpine rock slope instability need to be addressed. Faced with theses questions and challenges, this dissertation aims to improve our understanding of rock slope instability of alpine geomorphic systems with respect to different spatial and temporal scales. The primary aim of this research study is to better understand (i) the key rock slope destabilising controls, (ii) spatiotemporal activity of rockfall events after deglaciation and (iii) the geomorphic importance of bedrock instability for alpine sediment cascades based on a (iv) hierarchical scale approach. The specific geographic focus is on alpine systems in the Swiss Alps, which were formerly glaciated (Swiss National Park) or are still undergoing glacier retreat (Turtmann Valley). The following four major objectives will be addressed:

Objective 1: Identifying key controls for rock slope instability and rockfall initiation with respect to their relative importance at different spatial scales of alpine systems. Identifying linkages between lower and higher scales.

Objective 2: Identifying potential paraglacial scenarios of rock slope instability and quantifying the frequency-magnitude pattern of rockfall events at deglaciated rock slopes.

Objective 3: Evaluating the quantitative and qualitative significance of rock slope instability for the efficiency of alpine sediment cascading systems at different spatial scales.

Objective 4: (Re)developing and applying a hierarchical and holistic methodology that allows to account for the non-linear complexity and emergence of rock slope instability in geomorphic systems.

1.3 Chapter outline and chapter summary

This thesis is divided into three main parts (Figure 1.1). After an overview of the overall research motivation and aims of this study (previous chapters), **Part A** outlines the current state of the art in the research of mountain rock slope instabilities and presents the broad conceptual and methodological approach of this dissertation.

In **Chapter 2,** the state of the art is structured into 'form, material and process' characteristics of high alpine rock slope systems. The current process understanding of the form and hierarchical nature (**Section 2.1**), the mechanical and thermal material properties (**Section 2.2**) as well as the major bedrock destabilising processes (**Section 2.3**) and processes and storage of rockfall sediment cascades (**Section 2.4**) are described at different scales. These chapters serve to define the terminology, to introduce methodological approaches, to provide an overview on major theories and changing paradigms, while conjointly identifying limitations to our existing understanding.

In **Chapter 3,** the broad conceptual and methodological approach of this thesis is presented. Based on the previous literature review, four key knowledge gaps and methodological shortcomings are identified. This leads to eight overal research hypotheses (**Section 3.1**) concerning (i) the controls and (ii) paraglacial activity of rock slope instability and rockfall initiation, (iii) their geomorphic importance for alpine sediment cascades and (iv) the (methodological) question of scale. A multi-scale methodology is proposed **(Section 3.2)** that addresses three levels of system complexity by combining regional-scale modelling, local rockwall-talus surveys and small-scale laboratory experiments. As different study sites in the Swiss Alps are investigated in this thesis, a brief overview to their geographic, geological and geomorphological setting is given (**Section 3.3**).

Part B combines five empirical studies, three of which are published as journal articles and one currently under review. Each study is presented in an individual chapter and addresses different scales of rock slope instability in geomorphic systems, decreasing from the regional scale, over the hanging valley and rockwall-talus scale to the smallest level of the rock mass.

Chapter 4 explores regional-scale controls of rock slope instability in the 110 km² large Turtmann Valley and addresses the higher-scale system complexity and emergence of mountain valleys affected by permafrost degradation and glacier retreat. For the first time, a decision-tree based random forest algorithm is applied in rockfall research in combination with a principal component logistic regression model of an inventory of 220 talus slopes. The study presents new scientific insights into the discussion whether periglacial rockfall events are controlled more by topo-climatic, cryospheric, paraglacial or/and rock mechanical properties.

Chapter 5 addresses the geomorphic consequences of regional-scale rock slope instability and explores their influence on alpine sediment cascades in a deglaciated valley of the Swiss National Park. Pathways of sediment routing from unstable rockwalls to the stream and the degree of sediment connectivity are evaluated using a morphometry-based GIS algorithm. The DTM-based results are tested against a geomorphic map derived from field investigations. The indispensability of geomorphic field mapping in an emerging GIS world for a holistic understanding of alpine systems is discussed. The study emphasises the key role of rockfall processes from deglaciated rock slopes for the short- and long-term efficiency of sediment routing as well as the decoupling effect of the glacial bedrock topography in mountain valleys.

Chapter 6 builds on findings of the previous two studies and explores the linkage between rock weathering, rockwall instability and rockfall sediment cascades in three hanging valleys of the

Turtmann Valley. In a principal component analysis, regional-scale system components and small-scale thermo-mechanical characteristics of twelve rockwalls are evaluated with respect to sediment production and rockfall sediment storage after glacier retreat. The combined GIS-, field- and modelling-results reveal the first-order control of frost cracking intensity and permafrost probability at deglaciated, near-vertical rockwalls. The presented findings have implications for future sediment cascade research as they highlight the need to pay more attention to source rockwalls.

Chapter 7 investigates the rock-mass scale controls identified in chapter 6 in more detail and quantifies the associated local rockfall frequency-magnitude pattern at two rockwall-talus systems at the north-exposed Hungerli Peak. A new holistic approach is presented that integrates deductive geotechnical and 2-years thermal investigations of the source rockwalls as well as frost cracking modelling with abductive surveys of rockfall deposits. The results emphasise the significance of small- to medium-size rockfall events for local frequency-magnitude pattern. A new research agenda for future geomorphic rockfall research is proposed that incorporates small-scale structural and thermal rockwall properties rather than only climatic and meteorological triggers.

Chapter 8 addresses hypothesis on the efficiency of small-scale rock weathering processes at the near-surface of alpine rock slopes posed in previous chapters. In a novel two-phase weathering simulation, the individual and synergistic mechanical effects of repeated thermal cycling and high-frequency diurnal ice crystallisation is studied based on low-porosity mica schist samples from the Turtmann Valley. Rock monitoring of open porosity, p-wave velocity, surface hardness and thin sections reveals clear signs of (pore-scale) rock damage after exposure to repeated frost events, but particularly if rocks were thermally pre-stressed. The documented rock responses have implications for current research debates about the role of sun-induced vs. frost-induced failures of metamorphic rocks slopes with contrasting cleavage orientation.

In the last **Part C**, **Chapter 9** provides a synoptic discussion of the major outcomes of all five empirical studies using the multi-scale conceptual frameworks outlined in chapter 3. To come back to the initial objectives and hypotheses of this thesis, the scale-dependent role of rock slope destabilising factors, different scenarios of paraglacial rockfall activity and the downslope consequences for alpine sediment cacades will be discussed. Practical and philosophical recommendations for future rock slope instability research are provided. Finally, **Chapter 10** concludes the main systemic and practical contribution of this research to our multi-scale understanding of rock weathering, rock slope instability and geomorphic sediment cascades in alpine systems and closes with an outlook for a future research agenda.

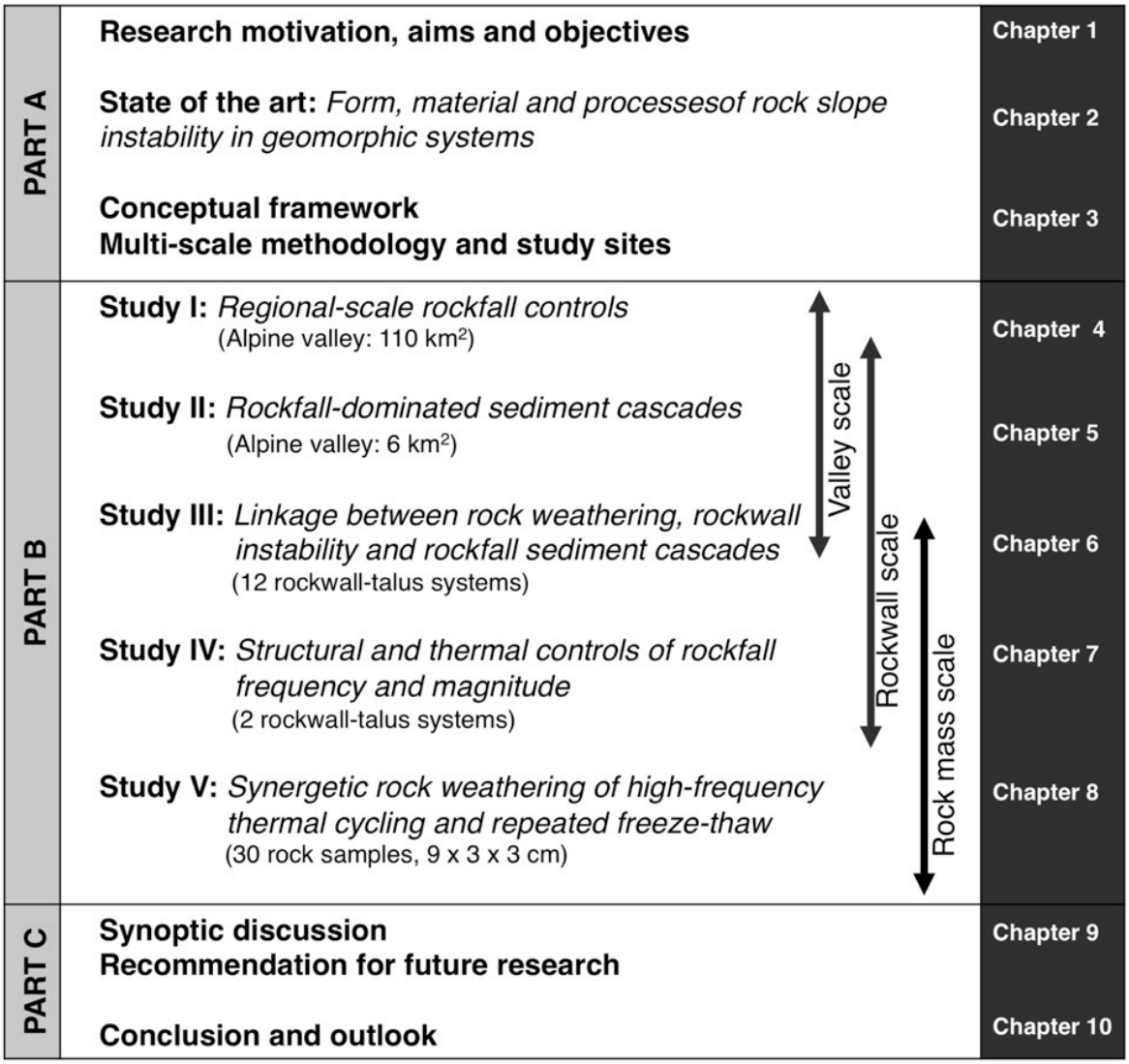

Figure 1.1: Thesis structure and chapter outline.

Chapter 2

STATE OF THE ART: THE NATURE OF HIGH ALPINE ROCK SLOPE SYSTEMS

"A geomopric system is a structure of interacting processes and landforms that function individually and djointly to form a landscape complex"' (Chorley et al. 1985, p. 5). According to the systems approach proposed by Chorley, Schumm and Sudgen, a rock slope represents a landform or sub-system within a larger geomorphic process-response system. It is crucially dependent upon inputs, throughputs and outputs of material (sediment) and energy (cascading systems). In this way, any change of input can result in changing outputs in form of form modification or altered internal components. within both the large-scale geomorphic system and the rock slope system. Following this idea, research on rock slope instability must therefore involve a description and understanding of the processes and controls involved, potential inputs, throughputs and outputs, as well as their evolution over time. To provide an overview on our current systems understanding of alpine rock slopes and to identify knowledge gaps, the following chapters outline the state of the art in the research of mountain rock slope instabilities with respect to landform, material, and processes characteristics of alpine rock slope systems.

2.1 Landform and hierarchical relief characteristics

Alpine or mountain[1] rock slope systems show distinct forms and hierarchical relief characteristics. Geomorphometric description of (high) mountain or alpine systems dates back to Alexander von Humboldt (1814) followed by pioneering work by e.g. Ritter (1852), Sonklar (1873) or Penck (1896). According to Barsch and Caine (1984), the most prominent geomorphometric features of high mountain systems are slopes steeper than 60° and elevation ranges of more than 1000 m between summits and valley floors. Rockwall profiles are usually stepped in response to internal structural controls (Caine, 1974). In comparison, geomorphometry of high-mountains is clearly distinguished from that of mountain systems. Due to their local relief of > 1000 m and slopes steeper than 45°, high-mountains systems are described as high-energy environments (Barsch and Caine, 1984; Owens and Slaymaker, 2004), where the distinctively bedrock-dominated relief is linked to a high potential energy for bedrock erosion, a dominance of rapid gravitational processes and unique coarse-grained landforms such as talus slopes (Caine, 1976; Chorley et al., 1984).

Alpine or mountain systems have been widely recognised to represent a nested, hierarchical aggregation of individual landforms (Penck, 1896; Dikau, 1989; Brunsden, 1996). In this so-called 'landform palimpsest', a term introduced by Chorley et al. (1984), the dimension (form, shape) and key morphometric attributes of landforms are scale-dependent and linked to different lifetimes (Brunsden, 1996). Dikau (1992), following Kugler (1964), proposed a geomorphometric hierarchical conceptualisation of landform (or relief) types at

[1] In this thesis, 'alpine' and 'mountain' will be adequately used when describing rock slope systems.

different spatial scales. In Table 2.1, Dikau's approach is transferred to mountain rock slope systems based on the example of the Turtmann Valley in the Swiss Alps.

Table 2.1: *Relief characteristics and key morphometric attributes of mountain systems at different spatial scales according to the hierarchical approach proposed by Dikau (1989, 1992). Example landforms and key morphometric attributes are illustrated for the Turtmann Valley.*

	Width (m)	Area (m^2)	Example landform		Key morphometric attributes
Macrorelief B	10^6	10^{12}	Mountain range: Swiss Alps	*Relief form association*	• Altitude • Hillslope profile • Valley profile • Topological position • Distance to watershed • Surface roughness • Attribute variability
Macrorelief A	10^5	10^{10}	Glacial Valley: Turtmann Valley		
Mesorelief C	10^4	10^8	Hanging valley (e.g Hungerli Valley)		
Mesorelief B	10^3	10^6	Mountain hillslope (i.e. rockwall-talus systems)		
Mesorelief A	10^2	10^4	Rockwall, talus slope	*Relief form*	• Surface roughness • Attribute variability
Microrelief B	10^1	10^2	Rockwall foot, crest talus apex, mid slope	*Form element*	• Plan curvature • Profile curvature
Microrelief A	10^0	10^0	Jointed rock mass	*(Form elements) Form facets*	• (Plan curvature) • (Profile curvature) • Slope angle • Slope aspect
Nanorelief	10^{-2}	10^{-4}	Intact rock, joint, Rockfall block, flakes Talus erosional rills		

The smallest spatial scales (Nanorelief, Microrelief A in Table 2.1) are mainly composed of simple form facets with uniform slope angle and aspect. Examples of Nanorelief are small areas of 10^{-4}-10^0 m^2 of intact rock (without joints) or single rockfall blocks at the foot of talus slopes. As soon as joints are present, the jointed bedrock (rock mass) represents form facet of the microrelief (10^0 – 10^2 m^2). One hierarchical level higher (Microrelief B) uniform plan or profile curvature represents the key morphometric attribute, leading to a form element of 10^2-10^4 m^2. Typical examples are the lower rockwall foot or segments of a talus slopes such as the apex or mid slope. On a higher scale (Mesorelief A) the association of homogenous form elements leads to a relief form of > 10^4 m^2, with a complex surface roughness and geometrical attribute variability. In mountain

systems the rockwall and talus slope are major landform types. At a higher scale, mountain hillslopes (i.e. rockwall-talus systems), the glacial valley with its lower-scale hanging valleys as well as the mountain range of the Swiss Alps represent more complex relief form associations. For a geomorphometric description of those Meso- and Macroscale entities (10^2 -10^6 m^2) the importance of local slope gradient or curvature decreases in favour of more synoptic, regional attributes such as altitude, hillslope profile, valley profile, topological position and distance to watershed (Dikau, 1994).

2.2 Mechanical material characteristics

Since joints are among the most important causes of excessive overbreak and of trouble with water, they always deserve careful consideration. (Terzaghi, 1946 in Palmström, 2005, p. 2)

2.2.1 Preliminary considerations of the anisotropy of mountain rock mass

The mechanical material of mountain rock slopes is solid, anisotropic rock mass that is defined to be composed of (i) the intact rock and (ii) the three-dimensional discontinuity pattern. In geology, the intact rock refers to the unfractured blocks between structural discontinuities and may range from a few millimetres to several metres in size. The intact rock is characterised by its physical characteristics such as mineral composition, texture, grain size and porosity as well as its mechanical characteristics such as hardness, brittle behaviour or plasticity (Singh and Goel, 2011). Therefore, even without (microscopic) discontinuity structures, the homogenous intact rock owns a distinct mineral-controlled anisotropy (Goodman, 1989). In this study, major focus will be on low-porosity, mica-rich metamorphic rocks. As result of regional Alpine folding processes and tectonic stresses, the paragneiss' intact rock is highly anisotropic and dominated by a pronounced, slightly wavy schistocity. This parallel arrangement of platy mineral grains (i.e. mica) creates major zones of weakness (Wyllie and Mah, 2004) and is linked to a highly directional deformability (Goodman, 1989).

As highlighted by the above quotation of Terzaghi (1946), the stability of mountain rock slopes is never solely controlled by the intact rock mass, but essentially by the three-dimensional structures of discontinuities. The structural control is scale-dependent, as discontinuities can occur as fissures, fractures, cracks, bedding planes, faults etc., either singularly or in a set or system. Commonly, *discontinuity* or *joints* are used as collective terms for the whole range of mechanical defects (Priest, 1993). Metamorphic rocks, for instance, are typically dominated by micro-scale tectonic joint systems, which can be visible over considerable distances with uniform orientations independent from lithology parallel to the regional-scale tectonic layering of Alpine nappes. However, if no evidence of genesis or geological origin has been made (e.g. tectonic bedding, thermal cracks), joints and discontinuities will be used synonymously in this thesis.

2.2.2 Valley and rockwall scale: In-situ stress field

The in-situ stress field of steep mountain valley flanks is crucial for the understanding of joint evolution and the deformation behaviour of rock mass, i.e. in the paraglacial context (see chapter 2.4). As illustrated in Figure

2.1, it can be approximated by the orientation and magnitude of the vertical and horizontal component of the (three) principal stresses, where the major principal stress σ_1 always acts horizontally parallel to the surface. The major stress can be expressed by:

$$\sigma_1 = \gamma H \qquad (2.1)$$

Where H is the depth [m] below the ground surface and γ is the unit weight [MN/m³] (Wyllie and Mah, 2004). Equation 2.1 reveals that the horizontal stress magnitude σ_1 is mainly controlled by the weight of overburden at a particular depth and increases linearly with depth. As shown in Figure 2.1 the minor principal stress component σ_3 acts perpendicular to the rock slope in the vertical direction. It results from the lateral confinement provided by the surrounding and overlaying rock mass (Wyllie and Mah, 2004; Prinz and Strauß, 2011).

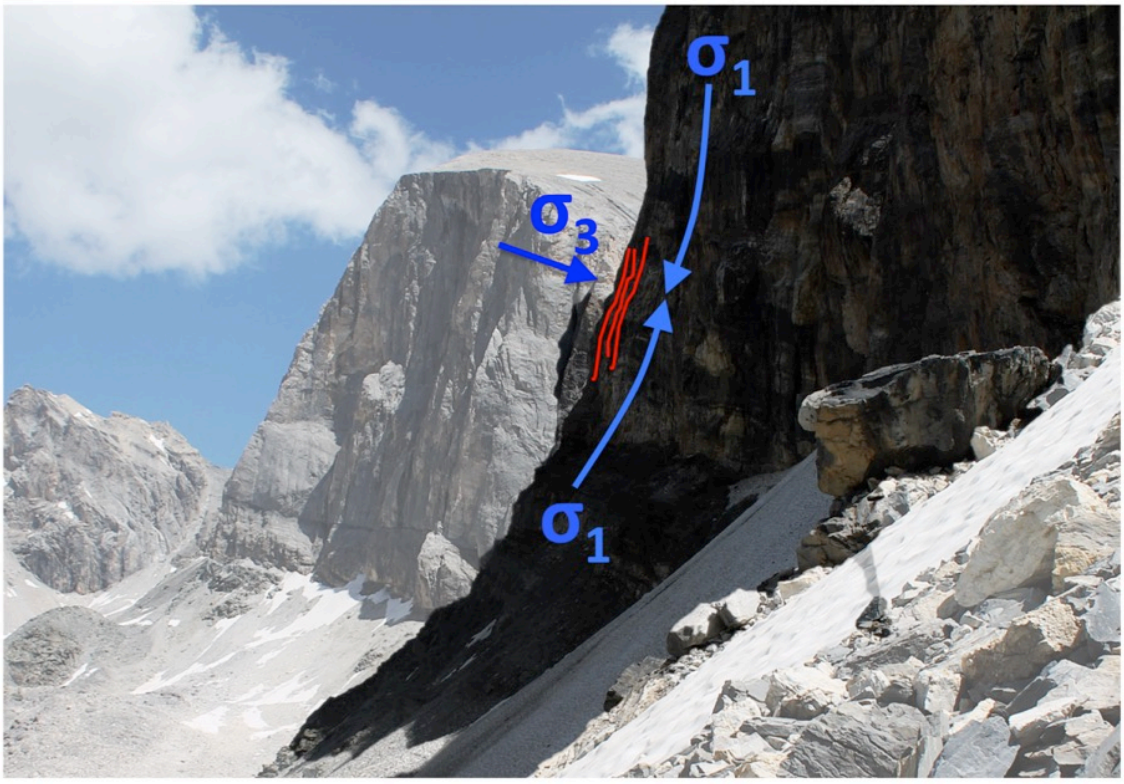

Figure 2.1: *Schematic illustration of in-situ stress field (σ_1 = maximum principal stress, σ_3 = minimum principal/gravitational stress) of mountain valley flanks. High horizontal to vertical stress ratios (σ_1/ σ_3) can be the reason for the formation of sheeting joints (red signature) due to stress release.*

The existing stress field of a rock slope is therefore primarily a function of the rock depth and the ratio between the horizontal stress and vertical stress. However, the stress trajectories can be influenced by the discontinuity pattern (i.e. schistosity), the local long-term geological, tectonic (i.e. overconsolidation) and glacial history, and can vary highly with valley or slope topography (Hencher et al., 2011; McColl, 2012; Leith et al., 2014a). High horizontal to vertical stress ratios (σ_1/ σ_3) can be the reason for the development of surface-parallel exfoliation, stress-relief, stress release joints or sheeting joints (Figure 2.1). The latter term is preferred

if no reference to the process of formation should be made (McColl, 2012). It is widely accepted that their formation is the consequence of tensile stresses, which develop due to the removal of overburden caused e.g. by long-term erosion of surrounding rock mass or - in (de)glaciated mountain valleys - by glacial unloading (see chapter 2.4). Normally, the overburden of surrounding rock mass provides sufficient confining pressures, which prevent the development of sheeting joints. However, if the overburden is removed the confining load decreases and results in a redistribution of the principal stresses. Typically, the slope-parallel stress component σ_1 distinctly increases in magnitude relative to the vertical stress σ_3 (Figure 2.1). As a consequence, high tensile stresses occur, which can - if exceeding the tensile strength of the rock - trigger the formation of joints and their propagation in surface-parallel direction (Brunner and Scheidegger, 1973; Twidale, 1973; Nichols, 1980; Hencher et al., 2011).

In deglaciated mountain valleys, sheeting joints have been recognised to play a major role for post-glacial rock slope failures, particularly in massive granite and gneiss rocks (Balk, 1939; Brunner and Scheidegger, 1973; Jarman, 2006; McColl, 2012). They can occur up to 100 m rock depth – although spacing increases with depth - and can often be traced laterally for several hundreds of meters nearly parallel to the ground surface. Their slope-parallel orientation, their long persistences and the lack of intact rock bridges are distinct characteristics to differentiate these geologically young structures from most pre-existing tectonic joints (Hencher et al., 2011).

2.2.3 Rockwall scale: Rock mass strength and its field classification

In consideration of the rock mass strength of mountain rock slopes, careful distinction has to be made between the (i) the rockwall-scale strength of a jointed rock mass and the (ii) lower-scale strength of intact rock without discontinuities.

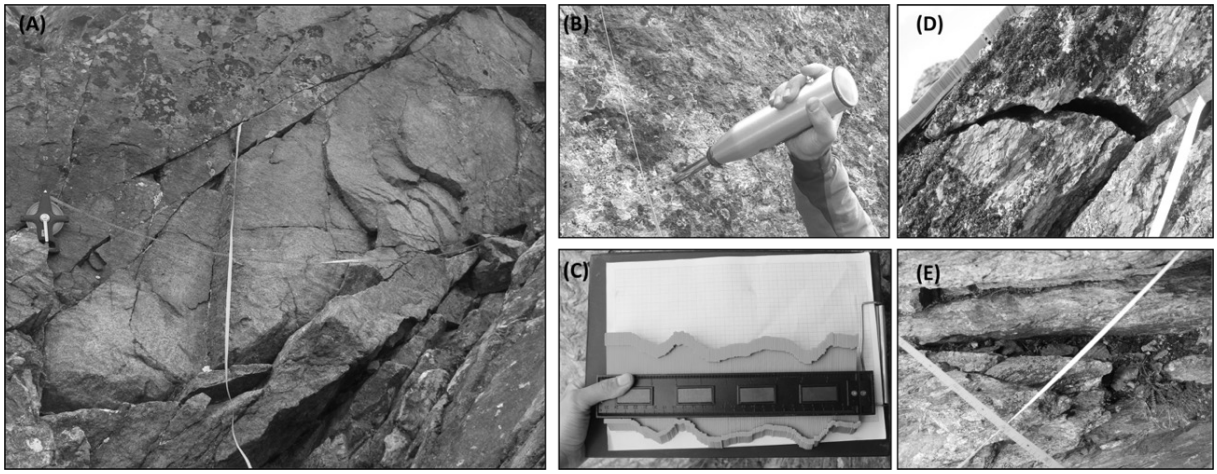

Figure 2.2: *Vertical and horizontal scanline transect (A) to quantify intact rock strength by using the Schmidt Hammer (B) as well as geotechnical and geometrical joint parameters such as joint spacing, persistence (A), joint roughness (C), opening (D) and infilling (E).*

The rock mass strength is usually characterised based on semi-quantitative classification of the mechanical and geometrical rock mass properties. The result is therefore a holistic semi-quantitative estimate of the slope-scale rockwall stability, from which values can be subsequently used to calculate the rockwall's failure criterion.

Different classification approaches have been proposed, in particular for civil engineering applications, such as the RMR system of Bieniawski (1987) and the Q-system of Barton (2006). A detailed summary of different approaches of rock mass strength classification is provided e.g. Edelbro (2003). For geomorphic purposes, the rock mass strength classification system (RMS) of Selby (1980); Selby (1982a) is probably the most widely known. Like the engineering approaches, Selby's RMS approach accounts for most of the above joint parameters as well as the intact rock strength and the weathering state of the rock mass.

A total of eight parameters needs to be assessed along vertical and horizontal transects on accessible rockwalls (Figure 2.2A), by using simple field methods such as a tape measure, an inclinometer, a compass and a Schmidt Hammer (Figure 2.2B) and occasionally a roughness measure (Figure 2.2C) (Selby, 1993). For weak rocks it is appropriate to use the 'L' type Schmidt Hammer to evaluate the intact rock strength. Generally, the higher the rebound R value, the harder and more intact the rock (Viles et al., 2011). Based on the scheme in Table 2.2, each parameter is rated according to its perceived influence on rock stability (or see refinement by Moon, 1984).

Table 2.2: *Rock mass strength classification system proposed by Selby (1980), refined by Moon (1984).*

Criteria	(1) Very strong	(2) Strong	(3) Moderate	(4) Weak	(5) Very weak
Intact rock strength N-type Schmidt Hammer	100-60	60-50	50-40	40-35	35-10
Rating	***20***	***18***	***14***	***10***	***5***
Weathering	Unweathered	Slightly weathered	Moderately weathered	Highly weathered	Completely weathered
Rating	***10***	***9***	***7***	***5***	***3***
Joint spacing	> 3 m	3-1 m	1-0.3 m	0.3-0.05 m	< 0.05 m
Rating	***30***	***28***	***21***	***15***	***8***
Joint orientation	> 30° into slope	< 30° into slope	Horizontal or vertical	< 30° out of slope	> 30° out of slope
Rating	***20***	***18***	***14***	***9***	***5***
Joint width	< 0.1 mm	< 0.1-1 mm	1-5 mm	5-20 mm	> 20 mm
Rating	***7***	***6***	***5***	***4***	***2***
Joint continuity (or persistence)	None continuous	Few continuous	Continuous, no infill	Continuous, thin infill	Continuous, thick infill
Rating	***7***	***6***	***5***	***4***	***1***
Groundwater outflow	None	Trace	Slight	Moderate	Great
Rating	***6***	***5***	***4***	***3***	***1***
Total rating	**100-91**	**90-71**	**70-51**	**50-26**	**<26**

As shown in Table 2.2 greatest importance is given to the intact rock strength, joint spacing and joint orientation with maximum ratings of 30. The sum of the individual weightings then results in a final RMS value ranging from very strong (> 91) to very weak (< 26). Today, Selby's classification scheme has been proven to be a reliable and easy method of rock mass classification that can keep up with engineering schemes, particularly in the study of highly weathered rock slopes (cf. Goudie, 2004 p. 879). Over the past 30 years, it has significantly improved our understanding of the instability and morphology of rock slopes in different lithological and climatic environments such as Antarctica (Selby, 1980), New Zealand (Augustinus, 1992; Brook and Hutchinson, 2008), Western Australia (Allison and Goudie, 1990), Southern Africa (Moon and Selby, 1983) and the European Alps (Krautblatter et al., 2012; Heckmann et al. 2016).

2.2.4 Rock mass scale: Key geometrical and mechanical joint properties

The stability of mountain rock slopes is directly influenced by the geometrical pattern of joints and their mechanical characteristics. As illustrated in Figure 2.3, joints occur on all scales, either occurring as random, individual or as parallel sets of joints with similar orientation. Thus, on all scales, they represent significant zones of weakness in the much stronger intact rock so that rock failures preferentially occur along these planes (Goodman, 1989). Figure 2.4 displays the essential geometrical properties of joints, which have been described in detail by e.g. Wyllie and Mah (2004) and Selby (1993). Field description of joint properties is commonly performed in geotechnical scanline or transect surveys, quantitatively, according to the suggested methods of the International Society of Rock Mechanics (ISRM, 1978) or, semi-quantitatively with focus on the higher-scale rock mass strength, after the geomorphic classification of Selby (1993).

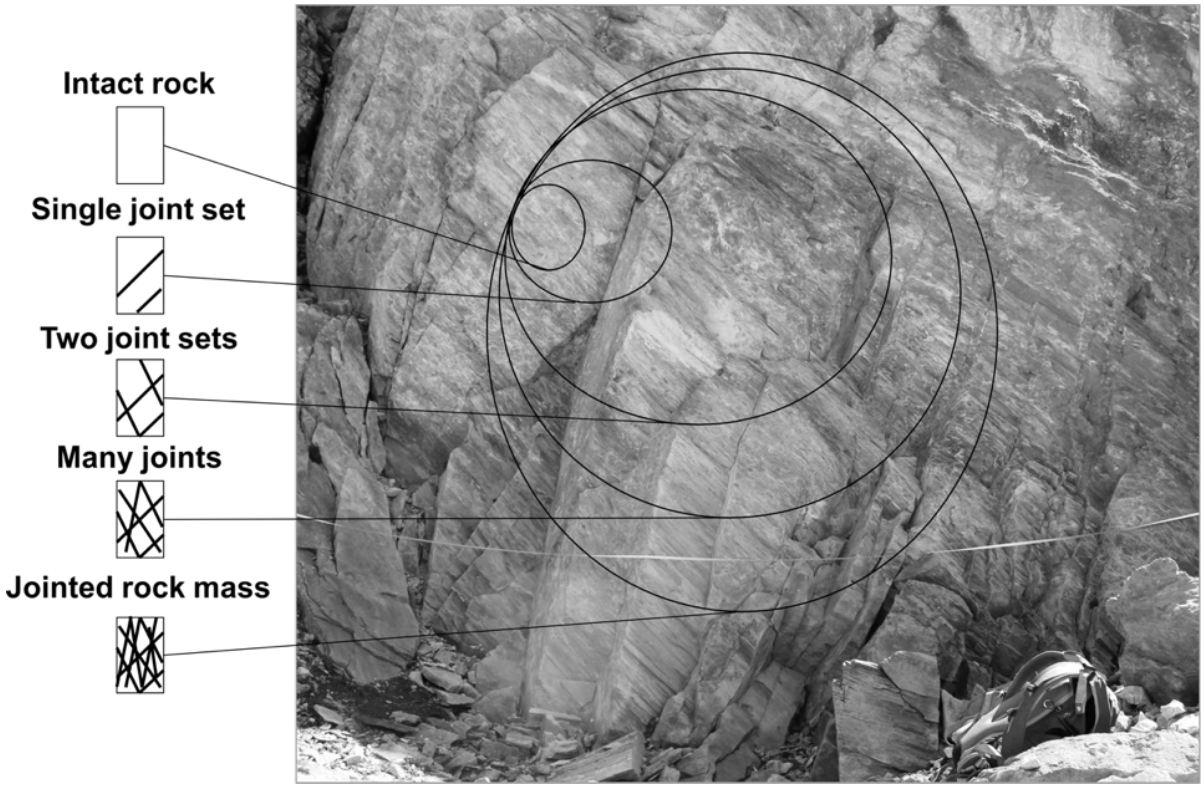

Figure 2.3: *Photograph of a geotechnical transect along a natural rock slope exposure (Hungerli Valley) and schematic illustration of the scale-dependent transition from intact rock to jointed rock mass. Schematic illustration derives from Wyllie and Mah (2004, p. 74) .*

Joint orientation

The orientation of a joint can be described by its dip and dip direction. The dip refers to the maximum angle of the plane to the horizontal, whereas the dip direction defines the horizontal line of the dip clockwise from north (Figure 2.4). Parallel oriented joints form a joint set. Commonly, a geotechnical description of joint orientation is made quantitatively according to the suggested methods of ISRM (1978). For geomorphic purposes, however, joint orientation is often qualitatively described by considering its relationship with the slope surface (Selby, 1993). Knowledge about joint orientation relative to the slope surface is of crucial importance as it significantly defines the probability of instability (Moore et al., 2009) and the mode of rock failure (Terzaghi, 1962; Cruden and Hu, 1994). Whether rockfall will be released by e.g. toppling or sliding can be identified by means of kinematic analysis of stereographic projections. Most commonly, equal area projections such as the Schmidt nets are used as they allow a 2D representation of the three-dimensional joint data in form of poles and great circles. Specific examples will be given in section 2.5.2.

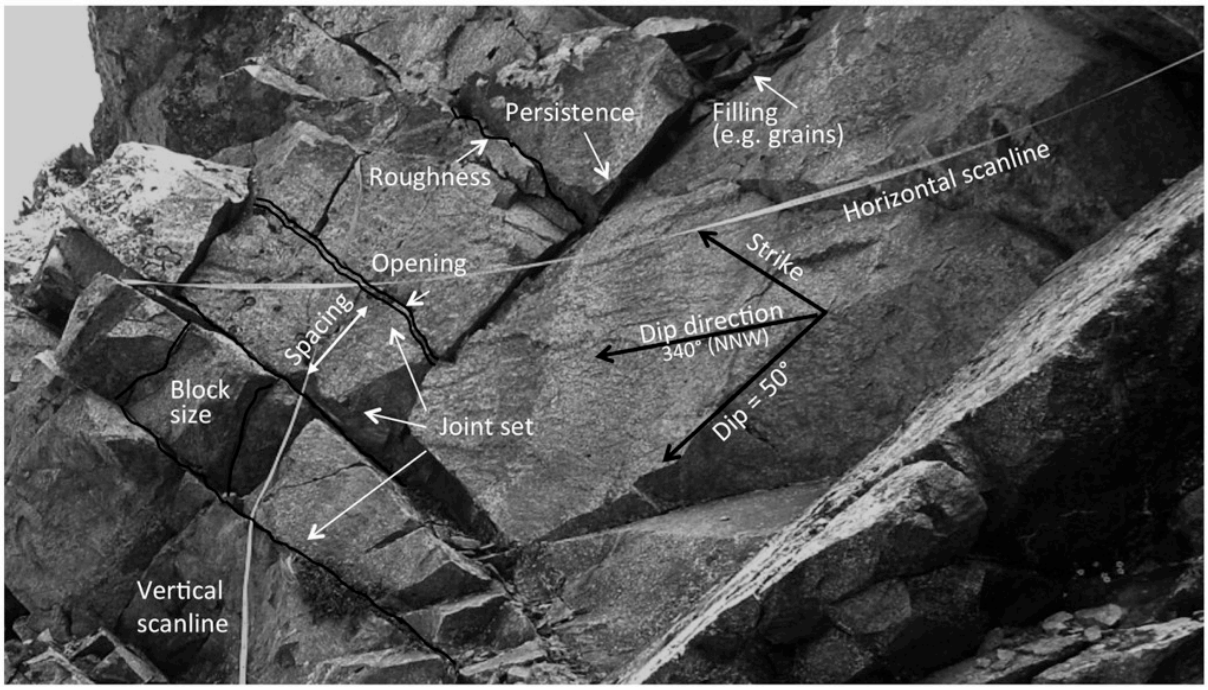

Figure 2.4: *Schematic illustration of the key joint properties analysed in this study. Field description of joints is commonly performed along geotechnical scanline or transect surveys.*

Joint spacing or density (block volume)

Joint spacing defines the perpendicular distance between two parallel joints of one set (Figure 2.4), which can range from extremely close spacing (< 6 mm) to extremely wide (> 2 m) (ISRM, 1978). If the 'apparent' spacing is measured along scanline transects, as shown in Figure 2.2, correction by the angle between face and joint strike is necessary. Joint spacing directly affects the entire rock stability in comparison with the intact rock material. In particular, it has been demonstrated that compressive rock strength and the potential of water pressures or hydraulic conductivity is inversely proportional to the spacing of joint sets (Deere and Miller, 1966; Bieniawski, 1987). Moreover, joint spacing largely controls the individual block size (Figure 2.2) of the

intact rock, ranging from crushed rock of cm^3 to several m^3 in massive rock (Dearman, 1991). The block size in turn can determine whether failure will occur translational as continuous (bulk) material, or e.g. as circular rotation of a discontinuous material (ISRM, 1978; Barton, 1990). Palmstrom (1982) introduced the volumetric joint count Jv as a quantitative measure to define the total number of joints intersecting a cubic metre of rock mass. Jv can range from very low (< 1) to crushed (< 60). Ideally, in rock mass with at least three well-defined joint sets (S1, S2, S3), Jv can be calculated as (Palmstrom, 2005):

$$Jv = 1/S1 + 1/S2 + 1/S3 \qquad (2.2)$$

Where γ1, γ2, γ3 are the angles between the three joint sets S1, S2, S3. Then, block size V (m^3) with respect to three different block shapes (cubic, elongated, platy) can be inferred from a chart provided by Palmstrom (1982). As joint sets rarely intersect at 90° angles, final block size Vb must be adjusted by the intersecting angles (a, b, c) between each joint set:

$$Vb = V \times 1/\sin a \times 1/\sin b \times 1/\sin c \qquad (2.3)$$

Persistence

The persistence, which is often synonymously described as 'continuity' e.g. by Selby (1980), defines the continuous length or area of a discontinuity (Figure 2.4). Categories of the ISRM (1978) range from very low (< 1 m) to very high (> 20 m) persistence. The persistence is of crucial importance for the effective cohesion of rock mass (Terzaghi, 1962) and the rock bridges of intact rock (Einstein et al., 1983; Eberhardt et al., 2004). Specifically, more persistent joints represent significant shear zones as they reduce the cohesive rock strength and permit the circulation of water into depth (Selby, 1993). However, in metamorphic rocks, joints are rarely fully persistent. Here, the importance of joint persistence is mainly the geometrical interaction with the joint spacing and orientation, as it crucially determines the released block size and shape.

Aperture, filling and seepage

The aperture is the perpendicular distance separating the adjacent walls of an open joint (Figure 2.4). It may range from < 0.1 mm to > 1m and is therefore significant to rock stability. It crucially affects the hydraulic conductivity and deformation the rock mass under stress changes (Wyllie and Mah, 2004). Aperture is often distinguished from the 'width' of a filled discontinuity (ISRM, 1978). In widely opened and filled joints, the rock mass stability is mainly controlled by the inherent strength of filling material. This is most significant where the infill is clay. In contrast, highest frictional and cohesive strength occurs in rock mass with nearly closed joints (Barton, 2013).

Furthermore, water flow or seepage through porous and jointed rock mass can significantly control the rock stability in different ways. Pore water in intact rock can decrease its compressive strength, while pore

water in joint filling materials can reduce the cohesive and frictional strength of the infill. Likewise, cleft-water pressures along joint surfaces can produce uplift forces along potential failure planes (Selby, 1993).

Roughness

All (open) joints display inner surfaces (Figure 2.4) with different degrees of surface roughness ranging from stepped to undulated, very smooth or planar slickenside (ISRM, 1978). The roughness degree of a discontinuity surface is of major importance for the deformation behaviour of bedrock and its resistance to stress, especially where joints are unfilled. In turn, the importance of surface roughness decreases with increasing joint opening, infilling thickness or if previous displacement occurred (Wyllie and Mah, 2004). The effect of joint roughness is scale dependent. Small-scale asperities or 'unevenness' normally affects the shear strength of sample-size rock mass (e.g. in laboratory tests). In contrast, larger scale undulations or ‚waviness', where asperities are interlocked and too large to be sheared off can cause dilation during shear displacement (Patton, 1966; Selby, 1993). The roughness (or dilatation) can be expressed by the average angle *i* of the asperities (see chapter 2.5.1) along the joint surface (Patton, 1966).

2.3 Thermal material characteristics

2.3.1 Valley and rockwall scale variability of rock temperature

In geomorphic research, the thermal material characteristics of mountain rock slopes have become increasingly important when it comes to understanding the spatiotemporal pattern destabilisation of rock failures. During the last two decades, quantitative measurements of rock slope temperatures have been emerged – although slowly. Particularly in the European Alps, those thermal studies significantly strengthen the assumed relationship between bedrock instability, rockfall activity and the bedrock temperature-depth field (e.g. Coutard and Francou, 1989; Wegmann et al., 1998; Gruber et al., 2004b; Gruber and Haeberli, 2007; Matsuoka, 2008; Hasler et al., 2011b; Haberkorn et al., 2015a; Haberkorn et al., 2015b; Magnin et al., 2015a; Phillips et al., 2016).

In permafrost-affected areas, several rock slopes are instrumented with boreholes to monitor the spatiotemporal evolution of the ground thermal regime and to evaluate the resulting mechanical behaviour of the rock mass. Largest monitoring projects are e.g. the European Union PACE project (Harris et al., 2001; Harris et al., 2009), the Swiss Permafrost Network (PERMOS, 2016), PermaNET (Mair et al., 2011) or MOREXPERT (Keuschnig et al., 2011). Despite their unique insights into permafrost and temperature changes at depth of 15-100 m, however, cost-intense borehole projects are usually scant and the thermal records are restricted to individual major mountain peaks like the Zugspitze, Matterhorn, Aiguille du Midi or Kitzsteinhorn.

Miniature data loggers such as iButtons ® (Figure 2.5A) with diameters of only 17 mm provide promising commercial low-cost devices to study the near-surface temperatures of unstable rock slopes. Depending on the research purpose, they can be easily installed at the upper 10-100 cm of bedrock surface in different

topographic and lithological settings. Given their accuracy of ±0.5 °C at an operating temperature range of -10 °C to +65 °C (e.g. iButtons ® type DS1922L (Hartmeyer et al., 2012), miniature loggers provide high-resolution temperature data that are comparable to more expensive UTL3 loggers (±0.1 °C).

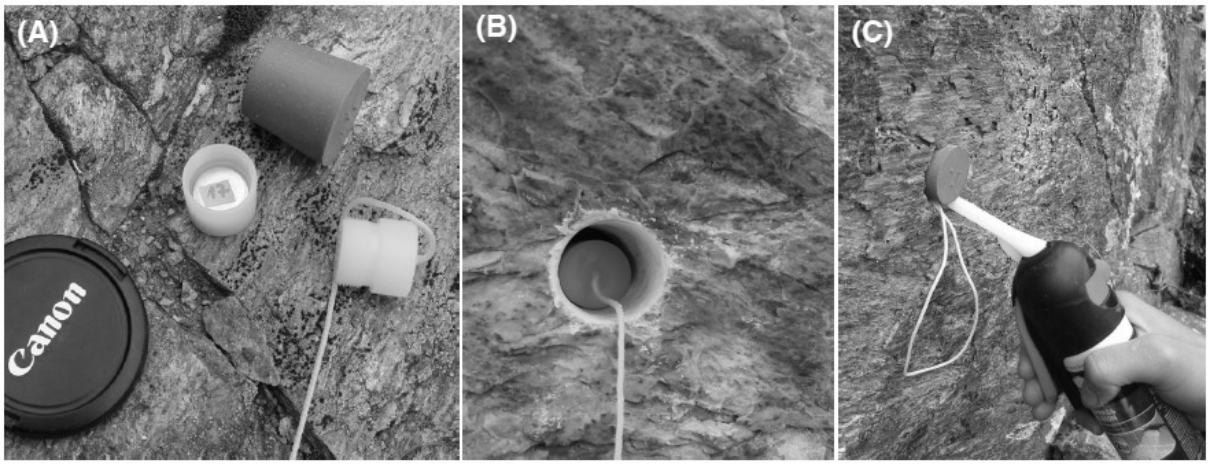

Figure 2.5: *Field installation of miniature temperature loggers at high-mountain rockwalls according to the strategy proposed by Gruber et al. (2003). (A) iButtons ® type DS1922L with diameter of 17 mm is enclosed in waterproof (and thermally coupling) polyethylene capsules to avoid water intake and (B) drilled into 10 cm bedrock depth. Finally, (C) drilling openings is sealed by a rubber plug and silicone to avoid air- or water-intake into borehole.*

Commonly, field instrumentation of data loggers is performed as proposed by Gruber et al. (2003). As emphasised by Hipp et al. (2014), using the similar installation design maintains consistency with previous work and allows comparison of Alpine temperature records (Gruber et al., 2004b; Haberkorn et al., 2015a; Magnin et al., 2015a) with e.g. data from Scandinavia (Hipp et al., 2014) or New Zealand (Allen et al., 2009). Following the strategy of Gruber et al. (2003), loggers are enclosed e.g. in waterproof polyethylene capsules (Figure 2.5A) and installed at 10 cm bedrock depth at locations representative for the whole rock slope. A small drilling diameter (18 mm, Figure 2.5B) guarantees good coupling between rock and logger. Finally, sealing of drilling opening prevents air- or water-transfer into the borehole (Figure 2.5C).

In comparison to borehole transects, the easy and low-cost installation of miniature loggers permits temperature monitoring over many square kilometres within mountain valleys. One of the spatially most extensive applications of iButtons exists for the Corvatch area (Swiss Eastern Alps). Wwithin an area of approximately 16 km², Gubler et al. (2011) and Schmid et al. (2012) have installed and analysed 39 and 390 loggers (but mostly below loose debris), respectively. Although logger data are restricted to the upper meter of bedrock surface, their interpretation with respect to site-specific topographic, climatic and mechanical characteristics allows extrapolating the bedrock temperature field as well as depth-distribution of permafrost in time and space.

Previous studies both from Alpine and Artic environments demonstrate that rock temperatures highly vary in time and space. In fact, this spatiotemporal variation is interpreted as evidence for the strong dependence on topographic and climatic controls. For instance, mean annual rock temperature (MART) of e.g. two E-W

oriented ridges have been found to differ by more than 5 °C in mid-latitudes (Swiss Alps, Gruber et al., 2004b; New Zealand, Allen et al., 2009) or by up to 10 °C in slightly higher latitudes (Norway, Hipp et al., 2014) albeit similar aspect, slope or elevation. MART differences between mountain valleys appear therefore to be primarily governed by contrasting geographic settings (altitude, latitude) and macro-scale climatic or meteorological influences such as sun angle, intensities of solar radiation, wind and precipitation systems (Hasler et al., 2015).

Likewise, by comparing different mountain peaks within one mountain valley, elevation difference of only 200 m have been found to cause MART differences of 6-8 °C between sites which are otherwise comparable (Gruber, 2005). In turn, temperatures of rockwalls within a similar elevation belt, but with contrasting aspects, can differ significantly due to the key role of the net short-wave radiation (Hall, 1997; Hall and André, 2001; Lewkowicz, 2001). Generally, MARTs of N-facing rock slopes are several degrees lower than those of southern sun-exposed bedrock at comparable elevations; with N-S differences of 5-8 °C in the European Alps (Gruber et al., 2004b; Gubler et al., 2011; Hasler et al., 2015) or e.g. 3-3.5 °C in Norway (Hipp et al., 2014). Occasionally, even small E-W temperature differences may occur, which can be linked e.g. to the influence of cloud cover (Gunzburger and Merrien-Soukatchoff, 2011), the shading of surrounding topography or nearby glaciers or snow packs that amplify the incoming short-wave radiation (Lewkowicz, 2001; Allen et al., 2009; Hasler et al., 2011b). However, the aspect-related difference largely disappears during winter and all aspects have broadly similar rock temperatures due to the lower sun angle.

Rock temperatures can also highly differ along one rock slope of homogenous aspect or slope angle, primarily due to the strong influence of the rockwall micro-morphometry and the associated microclimate. Noetzli and Gruber (2009) demonstrate, for instance, that rock temperatures may react faster to changing air temperatures at concave and steep slopes, as thermal fluxes have to penetrate shorter distances into the rock depth than in flat and convex terrain. Similarly, as discussed later, rockwalls with pronounced micro-topography, where snow can efficiently accumulate, have usually 2-3 °C higher MART and distinctly smoothed daily temperature amplitudes during winter in comparison to snow-free sites (Coutard and Francou, 1989; Matsuoka and Sakai, 1999; Pogliotti, 2001; Haberkorn et al., 2015a; Hasler et al., 2015; Magnin et al., 2015a). Figure 2.6 summarises above stated topoclimatic variations of near-surface rock temperature with respect to Dikau's (1996) hierarchical relief approach presented in Table 2.1. Accordingly, from a topoclimatic perspective, the temperature signal measured e.g. by iButtons ® may be the result of (Figure 2.6A) macro-scale geographic and climatic/meteorological influences, (Figure 2.6B) local topoclimatic characteristics and (Figure 2.6C) the micro-morphometry and-climate of mountain rock slopes.

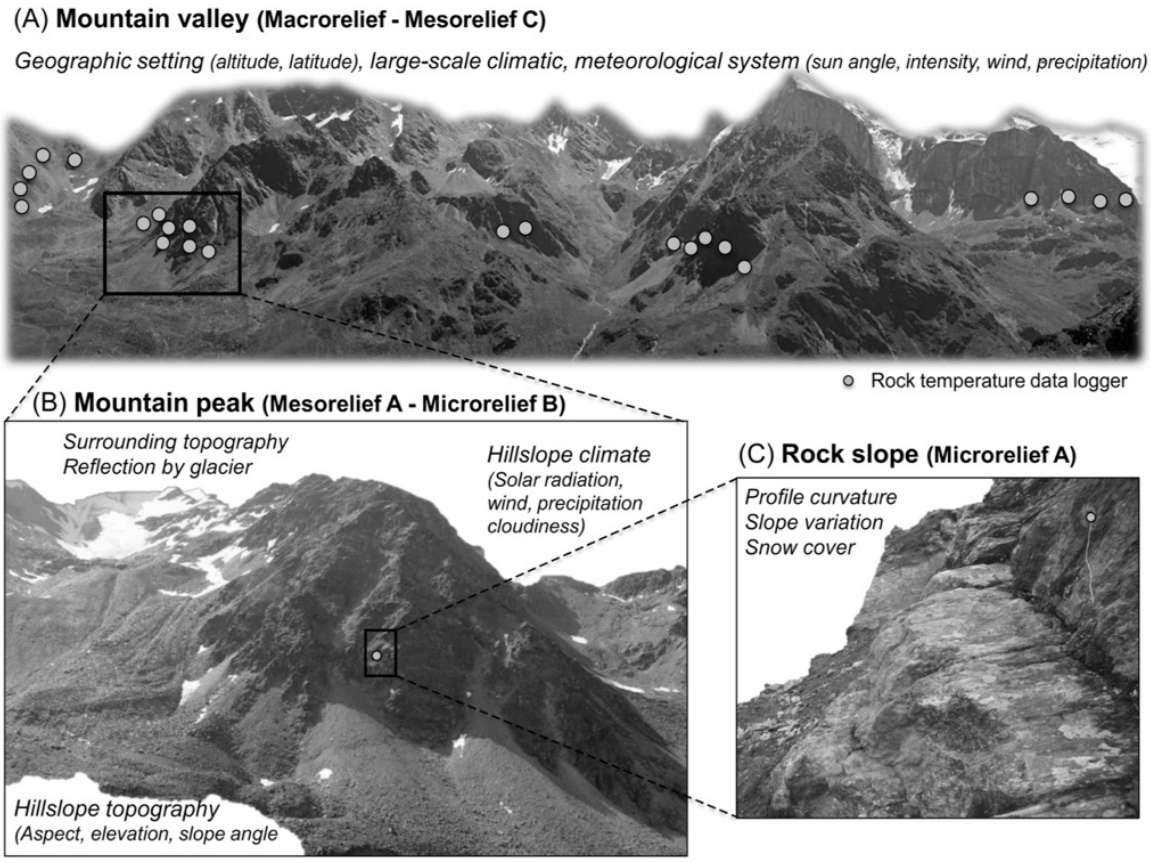

Figure 2.6: *Schematic hierarchical concept of topoclimatic dependence of rock temperatures with respect to different relief characteristics according to the nomenclature and approach of Dikau (1996). So far existing studies clearly demonstrate that near-surface and ground bedrock temperatures significantly vary in time and space as result of (A) macro-scale geographic and climatic/meteorological influences, (B) local topoclimatic characteristics and (C) the micro-morphometry and micro-climate of mountain rock slopes.*

2.3.2 Rockwall scale: Energy exchange between atmosphere and ground surface

The ground thermal material characteristics or regime of high-mountain rockwalls are the result of heat and moisture fluxes that exchange between the atmosphere and the ground surface, as shown in Figure 2.7 (based on Krautblatter, 2009). Furthermore, the thermal propagation into depth is governed by thermal properties of the ground material. In its simplest form, the net exchange of radiation Q* between atmosphere and rock surface involves three major components and can be expressed by following heat balance (Williams and Smith, 1989):

$$Q^* = Q_{LE} + Q_H + Q_G \qquad (2.4)$$

$$0 = Q^* \pm Q_{LE} \pm Q_H \pm Q_G \qquad (2.5)$$

Solar radiation provides the primary source of energy Q* (W/m²) and reaches the rock surface in form of shortwave $S_{in/out}$ and long-wave/infrared radiation $L_{in/out}$. Depending on the surface albedo, a percentage of radiation is reflected back (Barry and Chorley, 2010). The amount of incoming $L_{in/out}$ is relatively constant over large areas following large-scale atmospheric climatic conditions, whereas the $S_{in/out}$ highly varies in space and time depending on the sun's azimuth and zenith angle or sunshine duration (Oke, 1987; Gruber, 2005). The

term Q_{LE} defines the energy transfer that involves latent heat produced/consumed during evaporation (condensation) or melting (freezing) of water. Thus, latent heat is linked to a phase change of water, but no temperature change. The term Q_H refers to the turbulent transfer of sensible heat that is produced during air convection and advection. In mountain valleys, sensible heat transfer is most efficient when warm and strong valley winds are blown on rough (rock) surfaces that are colder than the air mass (Benn and Evans 2010). Finally, Q_G defines the ground heat flux through the solid rock (also valid for soil) to or from the surface (Williams and Smith, 1989).

Depending on the purpose, the heat balance in equations 2.4 and 2.5 can be extended by further components (e.g. snow, glacier) and can be applied to any time scale (e.g. annual, monthly, diurnal, hourly). Thereby, the relative importance of each heat component can spatially and temporally vary. Nevertheless, according to the conservation principle in equation 2.5, all heat fluxes towards the surface (energy input, '+') and away from the surface (energy loss, '-') must always balance. Consequently, if the intensity of one surface heat flux changes, there must be balancing modifications in another one (or more). This automatically leads to changing temperatures of the rock surface and ground (Williams and Smith, 1989; Barry and Chorley, 2010).

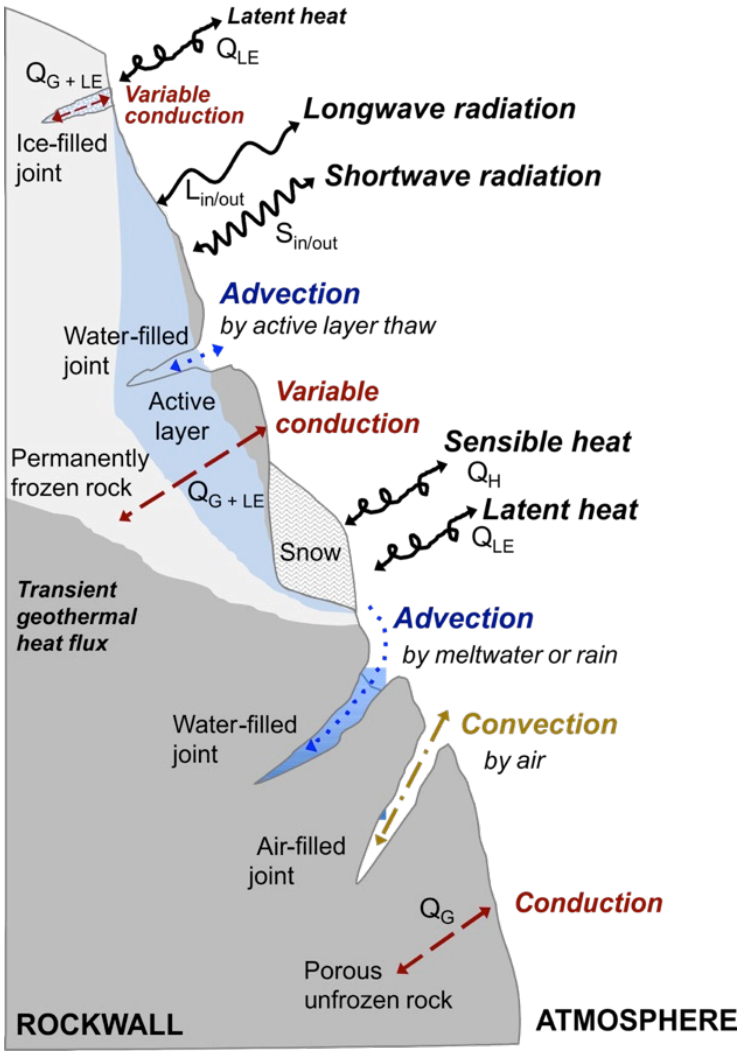

Figure 2.7: *Schematic diagram of the key thermal processes governing the thermal regime of permafrost- and snow-affected high-mountain rockwall. Illustration is based on the original figure of Krautblatter (2009, p. 15) and has been slightly modified.*

2.3.3 Rock mass scale: Conductive, convective and advective heat transfer

Figure 2.7 illustrates the major energy transfer processes on a rock mass scale, i.e. the conductive, convective and advective heat transfer caused by the lower-scale bedrock morphometry and rock mass anisotropy (Krautblatter, 2009). In geomorphic studies, rockwall temperatures are commonly understood by considering the rock mass as homogenous solid medium with air-, water- or ice-filled pores where conductive heat transfer in vertical direction dominates (Carslaw and Jaeger, 1986). The amount of conductive heat can be expressed by Fourier's law:

$$Q_G = - K (\Delta T / \Delta z) \qquad (2.6)$$

Equation 2.6 indicates that the actual rate of heat transfer largely depends on the thermal conductivity *K*. The negative sign of *K* is a consequence of the second law of thermodynamics, indicating that heat must flow in the direction z from higher to lower temperature *T*. Thus, for a given temperature gradient ΔT the more heat will flow through the rock, the higher the conductivity of a material is (Williams and Smith, 1989). For alpine metamorphic and igneous rocks typical *K* values range between 1.5 and 3.5 W m^{-1} K^{-1}, varying with temperature, porosity and foliation (Vosteen and Schellschmidt, 2003). Generally, the thermal conductivity increases with increasing water content and is greater in frozen than in unfrozen rock (Barry and Chorley, 2010).

Assuming conduction as major heat transfer has much practical value in geomorphic studies as it enables a reduction of the ground thermal regime of mountain bedrock to its most simple. For instance, application of the heat conduction theory has been proven to analyse the efficiency of frost cracking (e.g. Anderson, 1998; Hales and Roering, 2007) or the thermal conditions of permafrost rockwalls (Gold and Lachenbruch, 1973; Noetzli et al., 2007; Noetzli and Gruber, 2009; Hipp et al., 2014). In permafrost rockwalls, where the active layer behaves semi-conductive (Figure 2.7), thermal condition performs better in the frozen rock mass than in unfrozen rock with air-filled pores (Hasler et al., 2011a). Nevertheless, a purely conduction-based approach may exclude transient thermal effects on a longer timescale (Holocene: Little Ice Age, Quaternary: LGM) (Noetzli and Gruber, 2009) and overlook the true complexity of anisotropic mountain rock mass as illustrated in Figure 2.7. On a micro scale, for example, foliated rock types such as paragneiss typically create anisotropic heat transfer properties with contrasting thermal conductivity parallel and perpendicular to the bedding (anisotropy ratio = 1.5) (Vosteen and Schellschmidt, 2003; Clauser and Huenges, 2013). Likewise, melting/freezing of pore water can affect the conductive heat transfer through bedrock by the consumption or release of latent heat (334 joules per 1g of ice) (Benn and Evans 2010). On a higher scale, the conductive heat transfer system in mountain rockwalls is particularly disturbed by the existence of air-, water- or ice-filled discontinuities (Figure 2.7). Through joints, advective heat transfer by fluid flow and convective air circulation become efficient (Gruber and Haeberli, 2007; Krautblatter and Hauck, 2007; Krautblatter, 2009; Gischig et al., 2011a, b; Hasler et al., 2011a; Moore et al., 2011; Blikra and Christiansen, 2014; Phillips et al., 2016), especially in combination with seasonal snow and permafrost dynamics (Luetschg and Haeberli, 2005; Zhang, 2005; Luetschg et al., 2008) and transient geothermal heat fluxes from past climatic changes (Kohl, 1999; Noetzli and Gruber, 2009).

A holistic concept of the key thermal processes in permafrost and snow-affected rockwalls and their mechanical consequences has been developed by Draebing et al. (2014). Based on this, Figure 2.8 displays a typical annual record of near-surface rockwall temperatures and a schematic illustration of the associated key heat fluxes (i-iv) on a seasonal scale:

(i) During autumn, when atmospheric temperatures decrease, conductive energy transfer through air-filled joints and rock pores dominate leading to progressive ground cooling. When the first snow cover accumulates at rockwall irregularities during late autumn the energy balance (equations 2.4 and 2.5) immediately changes (Wirz et al., 2011). The albedo and long-wave emissivity increase, whereas the thermal conductivity is reduced to approx. 0.1 (fresh snow) to 0.5 (old snow) W M^{-1} K^{-1} in comparison to snow-free rock (Zhang, 2005). As long as the snow cover is still thin (< 10-60 cm), conduction enhances progressive ground cooling (Figure 2.8) (Drebing et al., 2014).

(ii) During early winter, however, with increasing snow height and density (ca. 60-100 cm), the high thermal resistance thermally decouple the underground from the atmosphere (equation 2.4) (Keller and Gubler, 1993; Luetschg and Haeberli, 2005). Consequently, conductive as well as convective transfer processes distinctly decrease in magnitude until they finally stop (Draebing et al., 2014). With maximum snow cover, bedrock temperatures may remain constant at relatively high sub-zero temperatures over several month, as displayed in Figure 2.8 (e.g. Haberkorn et al., 2015a) and depth of active layer thaw is reduced (Luetschg and Haeberli, 2005). At comparable snow-free sites, on the other hand, open joints can act as chimneys that favour buoyancy-driven convective air ventilation into depth and enhance progressive cooling of the underground during winter (Gischig et al., 2011a; Moore et al., 2011). Similar phenomena has been reported e.g. by Delaloye and Lambiel (2005) from unconsolidated material of (frozen) talus slopes and rock glaciers bodies.

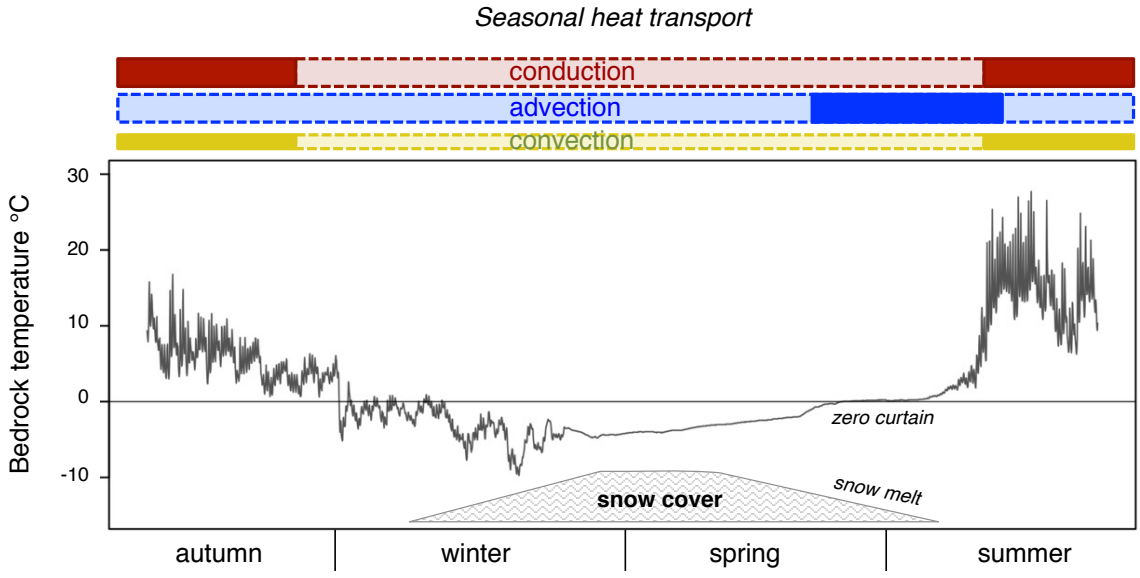

Figure 2.8: *Conceptual diagram of the temporal interplay of conductive, advective and convective heat fluxes in high-mountain rockwalls based on Draebing et al. (2014, p. 230) with respect to typical near-surface rock temperatures (10 cm bedrock depth) of the Turtmann Valley. For heat transfer, the same colors as in Figure 2.7 are used. Color intensity signifies intensity of seasonal heat transfer processes during the year.*

(iii) In late spring, when snow cover progressively thins, external heat is able to enter the underground again. Now conductive bedrock warming starts; it remains slow as incoming solar energy is consumed by melting of snow cover. Energetically, snowmelt acts as energy sink and consumes latent heat (Schmid et al., 2012; Draebing et al., 2014). During melt water infiltration into open joints systems, most heat transfer takes place by advection (Hasler et al., 2011a). The relatively warm water heats up the underground (Draebing et al., 2014). Rock temperatures can stagnate at 0 °C for several days to weeks during late spring (or early summer, Figure 2.8) indicating the zero curtain effect caused by latent heat consumption during snow melt (Schmid et al., 2012). If permafrost is present, advection additionally promotes large thaw corridors and ice erosion in fractures (Gruber and Haeberli, 2007; Krautblatter and Hauck, 2007; Krautblatter, 2009; Hasler et al., 2011a; Phillips et al., 2016).

(iv) During summer, advective processes rapidly stop, while conductive and convective intake of warm air starts warming up the comparatively still colder bedrock. Rock temperatures consequently increase (Figure 2.8) and twarming front slowly propagates into depth (Moore et al., 2011). Occasionally, thawing of the active permafrost layer or rainfall infiltration into joints can result in advective warming (Phillips et al., 2016), but only if water does actively flow (Draebing et al., 2014).

2.4 Rock slope destabilising processes - Theories and changing paradigms

> *The transition from a paradigm in crisis to a new one from which a new tradition of normal science can emerge is far from a cumulative process, one achieved by an articulation or extension of the old paradigm. Rather it is a reconstruction of the field from new fundamentals, a reconstruction that changes some of the field's most elementary theoretical generalizations as well as many of its paradigm methods and applications. During the transition period there will be a large but never complete overlap between the problems that can be solved by the old and by the new paradigm. But there will also be a decisive difference in the modes of solution. When the transition is complete, the profession will have changed its view of the field, its methods, and its goals. (*Thomas Kuhn, 1962, p. 84)

The following chapter provides an overview on major theories of rock slope destabilising processes and briefly explores past and on-going paradigms changes. The term paradigm goes back to Kuhn (1962). Although Kuhn did not provide an explicit definition of the term 'paradigm' in his 'Structure of Scientific Revolution', he understood it as an overarching framework of theories and beliefs. Kuhn argues that a paradigm determines the nature of scientific questions and also which scientific explanations seem to be acceptable. The strong point made by Kuhn is, that the awareness or definition of scientific problems changes over time depending on the prevailing social, scientific and economic context. According to Kuhn, what we as scientists do, is mostly 'normal science' with a bit of 'puzzle solving' – using standard techniques, applying standard concepts and providing almost standard answers. However, as soon as new observations and anomalies challenge our view on reality (or what we believe to see as reality) and existing concepts fail to explain them, we reach a 'scientific crisis'. We start to see the world from a different perspective. We need to choose a new paradigm, which is not yet fully elaborated (Kuhn 1962, p. 146). However, after increasing measurements, scientists return to routine and adopt the new paradigm. Although the concept of paradigms is controversially discussed (see Kennedy, 2006), such different stages of a 'paradigm shift 'can be observed in rock slope instability research e.g. with respects to theories or paradigms of bedrock permafrost, glacier retreat, frost weathering and thermal fatigue. For an in-depth discussion on paradigm shifts in (geomorphic) science

the author refers to Kuhn's 'Structure of Scientific Revolution', as well as to Kennedy (2006) and Inkpen and Wilson (2013).

2.4.1 Failure and deformation behaviour during imbalanced stress-strength ratios

The failure and deformation behaviour of mountain rock slopes is essentially controlled by the balance of downslope acting shear stress and the opposing stresses or strength of the rock-slope forming material that tend to resist the movement. For stability analysis, this ratio between driving forces to resisting forces per unit area can be expressed as 'factor of safety' (FS) where unstable rock slopes have FS < 1 (Glade and Crozier, 2005):

$$FS = \frac{shear\ strength}{shear\ stress} \qquad (2.7)$$

The most simple physical approach to estimate the ratio between resisting and driving forces per unit area is commonly a force-balance approach (infinite slope model) that reduces the complex three-dimensional problem of slope failure to a two-dimensional shear displacement. The rock mass of mountain rock slopes can be assumed to be a Mohr-Coulomb material, where two intrinsic material properties are the major controlling parameters: the cohesion c and the friction angle φ (Wyllie and Mah, 2004). For a sliding surface on which there is an effective normal stress σ' acting, the total resistance of the rock mass to shear at failure τ_f is given by:

$$\tau_f = c + \sigma' \tan\varphi = c + (\sigma - u) \tan\varphi \qquad (2.8)$$

$$\tau_f = c + \sigma' \tan\varphi + i \qquad (2.9)$$

The effective normal stress σ' enables consideration of the negative influence of pore-water pressure u on the normal stress. However, equation 2.8 represents a simplification of the failure criterion of natural, anisotropic rock slopes and is ideally valid for rock mass with either closed or micro-scale joints. To account

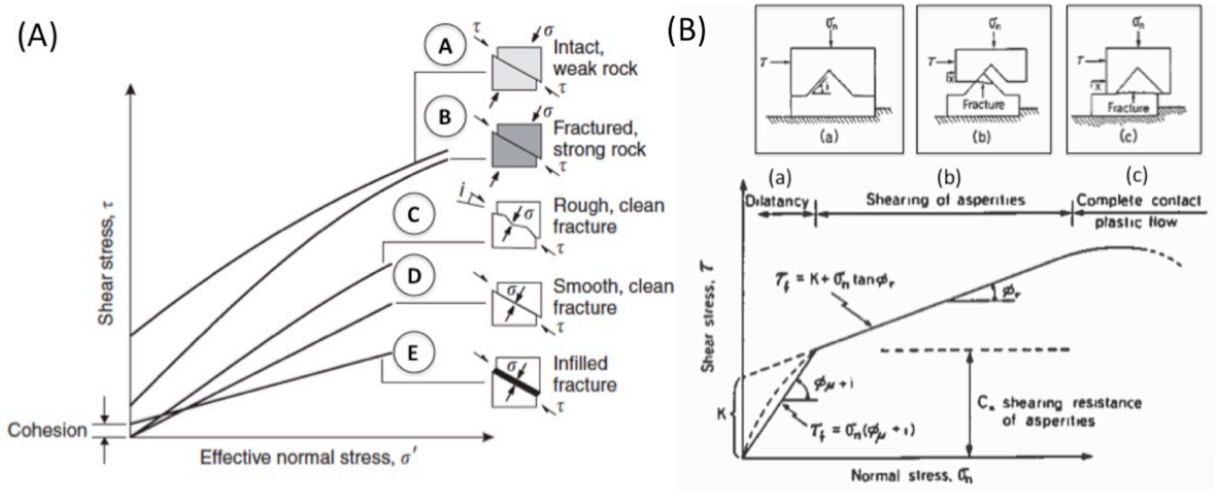

Figure 2.9: *(A) Relationships between shear and normal stresses on sliding surface for five different geological conditions and scales of asperities (A-E). Source: Wyllie and Mah (2004, p. 78).* **(B)** *Failure behaviour during direct shear test of a single joint asperity with increasing normal stress. The failure line represents three conditions: (a) dilatancy of joint according to a peak friction angle of φ+I, (b) dilatancy of joint with shearing of asperities and development of residual strength, and (c) plastic deformation with complete rock-to-rock contact. Images taken from Selby, (1993, p. 86).*

for the effect of joint roughness (and infilling) on the overall slope stability, Patton (1966) extended the Mohr-Coulomb criterion by the angle of asperities *i* as a quantitative parameter of dilatation (equation 2.9). The angle can be quantified after Barton and Choubey (1977) using the joint roughness coefficient (JRC) and the joint compressive strength (JCS).

The significant role of joint roughness on the rock mass failure behaviour is illustrated in Figure 2.9A, particularly with respect to the scale of asperities and infilling (Wyllie and Mah, 2004; Barton, 2013). In comparison to intact weak or fractured strong rock (curves A and B), even joints with small-scale and rather smooth unevenness (curve D) can lead to marginal reduction of shear strength, i.e. in laboratory situations where small cm-size rock samples are used. The frictional angle of the rock mass is particularly increased in bedrock with rough joint surfaces (curve C) shown e.g. in Figure 2.2C. Large-scale asperities, which are too large to be sheared off during shear displacement, will typically slide over one another. This causes dilatation (Selby, 1993).

Figure 2.9B shows that a rough, so far undisturbed joint surface will have a peak friction angle of φ+i. At low normal stresses, as normally necessary to initiate small size-rockfalls, rock deformation is the result of dilation following equation 2.8. Until this low-stress level, rock mass behaves ideally elastic. Then, with increasing normal stresses and exceeding shearing resistances of asperities, the interlocked asperities will shear off along their tips. This may result in bedrock fracturing and preferentially elastic-plastic bedrock failure. The failure line in Figure 2.3B displays that shearing leads to a progressive reduction of the friction angle until a minimum or residual friction angle of the rock is reached. Finally, complete rock-to-rock contact may occur with very high normal stresses and permanent plastic deformation occurs (Figure 2.9B). In foliated paragneiss with platy, mica minerals, creep may permit large plastic deformations before rupture occurs (Selby, 1993; Barton, 2013).

As stated above, the influence of joint roughness decreases with the size of asperities and becomes less important in bedrock with wide joint apertures that are filled with thick fillings as shown in Figure 2.2E. Depending on the thickness and material properties of the infilling both cohesion and friction angle of the rock mass can become progressively that which is due to the infill alone (curve E in Figure 2.9A). Particularly, clay-filled joints significantly decrease the frictional rock strength and can initiate large-scale rock failure as e.g. in 1963 in Vajont (Italy) (Veveakis et al., 2007; Ferri et al., 2011). Moreover, if permafrost is present (see below), the shear resistance is significantly controlled by ice-filled joints and their temperature (Mellor, 1973; Krautblatter et al., 2013).

Final failure of solid metamorphic rocks tends to occur in a brittle manner, due to a sudden loss of strength one the peak has been reached. Rarely, ductile failure may occur (Edelbro, 2003); this is more common for sedimentary weak rocks.

2.4.2 Paraglacial adjustment of steepened rockwalls: the mechanical perspective

In mountain valleys undergoing deglaciation or no longer occupied by glaciers, numerous researchers report a dominance of rock failures and/or active talus deposition in close distance to present-day or former glacier

margin (Bovis, 1990; Oppikofer et al., 2008; McColl and Davies, 2013; Cossart et al., 2014; Ostermann and Sanders, 2016). Likewise, interpretation of present-day rockfall rates in the light of total post-glacial talus volumes as well as cosmogenic data of large landslides reveal peaks of bedrock instabilities during early Holocene – thus immediately (or delayed with a time-lag) after deglaciation (Ivy-Ochs et al., 2009; Ballantyne and Stone, 2013; Ballantyne et al., 2014). This spatial and temporal rockfall clustering has been used for several decades as a strong argument that there is a direct link between bedrock instability and the site-specific (de)glaciation history. Rapp (1960a), for example, suggested that the massive slope failures in Kärkevagge cannot be solely attributed to frost action, but to its former glaciation.

One decade after Rapp's observation, the paraglacial concept was formulised by Church and Ryder (1972) to describe non-glacial processes conditioned by glaciation (see also Ryder, 1971); without referring to Godard (1965) who used the term 'paraglacial' five years earlier in his French thesis to describe terrain 'beyond the glacier'. Yet, in its original formulation, the paraglacial concept didn't define bedrock failures as glacially conditioned phenomena. It rather referred to the evolution of fluvial and alluvial fans such as deposited during the Late Wisconsin deglaciation in British Columbia (Church and Ryder, 1972). It is therefore no surprise that until the mid 1990s, the paraglacial concept was mainly adapted - although very slowly - to study fluvial and lacustrine sediment dynamics (Brierley and Hickin, 1985; Clague, 1986; Church and Slaymaker, 1989). Within this 'sediment-dominated' research, it seems that the work of Wyrwoll (1977) remained almost unnoticed. Wyrwoll was one of the first explicitly applying the paraglacial concept from a rock mechanical point of view in the context of post-glacial rockwall failures in Central Quebec-Labrador. From his mechanical analyses, he excluded a dominant influence of freeze-thaw activity, but favoured the role of glacially induced stress release. These outcomes did not only fuel the 'periglacial-paraglacial' debate (see e.g. Slaymaker, 2009), but also increasingly encouraged more geomorphologists to investigate mountain rockwalls with respect to their (de)glacial history (e.g. Bell, 1976; Carlsson and Olsson, 1982; Johnson, 1984; Bovis, 1990; Cruden and Hu, 1993).

It took a long time for the geomorphic community to accept the paraglacial paradigm. Only at the end of the 20th century, did its application suddenly increase (see publication statistics in Ballantyne, 2002a) far beyond the context of alluvial systems. To meet this diversification of paraglacial contexts, Ballantyne (2002a p. 1938) extended Church and Ryder's early approach by 'non-glacial earth-surface processes and sediment accumulations, landforms, landsystems and landscapes that are directly conditioned by glaciation and deglaciation'. Slaymaker (2009) however proposed to define paraglacial landforms or landscapes as 'transient' or 'transitional' due to the adjustment from glacial to non-glacial conditions' (p. 80-81). In this thesis, the working definition of McColl (2012) is preferred, as it combines elements of both Ballantyne and Slaymaker definitions and specifically refers to the failure of bedrock. Accordingly, paraglacial rock slope failures are defined as 'part of, or influences by, the transition from glacial conditions to non-glacial conditions' (McColl 2012, p. 2). In fact, paraglacial bedrock instabilities are spatially restricted to the maximum glacial extent (Slaymaker, 2009) and temporally, to the period between start of deglaciation (peak of activity) and approximation to geological 'norm' (Church and Ryder, 1972). However, it is often difficult to decide whether a post-glacial slope failure is a paraglacial phenomenon. McColl (2012, p. 13) points out that there are often

'grey areas', which require a 'certain amount of personal judgement'. Recent findings of McColl and Davies (2013), for example, suuggest reasons to mark the start during the actual glaciation.

Based on the terminology of Cruden and Varnes (1996), three major process types of paraglacial rock slope failure can be differentiated: (1) rapid to extremely rapid catastrophic rock slides that can develop into rock avalanches (Fischer et al., 2012; Ostermann and Sanders, 2016), (2) slow to extremely slow deep-seated gravitational slope deformation (DSGSD) with typical expression such as sackungen, toe bulging and anti-scarps (Ballantyne and Stone, 2013; McColl and Davies, 2013) and (3) very rapid to extremely rapid release of loose bedrock in form of rockfalls (Caine, 1982; André, 1997). In this study, only latter process type (3) is empirically addressed, but discussion is made in reference to type (1) and (2).

Today, the paraglacial concept is a common framework in geomorphology to investigate the reworking and the cascading flux of paraglacial sediments. It has been applied to different paraglacial gravitational processes such as shallow soil slips, debris flows, stream bank topples or thaw slumps on coasts. However, the number of studies addressing paraglacial failures that initiate in bedrock is still limited. The extensive review of McColl (2012, p. 6) highlights that the research on paraglacial rock slope instabilities is still faced with several misconceptions, disagreements and ambiguity with respect to the terminology, the underlying mechanisms and the spatio-temporal activity. According to McColl (2012) only few studies 'have managed to achieve a detailed investigation of the mechanism and causes of paraglacial rock slope failure' (p. 6), whereas most studies are based on assumptions and speculations. And the same criticism reappears five years later in Grämiger et al. (2017) pointing out that 'the mechanics of paraglacial rock slope damage remain poorly characterized' (p. 1).

Most critically, many researchers explain paraglacial bedrock failures in terms such as 'glacial oversteepening' (sensu Augustinus, 1992) and 'debutressing [2]' (Bovis, 1990; Holm et al., 2004; Cossart et al., 2008). However, McColl (2012, p. 2) criticizes that 'these terms are seldom justified in any detail'. For instance, in NE Tasmania, Caine (1982) identified most cliff topples along 'oversteepend', formerly glaciated cliffs. Likewise, Holm et al. (2004) found that recent catastrophic failures in NE British Columbia spatially dominate at rockwalls steeper than 40° just above the glacial trimline. Both Holm and Caine used the decreasing or absent number of failures in less inclined and little glaciated terrain as argument to imply glacial oversteepening and removal of ice buttress as major failure mechanism.

However, this reasoning can be misleading without any reference to the rockwall's mechanical regime that ultimately verify that the glacial processes were really critical for destabilisation. More convincing were e.g. Bell (1976) or Cruden and Hu (1993) arguing that glacial oversteepening and retreat can initiate rock failure when joints (i.e. schist layers) are unfavourably oriented and dip in the same direction as the slope. As shown in Figure 2.10, cataclinal slopes with underdip, dip or overdip joint conditions are highly sensitive, for detachment on planar failure planes (Cruden and Hu, 1998), while anaclinal slope with joints opposite to the surface might be relatively stable or more prone to toppling or wedge failure.

[2] According to Ballantyne (2002, p. 1939) debuttressing describes the ‚removal of the support of adjacent glacier ice during periods of downwastage'.

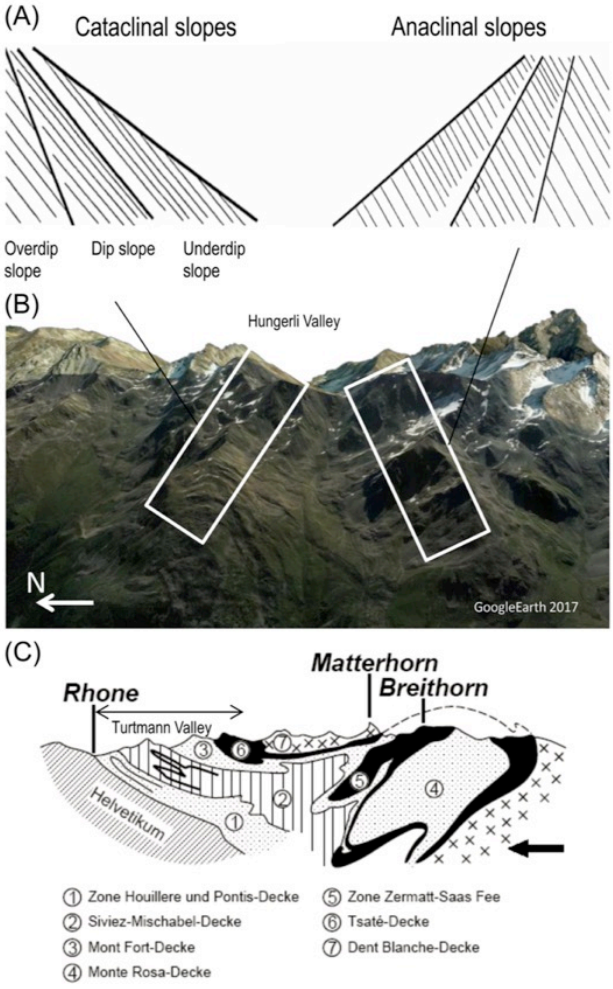

Figure 2.10: *Cataclinal and anaclinal joint conditions (adapted from Cruden and Hu 1998) (A) exemplified on S- and N-exposed rock slopes in the Hungerli Valley (B), a hanging valley of the Turtmann Valley. Here, due to the tectonic folding of the Alpine Nappes, i.e. Siviez-Mischabel Nappe (Labhart 2009, p. 94) (C) and the WE-oriented hanging valleys, joints and metamorphic layers dip either out or into the slopes.*

Nevertheless, McColl (2012) still questions the glacial origin of the slope gradient - it could also result from fluvial erosion, even in mountain valleys (Montgomery, 2002) - and emphasise the lack of information on other failure mechanisms. Moreover, squeezed glaciers adjacent to unstable rockwalls, as observed in New Zealand (McColl and Davies, 2013) cast doubt that glaciers can buttress a rock slope. Since ice is a ductile, highly viscos material, it is unlikely that glaciers provide sufficient rigid lateral support to adjacent, which is three times denser than bedrock (McColl et al., 2010). Instead, although temperature- and rheology-dependent, glaciers can deform at several mm/years under low strain rates caused e.g. by slow and large rockslides (Anderson and Anderson, 2012; McColl and Davies, 2013). Thus, glacial debutressing may certainly reduce the slope support, but the complete withdrawal of a glacier is probably no necessity for rock failures.

The above examples of previous findings and reasoning emphasise that glacial processes may influence mountain rock slopes in different ways and that their interplay with non-glacial factors needs to be considered. In response, McColl (2012) proposes to evaluate paraglacial rock slope instabilities in the light of Glade and Crozier (2005) concept of preconditioning, preparatory and triggering factors. As shown in Figure 2.11, it is useful to assume a 'paraglacial margin of stability' with three theoretical states of rock slope (in-)stability: stable, marginally stable and unstable. This perspective highlights two crucial points:

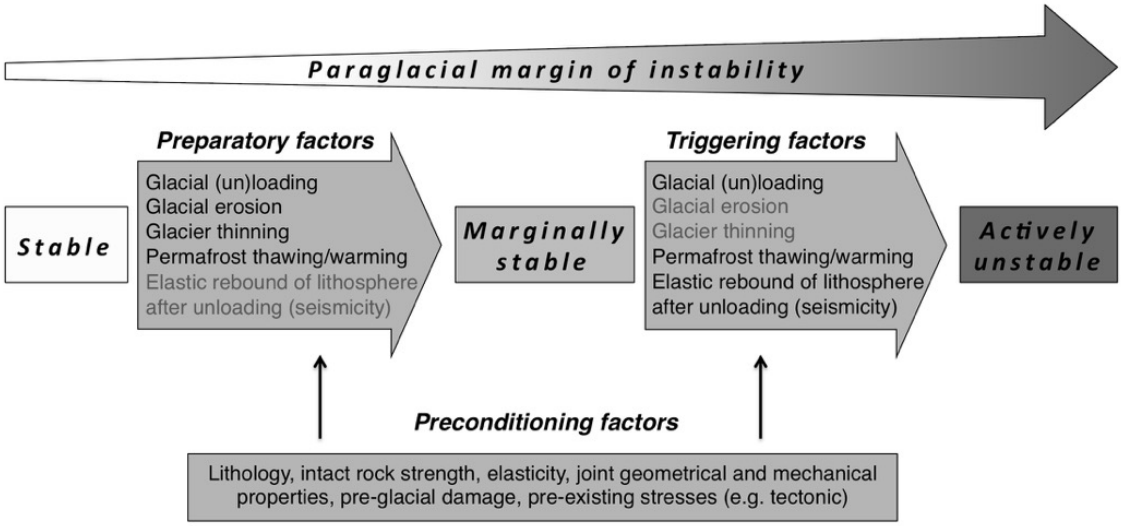

Figure 2.11: *Conceptual approach of preparatory, preconditioning and triggering factors after Glade and Crozier (2005) in the context of paraglacial rock slope instability (see text for details). Contrary to the original concept, sustaining factors are excluded for simplification and focus is on the 'instability'. Examples of controls are illustrated in black (very likely) and grey (less dominant) according to McColl 2012.*

First, predicting the failure of a glacially conditioned rock mass requires understanding of the inherent and almost static preconditioning factors (cf. McColl, 2012, p. 7) (Figure 2.11). Long before (de)glaciation, the bedrock stability is crucially conditioned by the rock mass strength, the mechanical and geometrical joint properties as well as the pre-glacial damage history. These factors control the overall ability of a rockwall to resist any form of dynamic glacial (and non-glacial) destabilising force (Terzaghi, 1962; Selby, 1980; Selby, 1982a; Bovis, 1990; Augustinus, 1992; Augustinus, 1995; Leith et al., 2014a, b; Stead and Wolter, 2015). For instance, Augustinus (1992, 1995) found that densely jointed metamorphic rocks with low RMS and outdipping joints are most sensitive for failure immediately after deglaciation, whereas Selby (1982, 1993) demonstrate that slopes with high RMS and anaclinal joint conditions can be in equilibrium despite steep inclinations.

Second, depending on the existing state of stability, any process linked to glaciation and deglaciation can either prepare or trigger a paraglacial rock failure. Mechanically, this occurs by a redistribution of the in-situ stress pattern within a rock slope resulting in progressive failure of rock bridges, joint propagation and formation of sheeting joints. Figure 2.12 illustrates several ways, in which (de-)glaciation can lead to high horizontal σ_1 to vertical σ_3 stress ratios:

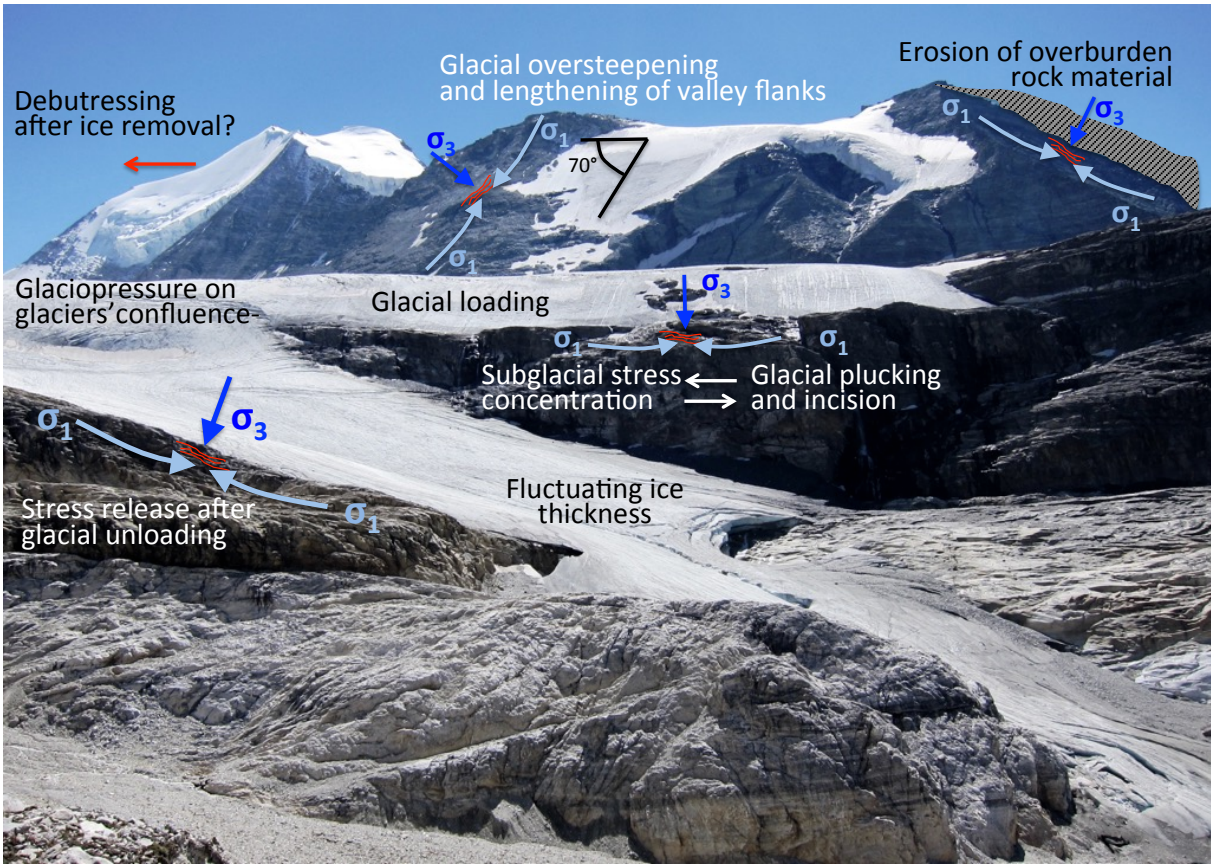

Figure 2.12: *Mechanical influences of glaciation and deglaciation on in-situ horizontal and vertical stress trajectories and thus rock slope stability (See text for details). Photograph from Brunegg glacier (August 2016) at around 2900 m asl with view to Brunegghorn and Bishorn. See text for a description.*

Stress redistribution by glacial modification of slope morphometry/geometry

It is accepted that long-term erosional activity of glaciers leads to deepening of mountain troughs, and thus to steepening and lengthening of rock slopes (Harbor, 1992). Due to the higher self-weight (overburden), the horizontally acting shear stresses increase over time to a critical point (Bovis, 1990). Many bedrock failures seem to predominately initiate at the lower part of the slope or at convex slope breaks (Augustinus, 1995; Holm et al., 2004; Cossart et al., 2008). Conceptual modelling for the Matter Valley imply a 'bottom-up' rockfall activity along valley flanks, where rockfalls initiate at different parts of the slope profile at different times (Leith et al., 2010a; Leith et al., 2010b). Leith and colleagues show that rock failures start at the toe, where maximum ice flow concentration resulted in highest erosion and stress redistribution, and then progress towards the trough shoulder. In that sense, glacial erosion acts as preparatory factor for bedrock instability, 'simply' by changing the slope profile without invoking stress release (Figure 2.12). But failure can occur long after ice removal, when further glacial or non-glacial processes (e.g. freeze-thaw weathering, seismic events) become the trigger and cause additional shear stresses that exceed the slope strength (McColl, 2012). Yet, in case of large and slow mass movements (e.g. rockslide), which are able to induce ductile creep and 'squeezing' of ice, glacial erosion can trigger failure as demonstrated by McColl et al. (2010).

Stress redistribution by glacial erosion of overburden material

The second way in which glacier erosion can reorganise the major principal stresses is through the removal of overburden rock material (Figure 2.12). The long-term erosion of surface material can release vertical elastic stresses in the rock slope, if the slope-parallel stresses remain at the same level due to the lateral confinement of the surrounding rock mass (Eberhardt et al., 2004). Additionally, glacial erosion exposes 'old' highly stressed bedrock under confined conditions with failure planes of pre-glacial origin (also old sheeting joints), which makes failure kinematically more feasible (Jarman, 2006). However, low glacial erosion rates of 0.4 mm/yr, as in the Yosemite Valley (Duhnforth et al., 2010), imply relatively little removal of overburden of < 30 m during the previous Würmian glacial cycle (Leith et al., 2014b). Yet, the finite difference model of Leith et al. (2014b) emphasises that differential stresses already accumulate beneath the ice and that glacial thinning can cause the development of a progressive fracture front in the subglacial bedrock. The consequence is a positive feedback, where subglacial bedrock weakening favours the glacial quarrying and further glacial incision, which in turn increases the stress concentration at the valley floor and thus again the bedrock fracturing.

Stress release following glacier unloading and loading

McColl (2012, p. 9) suggests that 'the loading and unloading of ice itself might be seldom sufficient to produce sheeting joints' and to destabilise rock slope. Instead most damage is likely produced either by glacial erosion or is even pre-glacial in origin (Brunner and Scheidegger, 1973). However, if mechanical preconditioning is sufficient e.g. due to regional tectonic stresses (Leith et al., 2010a) or horizontal stress evolution through subglacial erosion (Leith et al., 2014b), glacial loading and unloading can act as preparatory or triggering factor for bedrock failure. During glaciation, the weight of overlying ice increase the internal stress levels both on the valley bottom and on its flanks (Carlsson and Olsson, 1982). During unloading and removal of overburden ice weight, the vertical elastic stress component in Figure 2.12 increases, while the horizontal stresses may remain constant due to the lateral confinement of the surrounding rock material. This redistribution of the major principal stresses within the upper bedrock (up to 30 m) leads to release of high compressive stresses parallel to the slope surface (McColl, 2012). Thus, destabilisation does not occur due to the presumed 'buttressing effect' (McColl and Davies, 2013), but through the relaxation of strain energy or a 'rebound' as defined by Ballantyne (2002a). However, it is still debated whether paraglacial rock failure occur *after unloading* induced by stress release (Wyrwoll, 1977; Cossart et al., 2008) or already *during ice loading* e.g due to 'glaciopressure' at the confluence of glacier tongues (Panizza, 1973).

Stress redistribution due to fluctuating ice thickness during glacial cycles

Finally, a seldom-considered preparatory factor for paraglacial rock instabilities is the fluctuating ice thickness, especially over multiple glacial-interglacial cycles. In recent conceptual numerical model for the Great Aletsch Glacier, Grämiger et al. (2017), for instance, demonstrate that repeated glacier advance and melting can critically alter the stress trajectories in adjacent valley slopes and create cyclic stresses. Their model reveals most rock damage during the first deglaciation cycle (Eemian ice free conditions) when than the critically stressed mid-slope region becomes for the first time ice-free. Subsequently, fluctuating glacier elevation during each

modelled glacial cycle has been shown to result in progressive failure of intact rock bridges and slip-like rock deformation. Interestingly, Grämiger et al. (2017) found little damage when applying only pure mechanical loading and unloading in their slope model, supporting McColl's (2012) suggestion that glacial erosion or fluctuation is more efficient.

However, all above described (mechanical) effects of glacial processes always require evaluation relative to non-glacial causes. Latter can be defined as 'paraglacial causes' when they become active as a direct result of glaciation (Ballantyne, 2002a) or if they occur in the transition between glacial to non-glacial conditions (Slaymaker, 2009). Major mechanisms such as permafrost degradation and weathering by freeze-thaw and thermal stress are discussed below.

2.4.3 Paraglacial adjustment of permafrost rockwalls: the thermal perspective

Permafrost as an invisible, but very common, subsurface phenomenon in high-mountain rockwalls and its importance for slope (in-)stability is a relative young research topic (cf. Krautblatter and Leith, 2015), particularly in a paraglacial context. While the bedrock destabilising role of mountain glaciers have been recognised since several decades (Rapp, 1960a; Wyrwoll, 1977), comparatively little attention has been paid on the preconditioning or even triggering role of warming and thawing permafrost associated with glacier retreat (cf. McColl, 2012). First scientific investigations on mountain or alpine permafrost started in the late 1970s, particularly initiated in Switzerland by the geomorphologists D. Barsch and W. Haeberli. However, in this pioneering period, the major emphasis was on permafrost in unconsolidated sediment bodies (i.e. rock glaciers) due to their role as a (paleo-)climatic indicators, fresh water supplies (Barsch et al., 1979; Barsch, 1992; Haeberli, 1992; Haeberli et al., 2006) and their downslope sediment cascade and natural hazard potential (Haeberli et al., 1990; Rickenmann and Zimmermann, 1993).

It was in the late 1980s, that finally the severe instability problems of steep, perennially frozen rock slopes were also recognised. This was, amongst other, a result of the construction work of mountain railways such as the Gornergrat and the Jungerfraujoch (Keusen and Haeberli, 1983; King, 1996). In summer 2003 at the latest, observations of ice in fresh detachment zones of rock failures made the long 'hidden', but stability-relevant permafrost in rockwalls visible to both the public and geomorphic community (Dramis et al., 1995; Gruber and Haeberli, 2007). During the last two decades, the increasing number of spatial mapping campaign, geothermal monitoring field sites, geophysical ground surveys, numerical modelling and energy balance measurements as well as laboratory tests have contributed to better thermal, hydrological, mechanical and systemic understanding of permafrost rockwalls (Davies et al., 2001; Murton et al., 2001; Gruber et al., 2003; Noetzli et al., 2003; Gruber, 2005; Harris, 2005; Janke, 2005; Gruber and Haeberli, 2007; Krautblatter and Hauck, 2007; Noetzli et al., 2007; Fischer and Huggel, 2008; Krautblatter, 2009; Krautblatter et al., 2010; Hasler et al., 2011a; Hartmeyer et al., 2012; Krautblatter et al., 2013; Krautblatter and Draebing, 2014; Magnin et al., 2015a); not least as a result of the EU-funded PACE-project starting in 1997 (Harris et al., 2009).

With respect to the on-going temperature increase, those recent studies provide strong evidence that the past and present warming and thawing of rock permafrost is likely to be the key cause of many low- and

high-magnitude rockfalls recorded e.g. in the European Alps and Southern Alps in New Zealand (Sass, 2005c; Allen et al., 2009; Ravanel and Deline, 2011; Huggel et al., 2012; Allen and Huggel, 2013). However, Krautblatter and Leith (2015) point out that most of our current knowledge on rock permafrost and associated instabilities is still limited as it derives from a few study sites and relative short records of a few years. This might explain, why the (de)stabilising effect of permafrost has been little investigated from a paraglacial perspective, i.e. after LGM.

Permafrost is thermally defined on the basis of temperature and refers to ground material (soil or bedrock) that remains at or below 0 °C for at least two consecutive years, independent of its water and/or ice content (NRC-Permafrost-Subcommitee, 1988). Systemically, permafrost rockwalls contain perennial ice e.g. in pores, micro- and macro-joints. However, due to the effects of pore or joint size and filling as well as solute chemistry and pressures, the freezing point of rock may be significantly depressed by several degrees below 0 °C (Krautblatter et al., 2010; Krautblatter and Draebing, 2014). Therefore, while all perennially frozen ground is permafrost, not all permafrost rockwalls are necessarily perennially frozen. Even water-saturated, low-porosity bedrock at a temperature significantly below 0 °C may contain unfrozen water in supercooled form (up to -10 °C) (Mellor, 1973; NRC-Permafrost-Subcommitee, 1988).

The spatial presence or absence of permafrost in mountain rockwalls and its and temporal evolution ultimately depends on the energy exchange processes at the atmosphere-rock interface, as previously discussed and shown Figure 2.7. On a global scale it is mainly regulated by climate conditions, i.e. the total amount of incoming short-wave radiation, whereas the interplay of valley and rockwall topography, vegetation coverage and snow dynamics as well as (sub-)surface material properties modulates these energy exchange processes and their transfer into depth on a regional- and local scale (Williams and Smith, 1989). Consequently, the distributional pattern of permafrost within mountain valleys (Figure 2.13), can be highly heterogeneous over short distances (Gruber et al., 2004b) ranging from continuous (< 90%), discontinuous (50-90%), sporadic (10-50%) and isolated patches (< 10%).

On a metre to decametre scale the permafrost distribution is even more complex, ranging from a few meters to many hundreds of meters in depth (Marchenko and Etzelmüller, 2013). Due to the decreasing short-wave radiation, the permafrost thickness decreases with increasing altitude (Gruber, 2005). The typical vertical temperature regime of permafrost rockwalls is displayed in Figure 2.14. While the upper layer, called the active layer, seasonally freezes and thaws, the ground below the permafrost table remains constantly frozen. The active layer represents a thermal boundary layer, whose thickness and thaw dynamics are most controlled to diurnal and seasonal dynamics of surface temperatures. Below the boundary layer, mean annual temperatures increase monotonically following the geothermal gradient. The lower base of permafrost is defined by the depth, where temperatures re-crosses 0 °C. Here, the bedrock is again unfrozen (Williams and Smith, 1989; Anderson and Anderson, 2012).

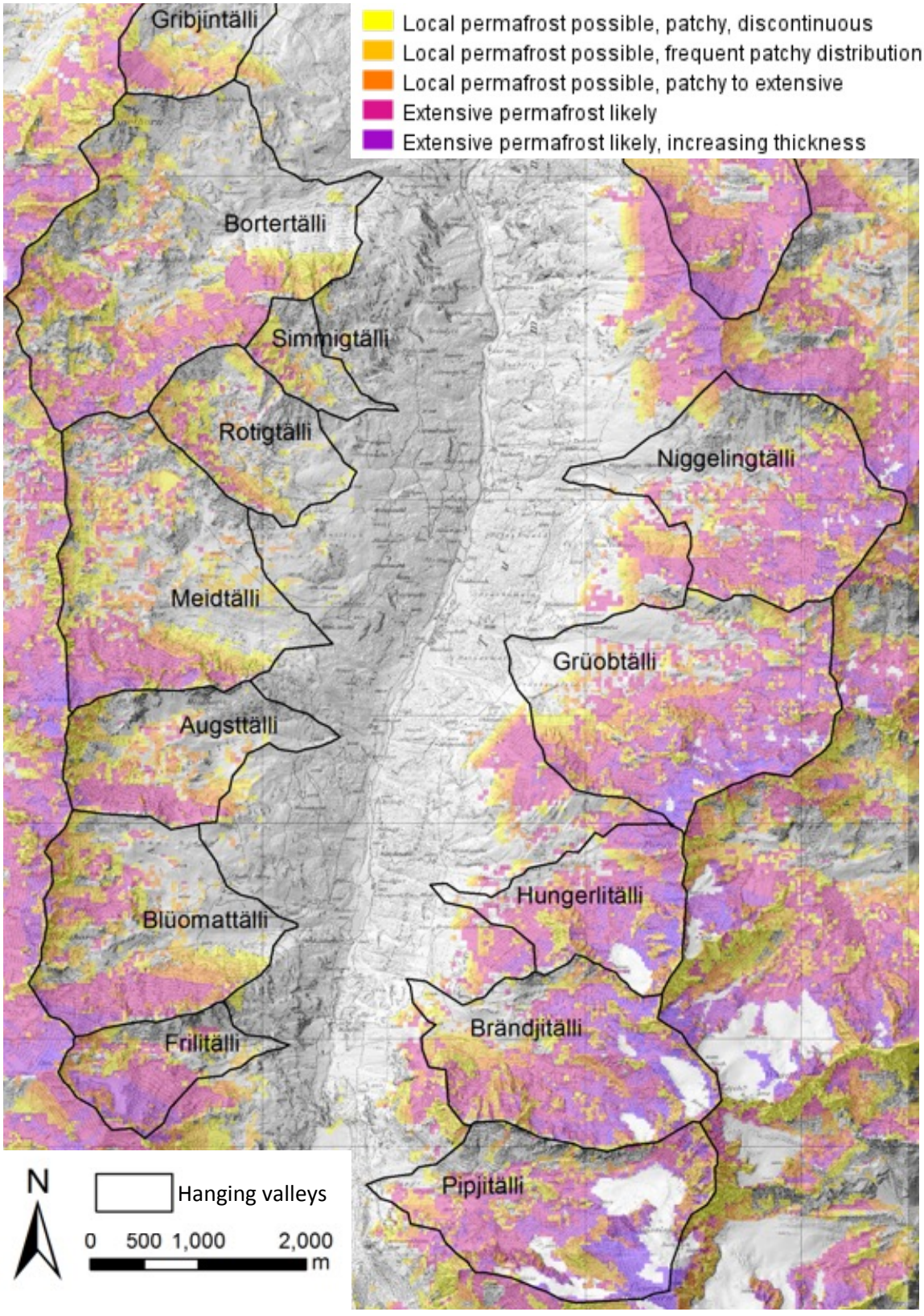

Figure 2.13: *Distributional pattern of permafrost (GIS layer taken from BAFU 2005) within mountain valleys shown for the 14 hanging valleys of the Turtmann Valley (Swiss Alps).*

With respect to time, mountain permafrost may persist from a few years to more than thousands of years. Due to the strong climatic dependence, the permafrost thickness reacts highly sensitively to any fluctuations of short-wave radiation and longer-term atmospheric warming (Williams and Smith, 1989). During the last century, a warming of 0.5 °C to 0.88 °C has been measured in the upper decametres of permafrost rockwalls (Harris et al., 2003). Shear box tests of Davies et al. (2001) indicate that this temperature rise is efficient to reduce the shear strength of ice-bonded joints and can decrease the slope's factor of safety lower than that of ice-free joints. Stability might be critically low even prior to complete thaw, when ice-bonded rocks are warmed up above -1.5 °C. Accordingly, seasonal or short-term permafrost dynamics (10^{0-2} yr) are hypothesised to be linked to a fast thermal and mechanical reaction of the upper < 10 m of bedrock. The exceptional activity of i.e. small- to medium-sized rockfalls during the extremely warm European summer of 2003 (+ 3 °C above norm) is frequently interpreted as indication of this rapid destabilisation during short-term permafrost dynamics (Gruber et al., 2004a; Fischer et al., 2006; Ravanel and Deline, 2011). In contrast to small recent warming of upper decametres, long-term warming in the order of several decades is assumed to cause deeper permafrost thaw up to several 100 m depths (Kohl, 1999; Kohl and Gruber, 2003; Noetzli et al., 2007). Noetzli and Gruber (2009) demonstrate that those transient effects of past climate periods additionally modify the present-day thermal regime of permafrost-rockwalls and might be associated with a delayed activation of deep detachment zones and thus, high-magnitude rock failures.

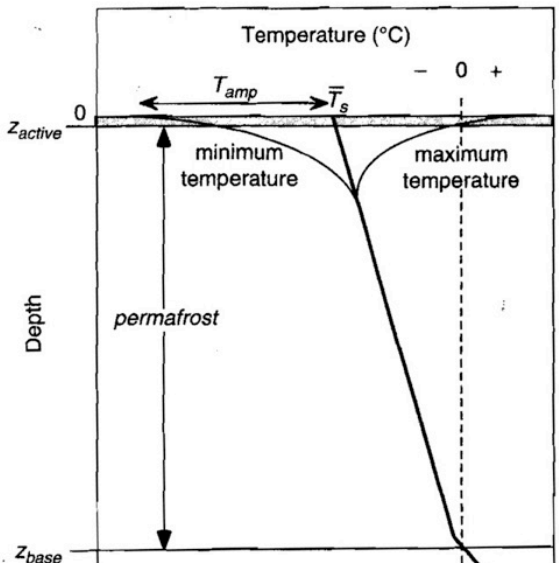

Figure 2.14: *Schematic depth profile of rock temperatures in permafrost rockwalls. Figure taken from Anderson and Anderson (2012, p. 274).*

Interestingly, in paraglacial literature, the interaction between glacier retreat and permafrost thaw in adjacent rockwalls has long been neglected (cf. Haeberli and Beniston, 1998; McColl et al., 2010). This shortcoming was addressed by Mercier (2008) and later by McColl (2012). While Mercier proposed to extend Ballantyne's original definition by the term 'paraperiglacial' to explicitly account for permafrost thaw-degradation during the paraglacial period, McColl underlines its crucial role as preparatory or triggering factor of paraglacial slope instability (see also Figure 2.11). Nevertheless, only a few paraglacial studies taken into account that glacier advance and retreat might not only be linked to a redistribution of the stress patterns across glaciated valleys, but also to time-dependent thermal (and thus mechanical) dynamics in formerly glaciated rockwalls (Lüthi and Funk, 1997; Wegmann et al., 1998; Fischer et al., 2006; Verleysdonk et al., 2011; Ballantyne et al., 2014).

Paraglacial rockwall adjustment to postglacial permafrost thaw and warming after ice removal has been recently discussed by Krautblatter and Leith (2015) with respect to the concept of 'reaction and relaxation time'

of Brunsden (2004) As shown in Figure 2.15, paraglacial rockfall activity at permafrost rockwalls is governed by different time-dependent ice-mechanical responses and the change in slope angle. A first ice-mechanical response occurs immediately after onset of deglaciation, but without initiation of rockfalls. Wegmann et al. (1998) demonstrate that the freezing front might first increase in depth after ice removal due to the bedrock exposure to cold atmospheric temperatures. This is supported by laboratory tests of Mellor (1973) showing that uniaxial compressive and tensile strength of saturated intact rock samples increase up to 50% and up to 70% respectively, when freezing to -10 °C. It is suggested that freezing of absorbed water in micro-cracks may lead to an effective grouting of the rock, although dependent on porosity and water content (Li et al., 2003; Krautblatter et al., 2013). Thus, the increasing permafrost thickness immediately after glacier retreat might temporally increase the slope stability and result in temporary slope equilibrium. This could explain the lag time commonly observed in many post-glacial rockfall data (McColl, 2012; Ballantyne and Stone, 2013) and the very steep angles of permafrost rock slope (Selby, 1982a; Augustinus, 1995; Gruber and Haeberli, 2007).

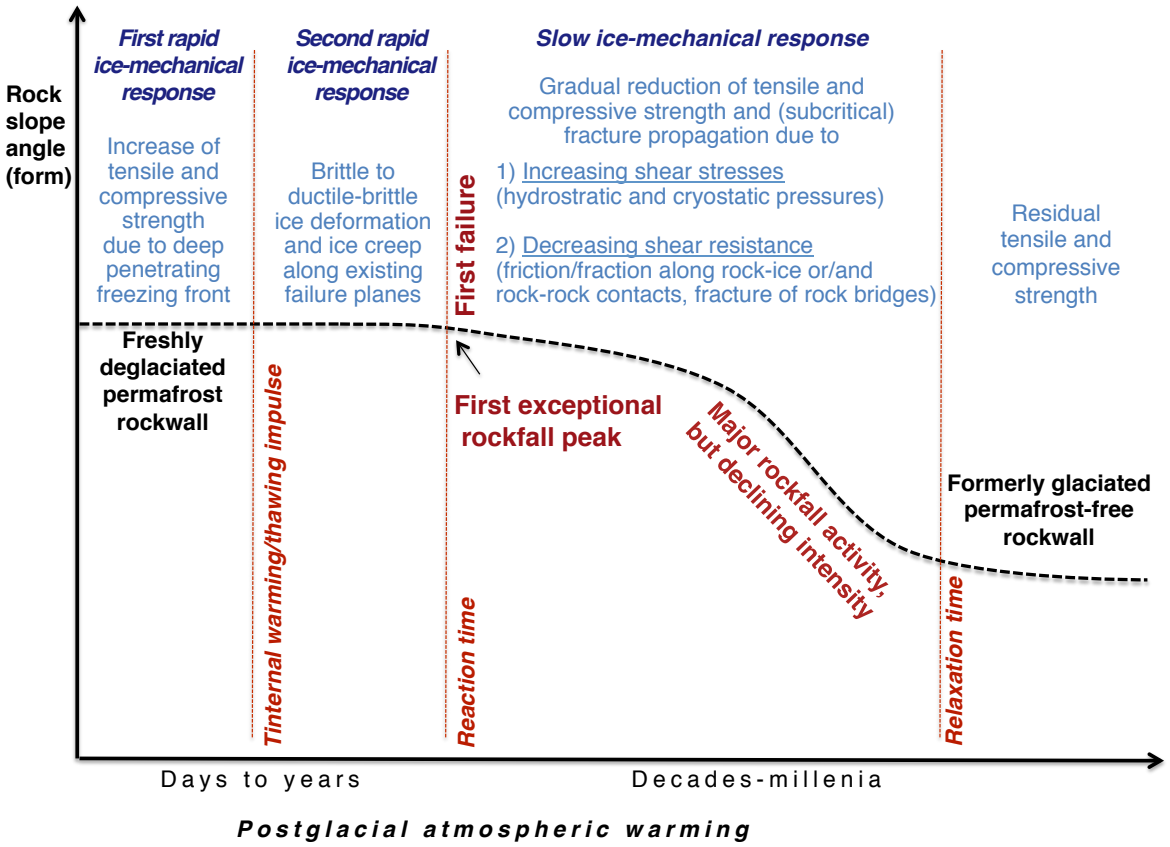

Figure 2.15: *Conceptual approach of paraglacial rockwall adjustment to postglacial permafrost thaw and warming after ice removal with respect to Brunsden's (2004) 'reaction and relaxation time' based on the concept proposed by Krautblatter and Leith (2015). Original figure taken from Krautblatter and Leith (2015, p. 160) and slightly modified.*

The second rapid response to the first sensible warming and thawing impulse occurs in form of enhanced creep and deformation of ice along existing failure planes (Figure 2.15). The reaction time and thus the first rock failure can be in a range of days to several years or decades. After this initial rockfall peak (Figure 2.15) the mechanical response of permafrost bedrock to further atmospheric warming might be more slowly dominated

by gradual subcritical fracture propagation and failure of rock bridges. It is therefore likely that final adjustment (relaxation time) to non-glacial conditions is achieved after hundred of years, when the thermal and mechanical regime of the bedrock has adapted to non-perennially frozen strength conditions or when slope angle reflects the equilibrium angle of permafrost-free rock slopes (Krautblatter and Leith, 2015).

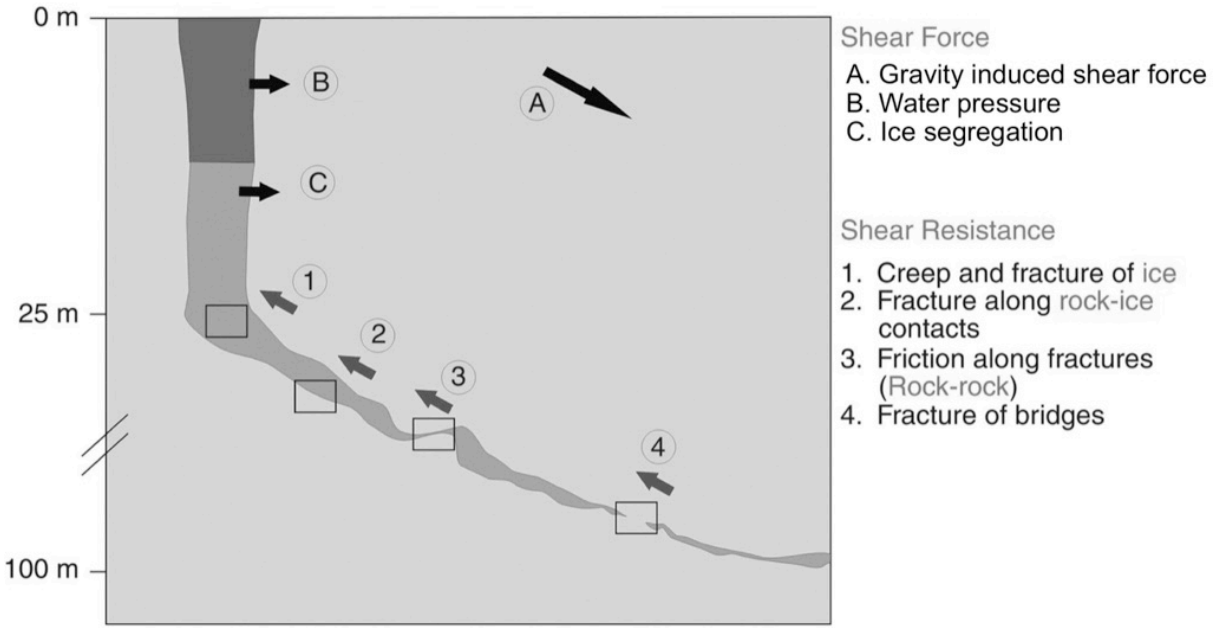

Figure 2.16: *Ice-rock mechanical model of Krautblatter et al. (2013) showing destabilising conditions of (i) increased shear stresses and/or (ii) decreased shear resistance in permafrost-affected bedrock. Image taken (and corrected: 'segregation') from Krautblatter and Leith (2015, p. 156).*

The ice-rock mechanical model of Krautblatter et al. (2013), shown in Figure 2.16, demonstrates that the initial failure (second rapid response) and the subsequent major rockfall activity (late-glacial slow response) can be caused by (i) increased shear stresses and/or (ii) decreased shear resistance due to the existence and/or progressive permafrost warming/thawing. Shear stresses can be increased by enhanced hydrostatic pressures associated with perched groundwater above permafrost (Krautblatter and Hauck, 2007; Fischer et al., 2010) or by bi-directional ice-segregation (Murton et al., 2001; Murton et al., 2016). As discussed in detail in section 2.4.4, latter mechanisms can lead to high cryostatic pressures of up to 30 MPa and deep progressive fracturing at the uppermost permafrost table and in the lower part of the active layer (Murton et al., 2006). In turn, four major individual or interacting mechanisms that can reduce the shear resistance (ii) of ice-filled fractures: (1) Fracture/deformation of cleft ice, (2) Friction/fracture along rock-ice contracts, (3) Friction/fracture along rock-rock contact and (4) Fracture of bridges. Figure 2.16 schematically displays all permafrost-related mechanisms that can influence the balance between shear stress and shear resistance in warming and thawing permafrost rockwalls. For a detailed discussion see Krautblatter et al. (2013).

(1) *Fracture/deformation of cleft ice*: Although dependent of the stress-strain condition and the rate of loading, ice can creep in a ductile, elastic manner when slowly compressed without initiating failure. Yet, as soon as a

certain threshold is exceeded (e.g. 5-10 MPa of compressive strength), brittle and ductile-brittle ice deformation can occur, which is typically followed by complete fracture (Sanderon, 1988; Krautblatter et al., 2013). Experiments of Davies et al. (2001) indicate that shear strength of ice-filled fractures is primarily dependent on ice temperature and declines particularly between -5 °C and 0 °C.

(2) *Friction/fracture along rock-ice contacts:* In constant stress experiments of concrete-ice samples, Krautblatter et al. (2013) demonstrate that rock failure is more likely to occur at the rock–ice interface than within the ice itself. For moderate levels of normal load (300 kPa), the maximum strength of rock-ice connection decreases linearly for temperatures between -3 °C and 0 °C.

(3) *Friction/fracture along rock-rock contact:* In permafrost rocks, uniaxial and tensile strength is significantly increased by up to 50-70% (Mellor, 1973) and fracture toughness is raised by 8-37% (Dwivedi et al., 1998). However, when ice in joints and micro-cracks starts to thaw, it has been shown that rock strength distinctly declines and subcritical fracture and friction occur, most significant between -10 °C and thawing point. Subsequent to thawing, frictional shear resistance of ice-free rock-rock surfaces decreases (Krautblatter et al., 2013).

(4) *Fracture of rock bridges:* In thawing permafrost, it is more likely that intact rock bridges fail when stresses exceed the fracture toughness and (sub-)critical crack growth occurs (Atkinson, 1982). While fracture toughness is increased when rocks are frozen to -10 °C (dependent on moisture content and temperature), thawing close to the equilibrium freezing point results in a decreasing fracture toughness (Mellor, 1973) and can enhance chemical fatigue effects at the crack tips (Krautblatter et al., 2013).

2.4.4 Ice segregation and its slow cracking of the volume expansion concept

Since the early 20th century, freezing and thawing of water in bedrock is considered the primary process responsible for crack evolution and rock breakdown (Jäckli, 1957; Matsuoka, 2008; Krautblatter et al., 2013) and rockfall initiation at mountain rockwalls (Rapp, 1960b; Sass, 2005b; Gruber and Haeberli, 2007). Due to the slow operation of frost weathering, the mechanism has rarely been directly analysed in the field and if so, it is often abductively inferred from visual field evidence such as shattered bedrock block fields and talus slopes (Lozinski, 1909; Hales and Roering, 2005). Instead, most of our present-day knowledge about the frost cracking process is founded on theoretical (Walder and Hallet, 1985; Hallet, 2006) and laboratory tests (Matsuoka, 1990; Hallet et al., 1991; Murton et al., 2006), and occasionally numerical models (Anderson, 1998; Hales and Roering, 2007; Gischig et al., 2011a) thought to replicate field situations. Apart from the question whether this anchored paradigm of frost weathering is still acceptable, two opposite – and we could say, also scale-dependent - hypotheses about the actual mechanism of frost cracking drive an on-going debate amongst geomorphologists.

According to the traditional theory, the prime cause of frost cracking is the volumetric expansion of 9% during the phase change of liquid water to ice (Lozinski 1909). When water freezes in confined pore spaces or micro-cracks, ice pressures of up to 207 MPa can ideally develop at a temperature of -22 °C. Since the tensile strength of most porous rocks is one to two orders of magnitudes smaller than 207 MPa, these ice-induced tensional stresses are theoretically effective enough to crack the bedrock (Davidson and Nye, 1985; Wegmann,

1998; Matsuoka and Murton, 2008). This first theory has become a paradigm supported by laboratory studies including the early simulation of grain-scale frost cracking by Tricart (1956), who later coined the terms macrogélivation and microgélivation (Tricart, 1970) and more recently, the frost fatigue tests of Jia et al. (2015). Latter study, for instance, suggest that ice volume expansion may act as sub-critical weathering process within the upper 20-50 cm of bedrock. Those laboratory results have been frequently used as strong argument that the repeated occurrence of volume expansion does promote, if not trigger, up to pebble-size rock disintegration (Matsuoka and Murton, 2008).

A more detailed examination of those experiments reveals that they have specific conditions in common to effectively simulate rock breakdown through volumetric ice expansion. First, many studies seal their samples to imitate a closed system where water cannot drain away and where ice expansion creates enough force (e.g. Jia et al., 2015). Ice extrusion of ice or water evaporation is also counteracted by simulation of rapid freezing rates down to -20 °C from all sides and ideally a high number of (e.g. 300) half-daily temperatures cycles, particularly in experiments favouring the open-system approach (Matsuoka, 1990; Nicholson and Nicholson, 2000). Furthermore, soft or/and highly porous rock samples are commonly selected to ensure detectable rock breakdown within time-restricted experiments. And finally, rock samples are fully or at least 50% water saturated to avoid compression of air and to generate maximum ice pressures (McGreevy and Whalley, 1985; Jia et al., 2015).

Given these common laboratory procedures, it does not surprise that the applicability of the volume expansion concept in natural conditions has been strongly questioned since the last three decades (Walder and Hallet, 1985; Hallet et al., 1991; Hall and Thorn, 2011). As a major source of criticism, natural rockwalls are barely closed systems, but rather best represented as open and permeable systems, where water can migrate, creep and extrude. Further, theoretically assumed maximum pressures of 207 MPa are particularly unrealistic because a) daily frost cycles are barely fast enough, b) rarely generate rock temperatures of -22 °C and c) penetrate only into the upper 30 cm (Matsuoka et al., 1998). Moreover, this near-surface area is exactly the zone of natural rockwalls most affected by high daily to seasonal moisture fluctuations (0-100%), as recently stressed again by Rode et al. (2016) in Figure 2.17. Only in deeper bedrock layers in annual water content constant at about 80% (Sass, 2004, 2005a). Thus, the critical degree of pore water saturation of e.g. 58-100% as suggested by Prick (1997) or 92% by Matsuoka (1990) is hardly ever reached in natural rockwalls, not even at shaded, rain-exposed exposures.

Although the weathering efficiency of the 9% volumetric ice expansion during phase change is no matter of doubt, its importance under natural conditions seems to decrease with bedrock depth; and when we leave the well-constructed laboratory setting. But surprisingly, despite this obvious gap between natural and experimental conditions, the ice volume expansion concept has been frequently transferred to the field (Church et al., 1979; Coutard and Francou, 1989; Matsuoka and Sakai, 1999) and is presented as dominant rock weathering mechanism in several German and English textbooks (e.g Zepp, 2008; Bierman and Montgomery, 2013). This general acceptance and somehow self-sustaining paradigm is – rather cynically – commented by Thorn (1992, p. 10) as 'story [… of] casual empiricism gathering respectability by repetition until it attained the stature of an article of faith'. However, if experiments do not adequately reproduce natural conditions, what can they tell us

about the efficiency of an assumed mechanism, such as volume ice expansion, for the weathering of natural rockwalls and initiation of rockfalls?

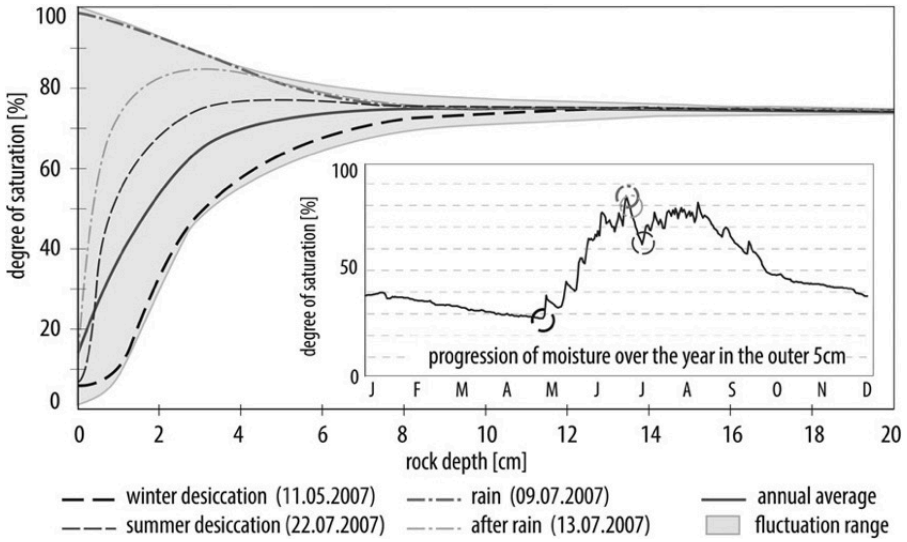

Figure 2.18: *Typical moisture depth profiles of mountain rock slopes during various weather conditions (Austrian Alps). Figure taken from Rohde et al. (2016, p. 1942).*

An alternative rock weathering mechanism that is independent from water-to-ice expansion, but linked to the pressures of growing segregation ice has been already proposed in the 1980s by Hallet et al. (1991) and (Walder and Hallet, 1985). In analogy to the ice lens growth in freezing soils (Taber, 1929) they argued that permeable and jointed bedrock may allow migration of liquid water through a frozen fringe towards ice lenses in crack tips, where it accretes (Fgure 2.18A-B). Water migration along grain boundaries is possible due to the temperature gradient-induced suction caused by thin (nm-scale) films of liquid water that may exist even at subfreezing temperatures in rock capillaries or absorbed on mineral surfaces. These films may exert an attractive force on pore water by cryosuction. Already a temperature drop of 1 °C induces a cryosuction of 1.2 MPa (Williams and Smith, 1989). Over time, the continuous segregation of ice increases the size of the ice lens,

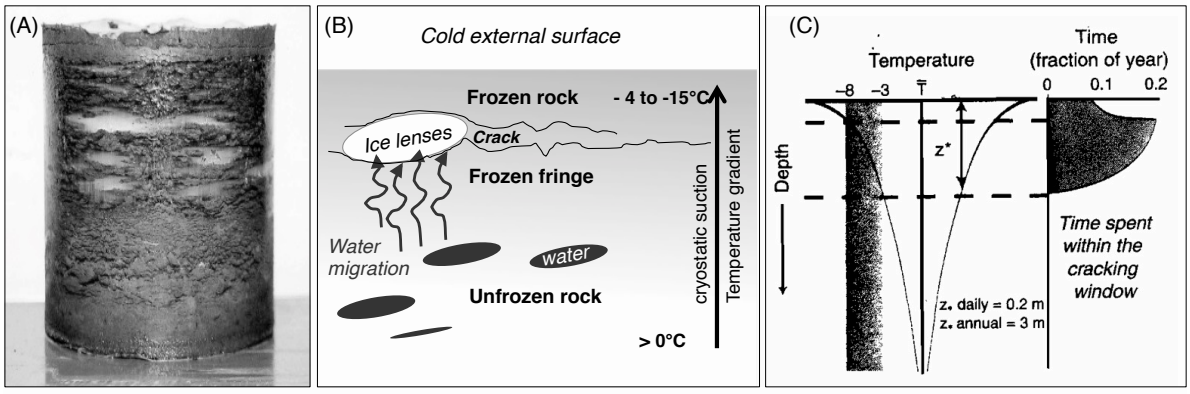

Figure 2.17: *Analogy between frost heave in soil (A) and frost cracking in permeable rocks (B and C). B: Schematic illustration of ice lens growth in permeable rocks adapted from Anderson and Anderson 2012, p. 174. C: Temperature depth profile through bedrock showing the optimal frost cracking window between -8 °C and -3 °C with respect to fraction of years (image taken from Anderson and Anderson 2012, p. 175). Source of photograph (A): http://civilengineersforum.com/wp-content/uploads/2014/12/ice-lenses.jpg.*

which in turn promotes the growth of the crack tip, and generates disjoining (intermolecular) pressures between ice and rock. Although depending on rock type (i.e. permeability, micro-fracturing), the optimal thermal range most conducive to ice-induced cracking is assumed to lie between -3 °C and -8 °C or -10 °C (Walder and Hallet, 1985; Hallet, 2006). Experiments of Hallet et al. (1991) indicate that most ice lens growth in fractures occurs as long as rock temperatures are maintained within this so-called 'frost-cracking window' (Figure 2.18C) and the rock has access to water. In turn, cracking rates may significantly decrease outside of this range because water is thermodynamically too stable to freeze at higher temperatures and, at lower temperatures, it becomes too viscose to efficiently migrate (see also Anderson and Anderson, 2012).

While the growth of segregation ice has long been accepted to be responsible for frost heave e.g. in Arctic soils, it took a number of clever laboratory experiments, numerical models and innovative field studies to convince the periglacial 'hard rock' community and to slowly crack the volume expansion paradigm. It appears, that the importance of ice segregation has been gained most recognition in research of mountain rockwalls in the context of current permafrost degradation (Gruber and Haeberli, 2007) and, particularly, after the prominent freezing experiments of Murton et al. (2001); Murton et al. (2006); Murton et al. (2016). In an environmental cabinet, Murton and his collegues exposed saturated chalk blocks to (A) top surface downward freezing as well as (B) both from top and upward freezing (Figure 2.19). By this distinction they aimed to simulate the seasonal differences at (A) permafrost-free with unidirectional heat and water transfer and (B) permafrost-affected rockwalls with bi-directional active layer effects. The experiments confirmed Walder and Hallet's (1985) concept and demonstrate that unidirectional freezing results in growth of segregation ice. However, after 30 cycles fracturing occurred only at the upper centimetre of bedrock surface. Contrarily, the blocks exposed to 24 cycles of bi-directional freezing displayed deeper and more intense frost cracking. The water transfer both downwards from the centre of the active layer and upwards towards to the rock surface resulted in ice-filled fractures at the uppermost permafrost and in the lower part of the active layer (Figure 2.19).

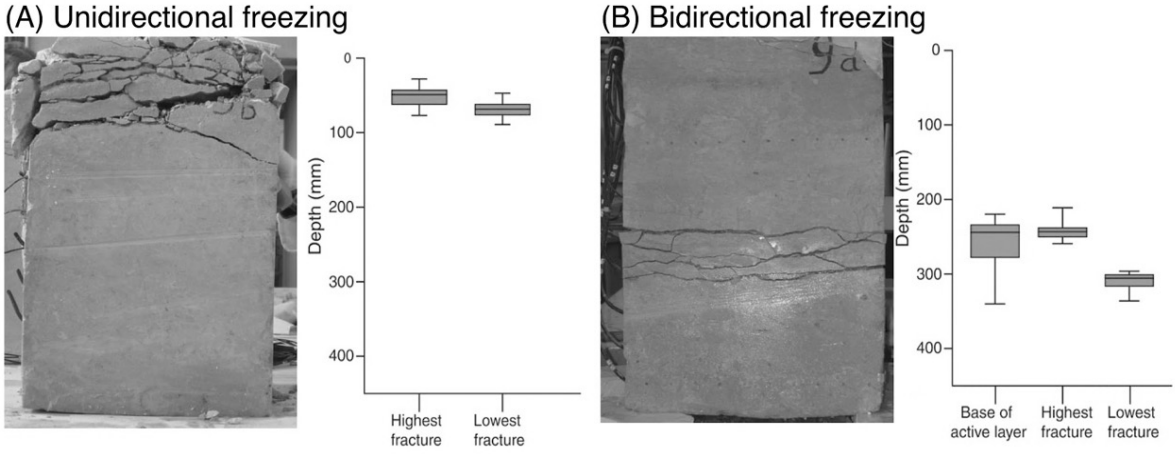

Figure 2.19: *Fracture formation within 450-mm-high blocks of chalk due to uni-directional freezing (A) and bi-directional freezing (B). Figures taken from Murton et al. (2006, p. 1228) and Matsuoka and Murton (2008, p. 202).*

With respect to mountain landscape evolution, the importance of ice segregation has been particularly recognised since insights from laboratory studies have been tested in numerical models. For instance, the use of a 1D heat conduction model (Anderson, 1998; Hales and Roering, 2007) allows predicting the monotonic decline of frost cracking intensity with depth. Hales and Roering (2007) transferred their findings to the Southern Alps of New Zealand and showed that their numerically predicted maximum frost cracking intensities coincide within a small elevation range (2300 m asl). Interestingly, this frost cracking belt is not only the approximate elevation of the highest peaks in this area but also the area with the highest rate of rockfall talus slope production (Hales and Roering, 2005). In a back-calculation, the authors also demonstrate that the zone of maximum frost cracking and thus most active rockfall release was likely 500 m lower in elevation during LGM, when temperatures were -2 °C and -4 °C cooler. These findings highlight that ice segregation can act as large-scale 'frost buzzsaw' that may counteract the uplift of active mountain ranges (Hales and Roering, 2009).

The likely most challenging task to bridge the gap between those laboratory and numerical studies to natural anisotropic rockwall systems is increasingly addressed since the last years, partially owned to new technologies. For instance, recent acoustic emission measurements at rockwalls in the Swiss Alps by Amitrano et al. (2012) and Girard et al. (2013) significantly improved our understanding of frost weathering under natural conditions. Their acoustic records underline well that sustained seasonal bedrock freezing result in much stronger frost cracking activity (due to slow water delivery), rather than the fast, repeated daily frost cycles. However, their results also emphasise that independent from lithology (gneiss, crystalline rock), frost cracking can occur over the full range of temperatures from 0 °C down to -15 °C, even under dry bedrock conditions. Their findings therefore underline that the heterogeneous thermal and hydrological bedrock properties highly complicate the conditions for ice segregation theoretically or numerically assumed.

To sum up, the evolution of the debate on the dominant frost weathering mechanism might be one of the best examples of how scientific paradigms can shift over time as consequence of theoretical, experimental, numerical and field investigations. At the same time, it shows the challenge to bridge the gap between theory and different empirical insights and transfer these back to reality: The natural rockwall system. Particularly, the field study of Girard et al. (2013) emphasises the importance of direct field observations for shifting a scientific paradigm such as volume expansion that is mainly founded on theoretical or laboratory arguments and even for providing constantly a new perspective on accepted facts (e.g. the frost cracking window).

2.4.5 Sun-induced thermal fatigue and thermal shock on 'cold' rock slopes

Another, albeit very tediously evolving paradigm shift in the research on bedrock failure is rock weathering by thermal stress. While thermal fatigue and thermal shock has already been implemented in research outside of geomorphology, it appeared long to be difficult to convince the geomorphic community that *heat* can be a major driver of rock breakdown and especially rockfall release in *cold* high mountains. Indeed, until a few years ago, it was hard to find any discussion in periglacial literature about rock weathering, landform evolution, not to mention, about rock slope instability, where freeze-thaw is not the sole basis for explanation (see discussion of e.g. Hall, 1999). This frost-dominated paradigm might be particularly founded on the repetition of 'circular

arguments devoid of relevant data' and unproven form-process causalities, as commented by Hall and Thorn (2011 p. 3). Specifically, the angularity of loose debris, characteristic for cold regions, has become the standard 'proof for the effectiveness of freeze-thaw weathering'. Yet, geomorphologists like Hall, Thorns and André do not question the general importance of freeze-thaw weathering in cold environments. But they are some of the few researchers criticising the freeze-thaw paradigm and encouraging the community to re-think our reasoning about weathering processes, form and material in cold regions (see critical review of Hall et al., 2002). The role of other potential mechanisms and their synergy seem to be 'filtered out' in most studies on rock weathering and slope instability in high-mountains. Hall (2006, p. 189) questions specifically "in how many of these descriptions [on frost weathering] can one find details regarding the high summer temperatures […] although the summer is […], in most cases, the period when the observer is actually there?".

Manifestation of the freeze-thaw paradigm may have started in the 1940s, when the experimental studies of Blackwelder (1933) and Griggs (1936) appeared to disprove the efficiency of thermal stress to breakdown rocks under cold conditions. While the unquestioning acceptance of these well-defined laboratory experiments contributed to periglacial geomorphologists moving away from the concept of thermal stress, interestingly, Blackwelder's and Grigg's studies had little impact on research outside of geomorphology (Hall and Thorn, 2011; Hall and Thorn, 2014). Here, during the last years, studies on ceramics (Tvergaard and Hutchinson, 1988; Han, 2007), building materials and concretes (Peng et al., 2008; Akentuna et al., 2016), even on human teeth (Brown et al., 1972) and more recently, extra-terrestrial research (Van Gasselt et al., 2005; Levy et al., 2010; Eppes et al., 2015) significantly improved our understanding of the physics of thermal weathering and its operational scales. In fact, those studies underline the importance to differentiating between thermal fatigue and thermal stresses (see literature in Hall and Thorn, 2014).

Thermal fatigue is a progressive and permanent structural damage of rock that is produced by repeated temperature changes whose stresses are often far below the actual rock strength (Wang and Liaw, 2008). Differential crystal expansion (warming) and contraction (cooling) lead to internal stresses that concentrate along crystal boundaries or nano-scale rock structures like bedding planes (Tvergaard and Hutchinson, 1988). If the stress intensity exceeds the elasticity of the rock material, it deforms by plastic strain (Yatsu, 1988). Thermal fatigue does therefore not generate *new* failure planes. It rather leads to micro-cracks along pre-existing weaknesses typical for sun-exposed rockwalls with pre-existing slope-parallel joints (Figure 2.20A-B). However, dependent on rock porosity and mineral association, thermally induced rock deformation may differ highly (Gómez-Heras et al., 2008). Light/heat transmission into depth and thermal expansion of rock may generally decrease with increasing porosity (Janio de Castro Lima and Paraguassú, 2004), but can significantly increase with increasing quartz content (Hall et al., 2008). Moreover, the large and anisotropic expansivity of quartz minerals highly complicate the thermal behaviour of many rocks (i.e. paragneiss); one mineral axis can contract while the others expand (Siegesmund et al., 2000; Luque et al., 2011). Nevertheless, given sufficient repetitions, final rock disintegration may be granular in form of individual grains (Gómez-Heras et al., 2006; Eppes and Griffing, 2010) or as thin near-surface exfoliation or flaking. Small, flake- or sheet-like deposits on the foot of unstable rockwalls could be typical evidence pointing to thermal stress fatigue (Figure 2.20D). It is important to state that latter terms such as 'exfoliation' do not express a *process* of weathering, but the *visible product* of weathering of rocks typically characterised by surface-parallel discontinuities (cf. Hall and Thorn, 2014).

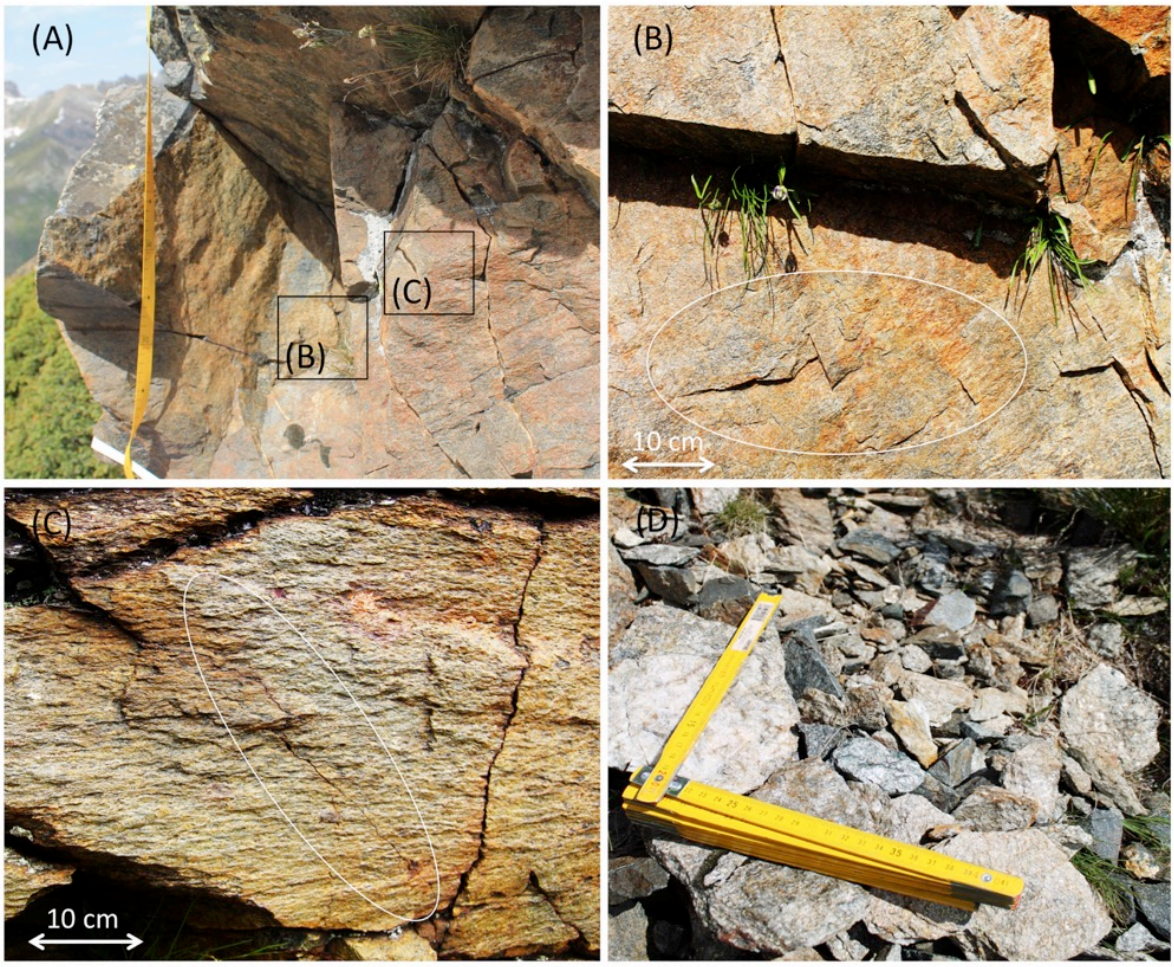

Figure 2.20: *A south-exposed, paragneiss rockwall in the Swiss Alps at approx. 2800 m asl (A) with typical fracture patterns (B, C) and detached material at the slope foot (D). In (B) Micro-cracks along pre-existing, slope-parallel foliation and bedding structures and thin flaking of bedrock near-surface could point to thermal stress fatigue. In (C) rectilinear orthogonal micro-cracks independent from schistosity and pre-existing joints could result from thermal shocks.*

Contrary, thermal shock is linked to one single stress event due to a sudden and large temperature change (Yatsu, 1988). Large cooling or heating rates can irreversibly deform the rock if the temperature-induced internal stresses suddenly exceed the capacity of the brittle material (Zhang et al., 2010). Thermal shocks produce unique and new 'catastrophic' diagnostic rock features, which, contrary to thermal fatigue, typically cut across pre-existing microcracks or crystal boundaries as shown in Figure 2.20C (Hasselman, 1969). Commonly reported diagnostic features are a hierarchical network of rectilinear (Bahr, 1986; Hall and André, 2001) or polygonal cracks (Levy et al., 2010; Levy et al., 2011). Thermal shock only occurs at a specific rate of temperature change ($\delta T/\delta t$). There is an on-going debate without general consensus about the actual threshold to initiate thermal shock (see review in (Hall and Thorn, 2014). Factors like the duration of the rate of change, rock properties and the size of rock surface highly complicate the fatigue behaviour of rock (Hall, 1999; Hall and André, 2003). Lanin and Fedik (2008), for example, show that stresses due to thermal shock decreases with decreasing rock surface size, because the rock thermal regime can adapt faster to surrounding air temperatures.

However, the comparison of previous laboratory studies seems to suggest a threshold of ≥ 2 °C/min, as proposed by Richter and Simmons (1974) to be the general minimum rate necessary for thermal shock.

Hence, thermal fatigue and thermal shock operate independently from each other and are linked to different driving forces and different diagnostic weathering features (Figure 2.20). Nevertheless, geomorphologists frequently simply summarise both processes by the term 'insolation weathering' (Hall and Thorn, 2014). However, Hall et al. (2012) point out that 'insolation does not weather'. The actual rock breakdown occurs due to internal thermal changes of the rock material. Certainly, insolation or the sun's radiation can be a *driving* force, but variations in wind speed or cloud cover can also result in significant temperature fluctuations within the shallow rock surface (4 mm) even when air temperatures and incoming solar radiation are constant (Hall and André, 2001; Gunzburger and Merrien-Soukatchoff, 2011). The term 'insolation weathering' is therefore not only erroneous, moreover following Hall (1999) its continued use may have greatly contributed to reject the feasibility of heat and thermal stresses as possible rock breakdown mechanisms in cold regions.

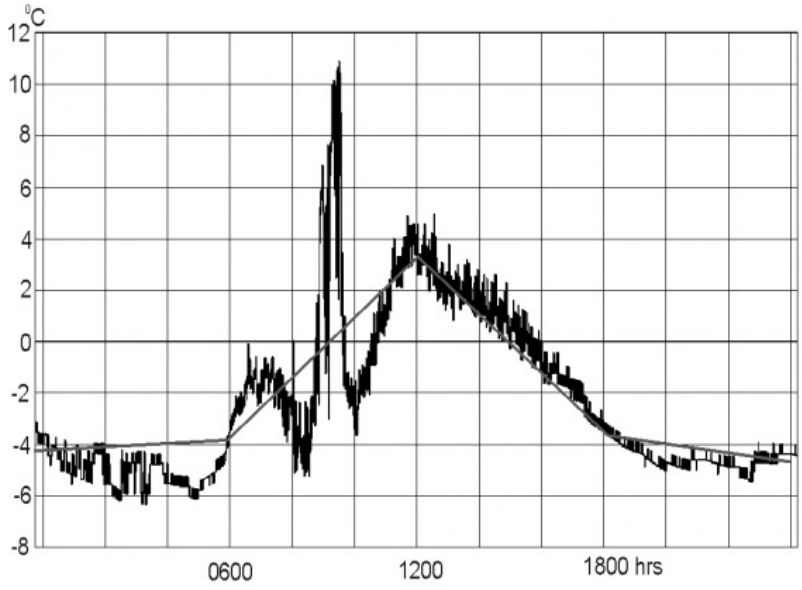

Figure 2.21: *Rock temperature data at one-minute interval (thick line) and six-hour interval (straight line) from Northern Canada. Figure taken from Hall (2006, p. 192). See Hall (2006) for an in-depth discussion.*

However at the turn of the 21st century, the role of thermal weathering suddenly received (again) increasing recognition in periglacial geomorphology, largely forwarded by field studies and the use of new technologies. Specifically, the use of high-resolution rock temperature data significantly changed the general perception of rock weathering in cold environments and offered new ways to address the scale of weathering (Thorn, 2003). For example, by monitoring rock temperatures at 1 min intervals in Antarctica, Hall and André (2001) could identify at least 16 crossings of 0 °C and numerous rapid thermal fluctuations during warm day-time with large $\Delta T/\Delta t$ changes of up 11 °C/min (Figure 2.12). While this information would have been 'hidden' in most low-frequency records (3-6h) and overlaid by the classic freeze-thaw cycle, the minute data clearly reflect thermal rates sufficient to cause thermal shock and thermal fatigue. While previous findings from Antarctica receive

from bedrock outcrops, however, it took long for the mechanism of thermal stress to also be addressed in the research of rockwall instability, particularly from a quantitative perspective. This is surprising given the frequent reports about rockfall events that occurred spontaneously during summertime without any of the typical triggers like earthquakes, rainfall, snow melt or freeze-thaw, as e.g. in the Yosemite National Park Area (Wieczorek et al., 1995; Stock et al., 2014; Collins and Stock, 2016). However, the few modelling and in situ field measurements from e.g. northern Japan (Ishikawa et al., 2004), Switzerland (Gischig et al., 2011a, b) and the French Alps (Gunzburger et al., 2005) suggest that daily surface temperature changes are effective to induce plastic deformation and gradual winding/lengthening of joints, when thermal stress intensities exceed the toughness of the material. Recently, Collins and Stock (2016) presented furthermore 3.5 years of rock deformation measurements form the Yosemite National Park indicating that exfoliated granitic rocks can expand by 1 cm per day. Their thermomechanical calculations demonstrate that cyclic thermal forcing on near rock surface, especially during hot summer days, can lead to progressive, non-reversible fracturing and rockfall events of cm to m-scale block size. Colin and Stock's findings therefore provide empirical support for the previous intuitive notion of Hall (1999) that also in mountain areas 'cracking cliffs can feel the heat' and fail, as phrased by Gischig (2016).

2.4.6 You only see what you look for – Other weathering processes

Even though this study will put emphasis on above described fracturing mechanisms, it is important to acknowledge that various other processes - which are either little considered in periglacial research, little understood or simply, still unfamiliar - could contribute to the weathering, fracturing and failure of mountain rock slopes. For instance, although working on the micro scale of joint tips or minerals, it could be likely that chemical processes promote bedrock fracturing and even failure, particularly in carbonate rich bedrock. The importance of chemical rock weathering and solution in periglacial environments was already underlined by Rapp (1960a) in Kärkevagge as well as by Caine (1976). Interestingly, although geomorphic studies always refer to those two seminal papers, chemical processes received little attention as potential control on mountain rock weathering and failure (cf. Hall et al., 2002). Nevertheless, recent investigations from the Italian Dolomites (Petley and Petley, 2005) and carbonate limestone rocks in the Bavarian Wetterstein mountain (Sass, 1998, 2005b; Krautblatter et al., 2012) reveal that dissolution processes, i.e. in limestone rockwalls can cause micro-scale fracturing of rock bridges, that can coalesce to larger-scale joints and favourable sliding planes for debris falls, cliff falls and high-magnitude rock slope failures such as in Vajont.

Likewise, a few laboratory and theoretical studies let assume that humidity variations (or even dew) at positive air temperatures could effectively promote deep wetting and drying cycles and anisotpric deformation in mountain bedrock due to repeated shrinkage and swelling (Fahey and Dagesse, 1984; Hamés et al., 1987; Hall and Hall, 1996; Prick, 1999). As wetting and drying processes are preferably active in a sub-surface zone where also frost weathering and thermal stress operate, Hall 1993 questions whether the dominance of frost weathering could be wrongly implied in some studies. However, due to the lack of empirical studies, i.e. from

the field, the significance of wetting and drying for the instability of mountain rock slopes remains little understood so far and requires future research.

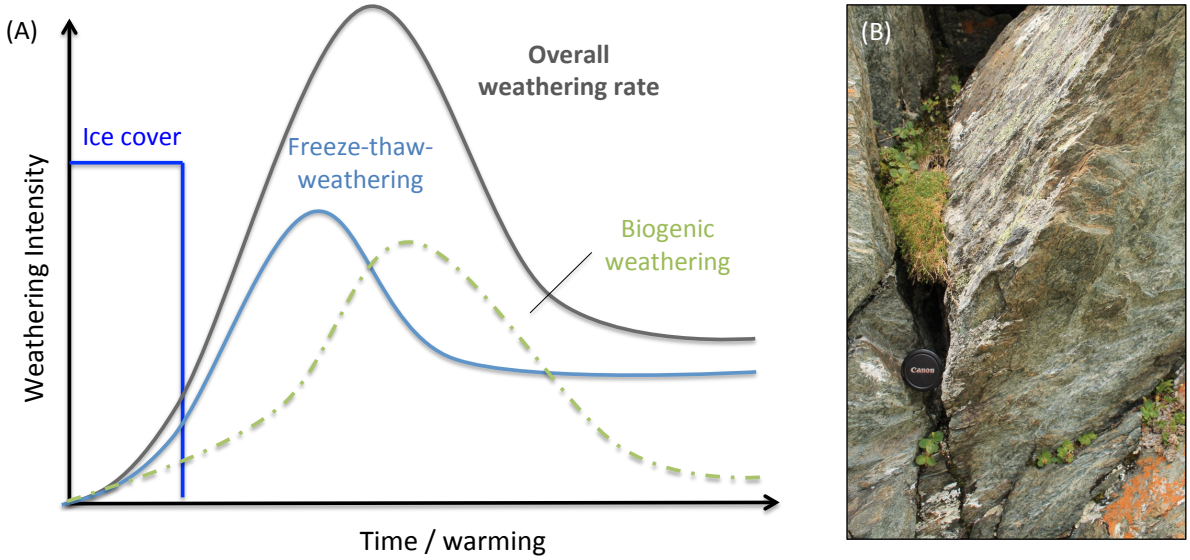

Figure 2.22: *Conceptual model (A) of the changing interaction between freeze-thaw weathering and biogenic weathering during the paraglacial period in high-mountain systems. Conceptual model adapted from Viles (2013, p. 18). (B) Example of biogenic joint filling and lichen rock coating.*

The same applies to biological weathering and i.e. the role of bacteria, mosses and lichens for surficial rock weathering or stability. While biological weathering has been identified in a variety of cold climate environments (e.g. Hall and Otte, 1990; Hall et al., 2002; Hall et al., 2005; Hall et al., 2008) it is still little understood whether their mechanical stresses (e.g. by roots), thermal (albedo) and chemical effects (oxidation) can contribute to the total long-term destabilisation and erosion of rockwalls as shown in Figure 2.22B (Viles, 2013b).

Therefore, as highlighted in the review paper of Viles (2013b), it is clear that the weathering and failure of mountain rock slopes is the result of multiple processes, which may act in succession or in synergy across different spatial and temporal scales. Table 2.3 summarises different processes of rock weathering and their major loci of operation as well as their visible product of weathering. The key point made by Viles (2013b) in Table 2.3 is that different weathering processes affect different spatial scales of rockwalls ranging from the near-surface to deep-seated joints, but their spatial synergy over different temporal scales will promote rock failures in very different mechanistic ways with likely very complex frequency-magnitude patterns. Particularly on larger temporal scales, e.g. the paraglacial period, it is likely that the relative role of individual weathering agents and their synergistic weathering efficiency change over time. A conceptual approach is presented in Figure 2.22A. However, rock weathering in context of paraglacial rock slope instability has been little addressed so far.

Table 2.3: *Linkage between weathering processes and rock slope instability (taken from Viles 2013, p. 65).*

(a) Weathering processes and their locii of action

Category	Agent/Process	Near surface	Along discontinuities	Across weathering profiles
Mechanical	Unloading	X	X	
	Gravitational stress	X	X	
	Tectonic residual stress	X	X	
	Thermal cycling stress	X		
	Frost weathering	X	X	
	Salt weathering	X	X	
Chemical	Hydration	X		X
	Hydrolysis	X		X
	Dissolution	X	X	X
Biological	Surface biofilms – biochemical	X		
	Surface biofilms – biophysical	X		
	Bacteria	X	X	X
	Plant roots		X	

(b) Weathering products and their characteristic scales

Weathering product	Near-surface	Deep-seated
Granular disintegration	X	
Sheeting	X	X
Cavernous weathering	X	X
Block detachment		X
Isovolumetric chemical transformation	X	X

Although acknowledging the operation of further weathering processes, the research of mountain rock slope instability is still faced to a problem central to all science: We commonly investigate only factors that we know, that we have seen or believe to see in the field. The British anthropologist Lubbock (1895) describes this problem of such 'predefined research glasses' with that 'in the same field the farmer will notice the crop, the geologists the fossils, botanists in the flowers, artists the colouring, sportmen the cover for the game. Though we may all look at the same things, […] but what we see depends on mainly what we look for'. Therefore, the true complexity of destabilising mechanisms might be still overlooked or better said, is still unknown. Because, as questioned by Hall et al. (2012), how shall we 'see' and thus investigate what we are unfamiliar with? Yet, as similarly demanded by Viles (2013b), our conventional view of bedrock weathering and fracturing in cold mountains needs a fundamental reconsideration of reality that must include non-linear and complex synergistic process relationships as well as not yet recognized mechanisms and emergent behaviour across scales.

2.5 Sediment cascading processes after bedrock failure

Once the internal and external stresses exceed the rock mass' resistance, rockwalls become unstable and the disintegrated material can be detached. In steep mountain terrain, rockfalls are the predominating process. Rockfalls are the free fall of weathered and detached rock down to the foot slope under the influence of gravity. Distinct evidences of rockfall activity are talus slope landforms at the rockwall foot. Therefore, the importance to study the mechanistic behaviour of rockfalls is based upon the fact that they are the primary agents of rockwall erosion, cascading sediment transfer and talus slope formation and account for one of the most serious natural hazards in mountain areas.

The following chapter provides a definition and terminological classification of rockfall processes, gives an overview on the tree major failure modes, the distinct transport pattern and fragmentation of rockfalls. Finally, the depositional evolution and material characteristics of talus slopes are described as they represent a key proxy for abductive reasoning of recent and post-glacial (i.e. LGM) rockfall activity in mountain environments.

2.5.1 Rockfall processes: Definition and classification

> *Rockfalls are probably the most frequently observed mass movement in mountain areas and yet few data are available on the frequency, size and controls of rockfall activity.* (Luckman, 1976, p. 287)

Rockfalls are defined as free downward movement of material detached from a steep slope, along joints or bedding planes on which little or no shear displacement takes place (Varnes, 1978; Cruden and Varnes, 1996). This definition is in accordance to the suggested classification of the International Geotechnical Societies' UNESCO Working Party on World Landslide Inventory (UNESCO, 1993). The detached material can be of any size and can encompass a single block, several blocks or a fragmented mass of rock, which typically moves en masse through the air. During the initial part of the trajectory, movement occurs as free fall before it turns into a bouncing, rolling and sliding at the foot of the slope (Flageollet and Weber, 1996). In comparison to other types of gravitational mass movement (see Varnes, 1978; Hungr et al., 2014), rockfalls usually occur suddenly and cover relatively rapid temporal scales of movement. Since the early 1960s, various classifications and nomenclatures of rockfalls have been proposed, each using different geomorphic and engineering criteria (Whalley, 1984; see summery in Flageollet and Weber, 1996). In order to clearly characterise the type of rock slope instability and to delimit the rockfall process from other gravitational processes, in this dissertation, rockfalls are classified and characterised according to six criteria (Figure 2.23).

(i) Depending on the **source material**, rockfalls can be subdivided into debris falls, when released from unconsolidated or weakly consolidated detritic rocks, or soil falls, when comprising fine material of soil e.g. from riverbanks (Nardi et al., 2012). However, this work deals with rock failures that originate in coherent, but jointed bedrock of steep mountain rockwalls.

(ii) Furthermore, distinction is made based on **timing or origin of rockfall release**. For that, a very useful approach of primary and secondary rockfalls was introduced by Matznetter (1956) and later adapted by several geomorphologists like Rapp (1960b, 1960a). While primary rockfalls represent freshly released events from

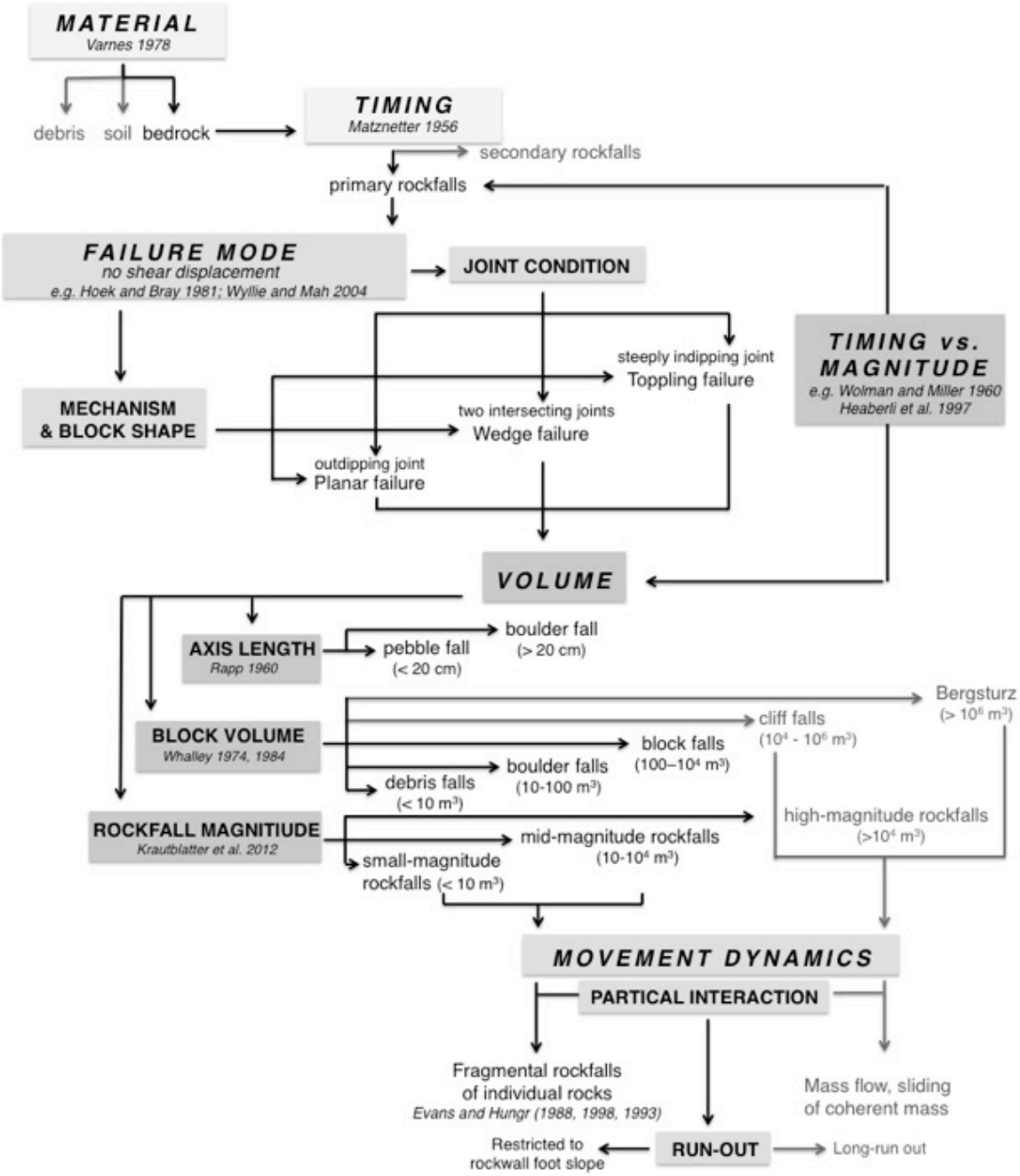

Figure 2.23: *Criteria of rockfall classification and characterisation of rock slope instability used in this study: (i) Type and origin of material, (ii) timing of detachment, (iii) failure mode at the source rockwall, (iv) volume of detached mass, (v) timing vs. magnitude and (vi) movement dynamics.*

rock slopes, secondary rockfalls are the delayed release of earlier detached material that have been accumulated in intermediate storages or in situ in bedrock irregularities. In geomorphic research, Matznetter's concept is still underrepresented, but has proven to be of major significance when it comes to explain the time lag of short-term rockfall activity and long-term rockwall erosion (e.g. Krautblatter and Dikau, 2007) or the non-linearity between rockfall release and its triggering event (Rapp, 1960b; Krautblatter and Moser, 2009). Similarly in engineering research, secondary rock release is still rarely part of natural hazard prediction, although as the gradual filling of intermediate rockwall storages and their abrupt depletion after snowmelt and heavy

rainstorms may represent a severe risk for humans and infrastructure, as shown e.g. in the Yosemite National Park (Guzzetti et al., 2003) and in Greece (Apostolou et al., 2015). Unless otherwise stated, this dissertation specifically focuses on **primary rockfall** processes.

(iii) Further classification is made according to the **failure mechanism** of the source area and associated block shape. From a geomorphological viewpoint, there has been previously little work done on classifying different failure modes (cf. Hungr et al., 2014). If at all, focus was (and is still) generally on rockfalls detached from planar shear surfaces, even though planar failure is often the exception. However, rock engineers contributed the terms 'wedge slide' (Londe, 1965; Hoek and Bray, 1981), for rockfalls released from two intersecting joints, as well as 'rock or flexural toppling' (Goodman and Bray, 1976) originating from joints that steeply dip into the slopes (Cruden and Varnes, 1996). In many textbooks, toppling processes are strictly defined as own process group distinct from planar or wedge failures due to their distinguishing process dynamics. However, as topples often culminate in an abrupt fall movement, especially on steep and high rock slopes (Dikau et al., 1996b), it is reasonable and necessary to consider topples as rockfall type in this dissertation.

(iv) Rockfalls can vary in size from small-size flakes, single pebbles to catastrophic events of several million m^3. Thus, particular emphasis has been on rockfalls according to their **event size and volume** (Gardner, 1970; Whalley, 1974; Douglas, 1980; Gardner, 1983; Whalley, 1984; Rochet, 1987). One of the earliest categorical systems dates back to 1960, to the Swedish geomorphologist Anders Rapp (1960a) suggesting a threshold block axis as distinguishing criterion to differ between pebble falls (< 20 cm) and boulder falls (> 20 cm). Later, the British geomorphologist Brian Whalley (1974) proposed a further subdivided volumetric classification that differentiates between debris falls (< 10 m^3), boulder falls (10-100 m^3), block falls (100-10^4 m^3) and cliff falls (10^4-10^6 m^3) and Bergsturz events (> 10^6 m^3). Several French and Italian authors also favour the approach of Rochet (1987) differentiating between single block falls (10^{-2} and 10^2 m^3), mass falls (10^2-10^5 m^3), very large mass falls (10^5-10^7 m^3) and mass displacement (> 10^7 m^3). However, in international rockfall research, Whalley's terminology is most common today. To simplify it, Krautblatter et al. (2012) suggested the terms 'small-magnitude rockfalls' for debris falls, 'mid-magnitude rockfall' for en bloc boulder and block falls, and summarised cliff falls and bergsturz events to 'high-magnitude rockfall'. The literature review highlights, that some authors occasionally include deep-seated events with failure planes of more than 50 m to the rockfall category, such as 'Sturzstrom' (Hsü, 1975), rock fragment flow or rock-fall avalanches (old classification of Varnes, 1958) and rock avalanches (Evans et al., 1989). However, given their distinguishing movement dynamics involved including longer travel distances, block interaction, lack of free fall of individual blocks (Erismann and Abele, 2001), those high-magnitude events are no focus of this dissertation.

(v) In geomorphic and natural hazard research, rockfall size is often plotted against time after release to characterise and predict the magnitude-frequency pattern of rock failure with respect to the concept of Wolman and Miller (1960) (see also Guthrie and Evans, 2004, 2007; Krautblatter et al., 2012). Figure 2.24 specifically address permafrost rockwalls and shows the relationship between timing of failure after permafrost warming and rockfall magnitude (Krautblatter and Leith, 2015). Commonly, small size debris or boulder falls can already initiate several days and weeks after intense permafrost warming events, as e.g. observed during

summer 2003 in the Swiss Alps (Gruber et al., 2004a). However, initiation of deep-seated failure planes occurs slowly due to the thermal propagation into depth and slow progressive fracturing. Therefore, the response time of high-magnitude cliff falls or Bergsturz events to external changes such as permafrost degradation can be often years to even millennia (Prager et al., 2008; Ravanel and Deline, 2011). In this study, particular interest is on the lower magnitude spectrum (<10^4 m^3) as it is supposed to be the predominating erosional and depositional process group in both study sites of this thesis (Swiss National Park, Turtmann Valley).

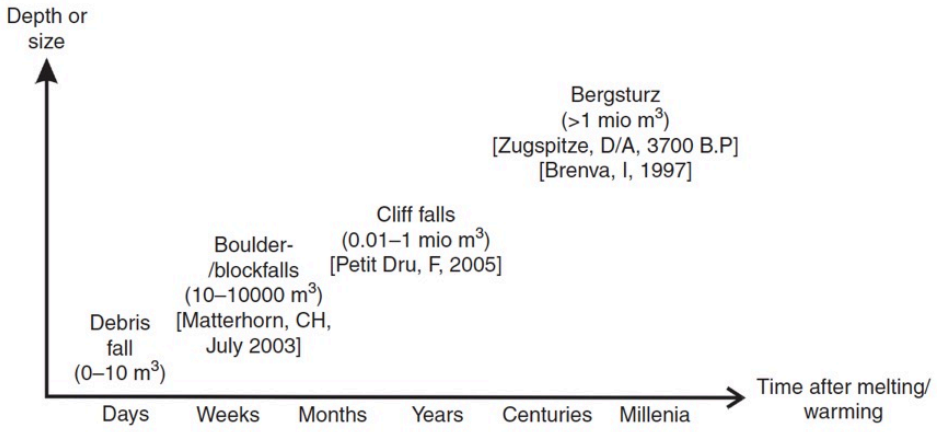

Figure 2.24: *Rockfall magnitudes released from permafrost rockwalls versus timing after permafrost warming and thawing. Image taken from Krautblatter and Leith (2015, p. 161) after Haeberli et al. (1997).*

(vi) Concerning this smaller rockfall size spectrum, the term **'fragmental rockfall'** will be additionally used, a term which was first introduced by Hungr and Evans (1988) in the Canadian Rocky Mountains. In fragmental rockfall events, the detached rock fragments move more or less independently downslope as ridged bodies (Evans and Hungr, 1993). This definition is favoured as it nicely stresses the negligible role of internal particle interaction during downslope movement of small-size rockfall events (similar to Rochet, 1987) and thus, makes a clear mechanistic distinction to mass flow or sliding of coherent or broken rock typical for deep-seated, high-magnitude failures.

2.5.2 Mechanics of rockfall erosion: Planar, wedge or toppling failure?

Release of rock fragments can occur in form of different failure modes, each associated with unique structural conditions of the source rockwall relative to its slope topography. The importance of identifying the failure mechanism is that different block shapes, sizes and spatiotemporal rockfall dynamics and consequently, different deposits are expected. Here, three major types of failure will be distinguished: planar failure, wedge failure and toppling. Kinematic analyses of joints detected in the fields by using steronets (e.g. Schmidt net, equal area projection), as shown in e.g. Figure 2.25C, are useful methods to identify joint sets critical for movement, potential failure modes, the shape of block release and the fall direction.

The simplest form of rockfall release is planar failure. Planar failure may occur in bedrock with persistent joints dipping out of the slope face or (nearly) parallel to it (Wyllie and Mah, 2004). In Figure 2.25A-B, joint set

A is favourable for planar sliding without or little shear displacement towards SW direction (Figure 2.25C). In contrast, there will be no failure on joints that dip steeper than the slope face and are not daylighting. In the seminal books on rock slope stability by Hoek and Bray (1981) and Norrish and Wyllie (1996), four key kinematic conditions are defined that have to be satisfied for plane failure to take place:

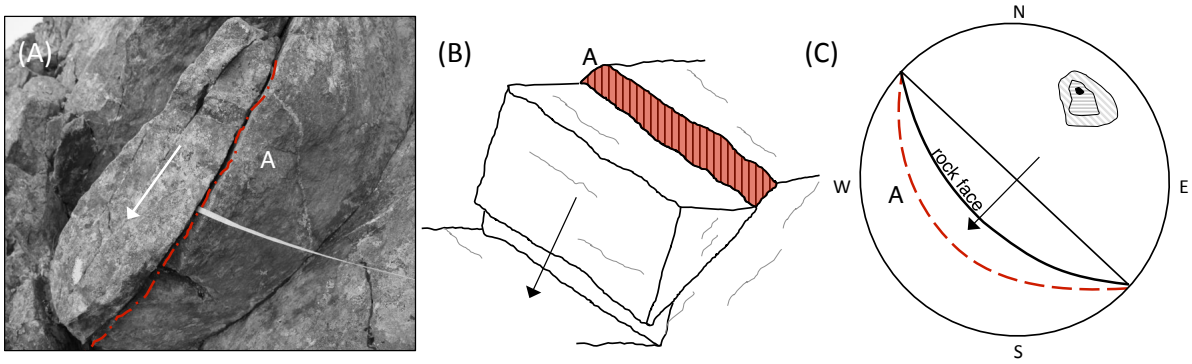

Figure 2.25: *Photograph (A), schematic illustration (B) and kinematic stereonet analysis (C) of planar failure. B and C based on Wyllie and Mah, 2004 p. 36.*

(i) The sliding surface dips less than the rockwall slope
(ii) The sliding surface daylights in the slope face (dips out of the slope)
(iii) The dip direction of the joint must be within +-20° of the dip direction of the rockwall
(iv) The dip of the sliding plane exceeds the angle of internal friction

Planar failures are lithologically independent and can occur in most geological settings, e.g. in granodiorite (Santana et al., 2012; Mavrouli and Corominas, 2016), andesite (Gokceoglu et al., 2000), limestone (Sellmeier et al., 2015) and foliated schist and gneiss (Derron et al., 2005). Nevertheless, rockfalls released from single planar failure surfaces are often the exception rather than the rule, because above-mentioned criteria are only occasionally present in rock slopes (Hoek and Bray, 1981 p. 150).

A more common failure mechanism is wedge failure, because rockwalls typically contain joints that intersect each other and dip obliquely to the slope. In Figure 2.26 a wedge-like rock fragment was previously contacted between the two planes A and B and was released on their daylighting line of intersection towards SSE. On the stereonet in Figure 2.26C, the line of intersection is defined by the intersecting point of the two great circles of the joints. Similar to planar sliding, specific kinematic conditions are required to induce wedge failure (Hoek and Bray, 1981; Norrish and Wyllie, 1996):

(i) The intersection line dips less then the dip of the slope face
(ii) The intersection line dips steeper than the average friction angle of the two joints
(iii) The trend of the intersection line approximates the dip direction of the slope

Thus, wedge failure can only occur if the trend of the intersection line lies within a range between αi (trend of intersection line) and αf (dip direction of face) (grey area in Figure 2.26C). If only one joint dips within this

range, wedge-like sliding will occur on its planar surface. If the dip directions of both joints however lie outside the angle between αi and αf, no wedge-type failure but planar sliding on both joint surfaces will occur.

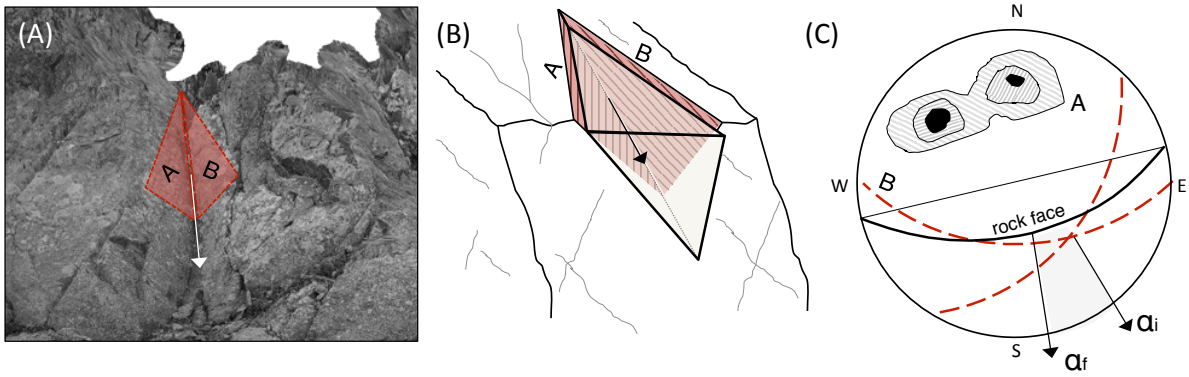

Figure 2.26: *Photograph (A), schematic illustration (B) and kinematic stereonet analysis (C) of wedge failure. B and C based on Wyllie and Mah, 2004 p. 36.*

In comparison to failure on single planar surfaces, rockfalls initiated by wedge failures occur more common and over a much wider range of structural and topographic settings. Early studies on wedge failures date back initially to engineers such as Goodman (1964), Londe (1965) and John (1970). However, recent geomorphic studies also highlight the significance of wedge failure on evolution of hlllslope morphology, sediment yield and frequency-magnitude relationships (Jaboyedoff et al., 2009; Loye et al., 2012; Matasci et al., 2015).

The third major failure condition associated with rockfall release is toppling on joints that dip into the slope (Figure 2.27). While the two previously mentioned failure modes involve a sliding movement, toppling failure represents a forward rotation of a block or column out of the slope about a fix point or axis below the centre of gravity of the displaced mass (Cruden and Varnes, 1996; Dikau et al., 1996b). The stereonet of Figure 2.7C shows the slope-indipping joint set A on which toppling failure can develop. According to Goodman and Bray (1976) following geometric and mechanical conditions must be fulfilled for initiating toppling events (see also Gokceoglu et al., 2000, p. 289):

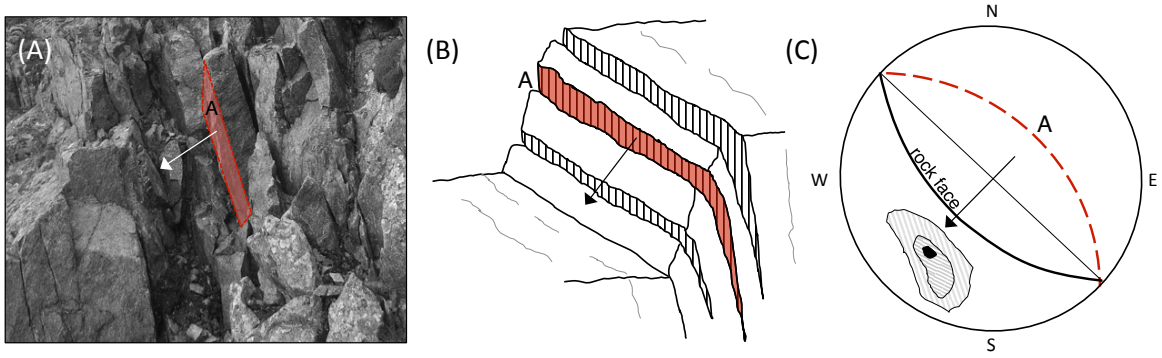

Figure 2.27: *Photograph (A), schematic illustration (B) and kinematic stereonet analysis (C) of toppling failure. B and C based on Wyllie and Mah, 2004 p. 36.*

(i) The rock slope has to be relatively steep and high
(ii) The controlling joint dips steeply enough into the slope for interlayer slip to occur
(iii) The dip direction of the joint lies within 150 and 210° to the rockwall's dip direction

For determining whether rock failure will occur by toppling or sliding, Freitas and Watters (1973) suggested the ratio between joint width and block height as well as the ratio between slope angle and its friction angle as the most critical criteria. More detailed description is given in Dikau et al. (1996b). Furthermore, Goodman and Bray (1976) differentiated between different types of topples, basically depending on the joint spacing, persistence and rock strength. Soft bedrock, for example, separated by long, near vertical and densely spaced joints is typically related to flexural toppling (Adhikary et al., 1997). In contrast, hard and equally jointed rockwalls, as shown in Figure 2.7A, are preferentially linked to block toppling of equally shaped columns or blocks (Brideau and Stead, 2010). Often, stairway rising from one cross-joint to the next higher up can be observed (Hoek and Bray, 1981).

Basal erosion of the toe of the slope allows the toppling process to start. After failure, the tilted mass or column can move onto the slope below and break up, bounce or start to slide downslope (Dikau et al. 1994). Occasionally, backward or reverse rotation is also possible when joints are rather parallel to the rock face and flatter cross-joints are relatively weak (Wyllie and Mah, 2004 p. 236). On steep, high mountain rockwalls, topples commonly culminate into a fall process.

One of the earliest studies on rock topples dates back to Müller (1968) identifying it as a key contributory or persecutory failure mechanism of the Vajont slide. Since then, toppling failure have been studied in schist (Halliday, 2010), calcareous rocks (Frayssines and Hantz, 2006) sandstone-claystone sedimentary formations (Evans, 1981; Alejano et al., 2010) and igneous rocks (Ballantyne, 1986). However, focus is rarely on those toppling mechanism that culminate into small-size rockfall events.

2.5.3 Downslope rockfall transfer: Kinematics and travel dynamics

After failure of rock slopes, the detached rock fragments move down the slope driven by gravity, passing through different modes of motion. There are three major modes of motion, which were first stated by Ritchie (1963) in experimental tests: free fall through air, followed by bouncing, rolling or sliding over the slope surface (Figure 2.28). Although rockfall dynamics and kinematics are no specific focus of this dissertation, it is important to give a short overview to understand the complex form evolution and (sub-)surface material characteristics of talus slopes. Only by understanding the dynamics and kinematics involved in talus slope deposition, can the latter be used as a proxy for conclusions on the instability of their rockwall source area.

If mean slope gradient of a rock slope exceeds around 70-76° (Ritchie, 1963), free fall of rock fragments occurs (Figure 2.28) - although varying in specific field situations (Dorren, 2003). As previously stated, any interruption of the free fall makes the process a secondary fall (Matznetter, 1956). Filling of intermediate sediment storages within rockwalls leads to short time lags of the rockfall sediment cascade. However, as soon

as movement starts, whether released as primary or secondary event, potential energy of blocks is converted into kinetic energy resulting in a gain of velocity (Frattini et al., 2012). Critical controls (Table 2.4) on rockfall velocity are rockwall height, volume (or mass) and shape of rock fragments, mechanical block properties and air friction (Bozzolo and Pamini, 1986). Numerical modelling by Crosta and Agliardi (2004) emphasises the strong influence of 3D rockwall effects, i.e. linked to micro-topography (roughness). Their simulation indicates that already small-scale bedrock convexities and ridges can affect both the trajectories of the free fall and the partition of total kinetic block energy into its translational and rotational components. Particularly, blocks that rotate during fall can reach long travel distances far away from the source area (Agliardi and Crosta, 2003; Dorren, 2003).

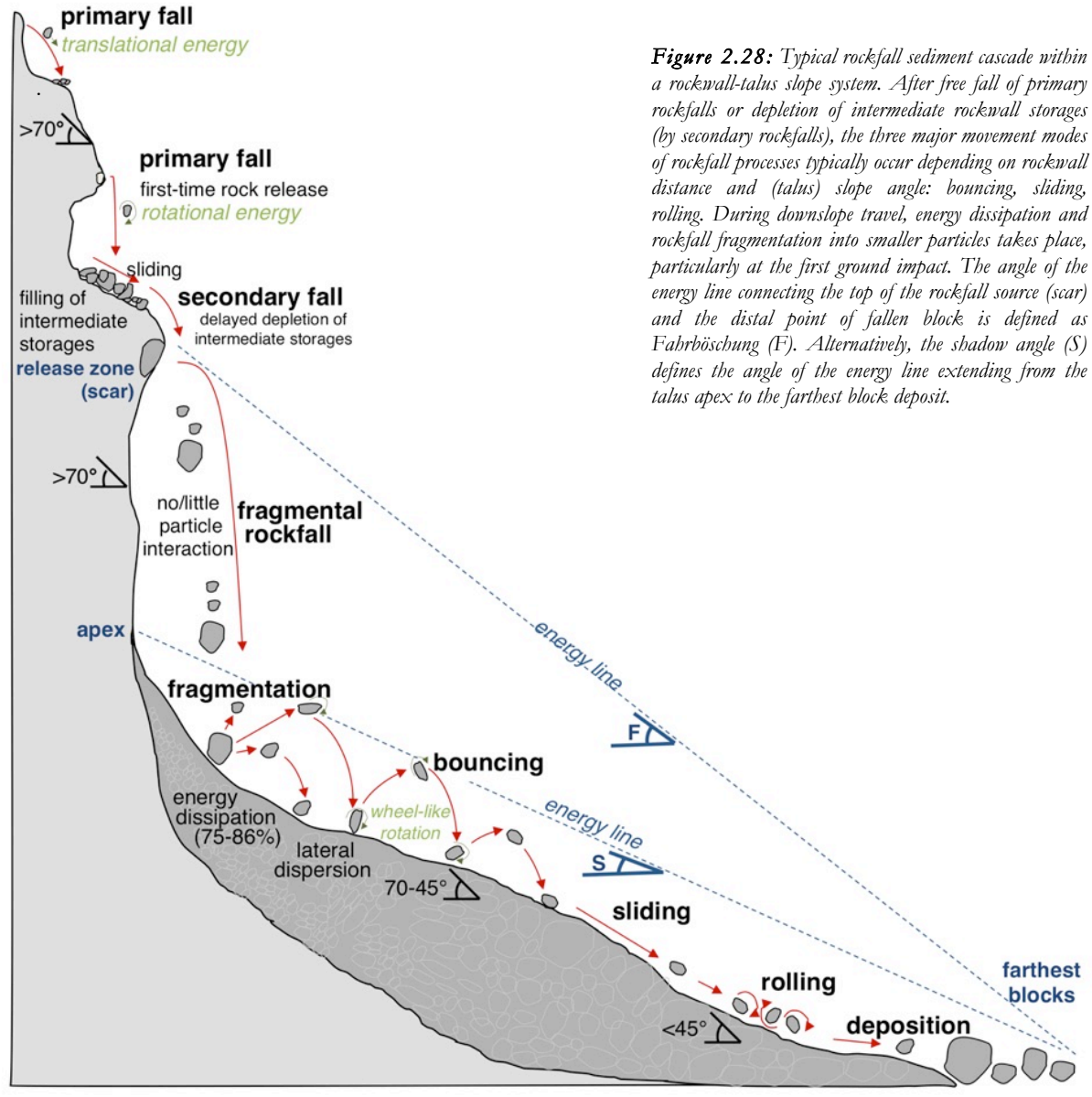

Figure 2.28: *Typical rockfall sediment cascade within a rockwall-talus slope system. After free fall of primary rockfalls or depletion of intermediate rockwall storages (by secondary rockfalls), the three major movement modes of rockfall processes typically occur depending on rockwall distance and (talus) slope angle: bouncing, sliding, rolling. During downslope travel, energy dissipation and rockfall fragmentation into smaller particles takes place, particularly at the first ground impact. The angle of the energy line connecting the top of the rockfall source (scar) and the distal point of fallen block is defined as Fahrböschung (F). Alternatively, the shadow angle (S) defines the angle of the energy line extending from the talus apex to the farthest block deposit.*

With the rock fragments' first impact at the base of the rockwall, maximum momentum is reached (Figure 2.8). According to experiments of Broili (1974), around 75-86% of the kinetic energy gained in the initial fall is lost by the first contact with the surface (Evans and Hungr, 1993). Simultaneously, rockfall blocks commonly disintegrate into several smaller rock pieces on their first ground impact. The mechanism of fragmentation is

complex and is linked to impact induced stress propagation, generation of thermal energy and plastic behaviour in the impacted ground material (Wang and Tonon, 2011; Gili et al., 2016). Latter authors note that rockfall fragmentation is, however, often purely explained based on the relationship between kinetic energy during impact and the threshold fragmentation energy obtained from intact rock strength (Chau et al., 2003a; Giacomini et al., 2009). Although those energetic considerations may be justified, it has been shown that fragmentation is also critically controlled by mechanical material properties of the impacting block (Table 2.4) such as block mass, rock compressive strength and Young modulus (Chau et al., 2003a; Asteriou et al., 2012). On a micro-scale, Wang and Tonon (2011) additionally emphasise the importance of pre-existing joints and micro-fractures in the impacting block. Using discrete element modelling, they found that blocks with closed, but highly persistent pre-existing joints tend to fragment into large pieces after their first impact. Instead, blocks with less than 80% joint persistence can only produce large fragments when joints are open. Furthermore, they provided evidence that the number and shape of fragments generated is mainly a function of the fracture orientation with respect to the angle of impact (Table 2.4). However, the role of rock mechanical properties on fragmentation is still poorly understood and particularly challenges the modelling and hazard prediction of rockfall run-out and impact energy (cf. Ruiz-Carulla et al., 2015).

After the first impact, the fragmented blocks can either arrest or, more typically, start to disperse laterally in different trajectories over the slope (Evans and Hungr, 1993; Crosta and Agliardi, 2004). With decreasing mean slope gradient below 70° (Figure 2.8) rockfall trajectory commonly continues into a bouncing (Ritchie, 1963). With each ground rebound, energy is absorbed by the shock or transformed into rotation energy (Prisco and Vecchiotti, 2006). Block sizes and shapes as well as its nature of ground impact are most critical for velocity and bouncing behaviour (Table 2.4) resulting in irregular downslope trajectories (Ferrari et al., 2016). Highest rotational energy is linked to disk-shaped or ellipsoid blocks (Azzoni et al., 1995). When landing on their long vertical axis, wheel-like bouncing is typical (Leine et al., 2014). It has been frequently observed that mainly the edge with the longest axis maintains contact to the ground. In turn, when landing on their smaller side, discoid blocks may preferentially slide and often stop after short distances (Dorren, 2003; Luckman, 2013). Energetically, most block velocity is lost in this proximal rockfall travel. This is because the energy dissipates proportional to the velocity of impact, as shown in experiments of Pfeiffer and Bowen (1989). Most important factors influencing the energy dissipation are fall (or bounce) height and angle of impact (Li et al., 2016), block shape (Glover et al., 2015), density and weight of falling block (Vilajosana et al., 2008) and mutual block collision during movement (Erismann and Abele, 2001) (Table 2.4). Moreover, energy dissipation is highly controlled by the rock properties and buffering capacity of the underlying material on which impact occurs (Pichler et al., 2005; Schellenberg et al., 2008). Here, most controlling parameters (Table 2.4) are grain size, shape, rock strength and (micro-)fractures, elasticity, as well as the voids between blocks, snow and vegetation cover (Crosta and Agliardi, 2004; Dorren et al., 2006; Frattini et al., 2012).

When mean gradient decreases below < 45° towards the talus toe, rock fragments again gain rotational energy. Typically, bouncing stops and the blocks start to roll (Figure 2.8) along the slope surface (Bozzolo and Pamini, 1986; Dorren, 2003). Volkwein et al. (2011) point out that pure rolling rarely takes place, predominantly linked to soft, elastic rock materials. Instead, alternating periods of bouncing and rolling are more frequent. During this final travel path, total kinetic energy dissipates to a minimum and rockfall

movement finally stops. Depending on the block size and its kinetic energy, rockfall can arrest everywhere along the talus slope due to the stationary slope gradient or due to increasing surface roughness of underlying material (Table 2.4). Particularly, movement is forced to stop earlier due to obstacles such as larger blocks, higher vegetation cover or trees (Dorren, 2003; Volkwein et al., 2011).

Table 2.4: *Controlling factors on kinematics and dynamics of rockfall movement (free fall, bouncing, sliding, rolling), fragmentation, energy dissipation and deposition within respect to different elements of rockfall sediment cascade (rockwall, detached block, talus slope).*

		Controlling factors	Kinematics and dynamics of free fall	bouncing	sliding	rolling	Fragmentation	Energy dissipation	Deposition
Elements of rockfall sediment cassade	Rockwall	*mean slope (>70°)*	+				+	+	
		length or height	+				+	+	
		micro-morphometry	x				x	x	
	Detached block	*mass or volume*	x	x	x	x	x	x	x
		density or porosity	x	x	x	x	x	x	
		elasticity (E modulus)		x			x	x	
		shape (axis ratio)	x	x	x	x			x
		compressive strength		x			x	x	
		(micro)jointing		x			+		
		angle of impact		x	x	x	x	x	x
	Talus slope	*compressive strength of material*		x			+	x	
		(micro)jointing of material		x			+	x	x
		vegetation cover		-	x	x	-	x	+
		snow cover		-	x	x	-	+	-
		moisture, saturation		(-)		x	-	x	x
		voids/interstices		x	x	x	x	+	x
		block sizes			x	x			x
		mean slope (70-45°)		+	+		+	+	-
		mean slope (<45°)		(-)	(+)	+		(+)	+

As shown in Figure 2.8, the maximum distance that rockfalls can travel and will be accumulated can be commonly approximated by two empirical approaches: The Fahrböschung (F) refers to the angle of the energy line connecting the top of the rockfall source (scar) and the distal point of fallen block (Heim, 1932; Toppe, 1987). Occasionally, the Fahrböschung is also known as travel angle (Cruden and Varnes, 1996) or reach angle (Corominas, 1996). Alternatively, if no data on the release zone are available, the shadow angle (S) enables an estimation of the maximum zone of rockfall activity (Scheidegger, 1973; Evans and Hungr, 1993). In Figure 2.8, it is the dip angle of the energy line extending from the apex of the talus slope to the farthest block deposited in the past. So far, a wide range of different minimum shadow angles have been reported from individual talus slopes, ranging from, in minimum, 17° (Domaas, 1994) and 21° (Holm and Jakob, 2009) to maximum values of 36.9° (Copons et al., 2009). Due to its simple parameter assumptions and easy implementation in geographic information systems (GIS), the shadow angle approach has also been widely used for regional-scale prediction of rockfall trajectories and associated hazard zones (Jaboyedoff and Labiouse, 2011). However, considering the wide spectrum of angles found by different studies, the concept's limitation is obvious. Apparently, rockfall run-out depends rather more on complex rockwall-scale and valley-scale rock mechanical and topographic characteristics (see Fig. 22.2 in Frattini et al., 2012).

2.5.4 Talus slope deposition: Morphology and material characteristics

Simplicity is not a feature of talus accumulations. The diversity of talus-forming processes, diversity of [source] material and diversity in talus age […] make any model based on single mechanism inadequate. Selby (1993, p. 351, 355)

The long-term rockfall release and the site-specific sediment deposition along the rockwall foot is linked to the gradual accumulation of sediment storage landforms, so called talus slopes (American term) or scree slopes (English term). In this work, the American term is favoured. In geomorphic research, the study of talus slopes has a long tradition with pioneering work by Piwowar (1902) in the Swiss Alps and (Harker, 1904, 1905) in Skye (Scotland). Although talus slopes can be observed all over the world where rockwalls become unstable and erode, they are certainly most prominent for recently or previously glaciated mountainous environments.

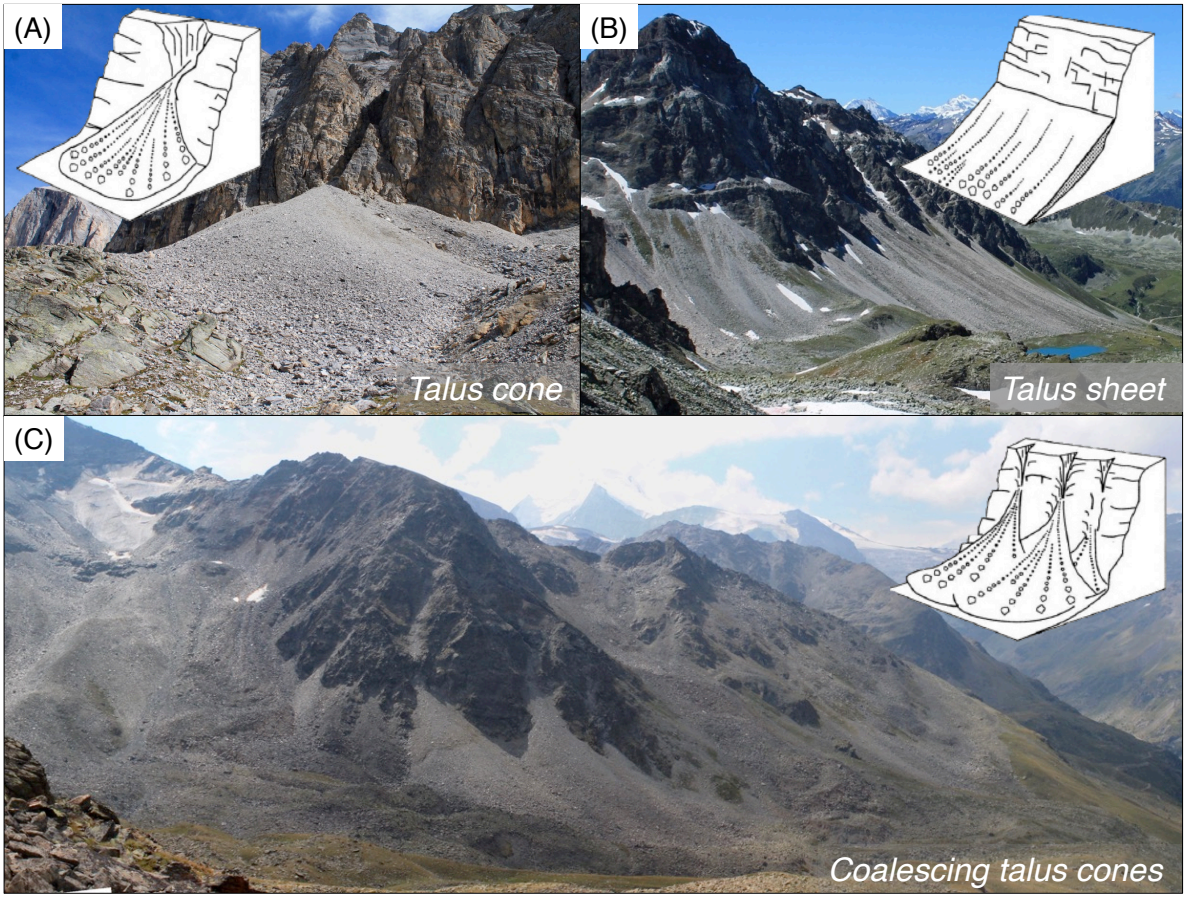

Figure 2.29: *Major types of rockfall talus slopes with examples from the Turtmann Valley: (A) Talus cones along intersected rockwalls (Pipitälli, August 2014); (B) Talus sheets along relatively featureless rock faces (Meidtälli, August 2013); (C) Coalescing talus cones develop (Hungerlitälli, August 2015). Schematic illustrations of talus slopes taken from Ballantyne and Harris (1994, p. 220).*

In plan view (Figure 2.29) three types of rockfall talus slopes can be ideally distinguished being a simple reflection of the (micro-)topography of the source rockwall and the underlying slope profile on which the sediments accumulate (see overview in e.g. Selby, 1993; Ballantyne and Harris, 1994; Luckman, 2013). On rockwalls with a complex or dissected topography, for example, talus cones dominate. As shown in Figure 2.29A, gullies and chutes within rockwalls force rockfalls to become channelled and concentrated to fan-like deposition. By contrast, relatively featureless rock faces of uniform or homogenous geology and with spatially

uniform sediment supply tend to produce straight talus sheets (Figure 2.29B). When single talus cones intersect laterally, coalescing talus cones develop (Figure 2.29C). However, all three types are most often transitional and therefore, no specific form distinction will be made in this work and the collective term 'talus slope' is used.

In long profile, rockfall-dominated and unmodified talus slopes, as shown in Figure 2.30A, are typically described by bi-segmented profiles with an upper rectilinear unit of an overall gradient of 33-35° (Chandler, 1973) and a concave basal zone of around 30° to 5° (Francou and Manté, 1990; Wilson, 2009). Occasionally, a small convexity immediately below the apex can be observed as e.g. by Church et al. (1979) on Baffin Island talus slopes. It has been assumed that the upper straight segment reflect the angle of repose, thus the gradient at which loose, unconsolidated debris comes to rest after periodical redistribution by i.e. dry avalanching or grain flows (Bakker and Le Heux, 1947; Rapp, 1960b; Statham, 1973; Van Steijn et al., 2002). This traditional hypothesis was particularly supported by laboratory tilting-box tests of Carson (1977) and by field studies of Church et al. (1979). Yet, Statham (1976, 1977) and others questioned this concept, given that the angle of repose is often 5-15° higher than most talus gradients.

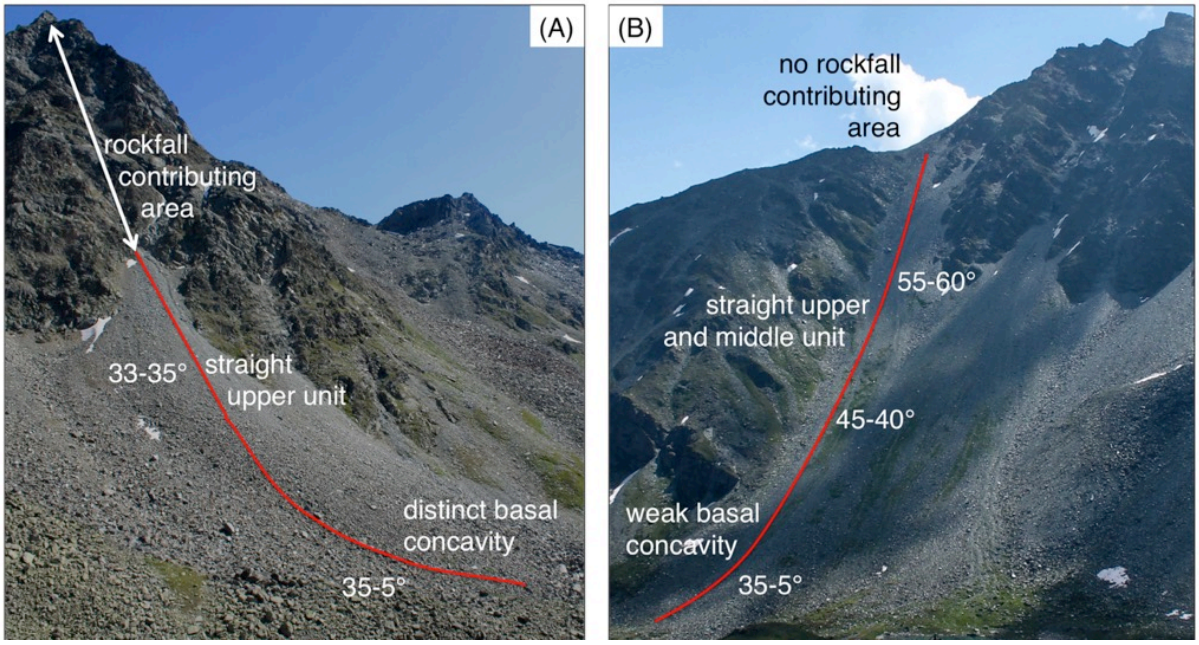

Figure 2.30: *Typical long profile morphometry of talus slopes in their early (A) and late (B) evolutional stage. (A) Rockfall-dominated and unmodified talus slopes are typically characterised by a bi-segmented profile with an upper rectilinear unit (33-35°) and a basal concavity (35-5°). (B) With increasing talus maturity, talus debris progressively covers most of the contributing rockwall area and talus gradient steepens close to the angle of repose (45-40°) resulting in redistribution of talus material.*

Obviously, the frictional strength of the unconsolidated debris is still too high to favour redistribution of dry avalanching. As an alternative, Statham proposed the 'discrete rockfall model' where impact energy of falling fragments and their associated travel distances are the major controls. Following this idea, laboratory and numerical analyses of Kirkby and Statham (1975) as well as field studies of Francou and Manté (1990) indicated that the basal concavity develops only in the early talus evolution; i.e., when the rock face is still high enough to favour high impact energy of rockfalls. Afterwards, with increasing talus maturity, when talus debris progressively covers most of the contributing rockwall area, as shown in Figure 2.30B, rockfall impact energy

decreases and the talus gradient steepens. Therefore, it may be only in the late evolutional stage that talus gradient is close to the angle of repose and that dry avalanching is plausible to become a redistributive process.

The long-term rockfall deposition is associated with site-specific surface and subsurface material characteristics. Most researchers report a tendency of downslope increasing block sizes with the finest particles below the rockwall apex and the largest boulders covering the talus toe (Caine, 1969; Kirkby and Statham, 1975; Albjär et al., 1979; Pérez, 1989, 1993, 1998; Jomelli and Francou, 2000). This so-called fall sorting can be attributed either to the downslope increasing frictional resistance of the talus surface and the great kinetic energy of large boulders. Once fall sorting has been established, the coarse openwork surface texture acts like a sieve (Carniel and Scheidegger, 1974). The laboratory experiments of De Blasio and Sæter (2009) highlight very well how this sieve effect makes talus sedimentation a self-organised process. While large blocks can move over smaller ones and will preferably stop in zones, where they reach blocks of similar size to their own, smaller particles are trapped or washed into voids. As consequence, most talus slopes typically contain large quantities of interstitial fine material at depth. Furthermore, the exhaustive surveys of Pérez (1985, 1989, 1993, 1998) in Northern California reveal that fall sorting is typically associated with a characteristic longitudinal arrangement of block shapes and preferred downslope orientation of clasts. While platy and elongated blocks rapidly lose momentum during travel and, thus, primarily cover the upper talus segment, block shapes tends to become more spherical or equidimensional towards the talus toe due to their higher kinetic energy.

However, the above described systematic across-slope variations of surface material are not universal. They are mostly diagnostic for unmodified talus slopes where rockfalls are still the dominant sediment supply and depositional mechanism, as e.g. shown in Figure 2.30A. By contrast, on rock slopes where rockfall activity has diminished and/or the effective rockfall contributing area is covered by talus debris (Figure 2.30B), reworking and additional sediment input by secondary processes commonly start to alter the downslope depositional pattern (Sass and Krautblatter, 2007). For example, Åkerman (1984) and Hétu (1995) reported reversed particle sorting due to the influence of running water and supranival aeolian transport (see also review of Van Steijn et al., 1995). Similarly, Caine (1967) and Gardner (1972) detected absent material sorting along talus slopes in the Southern Alps of New Zealand and Canadian Rocky Mountains. Both identified the dominance of fine-grained sediment input by episodic snow avalanches and debris flows as major reason.

2.5.5 Talus slopes as proxy for short-term and paraglacial rock slope instability

Talus slopes that have been accumulated in closed basins and that are disconnected from the major sediment cascade, e.g. by moraine ridges or bedrock outcrops, represent valuable proxies for a retrogressive assessment of their source rockwall. Numerous field-based, numerical and theoretical models have been performed to determine the spatiotemporal activity rock slope instability and their controlling factors at different temporal and spatial scales:

Local information on diurnal and seasonal variations of rockfall supply, often with respect to their event magnitude, have been derived from continuous records of rockfall debris accumulated onto talus slopes. Conventional and relatively cheap techniques include the use of plastic sheets (Krautblatter and Moser, 2009), seasonal snow cover (Matsuoka and Sakai, 1999), nets or natural traps (Gardner, 1972; Sass, 1998; Vehling et

al., 2015). Those measurements can provide continuous time series of 10-15 years. Although such studies rarely consider site-specific effects of talus slope deposition, they indicate distinct rockfall peaks during spring and autumn, i.e. of smaller event magnitude (< debris falls). It is assumed that recent, short-term rockfall supply is highest during/after intense freeze-thawing of bedrock and/or heavy precipitation events released by secondary events (Krautblatter and Moser, 2009). However, active talus slopes in frost-free and relatively dry environments suggest that other mechanisms may also be important for rockwall erosion and rockfall supply. Unfortunately, periglacial talus and rockfall studies are still driven by a frost-dominated paradigm and talus forming processes such as thermal fatigue or biogenic processes are rarely considered yet (André, 1997; Hall et al., 2002).

On a decadal-scale (Late-Holocene), dendrochronological studies and systematic lichonometry on individual rockfall blocks have been performed across talus slopes to determine the relationship between rockfall magnitude and return frequency (McCarroll et al., 1998; Corominas and Moya, 2010) as well as the spatial occurrence of rockfall hazard in mountain valleys (Stoffel, 2006; Sass, 2010). Evans and Hungr (1993) derived frequency-magnitude curves from detailed block size data of talus slope profiles. In their detailed examination of 16 talus slopes in British Columbia, they revealed that rockfall shadow angle is particularly dominated by larger events with return periods of 1000 years.

On longer time scales, stratigraphic investigations of talus subsurface material e.g. exposed at gullies incised within talus crests or artificial trenches can provide valuable insights in rockfall intensity and associated driving factors during Holocene. It has been shown that most talus slopes are composed of alternating layers of openwork clasts with finer graded deposits. C14 dating of intercalated paleosoils or peats suggest that subsurface material variations may result from alternating periods of rockfall activity and reworking processes due to Holocene climate fluctuations (Hinchliffe, 1999; Hétu and Gray, 2000; Curry and Black, 2003; Curry and Morris, 2004) or forest fires (García-Ruiz et al., 2001). However, accessible exposures of alpine talus slope subsurface are sparse, and artificial excavations and drillings are often expensive or difficult to perform due to the steep and loose sediments. Recently, the increasing application of high-resolution geophysical ground surveys in mountain geomorphologic research provided new insights into subsurface material (as well as permafrost) characteristics of stratified talus slope bodies and allow to identify their associated forming drivers (Schrott and Hoffmann, 2003; Otto and Sass, 2006; Sass, 2007; Sass and Krautblatter, 2007; Schrott and Sass, 2008; Scapozza et al., 2011). By using ground penetrating radar in different talus slopes in the Eastern European Alps, for example, Sass and Krautblatter (2007), identified discordant layers at depth. Their geophysical data support the previous notion that enhanced freeze-thaw activity, like during the Little Ice Age, promoted the supply of coarse rockfall-originating debris. On contrary, fine-grained deposits have been interpreted to result from sediment redistribution (by debris flows or dry grain flows) or the depletion of intermediate rockwall sediment fills after intensified rainstorms periods during warmer climates. Nevertheless, both direct and indirect subsurface surveys on talus material suffer from the problems of degradation (erosion) of sediment records and again, the form convergence of different geomorphic processes.

At millennial timescales, in formerly and still glaciated valleys particular emphasis has been placed on talus slopes that are completely vegetated and seem to be relict features (Kershaw and Gardner, 1986; Ballantyne and

Benn, 1994; Hinchliffe, 1999; Hinchliffe and Ballantyne, 1999; Hétu and Gray, 2000; Wilson, 2009). Numerous attempts have been made to calculate talus slope volumes (or thicknesses) and regolith-bedrock boundary to infer postglacial rates of rockwall erosion and rockfall supply; either by using geophysical field surveys, theoretical and geometrical-numerical modelling approaches (Sass and Wollny, 2001; André, 2002; Hoffmann and Schrott, 2002; Krautblatter and Dikau, 2007; Moore et al., 2009; Otto et al., 2009). Although varying with geomorphic-lithological setting and technique, the average postglacial rates determined both from Alpine and Antarctic talus slopes cover similar values ranging from 0.1-0.3 mm/a in the German Karwendelgebirge and Zugspitz area (Sass and Wollny, 2001), 0.1-0.16 mm/a on Svalbard (André, 2002), 0.28 mm/a in Yosemite National Park (Moore et al., 2009), 0.24-0.25 mm/a on Isle of Skye, Scotland (Hinchliffe and Ballantyne, 1999), 0.5 mm/a in the Reintal (Hoffmann and Schrott, 2002) to 0.7 mm/a in the Turtmann Valley (Otto and Sass, 2006). Although these postglacial rockwall erosion rates appear fairly low, they are still one order of magnitude higher than most of the recent rates (Curry and Morris, 2004).

This data discrepancy has prompted geomorphologists to suggest that much of the talus accumulation is of paraglacial origin, thus conditioned by previous glaciation of rockwall source area. It is assumed that rockfall supply onto talus slopes was significantly higher immediately after deglaciation of their source rockwall, when stress release of bedrock and its exposure to atmospheric influences resulted in a high susceptibility to failure (Hinchliffe and Ballantyne, 1999; McColl, 2012). After this first intensity in talus slope deposition, rockfall supply is assumed to progressively diminish due to equilibration of the rockwall to non-glacial strength conditions. To describe the paraglacial evolution of talus slopes, Hinchliffe and Ballantyne (1999) proposed a three-stage model, as illustrated in Figure 2.31, with (A) initial rockfall-dominated accumulation, (B) near-cessation of rockfalls, with initial reworking of upper slope sediment by debris flows and slopewash and (C) vegetation coverage and incision of deep, often still active gullies into the talus crest with associated transfer of upper sediments to the foot. Dating of paleosoils in relict talus material in South Wales suggest that around 50% of talus deposition may have occurred within 1000 years (Curry and Morris, 2004) and that the period of rockfall-dominated input was likely terminated within ca. 5-6 kyrs after deglaciation (Hinchliffe and Ballantyne, 1999).

However, the manner in which rockfall intensity and talus slope supply changes between onset of deglacations and adjustment to non-glacial conditions is still little understood, i.e. on a valley scale (Figure 2.31D). Five models - although mainly in the context of large-scale rock failures - are currently discussed and illustrated in Figure 2.31E. Cruden and Hu (1993) proposed two possibilities tested on glacially steepened slopes in the Rocky Mountains: In (i) a 'constant frequency (steady state) model the frequency of rock instabilities is constant with time and not influenced by glacial retreat, but by geological and geotechnical properties of the rock slope. Contrary to this, the exhaustion model (ii) postulates a rapid and intensified period of rock failures (50%) immediately (ca. 5.7 ka) after deglaciation followed by an exponential decrease in failure activity with time. The underlying assumption of latter model is a simple kinematic exhaustion due to the progressive reduction of potential failure sites following deglaciation (Cruden and Hu, 1993). An alternative model may be a (ii) 'rapid response' in which nearly all rockfalls occur within a few centuries after glacier retreat, given data from sites recently undergoing deglaciation (Evans and Clague, 1994; Allen et al., 2011). For completeness, Ballantyne and Stone (2013) further propose a (iv) 'steady state decline model', in which the

paraglacial rockfall activity declines approximately linearly within a given area. Finally, cosmogenic data and lake sediments let suggest a bimodal or even (v) multimodal pattern, with two major peaks of rockfall activity; the first immediately (ca. 1-2 kyrs) after onset of deglaciation and the second at approx. 4-2 kyr BP (Strasser et al., 2013; Ballantyne et al., 2014).

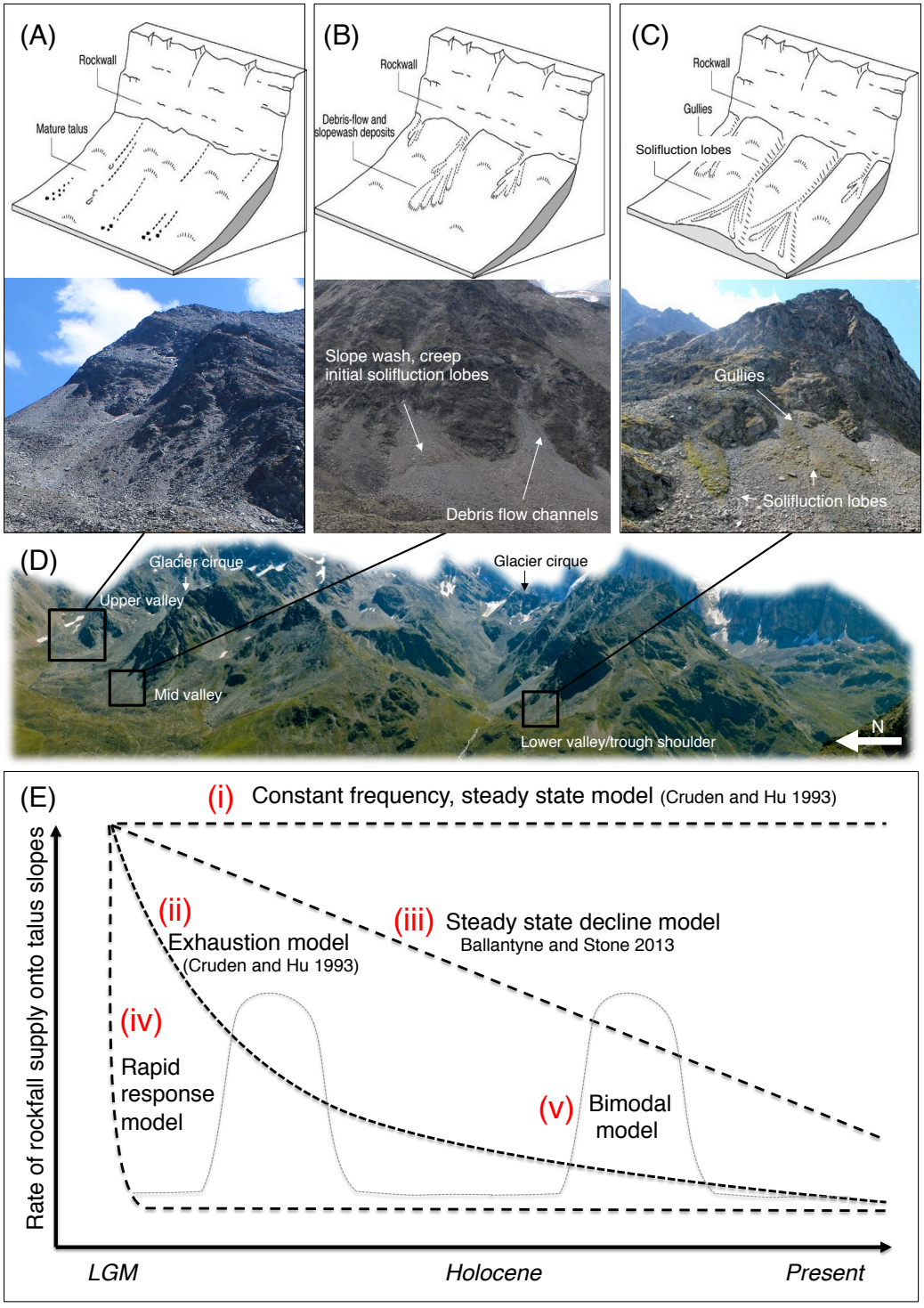

Figure 2.31: *Paraglacial evolution of talus slopes according to the three-stage model of Hinchliffe and Ballantyne (1999). (A) Initial rockfall-dominated accumulation, (B) near-cessation of rockfall, with initial reworking of upper slope sediment by debris flows and slopewash and (C) vegetation coverage and incision of deep, often still active gullies into the talus crest with associated transfer of upper sediments to the foot. Schematic illustrations of talus slopes taken from Hinchliffe and Ballantyne (1999). (D) Spatial distribution of talus slopes at the regional scale. (E) Five potential models of paraglacial rock slope adjustment and paraglacial rockfall activity (for a description see text).*

To sum up, the previous chapter highlights that talus slopes represent valuable recent and postglacial proxies on rock slope instability and their controlling factors. Nevertheless, caution is necessary when it comes to extrapolate findings and to make general conclusions. All empirical and theoretical models are challenged by the fact that talus slope can vary considerably in form, morphology and (sub-)surface material characteristics amongst different study sites and even within one single mountain valley. As nicely stated by Selby (1993 p. 351) 'Simplicity [..] is not a feature of talus accumulations'. Hence, rather than searching for a simple universal model of talus evolution, it is more appropriate to start interpreting talus landforms as a site-specific and complex proxy of different variables. Particularly with respect to the paraglacial interpretation on rock slope instabilities, McColl (2012) emphasises a careful interpretation and not to use the paraglacial concept as 'panacea' for the total postglacial rockwall erosion and talus supply. Only if the interplay of factors such as e.g. periglacial (Holocene) fluctuations, landform maturity, rockwall-talus coupling, micro-scale rockwall properties and the non-linear-complex system behaviour are considered – either theoretically, by exclusion or empirically – talus slopes can be used as valuable indirect archives for their source rockwall. Then, retrogressive conclusions are possible on rockwall erosion rates, spatiotemporal rockfall occurrence, frequency-magnitude relationships and associated hazard, significance of rockfalls in mountain sediment cascades and above all, the key bedrock destabilising factors.

----- BLANK -----

Chapter 3
CONCEPTUAL AND METHODOLOGICAL RESEARCH APPROACH OF THIS THESIS

3.1 Knowledge gaps and hypotheses

Please, at least ten hypotheses for the origin of this sinkhole! Think and discuss!
(Richard Dikau to his students at one of his field excursions)

With regard to the outlined state of the art, specific systemic and methodological shortcomings in the research of rock slope instability in geomorphic systems become clear. At least, four major knowledge gaps can be identified linked to eight overal research hypotheses:

(i) Controls of rock slope instability and rockfall initiation

Although the increasing number of field, modelling and laboratory studies is constantly improving our mechanistic understanding of rock slope instabilities and rockfall initiation, the relative importance of controlling factors within their complex interplay is insufficiently understood. This knowledge gap is best reflected by the on-going debate as to whether the instability of mountain rock slopes is more driven by topoclimatic, cryospheric, paraglacial and/or mechanical controls. While some researchers explain rock failures primary by large-scale topoclimatic parameters such as solar radiation, slope aspect and associated frost weathering and permafrost dynamics and, to a lesser extent, surficial thermal fatigue, other studies identified structural controls of the rock mass and its joints as most critical. And further researchers emphasise the key role of historicity and particularly the paraglacial bedrock adjustment to the former glaciation and the subsequent ice retreat. However, since those outcomes typically result from studies where only *one* individual factor at only *one* scale has been investigated, a satisfactory answer to the debate about the key control(s) is still missing; or might be virtually impossible? In fact, when referring to Harrison (2001) and Phillips (2003b), it is reasonable to assume that due the complexity and non-linearity of mountain systems, at each scale, new and often unknown system properties and causalities emerge and interact (Figure 3.1). Consequently, to bring further light into the debate about the *key* controls and their *relative* role for rock slope instability, future research needs to address both the interplay of multiple factors and much more, the question of their scale-dependency. With respect to Figure 3.1, two hypotheses arise:

Hypothesis 1: Due to the emergent and often non-linear complex nature of mountain systems the key rock-mass scale system properties or processes responsible for rock slope instability contrast to those being dominant at the higher scales such as of individual rockwalls and mountain valleys. Thus, the relative importance of rockfall controlling factors is likely to be scale-dependent.

Hypothesis 2: Rock slope instability results from scale-linkages between controlling factors.

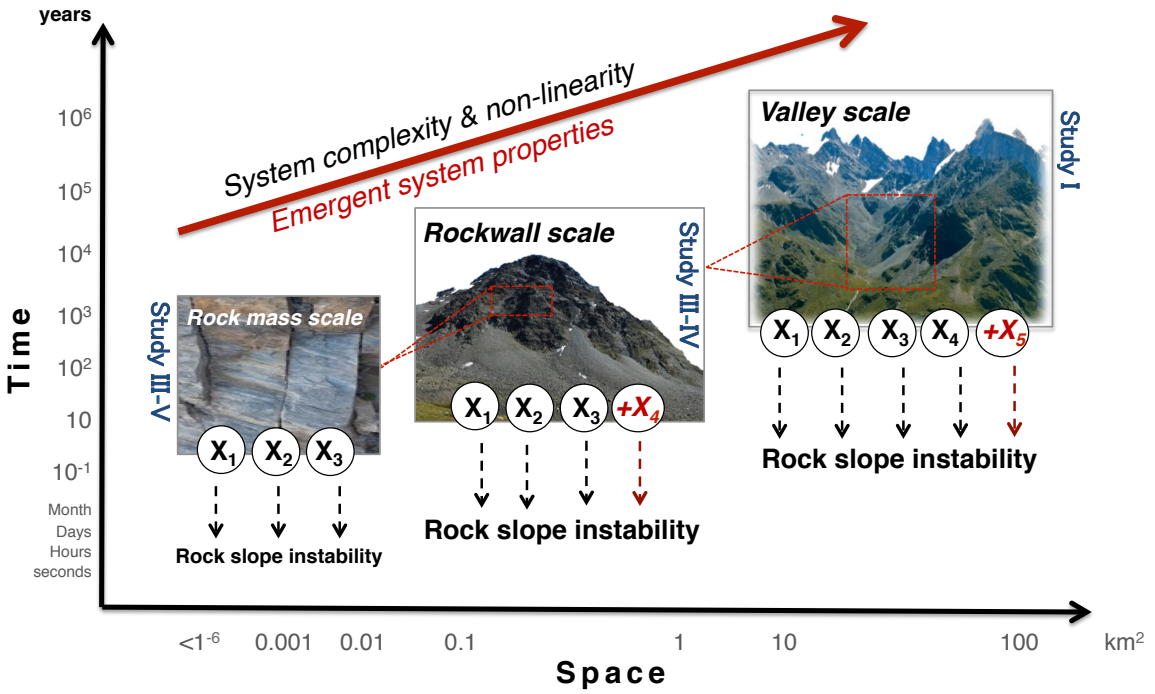

Figure 3.1: *Conceptual framework of this thesis assuming a scale-dependency of key controls of rock slope instability due to the non-linear complexity of emergent geomorphic systems according to Philipps (2003) and Harrison (2001).*

(ii) Paraglacial activity and magnitude-frequency pattern of small-size rockfalls

The literature review shows that geomorphic and geological investigations of mountain rock slopes mainly focus on rare and catastrophic landslide or rockfall events with deep-seated failure zones and large volumes of > 10^4 m^3. In comparison, there is still scant scientific attention on small-size failures such as debris falls of < 10 m^3 and boulder falls of 10-10^2 m^3. Consequently, our understanding of rockfall activity at the lower magnitude spectrum is still incomplete. This shortcoming is surprising, given their frequent occurrence of small-size failures in most alpine regions, thus their evident geomorphic relevance for landscape evolution, and their hazardous risk as became obvious most recently in summer 2003. This knowledge gap refers to both the annual to decadal magnitude-frequency pattern as well as the rockfall activity after LGM. Particularly with respect to the past and present-day deglaciation of mountain valleys, it is little explored whether the timing and intensity of paraglacial rockfalls follows either an exhaustion, linearly decreasing, constant steady state or even an yet unknown path (Figure 3.2). However, transferring previous findings from large-scale gravitational mass movements to small-size rock instabilities might be highly problematic due to different mechanisms involved either in the activation of deep-seated or near-surface detachment zones. Moreover, the paraglacial framework has been rarely applied from a rock mechanical perspective, nor at different scales, so that paraglacial rock slope instability is little understood. Therefore, future research is needed hat specifically address small-size rock slope instabilities and test the paraglacial concept of Church and Ryder (1972) from a rock mechcnical perspective at different scales. Based on Figure 3.2, two contrasting hypotheses should be tested:

Hypothesis 3: *Paraglacial rock slope adjustment and thus the timing and intensity of rockfalls after glacier retreat follows an exhaustion model, with a peak immediately after LGM and an exponential decrease with increasing time after deglaciation.*

Hypothesis 4: *The timing and intensity of paraglacial rockfall activity in alpine valleys is governed by mechanical characteristics of the source rockwall.*

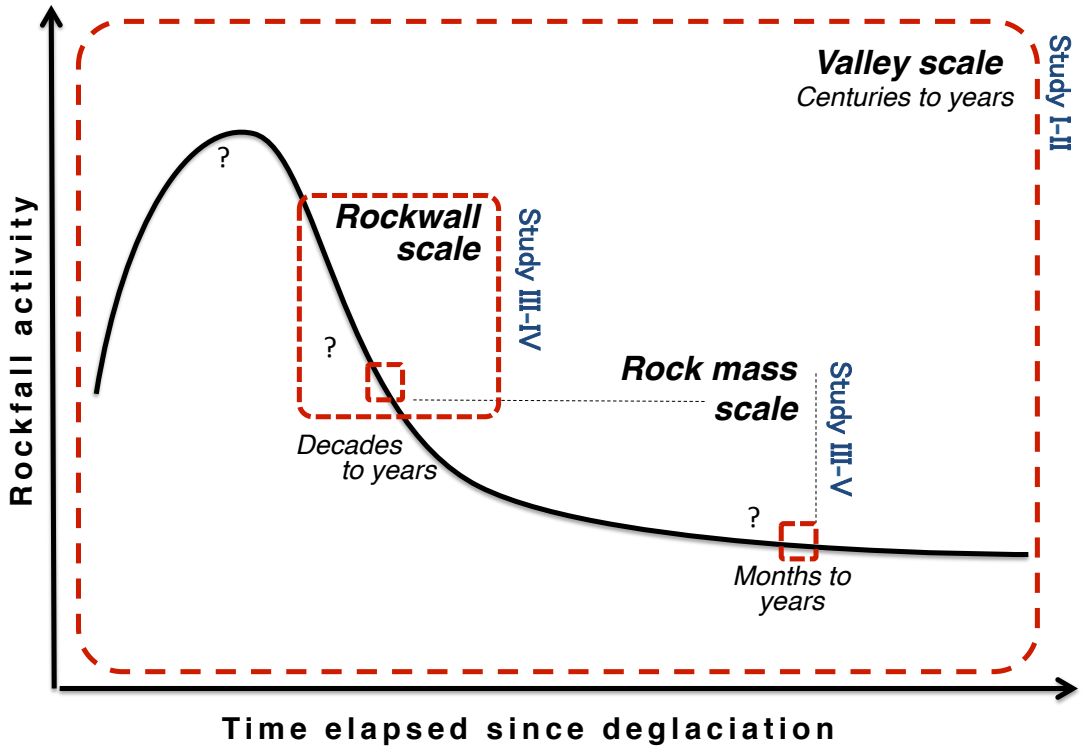

Figure 3.2: *Conceptual framework of this thesis assuming a scale-dependent activity of small-size rockfalls from unstable rockwalls on different temporal scales after glacier retreat.*

(iii) Geomorphic importance of unstable rock slopes for alpine sediment cascades

In its tradition, (mountain) geomorphology represents a strongly 'sediment-dominated' research discipline that developed over time alongside engineering geology. Particularly since early work of Jäckli (1957) and Rapp (1960a,b), geomorphologists put much emphasise on sediment budget studies in mountain valleys as there was the leading agenda to characterise and quantify the sources, sinks and pathways of clastic sediments in space and time. This was also the time that the paraglacial concept became a common framework for investigating the reworking of postglacial sediments. However, within this geomorphic enthusiasm of budgeting postglacial sediments, the unstable source rockwall is often oversimplified and if not even neglected. The geometric, material and process characteristics of the unstable and weathered rock mass are not implemented in a meaningful way in sediment cascade studies, neither theoretically nor empirically. Particularly the paraglacial concept has rarely been applied from a rock mechanical perspective, despite the fact that it is the key source of

paraglacial sediment storages. Thus, the question arises whether we can really tackle the increasing number of associated applied environmental problems in mountain valleys, solely by budgeting sediments? Or do we need much more to address also the role of rock slope instability and weathering in mountain sediment cascades? As shown in Figure 3.3, it is hypothesised:

Hypothesis 5: In mountain valleys undergoing glacier retreat, small-size rock failures are significant drivers for sediment production and downslope sediment transfer.

Hypothesis 6: Rock slope instability is of major significance for alpine sediment cascades. The role of unstable rock mass is evident at all scales of geomorphic cascading systems, including the rockwall-talus system and alpine catchments.

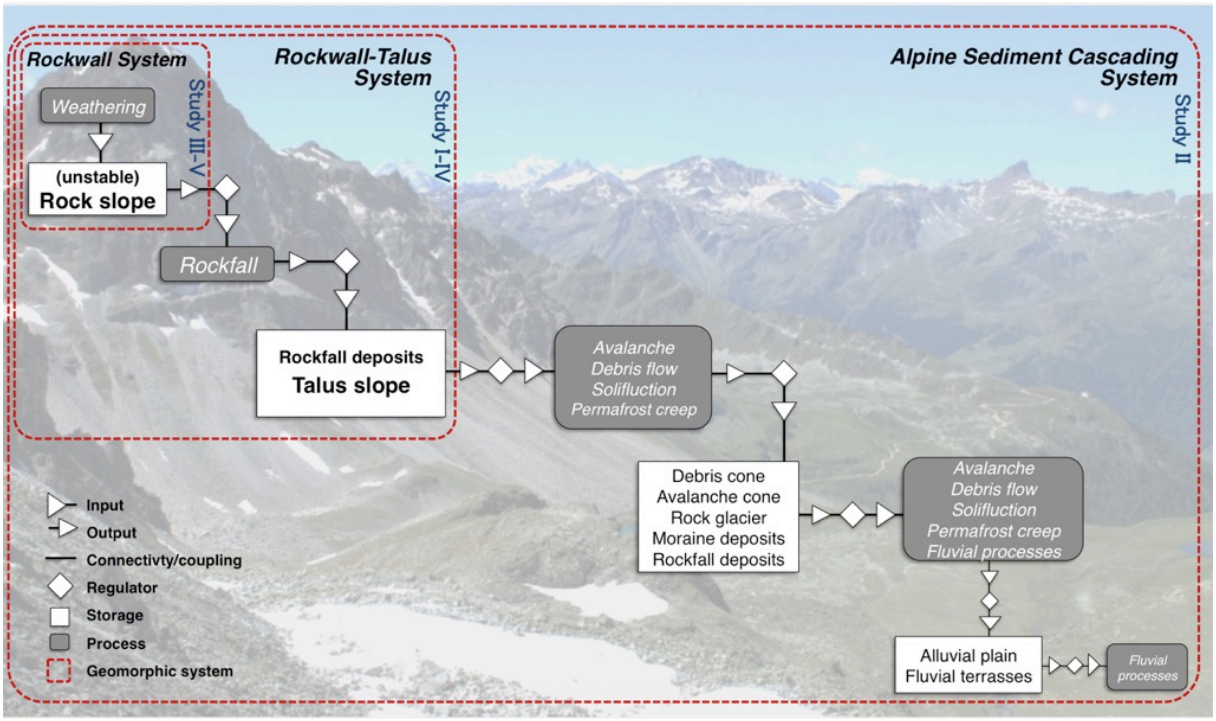

Figure 3.3: *Conceptual framework of this thesis addressing the role of rock slope instability and weathering at different scales within alpine sediment cascades following the illustration and concept of Schrott et al. 2002.*

(iv) Methodological multi-scale approach

During the last few years, an upcoming interest in novel GIS-based statistical and numerical algorithms is noticeable in geomorphology, specifically on a valley and mountain scale. On those higher scales, methodical shortcomings still exist in the research on small-size rockfalls, but GIS approaches such as sediment connectivity models and machine learning could be promising tools. Nevertheless, such technological developments can become problematic from a systemic perspective. Far too often pixel-based and statistical model outcomes are downscaled without field-based knowledge to explain the complex nature of individual rockwalls. This problem of reductionism has long been noticeable in laboratory weathering studies, where

findings from small rock samples derived from experimental conditions are commonly up-scaled without meaningful scale-linkage to rock slope instabilities under natural conditions. Within this trend of increasing 'data accumulation' in geomorphic sience, there is much more the need to ask for the little addressed epistemological consequences of emergent and complex geomorphic system behaviour for investigating mountain rock slopes. Two methodological hypotheses with major systemic implications for our process understanding should be tested:

Hypothesis 7: *The scale-dependency and non-linear complexity of geomorphic systems (H1) additionally makes investigating rock slope instabilities a methodological question of scale that requires* different types of scientific explanation at each scale. Hierarchical scale approaches and ergodic reasoning provide valuable systems approaches to investigate rock slope instability.

Hypothesis 8: *Discontinuities (or joints) of rock slopes are a key systemic and methodological link between different hierarchical levels of rock slope systems.*

3.2 Methodological multi-scale approach

sseWhen it comes to testing the previously stated hypotheses and to investigating the objectives of this thesis, the question of scale becomes a major methodological challenge. In this dissertation, a new hierarchical methodology is proposed that address – individually and in synthesis – three levels of rock slope instability and alpine sediment cascades (Figure 3.4):

At the **valley scale**, a novel combination of a decision-tree based random forest algorithm and a principal component logistic regression model is applied to identify major region-scale controls on rock slope instability and talus slope deposition in glaciated alpine valleys (*Study I*). Furthermore, a morphometry-based GIS connectivity algorithm is combined with a heuristic geomorphic field map of sediment storage toposequences to assess pathways and controls of sediment cascades from unstable through sediment cascading systems (*Study II*).

At the **rockwall scale**, a new holistic approach is presented to explore the influence of topoclimatic, mechanical, thermal and paraglacial rock destabilizing factors on rockfall activity in rockwall-talus systems. Source rockwalls (*Studies III-IV*) are assessed through detailed rock mass strength classification, geotechnical joint surveys, joint volumetric count and kinematic failure analyses. Deductive rockwall studies are integrated with abductive sedimentological surveys at the surface of their respective talus slope landforms. To transfer those findings to the higher valley scale, a total number of twelve rockwall-talus systems is investigated at different locations and at different topological hillslope toposequences in three hanging valleys of the Turtmann Valley.

At the **intact rock scale**, near surface rock temperatures are monitored in the field for two years and to model the seasonal frost cracking intensity within rockwall-talus systems (*Studies III-IV*). In a large-scale monitoring network of twelve logger sites across three hanging valleys of the Turtmann Valley, temperature data from the intact rock mass are linked to geotechnical and geomorphological rockwall surveys, which allows conclusion on the rockwall thermal regime. Furthermore, a novel two-phase laboratory weathering experiment (*Study V*) is designed to simulate individual and synergistic rock weathering by repeated thermal cycling and frequent diurnal ice crystallization. Low-porosity mica schist samples from the Swiss Alps are exposed in a climate cabinet to 120 8h-thermal cycles and 80 half-daily frost events. Rock decay is assessed through monitoring of open porosity, p-wave velocity, surface hardness and thin sections analyses.

Figure 3.4 provides an overview about the various methodological approaches applied at each scale of rock slope instability and different systems of alpine sediment cascades with respect to the four key objectives of this thesis. All methods are explained in more detail in each method section of subsequent chapters 4 to 8.

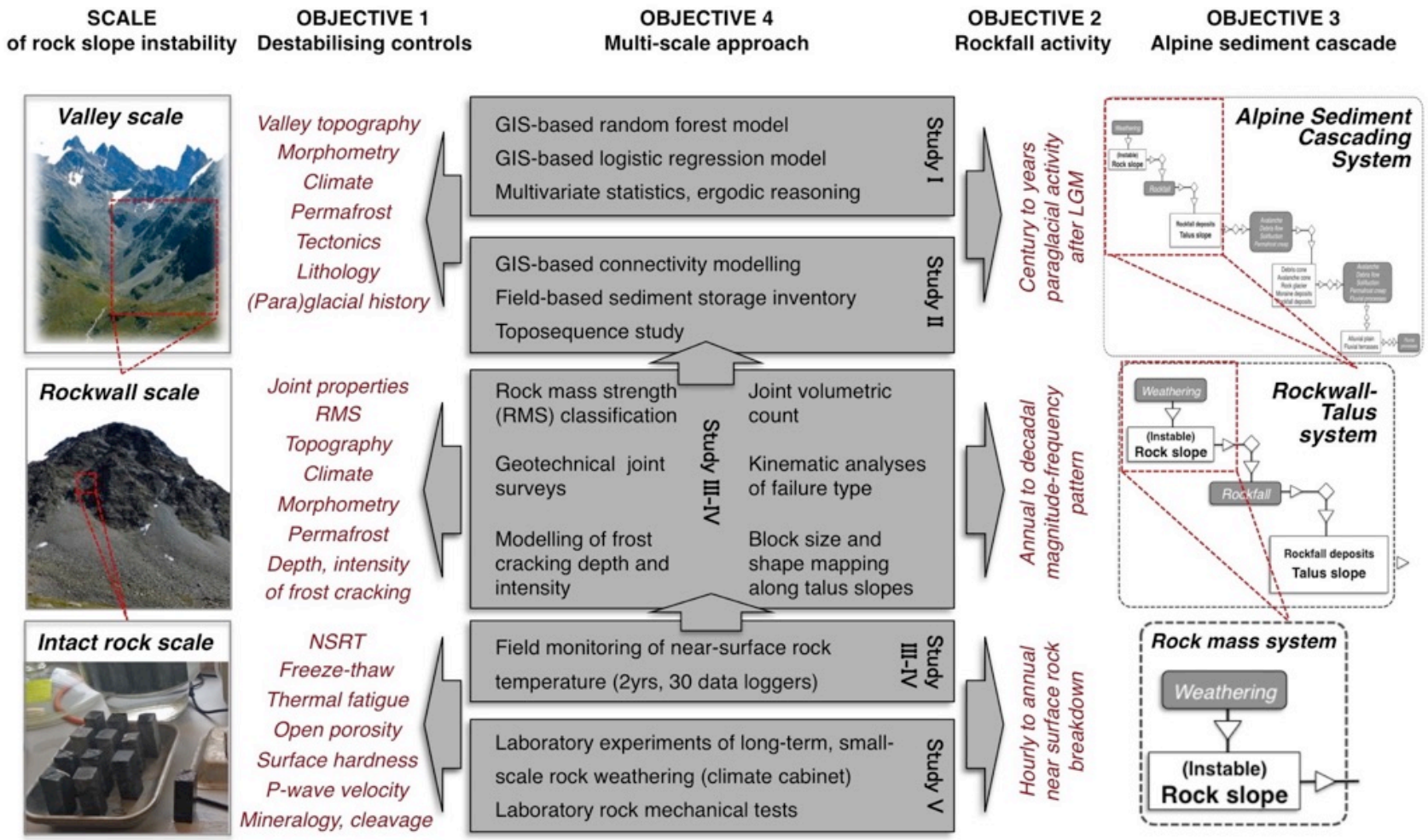

Figure 3.4: *Multi-scale methodological approach of this thesis, combining laboratory, field and modelling studies at the rock mass, rockwall and valley scale. At each level, the key systemic and methodical objectives (1-4) and hypotheses are addressed. The multi-scale approach allows to account for the scale-dependency and emergence of rock slope systems .*

3.3 Overview of study sites

In order to account for different degree of geomorphic system complexity as well as to consider different system components of the alpine sediment cascade, research is conducted in different study sites in the Swiss Alps, as shown in Figure 3.5.

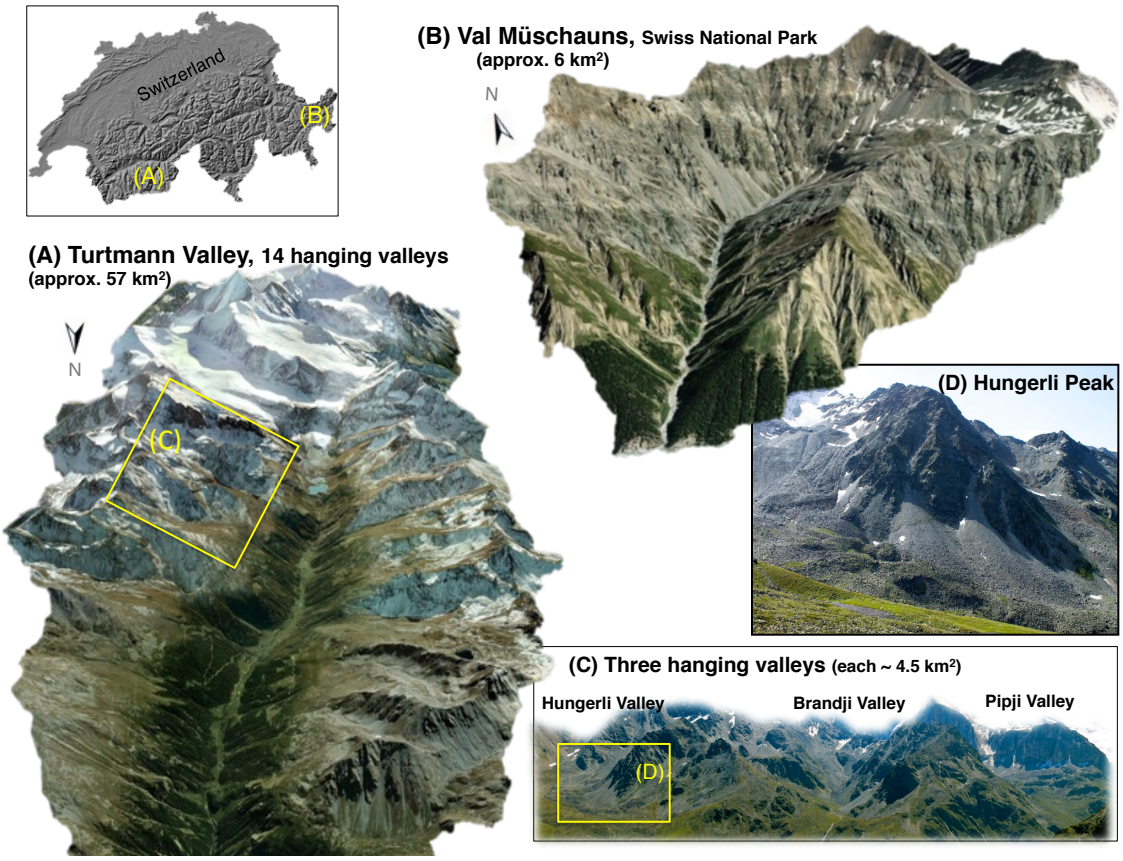

Figure 3.5: *Overview on different study sites of this thesis: A) The Turtmann Valley in the SW Valais Alps, B) Val Müschauns in the Swiss National Park, C) three hanging valleys of the Turtmann Valley and D) the north-exposed Hungerli Peak in the Hungerli Valley.*

Principal study site is the Turtmann Valley (Figure 3.5A) situated in the SW Swiss Alps between the Matter Valley and the Val d'Anniviers in the Swiss Canton Valais. As a southern tributary of the Rhône Valley, the Turtmann Valley is a high-alpine valley with a distinct variety of processes of rock slope instability, geomorphic processes of sediment transfer and sediment landforms. The 15 km long and 110 km² large valley is a typical Pleistocene glacial through (in the southern part) with the Turtmann Glacier and the Brunegg glacier at the southern valley head. At each side of the NS- oriented main valley, more than 14 hanging valleys are lying on either side of the through shoulders ranging from approx. 2300 to 4200 m asl. The pronounced N- or S-exposition of the valley flanks, the distinct SW striking of tectonic layers, the ongoing rock slope deglaciation since LGM and the diverse lithology make the evaluation of the relative importance of rock slope destabilising factors highly interesting. In this thesis, modelling, field and laboratory studies address the entire Turtmann

Valley (Figure 3.5A), three hanging valleys and the N-exposed Hungerli Peak in the Hungerli Valley (Figure 3.5D).

Geomorphic research in the Turtmann Valley has a long tradition dating back to first field observations of R. Dikau in the late 1980s. During the last 30 years, numerous geomorphic and interdisciplinary studies have been performed, particularly in the framework of the Research Training group 436 (see e.g. Otto and Dikau, 2010). Previous work focused, amongst others, on vegetation characteristics (Hörsch, 2002), geomorphometry and landform toposequences (Rasemann, 2004), rock glacier distribution and kinematics (Nyenhuis et al., 2005; Roer, 2005), scale-dependent biogeomorphic dynamics in the Turtmann glacier forfield (Eichel, 2016), as on permafrost both with respect to its regional distribution (Van Tatenhove and Dikau, 1990; Nyenhuis, 2005) and its local thermomechanical effects on rock slopes (Krautblatter, 2009; Draebing, 2014). In particular, the meso-scale inventory of paraglacial sediment storages compiled by Otto (2006) represents an important linking point for this thesis. Although it neglects the rockwall source areas, Otto's work is a fundamental knowledge and data basis that needs to be extended. The total number of 220 active talus slopes accounting for more than 12% of the tributaries' total sediment volume (Otto et al., 2009) significantly emphasises the activity of (small-size) rock slope failures. However, so far, only Krautblatter (2009) and Draebing (2014) investigated bedrock instabilities in the Turtmann Valley, with focus on deep-seated and slow bedrock deformation of the permafrost- and snow-affected Steintälli.

Second research site (Figure 3.5B) is the high-alpine valley Val Müschauns in the Swiss National Park. The formerly glaciated valley is situated in the Engadine region in the Swiss Canton Graubünden and covers a catchment area of 6.2 km² ranging from 1869 m to 3154 m asl Contrary to the Turtmann Valley, the basin is naturally drained by a mountain stream (Ova da Trupchun) making the study of hillslope sediment transfer to the valley outlet highly interesting. Similar to the Turtmann Valley, Val Müschauns hosts a variety of geomorphic processes and sediment storage landforms. While debris flows are most active in the lower V-shaped valley part, low-magnitude rockfall events are most dominant in the two upper EW-oriented and bedrock dominated hanging valleys. Here, the steep, elongated carbonate rockwalls and the pronounced glacial valley morphology are dominant form characteristics. First geomorphic studies in Val Müschauns have been performed by Schoch (2013) and Messenzehl (2013). In this thesis, the valley will be studied by both modelling and geomorphic field mapping to address the role of rock slope failures for sediment cascades in formerly glaciated high-alpine terrain. In the following chapters, all study sites will be described in more detail in the context of the respective research studies.

----- BLANK -----

PART B

Barrhorn

----- BLANK -----

Chapter 4

STUDY I - CONTROLS ON REGIONAL-SCALE ROCKFALL ACTIVITY IN ALPINE VALLEYS

This chapter is based on the published journal article: Messenzehl, K., Meyer, H., Otto, J.-C., Hoffmann, T., Dikau, R. (2017): Regional-scale controls on the spatial activity of rockfalls (Turtmann valley, Swiss Alps) - A multivariate modelling approach. In: Geomorphology 287: 29-45. DOI: 10.1016/j.geomorph.2016.01.008.

Abstract

In mountain geosystems, rockfalls are among the most effective sediment transfer processes, reflected in the regional-scale distribution of talus slopes. However, the understanding of the key controlling factors seems to decrease with increasing spatial scale, due to emergent and complex system behaviour and not least to recent methodological shortcomings in rockfall modelling research. In this study, we aim (i) to develop a new approach to identify major regional-scale rockfall controls and (ii) to quantify the relative importance of these controls. Using a talus slope inventory in the Turtmann Valley (Swiss Alps), we applied for the first time the decision-tree based random forest algorithm (RF) in combination with a principal component logistic regression (PCLR) to evaluate the spatial distribution of rockfall activity. This study presents new insights into the discussion on whether periglacial rockfall events are controlled more by topo-climatic, cryospheric, paraglacial or/and rock mechanical properties.

(i) Both models explain the spatial rockfall pattern very well, given the high areas under the Receiver Operating Characteristic (ROC) curves of > 0.83. Highest accuracy was obtained by the RF, correctly predicting 88% of the rockfall source areas. The RF appears to have a great potential in geomorphic research involving multicollinear data.

(ii) The regional permafrost distribution, coupled to the bedrock curvature and valley topography, was detected to be the primary rockfall control. Rockfall source areas cluster within a low-radiation elevation belt (2900-3300 m a.s.l,) consistent with a permafrost probability of > 90%. The second most important factor is the time since deglaciation, reflected by the high abundance of rockfalls along recently deglaciated (< 100 years), north-facing slopes. However, our findings also indicate a strong rock mechanical control on the paraglacial rockfall activity, declining either exponentially or linearly since deglaciation.

The study demonstrates the benefit of combined statistical approaches for predicting rockfall activity in deglaciated, permafrost-affected mountain valleys and highlights the complex interplay between rock mechanical, paraglacial and topo-climatic controls at the regional scale.

4.1 Introduction

Rockfalls from steep rock slopes are frequent in cold mountain environments (Rapp, 1960b; Whalley, 1984), where they represent a considerable natural hazard (Hungr et al., 1999; Ravanel and Deline, 2015). From a geomorphological perspective, detailed knowledge of the key factors controlling rockfalls is important as rockfalls efficiently contribute to bedrock denudation (Heim, 1932; Selby, 1982b; Krautblatter et al., 2012), accumulate massive talus deposits at the footslopes (Caine, 1974; Messenzehl et al., 2014) and play a major role in the sediment flux in mountain geosystems (Jäckli, 1957; Hoffmann et al., 2013; Heckmann et al., 2016). The spatial occurrence of rockfalls, i.e. covering debris falls (<10 m^3), boulder falls (10-10^2 m^3) and block falls (10^2-10^4 m^3) (nomenclature after Krautblatter et al. 2012), is best indicated by the presence of talus slopes (Hales and Roering, 2005; Sass, 2005c; Moore et al., 2009) integrating a long-term average of rockfall history over longer time scales such as the Holocene (Krautblatter and Dikau, 2007). However, the heterogeneous spatial distribution of talus landforms within mountain landscapes as well as their varying volumes and material properties (Gerber, 1974; Schrott and Hoffmann, 2003; Sass, 2010) reflect a complex interplay of numerous causative factors, collectively defining the sensitivity of rockwalls to fail at different spatial and temporal process scales (Figure 4.1).

At small scales, the balance between shear stresses and shearing resistance of the rock mass (Terzaghi, 1962) is determined by the highly spatio-temporal variable interplay between mechanical, thermal and hydrological bedrock characteristics (Hoek and Brown, 1997; Wyllie and Mah, 2004) as well as rock breakdown processes

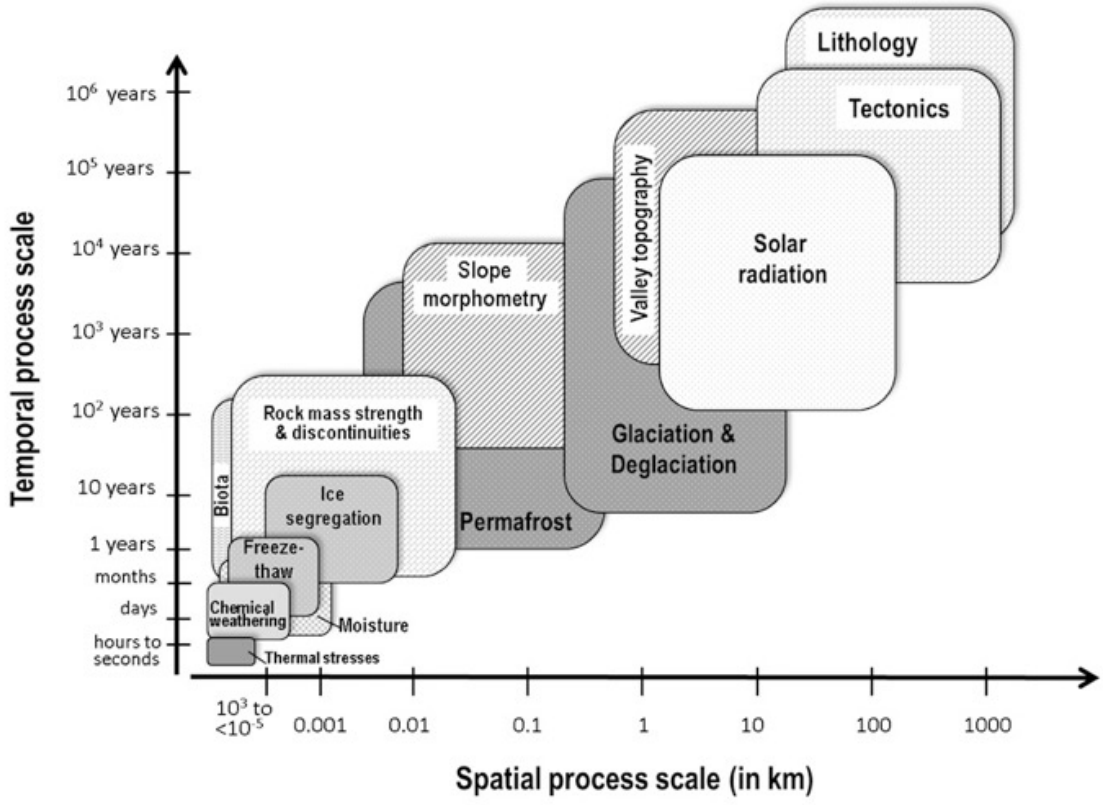

Figure 4.1: *Process-scale of potential rockfall controls with respect their temporal and spatial variability. So far, limited knowledge exists on the relative importance of topo-climatic, morphometric, paraglacial and rock mechanical factors for the regional-scale rockfall activity.*

(e.g. Dixon and Thorn, 2005; Gunzburger et al., 2005; Matsuoka and Murton, 2008; Hall and Thorn, 2014). Rockfalls are particularly found to correlate directly with a low intact rock strength (Selby, 1980; Vehling et al., 2015), an unfavourable joint orientation in relation to slope surface (Cruden and Hu, 1994; Moore et al., 2009) and a high joint density (Sass, 2005b; Loye et al., 2012). Sheeting joints parallel to the slope surface are often associated to stress relaxation after glacial unloading of rock slopes during paraglacial conditions (Brunner and Scheidegger, 1973; Augustinus, 1992). Although the synergy of multiple weathering processes is increasingly acknowledged (Hall, 2006; Hall et al., 2012; Viles, 2013b), daily freeze-thaw cycles (Matsuoka, 1994; Sass, 1998) and seasonal or multi-annual segregation ice growth are supposed to be the prime destabilising agents in cold environments (Hallet et al., 1991; Matsuoka and Sakai, 1999; Murton et al., 2006). The efficiency of freeze-thaw action significantly depends on bedrock moisture (Coutard and Francou, 1989; Prick, 1997) and the thermal behaviour of permafrost (Allen et al., 2009; Krautblatter et al., 2013). Likewise, the specific bedrock roughness and morphometry, e.g. by convex overhangs, can lead to spatially variable, but persistent stress fields (Gerber and Scheidegger, 1969).

With increasing scale, the spatio-temporal variability of most rockfall controls generally decreases pre-disposing the rock slope to fail (Crozier, 1989). Key factors seem to be primary geology and topo-climate (Figure 4.1) considering that instabilities predominantly occur on cold, shaded slopes, steeper than 40° (Dorren and Seijmonsbergen, 2003; Wichmann et al., 2009). These sites are often congruent with an altitudinal belt of low solar radiation (Noetzli et al., 2003; Fischer et al., 2012), where frost cracking over the active permafrost layer might be highly effective (Gruber, 2005; Hales and Roering, 2009). Over geological time scales, the lithological and tectonic settings cause an inherent preconditioning of rockwalls for failures (Cruden and Hu, 1998; Coe and Harp, 2007). A particular bedrock pre-disposition is linked to the impact of glaciation during LGM due to slope oversteepening as well as subsequent paraglacial adjustment processes including slope debuttressing, stress release, permafrost degradation and isostatic rebound (Ballantyne, 2002a; McColl, 2012; Leith et al., 2014b).

Despite our knowledge on the process scale of rockfall causative factors (Figure 4.1), their relative importance within their complex interplay is insufficiently understood. A major challenge is that the relative roles of rockfall controls probably change depending on scale. According to Harrison (2001) and Phillips (1988, 2003b) it must be supposed that the local-scale causes for failure of individual rock slopes likely contrast with those being causative at the regional scale of mountain catchments due to emergent system behaviour and increasing system complexity (and often non-linearity) with increasing spatial scale (Figure 4.2B-D). Harrison (2001) even assumes that at each scale, new, often unknown system properties and causalities emerge ("*?*" in Figure 4.2D) being insensitive to changes at lower levels of this hierarchical structure (see also De Boer, 1992; Church, 1996). However, compared to the slope scale, the understanding of bedrock destabilising factors at regional scales is still very limited as shown by the recent debate on whether rockfall activity is dominated either by topo-climatic forcing (Tricart and Cailleux, 1972; Büdel, 1977; Hales and Roering, 2005), paraglacial adjustment (Cossart et al., 2014; Feuillet et al., 2014) or rock mechanical properties (Duarte and Marquinez, 2002; Fischer et al., 2006).

To some extent, this limited systemic knowledge may be due to methodological shortcomings. While most work focuses on local rock instabilities, few studies have examined regional-scale rockfall controls so far (e.g. Duarte and Marquinez, 2002; Hales and Roering, 2005; Frattini et al., 2008; Michoud et al., 2012). We argue that the appropriate research design to identify key rockfall controls is dictated by the specific scale of interest. While reductionist, process-based field surveys are appropriate to study local parameters (Krautblatter and Moore, 2014), the complex and emergent behaviour of destabilising factors at a larger scale might be best understood by abductive approaches (Peirce, 1902) using e.g. inventories of talus slopes (e.g. Moore et al., 2009; Tanarro and Muñoz, 2012). Here, GIS-based multiple logistic regressions provide a powerful statistical method that has been successfully applied in the mapping of permafrost (Janke, 2005) and patterned grounds (Luoto and Hjort, 2005), soil erosion (Vanwalleghem et al., 2008) and extensively of landslide susceptibility (Guzzetti et al., 1999; Ohlmacher and Davis, 2003; Vanacker et al., 2003; e.g. Bai et al., 2010; Borgomeo et al., 2014). More recently, machine learning algorithms such as random forests (Breiman, 2001), mainly known from ecological studies (Cutler et al., 2007) and climate modelling (Meyer et al.; Kühnlein et al., 2014) are receiving increased attention in landslide studies (Brenning, 2005; Stumpf and Kerle, 2011; Vorpahl et al., 2012; Catani et al., 2013). However, since knowledge of deep-seated gravitational mass movements cannot be automatically transferred to rockfall processes, adequate approaches are needed specifically for rockfall research.

To address the recent systemic and methodical shortcomings, we investigate the spatial rockfall activity in the Turtmann Valley (Swiss Alps). Our objectives are *(i)* to develop an appropriate approach to identify major factors controlling the regional-scale occurrence of rockfall processes and *(ii)* to evaluate the relative importance of rock mechanical, paraglacial and topo-climatic influences within this complex interplay. Using an inventory of 220 talus slopes, we combine a classical logistic regression model based on principal components and a novel random forests classification to examine the relative causality between the slopes' rockfall susceptibly and ten potential destabilising parameters.

4.2 Characteristics of the study area

The Turtmann Valley is located in the Valais Alps (Switzerland) between the Matter Valley and the Anniviers Valley (Figure 4.2) covering a catchment area of 110 km² at altitudes ranging from 620 m to 4200 m above sea level (asl) (Otto et al., 2009). The 15 km long valley is a typical Pleistocene glacial trough with the Turtmann Glacier at the valley head. While the rock slopes of the trunk valley are mainly affected by deep-seated gravitation processes, rockfalls predominate in the 14 strongly W-E-oriented hanging valleys, lying on either side of the trough shoulders at 2300-2600 m asl

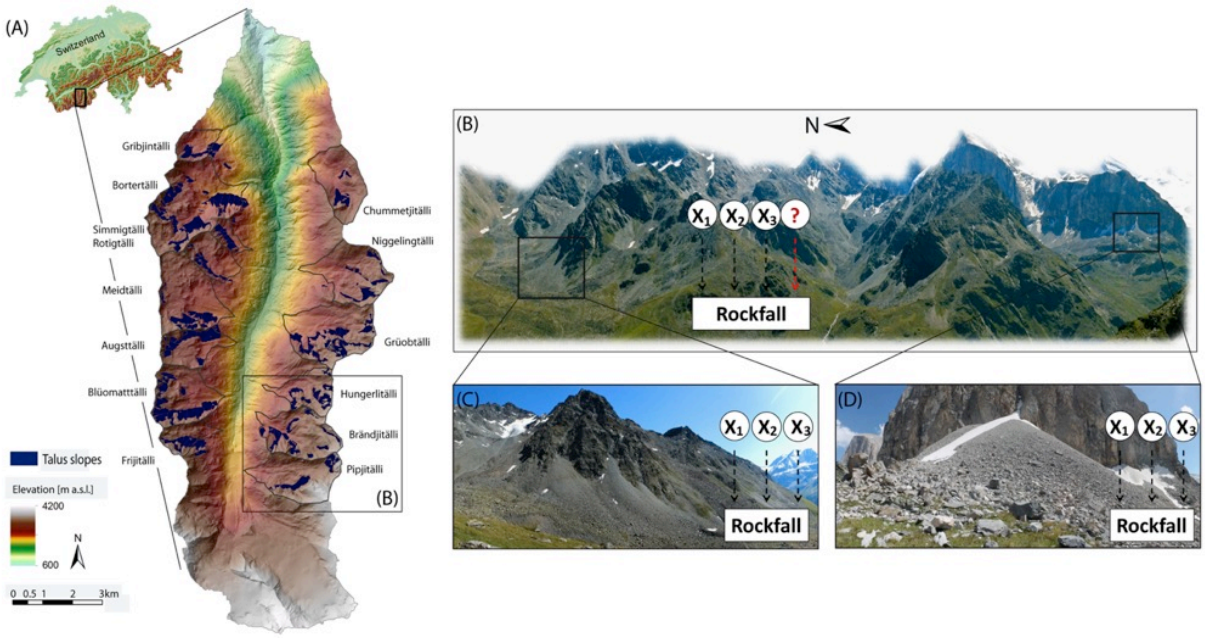

Figure 4.2: *Study area. A total of 220 Talus slopes (mapped in blue) are deposited in the 14 hanging valleys of the Turtmann Valley, southern Swiss Alps (A). It is supposed that the relative role of regional-scale rockfall controls (X_1, X_2, X_3, ?) (B) contrasts to destabilising factors (X_1, X_2, X_3) at the local scale (C, D) due to emergent and complex behaviour of geosystems with increasing spatial scale.*

The lithology of the hanging valleys is dominated by metamorphic rocks (penninic Siviez-Mischabel nappe) consisting of Palaeozoic micashists and paragneisses (ca. 72%), which form most of the bedrock in the northern and eastern hanging valleys located in the NE (Labhart, 2009). Thin layers of amphibolite (0.20%), quarzites (0.53%) and apatite (6.23%) are incorporated. As result of the tectonic folding, the metamorphic rocks generally strike in a south-west direction with a dip of 20-30° (Bearth, 1980). Overlying the crystalline rocks, mesozoic dolomites, limestones and marbles with clay layers (Barrhorn series and Frilihorn series) occur in the western (Meidtälli) and south-eastern hanging valleys (Pipjitälli) (Labhart, 2009).

Due to the inner alpine location, the climatic situation of the study area is characterised by dry continental conditions with mean annual precipitation of ca. 600-900 mm at 2000 m asl (Gärtner-Roer et al., 2013) and a snow line at ca. 3450 m (Escher, 1970). The 0 °C isotherm of the mean annual air temperature might be at ca. 2550 m asl (Van Tatenhove and Dikau, 1990). According to a local permafrost model (Nyenhuis et al., 2005), 37 km² or 33% of the catchment area is very likely affected by permafrost (> 60% probability), with a lower limit ranging from 2500 m asl (N-orientations) to 3000 m asl (S-orientations).

The ice surface of the Late-Glacial maximum (LGM) is supposed to have reached up to 2600 m asl in the main valley, rising towards the cirques of the hanging valleys and the Bishorn peak (4058 m) (Kelly et al., 2004b). At ca. 24-21 kyrs BP, rock slopes were likely ice covered by local hanging glaciers and only the peaks were ice-free nunataks. After ca. 18 kyrs BP, deglaciation started in the main trough and subsequently in the hanging valleys (Kelly et al., 2004b; Schlüchter, 2004), successively exposing the slopes above the trough shoulders. However, no data on the timing of glacier recession in the study area exist. With respect to the Late Glacial advance, the Younger Dryas glacier (ca. 12-8 kyrs) probably did not affect the rock faces of the hanging

valleys (Ivy-Ochs et al., 2009) indicated by the well-preserved Egesen (Younger Dryas) moraines within the hanging valleys at ca. 2600 m (Otto and Dikau, 2004). Today, the few glaciers still existing in some of the hanging valleys are affected by a significant recession trend due to atmospheric warming in the last decades.

Rockfall events of small (< 10 m^3) and medium magnitude (10-10^4 m^3) (Messenzehl and Draebing, 2015) are some of the most active processes in the hanging valleys leading to a postglacial denudation rate of around 0.7-2.2 mm/a (Otto et al., 2009). A total number of 220 active talus slopes (including sheets and cones) accounts for ca. 8.7-12.3% of the tributaries' total sediment volume (Otto et al., 2009), representing major sources for rock glaciers and debris flows in the sediment cascade. Sediment output from the tributaries to the main drainage system is largely disconnected due to the bedrock trough shoulders and geomorphic buffers such as moraine landforms (compare to Messenzehl et al., 2014).

4.3 Modelling approach

4.3.1 Data selection and pre-processing

Response variable

An inventory of 220 talus slopes (Otto et al., 2009) was used to deduce abductively the rockfall activity of the associated rock slope. Since rockfalls predominantly occur in the hanging valleys, the trunk valley was excluded from further investigations. The presently absent or negligible vegetation cover on talus deposits indicates active rockfalls. Rockfall source areas in bedrock were automatically extracted from a 1 m HRSC-Digital Elevation Model (DEM, Otto et al., 2007) using the hydrological algorithm of the D8 flow routing in SAGA GIS (Martz and Garbrecht, 1992). The talus slopes served as sinks to determine their contributing areas. Our approach is in accordance with Frattini et al. (2008) and Marquínez et al. (2003) similarly using inventories of talus slopes to deduce associated grid cells of rockfall source area polygons. To derive rockfall initiation zones exclusively on bedrock, we furthermore intersected the contributing areas with the bedrock outcrop derived from a digital geological map 1:25,000 (© Swiss Topo, based on Bearth, 1980). To correct the planimetric area of the rockfall source areas for the actual surface area, each raster cell was multiplied by the cosine of the slope gradient. For subsequent modelling, source areas were transformed into a binary raster grid (1 = presence of rockfall source area, 0 = no rockfall source area) and used as dependent response variable. A ground truthing based on field observations (e.g. fresh rockfall detachment zones, or freshly weathered bedrock) and interpretation of HRSC-aerial images (ground resolution 50cm) suggest reasonable results of the automatic mapping.

Predictor variables

Based on systemic process understanding and data availability, ten variables were considered to be potentially causative for the spatial rockfall distribution (Table 4.1). Topographic and morphometric parameters including elevation, slope gradient (Figure 4.3A), aspect, profile curvature and surface roughness (Figure 4.3B) were derived from the 1 m DTM using ArcGIS (ESRI, 2006). Considering climatic and cryospheric variables (Figure 4.3C, D), the potential annual sum of solar radiation in watt hours per square meter (WH/m^2) was modelled

for every pixel using a hemispherical viewshed algorithm provided in ArcGIS (Fu and Rich, 2002). A layer of permafrost probability was derived from the empirical-statistical model PSIM (Permafrost Simulation Indication Model) by Nyenhuis (2005). Here, a local inventory of active and relict rock glaciers is related to potential direct solar radiation and mean annual air temperature (represented by altitude) (Nyenhuis et al., 2005). In contrast with other permafrost models, shadowing effects due to relief and solar variations are considered.

Table 4.1: *Overview on response and predictor variables with respect to geomorphic type, data source, variable scale, decoding scheme (classes with rockfall density RD) and their implication for slope (in)stability based on a selection of related rockfall and rockwall instability studies.*

Type and name of variable		Data source	Variable scale	Decoding	Implication for slope stability *(referring to a selection of local-and regional-scale rockfall and rockwall instability studies)*	
Response variable (dependent variable)						
	Rockfall source areas	Talus slope inventory (Otto et al., 2009)	binary			
Predictor variable (independent variables)						
Topography	Elevation	DEM (1m)	metric		• Sum and variability of incoming solar radiation • Efficiency of weathering activity • Bedrock permafrost • Bedrock hydrology • Snow coverage • Joint orientation	(Sass, 1998; André, 2002; Dorren and Seijmonsbergen, 2003; Dixon and Thorn, 2005; Gunzburger et al., 2005; Sass, 2005b; Santi et al., 2009; Wichmann et al., 2009)
	Slope	DEM (1m)	ordinal	radians		
	Aspect	DEM (1m)	ordinal	6 classes (45° units) with RD		
Morphometry	Profile curvature	DEM (1m)	ordinal	3 classes (convex. concave. planar) with RD	• Local stress fields • Sediment storage inside bedrock • Shadowing effects • Local moisture patterns • Snow accumulation • Permafrost distribution	(Terzaghi, 1962; Gerber and Scheidegger, 1969; Coutard and Francou, 1989; Prick, 1997; Sass, 2005a; Matsuoka, 2008; Shirzadi et al., 2012)
	Surface roughness	DEM (1m)	metric			
Climate and Cryosphere	Annual sum of incoming solar radiation	DEM (1m)	metric		• Intensity of frost cracking • Thermal weathering processes • Permafrost depth and thermal behaviour • Snow melt and deposition • Bedrock moisture supply • Plant colonisation	(Hallet et al., 1991; Matsuoka and Sakai, 1999; Noetzli et al., 2003; Gruber, 2005; Hall, 2006; Murton et al., 2006; Hales and Roering, 2007; Matsuoka and Murton, 2008; Allen et al., 2009; Sass, 2010; Hall et al., 2012; Krautblatter et al., 2013; Viles, 2013; Hall and Thorn, 2014),
	Permafrost probability	DEM (1m) based on PSIM model (Nyenhuis, 2006)	metric			
Rock mechanics	Lithology type	Geological map 1:25,000 Swiss Topo. (Bearth, 1980)	nominal	6 lithological classes with RD	• Rock mass strength • Rock porosity • Moisture distribution • Weathering efficiency • Rockfall type • Rockfall block size • Rockfall frequency (historicity)	(Selby, 1980; Selby, 1982; Cruden and Hu, 1994; Hoek and Brown, 1997; Cruden and Hu, 1998; Sass, 1998; Wyllie and Mah, 2004; Coe and Harp, 2007; Moore et al., 2009; Fischer et al., 2012)
	Joint orientation (in relation to slope)	Geological map 1:25,000 Swiss Topo, (Bearth, 1980)	nominal	5 joint classes with RD		

Rock mechanical characteristics including lithology and overall joint orientation were extracted from the digital geological vector map at 1:25,000 scale (© Swiss Topo, based on Bearth, 1980). Six lithological classes (Figure 4.3E) were identified: 1) marble and limestone, 2) paragneiss and micaschist, 3) amphibolite, 3) apatite, 4) quartzite and 5) basalt. Quaternary deposits are not included. Additionally, overall joint orientation (dip and dip direction) was extracted for those rock faces, where geotechnical information was available, and evaluated in relation to the specific slope gradients following Selby (1980) and Cruden and Hu (1994). Following classes are used:

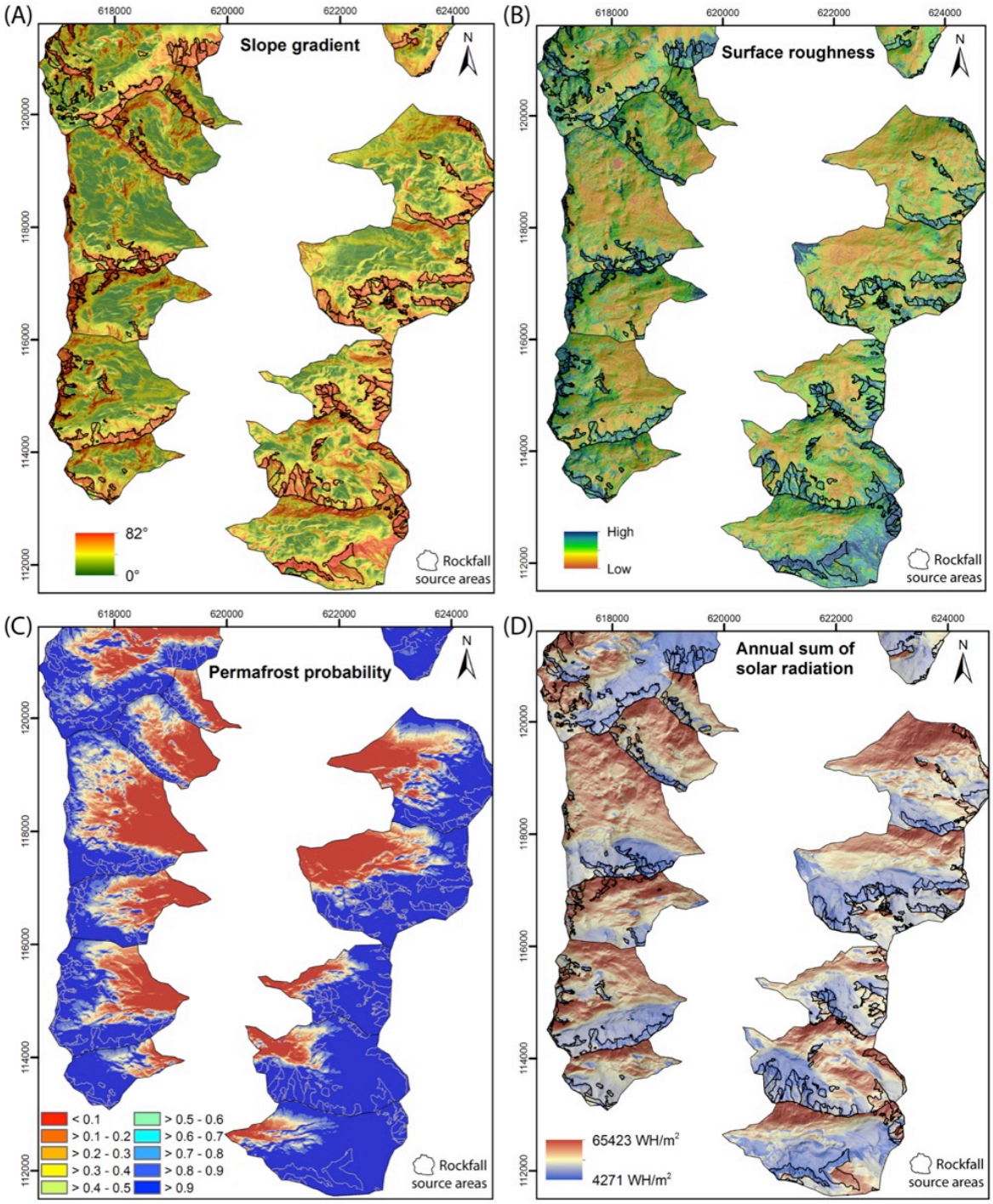

Figure 4.3: *Selection of predictor variables representative for topography (A: Slope gradient), morphometry (B: Surface roughness). (C): Permafrost probability modelled by Nyenhuis 2005, D: Annual sum of incoming solar radiation). Sub-figures E-F continued on next page.*

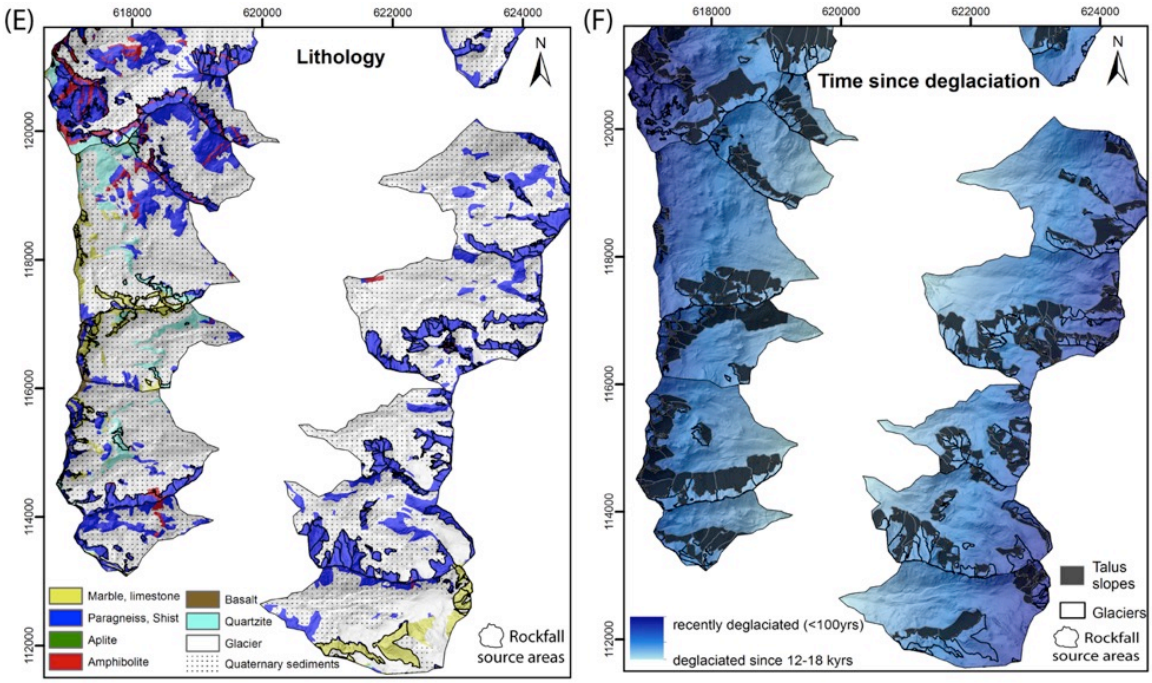

Figure 4.3 (continued): *Predictor variables representative for rock mechanical properties (D: Lithology) and paraglacial adjustment (F: Relative time since deglaciation).*

1) Steep joint dipping into the slope (> 30°)
2) Moderate joint dipping into the slope (30°-horizontal)
3) Horizontal joint layering
4) Moderate joint dipping out of the slope (< 30°)
5) Overdip slope (> 30°)

To consider paraglacial rock slope adjustment after LGM we assume that rockfall activity is highest immediately (or with a short time lag) after deglaciation and is declining (exponentially or linearly) with time (e.g. Curry and Morris, 2004). Due to absent data on glacial retreat stages in the study area, we applied the ergodic reasoning or space-for-time-substitution (Paine, 1985; Pickett, 1989): The time elapsed since deglaciation of rock slopes was approximated by their relative distance from the cirque assuming a gradual retreat of LGM ice from the trough shoulders (Kelly et al., 2004b; Ivy-Ochs et al., 2009). For each hanging valley, the relative distance of rockwalls to the cirque was calculated by the normalised Euclidean distance (Figure 4.3E) ranging from 1 (outlet = deglaciated since ca. 12-18 kyrs BP) to 0 (cirque = recently deglaciated since < 100 yrs). Additionally, to consider ice thinning during deglaciation, which is considerably accelerated on steep relief and retarded on flat terrain, a topographic factor was incorporated in the Euclidian distance calculation. Therefore, the horizontal surface distance to the cirque was weighted by the slope angle at each cell of the 1m DEM. For modelling purposes, all non-metric predictors were converted to metric, except slope gradient, which was recalculated to radians. Non-metric variables were decoded (Table 4.1) using the rockfall densities (RD), as proposed by Bai et al. (2010):

$$RD = \frac{\frac{B_i}{A_i}}{\sum_{i=1}^{N} \frac{B_i}{A_i}} \qquad (4.1)$$

where A_i is the area of the ith class of the specific variable, B_i is the total rockfall source area of the ith class, and N is the number of variable classes. Contrary to dummy variables, this approach keeps the original number of predictors. To evaluate the spatial characteristics of rockwalls contributing to talus landforms, the density percentage of the rockfall source areas was calculated for each predictor variable.

4.3.2 Validation methodology

To avoid overfitting during modelling, we split the total dataset into a training data set containing 20% of the pixels, and a validation set containing the remaining 80% of the pixels of the 1 m DTM. Data splitting was done by stratified random sampling to obtain the same distribution of the response variable in both subsets. To validate and compare both model approaches, we estimated three different validation measures: The accuracy (overall rate of correct classification), the Probability of Detection POD (fraction of observed rockfall source areas that is predicted correctly) and the Probability of False Detection POFD (fraction of observed absent source areas that is predicted falsely as rockfall source areas). The values of validation measures range between 0 and 1, with POD = 1 and POFD = 0 indicating perfect score (Wilks, 2006). Additionally, a Receiver Operating Characteristic curve (ROC curve) and the specific area under the curve (AUC) serve to visualise the accuracy and prediction power of the model over the complete range. Here, the sensitivity or POD (true-positive fraction) is plotted against the specificity or POFD (false-positive fraction) (Bradley, 1997).

4.3.3 Principal component analysis and logistic regression modelling

When using the multiple logistic regression (LR), our focus is not on the spatial prediction of rockfall probability or susceptibility based on a number of independent predictor variables, but instead on ranking the predictors with respect to their relative importance for the binary dependent response (i.e. presence/absence of rockfall initiation zones). Our algorithm of the principal component logistic regression (PCLR) model was computed using R software packages, based on eight main steps (Figure 4.4).

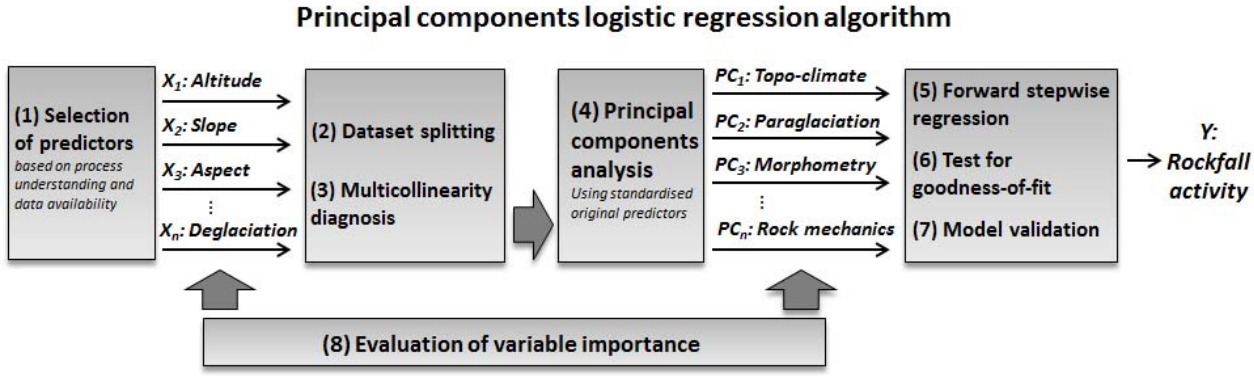

Figure 4.4: *Modelling approach of the multiple logistic regression using uncorrelated principal components (PC) instead of the original, intercorrelated predictor variables X.*

Using a logit transformation, the natural log odds (logit) was calculated, being the ratio of the probability of rockfalls (= presence of rockfall source areas) to that of absence. The LR represents a generalised linear regression and can be written as (Atkinson et al., 1998):

$$Y = logit\,(p_i) = \log\frac{p_i}{1-p_i} = \beta_0 + \beta_1 X_1 + \beta_2 X_2 + \cdots + \beta_n X_n \qquad (4.2)$$

where Y is the dependent variable, p_i is the rockfall probability (0 to 1), β_i (i =1,2,3…n) is the coefficient of the model, n is the number of independent predictors X_i (i = 1,2,3…n).

To identify multicollinearity, the Tolerance (TOL) and the Variation Inflation Factors (VIF) were calculated. Variables with VIF > 2 and TOL < 0.4 might be highly dependent on other predictors (Allison, 2001) and are usually excluded in most regression analyses. The inter-correlation between the permafrost distribution and the time since deglaciation is rather small. This is also supported by their contrasting spatial distribution of these variables shown in Figure 4.3C and Figure 4.3F. In contrast, we detected a moderate inter-correlation between the permafrost probability, slope and aspect (Table 4.2). To solve this problem without a loss of original input data, we used a reduced set of uncorrelated PCs representing linear combinations of the ten original standardised data with a maximum possible variance (Escabias et al., 2005; Aguilera et al., 2006).

Table 4.2: *Diagnostics statistics of multicollinearity between independent predictors using the Tolerance (TOL) and the Variation Inflation Factors (VIF). VIF of > 2 and TOL of < 0.4 point to variable intercorrelation.*

Predictor variables	VIF	TOL
Elevation	1.95	0.51
Slope	4.96	0.20
Aspect	4.24	0.31
Curvature	1.01	0.99
Roughness	1.42	0.71
Solar Radiation sum	2.96	0.30
Permafrost probability	6.16	0.16
Lithology	1.17	0.85
Joints	1.10	0.90
Deglaciation	1.94	0.51

To select only those principal components (PCs) with statistically significant contribution to rockfall activity a forward stepwise method was applied using maximum likelihood ratio (-2ln$L$) tests together with the Akaike Information Criterion (AIC) value. Here, PCs were selected based on their predictive ability and not on the largest variance (Aguilera et al., 2006). Starting with the null-model (intercept only), PCs were successively added until further additions did not result in a lower -2ln$L$ and AIC value. Using the Wald X^2 statistics, the predictors' coefficients were estimated to be statistically significant, if the tested null hypothesis (H_o: the estimated coefficient is 0) could be rejected at a p = 0.001 significance level (Kleinbaum et al., 1998). The association between the predicted probability and the observed responses (goodness-of-fit) was tested over the training dataset using the X^2 value (based on -2ln$L$) of the Hosmer-Lemeshow test, the -2ln$L$ and the AIC value (Hosmer and Lemeshow, 2005).

For validation of the fitted logistic regression model we used a contingency table using the validation data set based on a cut-off value of 0.509. This threshold was determined by finding the best trade-off between sensitivity (Probability of Detection) and specificity (1- Probability of False Detection) of the predicted probabilities, i.e. the trade-off between failing to detect rockfall against the costs of raising false alarms. The strength of association between response and each predictor was determined by means of the Odds ratios (OR) of the varimax-rotated PCs (Kaiser, 1958) with respect to the loadings of the original standardised predictors. The OR is the exponential of the regression coefficient (e^{β_i}) associated with a one-unit increase in X_i. If a coefficient is positive, then OR is > 1 and thus, rockfalls are more likely to occur. In turn, the likelihood of rockfalls decreases with negative coefficients and OR < 1. In case of no or weak causal link between predictors and response, OR is ~ 1 (Atkinson et al., 1998).

4.3.4 Random forest model

Machine learning algorithms such as the random forest algorithm of Breiman (2001) are known as being able to deal with complex interacting as well as highly correlated predictor variables. The RF model is based on the concept of classification trees. Tree-based models consist of a series of nested decision rules for the predictors that determine the response. Random forest repeatedly builds trees from random samples of the training data. Each tree is treated as a separate model of the ensemble. The majority class of all trees is taken as final estimate of the model. To overcome correlation between trees, a certain number of predictors (commonly abbreviated as 'MTRY' in the random forest literature) are randomly selected at each split of a tree. The best predictor from the random subset is used at the respective split to partition the data. MTRY is a parameter, which must be adapted to the respective model data. We used the R implementation of the random forest algorithm (Liaw and Wiener, 2002) to classify the rockfall source areas based on the set of predictor variables. Following the suggestion of Kuhn and Johnson (2013), MTRY was tuned between 2 and the number of predictors. The training was performed using a stratified 10 fold cross-validation. Therefore, models were fitted by repeatedly leaving one of the folds out. The performance of each model was determined by predicting on the respective withheld fold. The ROC from the withheld iterations was averaged to the overall performance for the respective value of MTRY. The model resulting from the best set of tuning parameters was used as the final model for prediction on the test data. Variable importance was further calculated as described in Liaw and Wiener (2002), using the mean decrease in GINI index. The GINI index is a criterion of impurity of a node in the RF model (Breiman, 2001). At every split of a node, one of the randomly chosen variables is used to form the split, which results in a decrease in the GINI index. Thus, the mean decrease in GINI index over all trees in the forests indicates how much the given predictor variable contributes to the impurity of nodes in the model. The higher the decrease in GINI index, the higher the purity of the final RF model, and thus the more important is the predictor variable.

4.4 Results

4.4.1 Spatial characteristics of rockfall source areas (rockfall density statistics)

The rockfall density percentage (RD in %) of active initiation zones with respect to each predictor variable is shown in Figure 4.5. Around 11% of the total bedrock area in the hanging valleys represents active rockfall source areas contributing to active talus landforms. The rockfall source zones predominate on NNE-NNW-exposed slopes (41% RD, Figure 4.5C) with slope gradients > 40° (93% RD, Figure 4.5B).

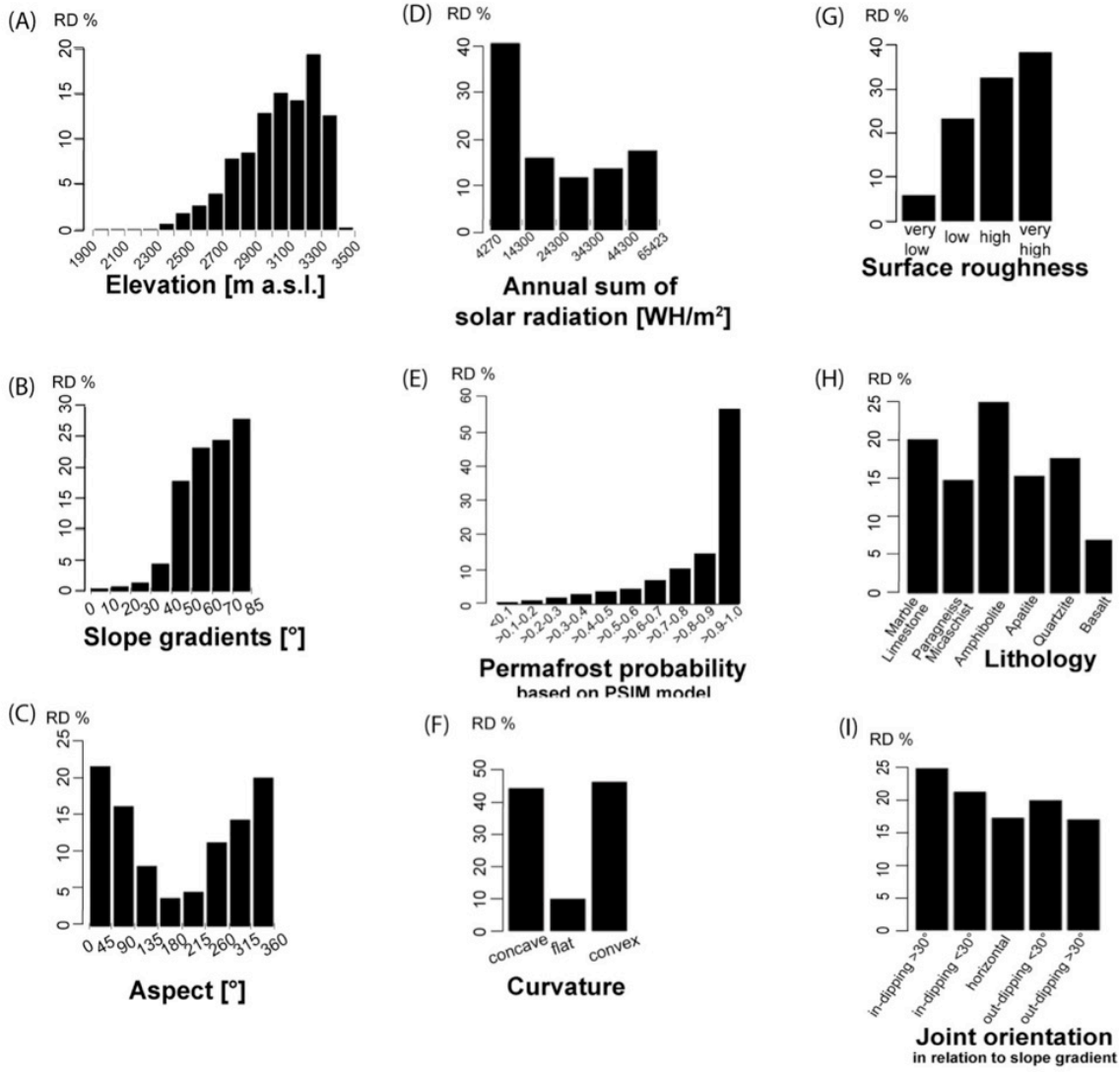

Figure 4.5: Rockfall densities (RD in %) of predictor variables including topographic (A-C), climatic and cryospheric (D-E), morphometric (F-G), rock mechanical (H-I) and paraglacial (J) properties.

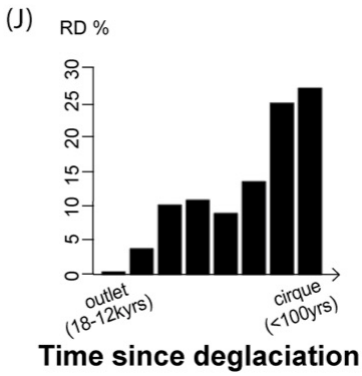

The dominance of north-facing initiation zones is independent of the morphometric configuration of the study area, given the relatively uniform orientation of the total bedrock area across the hanging valleys. Half of the active rockfall source areas receive very low incoming solar radiation of less than 14300 WH/m² per year (Figure 4.5D). The majority of rockfalls

occur in the upper half of the hanging valleys (Figure 4.5J), although bedrock slopes dominate in the middle basin at 2500-2800 m asl About 74% of the rockfall initiation zones are primarily concentrated within an elevation belt at 2900-3300 m asl (Figure 4.5A). This is consistent to the lower boundary of the modelled permafrost distribution. Particularly, 57% of the unstable rockwalls correlate with a 90-100% permafrost probability Figure 4.5E). Considering the micro-topography, active rockfall source areas are equally concave and convex and ~70% are characterised by very rough bedrock surfaces (Figure 4.5F, G). Despite the dominance of paragneiss and micashist in the study area, only 14% of the active rock slopes can be found there (Figure 4.5H). Instead, failures mostly occur in amphibolite (25% RD) and limestone (20% RD), contrasting to their small relative catchment areas (0.2% amphibolite, 12% limestone). Finally, half of the rockfall initiation zones lie at anaclinal slopes with moderately and steeply in-dipping joints, while 36% are linked to cataclinal slopes with out-dipping joints (Figure 4.5I).

4.4.2 Principal components and geomorphic meaning

The first eight varimax-rotated principal components account for around 98% of the total variability of the original, standardised predictor dataset (Figure 4.3). Most of the variance is explained by PC1 (20%) and PC3 (18%), respectively, while the contribution of PC9 and PC10 is < 1%. PC1, PC3 and PC9 represent topo-climatic characteristics. The first component is strongly related to steep slope gradients (loading of 0.95) and a high probability of permafrost (loading of 0.85). PC3 is highly associated with convex S-exposed slopes and high annual solar radiation sums, but negatively correlated with permafrost occurrence. PC2 denotes paraglacial adjustment given the high loading of the time since deglaciation. Likewise, PC8 is strongly correlated with elevation and, to minor extent, with the time since deglaciation. The bedrock morphometry is represented both in PC5 and PC7, with a high positive loading of curvature (0.98 in PC5) and roughness (0.93 in PC7). PC4 describes rock mechanical properties, given the very high loading of in-dipping joints. The lithology is characterised by PC6, strongly associated with amphibolite and limestone rocks. Finally, PC9 summarises N-facing, low-radiation slopes, whereas PC10 stands for permafrost occurrence; but the predictor loadings are very low (< 0.26).

4.4.3 PCLR model and importance of PCs

In the stepwise logistic regression procedure (stepwise model I), PC4, PC9 and PC10 were excluded, since their elimination lead to a significant reduction ($p=0.001$) of -2lnL and AIC. This decrease of significance was greater compared to the full model including these three PCs (Table 4.4).

To evaluate the goodness-of-fit when integrating rock mechanical properties (PC4), we additionally tested a stepwise model II. Both stepwise models seem to perform very well as a significant decrease of -2ln$L$ and AIC was obtained in each stepwise procedure in comparison with the full model (containing all PCs) and the null-model with intercept only. Additionally, the Wald X^2 statistics indicate an acceptable model performance of the stepwise models at a significance larger than 0.001. However, the incorporation of PC4 does not result in a distinctly better model fitting, indicating that the joint orientation might not be necessarily causative for the

Table 4.3: *Varimax-rotated principal components of original standardised predictor variables. Geomorphic meaning of PCs is based on strength of factor loading of original predictors. PC1, PC2, PC3, PC5, PC6 and PC7 were selected to be significantly causative with the response variable in a stepwise regression modelling based on the -2LnL and AIC value.*

	PC1	**PC2**	**PC3**	**PC4**	**PC5**	**PC6**	**PC7**	**PC8**	**PC9**	**PC10**
Geomorphic meaning	**Topo-climate**	**Paraglacial adjustment**	**Topo-climate**	**Rock mechanics**	**Bedrock morphometry**	**Lithology**	**Bedrock morphometry**	**Paraglacial adjustment**	**Topo-climate**	**Permafrost**
	Steep slopes, high permafrost probability	*Very short time since deglaciation, high elevation*	*S-exp. slopes, high solar radiation, medium permafrost probability*	*In-dipping (>30°) joints*	*Convex bedrock profiles*	*Amphibolite and limestone rock types*	*Very rough bedrock surface*	*High elevation, Short-medium time since deglaciation*	*N-exp. slopes with low-medium solar radiation*	*Low to medium permafrost probability*
Elevation	0.14	**0.36**	0.12	0.06	0.02	0.17	0.07	**0.91**	0.01	0.00
Slope	***0.95***	-0.01	0.18	-0.03	0.10	0.12	0.20	0.12	-0.02	0.15
Aspect	0.25	-0.04	**-0.76**	0.03	0.00	0.04	0.02	0.05	**0.23**	-0.03
Curvature	0.10	0.02	**0.72**	-0.01	**0.98**	0.03	0.14	0.02	0.00	0.00
Roughness	0.30	0.03	0.07	-0.04	0.17	0.08	**0.93**	0.06	0.00	-0.01
Solar radiation sum	0.25	0.03	**0.95**	-0.03	-0.03	-0.06	-0.06	0.07	**0.23**	-0.02
Permafrost probability	***0.85***	0.07	**-0.43**	0.05	-0.08	-0.07	-0.20	0.00	-0.03	**0.26**
Lithology	0.14	0.06	0.08	-0.10	0.03	**0.97**	0.07	0.14	0.00	0.00
Joints	-0.06	0.10	0.05	**0.99**	-0.01	-0.09	-0.04	0.05	0.00	0.00
Time since deglaciation	0.06	**0.94**	0.05	0.11	0.01	0.06	0.02	**0.31**	0.00	0.00
Eigenvalues	2.98	1.03	1.03	1.01	1.01	1.01	0.98	0.96	0.11	0.09
Explained Variance	0.20	0.10	0.18	0.10	0.10	0.10	0.10	0.10	0.01	0.01
Cumulative Variance	0.20	0.30	0.48	0.58	0.68	0.78	0.88	0.98	0.99	1

spatial rockfall pattern. This is also demonstrated by the AUC value of stepwise model II, which is 1% lower compared to stepwise model I. Consequently, we decided to exclude PC4 from the final regression. Therefore, the best LR model for predicting the spatial pattern of rockfalls includes seven PCs (based on equation 4.2):

$$\begin{aligned}\text{Logit}(p) = \log(p/1\text{-}p) = 0.23 \quad & + 1.08\ \text{PC1}\ \textit{(“Topo-climate”)} \\ & + 0.26\ \text{PC2}\ \textit{(“Paraglacial adjustment”)} \\ & - 0.89\ \text{PC3}\ \textit{(“Topo-climate”)} \\ & + 0.11\ \text{PC5}\ \textit{(“Bedrock morphometry”)} \\ & + 0.29\ \text{PC6}\ \textit{(“Lithology”)} \\ & + 0.28\ \text{PC7}\ \textit{(“Bedrock morphometry”)} \\ & + 0.38\ \text{PC8}\ \textit{(“Paraglacial adjustment”)}\end{aligned} \qquad (4.3)$$

The Wald X^2 statistics reveal that all coefficients are statistically significant at $p < 0.001$. Comparing the ORs of the PCs (Table 4.3), PC1 was detected to be most strongly associated with the spatial rockfall activity, directly followed by PC3. One-unit increase of these topo-climatic PCs therefore leads to a 2.94 times higher or 0.41 lower rockfall likelihood, respectively. Table 4.3 displays that the third most important control is PC8, increasing the odds of rockfalls by 1.47 times. The ORs of PC2, PC6 and PC7 range between 1.34 and 1.29 indicating a positive, but comparatively moderate impact on the spatial rockfall pattern. Finally, the OR of PC5 is relative close to 1, indicating a weak power to explain the response variable.

4.4.4 Random forest model and variable importance

The tuning of the random forest model revealed an optimal MTRY value of 8. The variable importance indicated by the GINI decrease denotes the regional distribution of permafrost as the most important predictor (Figure 4.6). Further, the time since deglaciation and the elevation are shown to have considerable influence on the classification result. Furthermore, the sum of solar radiation, the slope gradient, bedrock roughness and slope aspect are linked to a medium relative variable importance. The two rock mechanical predictors including joint orientation and lithology, followed by curvature, were ranked as least important for the spatial distribution of rockfall source areas.

Table 4.4: *Test for goodness-of-fit using the -2log likelihood ratio tests (-2LnL), Akaike Information Criterion (AIC), X^2 and area under the ROC curve (AUC).*

Model	-2Ln*L*	AIC	X^2	Pr(>I X^2I)	AUC
Null model (intercept only)		25811			0.50
Full model (with all PCs)	19258	19275	19257	<0.0001	0.80
Stepwise model I PC1. PC2. PC3. PC5. PC6. PC7. PC8	19247	19265	19247	<0.0001	0.83
Stepwise model II PC1. PC2. PC3. *PC4.* PC5. PC6. PC7. PC8	19247	19266	19247	<0.0001	0.82

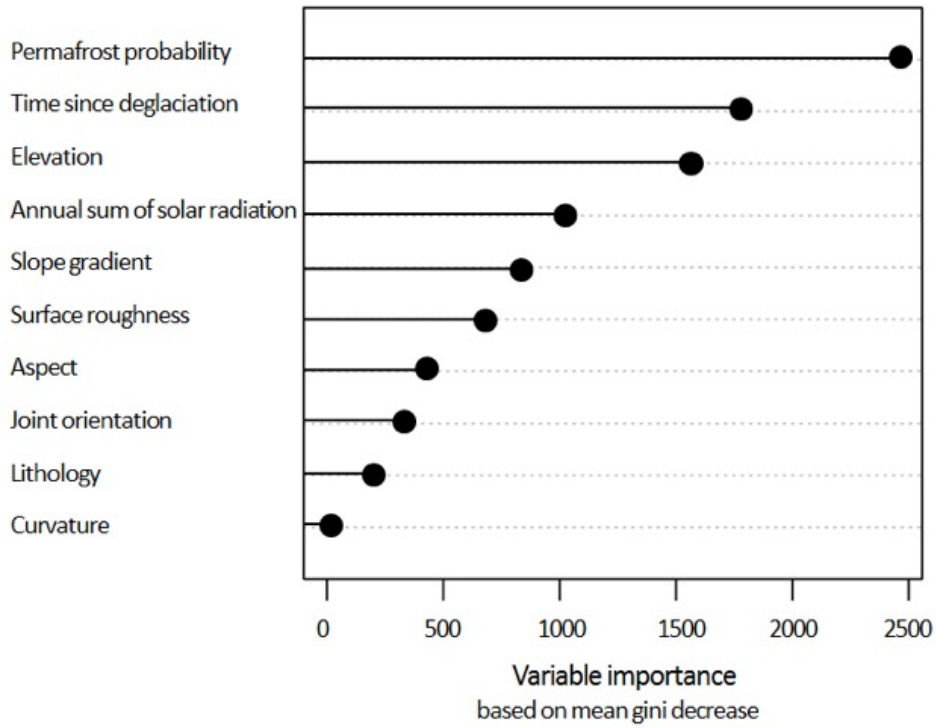

Figure 4.6: Variable importance quantified by means of the random forest mode using the mean decrease in GINI index. The higher the decrease in GINI index, the more important is the variable for the spatial activity of rockfalls.

4.4.5 Validation and evaluation of model performances

To validate the two models with respect to each other we estimated the same validation measures using the same validation data set (Table 4.6). For the PCLR, the overall rate of correct classification is estimated as 75.52%, which is considered to be very acceptable. While 73.71% of the rockfall initiation zones are correctly predicted (POD), the POFD is 22.48%. A comparatively better accuracy is estimated for the RF as 88.40% of the positive and negative observations are correctly predicted. Likewise, the RF results with 88.40% in a comparatively higher POD and only 11.60% is false alarm (POFD). The validation by means of the ROC curves (Figure 4.7) reveals for both models a very good performance given their high AUC values > 0.80 (Swets, 1988). However, the AUC value of the RF model (AUC = 0.95) is slightly higher compared to the PCLR (AUC = 0.83), reflecting a slightly better performance of the machine learning algorithm.

4.5 Discussion

4.5.1 Evaluation of the methodological approach

Given the large areas under the ROC curves of 0.83 and 0.95 (Figure 4.7), respectively, the logistic regression and the random forest classification have proven to be very effective techniques to explain the spatial rockfall pattern in the Turtmann Valley. Nevertheless, there are some systemic uncertainties and limitations underlying our approach. Admittedly, using an inventory of presently vegetation-free talus slopes as proxy to infer potential rockfall initiation zones and their controlling factors is only valid under the assumption that recent

talus slope deposition very likely resulted from the same conditions, which have been causative in the past (Varnes, 1984; Carrara et al., 1999). This abductive reasoning might be true regarding large-scale, relatively static tectonic, lithological and topographic settings; but obviously, weathering history (Viles, 2013b), climatic and cryospheric conditions (Gruber and Haeberli, 2007), bedrock morphometry and rock mechanical properties (Verleysdonk et al., 2011) highly evolved since the LGM (Figure 4.1), all integrated in the evolution of talus slopes. However, the changing relative contribution of rockfall controls over time remains difficult to quantify (Church, 1996; Guzzetti et al., 1999) and we must argue actualistically and often narratively. Similarly, it is important to note that the spatial occurrence of rockfalls crucially depends on the point of observation time. Rock slopes, which we identified as being recently inactive, were likely affected by rockfalls in previous times, e.g. when the permafrost boundary was lower than today. To overcome this, our approach implements an ergodic reasoning to use the spatial pattern of active/inactive rockwalls for the temporal shift in rockfall activity since LGM. Further, the detection of rockfall source areas using the hydrological GIS approach is linked to some restrictions, as falling of rock fragments from steep slopes cannot be simply equated by the water-driven flow paths. However, Duarte and Marquinez (2002) found a good agreement between a similar automatic method and a manual mapping of detachment zones,implying that our approach might be applicable at larger scales. Alternatively, it would have been possible to use the approach proposed by Heckmann et al. (2016), who delineated potential rockfall source areas by combining their slope angle distribution derived from a high resolution DEM (Loye et al., 2009) with a field-based geomorphological map.

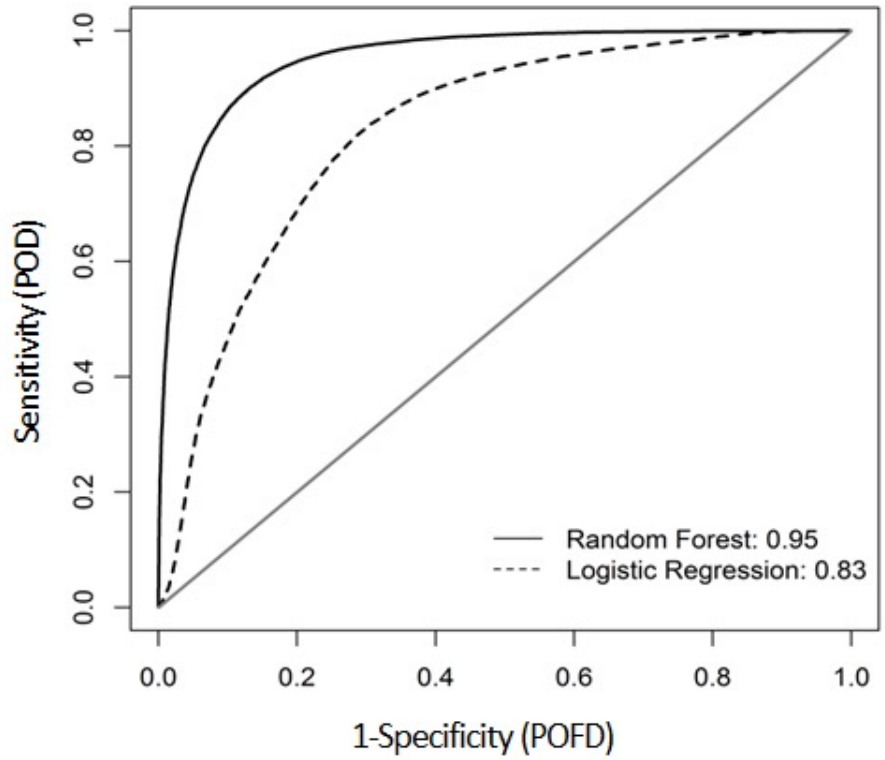

Figure 4.7: *Receiver Operating Characteristic (ROC) curves and values of the corresponding areas under the curve (AUC) of the random forest and logistic regression model.*

Table 4.5: *Coefficient statistics: β= logistic regression coefficient of PC. S.E. (β)=standard error on β. Wald χ^2, P (>$|\chi^2|$), odds ratio= e^{β} with a S.E. of ±1.96 and a 95% confidence interval (C.I.). Variable importance was ranked from I (most important) to VII (less important) based on the odds ratio.*

	β	S.E. (β)	Wald X^2	Pr(>| X^2 |)	OR	95% C.I.			Variable importance ranking (I-VII)
(Intercept)	0.23	0.02	13.00	<0.0001					
PC1	1.08	0.02	50.40	<0.0001	2.94	2.82	-	3.07	I
PC2	0.26	0.02	14.11	<0.0001	1.29	1.25	-	1.34	VI
PC3	-0.89	0.02	-47.79	<0.0001	0.41	0.40	-	0.43	II
PC5	0.11	0.02	6.09	<0.0001	1.12	1.08	-	1.16	VII
PC6	0.29	0.02	15.57	<0.0001	1.34	1.29	-	1.39	IV
PC7	0.28	0.02	13.97	<0.0001	1.32	1.27	-	1.38	V
PC8	0.38	0.02	21.38	<0.0001	1.47	1.42	-	1.52	III

Additionally, the pre-selection of predictors certainly depends on data availability, raster resolution and technical restrictions typical for spatial modelling (Carrara et al., 1999). For instance, we compensated the missing data on timing of deglaciation by the relative Euclidean distance to the cirques. This ergodic reasoning has been successfully applied for studying hillslope evolution (Carson and Petley, 1970; Brunsden and Kesel, 1973; Obanawa et al., 2009), river system changes (Fryirs et al., 2012) and vegetation succession (Cammeraat et al., 2005). Further, the calculation of solar radiation by means of the hemispherical viewshed GIS algorithm (Fu and Rich, 2002) might be rather idealised, as a disturbed solar transmission through atmosphere and topographic shadowing effects are not taken into account (Allen et al., 2009). The permafrost validation of the PSIM by means of a local rock glacier inventory revealed a good agreement of ca. 87%, which was even larger when using classical methods like ROGMOD or PERMAMAP (Nyenhuis et al., 2005). However, the rock glacier based modelling probably underestimates the subsurface temperatures of steep rock slopes and the lower limit of permafrost is probably higher than in more gentle terrain (Magnin et al., 2015b), given the specific conductive and advective thermal fields inside the anisotropic rock mass (Gruber, 2005; Noetzli and Gruber, 2009). Likewise, despite their recognised relevance for slope instability, bedrock moisture (Sass, 2004, 2005a), snow cover (Draebing et al., 2014), biological influences (Chen et al., 2000; Hall et al., 2005) or discontinuities at a cm-dm scale resulting from thermal fatigue (Hall and Thorn, 2014) and stress release (Augustinus, 1995) cannot be portrayed at the regional scale. Besides methodical limitations, variable selection also arises from a prior systemic knowledge on rockfall mechanisms, leading to the risk filtering out any factors being underestimated in their efficiency or unknown so far (Hall, 2006).

Finally, with respect to our sampling strategy (20%-80% sample splitting on pixel basis), it is to note that the cross validation error metrics might tend to be somewhat overoptimistic. Assuming that the neighbouring pixels in the vicinity of the rockfall initiation zones have similar properties, the samples are not completely independent. To overcome this issue, it might be an option to consider stricter cross validation methods in upcoming studies. However, since the main aim of this study is not to predict the spatial distribution of rockfall activity, but to quantify the relative importance of various controlling factors, the cross validation does not change the general outcome of this study.

Taking into account these uncertainties, our proposed modelling approach is promising to evaluate the regional-scale causality between rockfalls and potential key drivers. Instead of avoiding multicollinearity of data, which is often ambiguous or intuition driven by the researcher's pre-existing hypotheses, far more importance should be given to its evaluation (cf. Graham, 2003), as multicollinearity is typical in complex non-linear geomorphic systems. Using PCs as covariates in the logistic regression allowed keeping all original predictors in the regression and preventing a substantial loss of explanatory power, as reflected very well by the high POF (75%) and low POFD (22%) of our final LR model (Table 4.6) Furthermore, while most (landslide susceptibility) studies treat the relative predictor importance as "by-product" of the logistic regression modelling, our PCLR algorithm (Figure 4.4) has proven to be a powerful tool to identify characteristic synergistic combinations of different rockfall controls with respect to the strength and direction of their association. The PCs' varying predictor loadings (Figure 4.3) efficiently contribute to a better understanding of whether rockfalls are more affected by rock mechanical, paraglacial or topo-climatic characteristics. Admittedly, the geomorphic interpretation of the association between response and predictors is less straightforward and needs a profound systemic knowledge.

To complement the PCLR model and to compensate some constraints in interpretation we applied a second modelling, the decision-tree based random forest algorithm, which is one of the most precise machine learning algorithms. To the authors' knowledge, we are the first to use the RF model for rockfall analyses. Compared to the LR, all validation indices (Table 4.6, Figure 4.6) imply an overall better performance and higher accuracy of the RF when explaining the spatial rockfall pattern in our study area. With respect to the computation time, it is to note that logistic regression training and prediction took 17 seconds on one core while the RF modelling took 15 minutes even on 4 cores. However, the computational complexity of the tree-based classification is compensated by the relatively rapid quantification and interpretation of the predictors' relative importance (Figure 4.6). While the decision-tree based model works more like a "black-box", the PCLR requires a conceptual understanding of the geomorphic system to name and identify the principle components. The RF approach is also highly attractive since it accepts the multicollinearity in our dataset without using PCs, and allows mixing of categorical and metric variables without decoding (Catani et al., 2013). Our study demonstrates therefore the great potential of the RF algorithm for future applications in rockfall research.

Given the coherent results of both models, we conclude that the classical logistic regression can perform comparably with the novel, but often time-consuming and technically challenging machine learning approaches (sensu Brenning, 2005; Vorpahl et al., 2012). However, to achieve reliable results we favour the application of multiple models relying on different degree of systemic knowledge on the geomorphic system. Here, by combining a random forest black-box approach with a strongly knowledge- and theory-based logistic regression of principal components we hope to avoid filtering out anything that we do not expect or do not want to see (Hall, 2006) as well as to argue purely driven by statistics.

4.5.2 Regional-scale controls on rockfall activity

4.5.2.1 The predisposing effect of rock mechanical characteristics

The influence of structural and lithological properties on the regional-scale rockfall activity is poorly studied and largely underestimated, hampered by the prevailing idea of environmental forcing or due to the methodical challenge of spatial extrapolation of geotechnical data. However, the growing availability of high-resolution DEMs and digital geological maps as well as the improvements in GIS and image analyses technology promise considerable advances for regionalisation of structural bedrock characteristics, even in steep mountain terrain (Jaboyedoff et al., 2007; Günther et al., 2012; Matasci et al., 2015). In the hanging valleys of the Turtmann Valley, the lithological and structural control is reflected very well in our results. Despite the dominance of metamorphic rocks, amphibolite and limestone are found to be most sensitive to rockfalls (Figure 4.6H). These findings may seem surprising as their high compressive strength (Selby, 1980; Wyllie and Mah, 2004) and low joint density (Sass, 2005b) would suggest a relatively low erodibility. In the Cantabria Mountains, e.g., Duarte and Marquinez (2002) showed that siliciclastic rocks with a high density of open joints are more affected by rockfalls than limestone of lower joint densities. However, as stated by Fischer (2010), it is often exactly the small-scale transitions between different lithological units that effectively promote failure due to the contrasting hydraulic regimes and stress-strength conditions (Evans and Hungr, 1993).

Table 4.6: *Contingency table for (A) principal component logistic regression model and (B) random forest model. Three verification measures were estimated: Accuracy, Probability of Detection (POD) and Probability of False Detection (POFD).*

(A) PCLR		**Observed**		
		Yes (1)	**No (0)**	**Total**
Predicted	**Yes (1)**	33.71	12.11	45.82
	No (0)	12.36	41.76	54.12
	Total	46.07	53.87	99.94
***Accuracy*=(33.71+41.76)/99.94; *POD* = 33.71/46.07; *POFD*=41.76/53.87**				

(B) RF		**Observed**		
		Yes (1)	**No (0)**	**Total**
Predicted	**Yes (1)**	40.78	6,25	47.03
	No (0)	5.35	47.62	52.97
	Total	46.13	53.87	100
***Accuracy*=(40.78+47.62)/100; *POD* = 40.78/46.13; *POFD*=47.62/53.87**				

We furthermore found a relatively strong relationship between rockfall scars and in-dipping joints Figure 4.6H, I). This also contrasts to common rock mechanical studies (Selby, 1982a; e.g. Moore et al., 2009), identifying cataclinal slopes with surface-parallel joints as more sensitive for instability due to the pre-existence

of sliding planes (Cruden and Hu, 1998). However, failure mechanisms in our study site differ from those in other studies. Resulting from the high compressive strength (e.g. amphibolite) and in-dipping, widely spaced joints, detachment mostly occurs through toppling processes of large blocks, as being reflected in the large and cubic blocks on talus slopes (Figure 4.8A). In contrast, highly weathered paragneiss coupled with cataclinal bedding and high joint densities is linked with surficial flaking off, which is only effective enough to accumulate block slopes of platy, small-size debris, as observable on the southern valley flanks (Figure 4.8B). Compared to topo-climatic and paraglacial variables, the relative contribution of rock mechanical properties to the regional-scale rockfall pattern in the Turtmann Valley was minor. Although the existence of amphibolite and limestone rocks can increase the susceptibility for bedrock failure by a factor of 1.34 times (Table 4.5), this is low relative to the other predictors' impact in the PCLR model. Similar findings were obtained by the RF model, relating joint orientation, lithology and curvature (leading to local stress fields) to the lowest explanatory power (Figure 4.6). However, although our modelling might reveal that rock mechanical properties are currently not the most effective rockfall driver at regional scale, lithology and joint orientation certainly have a major predisposing control, as also shown for catchments in the Eastern Italian Alps (Frattini et al., 2008) and Norway (Böhme et al., 2014). Below, we will further evaluate how the relative contribution of paraglacial and environmental factors is significantly preconditioned by the rockwalls' mechanical properties.

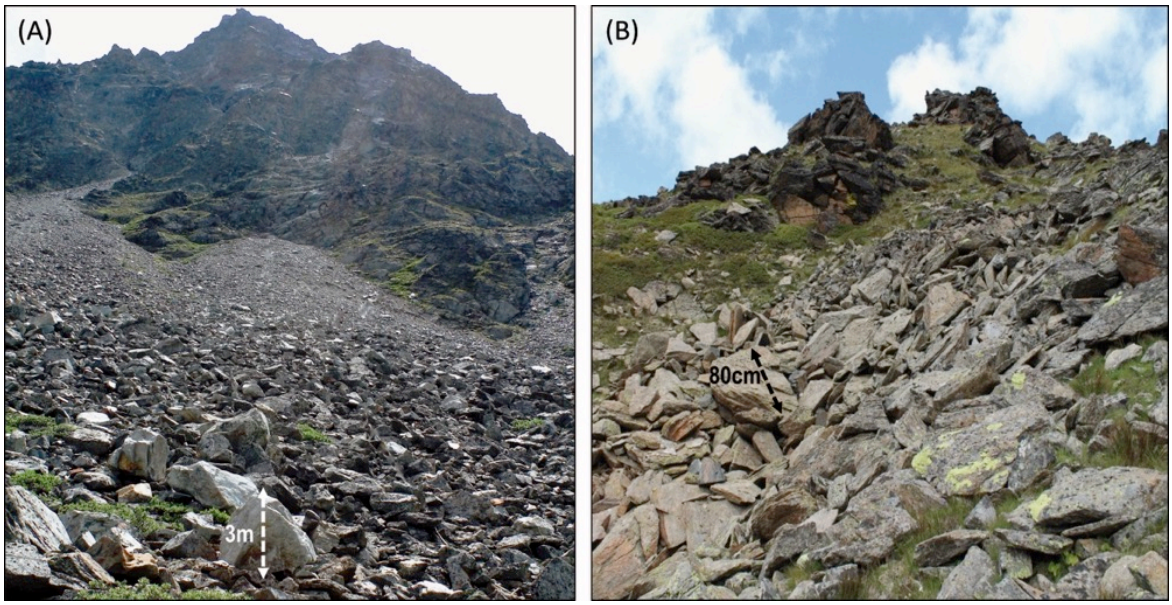

Figure 4.8: *Typical examples for active talus slope deposition along north-exposed rockwalls (A) and mainly inactive, vegetated rockfall deposits along south-exposed rock slopes (mainly outcrops) (B). At north-facing, probably permafrost-affected rockwalls, high compressive strength of amphibolite (and limestone) and in-dipping joint bedding might temporary increase the rock slope stability. However, if rock breakdown e.g. by frost cracking occurs, toppling processes of large block sizes (10-10⁴m³) are supposed to be the major failure mechanism, reflected by the large block sizes (~3m in b-axis) and cubic forms of the talus slope material. At sun-faced slopes, low compressive strength of paragneiss rocks and cataclinal bedding in combination with frequent thermal, but dry cycles mostly result in flaking off of near-surface bedrock (cm-mm). As results, talus slopes are mainly made of small-sized (~80 cm in b.axis) and platy rock material. The lichen cover might reflect the inactivity of rockwall today, however, it is also to note that it might be caused by the warmer climate conditions at the south-exposed slopes.*

4.5.2.2 Paraglacial adjustment processes as system inherent controls

The obvious dominance of rock slope failures in deglaciated mountain geosystems is often causally linked to the disappearance of glaciers (Bovis, 1990; Cossart, 2008; Ballantyne and Stone, 2013). Former glaciation and subsequent deglaciation is assumed to have conditioned mountain rock slopes, rapidly adjusting to a nonglacial equilibrium through enhanced rockfall events (Church and Ryder, 1972; Ballantyne, 2002a). However, compared to non-glacial factors, the specific role of paraglacial bedrock adjustment for both local- and regional-scale rockfall activity is still subject to major uncertainties (McColl, 2012).

Our analyses give strong evidence for a paraglacial forcing on rockwalls in the Turtmann Valley. In the RF model, the time since deglaciation is the second most important predictor (Figure 4.6). A similar explanatory power was detected in the PCLR model, where PC8 (paraglacial adjustment) is the covariate with the third highest odds ratio (Table 4.5). With decreasing time elapsed since deglaciation and increasing elevation, failure susceptibility of bedrock can increase up to 1.29 (PC2) and 1.47 times (PC8), which is comparable to findings from Great Britain (Hinchliffe and Ballantyne, 1999; Curry and Morris, 2004) and Svalbard (André, 1997). The paraglacial bedrock adjustment is reflected very well in the characteristic rockfall pattern showing a significant overrepresentation in the upper basins (Figure 4.5J), where rock slopes have been deglaciated during the last <100 years. In turn, rock faces near the trough shoulders, where deglaciation started earlier ca. 18-12 kyrs ago, might have already worked off the paraglacial signal, given the recent rockfall inactivity there. With respect to the timing of paraglacial rock slope adjustment, the regional-scale activity of rockfalls, shown in Figure 4.5J, appears to confirm the exhaustion model proposed by Cruden and Hu (1998), assuming a rockfall peak immediately after deglaciation and a fast decline (Figure 4.9 curve A). While most large-scale paraglacial studies ignore or avoid possible rock mechanical influences (Ballantyne and Stone, 2013; Ballantyne et al., 2014), our data reveal that the timing and intensity of paraglacial rockfall events might depend on the specific tectonic and geological settings, i.e. on the general SW-dipping of the metamorphic rocks. At a slope scale, the comparatively lower rockfall susceptibility of recently deglaciated south-facing rockwalls (Figure 4.5C) could imply that cataclinal slopes with low compressive strength (e.g. weathered paragneiss) favour a very rapid paraglacial response due to the prompt initiation of pre-existing shear planes. As soon as the weathered rocks are eroded, the slopes may immediately adjust to a non-glacial strength equilibrium (Figure 4.9, curve C). In contrast, it is reasonable to assume that along north-exposed rockwalls, whose stability is temporally increased due to high internal strength of amphibolite and anaclinal bedding opposite to the general SW-oriented tectonic rock layering, rockfalls may start delayed, rather weaker (Figure 4.9, curve B) after deglaciation. As consequence, paraglacial rockfall activity likely diminished more linearly, supporting Cruden and Hu's (1998) idea of a constant frequency (steady state) model.

Today, the process interplay responsible for paraglacial adjustment is still disputed and shows a significant time- and scale-dependence (McColl, 2012). At the scale of individual rock slopes, our modelling analyses do not allow further conclusions on whether glacial unloading of rockwalls and post-glacial debuttressing resulted in relaxation of internal stresses (Evans and Clague, 1994; Augustinus, 1995) and in propagation of stress-release joints parallel to the former glacier contact zone (Lewis, 1954; Bovis, 1990; Hencher et al., 2011).

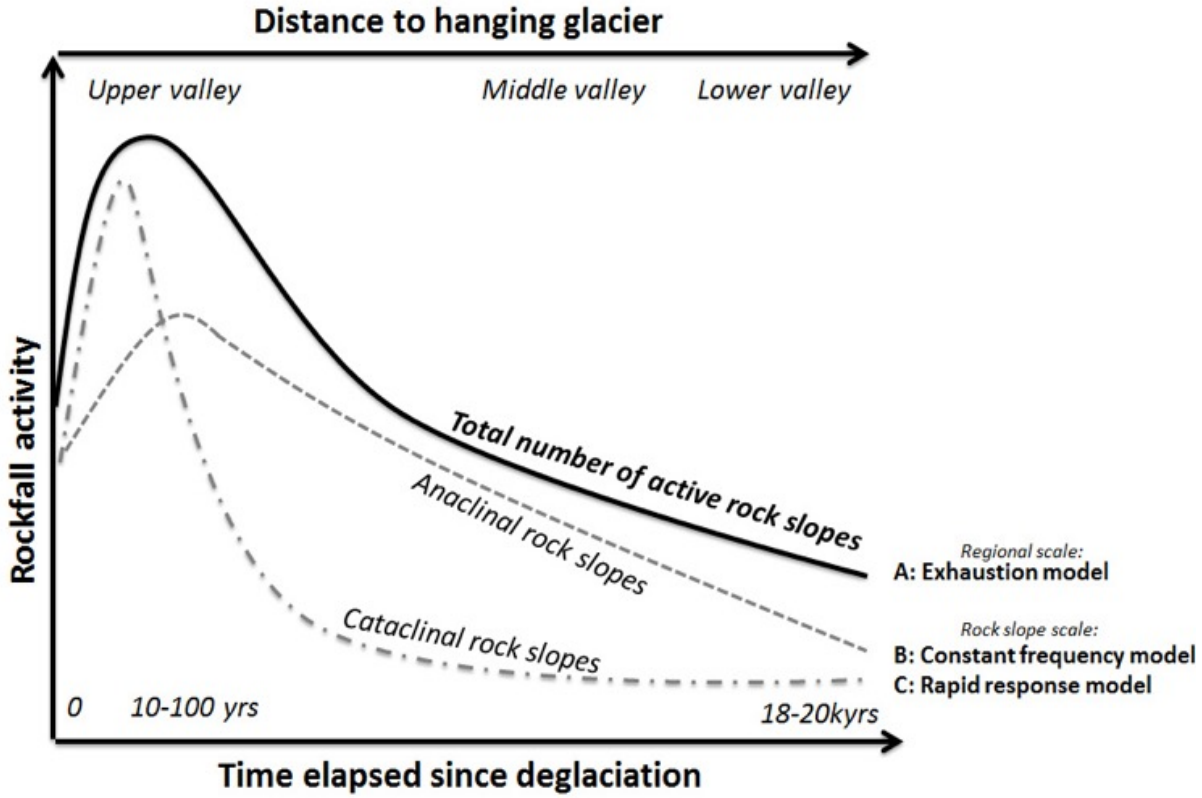

Figure 4.9: *Possible models for the timing of paraglacial rockfall activity in the Turtmann Valley referring to Ballantyne and Stone (2013, p. 151). Depending on the spatial scale (regional scale vs. individual slope scale) and rock mechanical settings with respect to slope aspect, paraglacial bedrock instability may evolve rapidly or more linearly from glacial to non-glacial conditions. For explanation, see text.*

Yet at larger scales, the obvious higher rockfall activity detected at nearly vertical slopes (> 60°, Figure 4.5B) appears to support the hypothesis that glacial over-steepening relative to the internal rock mass strength is a major paraglacial driver in our study area (Augustinus, 1992; Leith et al., 2014b). Furthermore, glacio-isostatic rebound might be plausible for landslides clustering over large geographic areas, as calculated by Feuillet et al. (2014) and Cossart et al. (2014) for northern Iceland, but can likely be precluded here. Post-glacial uplift of hanging valleys is probably not variable enough to produce the heterogeneous rockfall pattern or is likely overlain by the large-scale uplift of the Rhone valley (0.2-1.6 mm/a Gudmundsson, 1994; Schlunegger and Hinderer, 2001). Instead, paraglacial rockwall adjustment appears to be strongly related to warming and thawing of permafrost, given the obvious dominance of rockfall scars within a low-solar elevation belt between 2900-3300 m (Figure 4.5A, D), consistent with the regional permafrost distribution (Nyenhuis, 2005). In findings from the Southern Alps of New Zealand (e.g. Davies et al., 2001; Hales and Roering, 2007; e.g. Allen et al., 2009), glacier retreat after LGM was probably accompanied by a gradual rise of the lower permafrost level and, concurrently, of the frost cracking window; even though this may not be necessarily true for S-facing slopes. According to calculations by Hales and Roering (2009), a temperature drop of 4 °C, consistent with possible climatic conditions during LGM in the New Zealand Alps, would lead to 500 m lowering of the zone, where warming and thawing of permafrost effectively promote changes in internal rock shear strength and water pressure (Krautblatter et al., 2013). This could explain the former rockfall activity of the vegetated

hillslopes near the trough shoulders (Figure 4.5J, B). Therefore, when evaluating the causality between climate change, permafrost degradation and rockfalls, the rock mass' memory effect must be considered, as slope instability is often a delayed response to paraglacial forcing on rock mechanical and thermal systems (Krautblatter and Moore, 2014).

4.5.2.3 Topo-climatic forcing on permafrost rockwalls

For the last two decades, a significant correlation of warm periods and intensified episodes of rock slope failures is found in the European Alps (Ravanel and Deline, 2015) and in the New Zealand Alps (Allen and Huggel, 2013). This trend is often associated with warming and thawing of bedrock permafrost, due to its high sensitivity to past and ongoing atmospheric warming (Gruber and Haeberli, 2007; Huggel et al., 2012). During the 20th century, the mean annual temperature of mid-latitude Alpine settings has increased by more than 1 °C, especially since the Little Ice Age. For 2055, a warming of 2-3 °C (B1 global environmental scenario) or 3-4 °C (A1FI global economic scenario) is projected in comparison with the recorded 20th century average (Nogués-Bravo et al., 2007). In the Turtmann Valley, the regional permafrost distribution was detected to be the most important factor controlling the spatial rockfall activity, indicated by the RF model (Figure 4.6) as well as by the high ODs of PC1 and PC3 in the PCLR (Table 4.5). More than two thirds of rockfall source areas lie within a uniform altitudinal belt at ca. 2900-3300 m asl, immediately above the predicted lower permafrost boundary (Figure 4.5). In this zone, frozen bedrock plays a decisive role for slope stability, because changes of its thermal and hydrostatic state can significantly promote rockfalls (Krautblatter et al., 2013). Seasonal and multiannual freezing and thawing can lead to intense bedrock fracturing (Matsuoka and Murton, 2008), warming of subsurface temperatures may reduce the shear strength of ice-bonded discontinuities (Davies et al., 2001) and water seepage from melting permafrost bodies can increase hydrostatic pressures (Gruber and Haeberli, 2007; Krautblatter and Hauck, 2007). Our findings are consistent with studies from the European Alps (Sass, 2005b; Ravanel and Deline, 2011; Fischer et al., 2012), observing a similar altitudinal clustering of rockfall scars in a zonal window, where freeze-thaw cycles are highly effective. Assuming the existence of permafrost in our study area, it might be reasonable to infer that seasonal ice segregation in near-surface permafrost is one of the primary rock breakdown mechanisms in the hanging valleys. The bi-directional freezing progress over a period of several months and penetrates to depth of several meters (Hallet et al., 1991; Murton et al., 2006). This slow formation of segregation ice results in progressive fracture of the upper permafrost layer and the base of the active layer promoting rockfalls of low frequency, but of block sizes of decimeters to several meters in diameter. Even though data on frost cycles are missing in our study area, our assumption seems to be supported by field observations of the talus material along the permafrost-affected rock slopes (Figure 4.8A).

The obvious dominance of large block sizes might reflect the activity of large magnitude toppling events, which needs to be prepared by annual or decadal frost cycles with meter-scale freezing (Matsuoka and Murton, 2008). In contrast, rock fragments resulting from high-frequency diurnal frost cycles affecting the outermost decimeters of bedrock tend to be much smaller and are found primarily near the apex of the talus slopes. Following Hales and Roering (2007; 2009), the regional-sale cracking intensity of segregation ice is likely highest in a rock temperature window between -3 and -8 °C, provided that water is available in the system, e.g.

from the surface or from the active layer of permafrost. However, recent field studies of frost cracking inferred from acoustic emissions in natural Alpine rockwalls reveal slightly different temperature ranges. For instance, Amitrano et al. (2012) reported a rising of rock damage between 0 °C and -5 °C (granitic gneisses), while Girard et al. (2013) found frost cracking events occurring over the full range of temperatures from 0 °C down to −15 °C (crystalline rock). These field findings reveal that transferring the theoretical and laboratory-based frost cracking window concept (Walder and Hallet, 1985) to natural conditions is not trivial due to the mechanical and hydrological heterogeneity of bedrock. This is particularly the case when trying to upscale the frost cracking to larger spatial scales, where the relative importance of bedrock characteristics is difficult to evaluate or is simply underestimated. However, based on the datasets presented in this study, we cannot quantify the role of seasonal ice segregation opposite to other weathering processes such as daily frost action of the bedrock near-surface or thermal fatigue. To test our initial hypothesis that ice segregation is a major key driver for rockfall events, field data of bedrock temperature are needed in upcoming research to evaluate the penetration depth and timing of freeze-thaw cycles at the regional scale.

Furthermore, the PCs of the LR model provide insights into the strength and direction of the interaction between bedrock permafrost and other factors governing rockfall activity. For instance, the factor loadings in PC3 (Table 4.5) support the notion that permafrost degradation through lateral heat fluxes is efficiently accelerated along convex topography, which is well exposed to high incoming solar radiation (Ravanel and Deline, 2011). However, the relative contribution of micro-scale bedrock roughness and curvature for the large-scale rockfall pattern in the Turtmann Valley was classified to be small (Figure 4.5) contrary to the important role of overall valley topography. Permafrost-related rockfalls seem to be promoted most by steep terrain (up to 2.94 times, Table 4.5) linked to the higher shear stresses (Wyllie and Mah, 2004) and to the shorter penetration distance of the warming signal into the interior of the rock mass (Noetzli and Gruber, 2009). The critical slope threshold for failure of permafrost-affected bedrock was found to be > 40° (Figure 4.5B), typical for Alpine rockfall events (Noetzli et al., 2003). Furthermore, our results expose an aspect-driven rockfall activity. South-facing slopes show a decrease in rockfall activity. These slopes are characterised by higher solar radiation input and increased surface temperatures that increase the permafrost limit significantly compared to north-facing slopes (Table 4.3, PC3). Between N- and S-orientations, significant differences in mean annual rock surface temperature of up to 6 °C and in moisture supply are likely, as found by Coutard and Francou (1989) and Sass (2005a). The consequences for frost weathering intensity (Hales and Roering, 2007) and resulting rockfall size and shape (Matsuoka, 2001b; Hall and Thorn, 2011) are observable in the hanging valleys (Fiure 4.8). Although temperature fluctuations around 0 °C are probably highest at S-slopes, these dry thermal cycles might be only effective to weaken the outermost decimeter of bedrock, leading to the flaking off of small rock fragments (Hall and André, 2001; Prick, 2003). In contrast, seasonal freezing might advance much more slowly, but deeper along north-facing rockwalls up to several meters, significantly enhanced by the bi-directional moisture supply (Sass, 2005b; Murton et al., 2006; Matsuoka and Murton, 2008). Consequently, rockfalls predominantly are expected to occur as large-magnitude, seasonal toppling events (Figure 4.8A).

Our study gives therefore evidence that the dependence of rockfall activity on aspect is probably not exclusively climatic, but rock mechanically predefined. Along north-facing slopes, in-dipping joints may favor

moisture retention within the bedrock and allow subsurface advective heat fluxes to penetrate much faster and deeper through running melt water (Hasler et al., 2011a; Hasler et al., 2011b). Besides predefining the block size and shape, the joint orientation with respect to aspect might significantly control the development of thaw corridors in permafrost and the efficiency of freeze-thaw cycles (Gruber and Haeberli, 2007). Therefore, our modeling results reveal that the influence of permafrost on rock slope stability can never be studied decoupled from other interacting factors, as its thermal and mechanical behaviour is considerably governed by the overall valley topography as well as small-scale morphometric and rock mechanical properties.

4.6 Perspectives

Coming back to Harrison (2001) stating that the relative role of rockfall controls can change with increasing scale due to emergent and complex system behaviour, leads us to the questions: "Would the findings of this study have been significantly different at the local scale?" And moreover, "would the key rockfall controls identified in our study area contrast with other mountain environments? To examine these questions further research is needed in future. As each level requires its own scientific explanation, we cannot simply upscale local-scale knowledge and, in turn, we cannot downscale the regional-scale knowledge obtained from this study to smaller phenomena. Thus, we hereby appeal to enlarge the research activities at each geomorphic scale. There is a need for both deductive studies to improve the mechanistic understanding of slope stability with respect to climate change and research at larger geomorphic scales; even if the latter may be associated to more narrative and abductive reasoning. A final goal must be an upscaling causation linking the local-scale rockfall controls to regional-scale conditions. Considering that the regional-scale importance of paraglacial and rock mechanical factors has been probably underestimated far too long, there is a particular need to consider more intensely those parameters in future geomorphic research. Here, we specifically aim to stress the great potential of the random forest algorithm for novel applications in studying complex, collinear geomorphic system behaviour. Ideally, the classification results need to be tested against a method, which is not so much a black-box like the RF and which gives additional information on the strength of association between the interacting factors, such as a classical logistic regression using principal components. To overcome some sources of uncertainties, forthcoming work will comprise the validation of the lower permafrost boundary adjusted to the steep terrain and bedrock anisotropy by local field surveys. Similarly, local data of bedrock temperature are needed for more insight into the regional-scale intensity of frost cracking and its effective depth for rock breakdown.

As a future step, it is desirable to test both our methods and the corresponding predictor variables in other mountain valleys where permafrost degradation and glacier retreat is dominant. Particularly in environments with vulnerable settlements and tourist infrastructure, using the approach developed in our study allows a relatively simple and time-efficient prediction of rockwalls most vulnerable to rockfall initiation. This in turn can be used as a key basis of information for regional hazard mitigation and sediment management in cold mountain regions that face ongoing atmospheric warming.

4.7 Conclusion

Rockfalls are among the most hazardous natural hazards and represent a first-order geomorphic agent in the sediment cascade of cold-mountain geosystems. Detailed knowledge on the critical factors controlling rockfalls is important for geomorphologists, engineers and decision makers. While most effort is obtained locally, the relative importance of potential rockfall controls at regional scales is still poorly understood. To bring further insight into the debate whether regional-scale rockfall activity is driven by (a) topo-climatic, (b) paraglacial (c) or rock mechanical factors, we designed a new spatial modelling approach using an inventory of 220 talus slopes in the Turtmann Valley (Swiss Alps). In this study, the classification-tree based random forest algorithm by Breiman (2001) was applied for the first time for a rockfall-related purpose and combined with a classical logistic regression model using principal components. Major findings are:

a) The regional permafrost distribution was identified as the major control on the spatial rockfall activity. The clustering of rockfall source areas within a low-radiation altitudinal belt at 2900-3300 m asl, consistent to the modelled permafrost probability of > 90%, suggests that seasonal ice segregation growth in the near-surface permafrost might be one of the key rock breakdown mechanism. However, the relative contribution of permafrost strongly depends on a complex interaction with small-scale bedrock morphometry and overall valley topography. Permafrost-affected rockfalls were found to be linked to convex, steep terrain (> 40°) and north-facing valley flanks, promoting surficial moisture supply and subsurface lateral heat fluxes.

b) The paraglacial adjustment of rock slopes to the LGM glaciation and subsequent deglaciation was modelled to be the second most critical variable. Using ergodic reasoning, we detected an increasing rockfall probability with decreasing time since bedrock deglaciation. Besides glacially induced slope oversteepening relative to the specific rock mass strength, the gradual altitudinal rise of the frost cracking window during postglacial permafrost degradation is supposed to be the major large-scale paraglacial driver

c) The relative importance of rock mechanical properties for the regional-scale rockfall pattern was shown to be subdued compared to topo-climatic and paraglacial factors. Nevertheless, we proposed different hypothetical models, where the timing and intensity of paraglacial rockwall adjustment might evolve either exponentially or more linearly after LGM, dependent on the rock mass strength and the tectonically-derived dip direction of joints.

Therefore, our study emphasises that periglacial rockfalls cannot be mono-causally explained as they result from a complex synergistic interplay of topo-climatic, paraglacial and rock mechanical factors at different spatial and temporal scales. When evaluating bedrock instabilities with respect to past and recent deglaciation and permafrost degradation, our study demonstrates that it is never only the influence of changing climatic conditions, but rather the dependence on the topography and the structural geology of mountain valleys as well as the rock mass' memory effect on paraglacial forcing.

Acknowledgements

We greatly appreciate the funding provided by the British Society for Geomorphology, the Humboldt-Ritter-Penck Foundation by the Gesellschaft für Erdkunde zu Berlin and the AK Geomorphologie. Furthermore, we thank Carina Schmitz for fruitful discussions on paraglacial geomorphology and her comments on the manuscript. We highly appreciate the previous achievements of the Research Training Group 437 – Landform, a structured and variable boundary layer at the Department of Geography, University (Otto and Dikau, 2010), especially Michael Nyenhuis for providing the permafrost modelling data. Finally, we would like to thank Sam McColl, Oliver Sass and the anonymous reviewer as well as the editors David Morche and, especially, Adrian Michael Harvey for their very constructive reviews that have significantly contributed to improve the manuscript.

----- BLANK -----

Chapter 5

STUDY II - VALLEY-SCALE SEDIMENT STORAGE AND CONNECTIVITY IN ROCKFALL-DOMINATED, HIGH-ALPINE SYSTEMS

This chapter is based on the published journal article: Messenzehl, K., Hoffmann, T., Dikau, R. (2014): Sediment connectivity in the high-alpine valley of Val Müschauns, Swiss National Park - linking geomorphic field mapping with geomorphometric modelling. In: Geomorphology 221: 215-229. DOI: 10.1016/j.geomorph.2014.05.033.

Abstract

The efficiency of sediment routing through mountain sediment cascades is controlled by the connectivity of hillslopes to the main river system. A lack of connectivity may cause long-term sediment storage and exclude large fractions of a basin from the sediment flux system for several thousand years. Here, we studied sediment transfer dynamics in a small, formerly glaciated valley in the Swiss Alps. To characterise the sediment connectivity to the stream, we calculated a morphometric index using a GIS algorithm. The modelling results were tested against a field based geomorphic mapping of topological hillslope sequences of sediment storages, which were evaluated with respect to their state of (de)coupling. In accordance to the field diagnostics, the modelling results indicate very well that the present-day sediment flux is conditioned by the glacial valley morphometry inherited through Pleistocene glaciation. Especially in the upper hanging valleys, the connectivity index is reduced noticeably due to the glacial cirque morphology. Based on the field based mapping, 30% of the hillslope sediment cascades are interrupted and 20% of the storage boundaries are currently affected by a lack of material transfer. As a consequence, ~29% of the basin surface is currently disconnected from the main river. Nevertheless, the GIS algorithm overestimates the connectivity within the basin, because it fails to calculate decoupling between neighbouring pixels in digital terrain models (DTM). Around 35% of the basin surface, which has been mapped in the field as being decoupled, is related to relative high connectivity. Our study highlights the potential of morphometric GIS modelling for studying sediment connectivity, but additionally emphasises the indispensability of geomorphic field mapping for a holistic understanding of mountain cascading systems.

5.1 Introduction

Mountain environments are characterised by some of the highest erosion rates on earth (Walling and Webb, 1996; Hinderer, 2001). This erosional activity is related to the nature of mountain geosystems including high their relief, steep slopes, low temperatures, thin vegetation cover and increased precipitation amounts compared to low terrains (Caine, 1974; Barsch and Caine, 1984; Owens and Slaymaker, 2004). Globally, mountains are therefore regarded as one of the main sediment sources for lowlands and oceans (Milliman and Syvitski, 1992).

However, most mountain valleys are affected by an imbalance between the local erosion rates and the sediment yields measured at the basin outlet (Walling, 1983; Church and Slaymaker, 1989), as the sediment transfer is attenuated by sediment storage and subsequent reworking (Dietrich and Dunne, 1978; Caine, 1986; Phillips, 2003a; Straumann and Korup, 2009; Tunnicliffe and Church, 2011). Thus, mountain basins can be considered as cascading systems (Chorley and Kennedy, 1971; Caine, 1974; Burt and Allison, 2010). Once sediment is detached from steep, weathered rock cliffs, it is being conveyed downslope by different geomorphic processes along topological sequences of neighbouring storage compartments including talus slopes, debris cones and alluvial plains, until it will finally be exported to the stream network (Schrott et al., 2002; 2003; Church, 2010).

The rate of sediment transport, storage and reworking in sediment cascades is controlled by the strength of coupling between neighbouring storages on hillslope and the connectivity to the stream channel (Caine and Swanson, 1989; Harvey, 2001; 2002; Brierley et al., 2006; Fryirs, 2013). Coupling results from the physical linkage of adjacent sediment stores as well as from the sediment transfer across their separating boundary by different geomorphic processes (Schrott et al., 2003; Faulkner, 2008; Jain and Tandon, 2010; Wainwright et al., 2011). Those coupling mechanisms are related to varying spatio-temporal activity, e.g. frequent small-scale rockfalls, episodic high-magnitude debris flows or periodic snow avalanches. In contrast, connectivity denotes the potential that sediment is routed from the hillslope system to the basin outlet (sensu Hooke, 2003; Brierley et al., 2006). While the coupling term is generally used to describe the relationship between local scale landforms or compartments, connectivity is frequently used as a system property on a meso- (> 10 km^2) and macro-scale (> 1000 km^2) (Harvey, 2001; Faulkner, 2008; Heckmann and Schwanghart, 2013).

Therefore, the discrepancy between catchment erosion and sediment yield at a valley's outlet can be attributed to a temporary lack of lateral (hillslope-channel) and longitudinal (within a channel) sediment exchange between neighbouring storages (Lexartza-Artza and Wainwright, 2009) as well as to a single landform or sediment storage interrupting the sediment pathway (Fryirs, 2013). On the basin scale, the integral effect of storage decoupling may go along with disconnectivity of the hillslopes to the main river system (Heckmann and Schwanghart, 2013). Referring to Fryirs et al. (2007), key drivers influencing the sediment conveyance on hillslope are local-scale buffers like outcropping rocks or sediment storages themselves such as vegetated talus slopes, moraine deposits as well as debris fans and alluvial plains acting as areas of low transport capacity or breaks within the sediment cascade (Harvey, 2010, 2012). On a larger scale, the often glacially inherited valley geomorphometry, i.e. the valley cross profile or the existence of stepped longitudinal profile, might remarkably affect the connectivity of the hillslopes to the stream channel (Brardinoni and Hassan, 2006; Cavalli et al., 2013; Kuo and Brierley, 2013; Hoffmann et al., 2014a). These catchment specific factors may generate sediment storages with residence times ranging from minutes (e.g. covering single flood and debris flow events) to thousands of years (Dietrich and Dunne, 1978; Harvey, 2002). In the Turtmann valley (Swiss Alps), for instance, Otto et al. (2009) examined that 60% of the sediment deposited since deglaciation is presently still stored within the hanging valleys (typically < 10 km^2) due to their characteristic, glacially shaped topography; this is in agreement with studies in headwater basins in the Canadian Rockies (Hoffmann et al., 2014a). From this, we state that only a fraction of the sediment recently stored within mountain headwater basins will make

its way to the outlet and will contribute to the sediment flux system due to a low degree of geomorphic coupling and connectivity.

Since the seminal work by Caine and Swanson (1989), numerous studies in contrasting environments have recognised the major relevance of geomorphic coupling and connectivity for i) sediment budget studies (e.g. Smith and Dragovich, 2008; Warburton, 2010), ii) the explanation of changes of channel morphology (e.g. Montgomery and Buffington, 1997; Chiverrell et al., 2009; Harvey, 2012) and of iii) river ecology (e.g. Sandercock and Hooke, 2011) as well as iv) for the estimation of a system's sensitivity towards changes of land use, tectonic or climate (e.g. Brunsden and Thornes, 1979; Brunsden, 2001; Harvey, 2001; Cossart, 2008). Mountain sediment cascades have been studied by a number of various methods, each with different purposes: For instance, the volume of sediment storage landforms is commonly quantified using geophysical surveys (e.g. Schrott et al., 2002), core drillings (e.g. Götz et al., 2013) and morphometric GIS approaches (Moore et al., 2009; Tunnicliffe and Church, 2011; Hoffmann et al., 2014a). The process rates and geomorphic activity of sediment erosion and transfer processes are quantified by topographic change detection based on photogrammetry (e.g. Schrott et al., 2006; Schlunegger et al., 2009) or repeated airborne and terrestrial laser scanning (e.g. Morche et al., 2008; Carrivick et al., 2013) as well as by using cosmogenic nuclides (e.g. von Blanckenburg, 2006) and dendrogeomorphic methods (e.g. Savi et al., 2013). In contrast, geomorphic field mapping provides a holistic cartographic description and analysis of sediment transfer pathways, the spatial configuration of storage compartments and the state of coupling and connectivity (e.g. Cossart, 2008; Schlunegger et al., 2009; Theler et al., 2010; Beel et al., 2011). In the last few years, an upcoming interest in remote sensing and GIS techniques is noticeable in the study of geomorphic cascading systems (e.g. Borselli et al., 2008; Wichmann et al., 2009; Sougnez et al., 2011; Thiel et al., 2011; Cavalli et al., 2013; Heckmann and Schwanghart, 2013; López-Vicente et al., 2013; Heckmann et al., 2014). Heckmann and Schwanghart (2013), for instance, applied mathematical graph theory to analyse the geomorphic coupling between adjacent landforms through rockfalls, debris flows and fluvial processes in an alpine valley. In the context of soil erosion in lowlands, Borselli et al. (2008) proposed a connectivity index (*IC*) based on digital terrain models (DTMs). Cavalli et al. (2013) adapted the *IC* for studying mountain regions, where small-scale topography is a major control on sediment conveyance. These recent methodical developments in geomorphology have been commented by Bishop et al. (2012: 5) claiming that new "geocomputational algorithms and approaches now permit Earth scientists to go far beyond the traditional mapping". However, the question arises whether GIS approaches, such as the DTM based connectivity index by Cavalli et al. (2013), are able to sufficiently explain the complex nature of mountain sediment cascades and whether quantitative GIS techniques are able to replace the expert knowledge and ability of experienced geomorphologist to recognise contingent patterns of geomorphic forms, processes and near surface sediments, which are typical for heterogeneous mountain environments (Hoffmann et al., 2014b). We state that without field based diagnostics, morphometric GIS modelling approaches might insufficiently explain the sediment connectivity in mountain catchments.

To characterise the present-day pattern of sediment connectivity in formerly glaciated headwater valleys and to test the value of traditional geomorphic field mapping, we studied the sediment dynamics in the small, de-glaciated alpine valley Val Müschauns (6.2 km^2) in the Swiss Alps. We combined i) geomorphic field mapping and the analysis of topological storage sequences (toposequences) with ii) a morphometric GIS modelling of

the connectivity index by Cavalli et al. (2013). The objectives of this study are, first, to evaluate the morphometric GIS modelling results against the field based geomorphic map, second, to decipher key controls on the present-day sediment flux in a small, de-glaciated mountain valley and third, to address the question of whether traditional geomorphic field maps have become indispensable today when studying mountain cascading systems.

5.2 Toposequences as concept for studying mountain sediment cascades

Sediment storages such as talus slopes, debris cones and alluvial plains are often arranged in a nested hierarchy, or palimpsest as stated by Chorley et al. (1984), displaying neighbouring and overlapping structures of different age and different genesis (Brunsden, 1996; Dikau, 1996, 2006; Otto, 2006). This complex spatial organisation impedes the understanding of mountain sediment cascades. To address this challenge, Dikau (1996), MacMillan and Shary (2009) and Evans (2012) proposed a systematic classification and segmentation of hillslope sequences, which subdivide this complex spatial pattern into homogeneous, neighbouring sediment storage

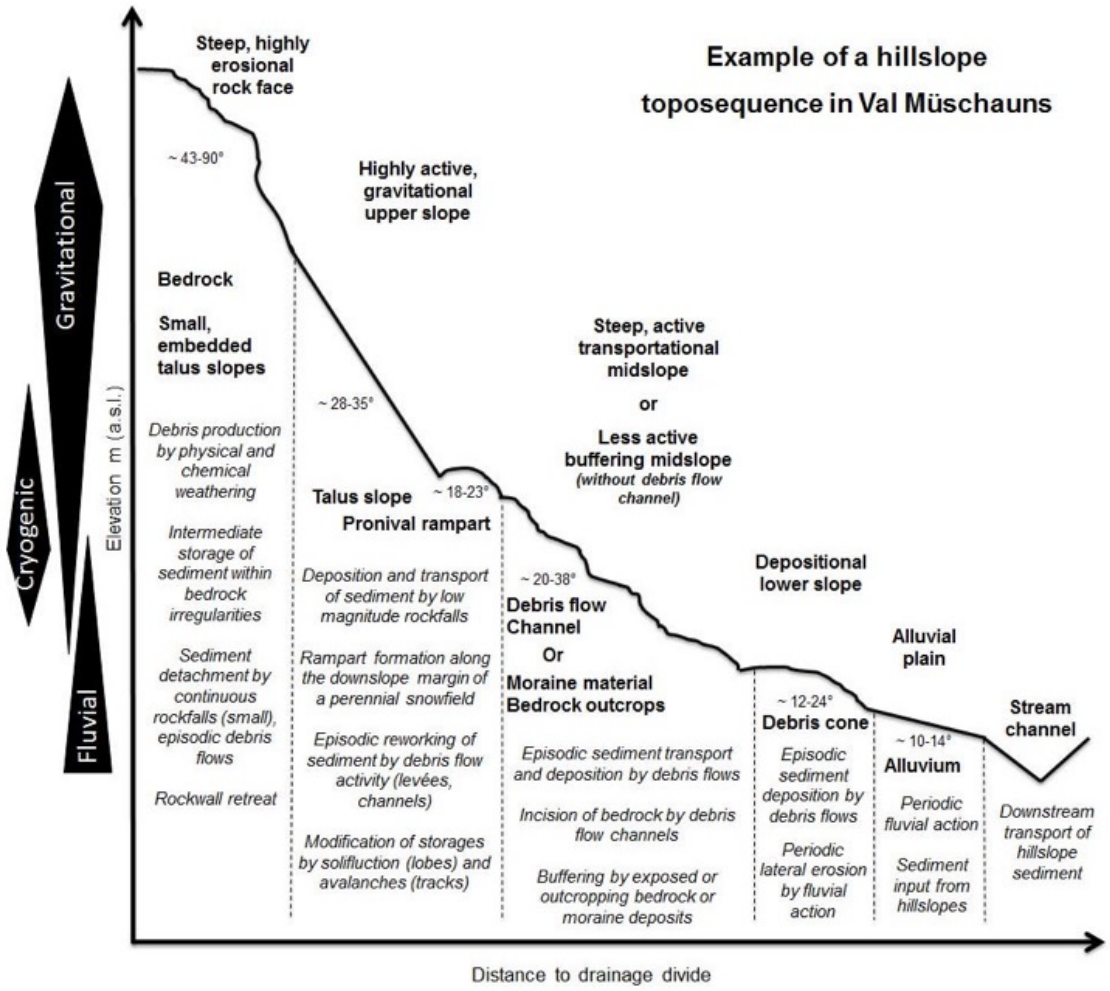

Figure 5.1: *A typical toposequence in mountain valleys. Each hillslope segment between the local divide and the valley bottom is related to specific geomorphometric attributes, geomorphic processes and depositional landforms (graphical illustration based on Dalrymple et al., 1968; Conacher and Dalrymple, 1977; Slaymaker, 1993).*

units. Originally derived from the soil science, the concept of toposequences permits to conceptualise hillslope sediment cascades as individual sequences of sediment storage units between drainage divide and stream channel (Dikau, 1993; Schmidt and Dikau, 1999). Based on the principle of the soil catena (Milne, 1935), toposequences segments a hillslope between the local divide and the valley bottom into homogeneous terrain units (Figure 5.1) each related to specific geomorphometric attributes, geomorphic processes and depositional landforms, vegetation cover and soil properties (sensu Rasemann, 2004; Francke et al., 2008). Therefore, the application of the toposequence approach is not exclusively restricted to soil properties, but can also involve objects of uniform morphometry and process domains such as sediment storage landforms (Francke et al., 2008).

Several models of toposequences have been developed (e.g. Speight, 1974; Ruhe and Walker, 1986; Pennock et al., 1987; Speight, 1990; see also summery in Ventura and Irvin, 2000). One of the key concepts applied in a geomorphic context was presented by Conacher and Dalrymple (1977) and Dalrymple et al. (1968). They divided a hillslope into nine units, each of which is related to specific geomorphic processes of water and sediment transfer, e.g., soil creep, rockfalls and slumps (see illustration in Goudie, 2004, p. 520). Based on the key ideas of the toposequence concept, the topological delineation of sediment cascades into neighbouring storage units is recently performed quantitatively based on DTMs using available GIS routines (Dikau, 1993; Schmidt and Hewitt, 2004; MacMillan and Shary, 2009; Evans, 2012). Schmidt and Dikau (1999), identified representative geomorphometric parameters including slope angle, altitude, curvature and distances to drainage divide in order define landforms. Rasemann (2004) extracted different types of toposequences from a DTM using specific geomorphometric attributes along hillslope transects and applying flow routing algorithms. Otto et al. (2009) successfully determined various toposequence types consisting of neighbouring sediment storages by a semi-quantitative procedure that is based on field observations and geomorphometric derivatives of the DTM.

The delineation of toposequences, both automatically and manually, may have a high potential in the analysis of mountain cascading systems. Each topological succession of sediment storages may represent a potential sediment routing trajectory from valley crest to the stream channel. Additionally, the toposequence concept may provide a valuable tool to evaluate the (de)coupling relationships of hillslope sediment cascades and, finally as integral effect, the connectivity to the main river system. With respect to the concept by Lexartza-Artza and Wainwright (2009) and Wainwright et al. (2011) toposequences may help to explain the structural and functional connectivity in mountain catchments. Both the potential coupling of adjacent, physically linked storage units (= structural) as well as coupling through de-facto sediment transfer by geomorphic processes (= functional) can be analysed based on the topological sequences along altitudinal gradients.

5.3 Study site

The study site Val Müschauns is part of the Swiss National Park (SNP), which is located in the Engadine region in Switzerland's easternmost canton Graubünden (Figure 5.2A). Covering an area of around 170 km², the park

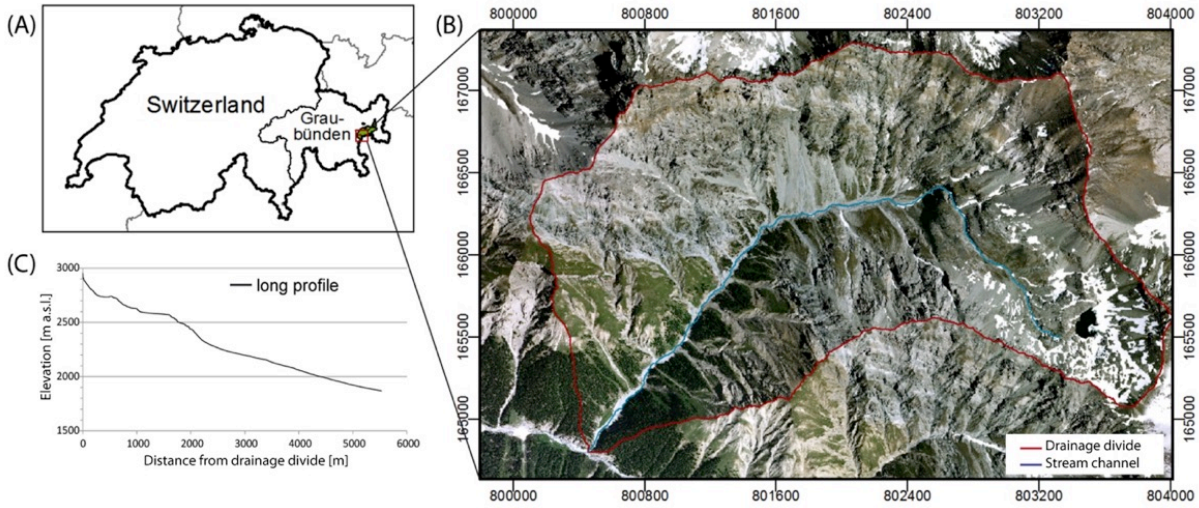

Figure 5.2: *Location of the study site in Switzerland's easternmost canton Graubünden (A) and aerial photograph (© GoogleEarth 2012) of the basin of Val Müschauns (B). Pleistocene glacial erosion exerted a strong influence on the valley'smorphology demonstrated by the glacial cirque morphology of the two hanging valleys in the upper basin. The long profile of the catchment (C), provided by A. Schoch in 2013, reflects a visibly stepped topography, which is characteristic for formerly glaciated mountainous basins.*

is the largest protected region of Switzerland today. Val Müschauns is a formerly glaciated valley located in the SW of the SNP (Figure 5.2B). The 6.2 km² large basin is drained by the Ova dal Müschauns, which is a tributary of the Ova da Trupchun, one of the park's major streams. The elevation ranges from 1869 m (basin outlet) to 3154 m (Piz Quattervals) above sea level (asl). The catchment is characterised by a striking change in orientation primarily controlled by the geological setting. While the lower basin has a NE-SW orientation, the upper valley is basically oriented E-W.

As a part of the Upper Austroalpine nappe, the SNP is situated in the Engadine Dolomites. The dominating lithology of this region is made up of relatively brittle rock with a high susceptibility to weathering and erosion (Laphart, 1992). The lithology of the study area is principally composed of two different Triassic

Figure 5.3: *Upper hanging valleys of Val Müschauns with typical glacial cirque morphology. The extensive alluvial valley plain in the foreground and the elongated bedrock slopes in the background noticeably reduce the overall sediment connectivity to the main river system. The bedrock step of the glacial cirque (arrow) decouples the sediment deposited in the uppermost hanging valley from the sediment flux system of the lower catchment area.*

nappes, which have been obducted along the E-W-oriented thrust-fold. The Ortler nappe in the lower basin is dominated by grey stratified, partly siliceous limestone with intercalated layers of marl und breccia. In contrast, grey-banked dolomites of the Scharl nappe with limestone and shale intrusions built up the upper valley (Trümpy et al., 1997).

Figure 5.4: *Middle basin of Val Müschauns. Talus slopes and hillslope debris flows are well coupled with the stream network indicated by intense lateral erosion of footslopes. Failure of accumulated debris cones by reworking may provide short-term and intense inputs of hillslope sediments to the river channel (photograph by T. Müller in 2012).*

During Pleistocene, glacial erosion exerted a strong influence on the valley's morphology demonstrated by the present-day mountainous character of Val Müschauns. While the lower valley has a characteristic V-shaped cross section, the middle part gradually broadens to a typical glacial trough with concave slope profiles. The upper basin consists of two hanging valleys characterised by glacial cirque morphology with concave slopes and wide floors. Thus, the long profile is visibly stepped (Figure 5.2C, Figure 5.3). In the uppermost hanging valley, the lake Lai Müschauns is located in the overdeepened basin of the relict glacial cirque, which is bounded upstream by a distinct bedrock step (Figure 5.3).

Today, Val Müschauns is ice-free and hosts a variety of high-alpine geomorphic processes and landforms largely undisturbed by human influences. Low-magnitude rockfall events frequently occur in middle basin and in the hanging valleys (see also Hartmann-Brenner, 1974). Debris flows are very active throughout the catchment (Figure 5.4), transporting talus sediments or deeply incising bedrock channels. Debris cones with large boulders are ubiquitous features along both sides of the thalweg (see also Stolz and Huggel, 2008). Cryogenic processes are active in higher altitudes above 2400 m asl (Trümpy et al., 1997). In sheltered positions, small amounts of sparsely vegetated moraine deposits are still preserved, but show signs of reworking through cryogenic creep. At the valley bottom, highly dynamic fluvial processes result in frequent lateral erosion of footslopes.

The climate of the study area is continental with a low mean annual precipitation of 680-800 mm/year and a mean annual air temperature of 1.3-5.3 °C (MeteoSwiss, 2013). Governed by the topography, the climatic

setting leads to typical vertical vegetation zoning in Val Müschauns. Below ca. 2200 m asl (subalpine zone), hillslopes are covered by relatively dense forest (e.g. *Pinus, Larix, Picea*). Above ca. 2200 m asl, grasses and low-growing shrubs dominate the alpine zone. Above ca. 2600 m asl (nival zone), where permafrost is assumed to occur, vegetation is reduced to scattered pioneer plants and lichens (Eck, 1994).

The high-alpine valley Val Müschauns is ideally suited to study mountain sediment cascades since it is located in the Swiss National Park and human impact can be neglected as a control on sediment dynamics. It hosts many landform features and characteristics that are typical for small, de-glaciated alpine headwaters in the European Alps. We therefore argue that our study area is representative of a larger number of mountain headwaters and that our approach can be easily transferred to other de-glaciated regions.

5.4 Methods

5.4.1 Geomorphic field mapping and geomorphometric characterisation of sediment storages

To identify storage compartments within the sediment cascades of Val Müschauns, an inventory of sediment stores was compiled based on geomorphic field mapping using interpretation of aerial photos and hillshades of a LiDAR-based 2m-DTM (© SwissTopo, 2013). The storage units were classified into eight storage types, based on Ballantyne and Harris (1994): Alluvium, colluvial creep deposit, moraine deposit, hillslope debris flow deposit, deposits within debris flow channels (incised in bedrock), debris cone, talus slope (comprising both sheets and slopes) and protalus rampart. To characterise the storage types, morphometric properties, i.e. the slope gradients and the normalised distance to the drainage divide, were derived from the DTM. While the slope of the landform provides information on its efficiency as buffer within the sediment conveyance (steep versus flat), the normalised distance represents the relative position of a landform unit within the toposequence between drainage divide (distance = 1) and stream channel (distance = 0). The DTM was previously smoothed by a moving window average filter (3 x 3 cells) in order to remove small surface roughness either caused by small elements (e.g. boulders) or DTM errors. After comparing different window sizes, the 3 x 3 window was selected as it proved to be the most suitable to delete surface irregularities without any loss of important information on surface objects.

5.4.2 Delineation of toposequences and evaluation of storage (de)coupling

Based on the storage inventory, toposequences were derived to assess the (de)coupling state of the sediment cascades and to evaluate the sediment connectivity in Val Müschauns. Due to the high variability of the mountainous terrain a GIS based delineation of toposequences with homogeneous hillslope units is problematic. Even the smoothing of the DTM cannot solve the issue, as important structural elements on hillslope can be lost (Rasemann, 2004). Therefore, a manual mapping procedure (similar to Otto et al. 2009) was applied in conjunction with the geomorphometry based connectivity index (see below). Using the sediment storage map, toposequences starting from the ridge crest and ending at the stream channel were manually identified in ArcGIS. Beginning from the drainage divide, each storage unit was linked with its lower neighbouring unit following a downslope gravitational gradient derived from the D8 flow routing algorithm

(Martz and Garbrecht, 1992). In total, 110 individual topological storage sequences were identified and classified into seven major types, consisting of up to six storage units (Figure 5.5).

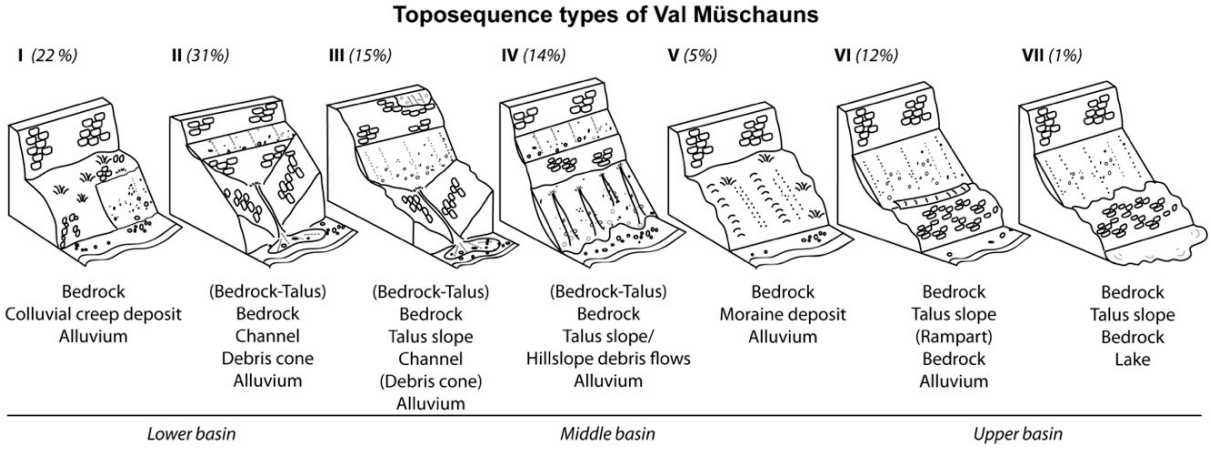

Figure 5.5: *Toposequence types (I-VII) in Val Müschauns with respect to their relative frequency (%) and their typical location within the catchment.*

Toposequences are static and simply an altitudinal succession of landform units. In order to define a toposequence as a sediment cascade, where sediment is routed from one storage to the lower one, the (de)coupling relationships were examined. Referring to Lexartza-Artza and Wainwright (2009), it is assumed that coupling takes place through the physical contact of two neighbouring sediment storages (= structural) as well as through active sediment transport across the separating boundary (= functional). To study the structural and functional (de)coupling, the mapped landform boundaries were extracted in ArcGIS and evaluated with respect to the sediment transfer. In the case of sediment input and/or output between a storage pair the boundary was mapped as coupled. In the case of a lacking sediment transfer, i.e. due to the presence of buffers or the inactivity of geomorphic processes, the separating boundary was defined as decoupled. Potential buffers that have been identified in the field include outcropping bedrock, the rocky step of the glacial cirque and alluvial floodplains (in accordance to Fryirs et al., 2007). Likewise, the activity of processes was evaluated using field observations of incoming and outgoing sediment transfer between adjacent storages. Referring to Schrott et al. (2002), major diagnostic criteria pointing to active sediment transport are no/low vegetation coverage, uprooted trees, fresh-looking detachment zones and scars on hillslope, no/low degree of weathering (e.g. lack of lichen cover) and freshly detached boulders as well as erosive/depositional microforms (e.g. rills, solifluction lobes).

Based on the (de)coupling relationships, the sediment connectivity to the stream was assessed. It is assumed that in the case of a decoupled landform boundary the whole sediment cascade will be interrupted there. Therefore, all storages of a toposequence situated uphill of such a boundary have been mapped as decoupled from its lower storage and, moreover, disconnected from the stream channel. Finally, the relative length of (de)coupled landform boundaries and the relative basin area of (dis)connected sediment storages were quantified.

5.4.3 Morphometric modelling of connectivity index

For studying the connectivity between different parts of the hillslopes and the fluvial system, an index of connectivity (*IC*) was modelled using the morphometric algorithm by Cavalli et al. (2013). This GIS method permits a relatively simple and rapid determination of the potential sediment connectivity in mountain terrain using high-resolution LiDAR DTMs. The *IC* represents the probability that sediment at a certain location of the hillslope will arrive in a specific sink, i.e. the stream channel, by considering the small-scale hillslope morphometry. The *IC* is calculated locally for each raster cell *i* of the DTM using an upslope and a downslope component (Figure 5.6).

The downslope component D_{dn} refers to the weighted sediment flow pathway from cell *i* to a user-specified target (e.g., stream channel, road, lake). Here, we used a polygon mask of the stream channel as the target. Weighting of each flow line segment between cell i and the stream channel is calculated using the slope gradient *S* and a weighting factor *W*, which is equivalent to the standardised roughness index *RI* (Cavalli et al., 2013):

$$W = 1 - \left(\frac{RI}{RI_{\max}}\right) \tag{5.1}$$

where RI_{max} it the maximum value. The *RI* was calculated according to Cavalli et al. (2008) and Cavalli and Marchi (2008), as standard deviation of the difference between the unsmoothed and smoothed DTM (= residual topography). The *RI* considers local obstructions to the sediment transfer such as bedrock roughness and outcrops or debris cover as it is typical in mountain areas (cf. Cavalli et al., 2013).

The upslope component D_{up} defines the potential for downslope transfer of sediment produced upslope and entering in cell *i*. D_{up} is determined by the contributing area of the cell *i* as well as by local properties including the slope gradient *S* and the *RI* (cf. Cavalli et al., 2013). Thus, the *IC* for each raster cell *i*, defined in the range of [-∞,∞+], is calculated by (equation 5.2):

$$IC = \log_{10}\left(\frac{D_{\mathrm{up}}}{D_{\mathrm{dn}}}\right) = \log_{10}\frac{\overline{W}\ \overline{S}\ \sqrt{A}}{\sum_i \frac{d_i}{W_i\ S_i}} \tag{5.2}$$

with the dimensionless weighting factor *W*, the slope gradient *S* (m/m), the upslope contributing area *A* (m^2) of cell *i* and the length d_i of the *i*th cell of the DTM along the steepest downslope pathway to its related target cell (Figure 5.6). The contributing area was derived by the multiple flow D-infinity algorithm (Tarboton, 1997) and a hydrologically corrected, unsmoothed LiDAR-based 2m-DTM. The *IC* was calculated using an ArcGIS toolbox that follows the approach described in Cavalli et al. (2013). The model was implemented through the Model Builder Application running in ArcGIS 10.1 (ESRI, 2006) using algorithms available in TauDem 5.0 (Tarboton, 2012). To avoid that *RI* becomes zero in the calculation of D_{dn}, a minimum value of 0.001 m/m was set in the calculation of *S*. In addition, a maximum slope of 1 m/m was used to reduce the effect of near-vertical rock faces (cf. Cavalli et al., 2013).

The resulting *IC* map was validated by the field based analyses of storage (de)coupling and (dis)connectivity of the toposequences. To identify a potential threshold *IC* value that might define disconnected DTM pixels in accordance to the field observations, the morphometric index was plotted along selected toposequences.

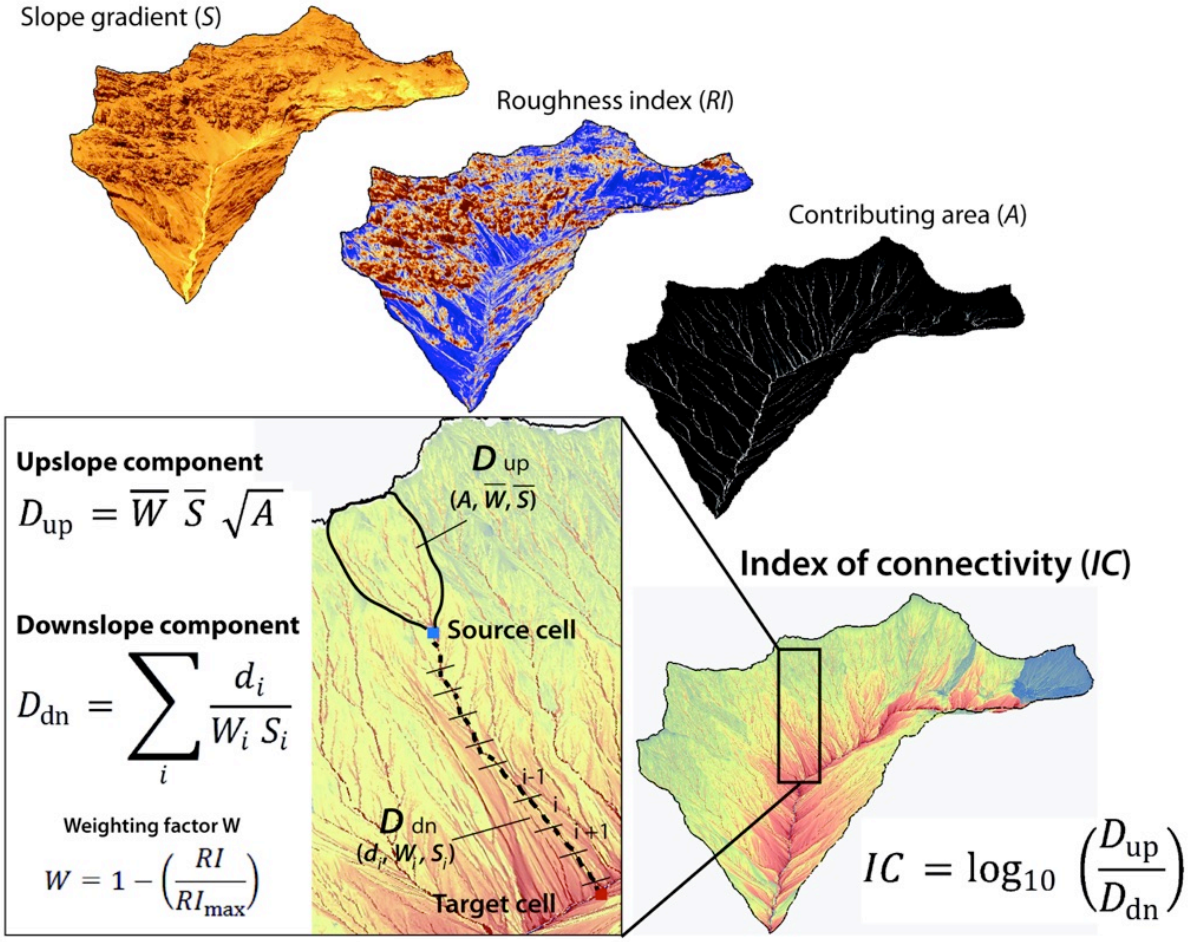

Figure 5.6: *Morphometrical GIS approach by Cavalli et al. (2013) combining an upslope and downslope component of the index of connectivity (IC). The variables are described in detail in the text.*

5.5 Results

5.5.1 Spatial pattern and morphometric attributes of sediment storage types

The geomorphic mapping reveals a distinct spatial distribution of sediment storages in Val Müschauns (Figure 5.7, Table 5.2). The major deposits are talus slopes (16%), i.e. located within the upper basin. This number represents a minimum estimate, because of numerous small-scale rockfall deposits inside rock wall irregularities, favoured by the horizontal bedding of the dolomitic rocks (Figure 5.2B). Colluvial creep deposits resulting from diffusive hillslope processes (i.e. shallow landsliding and creep processes) cover around 12% of the area (Table 5.1) mainly the lower valley. Moraine deposits and alluvium represent only a small proportion of the basin surface. The area associated with debris flow activity, e.g. cones, hillslope debris flow deposits and

material within bedrock channels, is relatively small (< 1%, Table 5.2). However, around 66% of the catchment consists of rockwalls and bedrock outcrops, dominantly within the upper basin (Figure 5.3, Table 5.1).

Slope gradients (Figure 5.8A) are steepest for bedrock cliffs and outcrops (the median as a representative measure for non-normally distributed slopes is ~43°), whereas alluvial deposits, i.e. in the upper hanging valley, have gentle gradients of ~14°. Debris cones exhibit comparatively steep gradients (median ~24°). Figure 5.8B displays an overall topological succession of the storage landforms between drainage divide and stream channel: While talus slopes dominate the upper slopes, the footslopes are covered by alluvium, often superimposed by debris cones and hillslope debris flow deposits. Colluvial creep deposits and bedrock channels are primarily related to the midslopes followed by moraine deposits at the lower slope. However, the overlapping slope positions for different storage landforms (Figure 5.8B) indicate that multiple topological landform sequences can be distinguished in Val Müschauns.

5.5.2 Toposequences types and storage (de)coupling

Seven major types of toposequences have been identified (Figure 5.7) each showing a distinct type locality within the catchment of Val Müschauns (Figure 5.5). The lower basin is dominated by type II toposequences (II in Figure 5.5) accounting for 31% of the 110 toposequences in the basin. Here, the rockwall is incised by a

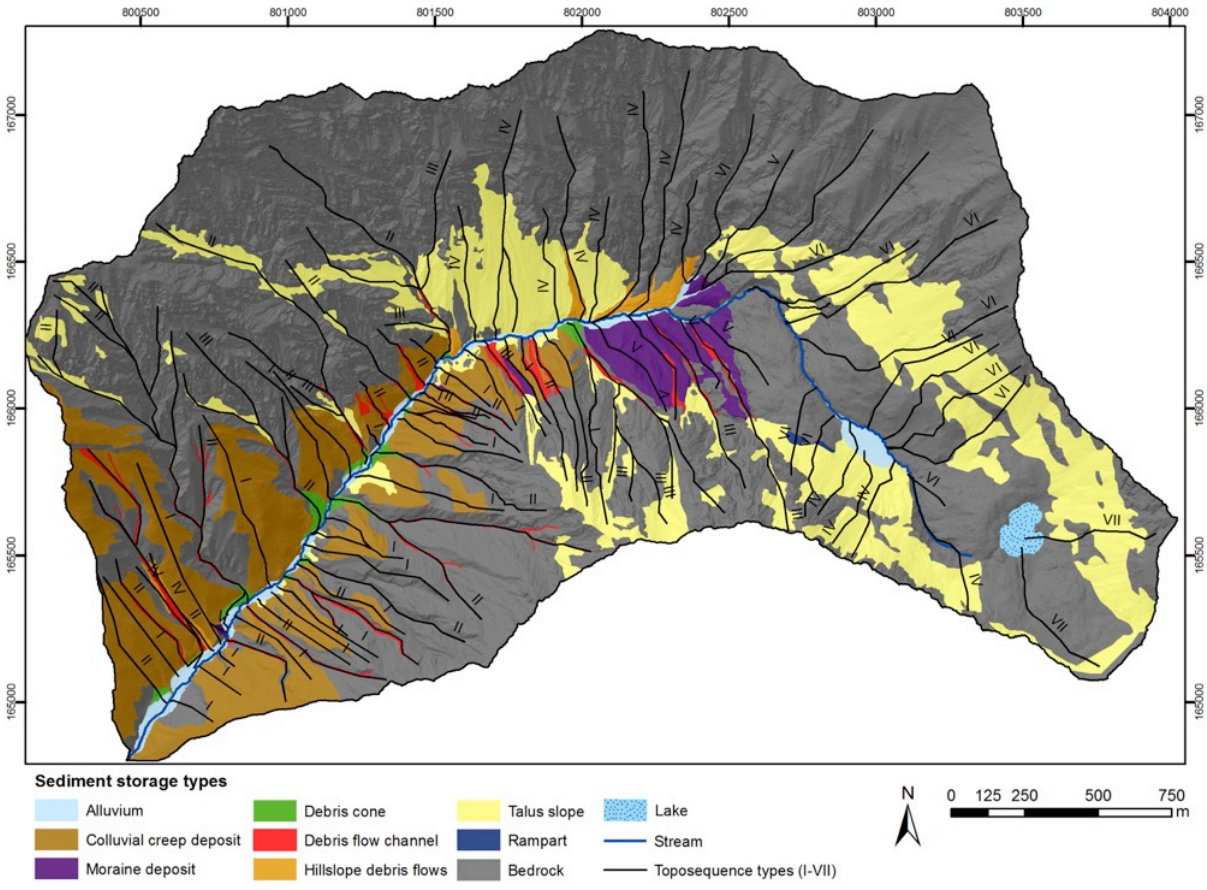

Figure 5.7: Spatial distribution of sediment storage types in Val Müschauns based on geomorphic field mapping. Seven different types of toposequences (black lines, I–VII) have been delineated.

steep debris flow channel (channel gradient > 0.5 mm^{-1}), leading over to a debris cone near the stream. In higher elevations, a small talus slope is stored inside the rock face. Further upstream of the thalweg, type III toposequences (III) prevail, comprising 15% of all toposequences. In contrast to type II, the source area of the debris flow channel is directly fed by the talus slope. Upslope, a small talus slope is commonly embedded inside the rock face. Around 14% of the 110 toposequences are typified as type IV (IV in Figure 5.5), primarily in the middle basin at the south-facing hillslopes. Extensive bedrock outcrops separate a talus slope lying on the lower slope from talus slopes situated above. The dominant topological sequence of the upper hanging valleys is toposequence type VI (12% in Figure 5.5), where a talus slope borders on exposed bedrock. As a special case (1%), the lake in the glacial cirque represents the final sediment sink of toposequence type VII (Figure 5.5)

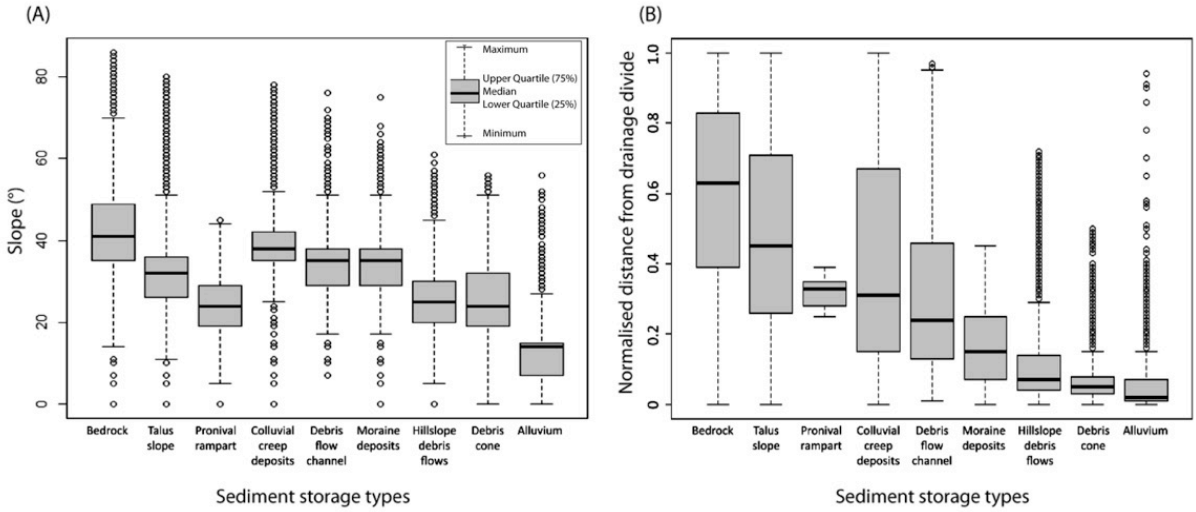

Figure 5.8: *Geomorphometric characteristics of sediment storage types in Val Müschauns, derived from the LiDAR-based 2m-DTM (© SwissTopo 2013). (A) Slope gradients (°) and (B) normalised distance from the drainage divide (1 = drainage divide, 0 = stream channel). The boxplots depict the minimum, maximum, median as well as the upper and lower quartile of the data for each landform.*

The analysis of storage boundaries reveals a total number of 26 combinations of storage pairs in Val Müschauns (Table 5.2). A relative length of 79.8% of the basin's storage boundaries (or 22 storage pairs) is presently coupled due to active sediment transfer. The most frequent storage coupling occurs between bedrock and talus slopes encompassing a relative boundary length of 29.9%. Here, sediment flux takes primarily place by low-magnitude rockfall events. In turn, 20.2% of the storage boundaries are currently affected by a lack of material exchange (thick double lines in Figure 5.9, Table 5.2). The transition from talus slopes to bedrock accounts for 19% of the storage boundaries without sediment flux and represents the main cause of storage decoupling. Consequently, 33 toposequences (or 30%) are interrupted and do not represent continuous sediment cascades from the crests to the main stream (Figure 5.9).

Especially, the majority of toposequences in the upper basin (mainly type VI) are decoupled resulting in rather short sediment trajectories of less than 200m in length. Assuming that all units of the sediment cascade lying uphill of a decoupled storage boundary are disconnected from the lower part of the cascade, the relative basin surface disconnected from the fluvial system encompasses around 29% (crosshatched area in Figure 5.9,

Figure 5.10). This area comprises nearly the complete upper basin. The major landforms affected by this disconnectivity are talus slopes (68%) and the area made up of bedrock (24%).

5.5.3 Spatial pattern of sediment connectivity

The spatial pattern of the modelled connectivity index in Val Müschauns is illustrated in Figure 5.9. The lower and middle basin is characterised by comparatively high *IC*s with a distinct decline with increasing upslope distance to the stream channel. The highest values are calculated for the valley bottom and the lower slopes, covered by alluvium and debris cones (Figure 5.10). Similarly, very high *IC*s are related to steep debris flow channels. High indices are modelled for the steep south-facing slopes of the middle basin covered by talus slopes and hillslope debris flow deposits. Likewise, the moraine material is highly connected based on the model results. Low *IC*s are related to the upper slopes of the lower and middle valley, mainly consisting of steep rock faces. More than the half of the bedrock area has *IC*s lower than the basin's median *IC* Figure 5.10). Nevertheless, the small talus slopes stored inside the rock faces of the lower basin, which have been mapped as decoupled (Figure 5.9) are not severally recorded in the index (e.g. by a sharp decline). Instead, the modelling shows a dominantly smooth decrease of *IC* values in upslope direction (Figure 5.11, profile 1).

Table 5.1: Relative basin area of sediment storage types and relative sediment cover (%) without bedrock coverage (non-bedrock). Sediment deposited within the lake has not been included in this study.

	Sediment storage landform types	**Relative basin area (%)** (whole basin)	**Relative sediment cover (%)** (non-bedrock)
1	Alluvium	1.4	4.2
2	Colluvial creep deposit	11.9	34.9
3	Moraine deposit	1.9	5.7
4	Debris cone	0.5	1.3
5	Debris flow channel	0.9	2.6
6	Hillslope debris flows	0.6	1.9
7	Talus slope	16.4	48.3
8	Rampart	0.1	0.2
9	Bedrock	66.0	-
	(Lake)	*(0.3)*	-

Table 5.2: *Coupled and decoupled landform pairs (based on adjacency and active sediment transfer) in Val Müschauns with respect to the relative length of separating boundaries (%) and the major geomorphic processes of sediment transfer evaluated in the field.*

	Pairs of adjacent landforms (upper storage – lower storage)	Relative length of storage boundaries (%)	Major geomorphic processes of sediment transfer (based on field mapping)
Coupled	Bedrock-Talus slope	29.9	Rockfalls (primary and secondary)
	Bedrock-Colluvium creep deposits	12.4	Debris flows, rockfalls avalanches, creep
	Bedrock-Debris flow channel	10.7	Debris flows (rockfalls)
	19 other combinations, each with a relative boundary length of < 2%	26.8	Rockfalls, debris flows, avalanches, creep solifluction, rill erosion
	Sum ∑	**79.8**	
Decoupled	Talus slope-Bedrock	19.0	
	Bedrock-Bedrock (glacial cirque step)	0.6	currently, no active transfer process
	Talus-Alluvium	0.5	
	Rampart-Bedrock	0.3	
	Sum ∑	**20.2**	

In the upper valley, the *IC* is remarkably reduced (Figure 5.9, crosshatched area). Around half of the talus slopes in this area are related to indices lower than the basin's median *IC* (Figure 5.10). In particular, extremely low values are calculated within the uppermost trough, where the *IC* decreases abruptly at the glacial cirque step in downslope (Fiugure 5.11, profile 2) and downstream direction. However, there is no sharp decline of the *IC* at the boundary between the flat alluvial plain and the higher situated talus slopes (Figure 5.11, profile 3). Similarly, even though the *IC*s of hillslopes visibly decrease along bedrock exposed on hillslope (Figure 5.11, profile 4), the modelling calculates no distinct drop of *IC* values for the talus slopes situated uphill, which were mapped as decoupled.

Given Figure 5.10 (right-hand side), the overall connectivity degree is calculated remarkably higher by the GIS modelling compared to the calculations made by the field based toposequence study. Around 35% of the basin surface, which has been mapped as being decoupled, is related to *IC*s higher than the basin's median *IC* value. To identify a potential threshold *IC* value for disconnected DTM pixels, the morphometric index was plotted along selected toposequences (Figure 5.11). No uniform *IC* is recorded at locations, where decoupled storage boundaries were mapped (vertical dashed lines in Figure 5.11), precluding the definition of a consistent *IC*, below which decoupling occurs. All equivalent *IC* values are negative, scattering between -4.1 and -2.1.

5.6 Discussion

5.6.1 Evaluation of the GIS modelling results with respect to field based investigations

On the basin scale, the *IC* displays a spatial pattern of connectivity in Val Müschauns that is in good accordance to our field based investigations (Figure 5.9). While the confined channel and the steep slope profiles of the lower and middle basin are associated with short and well-connected sediment trajectories (low *IC*s), the sediment delivery within the upper basin is attenuated noticeably by the elongated and less inclined slopes. In particular, the extremely low indices in the upper hanging valleys coincide very well with the talus slopes and rock faces (Figure 5.9, Figure 5.10) which have been mapped in the field as being decoupled. Here,

field evidence reveals that the flat alluvial valley plain (Gigure 5.8B) and the glacial cirque act as local buffer (Figure 5.39) within the lateral sediment flux and prevent most of hillslope sediments from entering the river system (Figure 5.11, profile 2 and 3). Moreover, given the abrupt drop of the *IC*, the step of the glacial cirque constitutes a topographic barrier within the longitudinal sediment transfer separating the upper trough from the remaining lower basin. Therefore, the GIS model reflects very well the influence of the overall mountain valley morphometry on the sediment conveyance in Val Müschauns.

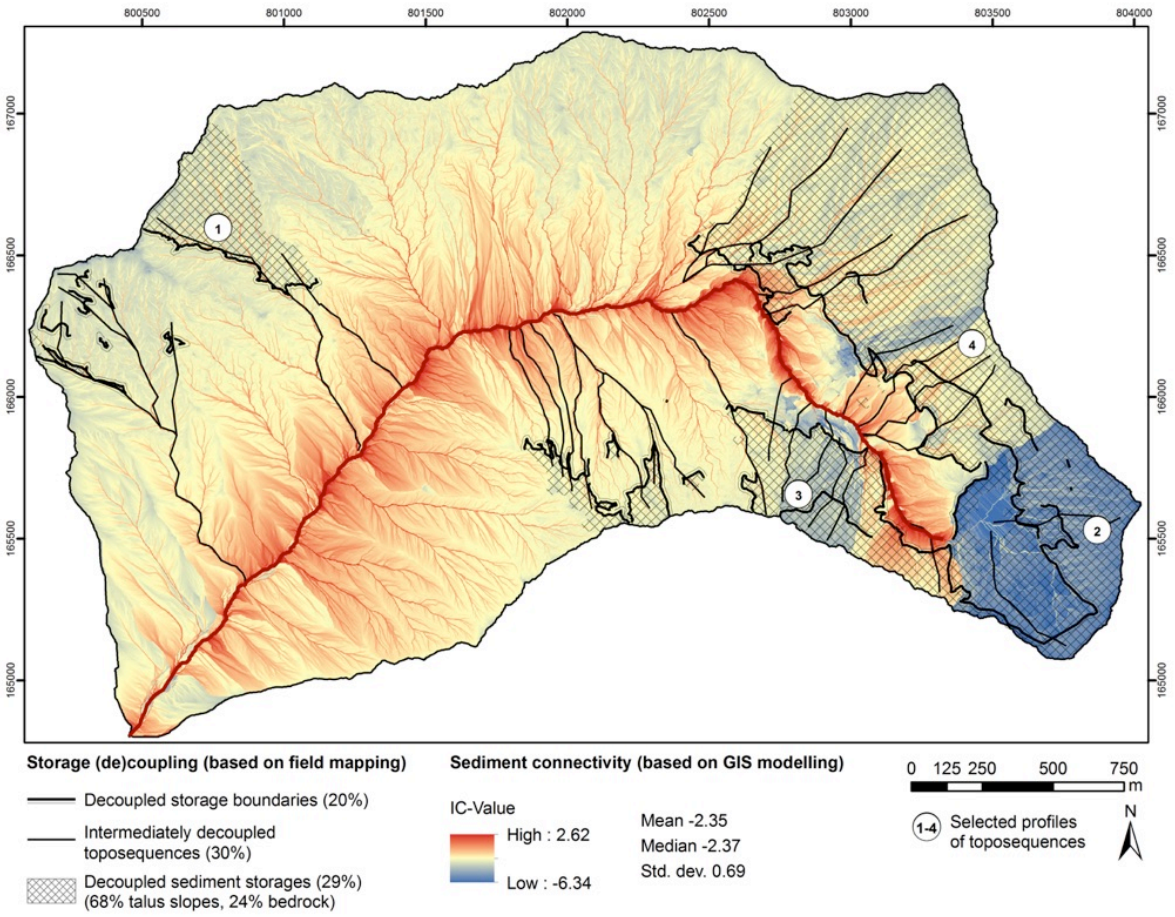

Figure 5.9: *Storage coupling, according to the field-based analysis of toposequences, and index of connectivity (IC), calculated by the GIS modelling approach (2m-DTM © SwissTopo 2013). Thick double lines show storage boundaries qualitatively defined as decoupled due to lacking sediment transfer between adjacent landforms caused by inactivity of geomorphic processes or the occurrence of buffers. As a consequence, around 29% of the basin surface has no connectivity to the fluvial system (crosshatched area). Among them, 68% of the talus slopes and 24% of the bedrock-coverage are affected by this disconnectivity.*

However, on the local scale, some spatial patterns of the *IC* are not geomorphologically interpretable or meaningful. The model outputs simply occur for morphometric reasons, disregarding the (in)activity of any geomorphic processes. This is most obvious in the proximity of debris flow channels (Figure 5.10). Their high *IC*s coincide with the high activity of periodic debris flows entraining large volumes of sediments to the trunk stream as a result of the steep gradients (Figure 5.8A) and large contributing areas. Yet, high *IC*s and high debris flow activity are not causally linked. Likewise, the high *IC*s of most of the lower slopes seem to be supported by field evidence of lateral undercutting and sedimentation caused by frequent shifts of the stream (Figure 5.4). The high gradients of debris cones (Figure 5.8A) imply intense hillslope-channel linkages through

fluvial erosion at the cone foot (see also Harvey, 2001; Harvey, 2002). However, the algorithm does not predict the fluvial process that increase the strength of connectivity, but it is controlled by the closeness to the stream channel (Figure 5.8B). The same applies for the rock faces of the upper slopes. Based on field mapping, a significant amount of rockfall particles are presently deposited inside couloirs of the rockwalls (Figure 5.5., Figure 5.8B) might be only infrequently connected with the stream via secondary rockfalls (Caine, 2001; Krautblatter and Dikau, 2007). Although these field observations seem to be supported by the relatively low *IC*s, they occur simply due to the long routing distances and the high surface roughness, which affect the calculation of D_{up} and D_{dn} in the algorithm of equation 5.2.

Therefore, the GIS approach, which is based on morphometric DTM derivatives, might insufficiently represent the role of geomorphic transfer processes as (dis)connecting mechanism within the sediment conveyance of Val Müschauns. Frequency and magnitude characteristics are neglected in the model, although they might be crucial for the strength and timescale of connectivity (Wolman and Miller, 1960; Harvey, 2002; Fryirs et al., 2007). For instance, the high indices of moraine deposits (Figure 5.10) do not match with field evidence, despite their steepness (Figure 5.8A) and neighbourhood to the stream channel (Figure 5.8B). Here, cryogenic creep, being the dominant sediment transfer process, might operate at extremely low rates < 1 mm/year (cf. Matsuoka, 2001c) due to the stabilising effect of vegetation. Thus, hillslope-channel connectivity might be greatly reduced (Caine and Swanson, 1989). These model limitations have been also emphasised by Cavalli et al. (2013) attributing them to the simplicity of the method and the complex mountain terrain. We propose to include the vegetation structure, type and coverage as additional weighting factors, as they considerably control the sediment conveyance on mountain hillslopes by minimizing process activity and by stabilizing non-consolidated sediment through its root system (Borselli et al., 2008; Theler et al., 2010; Corenblit et al., 2011). For a better representation of rockfall events, a threshold slope gradient of ca. 43° (Figure 5.8A) that defines potential initiation sites could be involved in the algorithm (Wichmann et al., 2009; Heckmann and Schwanghart, 2013).

Our assumption, that the DTM based model does not sufficiently characterise the local sediment cascades in Val Müschauns, is confirmed when comparing the *IC* map with the results of the field based toposequence study (Figure 5.11). While the latter provides information on the coupling relationships between adjacent storage compartments due to active geomorphic transfer processes, the pixel-based index obviously fails to model boundary effects and to calculate decoupling between neighbouring DTM pixels. Instead of a visible change or a sharp decline of *IC* values, most of the decoupled boundaries mapped in the field (Figure 5.9, Table 5.2) are related to a smooth decrease. Although the GIS algorithm correctly predicts the buffering effect of the hillslope topography (Figure 5.11, profiles 2 and 4), it does not consider morphologically "invisible" buffers, which are not represented by an abrupt change of topographic properties in the DTM, such as elongated bedrock slopes (Figure 5.11„ profiles 1 and 3) or vegetated moraine deposits. On the other hand, the index might also overvalue the efficiency of local topography, as large boulders or debris flows can cross even very rough bedrock outcrops when having sufficient kinetic energy (Iverson, 1997). As a consequence, the *IC* does not adequately show that 29% of the basin surface is currently disconnected from the stream network, as have been calculated based on the field map. Thus, the morphometric index overestimates the overall degree of

connectivity in Val Müschauns; 35% of the basin area qualitatively assessed as decoupled is represented by *IC*s higher than the median (Figure 5.10, right-hand side).

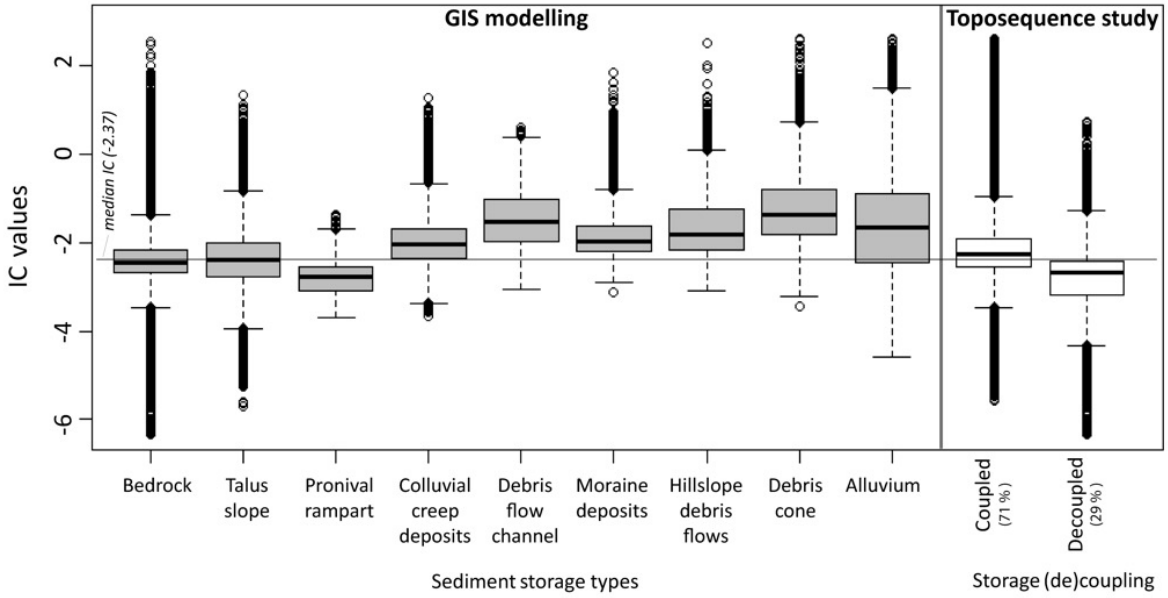

Figure 5.10: *IC-values of sediment storage types in Val Müschauns and comparison between the modelling results (grey boxplots, left-hand side) and the field-based mapping results of the toposequence study (white boxplots right-hand side). Around 35% of the basin surface, which has been qualitatively classified as being decoupled, is related to IC-values higher than the basin's median IC*

In general, these discrepancies between field and model evidence imply therefore the need to improve the representation of buffering effects in the GIS algorithm; for instance, by the implementation of blockade targets, which set the *IC* of the upslope flowpath to zero signifying a disconnectivity to the stream network. However, Figure 5.11 indicates that the automated extraction of a uniform *IC* threshold defining blockade objects exclusively derived from DTMs might be problematic, especially if they are morphologically undetectable. Instead, field evidence obtained by geomorphic field maps appears to be the most suitable way to implement targets of buffers in the connectivity model.

5.6.2 Key controls on the sediment transfer in formerly glaciated mountain valleys

Mountain environments are characterised by a variety of geomorphic processes that mobilise, transfer and deposit sediments along cascading trajectories downslope to the basin outlet (Chorley and Kennedy, 1971; Burt and Allison, 2010). In the high-alpine valley of Val Müschauns, rockfall derived talus slopes dominate the landform inventory (Figure 5.7, Table 5.1). The high rockfall activity is also demonstrated by the toposequence analysis (Table 5.2) as more than 29% of the basin's landform boundaries are dominated by sediment transfer by low-magnitude rockfall events. This dominance is in good accordance to other studies performed in small mountain headwater valleys (< 30 km²) (Rapp, 1960a, b; Caine, 1986; Schrott et al., 2003; Krautblatter et al., 2012).

The analysis of toposequences implies a distinct spatial pattern of sediment cascades with respect to the downslope arrangement of storage units and their strength of coupling (Figure 5.5, Figure 5.7). Most of the sediment trajectories in the lower and middle basin are well connected through debris flow channels (I-IV in Figure 5.5). This emphasises the importance of debris flows as major sediment transfer process in mountain environments (Caine and Swanson, 1989; Benda and Dunne, 1997) and, particularly, as key driver for hillslope-channel connectivity (Brardinoni and Hassan, 2006; Hoffmann et al., 2014a). In a basin in the Austrian Alps, Heckmann and Schwanghart (2013) demonstrated using numerical graph models that debris flows are the most important processes connecting around 65% of the sediment cascades with the river channel. Moreover, debris cones represent important terrain features coupling the hillslopes with the stream channel of the lower basin of Val Müschauns. Whereas debris cones are commonly interpreted as local buffers within the sediment conveyance (e.g. Fryirs et al., 2007; Harvey, 2010), the decoupling effect of the debris cones in our study area may persist only temporary due to the high erosional activity of the stream (Figure 5.8A), which is favoured by the steep channel gradients and the confined valley morphology. Processes that rework those buffers result in a temporary increase of the sediment yield and strongly increase hillslope-channel connectivity (Davies and Korup, 2010).

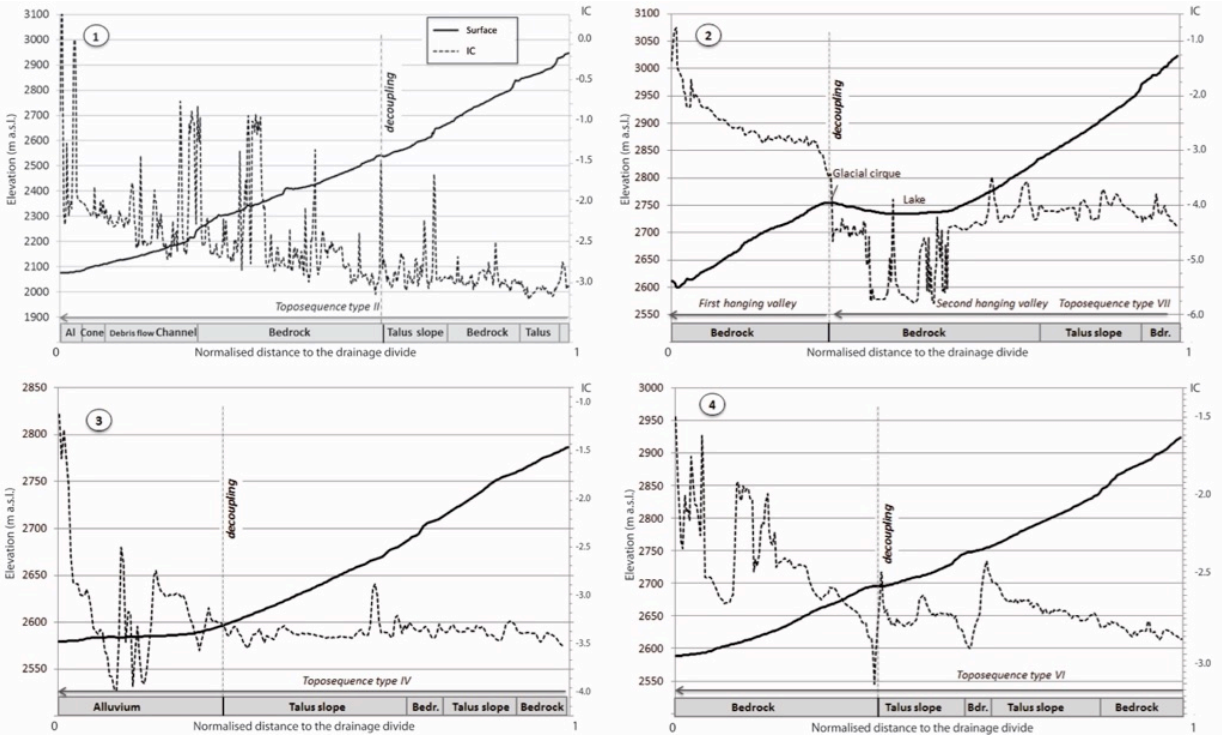

Figure 5.11: *Overlay of surface profiles of selected toposequences with the corresponding IC-values of the numerical connectivity map. Locations of the toposequences (profiles 1-4) are displayed in Fig. 5.8. The comparison between the storage boundaries mapped as decoupled and the related DTM-pixel of the connectivity raster results in no uniform IC-values ranging from -3.30 (profile 2), -0.87 (profile 3), -0.35 (profile 1) and -0.21 (profile 4).*

In the upper hanging valleys of Val Müschauns (Figure 5.3) the sediment cascades are largely decoupled (V-VII in Figure 5.5) due to small-scale topographic effects caused by the alluvial valley plain, the rocky step of the cirque and, in particular, by the elongated bedrock slopes (Figure 5.11, profiles 2-4). The dominance of bedrock in the basin (Table 5.1) especially exposed on midslopes, obstructs the sediment output from a significant proportion of the talus slopes' boundaries (Table 5.2). Thus, contrary to debris cones, bedrock constitutes a relatively static buffer delaying the sediment delivery to the river up to glacial-interglacial cycles (Table 1 and 2 in Fryirs et al., 2007). Probably, secondary rockfalls are of major significance in the basin (Krautblatter and Dikau, 2007), as they may compensate the long-term buffering effect of bedrock and may temporary connect the sediment stored inside rockwalls with the river system.

Given the field based analyses, one third of the basin area is currently disconnected from the main river system (Figure 5.9, Figure 5.10). This might be surprising when considering the small percentage of decoupled storage boundaries of around 20% in the valley (Table 5.2). However, most of the buffers are located on the midslopes or slope foots (Figure 5.5), in turn, disconnecting storages uphill from the sediment flux. As result, around one third of the basin's sediment trajectories are intermediately interrupted. This denotes that the relative area of buffers or length of decoupled boundaries are of secondary importance, but the location along a toposequence between drainage divide and river is decisive for the sediment delivery in mountain basins.

Considering the specific glacial history of Val Müschauns, our results imply that the present-day sediment flux of the basin is primary controlled by its specific valley topography inherited through Pleistocene glacial erosion. The two upper hanging valleys, comprising nearly 29% of the catchment area, are currently disconnected from the basin outlet due to their particular glacial cirque morphology reflecting strong glacial erosion. This percentage of disconnected basin area is supported by other quantitative investigations in headwater valleys of the European Alps, which range from 60% (Otto et al, 2009), 68-71% (Schlunegger et al., 2009) up to 84% (Heckmann and Schwanghart, 2013). Those values strongly contrast to non-glacial basins, as indicated by Hoffmann et al. (2014a). By comparing 57 tributary valleys of the Rocky Mountains, Hoffmann et al. (2014a) assessed reasonably smaller sediment delivery ratios (SDR) of < 15% in glacial basins compared to non-glacial basins with SDRs of > 28%. We argue that it is likely a unique characteristic of small, de-glaciated headwater basins that only a fraction of the eroded sediment will make its way to the basin outlet, as the glacial history still decreases the present degree of connectivity within the catchment (Hoffmann et al., 2014a). Although glacial headwater valleys are characterised by considerably higher erosion rates (Walling and Webb, 1996; Hinderer, 2001) than non-glacial headwaters or lowlands, the ability to export the relatively coarse sediment is hampered remarkably in glacial troughs due to the extensive valley bottom and the less efficient sediment transport of the streams occupying these valleys (in accordance to Montgomery, 2002). In Val Müschauns more than half of the talus slopes (68%) do currently not contribute to the sediment flux system (Figure 5.9, Figure 5.10); thus, most of the sediment produced since glacier retreat is stored within the upper trough, similar to the findings by Otto et al. (2009). How long this state of disconnectivity will persist and how it will change when the upper trough gradually fills with sediment remains unknown (cf. Hoffmann et al., 2014). As stated by Brardinioni and Hassan (2006), this impact of relict Pleistocene glacial erosion on the recent connectivity patterns can be very effective persisting until the onset of a next glaciation.

Therefore, our study emphasises the glacial legacy of small mountain headwater basins, as the sediment flux dynamics on hillslopes and within the river channel still adjust to the Pleistocene glacial erosion (Schumm, 1991; Ballantyne, 2002a; Verleysdonk et al., 2011). The sediment delivery problem (Walling, 1983) in glacial headwater regions might consequently derive from their transient state resulting from the Pleistocene glaciation. It is likely that the valley's history will also influence the system's sensitivity to future changes (Brunsden and Thornes, 1979; Brunsden, 2001; Usher, 2001). As a consequence of future global warming, the increasing frequencies and magnitudes of geomorphic processes (Harris, 2005; Gruber and Haeberli, 2007; Stott and Mount, 2007) might lead to rapid, if not catastrophic failure and depletion of sediment storages, which aggraded since the glacial retreat and had been decoupled since then (Koppes and Hallet, 2006; Meigs et al., 2006; Davies and Korup, 2010). If frequency of debris flow activity or magnitude and run-out length of rockfalls will increase in Val Müschauns, it is reasonable to assume that the two hanging valleys will response in future in form of a delayed rise of sediment delivery to the fluvial system.

5.6.3 Can traditional geomorphic field mapping be replaced by morphometric GIS approaches to understand mountain sediment cascades?

A major aim of this study is to evaluate the value of geomorphic field mapping in the study of mountain sediment cascades, in times of growing application of remote sensing and GIS techniques. Obviously, field mapping procedures are associated with certain limitations, which are rarely quantified. For instance, the real amount of intermediate storages of freshly detached rockfall material is rarely quantified on a catchment scale, and therefore, probably underestimated in geomorphic maps. Moreover, fieldwork is time consuming, particularly in mountain environments, and the resulting maps are affected by subjectivity and represent momentary snap shots of the present-day sediment dynamics (see also Van Asselen and Seijmonsbergen, 2006; Bishop et al., 2012). Due to the spatio-temporal variability of geomorphic processes in mountain basins, geomorphic mapsfa provide rather limited information on the long-term patterns of the sediment connectivity. Likewise, the vegetation cover is a restricted indicator for the activity of sediment transfer due to temporal and spatial dynamics of vegetation in high-alpine settings (Hörsch, 2002; Otto and Dikau, 2004). We are also aware of the fact that the field based toposequence mapping is only achievable in small catchments and that underlying conceptual assumptions are linked to some simplifications.

If referring to Bishop et al. (2012), the recent developments in GIS techniques as well as the high accuracy and resolution of LiDAR-based DTMs might compensate these limits of field mapping profoundly (see case studies in Hengl and Reuter, 2009). Thus, has geomorphic field mapping become dispensable today when studying mountain cascading systems? Apparently, the morphometric GIS approach used in this study stands out due to its simplicity and rapidity. Moreover, using a 2m-DTM and the multiple flow D-infinity algorithm realistically represent the sediment transfer and small-scale variations in mountain terrain (cf. Cavalli et al., 2013). Nonetheless, the evaluation of the model outputs by the field data underlines the difficulty to display the complicated structure of mountain sediment cascades using GIS algorithms, which is purely based on morphometric input parameters derived from the DTM. Although the connectivity index by Cavalli et al. (2013), adapted and modified from the approach by Borselli et al. (2008), is very well suited to examine the influence of the overall valley

topography on the mountain sediment flux, the model outputs are not sufficient to predict connectivity patterns that result from the physical linkage of neighbouring storage landforms and the de-facto sediment transfer. Consequently, landform-based approaches should be preferred over pixel-based approaches, as the latter might be less valuable to understand the (de)coupling relationships between the several landforms of a sediment cascade. Additionally, pixel-based approaches are characterised by a limited ability to recognise various geomorphic processes along the sediment cascade. Various geomorphic processes result in variable sediment fluxes and connectivity under a similar set of geomorphic parameters. Thus, process-related diagnostics have to take into account such as lateral fluvial undercutting of the slope foots (e.g. Harvey, 2010; Harvey, 2012), long run-out pathways of rockfalls (e.g Korup, 2005) or slow cryogenic creep (e.g. Caine and Swanson, 1989). In our study, the manual delineation of toposequences has proven to be a valuable approach to characterise the individual sediment cascades with respect to both geomorphic forms and processes. The method enabled to couple the sediment storages mapped in field by pathways of active sediment transfer or, in turn, to decouple them due to the occurrence of buffers or inactivity of processes.

Therefore, despite the increasing effort of quantitative GIS techniques, we cannot fully agree with the statement by Bishop et al. (2012: 5), for the reason that Earth scientists do still depend on heuristic, knowledge-based geomorphic field mapping – even in our modern pixel-dominated world. We argue that traditional geomorphic field maps remain indispensable for the validation and improvement of modelling results purely obtained from the morphometric derivatives of a DTM. The combined mapping of landforms, processes and material, as conducted by the geomorphic mapping approach, strongly relies on the present-day conditions in the field. However, it provides not only a short-term snap shot of the present-day conditions, but integrates the long-term landform evolution, since landforms, processes and materials are strongly inherited by past geomorphic events (i.e. the Pleistocene glaciation, see above).

To achieve a holistic understanding of sediment cascades, geomorphic field mapping and modelling approaches should ideally complement each other. Conceptual considerations gained by field maps in conjunction with, morphometric GIS approaches, such as the *IC* by Cavalli et al. (2013), provide a valuable representation of certain properties of mountain sediment cascades, particularly on a basin scale. Particularly, GIS techniques are very helpful in inaccessible areas, such as steep mountains. Mathematical graph models (e.g. Phillips, 2012b; Heckmann and Schwanghart, 2013; Heckmann et al., 2014) represent a novel approach in connectivity research. Here, the geomorphic field map can be used to identify and, i.e., to quantify the coupling relationships (edges or lines) between landforms (nodes or polygones) and to form network models of sediment cascades by numerical process modelling. Thus, even in our modern GIS world, traditional field mapping continues to remain an essential basis for a profound systemic understanding of geomorphic cascading systems and constitutes an essential input for quantitative models.

5.7 Conclusion

This study combines geomorphic field mapping with morphometric GIS modelling to characterise the sediment dynamics in the formerly glaciated alpine valley Val Müschauns. Our field based investigations indicate that the sediment delivery in mountain basins depends on the topology of neighbouring sediment storages and their mutual (de)coupling with respect to the active sediment transfer. It is shown that the

efficiency of buffers impeding the sediment flux remarkably depend on their specific location on hillslopes. On a basin scale, the overall valley morphology represents a key control on the sediment conveyance in mountain basins, as it is reflected very well by the DTM based connectivity index. While V-shaped valley cross-sections of the lower Val Müschauns are characterised by specific toposequences that support a strong sediment connectivity (consistent with high *IC*s), most of the toposequences (30 %) of the two upper hanging valleys of Val Müschauns, are currently disconnected from the main river network. Nearly one third of the basin area does not contribute any sediment to the thalweg due to the specific glacial cirque morphology. Our results support the notion that in formerly glaciated headwater basins, the sediment delivery is still conditioned by the Pleistocene glacial history. Therefore, a profound understanding of mountain sediment cascades, i.e. with respect to their (de)coupling relationships, will provide important knowledge for sediment budget studies and for future land-use and risk management activities in those highly dynamic systems.

Finally, we evaluated the value of field mapping in geomorphological research versus quantitative GIS techniques. The DTM based GIS approach by Cavalli et al. (2013) has proven to be very valuable to examine the influence of the overall valley morphology on the mountain sediment flux. However, not all modelling results can be interpreted as geomorphologically meaningful, because the model disregards the connectivity patterns that result from the physical linkage of neighbouring storages and their active sediment transfer, which are not expressed by a certain geomorphometry. This leads to an overestimation of the degree of connectivity within the basin. Our study demonstrates that process- and landform-based perspectives should be preferred over purely DTM- and pixel-based approaches when studying the complicate structure of cascading systems. The traditional geomorphic field mapping can fulfil this requirement, at least in a qualitative and descriptive way. Therefore, even in an automated, pixel-based GIS world, the traditional geomorphic field map and the ensuing systemic knowledge still remain indispensable to evaluate quantitative modelling outputs with respect to their geomorphic significance. A methodological framework, which combines geomorphic field mapping and morphometric GIS modelling, has proven to be an encouraging approach to obtain a holistic understanding of cascading sediment dynamics in a formerly glaciated mountain valley. A future step could be to use geomorphic field maps, far beyond the cartographic purpose, as input for numerical process models in order to quantify the sediment transfer dynamics and (de)coupling relationships in mountain cascading systems.

Acknowledgements

We greatly thank the staff of the Swiss National Park, especially R. Haller, for supporting the fieldwork in Val Müschauns and providing valuable GIS datasets. Furthermore, we acknowledge M. Cavalli for the valuable feedbacks and discussions as well as for providing a first version of the connectivity toolbox for ArcGIS, currently under development in the frame of the SedAlp Project (Alpine Space Programme). We also thank T. Heckmann and the other reviewer (anonymous) for their valuable comments on an earlier version of this manuscript.

----- BLANK -----

Chapter 6

STUDY III - LINKING ROCK WEATHERING, ROCKWALL INSTABILITY AND ROCKFALL SEDIMENT CASCADES IN GLACIATED HANGING VALLEYS

This chapter based on the journal article currently under review: Messenzehl, K., Viles, H., Otto, J.-C. Ewald, E., Dikau, R. (minor revisions): Linking rock weathering, rockwall instability and rockfall sediment cacasdes in partially glaciated hanging valleys (Swiss Alps). Submitted to Permafrost and periglacial processes.

Abstract

Sediment cascades in high-alpine valleys have received much recent scientific attention, with particular focus on the most active upland areas undergoing glacier retreat. However, when it comes to predicting paraglacial sediment fluxes and storages, deglaciated source rockwalls are often portrayed in an oversimplified way despite the fact that their instability and weathering are directly linked to landform and material characteristics of downslope sediment cascades. Here, we explore the role of source rockwalls in sediment production and deposition within twelve rockfall sediment cascades in three glaciated hanging valleys in the Swiss Alps. Principal component analysis is used to investigate the controls on rockfall sediment cascades, using data from talus slope surveys, and geotechnical surveys, rock temperature data, modelled frost cracking data and GIS-based topoclimatic analyses of their source rockwalls. The results show that four main factors (the intensity of seasonal frost cracking, permafrost probability in rockwalls, glacial slope profiles and mechanical preconditioning by joint spacing and joint orientation) combine to dictate paraglacial variability of sediment production, rockfall size and deposition. This study has major implications for future sediment cascade studies, as the identified rockwall parameters should enable better prediction and management of rockfall-dominated sediment fluxes in terrain adjusting to glacier retreat.

6.1 Introduction

Retreating glaciers in high-alpine valleys expose metastable or unstable, steepened rockwalls that are highly susceptible to external influences and internal modifications (Ballantyne, 2002b; McColl, 2012). To regain stability, deglaciated rockwalls usually react by a pulse of discrete rockfalls that can be enhanced for several centuries after the onset of deglaciation (Ballantyne et al., 2014; Krautblatter and Leith, 2015). As rockfall activity diminishes, the accumulated rockfall material of talus slope landforms is commonly remobilised by subsequent hillslope processes and is transported further downslope (Chorley and Kennedy, 1971; Ballantyne, 2003; Burt and Allison, 2010). Those sediment cascades from unstable rockwalls, over talus slopes, through alpine catchments can accordingly be described as 'paraglacial' as they are still reacting to the glacial signal to readjust to a non-glacial equilibrium (Church and Ryder, 1972; Ballantyne, 2002b).

Over the last few decades, the number of geomorphic studies on sediment cascades in formerly or still glaciated alpine terrain has significantly increased and substantial advances have been made in the budgeting of postglacial sediment storages and spatiotemporal prediction of often-hazardous fluxes after glacier retreat (Walling, 1983; Schrott et al., 2003; Slaymaker, 2003; Otto et al., 2009; Fryirs, 2013; Bennett et al., 2014; Messenzehl et al., 2014). Special attention has been paid to the rockfall-dominated, and typically most dynamic, part of paraglacial cascades in places including Great Britain (Curry and Black, 2003; Curry and Morris, 2004), New Zealand Alps (Hales and Roering, 2005, 2009), in Spitsbergen (Rapp, 1960b; Siewert et al., 2012) as well as in the Swiss and Austrian Alps (Schrott and Hoffmann, 2003; Sass, 2010; Götz et al., 2013; Heckmann et al., 2016). However, it appears that the focus of most sediment cascade studies is primarily on hillslope sediment storages such as talus slopes and their connectivity with the fluvial system, whilst the initial source area - the rockwall system - remains relatively neglected. Such a strong emphasis on sediment deposits is not only noticeable in field-based investigations, but similarly in catchment-scale research using e.g. photogrammetric and GIS-based sediment storage inventories (Schrott et al., 2002; Schrott et al., 2006; Otto et al., 2009; Micheletti et al., 2015), morphometric sediment connectivity indices (Cavalli et al., 2013; Tiranti et al., 2016) or numerical sediment flux algorithms (Heckmann and Schwanghart, 2013; Heckmann et al., 2016).

However, particularly in valleys undergoing glacier retreat, this exclusive view of storage and reworking of paraglacial sediments can be problematic without explicit linkage to the deglaciated bedrock area. As emphasised by McColl (2012), the relative importance of internal causes and weathering mechanisms of rockwall instability change notably as the paraglacial period evolves. This, in turn, has significant effects on the spatial and temporal variability of sediment production, on the material characteristics and volume of talus slopes, as well as further downslope, on the catchment-scale performance of alpine sediment cascades. When it comes to describing cascading sediment fluxes after glacier retreat, it is therefore not sufficient to focus exclusively on topoclimatic causes such as glacial topography or climate of alpine valleys (Tricart and Cailleux, 1972; Büdel, 1977; Schrott et al., 2003; Wichmann et al., 2009; Heckmann and Schwanghart, 2013; Delonca et al., 2014). Instead, additional information is needed on the rock mass and joint properties (Bovis, 1990; Selby, 1993; Augustinus, 1995; Grämiger et al., 2017), postglacial rockwall permafrost degradation (Haeberli et al., 1997; Wegmann et al., 1998; Krautblatter et al., 2013) and temporally changing efficiencies of weathering agents such as frost cracking and thermal fatigue (Hales and Roering, 2007; Viles, 2013b; Collins and Stock, 2016).

In this study, we explore the linkage between rock weathering, rockwall instability, sediment production and deposition after glacier retreat. Our aim is to better understand the role of rock weathering and rock slope instability in paraglacial rockfall-dominated sediment cascades. Using a combined field-, thermal modelling- and GIS-approach, twelve rockwalls and their resulting rockfall sediment cascades to talus slopes are investigated in three hanging valleys in the Swiss Alps undergoing deglaciation since the Last Glacial Maximum (LGM). Using ergodic reasoning, we demonstrate that frost cracking in near-vertical, permafrost-rich rockwalls is key to sediment production and deposition following glacier retreat. Structural preconditioning is also shown to be an important factor influencing paraglacial sediment cascades.

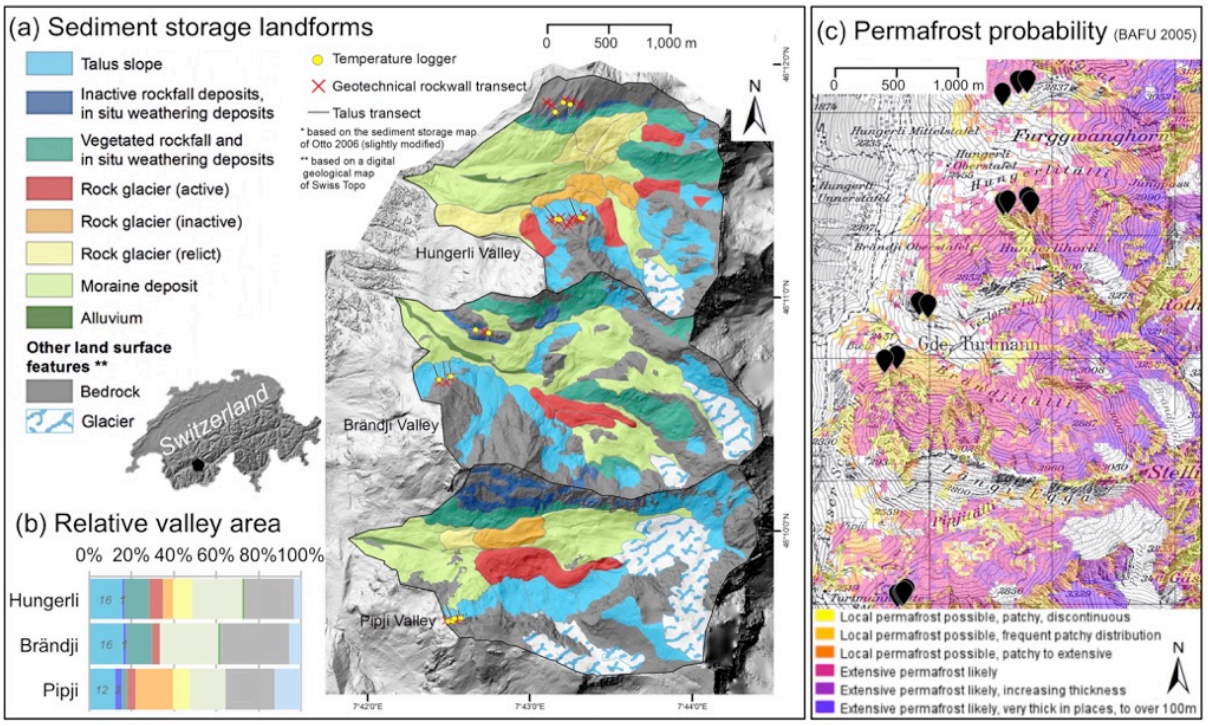

Figure 6.1: *(a) Inventory of sediment storages, rockwalls and glaciers and (b) relative storage surface area in the three hanging valleys of the Turtmann Valley in the Swiss Alps. Sediment storage map derives from previous work by Otto (2006) modified after geomorphic field mapping in summer 2013 to 2016. All investigation sites are displayed. (c) Potential permafrost distribution in the Turtmann Valley is displayed using the GIS layer of BAFU (2005) and overlain by investigated rockfall source areas.*

6.2 Sediment cascade systems of the study sites

The study sites are three neighbouring high-alpine hanging valleys in the Valais Alps, lying above the eastern shoulder of the NS-oriented Turtmann Valley (Figure 6.1a, c). Covering a mean valley area of 3.9 x 10^6 m^2, all valleys are characterised by a distinct EW-oriented central axis ranging from approx. 2300 m to 3590 m asl close to the border with the Matter Valley further East. During the LGM approx. 24–21 ka BP, it is assumed that most of the surface was covered by local hanging glaciers (up to 2800 m asl) (Kelly et al., 2004a). Remnants of hanging glaciers are located in the upper cirques today. Glacier retreat likely started around 18 kyrs BP (Ivy-Ochs et al., 2009), interrupted by a short re-advance during the Younger Dryas, approx. 12–9.5 kyrs BP, restricted to the lower valley floor (Leemann and Niessen, 1994; Kelly et al., 2004b). As a consequence

of post-glacial and recent atmospheric warming, glaciers today cover less than 5% (Brändji, Hungerli) and 12% (Pipji) of the valleys' surface. Dry continental climatic conditions with mean annual precipitation of less than 600–900 mm dominate the study sites (Gärtner-Roer et al., 2013; MeteoSwiss, 2016). According to the Swiss Permafrost map (BAFU, 2005) shown in Figure 6.1c, extensive and thick permafrost likely exists in sediment bodies in the upper partly glaciated basins and on higher north-exposed peaks, such as in the Pipji Valley. With decreasing altitude and/or increasing proximity to the valley outlet, permafrost distribution becomes patchy and discontinuous, but is still likely in shaded sediment bodies on the valley bottom and on N-exposed valley flanks higher than 2500 m asl (e.g. Brändji and Hungerli Valley). In contrast, S-exposed valley flanks in the lower and, to some extent, middle basins lying below 3000 m asl can be assumed to be largely permafrost-free (BAFU, 2005; Nyenhuis et al., 2005).

Around 26% of the total valley surface represents sediment-free bedrock, mainly in the form of steep and high rockwalls (shaded areas in Figure 6.1b). The three study sites display two main lithological and tectonic settings. Rockwalls in the Hungerli and Brändji Valleys are composed of Paleozoic micaschist and paragneiss of the Penninic Siviez-Mischabel Nappe with layers of amphibolite, quartzite and apatite. Metamorphic schistosity dips to the SE by 20-30°, parallel to the regional-scale tectonic folding of the Penninic nappes. In contrast, banked Mesozoic limestones and marbles of the Barrhorn and Frilihorn series dominate in the Pipji Valley (Bearth, 1980; Labhart, 2009).

On average, 66% of the surface in the three hanging valleys is covered by sediment storage landforms (Figure 6.1b). As shown in Figure 6.1a, the topological hillslope sequences of sediment landforms form typical high-alpine sediment cascades with glacial, periglacial and gravitational sediment transfer (see also Otto, 2006). In all three valleys, the most active sediment cascades occur via rockfalls from unstable rockwalls. Recent studies from Hungerli Peak reveal that the local frequency-magnitude pattern of rockfalls is dominated by boulder falls (14-61 m^3) and debris falls (< 14 m^3) with average annual to decadal return periods as well as seasonal surficial flaking (Messenzehl and Dikau, 2017). Rockfall activity is highest on north-facing, metamorphic rockwalls with anaclinal structural conditions (in-dipping orientiation of schistosity and main joint sets) in the middle and upper valleys (Figure 6.1a). This leads to a dominant pattern of active, N-exposed talus slopes (12-16% of land surface, Figure 6.1b), while inactive, often vegetated rockfall deposits predominate on south-exposed valley flanks (2-8% of land cover). As quantified by Otto et al. (2009), rockfall depositional landforms are either buffered at their lower foot by glacial moraine deposits or connected to rock glaciers of different activity states (Figure 6.1b).

6.3 Methodological approach

In the three studied hanging valleys, a holistic field approach of integrative rockwall-talus studies is applied, as previously developed on the northern flanks of the Hungerli Peak (Figure 6.2a) (Messenzehl and Dikau, 2017). Here, we further combined this integrative field approach with a GIS-based principal component analysis, which allows us to evaluate the relative importance of topoclimatic, paraglacial, cryospheric and mechanical controls on rockfall sediment cascades. In the field, twelve rockfall sediment cascades, each

consisting of a rockfall storage landform and its respective source rockwall, have been investigated at different locations within the three hanging valleys. As shown in Figure 6.2a, eight active rockfall sediment cascades on northern valley flanks with active rockfall supply onto talus slopes as well as four inactive cascades on southern flanks were studied. Major criteria for selection were: (i) accessibility and safety, (ii) comparable hillslope profiles on each valley flank (Figure 6.3) with respect to rockwall irregularities (curvature, mean slope) and talus slope length as well as (iii) comparable rockfall contributing area on each valley flank (quantified in Messenzehl et al., 2016). The latter two criteria are particularly important as they allow inter-site comparability with respect to overall sediment supply and rockfall fragmentation during deposition.

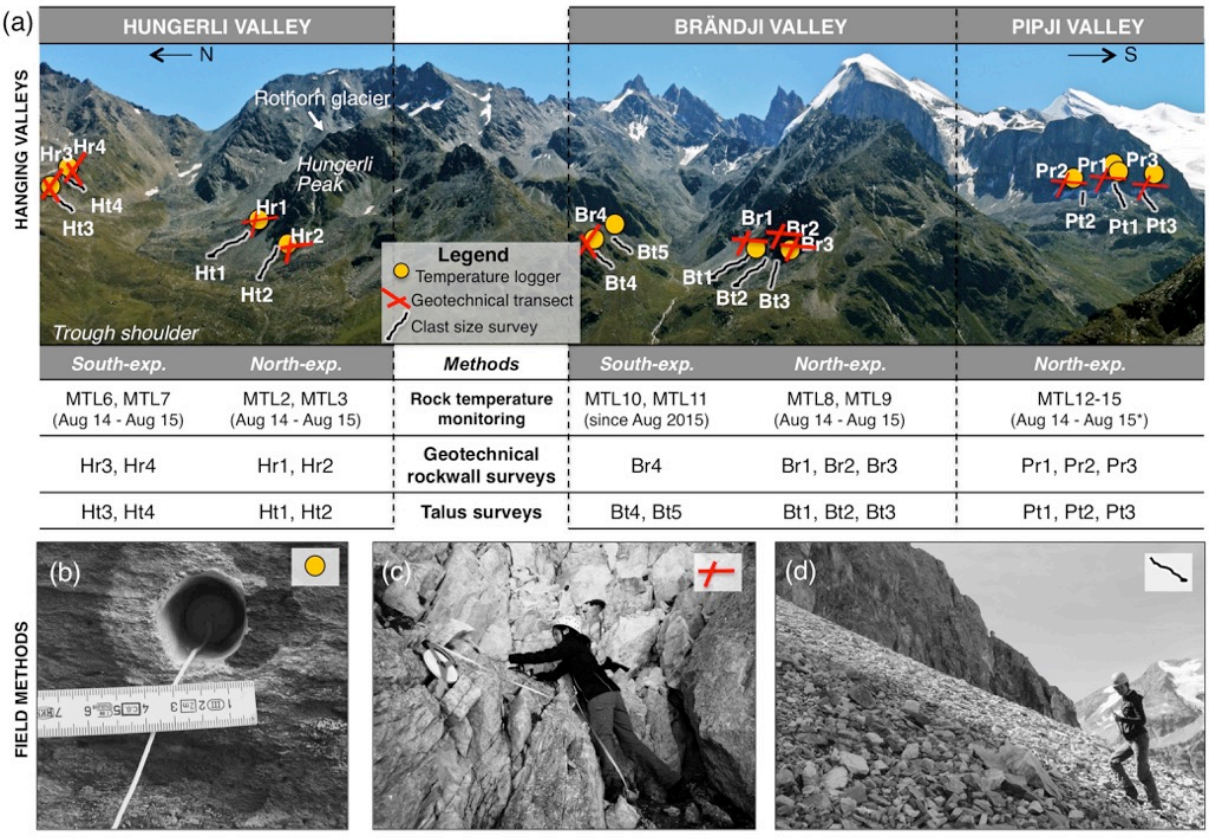

Figure 6.2: *Overview of field approach in three eastern hanging valleys of the Turtmann Valley (a). A total of 12 rockfall sediment cascades consisting of a source rockwall and rockfall sediment storage landform were investigated by combining (b) rock temperature monitoring (MTL = miniature temperature logger), (c) geotechnical rockwall surveys and (d) sedimentological transect surveys of rockfall deposits.*

6.3.1 Sedimentological transect surveys of rockfall sediment stores

Using talus slopes and surface sediment characteristics as an abductive proxy for rockfall activity and magnitude is a useful means to account for the multiplicity of potential key controls of their source rockwalls (Messenzehl and Dikau, 2017). Longitudinal variability in sediment size and shape on the surface of each storage landform has been quantified along twelve transects of varying length (150-50 m). Transects were placed from the apex to the toe of each site (Figure 6.2d). Care was taken to select transect areas within the

delivery area of primary rockfall events. Along each transect, sampling grids of 5 x 5 m with a grid size of 0.5 m were laid out every 25 m. At the grid intersects, each rockfall block or clast was measured with respect to its three axes (a-, b-, c-) (Caine, 1969; Pérez, 1993) leading to a maximum number (n) of 121 measured clasts per plot. On the foot slopes, this number was lower due to large boulder sizes with b-axis (> 0.5 m) larger than the mesh size. Similarly, at the apex, clasts smaller than 2 cm were not mapped so a minimum estimation was made. The approximate block volume V [m^3] was calculated using all three block axes (0.6 a*b*c) following the approach of Luckman and Fiske (1995). To evaluate the spatial heterogeneity of sediment sizes and shapes, the sorting index (standard deviation in phi, Folk and Ward (1957), the degree of sphericity (Goudie, 1981) and the degree of flatness were calculated (Gardiner and Dackombe, 1983).

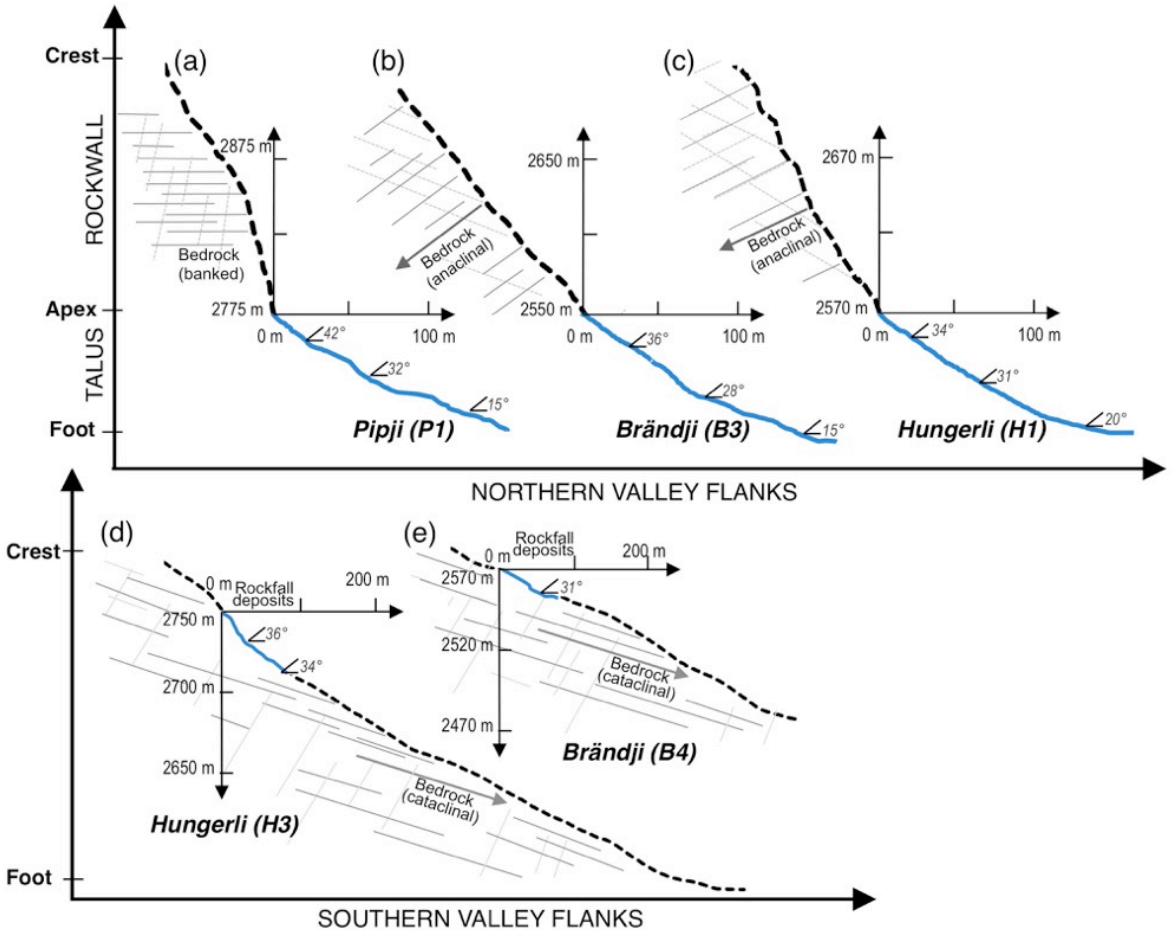

Figure 6.3: *Examples of hillslope profiles of rockfall sediment cascades on northern valley flanks (a-c) and southern valley flanks (d-e): Rockfall depositional areas (blue line signature and source rockwalls (black dashed line signature).*

6.3.2 Rock mass classification and joint volumetric count of source rockwalls

To add maximum information to the block surveys of rockfall sediment bodies, process-based geotechnical rock mass and joint surveys were performed on corresponding source rockwalls (Figure 6.2c). Following the standards of ISRM (1978), we recorded (i) true joint spacing, (ii) joint orientation, (iii) opening, (iv) persistence

and infilling, as well as (v) evidence of groundwater flow along horizontal (3-5 m) and vertical (2 m) transects. Intact rock strength was measured by a high impact L-type Schmidt Hammer (0.736 kN/m²) on different bedrock locations representative of the rockwall. A total of 20 readings was taken on lichen-free and un-jointed areas to calculate the mean rebound 'R' value (Aydin, 2015). Finally, using the semi-quantitative classification scheme of Selby (1980), we quantified the rock mass strength (RMS) index of each rockwall based on the individual ratings of measured joint and rock mass parameters. Furthermore, to estimate the potential rockfall block volume of the source rockwall, the volumetric joint count (Jv) was determined as an approximate measure of the joint density intersecting a m^3 volume of rock. According to ISRM (1978), Jv was calculated by:

$$Jv\ [joints/m^3] = S_1/l_h + S_2/l_h + S_n/l_v \qquad (6.1)$$

with S1, S2, Sn as joint counts of the dominant joint set (S) and with l_h and l_v as length of horizontal and vertical scanline transects. As proposed by ISRM (1978), corresponding block sizes can range from 'very large blocks' (Jv < 1.0) to 'very small blocks' (Jv > 30).

6.3.3 Near-surface rock temperature monitoring and frost cracking modelling

We furthermore extended our mechanical measurements with information on the thermal rockwall regime. Using miniature temperature loggers (MTL) near-surface rock temperatures (NSRTs) were recorded on each source rockwall between August 2014 and August 2016 (Figure 6.2a). Installation of calibrated iButtons® thermochrons (± 0.1 °C, Maxim DS1922) was performed following the design of Gruber et al. (2003) allowing comparability between individual MTL records. Moreover, it maintains consistency with previous work in other mountain areas (e.g. Allen et al., 2009; Hipp et al., 2014; Haberkorn et al., 2015a; Magnin et al., 2015b). The twelve MTLs were placed in boreholes of 10 cm depth on near-vertical (overhangs) and intact rock (Figure 6.2b) and a 3h measurement interval programmed. Water intake into boreholes and potential effects of heat advection were avoided by using waterproof polyethylene logger capsules, small drilling diameters (18 mm) and by sealing the borehole openings with a rubber plug and waterproof silicone.

For rockwalls where MTL records revealed constant winter temperatures (up to 100 days) between -3 °C and -9 °C, slow growth of seasonal segregation ice inside water-saturated pores and cracks is assumed (Hallet et al., 1991; Anderson, 1998). To predict the intensity and depth of associated bedrock cracking, the conduction-based heat flow model of Hales and Roering (2007) was applied. Although the model primarily considers heat transfer via conduction, it is suitable for application at this study site given the low-porosity of the paragneiss and limestone rocks (< 1% open porosity). Since the seasonal intensity of segregation ice growth is mainly a function of the thermal bedrock gradient (Everett, 1961; Worster and Wettlaufer, 1999), the depth-integrated frost cracking intensity [°C/cm] at each rockwall can be calculated using the following one-dimensional heat equation:

$$T(z,t) = MART + Ta\, e^{-z\sqrt{\frac{\pi}{\alpha P_y}}} \sin\left(\frac{2\pi t}{P_y} - z\sqrt{\frac{\pi}{\alpha P_y}}\right) \qquad (6.2)$$

where T is temperature, t is time, z is rock depth, MART is the mean annual near-surface rock temperature and Ta is the amplitude of the sinusoidal annual cycle Py (365 days). For thermal diffusivity α, depth-independent values of 1.3 mm^2/s (metamorphic rocks) and 2.1 mm^2/s (limestone) were assumed (Milanovic, 2004; Whittington et al., 2009). For simplification, sufficient rock moisture for ice growth is assumed given the transect surveys and MTL records. Likewise, micro-scale thermal effects caused by rock properties (mineralogy, porosity, schistosity) are neglected. Modelling was performed using the software R based on the mean statistics of the MTL records from 2014-2016 for all northern source rockwalls.

6.3.4 Statistical evaluation and data on potential controls

To evaluate the key controls on rockfall sediment cascades, a principal component analysis (PCA) has been applied to the sedimentological, mechanical and thermal data collected in the field as well as further GIS-based parameters (see below). PCA has been shown to be a useful eigenvector-based multivariate statistical method to find a reduced set of uncorrelated principal components (PCs) consisting of linear variable combinations with a maximum possible variance explained (Escabias et al., 2005; Aguilera et al., 2006). The cumulative proportion of variance explained of > 80% and an eigenvalue of > 1.0 were used as threshold criteria to select the minimum number of PCs with the maximum amount of explanatory power (Watanabe et al., 2017). Table 6.1 summarises all variables considered in the analysis as potential controls of bedrock weathering and instability, rockfall erosion and deposition. PCA was performed using R software packages (e.g. 'prcomp'). For comparability of PC vector lengths and directions, all variables were normalised (min-max method) on a scale of 0 to 1.

Values for external topographic and climatic variables were derived from GIS-based mean statistics of the rockfall source areas and include mean elevation, slope gradient, aspect and solar radiation sum. Rockfall source areas of depositional landforms have previously been calculated by Messenzehl et al. (2016) from a 1 m HRSC-Digital Elevation Model using, amongst others, the D8 low routing in SAGA GIS (Martz and Garbrecht, 1992). Mean solar radiation sum was identified by a hemispherical viewshed ArcGIS algorithm (Fu and Rich, 2002). For PCA, slope gradients were converted from degree to radians. Similarly, aspects were transformed to continuous measures of 'northness' by using the cosine (-1 = 180° to 1 = 0°). To implement internal thermal rockwall characteristics into the PCA, permafrost probability was estimated from a permafrost GIS-layer provided by BAFU (2005). Likewise, mean annual rockwall temperature (MART) recorded in the field (period 2014-2016), as well as modelled intensities of seasonal frost cracking, were considered.

Table 6.1: Field- and GIS-based input variables used in the principal component analysis to evaluate the key controls of rockfall sediment cascades.

Potential controls on rockfall sediment cascades	Variables (mean statistics)	Data source
Topoclimatic rockwall characteristics	Rockwall elevation [m] Rockwall length [m] Rockwall slope gradient [radians] Rockwall exposition [180°;0°] Solar radiation sum [WH/m^2]	Spatial characterisation of rockfall source areas in ArcGIS (derived from Messenzehl et al., 2016)
Thermal rockwall characteristics	Permafrost probability [patchy;extensive]	GIS Permafrost map of BAFU, 2005
	Mean annual rock temperature [°C]	Rock temperature records over the period 2014-2016 (this study)
	Intensity of frost cracking [°C/m]	Frost cracking modeling after Hales and Roering (2007) using MART and Ta recorded over the period 2014-2016 (this study)
Time since deglaciation	Relative time since deglaciation since LGM [1;0 ≙ today;LGM]	Topography-weighted Euclidean distance of rockfall source areas between hanging glaciers and valley outlet (derived from Messenzehl et al., 2016)
Rockwall mechanical characteristics	Lithology type [metamorphic, limestone] Overall orientation of main joint sets [0°;360°] Rock mass strength (RMS) [25;100]	Geotechnical rockwall surveys (this study)
Rockfall block size	Joint volumetric count (Jv) [3;20]	Geotechnical rockwall surveys (this study)

Furthermore, source rockwalls were parameterized according to their paraglacial adjustment status in order to evaluate the temporal activity of rockfall cascades after deglaciation. Since information on post-LGM glacial stages retreat in the study sites is missing, we inferred paraglacial adjustment stages by using ergodic reasoning or space-for-time substitution (Paine, 1985). Assuming a gradual glacier retreat starting on the trough shoulders at approx. 18 kyrs BP (Ivy-Ochs et al., 2009), the relative valley position of rockwalls between trough shoulder and present hanging glaciers was used as a substitute for the deglaciation time. It is assumed that rockfall activity declines with increasing deglaciation time (Ballantyne, 2002b) or, in space, with increasing distance from the glacier cirque (Messenzehl et al., 2016). Despite their simplifications, such topographic chronosequences have a long tradition in geomorphology and have been successfully applied to explain evolutionary stages of e.g. hillslope, river and coastal systems (Darwin, 1842; Davis, 1899; Brunsden and Kesel, 1973; Fryirs et al., 2012), especially when it comes to dealing with the lack of temporal data on a local deglaciation history (Messenzehl et al., 2016). The relative distance of source rockwalls to the cirque glaciers

was calculated in ArcGIS using the normalised and topography-weighted Euclidean distance ranging from 0 (trough shoulder, approx. 18 kyrs BP) to 1 (glacial cirque, recently glaciated or < 100 yrs). Topography-weighting was done by the slope angle in each DTM-cell to account for a relief-dependent ice thinning during deglaciation (Ballantyne and Benn, 1994). For easier interpretation, the rockwalls were grouped into three potential states of paraglacial adjustment: (i) intermediate, (ii) late and (iii) likely adjusted. An in-depth description of the GIS-based ergodic approach is provided by Messenzehl et al. (2016).

Finally, all major rock mechanical rockwall parameters identified in the field were used as input variables in the PCA (i.e. lithology, overall layering of main joint sets - banked, anaclinal, cataclinal, RMS indices and Jv results). Joint volumetric counts were inverted based on min-max-normalisation to allow better comparison with the last input variable, which is the median sediment size (in m^3) of each depositional landform.

6.4 Results

6.4.1 Sediment size and shape along active and inactive rockfall storage landforms

Figure 6.4 shows the longitudinal clast size distribution mapped along the surface of rockfall depositional landforms in the Brändji Valley (a-d), Hungerli Valley (e-f) and Pipji Valley (g-h). Independent of activity, lithology or slope aspect, all talus deposits have a relatively linear downslope increase from small clasts $<10^{-3}$ m^3 immediately beneath the rockwalls to large, mostly weathered boulders of around 10^{-1}-1 m^3 (median) at their concave slope toes (Figure 6.4b, d,f,h). Nevertheless, local variations are evident. Maximum block sizes have been found at northern paragneiss rockwalls, e.g. 28 m^3 at the foot of Bt3 (at 125 m in Figure 6.4b). In contrast, rockfall release from northern limestone cliffs in the Pipji Valley is linked to comparatively small rockfall volumes with interquartile ranges (IQR) from 4.5×10^{-4} to 1.3×10^{-2} m^3 (Figure 6.4h).

Additionally, Figure 6.5a-c displays distinct downslope variation in particle sorting (S.D. phi), block sphericitiy and flatness. Independent of lithology, active and north-exposed rockwalls (Ht1, Ht2, Pt1 in Figure 6.5a) are associated with relatively well-sorted upper slope segments (> 1.4 S.D. phi), while heterogeneity increases towards their lower segments. In comparison, relatively low clast sorting at the talus apex (< 1.4 S.D. phi) and a large size spectrum (Figure 6.4d,f) is characteristic of inactive and south-exposed rockwalls (Ht3, Ht4 in Figure 6.5a). With respect to lithology, metamorphic rockfall deposits (Ht1-Ht4 in Figure 6.5c) are dominantly flake-like at the upper slope (flatness index of < 0.65) and only become more spherical towards the slope foot (spherical index of > 1.45 in Figure 6.5b). In contrast, calcareous rockfall materials (Pt1 in Figure 6.5b) are markedly cubic across the entire storage surface, i.e. at equivalent apical and lower plots (sphericity index of <1.45).

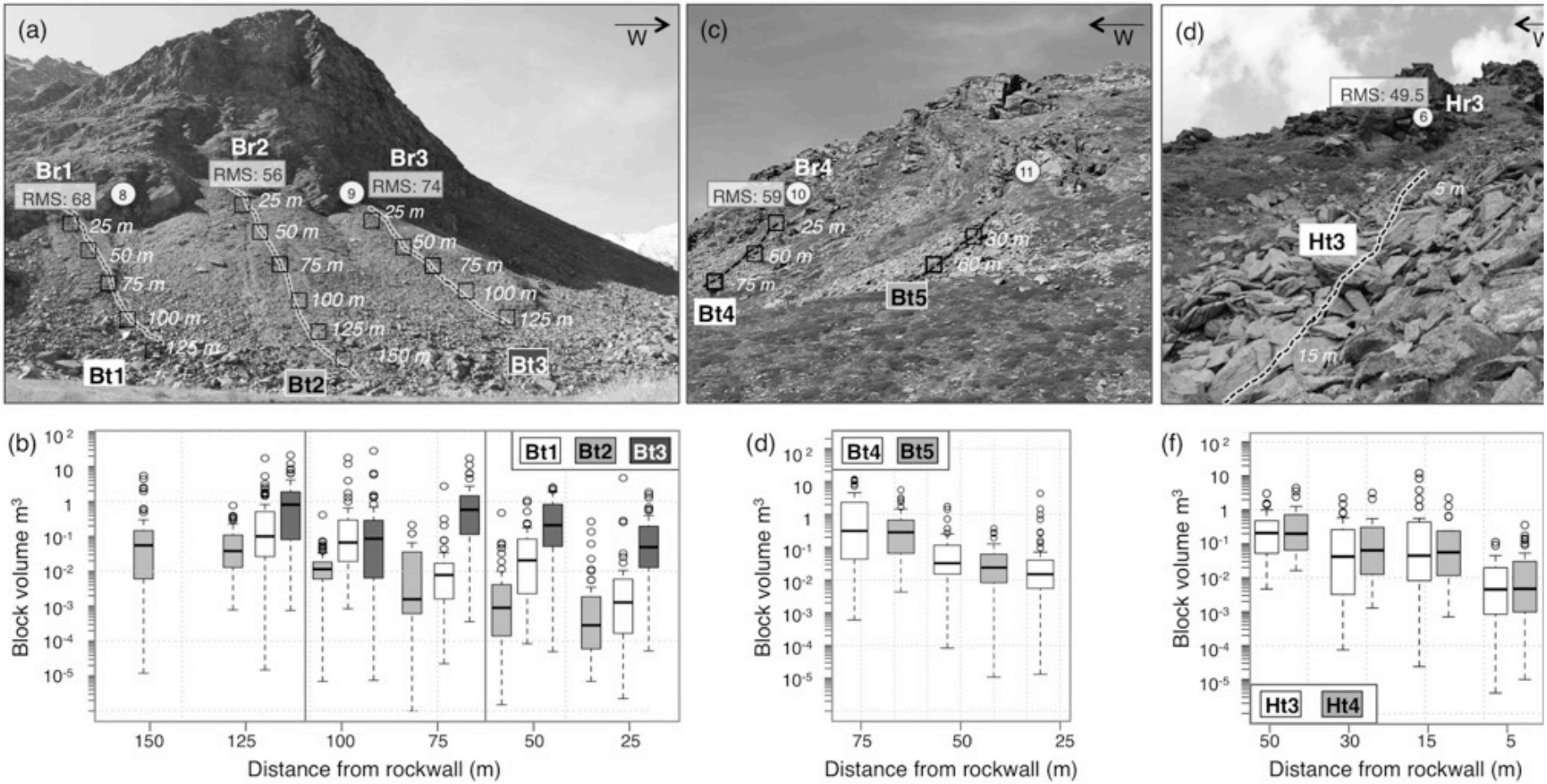

Figure 6.4: *Field sites of rockfall depositional landforms (upper photographs) and results of particle size distribution along field transect surveys (lower graphs shown as boxplots) for the Brändji Valley (a-b, c-d), Hungerli Valley (e-f) and Pipji Valley (g-h). Results of longitudinal block size distribution of Ht1 and Ht2 (Hungerli Valley) are presented in Messenzehl and Dikau (2017). Positions of Pt1, Pt3 and Ht4 are illustrated in Figure 6.1.*

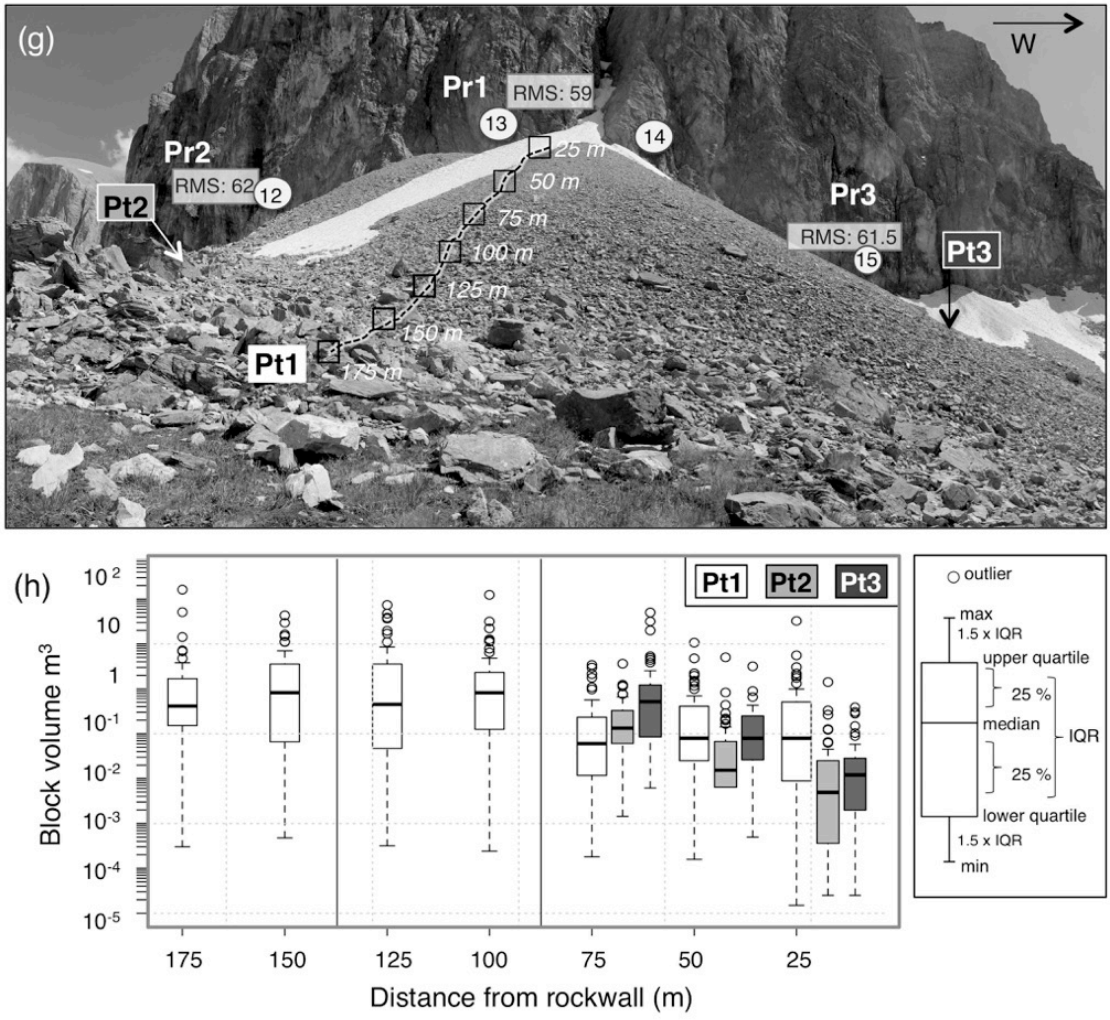

Figure 6.4 (continued: g-h).

6.4.2 Rock mass strength and potential rockfall sizes of source rockwalls

Table 6.2 displays results of the rock mass strength (RMS) classification of all rockwall source areas with respect to selected topoclimatic characteristics. Average RMS values are relatively comparable between all studied rockwalls and rated as moderate varying around a mean value of 61 (± 6). Nevertheless, spatial variations are evident. Moderate to strong RMS indices are generally linked to north-facing metamorphic rockwalls with comparable elevation (~2550 m asl) and mean inclination of ~ 75° (Ht1, Ht2 in Table 6.2a and Bt1-Bt3 in Table 6.2b). The highest RMS of up to 74 has been quantified at Br3 (Table 6.2b), where the largest rockfall clast sizes have been mapped (Figure 6.4b). By contrast, RMS of weathered paragneiss rockwalls such as along the higher-elevated (~2700 m asl) southern valley flanks is generally weak (e.g. Hr3 in Table 6.2a).

Table 6.2 shows that these local variations of RMS values are independent of the type of lithology, but mainly result from the individual (i) intact rock strength, (ii) surface weathering and the (iii) overall joint orientation relative to the surface. For example, moderate to slight surface weathering and relatively high Schmidt Hammer (SH) rebound values of > 50 (e.g. Hr1 in Table 6.2a and Br3 in Table 6.2b) generally increase

RMS, whilst stability is distinctly lowered on rockwalls with (very) weak intact rock strength and high surface weathering (e.g Hr4 in Table 6.2a). Furthermore, anaclinal (in-dipping) joint conditions, as on north-facing rockwalls, favour a high individual rating according to Selby's scheme (e.g. Hr1 in Table 6.2a), while cataclinal (out-dipping) conditions, typical for south-facing paragneiss, sites negatively influence rockwall stability (e.g. Hr3, Hr4 in Table 6.2a). Limestone rockwalls in the Pipji Valley are generally linked to a moderate RMS (59-62), positively influenced by horizontal joint layering and relatively low surface weathering.

With respect to potential block sizes, joint volumetric count (Jv) shows clear differences between sites correlated to joint spacing (Table 6.2). Generally small to medium block sizes dominate at limestone rockwalls (Pipji Valley). Here, small joint spacing of < 29 cm is associated with large Jv of up to 10.8 (e.g. Pr3 in Table 6.2c). In contrast, largest potential rockfall sizes were measured on paragneiss rockwalls, where average joint spacing often exceeds 1 m such as Hr1 and Hr2 on the Hungerli Peak (Jv: 3.4-3.1 in Table 6.2c) and at Br3 in the Brändji Valley (Jv: 2.3 in Table 6.2b). Jv of south-facing metamorphic rockwalls spans from small (e.g. Jv 19 at Br4 in Table 6.2b) to medium-sized blocks (e.g. Jv 5 at Hr4 in Table 6.2a).

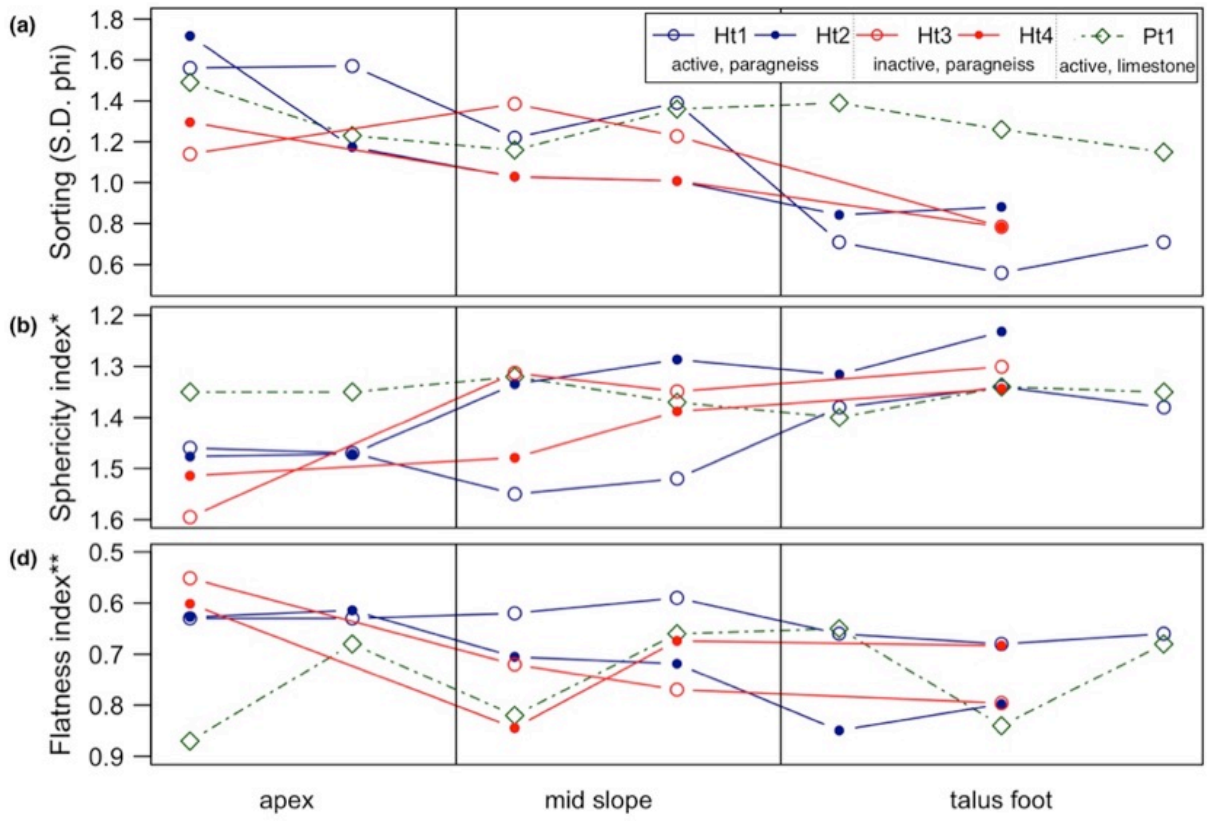

Figure 6.5: *Downslope distributional pattern of representative active (Ht1, Ht2, Pt1) and inactive (Ht3, Ht4) rockfall depositional landforms with respect to (a) degree of particle sorting, (b) degree of block sphericity and (c) flatness.*

Table 6.2: *Results of rock mass strength (RMS) classification, geotechnical joint mapping, joint volumetric count and selected topo-climatic characteristics of source rockwalls in the (a) Hungerli Valley, (b) Brändji Valley and (c) Pipji Valley.*

	(a) Hungerli Valley				(b) Brändji Valley				(c) Pipji Valley		
	Hr1 (N)	Hr2 (N)	Hr3 (S)	Hr4 (S)	Br1 (N)	Br2 (N)	Br3 (N)	Br4 (S)	Pr1 (N)	Pr2 (N)	Pr3 (N)
itude	2598 (±3m)	2573 (±4m)	2704 (±3m)	2711 (±3m)	2538 (±2m)	2551 (±4m)	2519 (± 1m)	2623 m (± 3 m)	2786 (±3m)	2788 (±7m)	2762 (± 7m)
t / Slope	10°/70°	340°/65°	123°/70°	120°/60°	326°/85°	6°/75°	18°/85°	243°/85°	310°/86°	350°/85°	346°/80°
ogy type	Paragneiss, schisty slate with amphibolite				Paragneiss, schisty slate with amphibolite				Marble, limestone		
olumetric ount nts/m³)	3.4 Large-medium-sized blocks	3.1 Large-medium-sized blocks	15.1 small blocks	5 Medium-sized blocks	13.7 Small blocks	5 Medium-sized blocks	2.3 Large blocks	19.0 Small blocks	6.7 Medium-sized blocks	10.8 Small blocks	3.7 Medium-sized blocks
ck strength R value	weak to moderate R: 30 - 52	Very weak to weak R: 9 - 37	Very weak to weak R: 19- 30	Very weak to weak R: 16- 29	Very weak to strong R: 23-50	Very weak to weak R: 18 - 37	Very weak to strong R: 23-54	Very weak to weak R: 17- 30	Very weak to weak R: 19 - 37	Very weak to moderate R: 16 - 46	Very weak to moderate R: 16 - 43
r:	***10 - 14***	***5 - 10***	***5***	***5***	***5 - 14***	***5 - 10***	***5 - 14***	***5***	***5 - 10***	***5 - 14***	***5 - 14***
eathering	Completely to slightly	Completely to moderately	Completely to highly	Completely to highly	Completely to moderately	Moderately	Completely to moderately	Completely to highly	Moderately	Unweathered to slightly	Unweathered to moderately
r:	***3 - 9***	***3 - 7***	***3-5***	***3-5***	***3 - 7***	***7***	***3 - 7***	***3-5***	***7***	***9 - 10***	***7- 10***
spacing	160 cm (± 85)	64 cm (± 5)	18 cm (± 10)	27 cm (± 37)	18 cm (± 15)	38 cm (± 31)	125 cm (± 21)	26 cm (± 12)	17 cm (± 27)	24 cm (± 21)	29 cm (± 10)
r:	***15 - 30***	***15 - 21***	***21***	***21***	***15 - 21***	***21***	***28***	***15-21***	***15 - 21***	***15 - 21***	***15 - 21***
rientation	90°/85° - 340/77°	90°/65° -330°/30°	340°/72° – 230°/36°	2°/23° – 190°/12°	95°/48° - 144/66°	305°/80 - 114°/73°	205°/29°-108°/71°	57°/42 – 188°/12°	28°/87° - horizontal	84°/67 - horizontal	92°/84° - horizontal
r:	***9 - 20***	***5 - 20***	***9-18***	***14-18***	***20***	***5 - 9***	***14- 20***	***9-18***	***9 - 14***	***5 - 14***	***5- 14***
opening	0.1 cm - 4 cm	0.1 cm – 1.9 cm	0.1 cm – 5 cm	0.1 cm – 6 cm	0.1 cm - 8 cm	0.1 cm – 3 cm	0.1 cm – 3 cm	0.1 cm – 6 cm	0.1 cm – 15 cm	0.1 cm - 44 cm	0.1 cm – 10 cm
r:	***2 - 7***	***2 - 7***	***2 - 7***	***2 - 7***	***2 - 7***	***2 - 7***	***2 - 7***	***2 - 7***	***2 - 7***	***2 - 7***	***2 - 7***
ontinuity nfilling	few (thin infill) to continous (cemented)	Continuous (no - thin infill)	Few (clear to thin infill)	Few (thin infill)	Few (thin infill) to continous (cemented)	Continuous (no - thick infill)	Continuous (no- thick infill)	Few to continous (thin infill)	Continuous (no – thin infill)	Continuous (no infill)	Few to continuous
r:	***4 - 6***	***5 - 6***	***6***	***6***	***4 - 6***	***1 - 5***	***1 - 5***	***4 - 6***	***4 - 5***	***5***	***5 - 6***
ndwater tflow	None to slight	None to slight	None	None	None	None	None	None	None	None	None
r:	***4 - 6***	***4 - 6***	***6***	***6***	***6***	***6***	***6***	***6***	***6***	***6***	***6***
k mass th (RMS)	**65 (± 13.9)**	**60 (± 9.9)**	**49.5**	**50**	**68**	**56**	**74**	**54**	**59**	**62**	**61.5**
	Moderate	**Moderate**	**Weak**	**Weak**	**Moderate**	**Moderate**	**Strong**	**Moderate**	**Moderate**	**Moderate**	**Moderate**

6.4.3 Rockwall thermal regime and frost cracking intensity

Figure 6.6 shows the near-surface rockwall temperatures (NSRT) recorded between August 2014 and August 2016 on all north-exposed monitoring sites. At MTL15, records are only available between August 2014 and August 2015. In 2014-2015, mean annual rock temperature (MART) was between 2.8 °C (Br1 in Figure 6.6b) and 0.67 °C (Pr2 in Figure 6.6d). One year later, MARTs dropped slightly to between 1.67 °C (Hr2 in Figure 6.6a) and 0.14 °C (Pr2 in Figure 6.6d). MART values just above 0 °C indicate permafrost boundary conditions.

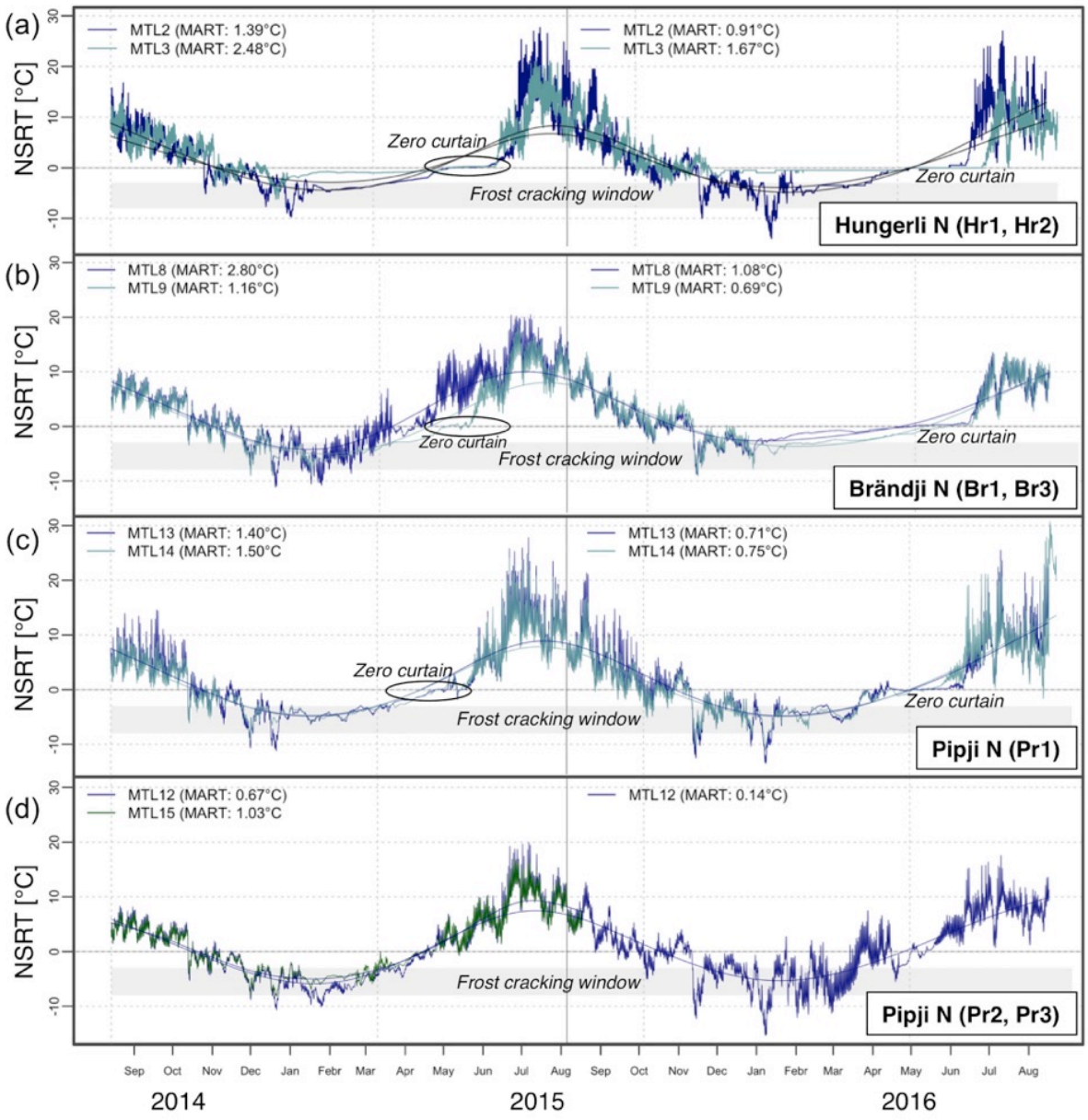

Figure 6.6: *Near-surface rock temperature (NSRT) records of all north-exposed monitoring sites in the (a) Hungerli, (b) Brändji and (c-d) Pipji Valley over the period August 2014 to August 2016.*

From late August in both 2014 and 2015 NSRTs of all north-facing rockwalls progressively cooled down with frequent temperature oscillations between approx. -5 °C and 5 °C during autumn (Figure 6.6a-d). The highest number of diurnal frost cycles (up to 87) has been recorded at Pr2 in the period 2014-2015 (Figure 6.6d) and at Hr2 in autumn 2015 (Figure 6.6a). During winter (i.e. January), NSRTs at the snow-free sites (Br1, Pt2, Pt3) progressively dropped to minimum values of -12 °C (MTL8 in Figure 6.6b) and -15 °C (Figure 6.6d). After this winter cooling, NSRTs rapidly increased followed by daily frost cycles in early spring (-5 °C to 7 °C). In contrast, constant NSRTs have been recorded for several winter months (~116 days) at the Hungerli Peak (Figure 6.6a), at Br3 (Figure 6.6b) and to some extent at Pr1 (Figure 6.6c). Stagnating winter temperatures between 0 °C and -9 °C recorded at those sites and the lack of temperature oscillations reveal an insulating rockwall snow cover that prevents progressive winter cooling and heat loss during spring. Snowmelt generally started between late April and early May as indicated by the MTLs' zero curtains (constant 0 °C in Figure 6.6a-c). With thinning snow cover, NSRTs progressively rise, due to the onset of atmospheric heat penetration and latent heat consumption. During summer, large diurnal thermal cycles between have been recorded at all sites with maxima of 32 °C (e.g. Pr1 in Figure 6.6d).

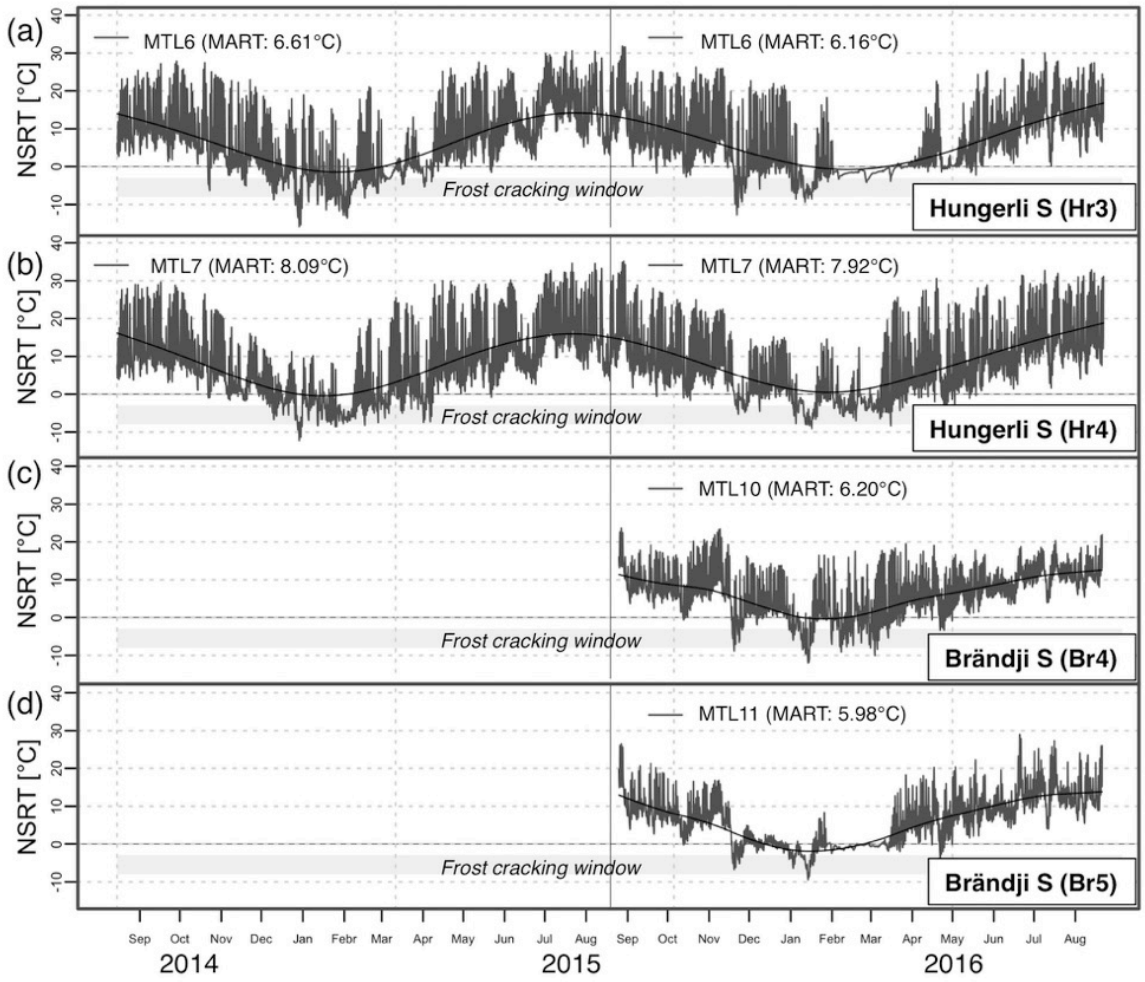

Figure 6.7: *Near-surface rock temperature (NSRT) records of all south-exposed monitoring sites in the (a) Hungerli and (c-d) Brändji Valley over the period August 2014 to August 2016.*

NSRT records from south-facing monitoring sites (Figure 6.7) display an inter-annual thermal regime governed by direct exposure to solar radiation and permafrost-free conditions. For instance, relatively high MARTs with average values of 7.35 °C (±0.74) have been recorded over the period 2014-2015, and 6.56 °C (±-0.79) over the period 2015-2016 (Figure 6.7a-d). From early spring until late summer, frequent diurnal and short-term (3h) thermal cycles are evident with maxima of 35.9 °C as in September 2015 (e.g. Hr4 in Figure 6.7b). Temperature peaks during summer are typically followed by immediate and rapid drops of more than 8.5 °C within 3h. During winter, southern rockwalls are similarly affected by a slow decrease in NSRT to minimum temperatures of e.g. -15.88 °C (Figure 6.7a). Between late November and early May, frequent frost cycles between approx. -12 °C and 25 °C, rather than constant sub-zero temperatures, dominate at all sites. The three short intervals of constant 0 °C (zero curtain) at Hr3 (Figure 6.7a) and Br5 (February - March 2016 in Figure 6.7d) indicate short accumulation of snow cover during early spring. Nevertheless, the short time intervals within the frost cracking window exclude the efficiency of segregation ice growth on those sites (Hallet et al., 1991; Prick, 1997).

Figure 6.8 displays the predicted depth-varying frost cracking intensity (°C/cm) of all northern rockwall sites, based on the MART and Ta recorded over the period between 2014 and 2016. Maximum cracking intensities and depths of segregation ice growth vary slightly between individual sites. Highest frost cracking intensities with peaks within the near-surface (~ 20 cm) have been predicted for paragneiss rockwalls in the Hungerli Valley (Figure 6.8). For limestone rockwalls in the Pipji Valley, deepest frost cracking depths of > 4 m have been calculated with peaks at 50 cm depth (Pr1, Pr2 in Figure 6.8). In the Brändji Valley, segregation ice growth occurs in comparatively shallower depths (< 2.5 m) and frost cracking is limited to the outermost few centimetres (Br1, Br3 in Figure 6.8).

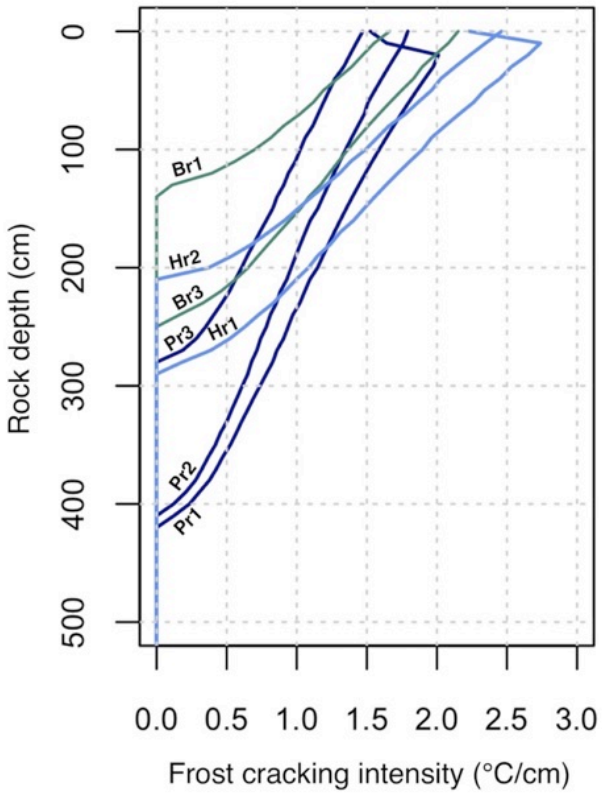

Figure 6.8: *Predicted seasonal frost cracking intensities of all north-exposed rockwall sites as function of the thermal gradient in [°C/cm] integrated over bedrock depth.*

6.4.4 Principal components

From the maximum number of 12 principal components, a reduced set of the first three PCs was selected which explain 89% of the total variability in the dataset (Table 6.3). The maximum amount of total variation (57%) is described by PC1 with an eigenvalue of 6.9. PC2 and PC3 explain an additional 21% and 9% of the dataset variability, respectively. Given the eigenvectors assigned to all variables, which are equal to their correlation coefficients with each PC, the individual variable combination can be interpreted as follows: PC1 represents the 'morphometric and thermal rockwall regime', due to its positive correlation with rockwall exposition, MART and annual solar radiation, and its strong negative association with frost cracking intensity, permafrost probability as well as slope gradients and rockwall profiles (bold eigenvalues in Table 6.3). PC2 defines the 'rock mechanical preconditioning' with respect to elevation, given the high eigenvectors of the RMS and the potential block size (or joint density). PC3 denotes the 'particle size on paraglacial sediment storage', due to the high positive correlation (> 0.60 in Table 6.3) with the deposited block size and paraglacial adjustment.

Table 6.3: First three uncorrelated principal components (PC1, PC2, PC3) explaining 87 % of the maximum variability in the dataset with an eigenvalue exceeding 1.07. Positive and negative eigenvectors assigned to the 12 variables within each PC are equal to the correlation coefficient with the PC. Geomorphic explanation of PCs is based on the highest positive and negative eigenvalues (bold values).

	PC1	PC2	PC3
Elevation	-0.17	**0.41**	-0.25
Length	**-0.36**	0.13	0.12
Slope	**-0.38**	-0.07	0.32
Exposition	**0.32**	0.25	0.08
Radiation	**0.37**	0.09	-0.03
Permafrost	**-0.34**	0.23	0.12
MART	**0.37**	0.02	-0.08
Frost cracking	**-0.33**	-0.15	-0.31
Paraglacial	-0.29	0.14	**-0.37**
RMS	-0.21	**-0.45**	0.20
Deposited block size	0.02	-0.36	**-0.66**
Potential block size	0.09	**-0.56**	0.14
Eigenvalue	6.9	2.58	1.07
Proportion of Variance %	57%	21%	9%
Cumulative Proportion %	57%	78%	87%
Geomorphic explanation	***Morphometric and thermal rockwall regime***	***Rock mechanical preconditioning***	***Particle size on paraglacial rockfall storage***

Figure 6.9a shows the ordination diagram of PC1 and PC2, which clusters all twelve rockfall sediment cascades into three groups dependent on lithology, overall joint orientation and exposition. All S-exposed rockfall deposits originating from cataclinal, metamorphic rockwalls are best described by their exposition, high radiation receipt and high MART of their source rockwalls (Ht3, Ht4, Bt4, Bt5 in Figure 6.9a). In contrast, north exposed rockfall cascades in anaclinal, metamorphic settings are best described by steep and high-elevated rockwalls with high frost cracking intensities and high RMS values (Ht1, Ht2, Bt1-Bt3 in Figure 6.9a).

Similarly, rockfall sediment cascades released from north-exposed limestone rockwalls are determined by high permafrost probability, long and near-vertical slope profiles and paraglacial adjustment (Pt1-Pt3 in Figure 6.9a).

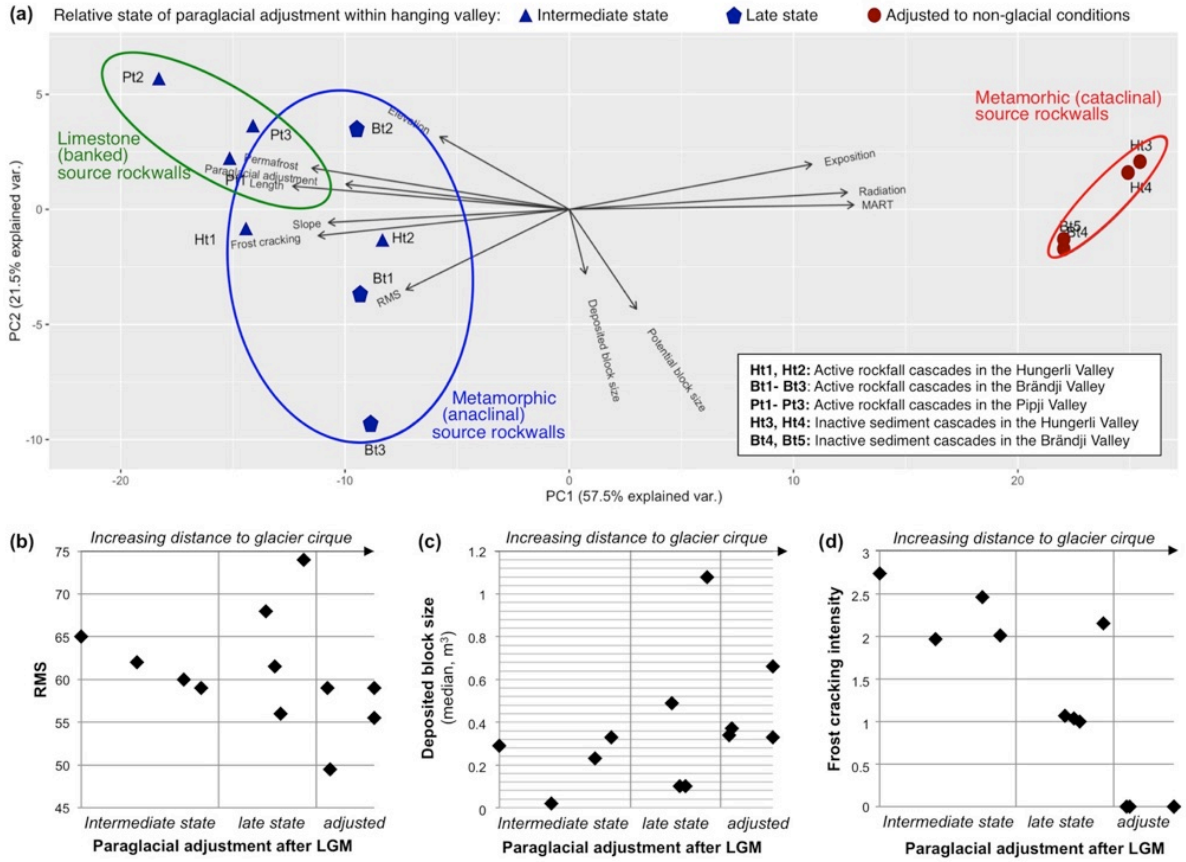

Figure 6.9: *(a) Ordination diagram of the principal component analysis grouping the rockfall depositional landforms investigated in the field by PC1 (x-axis) and PC2 (y-axis). Vector length and direction of the variables signify variable importance for the individual rockfall sediment cascades. Paraglacial adjustment after LGM (or distance from hanging glacier) has been plotted against RMS (b), median deposited block sizes (c) and frost cracking intensity (d) of source rockwalls.*

Figure 6.9a furthermore displays contrasts with respect to paraglacial adjustment state. While active sediment cascades in an intermediate paraglacial state (near the glacial cirque) are best explained by cryospheric and morphometric rockwall parameters (triangles in Figure 6.9a), sediment cascades within a late paraglacial state are structurally controlled by their RMS indices (hexagons in Figure 6.9a). In turn, inactive and paraglacially adjusted sediment cascades are best described by topoclimatic factors (dots in Figure 6.9a).

For better interpretation of mechanical and thermal variables with respect to the paraglacial adjustment of rockwalls, the latter has been plotted against RMS (Figure 6.9b), median deposited block size (Figure 6.9c) and frost cracking intensity (Figure 6.9d). Figure 6.9b illustrates no distinct paraglacial trend for the RMS, while Figure 6.9c reveals that deposited block sizes (median) slightly decrease with decreasing time since LGM. Figure 6.9d displays a statistically significant (inverse) paraglacial trend for frost cracking intensity, which increases with decreasing time since deglaciation (and distance to the glaciers).

6.5 Interpretation and Discussion

6.5.1 Evaluation of frost cracking model with respect to mechanical rockwall properties

The sustained sub-zero winter temperatures recorded at all northern MTL sites (Figure 6.6) even just below freezing, suggest favourable conditions for ice segregation in water-surrounded pores and/or cracks linked to effective disjoining forces (Hallet et al., 1991; Girard et al., 2013). On the basis of the 2014-2016 MART and Ta, our frost cracking modelling predicts efficient ice segregation growth up to 420 cm bedrock depth and highest frost cracking peaks in the uppermost 20-50 cm (Figure 6.8). These observations are in good accordance with previous field and modelling observations from both metamorphic and calcareous north-facing rockwalls in alpine places including the Japanese, Austrian and Southern New Zealand Alps (Matsuoka et al., 1997; Matsuoka and Sakai, 1999; Sass, 2005b; Hales and Roering, 2007). Hales and Roering (2007, p. F2033) emphasised that their frost cracking modelling approach particularly provides a first-order understanding of rockwall erosion and rockfall supply if coupled with field measurements of rockwall joint properties and spacing. Our integrative methodological approach allows consideration of both thermal and mechanical rockwall properties. The geotechnical findings shown in Table 6.2 suggest that the predicted frost cracking peaks cause small-sized bedrock instabilities in highly fractured rockwalls with large joint volumetric counts (e.g. Br1, Pr2). Rockwalls with low RMS and moderate to complete surface weathering (e.g. Br2, Pr in Table 6.2b, c) are in particular more susceptible to shallow bedrock erosion. As a consequence we expect small-sized, low-energetic rockfall sediment cascades to the upper talus segments. This is mirrored by the dominance of fresh platy talus sediments of 10^{-2} -10^{-1} m^3 mapped 25-50 m away from the rockwall (Figure 6.4a,b, Figure 6.5c).

Similar observations were reported in the neighbouring debris-flow dominated Illgraben, where frost-cracking was found to be the most effective processes for channel filling, particularly in combination with rockwall snow cover (Bennett et al., 2013). The thermal influence of local rockwall snow cover is also evident in most of our northern MTL records in Figure 6.8. Especially in the warm winter 2014-2015, when early and exceptional snow precipitation was recorded in the Valais Alps (MeteoSwiss, 2015), an insulating snow cover visibly decoupled the underground from the colder atmosphere given the constant and smoothed sub-zero NSRTs (Figure 6.6a, c). However, on those snow-covered rockwalls, one key limitation of the applied frost-cracking model is certainly the overestimation of conductive heat transfer (Luetschg, 2005; Luetschg et al., 2008), whereas advective heat fluxes during melt water infiltration and latent heat consumption in spring (zero curtains in Figure 6.6) are probably underestimated (Hasler et al., 2011a). Although application of the conduction-based approach is appropriate in our study given the low porosity (< 1%) and small joint openings (Table 6.2) of both paragneiss and limestone rocks (see e.g. Anderson, 1998), it is important to state that the quantified cracking intensities represent minimum values for snow-covered sites. Likewise, where MART's close to zero indicate permafrost boundary conditions, such as in the Pipji Valley (Figure 6.6c, d), our modelling results must be carefully interpreted. While the predicted near-surface frost peaks are still likely to cause cm- to dm-sized rockfall cascades (Figure 6.4g, h), large rockfall sizes due to bi-directional and deep-seated freezing over permafrost must also be considered (Murton et al., 2001; Murton et al. 2006). Especially in rockwalls with large joint spacing and Jv < 3, such as Br3 in the Brändji Valley (Table 6.2b), high-magnitude sediment

cascades with long run-out length are reasonable as reflected by block deposits of up to 28 m^3 found 125 m away from Br3. However, in comparison to rockfall release from weathered bedrock, high-magnitude rockfall cascades may occur infrequently, particularly where source rockwalls have high rock mass strength (e.g. Bt3 in Table 6.2b). Therefore, in agreement with Hales and Roering (2007), frost cracking modelling provides a simple, but highly useful, means to predict approximate block sizes and, in part, relative frequencies of rockfall sediment cascades, if modelling results are combined with geotechnical field data from source rockwalls.

6.5.2 Role of thermal and morphometric rockwall properties for rockfall cascades

The roots of geomorphic sediment cascade studies in formerly or still glaciated alpine valleys go back to the 1970s, particularly when the storage of postglacial sediments and their spatiotemporally delayed delivery to fluvial systems emerged as a key research question in geomorphology (Chorley and Kennedy, 1971; Church and Ryder, 1972; Church et al., 1979; Walling, 1983; Church and Slaymaker, 1989; Slaymaker, 2003). Yet, as stated earlier, within this 'sediment-dominated' research focus the deglaciated rockwall system is often only implicitly regarded as primary source of paraglacial sediments and driver for downslope sediment transfer. The observations of our study, however, emphasise the first-order control of thermal and morphometric rockwall properties on paraglacial rockfall cascades. In particular, our calculations show that the interplay of seasonal frost cracking and permafrost occurrence in shaded northern and near-vertical rockwalls explains 57% of the variability amongst the twelve rockfall cascades (PC1 in Table 6.3). The inverse trend between frost cracking intensity and time since LGM deglaciation in Figure 6.9d demonstrates that frost weathering is most important for sediment cascades close to the hanging glaciers, where source rockwalls are still adjusting to their former glaciation. These observations are consistent with previous regional-scale frost weathering studies in the Swiss Alps (Gruber et al., 2004b) and emphasise the importance of long-term frost cracking not only for postglacial bedrock erosion and relief evolution (Hales and Roering, 2009), but also for downslope paraglacial sediment fluxes (Ballantyne, 2002).

Besides frost cracking, Figure 6.9a reveals the importance of permafrost in deglaciated rockwalls as key control on paraglacially adjusting sediment cascades, particularly from near-vertical and still adjusting limestone cliffs such as in the Pipji Valley. Here, patchy (Pr1-Pt3) to extensive (Pr2, Pr3) permafrost conditions were estimated by BAFU (2005, Figure 6.1c) which seems likely given the recorded MARTs ranging between 1.5 °C and 0.14 °C (Figure 6.7). Thus, decreasing strength of rock mass and ice-filled joints in response to permafrost warming and thawing after ice removal (Davies et al., 2001; Krautblatter et al., 2013), combined with deep (> 4m) frost cracking (Pr2, Pr3 in Figure 6.8) may lead to high rockfall activity of different rockfall magnitudes (Fischer et al., 2006; Ravanel et al., 2017). At first glance, the distinctly small-sized sediment deposits on the surface of talus slopes in the Pipji Valley (Figure 6.4g,h) seem to exclude the recent release of high-magnitude rockfall sediment cascades (Figure 6.10a). However, from a kinematic perspective, given the exceptional rockwall heights of up to 280 m Table 6.2a) and the banked limestone's dense joint spacing of < 29 cm (Table 6.2c, Figure 6.10a), effective rockfall fragmentation into small cubic blocks after the first ground impact is plausible (Frattini et al., 2012; Ruiz-Carulla et al., 2015). Additionally, from a thermo-mechanical perspective, considering the relatively high RMS of ~60 and the steep gradients of > 85° (Table 6.2), it is reasonable that

extensive and cold permafrost conditions soon after deglaciation Table 6.2c) still stabilise the rock mass (Mellor, 1973) counteracting the detachment of large block magnitudes (Wegmann et al., 1998; Krautblatter et al., 2013; Krautblatter and Leith, 2015). This notion seems to be supported by Figure 6.9c showing a trend of decreasing block sizes with decreasing time since deglaciation and proximity to the glaciers where permafrost probability is relatively high (Figure 6.1c).

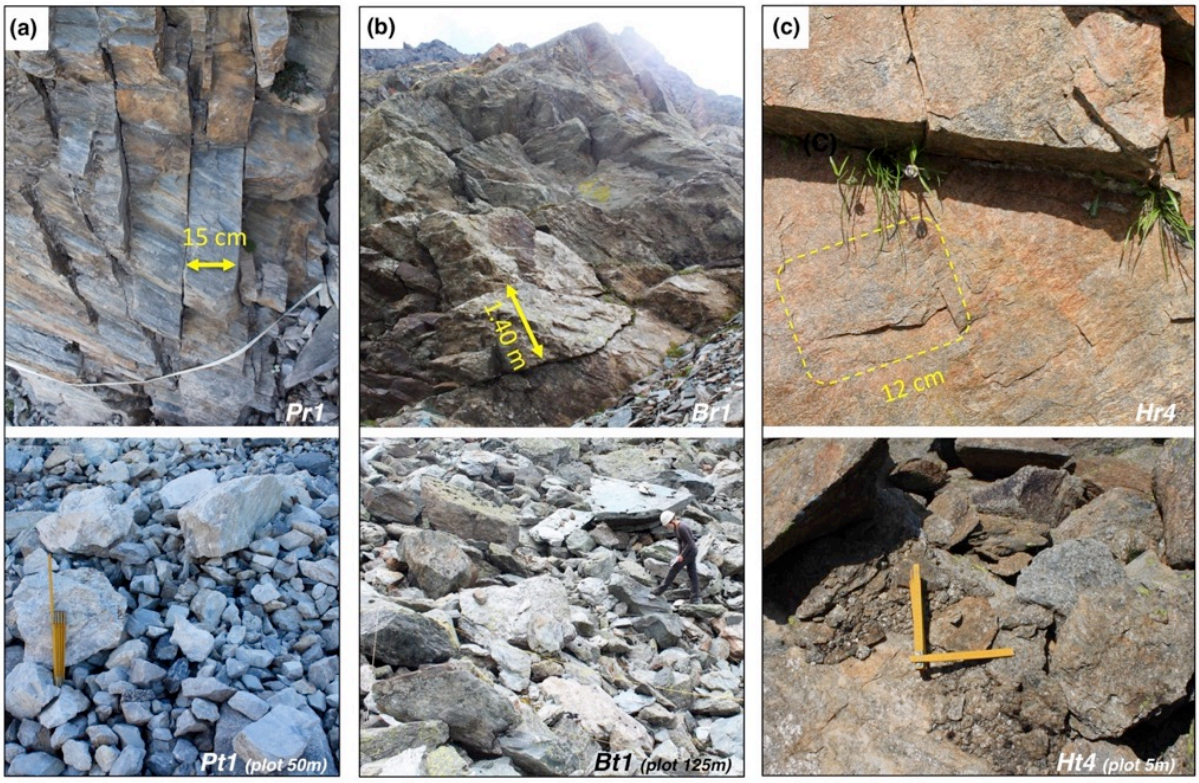

Figure 6.10: *Characteristic form-material relationships between rock mechanical properties of source rockwall (i.e. joint spacing) and block deposits on respective foot slopes. Examples from (a) densely banked limestone rocks, (b) widely spaced anaclinal paragneiss rockwalls and (c) south-exposed, cataclinal rockwalls with microfractures.*

Moreover, the dominance of active and still adjusting rockfall cascades from glacially steepened (> 75°) and lengthened (> 170 m) source rockwalls shown in Figure 9a (e.g. Pt1-Pt3) emphasises the inheritance of Pleistocene glacial erosion. As postulated in other high-alpine settings, we assume that horizontally acting shear stresses of those near-vertical sites are critically increased leading to high activity of rock failures and sediment supply to talus slopes (Bovis, 1990; Harbor, 1992). This shows, as noted by McColl (2012), that glacial erosion and the associated topographic modification is a key preparatory, if not triggering, factor for paraglacial rockwall failures and associated rockfall-dominated sediment fluxes after glacier retreat (Augustinus, 1992; Augustinus, 1995; Holm et al., 2004; Leith et al., 2014a).

In agreement with McColl (2012), our observations furthermore emphasise that the influences and causes of paraglacial rockwall adjustment and, thus, downslope sediment cascades change with increasing time since deglaciation. Using ergodic reasoning, our analyses demonstrate that permafrost and frost cracking decrease in relative importance where sediment cascades are adjusted to non-glacial conditions, whilst high solar radiation

sums coupled to high positive MART (Figure 6.7) become key controls (Figure 6.9a). Moreover, rockwall morphometry becomes one of the key factors limiting the efficiency of rockfall production and downslope sediment transfer. This is particularly evident on southern valley flanks in the Hungerli and Brändji Valley (Figure 6.9a), where missing gravitational fall sorting (e.g. Bt4, Ht3 Figure 6.4d,f) and low sorting degree of talus slopes (Figure 6.5a) indicate a terminated paraglacial adjustment (Ballantyne and Benn 1994) and transport-limited conditions (Richter, 1901; Lehmann, 1933; Bakker and LeHeux, 1952; Höllermann, 1983). Our field observations suggest inactivity of sediment cascades particularly due to low slope gradients of dissected source rockwalls (Figure 6.3d,e) and their coverage by rockfall or/and weathering debris (Figure 6.4c,e). Thus, contrary to active sediment cascades with long and geomorphologically efficient permafrost rockwalls such as in the Pipji Valley (Figure 6.3a-c), it appears that an increasing rockwall maturity and decreasing contributing area in the course of the paraglacial period are the key determining variables for inactivity of sediment production after adjustment to non-glacial conditions (Statham, 1976; Olyphant, 1983; Curry and Morris, 2004).

6.5.3 Mechanical preconditioning of paraglacial rockfall cascades

Steep hillslope gradients and high relief as well as high precipitation amounts, low atmospheric and rock temperatures are some of the often-cited characteristics of high-alpine environments (Barsch and Caine, 1984; Owens and Slaymaker, 2004). When it comes to describing associated high-energetic rockfall sediment supply to talus slopes, those external topoclimatic variables are commonly the most studied parameters in both field- and GIS-based geomorphic research (Schrott et al., 1999; Cavalli et al., 2013; Götz et al., 2013; Bennett et al., 2014; Tiranti et al., 2016). Likewise in our study, the contrasting depositional patterns of northern and southern talus slopes seem to reflect a topoclimatic-dependent trend of rockfall sediment cascades (Figure 6.4). While the efficiency of sediment cascades on southern, sun-exposed sites is mainly a function of solar radiation linked to high MART (Figure 6.9a), the typical longitudinal gravitational fall sorting on all northern talus slopes (Figure 6.4b,h) suggest active rockfall transfer from frost weathering dominated source rockwalls (Rapp, 1960b; Kirkby and Statham, 1975; Pérez, 1989, 1998). Thus, at first glance, this aspect-dependent depositional activity seems to support the prevailing topoclimatic hypothesis, favouring the combination of solar radiation, MART and freeze-thaw weathering (over permafrost) as the most important drivers for rockfall sediment cascades (Gardner, 1972; Gardner, 1983; Luckman, 1988; Hales and Roering, 2005; Sass, 2005b; Sass, 2010).

However, what remain little considered in previous sediment cascade research are rock mass and joint properties of source rockwalls. Our geotechnical field surveys (Table 6.2) provide evidence that the valley-scale topoclimatic pattern of rockfall sediment cascades is locally predefined by rock mechanical properties (PC2 in Table 6.3). In particular, Figure 6.9c displays a positive correlation between the median deposited sediment size and the potential rockfall size. Importantly, this trend is independent of any topo-climatic or lithological variable, as reflected by the vector orientations (Figure 6.9a). These observations imply that the likelihood of coarse-grained sediment cascades after ice retreat increases at rockwalls with increasing joint spacing (e.g. Figure 6.10b). A similar trend has been reported by André (1997) from metamorphic rocks in Svalbard and by Olyphant (1983) from igneous rockwalls in the Blanca Massif, where postglacial talus supply was best explained

by joint density rather than solely by topoclimatic factors. In our study sites, joint spacing (expressed as potential rockfall size) statistically explains an additional 24% (PC2) of the investigated rockfall sediment cascades, particularly in combination with the rock mass strength (Table 6.3). However, no significant paraglacial trend was found between RMS and rockfall activity and time since deglaciation (Figure 6.9b), contrary to observations by Moore et al. (2009) from granitic rocks in the Sierra Nevada/Yosemite area. Nevertheless, Figure 6.9a reveals that RMS becomes a prime driver of sediment cascades specifically within a late paraglacial adjustment state, where permafrost thaw and warming is most critical (e.g. Bt1). Moreover, our observations underline the strong dependence of paraglacial sediment supply on joint orientation relative to the slope surface, consistent with Moore et al. (2009) albeit with opposite effects. Interestingly, rockfall sediment cascades from cataclinal rockwalls were found to be inactive (Figure 6.9a), whereas active sediment transfer generally derives from rockwalls with horizontal (banked) and in-dipping joint orientations. These observations might seem surprising as the latter structural conditions are usually described as favourably stable and less prone for rockfall release (Selby, 1982a; Cruden and Hu, 1993; Cruden and Hu, 1998). However, previous regional-scale modelling by Messenzehl et al. (2016) showed that out-dipping (cataclinal) conditions are highly susceptible to fast bedrock adjustment and rapid exhaustion of rockfall supply immediately after deglaciation. In contrast, anaclinal structural conditions were postulated to favour overall bedrock stability so that rockfall supply further downslope can be enhanced several decades and centuries after ice retreat. Therefore, our field-based study also emphasises the significance of mechanical preconditioning on the paraglacial sediment flux system. They show that sediment production and downslope transfer can either rapidly decline if originating on cataclinal slopes with favourable failure planes, or can be time-delayed and still enhanced today on anaclinal and more competent rockwalls.

6.5.4 Evidence for thermal weathering as driver for small-sized sediment supply

While 87% of the spatial variability amongst the twelve investigated sediment cascades in the hanging valleys can be explained by the factors measured in this study other potential controls have not been considered yet but deserve more attention. For our study sites, we assumed seasonal freeze-thaw dynamics in the bedrock near-surface as a key destabilising mechanism. According to recent research, ice segregation is a more likely cause of frost cracking than diurnal freeze-thaw cycles (Hallet et al., 1991; Hallet, 2006; Amitrano et al., 2012; Andersen et al., 2015). Guided by assumptions on segregation ice growth in natural conditions, we modelled the depth-integrated frost cracking intensity using the approach by Hales and Roering (2007).

However, the 2-years NSRT monitoring in the study sites points to the potential importance of thermal cycling. Figures 6.6 and 6.7 illustrate the high frequency of large thermal variations in the range of 35.9 °C to 8.5 °C/3h during summer, not just on southern rockwalls. While the 3-hrs monitoring interval is too long to detect sudden thermal shock events (Hall and André, 2001), it provides evidence for rock weathering by sun-induced thermal fatigue (Yatsu, 1988; Wang and Liaw, 2008). Although this study lacks quantitative evidence of bedrock deformation by diurnal thermal stresses, both the geotechnical joint surveys and the depositional sediment data provide characteristic evidence of thermal fatigue. Particularly on southern, paraglacially adjusted rockwalls, distinct microfractures parallel to the schistosity are visible (Figure 6.10c). Similar crack patterns in

Antarctic and extra-terrestrial environments (Eppes et al., 2015; Eppes et al., 2016; Lamp et al., 2017) were interpreted as results of long-term, sub-critical stress accumulation in response to differential expansion and contraction along crystal boundaries or micro fractures (Tvergaard and Hutchinson, 1988). Figure 6.9 suggests that the ultimate detachment of cm- to dm-sized flakes is mechanically facilitated at cataclinal and southern/sun-exposed metamorphic rockwalls. Their relatively weak rock mass strength (< 60 in Table 6.2a,b) and the slope-parallel schistosity provide, in contrast to competent anaclinal rockwalls, multiple densely spaced detachment zones. Collins and Stock (2016) found that diurnal thermal forcing on sheeted (exfoliated) rocks is able to cause rock expansion by 1 cm per day and may be critical to trigger cm- to m-sized rockfall events. Therefore, the repetition of summer temperature variations as observed in all MTL records in our study sites must be assumed to be a potential mechanism for granular disintegration and thin flaking (Gómez-Heras et al., 2006; Eppes and Griffing, 2010; Walsh and Lomov, 2013). This means that the small particles and thin flakes detected on the upper talus segments (Figure 6.10c, Figure 6.5) need not exclusively derive from seasonal freeze-thaw in the upper bedrock meters, as predicted in Figure 6.8, but can also result from slow near-surface thermal fatigue (see also Hall, 2006).

With respect to the paraglacial timescale, our observations raise some final questions: Does repeated thermal cycling during summer play a significant role in long-term sediment production and deposition, albeit its slow and micro-scale operation in comparison to deep-seated frost cracking? Considering the trend in Figure 6.9d, does thermal micro-scale weathering particularly gain in importance at the end of the paraglacial period with increasing atmospheric warming, when the optimum location of frost cracking moves up in elevation (Hales and Roering, 2009) or shifts to shaded sites (Olyphant, 1983)? We believe these are important questions with relevance for our systemic understanding of rockfall sediment cascades and natural hazard prediction, which need to be addressed in future research.

6.6 Conclusion

In previous sediment cascade research much attention has been paid to paraglacial storage and reworking of hillslope sediments, whereas the formerly glaciated source rockwalls have often been portrayed in an oversimplified way. In this study, twelve rockfall-dominated sediment cascades of varying paraglacial adjustment state have been investigated in three Swiss hanging valleys in order to decipher the linkage between rock weathering, rockwall instability and sediment deposition. In a novel field-, modelling- and GIS-approach, material and form characteristics of deposited rockfall sediments were linked with their source rockwalls' topoclimatic and mechanical properties as well as near-surface thermal weathering regime. The main results can be summarised as follows:

- The combination of (i) seasonal frost cracking in (ii) shaded, permafrost-affected rockwalls with (iii) long and near-vertical profiles exerts a first-order control on paraglacial sediment production and deposition and explains 57% of the variability within alpine sediment cascades. At frozen, still adjusting rockwalls, deep ice segregation growth (up to 4 m depth) and near-surface (< 50 cm) cracking peaks lead today to both small-sized, short sediment cascades to the upper slopes and high-magnitude sediment supply with long run-out distances. However, with increasing time since

deglaciation, frost cracking and permafrost decrease in importance. Instead, high mean annual rock temperatures and rockwall morphometry become the key driving or limiting controls of sediment production and thus overall availability of sediment for downslope sediment transfer in alpine cascading systems at the end of the paraglacial period.

- The topoclimatic and paraglacial rockfall pattern is superimposed by a second-order variability that results from the (iv) mechanical preconditioning by the pre-existing joint spacing, individual rock mass strength and the valley-facing joint orientation. This interplay of mechanical properties of source rockwalls explains additional 21% of the variability of rockfall sediment cascades. The likelihood of coarse-grained sediment cascades increases with increasing joint spacing. No significant paraglacial trend has been found for the RMS. Instead, when combined with the overall joint orientation, both variables can dictate whether paraglacial rockfall fluxes rapidly decline immediately after deglaciation (cataclinal, weak slopes) or are still enhanced today (anaclinal, competent slopes).
- Near-surface rock temperature records from August 2014 to August 2016 reveal a high frequency of large thermal variations in the range of 8.5 °C to 35.9 °C during summer, particularly at southern sites. Given the distinct microfractures parallel to the metamorphic bedding, microscale weathering through sun-induced thermal stresses is considered to be a further frost-independent sediment source for cm- to dm-sized flakes. We believe that the mechanism of thermal fatigue in the context of the paraglacial framework represents an interesting and important issue for future research with relevance for our understanding for postglacial sediment cascades.

These findings highlight that sediment production and deposition in high-alpine systems are closely linked with rock weathering and instability of alpine rockwalls. Moreover, our study emphasises that causes and influences on rockfall sediment cascades can significantly change during the paraglacial period. This shows that the quantification of high-alpine sediment dynamics can be problematic if solely based on environmental or topographic data. Instead, future sediment cascade research should pay similar attention to rock weathering and instability of source rockwalls, particularly with respect to their adjustment to the former glaciation in form of permafrost thaw. Although the main focus of our study was on upslope rockfall-dominated cascades, the observations made in this study have important implications for catchment-scale sediment production, talus slope evolution and hillslope-channel connectivity. The implementation of the specific rockwall parameters (i-iv) identified in this study into future sediment cascade models should help, at both local and catchment-scales, improve the spatial and temporal prediction and management of cascading sediment fluxes after glacier retreat.

Acknowledgements

For financially supporting this study, the authors highly appreciate grants and scholarships by the British Society for Geomorphology (Postgraduate research grant), the Humboldt-Ritter-Penck Foundation of the Gesellschaft für Erdkunde zu Berlin, the German Exchange Service (DAAD), the Dr. Hohmann-Förderung of the Gesellschaft für Erdkunde zu Köln e.v. and the Studienstiftung des Deutschen Volkes. The authors would like to thank Arne Brandschwede, Luise Martin, Katharina Eibisch, Sebastian Unger, Katrin Hoffmann, Nikola Schulte-Kellinghaus, Nele Meyer, Daniel Dräbing and Jana Eichel for assistance during field campaigns in summers 2013 to 2016.

Chapter 7

STUDY IV - STRUCTURAL AND THERMAL CONTROLS OF ROCKFALL FREQUENCY AND MAGNITUDE WITHIN ROCKWALL-TALUS SYSTEMS

This chapter is based on the published journal article: Messenzehl, K., Dikau, R. (2017): Structural and thermal controls of rockfall frequency and magnitude within rockwall–talus systems (Swiss Alps). In: Earth Surface Processes and Landforms. DOI: 10.1002/esp.4155.

Abstract

Both from a systemic and natural hazard perspective, it is essential to understand the causes and frequency of rockfalls in mountain terrain and to predict the block sizes deposited at specific locations. Commonly, rockfalls are studied either retrospectively, using talus slopes, or directly by rockwall surveys. Nevertheless, our understanding of rockfall activity, particularly at the lower magnitude spectrum, is still incomplete. Moreover, the explanatory framework is rarely addressed explicitly. In this study, we investigate two rockwall-talus systems in the Swiss Alps to estimate the rockfall frequency-magnitude pattern and their key controls. We present a holistic approach that integrates deductive geotechnical and thermal investigations of the source rockwalls with abductive talus-based explanations of rockfall volume and frequency.

The rockwalls' 3D joint pattern indicates that 75% of the blocks may be released as debris fall (< 14 m^3) and boulder falls (14-61 m^3), which is mirrored in the corresponding talus material. Using 2-years records of near-surface rockwall temperatures as input for the frost cracking model of Hales and Roering (2007) underlines the destabilising role of seasonal ice segregation. Deepest frost cracking of 300 cm may occur on the NNE-exposed, snow-rich rockwall, with peaks at the outermost surface. The synthesis of all data suggests that infrequent, large planar slides (~ every 250 years) overlain by smaller, more frequent wedge and toppling failures (~ every 17-50 years) as well as high-frequency flake-like clasts (3-6 events/year) characterise the rockfall frequency-magnitude pattern at Hungerli Peak.

Here, we argue that small-size rockfalls need more scientific attention, particularly in discontinuous permafrost zones. Our study emphasises that future frequency-magnitude research should ideally incorporate site-specific structural and thermal properties, rather than just focusing on climatic or meteorological triggers. We discuss how holistic rockwall-talus approaches, as proposed here, could help to increase our process understanding of rockfalls in mountain environments.

7.1 Introduction

In steep mountain terrain, erosion of unstable rockwalls and downslope sediment supply commonly occurs by rockfalls of different block sizes and return periods Krautblatter and Dikau (2007). Once detached and if not intermediately stored the fragments move downslope through a combination of falling, rolling and bouncing (Varnes, 1984; Dorren, 2003) producing over time talus slope landforms with characteristic surface materials (Caine, 1969; Luckman, 1988). In particular, debris falls of < 10 m^3 and boulder falls of 10-10^2 m^3 (Whalley, 1984) can be key drivers of long-term landform evolution (Rapp, 1960a) and cascading sediment flux (Caine, 1976). Moreover, due to high-energy mobility and quasi-continuous activity, small-size rockfalls pose a significant natural hazard and an economic risk in mountain valleys (Heim, 1932; Hungr et al., 1999). To increase our process understanding of rockfalls, it is essential to evaluate the causes and timing of bedrock instability (Krautblatter et al., 2013) and to predict the block sizes deposited at specific locations (Hungr and Evans, 1988).

Surprisingly, unlike large cliff falls (10^4–10^6 m^3) and Bergsturz events (> 10^6 m^3), small-size rockfalls have received scant scientific attention. Consequently, their magnitude-frequency spectrum is still poorly defined (Luckman, 2013). In rockfall research, the frequency–magnitude concept of Wolman and Miller (1960) is primarily applied to failures > 10^4 m^3 using regional inventories, e.g. in North Ireland (Douglas, 1980), Great Britain (Barlow et al., 2012), the Canadian Rocky Mountains (Luckman, 1976; Gardner, 1980, 1983; Guthrie and Evans, 2004), Hong Kong (Chau et al., 2003b), the Yosemite Valley (Wieczorek et al., 1995; Stock et al. 2014) and the French Alps (Dussauge et al., 2003). Whether the observed power-law and negative log-normal distributions are also valid for events at the lower end of the magnitude spectrum is not clear. Undersampling of small block sizes in most inventories (Stark and Hovius, 2001) and different destabilizing factors affecting either deep-seated or near-surface detachment zones (Cruden and Varnes, 1996; Murton et al., 2006) may complicate the transferability to small-size rockfalls.

Geomorphologists commonly investigate unconsolidated talus materials to improve our knowledge of small-size rockfalls. In those abductive approaches (Inkpen and Wilson, 2013), the depositional 'effects' of rockfall supply onto talus slopes are used as a proxy to predict, in retrospect, a range of unknown 'causes' (Figure 7.1a) in terms of potential rockfall magnitudes and frequencies. For instance, quantification of rockfall volumes are achieved through mapping the block dimensions (Caine, 1967; Pérez, 1989) and downslope gravity sorting (Kirkby and Statham, 1975; Statham, 1976). Rockfall frequencies have been estimated on seasonal scales by measuring deposits on snow patches (Matsuoka and Sakai, 1999) or collectors (Rapp, 1960b; Vehling et al., 2016), and, on postglacial timescales, using vegetation indices (Harshberger, 1929; Corominas and Moya, 2010), rock weathering-rinds (Whitehouse and McSaveney, 1983) and lichen cover (McCarroll et al., 1998; Sass, 2010). Unfortunately, with few exceptions (Evans and Hungr, 1993; Krautblatter et al., 2012), the decreasing frequency of rockfall supply with increasing rockwall distance is rarely considered, which makes abductive reasoning from spatially selective talus examinations problematic.

Another key limitation of abduction from the sediment sink is that the properties of the source rockwall are often neglected or oversimplified (Figure 7.1a). This is problematic insofar as the volume of rockfall blocks significantly decreases due to collision and repeated impacts along the downslope movement path (Erismann

and Abele, 2001). The depositional talus pattern therefore allows only partial definition of the key controls or 'laws' governing the instability and failure of the source rockwall. Thus, to infer, in retrospect, from talus deposits to potential rockfall events, knowledge is necessary concerning the rockwall`s (a) static morphometric, lithological and mechanical properties as well as (b) the thermal and hydrological dynamics controlling the types and efficiency of rock weathering (Krautblatter and Dikau, 2007; Messenzehl et al., 2016).

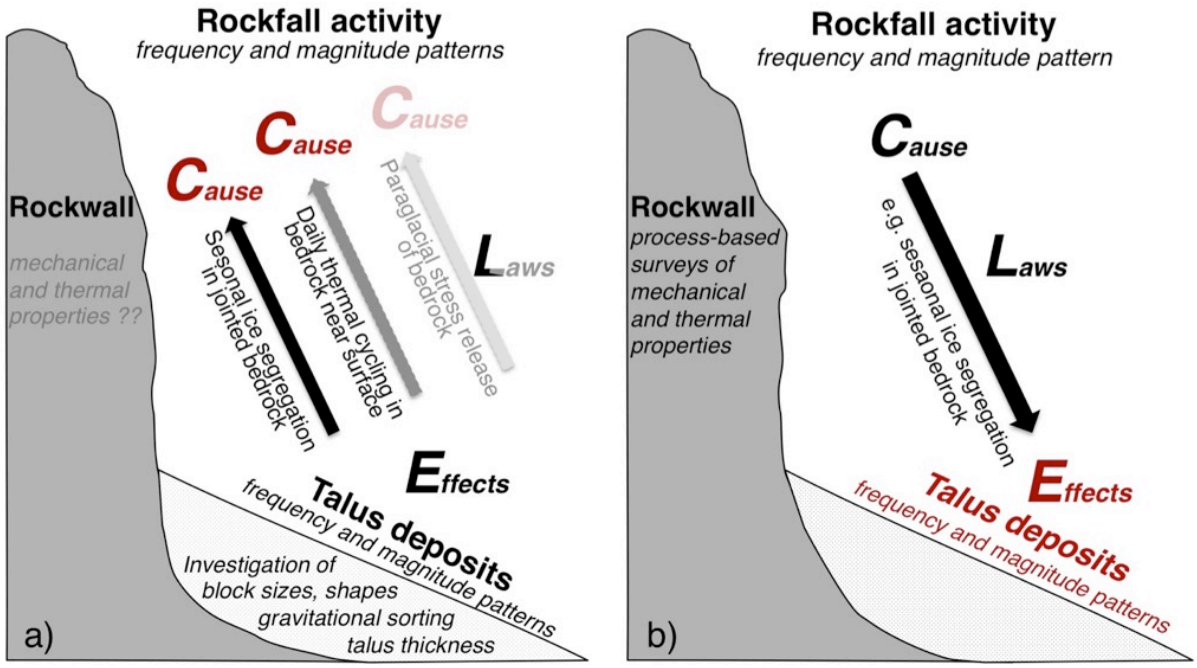

Figure 7.1: *Abductive (a) and deductive (b) reasoning of rockfall frequency and magnitude patterns, following Inkpen and Wilson (2013). In abduction, the potential magnitudes and frequencies of rockfall supply onto talus slopes are unknown (red colour). By investigating the visible effects of talus deposition and assuming plausible but partly uncertain laws of rock slope instability, different rockfall events can be found or hypothesised. The decreasing likelihood of laws and causes is shown by decreasing colour intensities. Due to the strong focus on the sediment sink, the mechanical and thermal properties of the source rockwall (light labelling) is often simplified or neglected in abductive approaches. In deduction, the depositional effects of rockfall activity are unknown (red colour), but are logically inferred from process-based investigations of the rockfall source rockwall. Unlike abduction, deduction commonly permits only one, certain link between cause and effect by referring to a potential law.*

To address these shortcomings in abductive reasoning, researchers increasingly favour deductive, process-based investigations of the rockfall source rockwall (Krautblatter and Moore, 2014). By determining the initial state of bedrock instability and the associated rockfall volume and frequency (= 'cause'), the aim is to logically predict different spatiotemporal 'effects' of rockfall supply onto talus slopes (Figure 7.1b). For instance, the availability of novel techniques, such as terrestrial or airborne photogrammetry (Abellán et al., 2014; Giordan et al., 2015), allow an accurate characterization of unstable rock masses and a quantification of rockfall volumes upwards of 10^{-4} m^3 (Lim et al., 2010). The logical basis of the cause-effect linkage is provided by reference to known controls or 'laws' of bedrock instability. While there is a tendency to correlate the detected rockfall events with regional topoclimatic or meteorological parameters (Guzzetti et al., 2003; D'Amato et al., 2016), in contrast, the installation of miniature temperature loggers e.g. at 10 cm bedrock depth, can provide high-resolution data on the near-surface thermal regime (Gruber et al., 2004b). Depending on the level of bedrock moisture and the presence of permafrost, conclusions can be made on failures of few cm^3 to many tens of m^3

on daily to decadal timescales (Hallet et al., 1991; Matsuoka, 1994; Sass, 1998; Matsuoka and Murton, 2008; Haberkorn et al., 2015a). Assuming that ice segregation is one key destabilizing mechanism in natural rockwall systems (Walder and Hallet, 1985; Hallet, 2006), numerical models allow estimation of depth-varying frost cracking intensity associated with seasonal freezing and thawing (Anderson, 1998; Hales and Roering, 2007; Andersen et al., 2015). Nevertheless, acknowledging the anisotropy of rock material at all scales, interpretation of thermal field and model data requires a careful geotechnical assessment. Specifically, the intact rock strength, the spacing and orientation of open joints (Selby, 1980, 1993; Sass, 2005b; Moore et al., 2009; Collins and Stock, 2016) can exercise significant control on heat transfer (Hasler et al., 2011a; Draebing et al., 2014), rockfall-prone block volume (Palmstrom, 1982) and movement types (Priest, 1993; Cruden and Hu, 1994).

However, the question arises at what level of simplification and reduction are those deductive examinations made to reduce the complexity of rockfall controls? In other words, can process-based rockwall surveys offset the shortcomings of abductive talus investigations? Or do we instead need combined approaches that integrate both abduction and deduction, as already recommended in the past by von Engelhardt and Zimmermann (1988)? And if so, how should such a methodological approach be designed to improve our geomorphic process understanding and hazard assessment in mountain areas?

Here, we propose a holistic rockwall-talus approach that accounts for, using different forms of reasoning, the entire rockfall cascade from the unstable source rockwall to the depositional sink. We investigate two rockwall-talus systems in the southern Swiss Alps and aim to evaluate their rockfall frequency-magnitude spectrum with respect to key controls. We combine (i) block size mapping and rockfall frequency estimation along the depositional areas with (ii) geotechnical transect surveys and a numerical frost cracking model using temperature data of the near-surface bedrock of two full consecutive years. By integrating deductive rockwall measurements (ii) into abductive explanations from talus deposits (i) we estimated the rockfall frequency-magnitude patterns at each landform complex, with 3D joint geometry and the depth-varying intensity of segregation ice as key controls. These findings emphasise the need to implement structural and thermal variations of the source rockwall, not just topoclimatic valley settings in rockfall frequency-magnitude research.

7.2 Regional-scale setting and local-scale characteristics of the study site

Our study site is situated in the Hungerli Valley, an eastern hanging valley of the Turtmann Valley in the Swiss Alps (Figure 7.2a, b). Recent modelling of regional-scale bedrock instability reveals that rockfalls predominate on steep, north-exposed metamorphic rockwalls with indipping joint bedding (Messenzehl et al., 2016) resulting in more than 220 talus slopes in the Turtmann valley (Otto et al., 2009). A paraglacial reaction of the deglaciated rockwalls (i.e. stress release) and a decreasing rock strength associated with postglacial and recent permafrost degradation are supposed to be major factors controlling the regional-scale occurrence of rockfalls (Messenzehl et al., 2016).

Here we focus on two rockwall-talus complexes (referred to hereafter as RT1, RT2), located along the northern, deglaciated hillslopes of Hungerli Peak (Figure 7.2a). Since the rockfall sediment cascade is largely disconnected due to an EW-extending inactive rock glacier bordering the talus' toes, the talus slopes provide

good proxies for assessing spatiotemporal rockfall activity. Covering a surface area of approx. 23,000 m², the talus slopes are approximately 180-200 m in length and extend from 2490 m asl up to 2570 m asl (apex). The 180 m high and 60-75° steep rockwalls cover a rockfall catchment area of 8715 m² (R1) and 8348 m² (R2) (Figure 7.3) (Messenzehl et al., 2016). They are composed of highly weathered and heavily folded Palaeozoic micaschists and paragneisses rocks (Labhart, 2009). Occasionally, amphibolite, quartzite and apatite are incorporated.

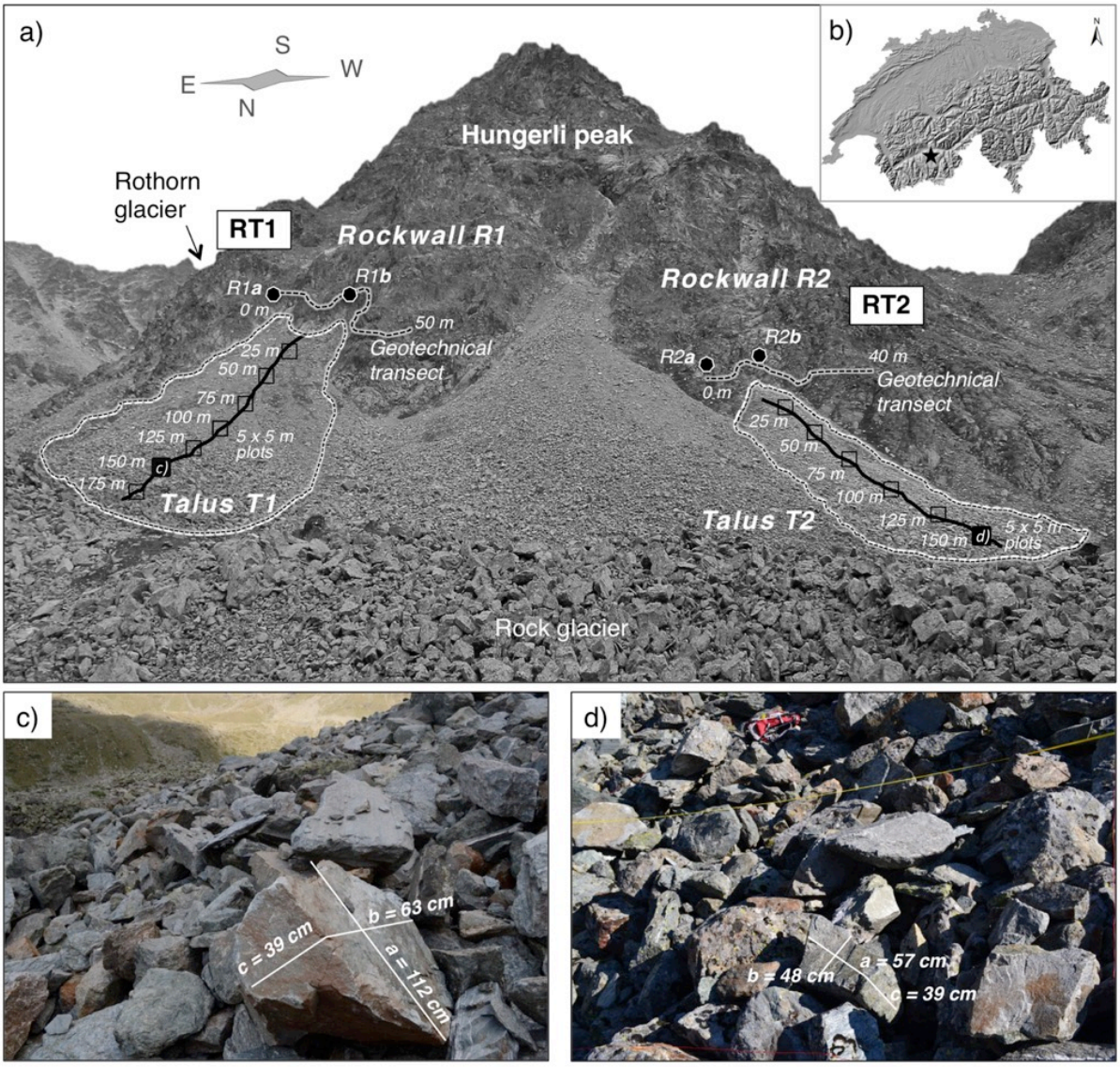

Figure 7.2: *Overview on the study site and the methodical field approach along (a) the N-exposed rockwalls (R1, R2) and talus slopes (T1, T2) of Hungerli Peak. The talus slopes extend from 2490 m asl, bordering on the rock glacier, up to 2570 m asl (apex). Both rockwalls are approx. 180 m high and 60-75° steep covering comparable catchment areas for rockfall release (b). The investigated landform complexes RT1 and RT2 are situated in the Hungerli Valley, a hanging valley of the Turtmann Valley (Swiss Alps). Despite lying in a similar regional-scale topoclimatic, geological and paraglacial setting, the rockfall deposits of (c) RT1 present a marked contrast to those being deposited along (d) RT2. The deposits shown in (c) and (d) represent typical block sizes and shapes of the talus foot (mapped at 150 m distance from the rockwall). Photographs (c,d) by N. Schulte-Kellinghaus, 2015.*

The metamorphic layers strike in a SW-direction slightly dipping into the slopes parallel to the tectonic folding of the Penninic Siviez-Mischabel Nappe (Bearth, 1980). Situated in a relative dry continental setting with a mean annual precipitation 500–600 mm, the rockwalls are exposed to direct rainfalls from northerly and easterly winds (MeteoSwiss, 2016) and low incoming solar radiation of <1430 kWH/m² per year (Messenzehl et al., 2016). A permafrost probability of 99% (rockwall) and 40-100% (talus slopes) were predicted by a rock glacier-based model (Nyenhuis, 2005), but as shown on Figure 7.3, permafrost boundary conditions are more likely according to the Swiss permafrost map (BAFU, 2005). Ground penetrating radar and seismic refraction surveys of Otto and Sass (2006) imply two different scenarios of mean postglacial rockwall backwathering rate of 2569 mm/ka and 1076 mm/ka.

Age information is missing with respect to the glaciation history, but data from neighbouring valleys suggest that our study site was likely ice covered by the local hanging glacier 24–21 kyrs BP ago. Remnants of the Rothorn glacier still exist in the uppermost cirque (Figure 7.2a). The glacier probably started to retreat with the onset of climate warming approx. 18 kyrs BP (Kelly et al., 2004b; Schlüchter, 2004). A second glaciation of Hungerli Peak during the Late Pleistocene ice re-advance (Younger Dryas) approx. 12 kyrs (Ivy-Ochs et al., 2009) is unlikely, as their moraines can only be found at approx. 2500 m. It is thus reasonable to assume that both rockwalls became ice-free between 18-12 kyrs BP. This was likely followed by a paraglacial adjustment of the rock mass, the onset of rockfalls and a gradual accumulation of talus slopes along rockwall bases.

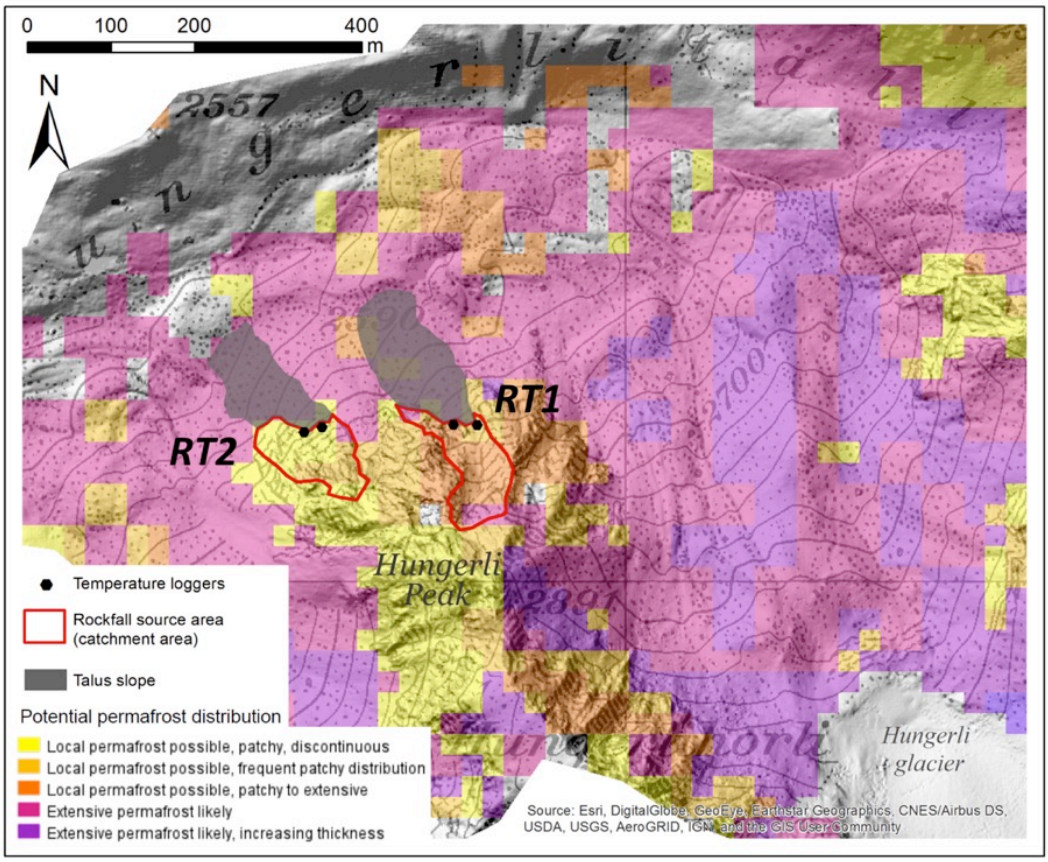

Figure 7.3: *Overview on Hungerli Valley and studied rockwall-talus complexes with respect to potential permafrost distribution (BAFU 2005) and size of rockfall source areas (red line). As calculated by Messenzehl et al. (2016) effective rockfall catchment areas (red line) are approx. 8715 m² (R1) and 8248 m² (R2).*

7.3 Methodological framework and key hypotheses

From the above discussion, it should be clear that both abductive and deductive research designs are valuable to decipher the cause-effect linkages between rockfall activity and talus slope deposition, but they are also linked to different degrees of uncertainty (Figure 7.1). In other words, both styles require additional information to select the valid explanation(s) (Inkpen and Wilson, 2013). Here we propose a methodological approach that integrates deductive rockwall studies with abductive talus assessments in order to constrain the potential pathways linking rockfall release and deposition. First, we estimate, in retrospect (Baker, 1996), potential rockfall frequency-magnitude patterns by quantifying the block size distribution and supply frequency of the talus slopes. The hypothetical event sizes and frequencies are then strengthened by process-based geotechnical surveys and rock temperature monitoring of the two corresponding source rockwalls.

In both frameworks, we refer to overarching theories or laws of bedrock instability to logically link cause and effect (Figure 7.1). Acknowledging the complex interplay of different destabilising factors in mountain systems, we aim to keep several variables constant to specifically test mechanical and thermal controls of the source rockwalls. For instance, the two N-exposed rockwalls characterised by a similar type of lithology and topography (slope, aspect), lie within the same elevation belt and receive similar intensities of rainfall, wind and incoming solar radiation (Figure 7.2a, Figure 7.3). Likewise, local permafrost conditions might be comparable and classified as 'patchy, discontinuous' at R2 and 'frequent patchy' at R1 (Figure 7.3). Furthermore, given the landforms' relative valley position and thus - in terms of a space-time-substitution - their concurrent onset of deglaciation (Messenzehl et al., 2016), similar degrees of paraglacial stress release or permafrost degradation are likely. Nevertheless, the block sizes and shapes of the corresponding talus slopes seem markedly different (Figure 7.2d). Consequently, if the depositional patterns of talus slopes are used as a first proxy for rockfall activity, the regional-scale topoclimatic, geological and paraglacial setting fails to explain the differences. We can also exclude differences in rockwall morphometry or surface area. As shown in Figure 7.3 the comparable bedrock catchment areas of talus slopes suggest similar stages of rockwall-talus maturity today. Following Kirkby and Statham (1975) the current rate of rockwall erosion and the spatial efficiency for rockfall release may be comparable at both sites. Likewise, the DEM reveals similar mean rockwall heights (Figure 7.3) as well as roughness and curvatures (Messenzehl et al., 2016). Although those properties significantly control rockfall energy, trajectories, run-out length and degree of final fragmentation (Gerber and Scheidegger, 1969; Crosta and Agliardi, 2004; Ruiz-Carulla et al., 2016), the comparable morphometric setting may provide similar kinematic and dynamic prerequisites. Therefore, as most potential rockfall controls provide no plausible explanation for the contrasting depositional rockfall patterns, we hypothesise that rockfall frequency-magnitude as well as the linked depositional talus pattern are primarily determined by structural and thermal properties of the source rockwalls.

7.3.1 Block size mapping and statistics of rockfall deposits

The rockfall blocks deposited on the talus surfaces were mapped along longitudinal profiles extending from the apices to the toes. The delivery areas of deep rockwall chutes or gullies were avoided in the selection of the

transect position to minimize the influence of secondary rockfalls, with these often linked to different magnitude-frequency patterns (Luckman, 2013). Moreover, areas obviously reworked by avalanches or debris flows were carefully excluded as were areas where plant coverage was higher than 10%. Talus morphometry was measured at 5 m intervals to include the topography of the depositional area influencing both rockfall run-out and fragmentation.

Beginning at the apices, a sampling plot (5 x 5 m) was laid out every 25 m (Figure 7.2a). For each block lying at the intersection of a 50 cm grid, the three dimensions (a-, b-, c-axis, Figure 7.2c, d) were systematically mapped (Caine, 1969; Pérez, 1993). At talus foots, the number of recorded blocks was distinctly lower due to their larger sizes and some axial lengths could only be estimated (3% of the data) due to their embedding. Similarly, where particles were too small (< 2 cm), i.e. at the apex, a minimum estimation was made. The axial block lengths were finally used to calculate the mean diameter (Caine, 1967) and to approximate the block volume V (0.6 a*b*c) as suggested by Luckman and Fiske (1995). Particle sorting was derived from the standard deviation (S.D.) in phi units (Folk and Ward, 1957). Following Pérez (1989), we calculated two different block shape indices: the degree of sphericity $(c^2/(a*b))^{0.333}$ (Goudie, 1981) and the degree of flatness (a+b/2*c) (Gardiner and Dackombe, 1983).

7.3.2 Estimation of rockfall supply frequency

To estimate the annual frequency of rockfall supply with respect to the downslope site, we follow the empirical approach proposed by Evans and Hungr (1993). Here, the frequency of a block falling per year on a particular area of the talus surface is calculated by relating the mean block diameter to the mean talus growth rate. This approach requires that the landform age is known. In mountain valleys, where sediments are generally removed from bedrock basins during a glacial cycle, it is reasonable to date the onset of talus production to the last rockwall deglaciation (Moore et al., 2009). Due to the proximity of both rockwalls, a concurrent onset of deglaciation and consequently talus production is likely. For simplicity, Evans and Hungr (1993) assume a uniform growth of talus thickness over time. Thus, Late-glacial and Holocene fluctuations in rockfall supply are averaged-out, similar to long-term erosional effect due to modifying talus processes (e.g. debris flows, avalanches, creep). However, the spatial proximity of both landforms and the pre-selection of talus transects imply comparable error ranges. Although temporary filling and depletion of intermediate rockwall storages are neglected, these might converge to uniform integral values on a longer timescale (Krautblatter and Dikau, 2007). The approach of Evans and Hungr (1993) neglects the progressive decrease of rockwall surface area or length linked to the gradual upslope growth of talus debris with increasing talus maturity. However, the comparable and relatively large catchment sizes (Figure 7.3) suggest only minor differences between both sites with respect to the general rockwall erosion or backweathering rate. We therefore assume a comparable rockfall efficiency and depositional activity at both sites (Kirkby and Statham, 1975). As the mean talus slope gradient remains almost constant during talus evolution (Statham, 1976) the mean time-averaged talus growth rate (G_n) in normal direction (m/year) can be calculated:

$$G_n = (d / t) * \cos(s) \qquad (7.1)$$

For the talus production time t, we used a mean value of 15 kyr, assuming a time interval between glacier retreat after the Last Glacial Maximum (LGM,approx. 18 kyrs BP) and the Younger Dryas time period (12 kyrs BP). The mean talus gradient s derived from our morphometric measurements in the field is 33° (T1) and 34° (T2). The individual landform thicknesses d was derived from unpublished geophysical field surveys performed in 2014 (data collection and processing was conducted by D. Draebing, TU Munich, Germany). Electrical resistivity tomography and seismic refraction tomography indicate a mean sediment thickness of approx. 24 m (T1) and 20 m (T2), which is in the range of previous findings from Hungerli Peak (15-29 m, Otto and Sass, 2006; Otto et al., 2009). Finally, by relating Gn to the mean block diameter D in m3 (b-axis) deposited on a specific position on the talus profile, we quantified the annual rockfall landing frequency F (event / (year * m²)) as:

$$F = G_n / D_{b\text{-}axis}^3 \qquad (7.2)$$

7.3.3 Geotechnical transect surveys and rock mass strength classification

The geotechnical properties of the intact rock mass and its joints (hereafter the term 'joints' is used for all types of discontinuities) were assessed in detail within a 40-50 m long and 1.5 m high transect window at the foot of each rockwall (Priest, 1993). The transect lengths were chosen both to cover the entire rockfall initiation zone (Figure 7.2a) and to account for rock mechanical variability over short distances. We assume that the empirical measured bedrock is representative for the whole rockwall. Following the standards of ISRM (1978) the dominant joints (excluding micro-cracks) were mapped with respect to their (i) position (along a horizontal and vertical measuring tape), (ii) dip and dip direction, (iii) spacing, (iv) opening, (v) persistence (or continuity), (vi) infilling and (vii) evidence of water flow (Table 7.1).

Sections of similar joint spacing were then summarized as sub-units and the degree of surface weathering was estimated (Selby, 1980). Intact rock strength was measured using a high impact 'L'-type Schmidt Hammer (0,736 kN/m²). The mean rebound value (R) was calculated based on all 20 readings taken on lichen-free and un-jointed areas (Aydin, 2015). The rock mass strength (RMS) of each sub-unit was finally calculated based on a semi-quantitative rating (r) of each parameter using the classification system of Selby (1980). Using Stereonet 9.5 (Cardozo and Allmendinger, 2013), the spherical data of joints were plotted in equal area stereonets to identify dominant joint sets, potential failure modes and angles of intersections.

7.3.4 Near-surface rock temperature monitoring

Near-surface rock temperatures (NSRT) were monitored in the field between August 2014 and August 2016. Within the framework of a large-scale rock temperature monitoring in the Turtmann valley, two miniature temperature loggers (iButtons®, Maxim DS1922, referred to hereafter as 'MTL') were installed at 10 cm depth at each rockwall following the design of Gruber et al. (2003). The MTL depth of 10 cm allow a good approximation of the near-surface temperature regime (Gruber et al., 2004b). The loggers were drilled at similar elevations of 2573 m asl (R1a, R1b) and 2590 m asl (R2a, R2b) at near-vertical bedrock with surface

orientations representative for each rockwall (Figure 7.2, Figure 7.3). To link NSRT to the geotechnical data, we carefully selected transect locations representative for the whole rock mass in terms of e.g. rock type, degree of schistosity and surface weathering. As recommended by Gruber et al. (2003), MTLs were drilled in homogenous, intact rock with at least 30 cm distance to joints. This sampling strategy does not reflect the importance of non-conductive heat transfer through joints, but allows comparability to previous MTL surveys in the Swiss Alps. Likewise, we avoided complex micro-topography from surrounding bedrock to minimize shadowing or concentration of surface runoff (after snowmelt). To guarantee the thermal coupling and to avoid heat advection by water or air, a small drilling diameter was chosen (18 mm). MTLs were waterproofed using polyethylene capsules. The borehole openings were closed with a rubber plug and sealed with waterproof silicone. MTLs recorded NSRT over 3-h intervals with an accuracy of around ± 0.1 °C (calibrated). To program the mission settings and to download data we used the smart phone "iAssist" software of Keller et al. (2010) allowing very fast data management (< 15 min data gap) in steep terrain.

Table 7.1: *Rock mass strength (RMS) index of rockwall R1 and R2 with semi-quantitative ratings (r) for intact rock mass and joint properties using the rating system of Selby (1980).*

	R1	**R2**
Intact rock strength	weak to moderate	very weak to weak
r:	***10 - 14***	***5 - 10***
Intact rock weathering	completely to slightly	completely to moderately
r:	***3 - 9***	***3 - 7***
Joint spacing	160 cm (± 85)	64 cm (± 5)
r:	***15 - 30***	***15 - 21***
Joint orientation	90°/85° - 340°/77°	90°/56° - 330°/30°
r:	***9 - 20***	***5 - 20***
Joint opening	0.1 mm - 4 cm	0.1 mm - 1.9 cm
r:	***2 - 7***	***2 - 7***
Joint continuity & infilling	few (thin infilling) to continuous	continuous (clear) to continuous (thin
r:	***4 - 6***	***5 - 6***
Groundwater outflow	none to slight	none to slight
r:	***4 - 6***	***4 - 6***
Average RMS	**65 (± 13.9)**	**60 (± 9.9)**

7.3.5 Numerical modelling of frost cracking depth and intensity

Here we assume that seasonal growth of segregation ice is the key destabilizing mechanism (or 'law' in Figure 7.2) in our study area. To estimate the depth at which segregation ice is likely efficient to cause stresses and to fracture bedrock, we applied the numerical frost cracking model of Hales and Roering (2007). While these authors used air temperature data from regional climate stations, we used the MTL data to obtain more realistic information on the intensity and depth of frost cracking variability in alpine rockwalls.

A temperature window between -3 °C and -8 °C might be the most conducive thermal range for frost cracking varying according to rock properties (e.g. lithology, porosity, jointing) (Walder and Hallet, 1985) as long as unfrozen water > 0°C is available in the system (Hallet et al., 1991; Anderson, 1998; Murton et al., 2006). To simplify the approach, we assume for both sites that water or rock moisture is no limiting factor. The major heat transfer considered in the model is heat diffusion in solid rock via conduction. Given a sinusoidal annual temperature cycle, Hales and Roering (2007) provide a simple one-dimensional heat conduction model:

$$T(z,t) = MART + Ta\, e^{-z\sqrt{\frac{\pi}{\alpha P_y}}} \sin\left(\frac{2\pi t}{P_y} - z\sqrt{\frac{\pi}{\alpha P_y}}\right) \qquad (7.3)$$

where T is temperature, t is time, z is rock depth, MART is the mean annual near-surface rock temperature and Ta is the amplitude of the sinusoidal cycle P_y (365 days). The thermal diffusivity α is set to be uniform with depth; we used a value of 1.3 $mm^2\ s^{-1}$ which is typical for micaschist and paragneiss (Whittington et al., 2009). Since water delivery to ice lenses and thus their growth rate depend on the thermal gradient (Everett, 1961; Worster and Wettlaufer, 1999), the frost cracking intensity can be modelled by summing the temperature gradients as a function of bedrock depth (Hales and Roering, 2007). Using the software R, we estimated the depth-integrated frost cracking intensity of each rockwall from their MTL records of the periods 2014-2015 and 2015-2016.

7.4 Results

7.4.1 Block sizes, shapes and annual supply of rockfall deposits

The longitudinal block volume distribution of the rockfall deposits (Figure 7.4a-c) and their associated shapes (Figure 7.4c-d) reflect certain regularities. Immediately beneath the rockwalls (25-50 m), the talus apices are equally covered by small, dominantly platy (flake-like) debris of $10^{-4}\ m^3$ (median) and a very fine, organic rich matrix. Their steep slopes gradients of 34-36° are associated with a high degree of particle sorting. Both talus slopes are subsequently characterized by a pronounced downslope increase in block volume and sphericity (Figure 7.4a,b), but the changes substantially differ between landforms. Along the approximately rectilinear profile of T1 (33-34°) median block volumes increase almost linearly from 3.9 x $10^{-3}\ m^3$ (lower mid slope) to 3.2 x $10^{-1}\ m^3$ (talus foot). Parallel, particle sorting decreases downslope, with this most evident at 150-175 m from the rockwall, where fine clasts of a few cm^3 are intercalated between large weathered boulders of up to 11 m^3 (Figure 7.4b). Block shapes remain relatively flat for most of its rectilinear long profile (Figure 7.4d). At T2, the transition from the mid slope to its foot is distinctly convex. Compared to equivalent plots on T1, this

convexity is linked to greater block volumes (10^{-2} - 10^{-1} m^3), poorer sorting and a higher sphericity index. Where T2 flattens out towards the toe median block sizes decrease to 6.4 x 10^{-2} m^3 with maximum blocks of < 1.73 m^3.

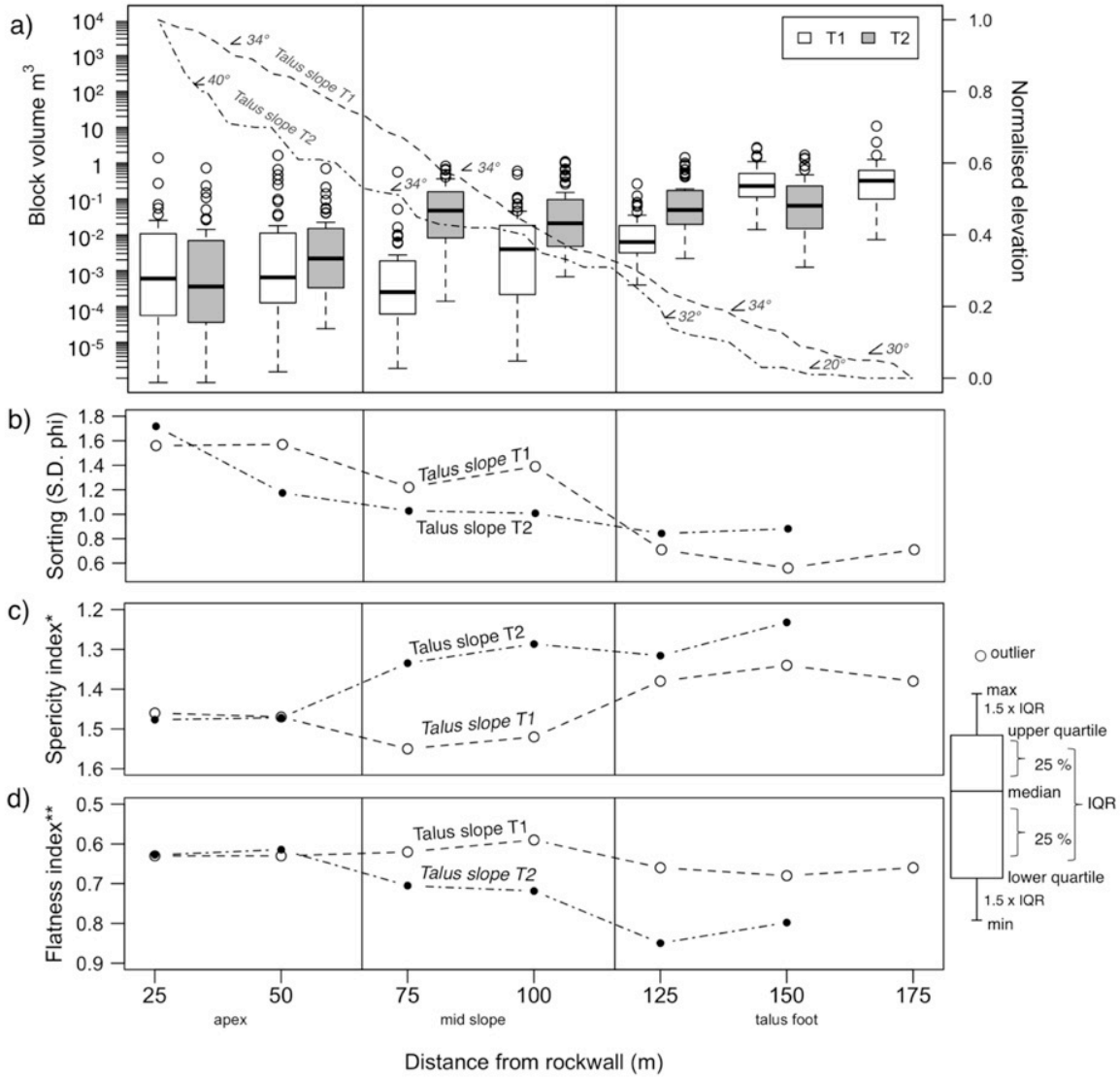

*Figure 7.4: Rockfall distributional pattern of talus slopes T1 and T2 with respect to the block volumes along the talus long profiles (a), degree of particle sorting, (b) degree of block sphericity (c) and flatness (d). Block volumes were calculated using the three block dimensions (a-, b-, c-axis) mapped every 25 m with a 5 x 5 m sampling plot (see Figure 7.2). Particle sorting was derived from the standard deviation (S.D.) in phi units. A decreasing index of sphericity (c2/(a*b))0.333 reveals a higher degree of roundness. An increasing degree of flatness is represented by an increasing index of flatness (a+b/2*c) (see text).*

Figure 7.5 shows the annual frequency and return period of the site-specific rockfall supply on T1 and T2. The first 25 m below the rockwalls are equally affected by frequent rockfall impacts of 4 - 6 events per year. Then, the depositional activity decreases with increasing distance to their source rockwalls, but non-linearly and with distinct landform-specific spatial variations. Along T2, the rockfall return period drops towards its mid slope (one event every 17-50 years) and remains relatively constant down to the toe. By contrast, the mid slope of T1 is affected by the highest rockfall supply with 5 (75 m) to 3 (100 m) events per year. Then, mean rockfall return periods remarkably decrease to approx. 250 years along the talus foot of T1.

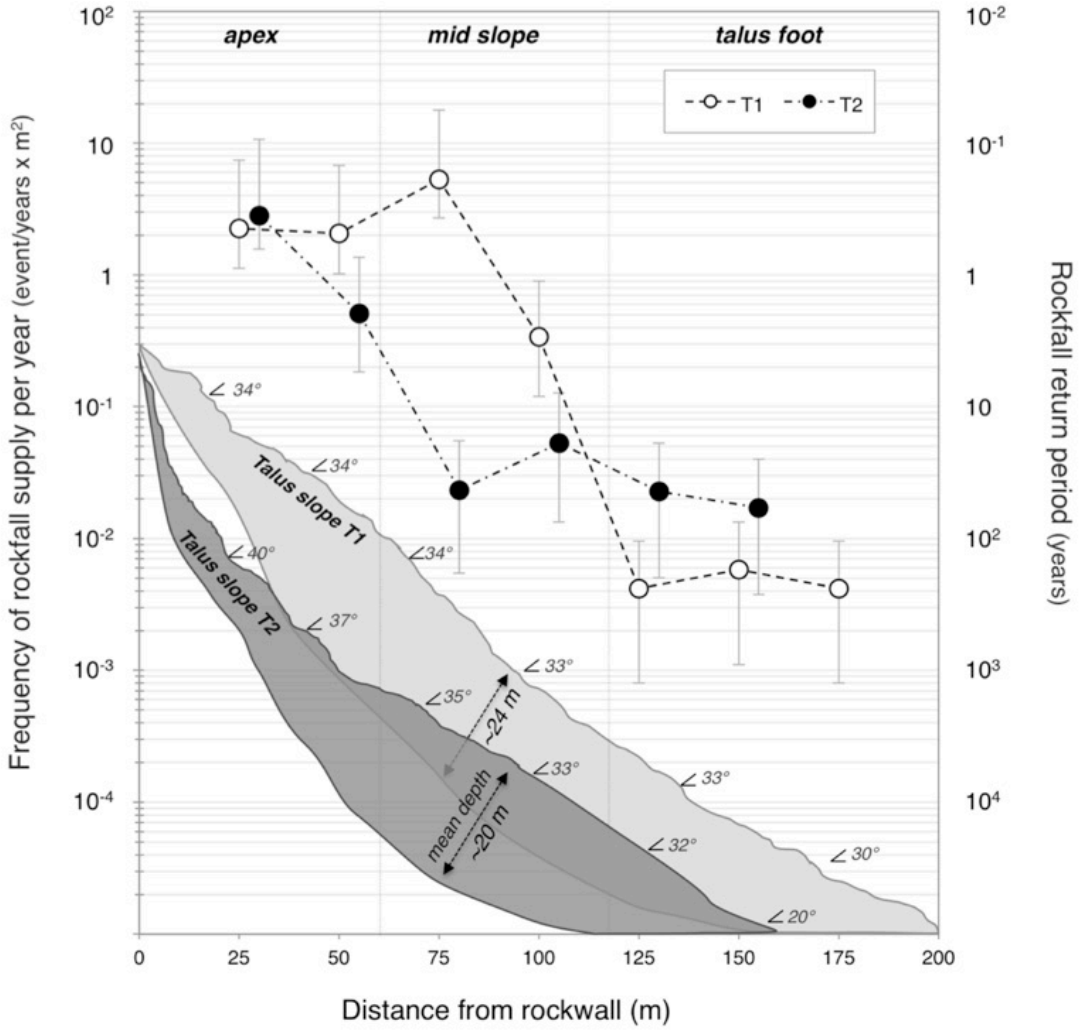

Figure 7.5: *Frequency and return period of rockfall supply per year on talus slope T1 and T2 Schematic illustration of approximate bedrock-sediment boundary and values for talus depth are based on Electric Resistivity Tomographies and Seismic Refraction Tomographies processed by D. Draebing, TU Munich, Germany. To calculate the rockfall frequency, a mean talus growth time of 15 kyr was assumed, error bars signify the range between the Younger Dryas (12 kyrs BP) and LGM (18 kyr) (Evans and Hungr, 1993).*

7.4.2 Structural properties, failure modes and potential block sizes of source rockwalls

The rockwalls are characterized, on average, by a moderate rock mass strength (Table 7.1), but transect data (Figure 7.6) reveal rock mechanical properties with a high spatial variability. At rockwall R1, in particular, RMS varies between 37 (V in (Figure 7.6a) and 81 (III in Figure 7.6a) and is rated, on average, as slightly stronger (RMS 65 ± 13.9) than R2 (RMS 60 ± 9.9) due to differences in intact rock strength, surface weathering and joint spacing. Weaker rock strength at R2, is linked to a heavily weathered surface with SH rebound values of 19-37 (Table 7.1).

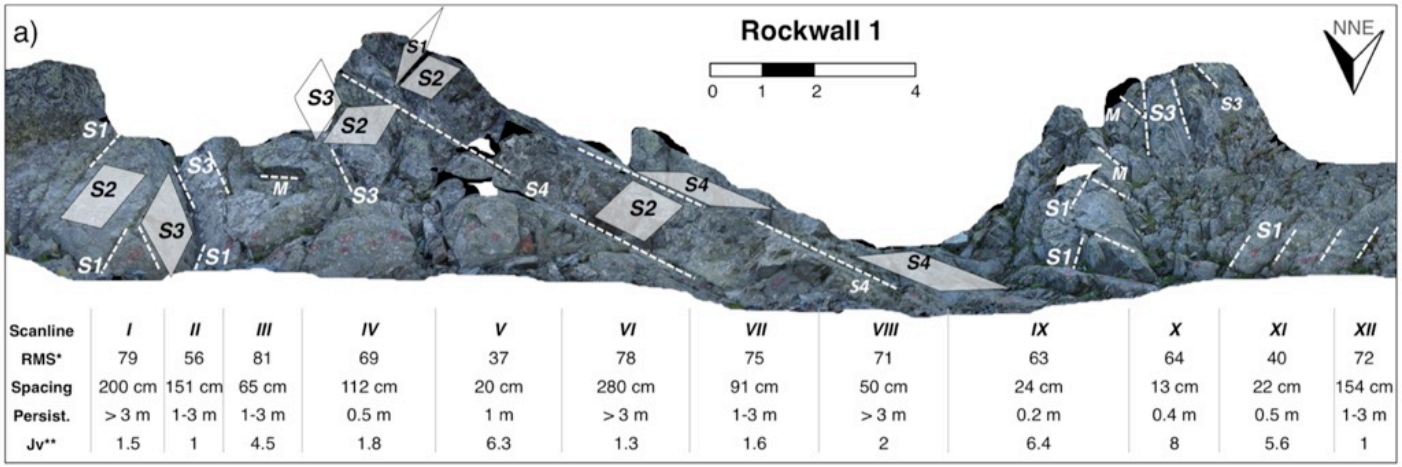

Scanline	I	II	III	IV	V	VI	VII	VIII	IX	X	XI	XII
RMS*	79	56	81	69	37	78	75	71	63	64	40	72
Spacing	200 cm	151 cm	65 cm	112 cm	20 cm	280 cm	91 cm	50 cm	24 cm	13 cm	22 cm	154 cm
Persist.	> 3 m	1-3 m	1-3 m	0.5 m	1 m	> 3 m	1-3 m	> 3 m	0.2 m	0.4 m	0.5 m	1-3 m
Jv**	1.5	1	4.5	1.8	6.3	1.3	1.6	2	6.4	8	5.6	1

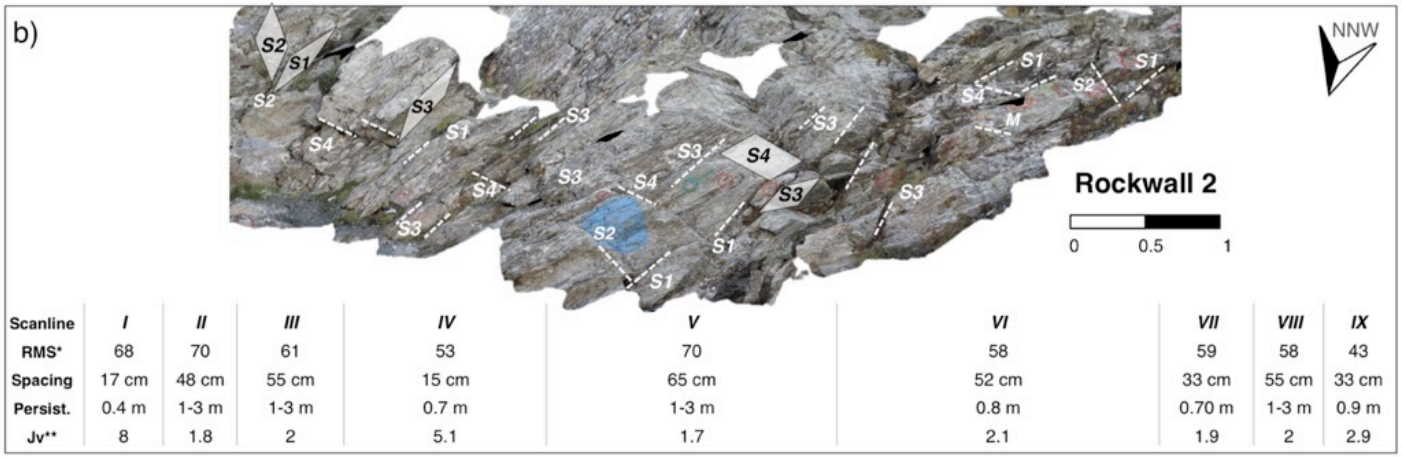

Scanline	I	II	III	IV	V	VI	VII	VIII	IX
RMS*	68	70	61	53	70	58	59	58	43
Spacing	17 cm	48 cm	55 cm	15 cm	65 cm	52 cm	33 cm	55 cm	33 cm
Persist.	0.4 m	1-3 m	1-3 m	0.7 m	1-3 m	0.8 m	0.70 m	1-3 m	0.9 m
Jv**	8	1.8	2	5.1	1.7	2.1	1.9	2	2.9

* Rock mass strength classification after Selby, 1980: Very strong (RMS 100-60), strong (RMS 60-50), moderate (50-40), weak (40-35), very weak (RMS 35-10)

** Corresponding block size descriptions of Jv (joints/m^3): Very large blocks (<1), large blocks (1-5), medium-sized blocks (5-10) based on ISRM, 1978.

Figure 7.6: *Photographs and selected rock mechanical and joint geometrical properties of R1 (a) and R2 (b). Transect sub-sections (I-XI) reveal a high rock mechanical variability over short distances (note: not the entire transect length of 40-50 m is shown). Different combinations of rock mass strength (RMS) or particularly, joint spacing and joint persistence (abbreviated as 'persists.') are associated with large to medium sized block sizes (Jv). Depending on the orientation (dip/dip direction) as well as intersection of the dominant joint sets (S1-S4) and metamorphic beddings (M), different failure modes are likely including planar sliding (i.e. R1), wedge failure and toppling processes (i.e. R2). Photographs of R1 (a) taken by J. Eichel (2015).*

Low RMS also often results from narrow joint spacing and short persistences (e.g. IV, VII, IX in Figure 7.6b). By contrast, at R1 joint spacing is more than twice as wide (160 cm), often coupled with long joint persistence (e.g. I in Figure 7.6a). At each rockwall, dip and dip direction of joints vary highly over short distances leading to either very favourable (56-85° indipping) or unfavourable (30°-77° outdipping) stability conditions (Table 7.1).

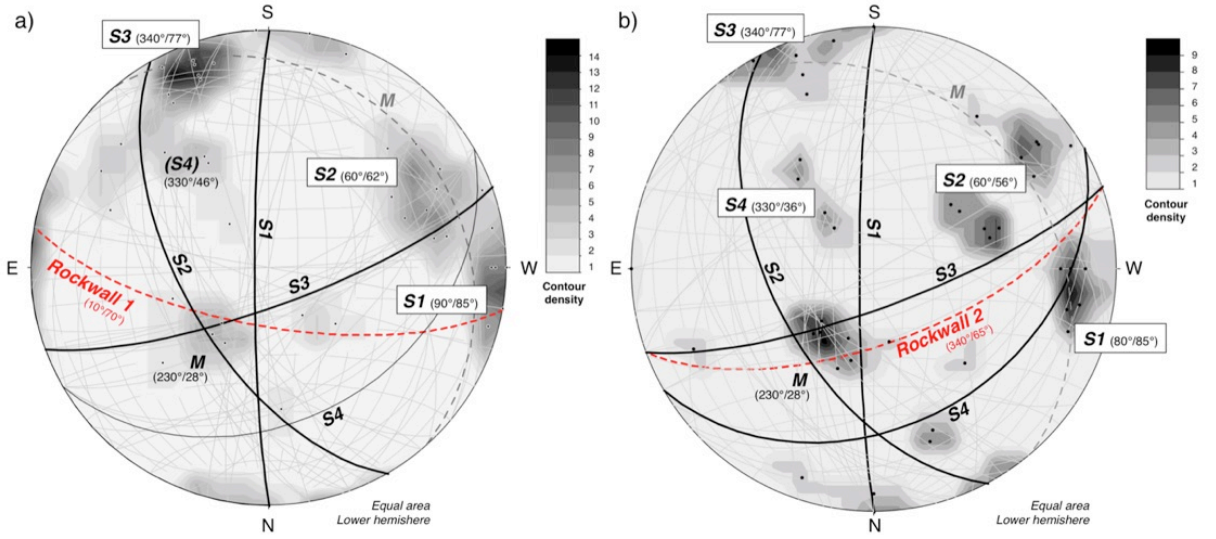

Figure 7.7: *Stereographic equal-area projections (lower hemisphere) for R1 (a) and R2 (b). The density of all poles (dotes) is shown in 1% contour intervals. The poles' respective great circles (black lines) represent the mean orientation of joint set S1, S2, S3 and S4. In both rockwalls, metamorphic (M) bedding planes (only some representatives have been mapped/displayed) are dipping into the slopes. Depending on the rockwalls' orientation (red dotted lines), the joint sets and their intersection result in different failure mechanisms ranging from mainly wedge failure and block slides (R1) to toppling processes (R2).*

The stereographic equal-area projection (Figure 7.7) shows the pole densities of joints and their great circles representative of the mean orientation of the given joint sets. In addition to the indipping metamorphic beddings (M, 230°/28°), four major joint sets have been identified. Most prominent are S1 (80-90°/85°) and S2 (60°/65-62°), both steeply dipping to NE/ENE. At their intersection, potential wedge failures are defined on the NNW-exposed R2 (Figure 7.7b), particularly where metamorphic layers dip in the opposite direction. Wedge failures often encompass large blocks (Jv 2-2.1) of medium spacing (55-52 cm) and strong rock mass strength (RMS 61-58) (III and VI in Figure 7.6b). At R1, joints of S2 occasionally act as failure planes for block slides dissected by S1 due to the rockwall's NNE-aspect (Figure 7.7a). In widely jointed bedrock sections (e.g. I and IV in Figure 7.6a), relatively large (Jv 1.5-1.8) and intact rock blocks (RMS 79-69) are expected to slide. Additionally, both rockwalls are dominated by steeply indipping planes (S3: 340°/77°), whose intersection leads to small-size wedge failures conditions at R1 (Figure 7.6a). At R2, by contrast, S3 is associated with toppling mechanisms due to the directly opposing slope aspect. Here, the shallow outdipping S4 (330°/36°) acts as a basal plane for relatively small-size topples (IV in Figure 7.6a). At R1, only a few planes of S4 are pronounced (Figure 7.7), but can result in large (Jv 1.3-2) block slides (VI-VIII in Figure 7.6a).

Joint volumetric counting indicates comparable rockfall-prone block volumes with median values of 9.6 m3 for cubic and 14.2 m^3 for platy blocks (Figure 7.8). Maximum block sizes of up to 103 m^3 may occur at R1,

associated with platy block shapes. However, while R2 covers an approximately uniform and small interquartile block range (IQR) of 5.6-12.2 m^3 (cubic) or 9-23.8 m^3 (platy), the size spectrum of R1 is broad. The IQR of R1 ranges from a few cm^3 up to 14.8 m^3 (cubic) or 60.9 m^3 (platy).

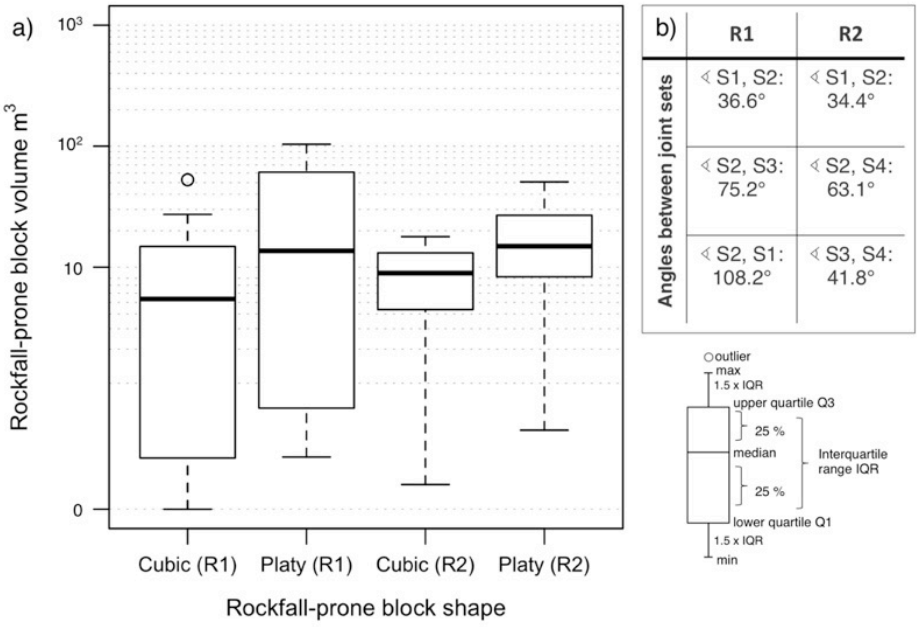

Figure 7.8: *Rockfall-prone volumes of cubic and platy (ratio 1:5:5) block detachments at R1 and R2 (a). Potential block volumes (m^3) have been estimated based on the corrected joint volumetric count (Jv) of each transect subsection (see Figure 7.6) and using the chart provided by Palmstrom (1982). Considering the angles (α, β, γ) of dominant joint intersections (b) block volumes have been adjusted with specific correction factors corr = $(1/\sin\alpha) * (1/\sin\beta) * (1/\sin\gamma)$ (Palmstrom, 1982).*

7.4.3 Near-surface rock temperature variability

Figure 7.9 displays 3-hourly near-surface rock temperature variations at R1 (a) and R2 (b) recorded from August 2014 to August 2016. During autumn (Oct-Nov), all sites experienced frequent diurnal temperature oscillations around 0 °C, particularly R2. In autumn 2015, the period of diurnal freezing started comparatively earlier compared to the previous year and the number of total diurnal frost cycles nearly doubled. From early winter onwards, R1a, R1b and R2a display temperatures curves typical for snow covered sites. Progressive cooling to sub-freezing conditions occurred until late December/mid January. The first winter cooling is then followed by approx. three (2015) or two (2016) months of stable conditions close to -3 °C (R1a), -5 °C (R1b) and -1 °C (R2a). Constant NSRTs below freezing point indicate local snow cover isolating the bedrock from further winter cooling and heat loss during spring.

Figure 7.9: *(Next page) Near-surface rock temperature variability (NRST) of (a) R1 and (b) R2 recorded in 3h intervals from 1st August 2014 until 25th August 2015. Positions of temperature loggers (R1a, R1b, R2a, R2b) are displayed in Figure 7.2a and Figure 7.3. Mean annual rock temperature (MART) and (half) annual sinusoidal amplitude (Ta) are displayed for each period and used as input for subsequent frost cracking modelling.*

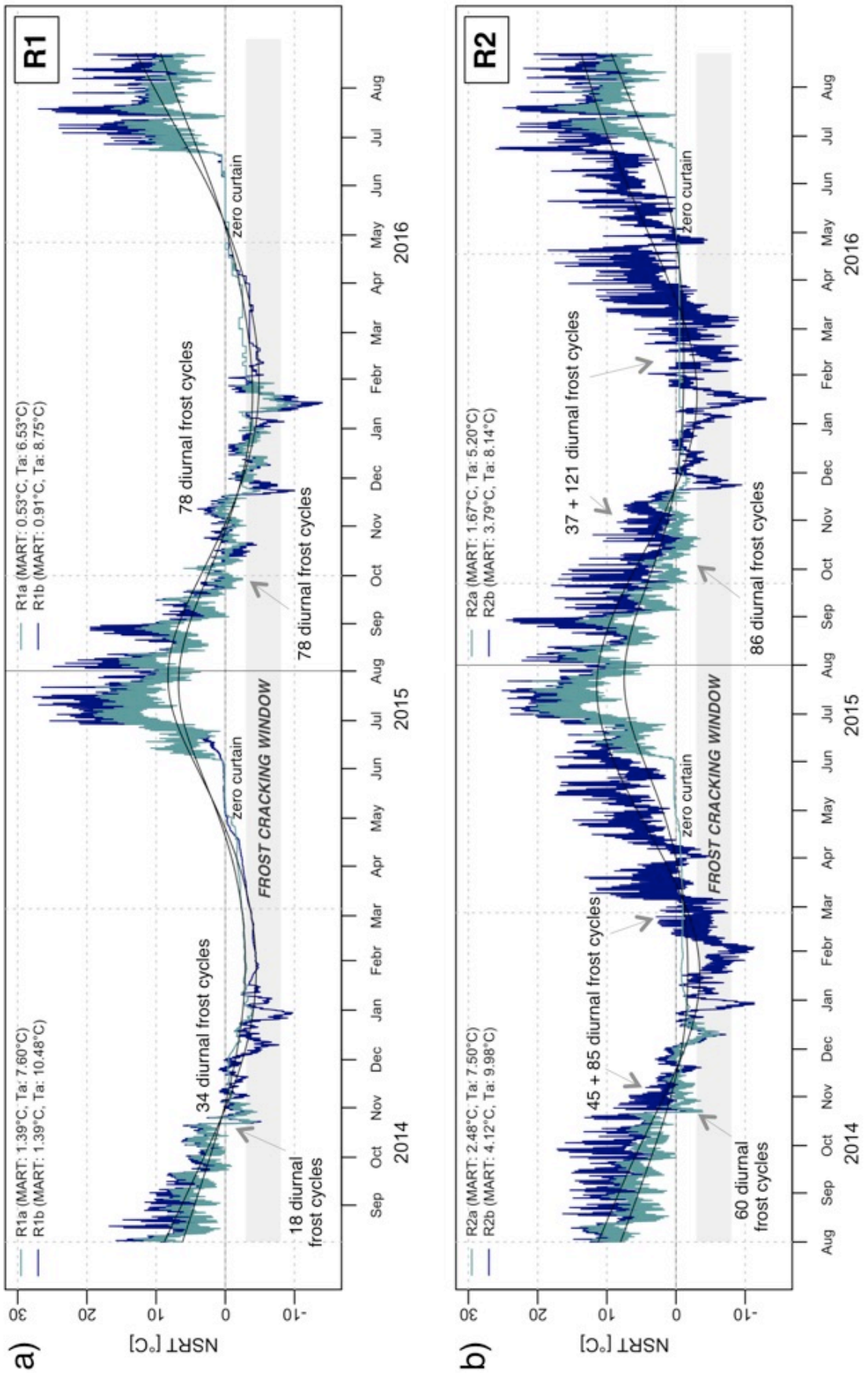
a)
R1
R1a (MART: 1.39°C, Ta: 7.60°C)
R1b (MART: 1.39°C, Ta: 10.48°C)
R1a (MART: 0.53°C, Ta: 6.53°C)
R1b (MART: 0.91°C, Ta: 8.75°C)
NSRT [°C]
30
20
10
0
-10
34 diurnal frost cycles
78 diurnal frost cycles
78 diurnal frost cycles
18 diurnal frost cycles
zero curtain
zero curtain
FROST CRACKING WINDOW
Sep Oct Nov Dec Jan Febr Mar Apr May Jun Jul Aug Sep Oct Nov Dec Jan Febr Mar Apr May Jun Jul Aug
2014
2015
2016
b)
R2
R2a (MART: 2.48°C, Ta: 7.50°C)
R2b (MART: 4.12°C, Ta: 9.98°C)
R2a (MART: 1.67°C, Ta: 5.20°C)
R2b (MART: 3.79°C, Ta: 8.14°C)
NSRT [°C]
30
20
10
0
-10
45 + 85 diurnal frost cycles
37 + 121 diurnal frost cycles
60 diurnal frost cycles
86 diurnal frost cycles
zero curtain
zero curtain
FROST CRACKING WINDOW
Aug Sep Oct Nov Dec Jan Febr Mar Apr May Jun Jul Aug Sep Oct Nov Dec Jan Febr Mar Apr May Jun Jul Aug
2014
2015
2016

By contrast, R2b recorded in both years steady cooling to lowest temperatures of -9.7 °C (January 2015) and -14 °C (February 2016), reflecting the lack of an isolating snow cover. Afterwards, the NSRT of snow-free bedrock rapidly became positive cycling between 2 °C to 18 °C until early April, whereas all other sites show constant temperatures around 0 °C over 1.5 months. The zero curtain effect in late April reflects the onset of snowmelt, allowing atmospheric heat fluxes to penetrate the ground surface and resulting in latent heat and subsurface warming. After spring, NSRTs became quickly positive reaching maxima of up to 23-27 °C (i.e. in July 2015) over several days during summer.

In both years, positive mean annual rock temperature (MART) and annual sinusoidal cycles (Ta) are evident, but differ between all sites and over both periods. In the first 12 months, the mean MART of R1a and R1b was 1.4 °C; nearly 2 °C lower than at R2 (Figure 7.9). July 2015 was the warmest month (mean of R2a and R2b: 15.2 °C) during the 2-year monitoring period. From August 2015 to August 2016, MART at all sites slightly decreased, similar to their Ta. This is primarily linked to lower summer temperatures and more intense autumn freezing compared to the previous year.

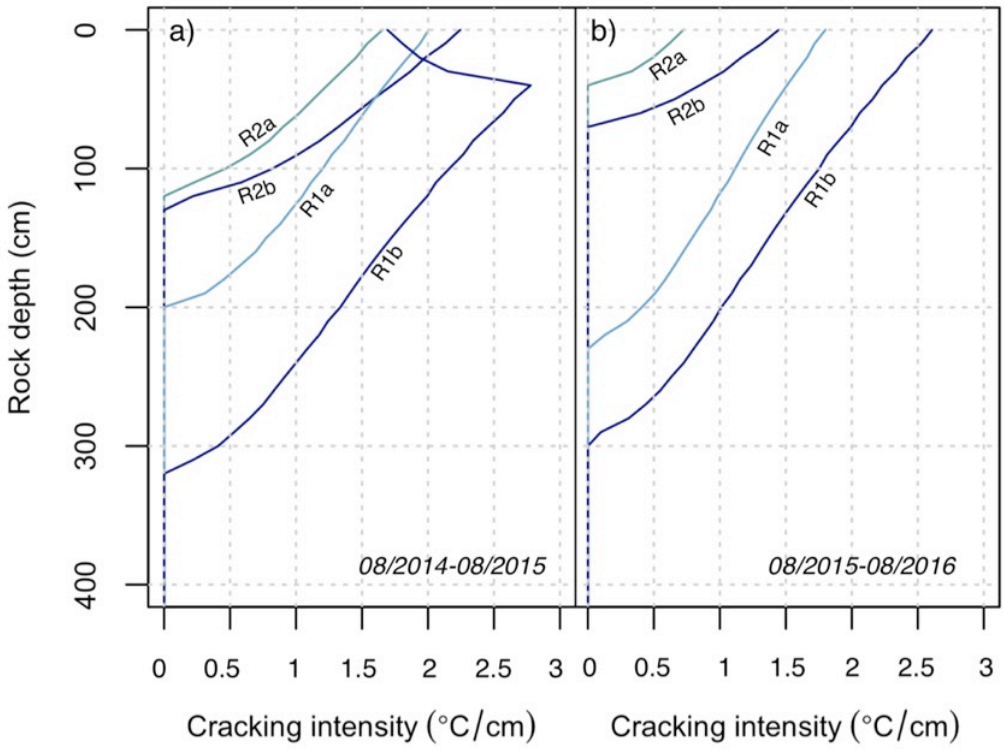

Figure 7.10: *Depth-integrated frost cracking intensity for the period 2014-2015 (a) and 2015-2016 (b) estimated using the one-dimensional heat conduction model of Hales and Roering (2007). Due to different MART and Ta values (shown in Figure 7.9) the maximum depths of segregation ice growth and the cracking intensities significantly differ between R1 and R2 as well as throughout the 2-year monitoring period.*

7.4.4 Maximum depth and intensity of segregation ice growth

Site-specific differences concerning the number of days of possible frost cracking are evident in Figure 7.9. From 2014-2015 to 2015-2016, the number of cumulative sub-freezing conditions slightly increased at most

sites, i.e. at R1 from 34 to 88 (R1a). Depending on the specific combination of MART and Ta, differences in the maximum depth of ice growth and the cracking intensity have been modelled at all sites and throughout the 2-year monitoring period (Figure 7.10). Both maximum depth and intensity of segregation ice growth are, on average, comparatively higher at R1 than at R2. During period 2014-2015 (Figure 7.10a), ice formed down to 190 cm (R1a) and 310 cm (R1b), with most intensive cracking at 40 cm and 10 cm, respectively. By contrast, the occurrence of segregation ice at R2 is limited to distinctively shallower depths of 110-120 cm and cracking is most intensive in the outermost centimetres of the bedrock surface. In the following year (Figure 7.10b), the total cracking intensity decreased by 0.1 °C/cm (R1) to 1.68 °C/cm (R2) then affecting only the outermost 0-30 cm of the bedrock surface.

7.5 Discussion

7.5.1 Frequency-magnitude pattern of rockfall supply onto talus slopes

Although rockfalls account for the dominant geomorphic process operating on steep mountain rockwalls (Rapp, 1960a; Caine, 1976; Messenzehl et al., 2014), the most effective event size and return period for the total rockwall erosion and downslope sediment supply are still poorly understood (cf. Krautblatter and Dikau, 2007). Particularly, quantitative data on small-magnitude rockfalls are scarce as their volumes are difficult to detect in laser scans and their deposits remain often unnoticed in regional-scale and/or short-term inventories (Krautblatter et al., 2012). Our study reveals that the long-term rockfall activity at Hungerli Peak leads to talus slopes covered by centimetre-sized flakes at the apices to boulders of up to 11 m^3 at the hillslopes' foot (Figure 7.4a). Platy and elongated clasts primarily cover the upper slope segments (Figure 7.4d) as they rapidly lose momentum during travel, whereas blocks tend to become more spherical towards the talus' toe (Figure 7.4c) reflecting their higher kinetic energies (Frattini et al., 2012). As this pronounced downslope sphericity increase and the gravitational fall sorting are typical indices observed on active rockfall-dominated talus slopes (Caine, 1967, 1969; Pérez, 1989; Jomelli and Francou, 2000), we argue that rockfalls are the key process governing the present-day rockwall erosion and talus supply at Hungerli Peak. Our data additionally suggest a dominance of low-magnitude rockfall events with mean volumes of approx. 10^{-1} m^3 (Figure 7.4a). This size range is consistent with observations from rockfall collectors below e.g. densely fractured magmatic rocks (Douglas, 1980) and banked limestone rockwalls (Sass, 1998; Krautblatter and Moser, 2009) where commonly > 60% of the weekly collected sediments are smaller than $10\text{-}10^{-1}$ m^3.

The overall dominance of small-size talus deposits is also mirrored by the potential rockfall volumes detected at their source rockwalls. Given the joint volumetric count (Figure 7.8a), 75% of expected block magnitudes correspond to Whalley's (1984) 'debris fall' (< 14 m^3) category, if cubic, or "boulder falls" category (14-61 m^3), if prismatic. This high probability of small-scale instabilities at Hungerli Peak corresponds well with previous measurements on deglaciated rock slopes in arctic and alpine environments (e.g. André, 1997; Sass, 2005b). In the Eastern Pyrenees, for instance, geotechnical analyses of Corominas et al. (2005) similarly show that 75% of the block volumes defined by joints are smaller than 12 m^3. A high activity of events of < 10 m^3 has also been directly observed in recent terrestrial laser surveys (Guerin et al., 2013; Abellán et al., 2014;

Carrea et al., 2015; Strunden et al., 2015). Figure 7.5 reveals furthermore that small magnitudes are linked, on average, to annual to century-scale return periods, with this distinctly varying downslope. With 3-6 events per year, flake-like to pebble-size events onto the upper talus segment are most frequent, whereas return periods of bigger boulders decrease non-linearly up to 250 years (on T1) with increasing distance to the source rockwalls. Following André (1997), the frequent supply of apical clasts could result from surficial rockwall flaking, although fragmentation of larger rockfall events after their first ground impact and associated dust clouds need to be taken into account (Gili et al., 2016).

Despite comparable areas and lengths of rockfall contributing areas (Figure 7.3), landform-specific differences in the depositional frequency and magnitude are evident. These appear to correspond well with the contrasting failure mechanisms of the source rockwalls and the involved block sizes. For instance, the approximately uniform rockfall-prone volume of 5.6-23.8 m^3 at R2 (IQR in Figure 7.8a), which is primarily linked to wedge and toppling conditions (Figure 7.6b, Figure 7.7b), is mirrored by relatively homogenous block size spectrum (10^{-2} -10^{-1} m^3) along its talus slope (T2 in Fiure 7.4a). Similar relationships are reported from thinly stratified limestone (Matasci et al., 2015) and crystalline rockwalls (Loye et al., 2012), respectively, where blocks of < 10 m^3 are primarily released by wedge failures. Conversely, the presence of relatively large sliding structures at R1 (Figure 7.6a, Figure 7.7a) may involve not only a comparatively larger erosional size-spectrum ranging from a few centimetres to a maximum of 103 m^3 (Figure 7.8a), but also larger block sizes and a higher heterogeneity along the adjacent talus slope (T1 in Figure 7.4a-b). The significance of large planar sliding of up to 250 m^3 for talus deposition is also observed in laser scans of granodiorite rockwalls in the Pyrenees by Santana et al. (2012). This supports the notion that regardless of the lithological setting (Stead and Wolter, 2015), rockfall events released by planar sliding may be more efficient than other failure types with respect to the amount of rock mass that is eroded and finally supplied downslope. In our study site, however, their return periods are presumably low with, on average, one event every 250 years (T1 in Figure 7.5). By contrast, despite the relative small magnitudes of singular wedge failures and topples, their sediment supply is likely more frequent covering annual to decadal time scales (T2 in Figure 7.5).

We hypothesise that boulder-size planar slides with decadal to century-scale return periods overlain by smaller, high-frequency wedge and toppling failures may be the key formative processes of rockwall erosion and talus evolution at Hungerli Peak. Nevertheless, it is important to state that the past occurrence of high-magnitude events cannot be excluded; although neither talus block sizes nor the joint volumetric count provide evidence for rockfall volumes of > 100 m^3. For instance, Krautblatter et al. (2012) showed that > 60% of the rockfalls from carbonate rockwalls in the German Alps occur as high-magnitude Bergsturz events and cliff falls. And even on hard low-porosity metamorphic and igneous rocks, a higher proportion of boulder and block falls has been previously reported (Jäckli, 1957; Rapp, 1960). Accordingly, we cannot discount that surface material of lower talus segment could originally result from high-magnitude failures. Particularly, the poor distal material sorting shown in Fifure 7.4b, where smaller sediments are frequently intercalated between highly weathered boulders, could point to gradual block disintegration after accumulation. Moreover, we have to take into account that the ground impacts of high-energetic events, i.e. when released from higher areas, can reduce the block volume up to several cubic meters (Chau et al., 2003a; Ruiz-Carulla et al., 2015). Although rockfall fragmentation may be comparable at both sites due to the similar rockwall/rockfall fall heights, the

pre-existing schistosity may increase the likelihood that blocks split along their platy, parallel-arranged minerals. Comparing the largest boulder of 11 m^3 at T1 (Figure 7.4) with the maximum joint volumetric count of its source rockwall (Figure 7.8a) suggests a block size decrease of up to 92%. Similar orders of rockfall fragmentation have been found by numerical (Wang and Tonon, 2011), experimental (Giacomini et al., 2009; Gili et al., 2016) and direct field observations (Corominas et al., 2005). Nevertheless, the intense surface weathering of large boulders at the talus toe (Figure 7.2b, c) may support our calculation in Figure 7.5 that boulder falls and larger events occur relatively rarely with long return periods of several 10-100 years.

7.5.2 Role of structural and thermal properties of the source rockwall

The review of the literature displays not only a wide spectrum of different findings on the rockfall frequencies and magnitudes in steep mountain terrain, but also diverse theories on the underlying key controls. While part of the variations certainly comes from the contrasting methods and databases, external meteorological and climatic influences, particularly exceptional rainfall events, have been frequently identified to be the key rockfall triggers (Luckman, 1976; Crozier and Glade, 1999; e.g. Chau et al., 2003b; Guzzetti et al., 2003; Krautblatter and Moser, 2009; Delonca et al., 2014; D'Amato et al., 2016). However, the predefining and preparing role of the source rockwall on event size and return period is still little explicitly addressed in geomorphic frequency-magnitude research.

Our investigations provide evidence that rockfall magnitude is primarily predefined by the joint spacing and joint density per m^3 of rock mass. The comparatively larger talus blocks along T1 in Figure 7.4a, where joint spacing and joint volumetric count of its source rockwall R1 is on average twice that of R2 (Table 7.1, Figure 7.8a), imply a tendency for increasing magnitudes with increasing joint spacing and/or decreasing joint density. While this relationship has been verified mainly for sedimentary rockwalls (Dussauge et al., 2003; Sass, 2005c; Matasci et al., 2015) and, rarely, for sheeted igneous rocks (Douglas, 1980; Olyphant, 1983), our study underlines the validity also for metamorphic rocks.

Furthermore, similar to findings of Moore et al. (2009) and Coe and Harp (2007), the importance of joint orientation or tectonic folding relative to the rockwall topography becomes evident in our data. Although both sites are dominated by same joint sets (S1 to S4), their stereographic equal-area projections in Figure 7.7 display contrasting failure modes due to small-scale variability in the rockwalls' exposition. While small-size wedges and larger planar sliding conditions primarily dominate the rockfall magnitude-frequency pattern of the NNE-rockwall R1, same joint dips and orientations favour small-magnitude toppling and wedge failures at the NNW-oriented site R2. Our findings therefore show that marginally contrasting rockwall orientations can lead to systematic variations in failure modes and magnitudes on one mountain peak, despite homogenous joint geometry and regional-scale tectonic setting.

However, previous studies emphasise that bedrock failures are not solely predefined by 3D joint geometry, but prepared, if not triggered, by their 'thermomechanical' interplay with the subsurface temperature field (Gunzburger et al., 2005; e.g. Gischig et al., 2011a; Gischig et al., 2011b). On a multi-annual to seasonal scale, the occurrence of rockfalls is often linked to permafrost degradation in rockwalls (Ravanel and Deline, 2015). At Hungerli Peak, the positive MART's of all MTL sites close to and above 0 °C (Figure 7.9) theoretically

indicate the absence or lower limit of permafrost on the northern slopes (Gruber and Haeberli, 2007). Our local rock temperatures are consistent to the regional-scale zonation of BAFU (2005) shown in Figure 7.3. This boundary zone is particularly sensitive for rockfalls of all magnitudes. As shown by Krautblatter et al. (2013), progressive permafrost warming and thawing effectively reduce the internal rock strength and friction, which can result in fast deformation along pre-existing shear planes. In higher elevated areas of Hungerli Peak, with presumably punctual existence of permafrost (BAFU, 2005), subcritical and deep rock failure is more likely (Krautblatter et al., 2013) due to bi-directional freezing over the active permafrost layer (Murton et al., 2001; Murton et al., 2006). This again supports the notion that slow, high-magnitude failures could infrequently contribute to the spatiotemporal rockfall pattern in our study area.

On an intra-annual scale, we consider different controls on rockfall activity. Our MTL data in Figure 7.5 display a high activity of hourly thermal cycles between 5 °C and 27 °C during summer. Recently, Collins and Stock (2016) showed that those high-frequency rock temperature fluctuations can favour high tensile stresses up to the point that they finally trigger rockfalls. However, while their findings derive from exfoliated, highly erosive granitic rockwalls in Yosemite Valley, daily thermal cycles in Hungerli paragneiss are probably insufficient to cause instabilities given the lack of surface-parallel fracturing (Figure 7.7). Nonetheless, we cannot rule out that their long-term activity is important for enhancing other weathering types e.g. by porosity increase or new micro-cracks, as recently shown by Eppes et al. (2016).

Alternatively, smaller rockfall deposits, as in our study sites, are often intuitively linked to repeated diurnal freeze-thaw cycles (Douglas, 1980; Matsuoka, 1994; Matsuoka and Sakai, 1999). Although all MTLs recorded frequent diurnal oscillations around 0 °C during autumn and spring (Figure 7.9), the theoretical model of Walder and Hallet (1985) suggests that they are insignificant for effective tensile stresses. Neither the prerequisite of a fully saturated closed system (Sass, 2005a) nor rapid freezing rates (Hallet, 2006) is present at Hungerli Peak to allow for volumetric ice expansion of 9%. Here we favour instead slow and seasonal growth of segregation ice as an alterative rock destabilising mechanism. Following laboratory tests (Murton et al., 2006; Krautblatter et al., 2013) and field monitoring of acoustic emissions (Hallet et al., 1991; Amitrano et al., 2012), the sustained sub-zero winter temperatures shown in Figure 7.9 may provide favourable conditions for progressive ice-induced rock deformation at both sites; even close to 0 °C as found by Girard et al. (2013). Application of the numerical model of Hales and Roering (2007) reveals most intense frost cracking in the outermost bedrock surface. This indication of effective shallow bedrock erosion seems to support our field-based calculation in Figure 7.5 that flake-like clasts are most frequently delivered to the first 25 m below the rockwalls. Nevertheless, in higher elevated permafrost-affected bedrock the 1D-conduction model may underestimate the cracking efficiency and the associated rockfall magnitude by several centimetres, as the effect of bi-directional freezing is not implemented (Matsuoka and Murton, 2008).

Due to site-specific variations in MART and Ta in our MTL records, Figure 7.10 displays different frost cracking depths and intensities at both rockwalls. Besides random effects caused e.g. by MTL drilling or rock properties (i.e. mineral conductivity), temperature differences may result from micro-topographic and snow cover effects. Particularly due to the drilling depth of 10 cm, NSRT is highly susceptible to atmospheric small-scale climatic variations (Hipp et al., 2014). Thus, although our number of four MTLs is too small to infer

small-scale thermal variability along one mountain peak, the analysis of 390 MTL by Gubler et al. (2011) indicates that NSRT can highly vary up to 6 °C even within an elevation belt of 300 m and at distances of less than 14 m. At Hungerli Peak, greatest frost cracking depths of 200-300 cm have been estimated at the NNE-exposed, snow-rich rockwall R1 (Figure 7.10), where hot summer extremes resulted in high annual Ta. In bedrock, where joint spacing of approx. 100-200 cm approximates these modelled maximum freezing depths (e.g. I, VI, XII in Figure 7.6a), rock failures of several m^3 are likely as e.g. deposited at the adjacent talus slope T1 (Figure 7.4a). However, as found by Moore et al. (2009) at rockwalls in the Sierra Nevada, probability or annual frequency of rock instability is probably counterbalanced by high RMS values of the amphibolite-rich rockwall R1 (Figure 7.6a, Table 7.1). At the NNW-exposed, less snow-affected rockwall R2, by contrast, frost cracking is restricted to the upper 110-70 cm due to a lower annual Ta and MART. This modelled surficial ice growth is likely still effective to promote smaller rockfall magnitudes, if the source bedrock is densely jointed and has relatively low RMS (e.g. IV, VII, IX in Figure 7.6b).

The above findings emphasise that the 1D-conduction model is highly sensitive to MART and the annual Ta, as they are assumed to be the first-order parameters on the availability of unfrozen water and its movement to the freezing front (Williams and Smith, 1989). Therefore, our results have to be carefully interpreted with respect to the thermo-isolating effect of snow cover detected at three MTL sites (Figure 7.10). Due to this, the diurnal temperature oscillations are significantly smoothed in comparison to the snow-free site R2b, often by 1.3 to 2.3 °C (Haberkorn et al., 2015a). This effect is particularly pronounced in Figure 7.9 end of 2014, when a relatively warm winter with exceptional snow precipitations was recorded in the Valais Alps (MeteoSwiss, 2015). In winter 2015-2016, less and later snow precipitation (MeteoSwiss, 2016) resulted in more intense winter bedrock freezing and lower MARTs (Figure 7.9). This shows that we likely overestimate the effect of conduction. Both during winter, when insulating snow cover prevents heat fluxes to penetrate into depth and in spring, when melt water infiltration into open joints produces latent heat (zero curtain) (Goodrich, 1982; Zhang, 2005; Phillips et al., 2016) and leads to heat advection (Hasler et al., 2011a; Blikra and Christiansen, 2014). It is therefore important to state that our approach simplifies the complex ground thermal regime of anisotropic mountain rock mass. Both the MTL installation at intact, unjointed bedrock and the 1D-conduction model do not reflect non-conductive heat fluxes through joints by air and i.e. melt water. However, the low rock porosity and permeability in our study site (see Table 1 in Draebing and Krautblatter, 2012) as well as the small apertures of mostly in-filled joints (Table 7.1, Figure 7.6) may still justify using a conduction model for our study site (Anderson, 1998).

7.5.3 Evaluation of explanatory framework: The integration of deductive rockwall surveys with abductive talus assessments

Previously, researchers commonly study either talus slope landforms or the unstable source rockwall to increase our knowledge of rockfall activity. However, the explanatory framework is rarely addressed explicitly. Moreover, talus- and rockwall-approaches seem to exist and develop largely alongside each other. While abduction from sediment archives is common in geological and geomorphic research (von Engelhardt and Zimmermann, 1988; Baker, 1996), this type of reasoning is increasingly rejected by those favouring process-

based rockwall investigations (Krautblatter and Moore, 2014). Here, we proposed a holistic rockwall-talus approach that combines abductive explanations of the depositional area with deductive stability assessments of the source rockwall (Figure 7.1).

Field mapping of talus block size and shape variations provided a valuable basis of arguments to infer past rockfall magnitudes ranging from cm-size flakes to debris and boulder falls. Their site-specific annual to multi-decadal rockfall return periods were estimated by the indirect approach of Evans and Hungr (1993). Our results underline that abduction from talus slopes is of central importance for particularly steep mountain terrain, where unpredictable and dangerous rockfalls are often difficult to observe. However, due to this lack of direct field observations, abduction requires to select a range of hypothetical conditions ('L' in Figure 7.1a) as there is no logical necessity that destabilising mechanisms such as near-surface bedrock flaking or permafrost degradation were really working in the past. In the words of Inkpen and Wilson (2013 p. 82), abduction requires a researcher who is able 'to tell a plausible story'. Advocators of process-based approaches may go even further by describing those explanations as 'lucky guessing' (cf. Baker, 1996 p. 70). Our above discussion emphasises that unknown intervening factors such as rockfall fragmentation or gradual weathering of talus deposits complicated our cause-effect causation. We therefore had to refer to additional information e.g. about rockwall height/length or efficiency of rockfall catchment area to evaluate the possibility of 'other unknowns' such as high-impact failures.

In order to strengthen our abductive hypotheses on rockfall activity at Hungerli Peak, we integrated deductive arguments from rockwall surveys in our explanatory framework. The synthesis of our structural and thermal data provided a valid basis to apply an overarching theory of rock instability, i.e. using the frost cracking model, and to predict logical rockfall sizes and frequencies. Normally, deduction seeks only one certain link between cause and effect (Figure 7.1b). But as our talus deposits permit multiple hypothetical rockfall sizes and frequencies, we tested different controls such as permafrost degradation, hourly thermal cycling, daily frost cycles and seasonal ice segregation. However, once we reach a particular degree of system complexity, our study also showed that deductive rockwall surveys rely upon a certain degree of simplification (Harrison, 2001; Phillips, 2003b). MTL installation at 10 cm depth of intact rock and application of 1D conduction model certainly simplifies the complex thermal regime of the anisotropic paragneiss with a high joint density. But it allowed comparability to previous studies and to narrowing our explanations on rockfall activity with respect to our initial research aim. Similarly, by selecting two landform complexes in comparable topoclimatic, paraglacial, geological and tectonic settings, we kept those influences on cause-effect linkage constant and reduced the complexity of controlling factors 'to a manageable proportion' (Baker, 1996 p. 60). This allowed us to exclusively assess the role of small-scale structural and thermal factors. This laboratory-like research is described by Inkpen and Wilson (2013 p. 90) as an inevitable and necessary 'human intervention into reality'. We are aware that it makes our cause-effect reasoning on rockfall activity to some degree a site-specific, if not a singular product. Therefore, we hereby appeal to enlarge the research activities on rockwall instability and talus deposition in different mountain settings, e.g. using similar rockwall-talus approaches.

To sum up, both abduction and deduction are linked to different degrees of certainty, but also likelihood concerning cause, effect and linking theories. Thus, as already recommended by von Engelhardt and

Zimmermann (1988), the best research design is about the interplay of abduction and deduction (and ideally induction). Our integrative study highlights that deductive information about the rockwall source area can strengthen the abductive hypothesis from sediment archives, and on the other hand, abduction can bring multi-causal interpretations into deductive structural and thermal findings (Figure 7.1). We believe that using holistic rockwall-talus approaches, such as proposed here building on previous studies (Rapp, 1960b; Olyphant, 1983; André, 1997; Krautblatter and Dikau, 2007; Moore et al., 2009) may significantly increase our confidence in explaining rockfall frequency and magnitude in mountains systems.

7.6 Summary and future perspectives

Despite the geomorphic importance and hazard potential of rockfalls in steep mountain terrain, understanding of their frequency-magnitude patterns and key controls is still incomplete, particularly at the lower end of the magnitude spectrum. In this study, we investigated two rockwall-talus complexes at the northern slopes of Hungerli Peak in the Swiss Alps proposing a holistic multi-method approach. By combining abductive reasoning based on block size and frequency estimations of talus deposits with deductive arguments from geotechnical and thermal investigations of the source rockwall, we aim to decipher (i) the rockfall frequency-magnitude pattern of each landform complex with respect to their (ii) key controlling factors.

(i) Pronounced downslope gravitational fall sorting and sphericity increase of talus material suggest that rockfalls are key drivers of present-day rockwall erosion and talus deposition at Hungerli Peak. Rockfall deposits reflect a dominance of low-magnitude events < 11 m^3, which is mirrored by the potential block sizes of the corresponding source rockwalls. 75% of the block volumes defined by joints represent debris fall (< 14 m^3) and boulder falls (14-61 m^3). Nevertheless, due to the likelihood of rockfall fragmentation and after-impact disintegration, the past occurrence of high-magnitude events cannot be excluded. Annual rockfall frequency was found to decrease non-linearly with increasing rockwall distance. Based on our kinematic joint analyses, we hypothesise that large planar slides with likely decadal to century-scale return periods (~250 years) overlain by smaller, frequent wedge and toppling failures (~17-50 years) as well as annual supply of flake-like clasts (~3-6 events/year) characterise the rockfall frequency-magnitude pattern of Hungerli Peak.

(ii) Our data emphasise the predefining role of 3D joint geometry, with a tendency for increasing rockfall magnitudes with increasing joint spacing and/or decreasing joint density. By integrating 2-year records of near-surface rock temperature into our abductive hypotheses, we evaluated different thermal controls. On a multi-annual to seasonal scale, MARTs close to 0 °C implies permafrost boundary conditions with a higher probability of rockfall activity. On an annual to seasonal scale, the numerical model reveals sustained bedrock freezing to -3 °C and -5 °C as key destabilising process. Greatest frost cracking depth of 200-300 cm has been estimated at the NNE-exposed, snow-rich rockwall, with peaks at outermost bedrock surface. We critically discuss

the model limitation to account for the thermo-isolating effect of snow cover on MAAT (decrease of 1.3-2.3 °C) detected at three MTL sites.

Our study underlines that rockfall processes, particularly of smaller magnitudes, need more attention in geomorphic research. With respect to ongoing atmospheric warming, major research should focus particularly on mountain slopes in discontinuous permafrost zones, where even small thermal variations may lead to different depths and intensities of bedrock deformation. For better prediction, we need to increase local networks of rock temperature monitoring in mountain valleys, e.g. by using a high number of rockwall miniature temperature loggers. Such data can then be further processed using numerical models to estimate ice-induced rockwall failures with a high spatiotemporal resolution. Furthermore, rather than focusing just on climatic or meteorological triggering events, future frequency-magnitude estimates should ideally incorporate the predefining role of site-specific structural and thermal properties of the rockwall source area. We showed that different kinematic and thermomechanical conditions may control local frequency-magnitude patterns, despite similar regional-scale topoclimatic, paraglacial, geological and tectonic settings. The integration of deductive small-scale surveys of rockwall instability into multi-causal explanations from abductive assessments of talus archives may provide a valid basis to proceed to this research agenda. We believe that the use of integrative and holistic rockwall-talus approaches, as proposed in our study, will contribute to a better systemic understanding of the geomorphic role of rockfalls and a better natural hazard prediction in mountain valleys.

Acknowledgments

We highly appreciate the funding for our field campaigns in 2014, 2015 and 2016 provided by the British Society for Geomorphology (Postgraduate research grant), the Humboldt-Ritter-Penck Foundation of the Gesellschaft für Erdkunde zu Berlin, the German exchange service (DAAD) and the Dr. Hohmann-Förderung of the Gesellschaft für Erdkunde zu Köln e.V. We thank Daniel Dräbing for assisting during MTL installation in summer 2014, Jana Eichel and Markus Wieland for help with photogrammetric image processing and Jan Blöthe for valuable support with R. Furthermore, we thank the two anonymous reviewers for their valuable comments that significantly contributed to improve the manuscript as well as Heather Viles, Vanessa Winchester and Martin Michette for final proof reading. Finally, all hard-working and faithful field helpers certainly deserve our greatest thanks! Many thanks to Andreas Ewald, Arne Brandschwede, Luise Martin, Nikola Schulte-Kellinghaus, Katharina Eibisch, Sebastian Unger and Katrin Hoffmann for assisting during fieldwork, carrying all equipment each day over several weeks to the hanging valley and making Geomorphology fun!

Chapter 8

STUDY V - LABORATORY WEATHERING EXPERIMENTS OF SYNERGISTIC THERMAL CYCLING AND FREEZE-THAW

This chapter is based laboratory experiments performed at the Oxford Rock Breakdown Laboratory in cooperation with Heather Viles and Martin Coombes. The described laboratory findings and discussed implications for synergistic rock weathering in steep alpine terrain will be addressed in a future publication.

Abstract

Frequent bedrock freezing and thawing is known to destabilise alpine rock slopes and to promote the release of rockfall events. While slow ice segregation seems to be a key weathering mechanism, it is still controversial as to whether diurnal, low-magnitude frost events can be efficient on their own or whether they only become active after previous stress accumulation. In parallel to this debate, there is increasing evidence that repeated sun-induced thermal cycling could be a further important weathering agent in cold environments, as has been long acknowledged for urban environments and hot deserts on Earth or Mars. However, little information exists about the efficiency of thermal fatigue in steep alpine terrain and even less for low-porosity metamorphic rocks. To address these two current debates, this laboratory study investigates the individual and synergistic mechanical effects of repeated thermal cycling and high-frequency diurnal ice crystallisation in low-porosity metamorphic rocks. A novel two-phase weathering simulation representative of realistic conditions was performed using mica schist samples from the Swiss Alps with contrasting cleavage orientation. The changes in rock properties were monitored across each phase through measurements of open porosity, p-wave velocity and surface hardness. After exposure to 120 thermal cycles (Phase A), an open porosity increase of up to 16% coupled with surface weakening and a p-wave decline by up to 10% are clear signs of pore-scale rock deterioration through differential and anisotropic crystal expansion and contraction. Across subsequent simulation of 80 half-daily frost cycles (Phase B), a two-stage structural damage behaviour was found for all exposed samples, with highest sensitivity found where schistosity was perpendicular to the surface. These findings clearly indicate that repeated frost events are generally capable of modifying rock properties even of low-porosity mica schists, initially at a pore-scale. In comparison, thermally pre-stressed samples recorded the greatest increase in open porosity (up to 50%) and the greatest decline in p-wave velocity (up to 40%) as compared with samples which had not experienced phase A. These findings demonstrate that both diurnal ice crystallisation between autumn and spring and sun-induced temperature variations during summer should receive more attention as individual and synergistic weathering mechanisms in cold environments, even more so when studying the near-surface instability of rockfall-prone rock slopes.

8.1 Introduction

8.1.1 Current debates and laboratory challenges in the research of small-scale rock slope weathering

Small-scale rock weathering processes are important drivers of the instability of larger-scale rock slopes, contributing to long-term relief evolution and sediment production across different climatic and tectonic settings (Selby, 1993; Robinson and Williams, 1994; Calcaterra and Parise, 2010; Viles, 2013b). On high-alpine rock slopes, the steep angles and high elevations that are typically associated with lower levels of insolation (Barsch and Caine, 1984) mean that freezing and thawing of bedrock is known to be a major destabilising mechanism (Matsuoka et al., 1997; Hall et al., 2002; Prick, 2003; Krautblatter and Moore, 2014). During autumn and spring, the ability of repeated ice crystallisation during diurnal frost cycles (Figure 8.1a) to cause breakdown is controversial, but has been shown to be efficient in almost saturated bedrock due to accumulation of sub-critical damage (Matsuoka, 2001a; Sass, 2005b; Jia et al., 2015). During and after constant winter temperatures close to below 0 °C (Figure 8.1a), rock weathering primary occurs due to water migration towards a freezing front and the slow growth of ice within the upper 5m of bedrock or even deeper, if permafrost is present (Matsuoka, 2001b; Hallet, 2006; Murton et al., 2006; Matsuoka and Murton, 2008; Amitrano et al., 2012; Girard et al., 2013). Thus, ice formation in bedrock is efficient in enlarging pores, in preparing failure planes by extending or creating (micro-)cracks, and triggeringultimate failure by enhancing shear stresses and/or reducing the rock strength to a critical state (Walder and Hallet, 1985; Hallet et al., 1991; Günzel, 2008; Krautblatter et al., 2013). Depending on the freeze-thaw depth and its temporal dynamics, associated slope failure can take many forms with varying hazardous potential spanning from seasonal peaks of flake-like clasts of few cm^2 (André, 2002), debris falls (<10 m^3) and boulder falls (10-10^2 m^3) (Rapp, 1960a; Ravanel and Deline, 2015; Messenzehl and Dikau, 2017) to deep-seated and catastrophic rock avalanches of > 10^6 m^3 (Hungr et al., 1999; Allen et al., 2011; Fischer et al., 2012). If occurring over a longer (e.g. postglacial) time scale, frost weathering becomes a major control on the sediment volume produced and stored in mountain valleys (Heim, 1932; Rapp, 1960b; Curry and Morris, 2004; Sass, 2010) and can determine, like a 'frost buzzsaw', the hillslope form and maximum elevation, even in tectonically active mountain belts (Hales and Roering, 2009; Andersen et al., 2015).

During the last few years, however, an increasing number of studies provide empirical evidence that sun-induced thermal cycling is a second, if not similarly important, near-surface weathering process to freeze–thaw cycling in the failure of high-alpine rock slopes. This awareness comes particularly from those mountain areas where rockfall events occur 'spontaneously' during summertime without any of the typical triggers like rainfall, earthquakes, permafrost degradation, snow melt or previous freeze-thaw (Gunzburger et al., 2005; Gischig et al., 2011a; Gunzburger and Merrien-Soukatchoff, 2011; Stock et al., 2014; Collins and Stock, 2016). For example, it has been shown that large diurnal or hourly temperature changes typical of summer rock temperatures, even on shaded and elevated bedrock (Figure 8.1a-b), can lead to thermal fatigue of the outermost mm to cm of bedrock (Hall and Thorn, 2014; Eppes and Keanini, 2017). Although these micro-scale stresses are often far below the inherent rock strength, their long-term concentration along pre-existing structural weaknesses can exceed the rock elasticity and may produce irreversible structural damage in the form

of porosity increases and micro-crack formation (Wang and Liaw, 2008). On granitic cliffs with slope-parallel exfoliation, thermal cycling has been even found to be sufficient to trigger rockfalls (Stock et al., 2012; Collins and Stock, 2016). However, in comparison to frost mechanisms, research on thermal weathering and its role for rock slope instabilities in cold environments is relatively scarce and often limited to granitic rocks. This is despite the fact that the debate about the significance of sun-driven rock weathering is not new in periglacial geomorphology; many researchers have questioned the often exclusive reference to freeze-thaw events and encourage more focus instead on its synergy with frost-independent processes (Hall et al., 2002; Hall and Thorn, 2011; Hall et al., 2012; Viles, 2013b). Therefore, many questions and hypotheses remain that are still to be addressed. In particular: (i) Can repeated thermal cycling alone be sufficient to cause mechanical changes in low porosity, foliated metamorphic rock? (ii) Can this 'pre-weathering' legacy of thermal cycling influence the subsequent action of repeated diurnal freeze-thaw that is generally assumed to be inefficient under natural conditions?

Due to the slow operation of both thermal cycling and freeze-thaw on natural rock slopes, laboratory experiments are a useful means of addressing those questions and simulating natural weathering conditions in high-alpine terrain. Experiments have already provided major insights into the mechanical and thermal effects of frost weathering on a range of different lithologies, rock properties and temperature regimes (McGreevy, 1985; McGreevy and Whalley, 1985; Hall, 1988; Matsuoka, 1990; Davies et al., 2000; Nicholson and Nicholson, 2000; Murton et al., 2006; Günzel, 2008; Matsuoka and Murton, 2008; Draebing and Krautblatter, 2012; Jia et al., 2015; Murton et al., 2016). In the case of thermal weathering, laboratory studies are mainly performed in a context of hot desert environments (Warke and Smith, 1998; Viles et al., 2010) and in material sciences with a focus on, for example, ceramics (Han, 2007) or building materials (Warke et al., 1996; Akentuna et al., 2016). However, regardless of whether thermal or frost weathering is addressed, experimental conditions rarely reflect the complex system of rock slopes in periglacial environments (Fahey, 1983). For example, experiments typically investigate the effects of one individual mechanism in isolation, whereas little emphasise has been given yet to the synergy of parallel or consecutive processes and their complex rock mechanical effects over time (Viles, 2013a). Furthermore, with few exceptions, many laboratory findings derive from soft, high-porosity rock samples such as limestone. Although this may guarantee fast and efficient rock breakdown within the often-limited investigation time, the transferability to low-porosity and competent bedrock as typical in many high-alpine settings is difficult. Similar problems may arise when results from homogenous or sedimentary rock samples are transferred to rock slopes with more complex rock textural structure (e.g. metamorphic cleavage) and are, moreover, up-scaled to rock mass with discontinuities. Therefore, each well-defined experiment is confronted with the challenge to transfer laboratory findings from small rock samples to natural rock slopes with complex mechanical properties and multiple destabilising processes (Figure 8.1b) (Matsuoka, 2001b).

8.1.2 Experimental aims

This laboratory study addresses the questions posed above and explores: (i) whether repeated thermal cycling can induce (trigger) mechanical changes in metamorphic rocks and whether; (ii) the efficiency of repeated diurnal freeze-thaw can be enhanced by its synergy with previous thermal cycling. By performing a two-phase

laboratory experiment (Figure 8.1c) of repeated thermal cycling followed by freeze-thaw cycles, the study aims to simulate consecutive weathering conditions typical for high-alpine rock slopes. By using low-porosity mica schist with preferred micro-scale foliation, the experiment also aimed to examine how the cleavage (or schistosity) orientation (relative to the exposed surface) can affect the response of metamorphic rocks to long-term sun- and frost-induced cycling.

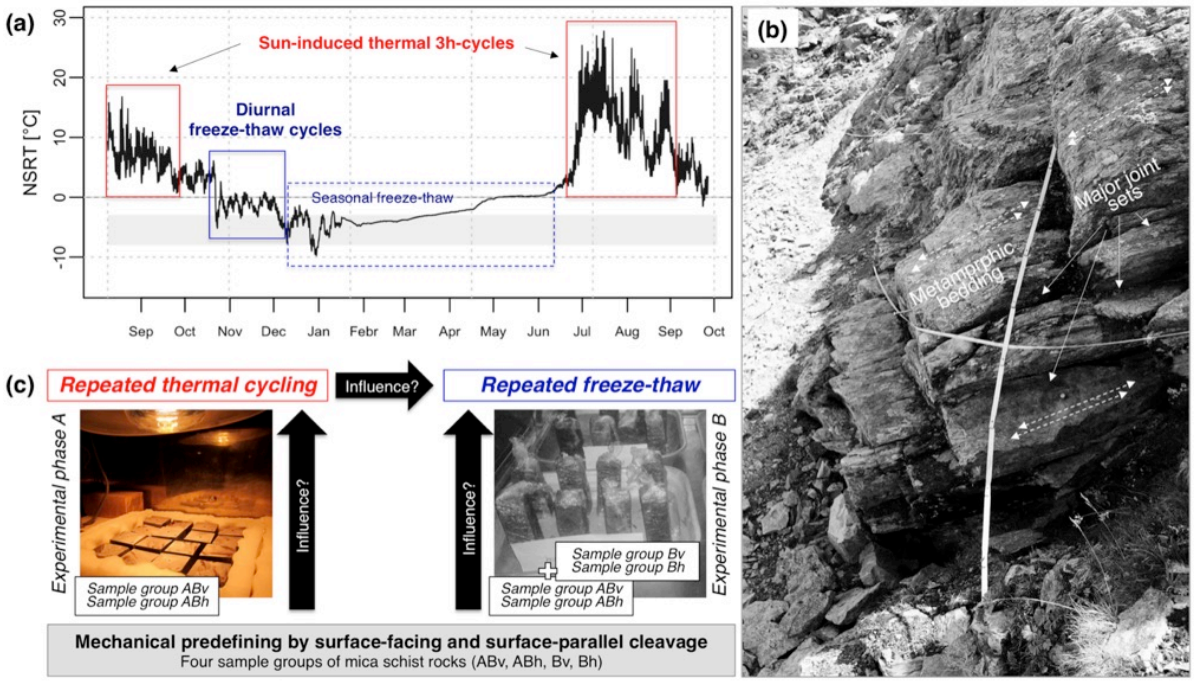

Figure 8.1: *a) Typical near-surface (10 cm) rock temperatures of north-exposed high-alpine rockwalls, recorded at b) metamorphic rock slope in the Swiss Alps (Hungerli Peak) with slope-facing discontinuities parallel to the metamorphic schistosity. c) Conceptual framework of this study addressing the synergistic and individual weathering effects of repeated thermal cycling and freeze-thaw on metamorphic rocks with pre-existing cleavage (and discontinuities) in slope-parallel or slope-facing direction.*

8.2 Experimental approach

8.2.1 Characterisation and preparation of rock samples

For the laboratory experiments, a strongly foliated and low-porosity (<1%) mica schist from the Turtmann Valley in the SW Swiss Alps has been used, where rockfalls from unstable metamorphic rock slopes are some of the most dominant geomorphic processes in the hanging valleys (Otto et al., 2009). While recent regional modelling (Messenzehl et al., 2016) and local-scale field studies (Messenzehl and Dikau, 2017) suggest freeze-thaw events are a key destabilising mechanism within the upper cm to meters of bedrock, Messenzehl et al. (in review) hypothesise a potential weathering efficacy of near-surface thermal cycling during summer.

Rock samples have been cut from intact and lichen-free bedrock of the north-exposed Hungerli Peak (at approx. 2700 m asl), which is composed of heavily folded and foliated Palaeozoic mica schist and paragneiss of the Penninic Siviez-Mischabel Nappe (Bearth, 1980). Similar low-porosity metamorphic alpine rocks, e.g. from Swiss or Japanese settings, have been also used in previous frost weathering experiments (e.g. Matsuoka, 1990; Draebing and Krautblatter, 2012).

Four boulder-sized field samples from the same rockwall were cut into 30 small specimens (9 cm x 3 cm x 3 cm). Only samples without visible cracks were selected. To account for the predisposition for breakdown by joints in natural rockwalls and, specifically, the role of joint orientation relative to the surface, one half of the sample set was cut with the blocks' longer side perpendicular to the planar schistosity, whereas the other half was cut parallel to it (Figure 8.2a).

Based on cross-polarized microscopic inspection of representative thin sections (FIgure 8.2b) the rock type can be characterised as a garnet-green schist facies typical for low pressure and low temperature regional metamorphosis. Green (i.e. chlorite) and white sheet silicates (phyllosilicates) as well as isotropic garnet and quartz account for 70-80% of the mineralogy with minor proportions of amphibole and haematite. The well-developed orientation and preferred alignment (cleavage) of the silicates (e.g. in a WS-direction in Figure 8.2c) create a distinct lepidoblastic (planar fabric) texture. Some minerals show rotational slip interrupting the general cleavage orientation (Figure 8.2b).

Analysis of micro-scale 3D surface roughness reveals that a foliation perpendicular to the surface (Figure 8.2c) causes a characteristic micro-scale surface roughness of linear 'valleys' (on smooth quartz) and linear 'peaks' (on e.g. mica crystals). In contrast, if bedding is horizontal (or parallel) to the rock surface (Figure 8.2d), no preferential roughness pattern is visible, but it is primarily dependent on the nano-scale roughness of the minerals. Particularly isotropic quartz has a smoothing effect, while micas generally produce rougher peaks, particularly if they are rotated.

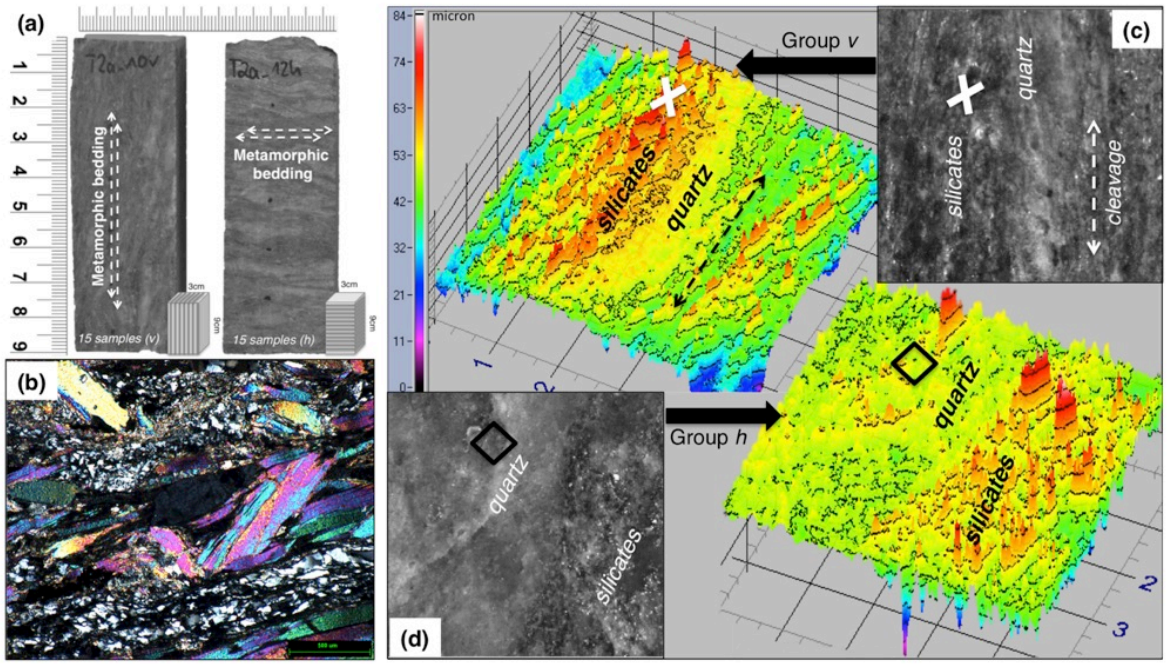

Figure 8.2: *a) Rock sample groups with vertical (v) and horizontal (h) orientation of metamorphic bedding (cleavage) relative to the top surface. b) Cross-polarized microscopy (40x magnification) of a representative thin section (Group h). Examples of 3D topography and corresponding visual images of surface roughness (in microns) from top surfaces of Group v (c) and Group h (d) using the Traceit ®.*

8.2.2 Rock weathering experiment

The laboratory weathering experiment was divided into two phases: Phase A consisted of 120 thermal 8h-cycles (summer condition) and Phase B consisted of 80 12h-cycles of freezing and thawing (winter condition). Thus, the experimental cycling was run for 40 + 40 days. For both phases, the total sample set was divided into four sample groups each comprising seven replicates with either horizontal (h) or vertical (v) cleavage, respectively (Figure 8.2a).

In Phase A, two groups (n = 7) with perpendicular (group ABv) and horizontal cleavage (group ABh), respectively, were exposed to repeated thermal cycling in an environmental cabinet (Sanyo-FE 300H/MP/R20). Samples were placed with their long side in an upright direction in a polystyrene box (with a 3 cm spacing between each block), so that the top surface was most affected by heating Figure 8.1c, Figure 8.3a). Beforehand, samples were oven-dried at 70 °C for 48h to reproduce low moisture content typical for high-alpine rockwalls during summer (Rode et al., 2016). Based on summer rock temperature data (i.e. July and August 2016) recorded at the Hungerli Peak (Messenzehl and Dikau, 2017), diurnal thermal cycles were simulated between 30 °C and 10 °C with a relative humidity of 70%. A total of 120 8h-cycles were run, with 2.5 hours of constant heating at 30°C and constant cooling at 10°C, respectively (Figure 8.3a). In order to reproduce specifically slow, low-magnitude stresses through thermal fatigue, the intermediate rate of temperature increase/ decrease was kept at 0.075 °C/min. Thus, this rate is well below the commonly-quoted minimum threshold of 2 °C/min required to induce thermal shocks (Richter and Simmons, 1974). During the heating phase, a 40 Watt infrared lamp positioned 35 cm from the samples was switched on for one hour in the middle of the heating period to simulate the effect of direct (conductive) heat fluxes via solar radiation (Warke and Smith 1998). Surrounding air circulation was programmed to simulate convective heat transfer (Viles et al., in review). Humidity and air temperature in the cabinet was monitored by hygrochrons (DS1923 Temperature/ Humidity Logger iButtons), and rock temperature was recorded at the centre (1.5 cm) of additional rock samples (Figure 8.b) using Tiny Tag probes (Coombes et al., 2017).

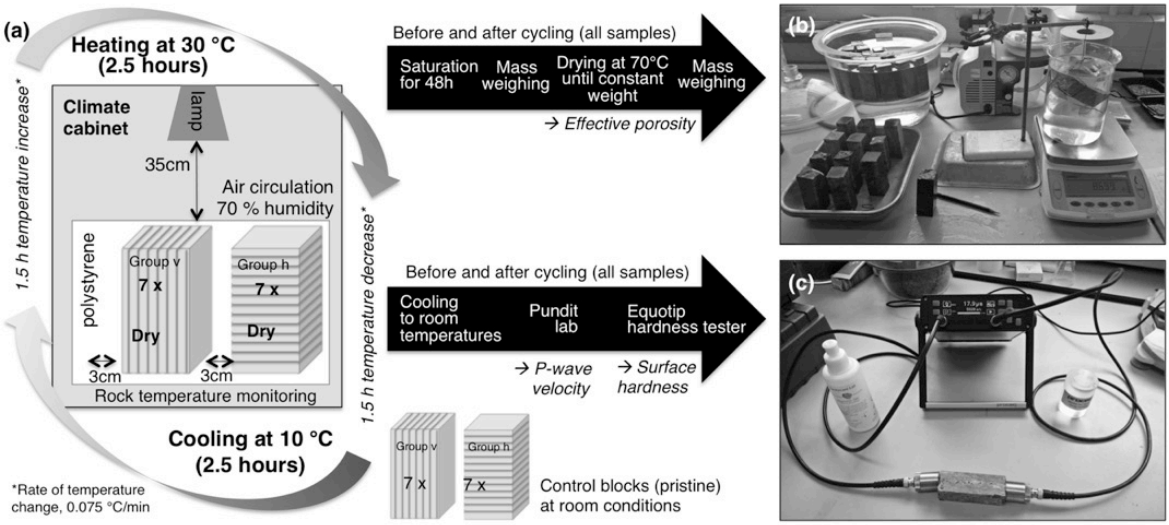

Figure 8.3: *a) Schematic illustration of the methodological approach of Phase A. Open porosity was determined before and after the experimental cycling (upper black arrow in (a) and picture of (b). P-wave velocities (c) and hardness were also assessed before and after the simulation (lower black arrow).*

In Phase B, the two pre-stressed sample groups (ABv, ABh) as well as additional two groups Bv and Bh of un-weathered blocks (each group: n=7) were exposed to intense freeze-thaw conditions. Before and after each measurement cycle (see below), all samples were saturated in water to 90-100% under vacuum conditions for 24 hours to reproduce typical winter near-surface rockwall moisture content favourable for ice growth (Sass, 2005a). Samples were then loosely sealed with plastic film to avoid drying and were placed (without contact) in an upright position on a metal tray. Based on winter rock temperature data from the Turtmann Valley (Messenzehl and Dikau, 2017) and following common cycling regimes used in previous frost weathering experiments (Matsuoka, 1990; Jia et al., 2015), samples were subjected to repeated 12-hours frost cycles between -10 °C and 25 °C. During freezing, temperature was kept constant at -10 °C for 5.5 hours. The chamber was then slowly warmed to 25 °C over 30 min and kept at this thawing temperature for an additional 5.5 hours (Figure 8.4a). Rock temperature monitoring during the frost experiment (Figure 8.4c) reveals that freezing and thawing according to the programmed air temperature penetrated into the centre of the rock samples, independently of the cleavage direction. Because of equipment malfunction, a short interruption of 6 hours was recorded at the 48th cycle.

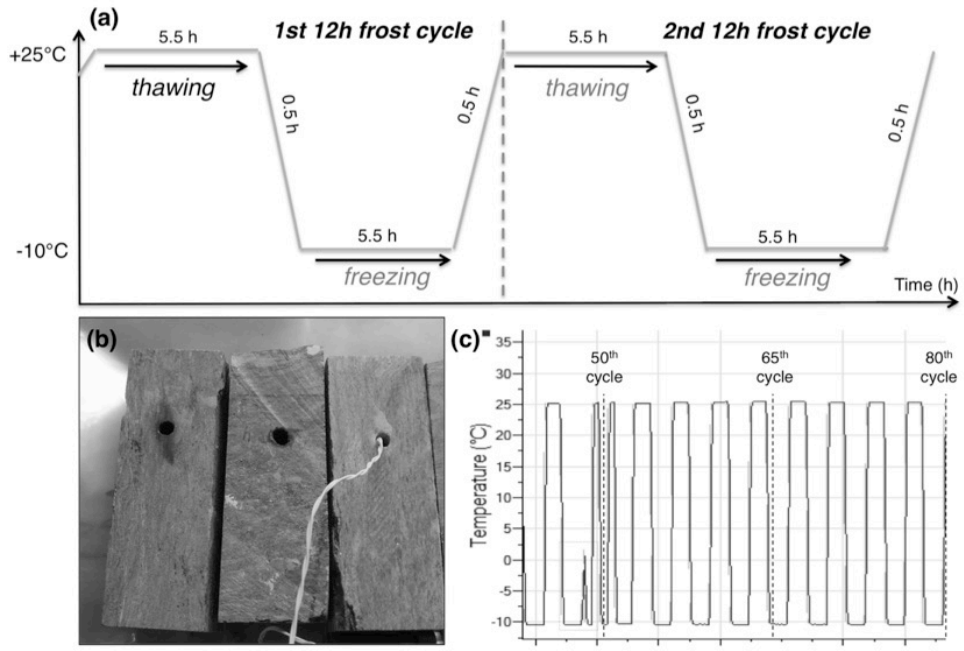

Figure 8.4: *a) Simulated temperature regime of Phase B. b) Rock temperatures recorded at 1.5 cm depth. c) Rock temperature profiles during 80 frost cycles.*

8.2.3 Monitoring of rock mechanical changes

To assess the individual and synergistic weathering effects of thermal cycling and freeze-thaw action, different indicative rock mechanical parameters were investigated before and after each experimental phase, as well as after the 50th and 65th freeze-thaw cycle. All measurements were conducted at room conditions (~ 22 °C) and with oven-dried (at 70 °C) rock samples to avoid influences of moisture and temperature. For measurements during Phase B, only four samples of each of the four pre-stressed and un-weathered groups were used, while the remaining samples were kept in the cabinet, exposed to uninterrupted frost cycling.

Open porosity

The open (or effective) porosity of all samples was quantified as a measure of all hydrologically linked open pores relative to the total rock volume or bulk volume (Draebing and Krautblatter, 2012). For that, samples were fully water saturated with deionized water under vacuum conditions for 24h in a desiccator (Figure 8.3b). Using an Oxford Research Plus balance (accuracy ±0.01), weights of saturated samples were measured under air condition and suspended in deionized water. Afterwards, samples were oven-dried at 70 °C until constant weight was reached (24h). Following Matsuoka (1990), open porosity (p) was calculated as:

$$p = \frac{W_s - W_d}{W_S - W_W} \quad (8.1)$$

where W_d is the oven-dried weight (at room temperature), W_S is the saturated weight after 24h of vacuum saturation and W_W is the saturated weight of the specimen submerged in water.

P-wave velocity

As a proxy for internal rock mechanical changes over time, (compressional) p-wave velocities were assessed using the Portable Ultrasonic Non-destructive Digital Indicating Tester (PUNDIT®). The pundit measures non-destructively the ultrasonic pulses travelling through a rock medium, which have been shown to correlate – under controlled laboratory conditions – with the compressive strength and the modulus of elasticity (Moses et al., 2014). As the transit time of p-waves is significantly affected by rock density and a range of elastic rock properties, and significantly decreases in air-filled pores and (micro-)cracks, the pundit has been widely used as a non-destructive method to identify invisible or subsurface changes resulting from weathering (Hall, 1988; Sobott, 2004; Warke et al., 2006). As shown in Figure 8.3c, direct transmission was measured using two transducers with a frequency of 54 kHz placed opposite each other on both 3 x 3 cm ends of the specimens. Thus, p-waves were assessed perpendicular to cleavage in group h and parallel to it in group v. The device was calibrated before each measurement. Only three repeat measurements were performed for each sample to calculate the mean p-wave velocity, as variations between different readings were consistent small (<10 m/s).

Surface hardness and microscopic analyses

To assess the mechanical weathering effects on the exposed rock surface, hardness change of top surfaces was measured using the Equotip impact device D as recommended by Viles et al. (2011). Similar to the Schmidt Hammer technique, the Equotip device is non-destructive and measures the electronic rebound value, but at a smaller impact energy (11 Nmm) and smaller impact area (Aoki and Matsukura, 2007). A total of 10 readings was taken across each top surface (randomly distributed within the 3 x 3 cm area and avoiding edge effects). The average hardness value of each sample is expressed in Leeb Hardness units (HL) representing the ratio of the rebound velocity to the impact velocity multiplied by 1000 (Viles et al., 2011). Thus, fully elastic rebound would result in a HL value of 1000 (max), while lower values indicate weaker rock surfaces.

In addition, thin sections of un-weathered (before phase A) and weathered rock surfaces (after Phase B) with both perpendicular and horizontal cleavage were prepared for visual inspection of breakdown. For microscopic analysis, a brightfield upright Olympus BX43 microscope at 40x magnification was used.

8.3 Results

8.3.1 Porosity change

Table 8.1 summarises the absolute values of the average open porosity (%) for all sample groups over phase A (after 120 thermal cycles, TC) and Phase B (after 50, 65 and 80 freeze-thaw cycles, FTC). Before the cabinet cycling (baseline conditions), mica schist samples are characterised by comparable, extremely low open porosity (0.45-0.65%). Despite the low porosity, Figure 8.5 displays statistically significant changes within each group relative to baseline conditions across the two experimental weathering phases. Dependent on cleavage orientation (v, h) and whether pre-weathering has been applied, different trajectories are visible.

Table 8.1: *Average values (and standard deviation) of open porosity (%) of all sample groups over the experimental phase A and B. TC = thermal cycles, FTC = freeze-thaw cycles).*

		Group Bh (pristine)	**Group Bv (pristine)**	**Group ABh (pre-stressed)**	**Group ABv (pre-stressed)**
	before	0.64 (±0.21)	0.46(±0.15)	0.48 (±0.12)	0.47 (±0.11)
Phase A	120 TC	-	-	0.51 (±0.15)	0.55 (±0.20)
Phase B	50 FTC	0.83 (±0.04)	0.54 (±0.19)	0.64 (±0.14)	0.62 (±0.05)
	65 FTC	0.71 (±0.02)	0.58 (±0.11)	0.63 (±0.13)	0.71 (±0.05)
	80 FTC	0.69 (±0.21)	0.55 (±0.13)	0.60 (±0.11)	0.69 (±0.25)

During phase A, the two sample groups exposed to thermal cycling ('pre-stressed' groups ABh and ABv in Table 8.1) increased in open porosity, with the greatest increase of 16% for rocks with vertical cleavage (group ABv in Figure 8.5). After further exposure to 50 freeze-thaw cycles (FTC), both pre-weathered and pristine sample groups (which were not exposed to thermal cycling) showed significant and consistent increases in porosity. The greatest increases were 31% and 28% (relative to the baseline) corresponding to the two groups with vertical cleavage (Group ABv). This increasing trend prevailed until the 65th freeze-thaw cycle in both v groups and was most expressed (+ 50% relative to baseline) in pre-stressed group ABv (solid blue line in Figure 8.5) while both h groups showed reductions in porosity between 50 and 65 cycles. Thus, the direction of change was consistent with bedding, and independent of pre-stressing. After the 80th FTC, open porosity slightly decreased by about 5% in three of the sample groups, with exception of group Bh also decreased very slightly (Figure 8.5). Therefore, at the end of Phase B, open porosity of all samples was significantly increased

relative to baseline conditions, with comparatively higher increases in rocks with vertical cleavage orientation, and that had also been exposed to the thermal cycling.

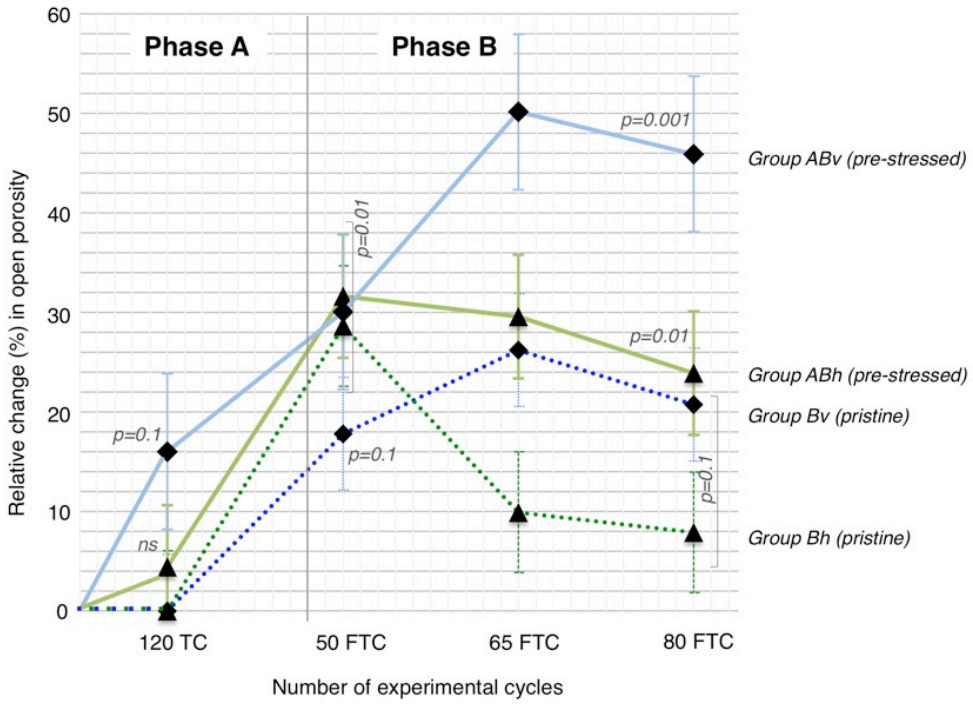

Figure 8.5: *Relative change (%) in open porosity (average ± SD) relative to baseline conditions (see Table 1) after 120 thermal cycles (TC) of Phase A and over Phase B after 50, 65 and 80 freeze-thaw cycles (FTC). Error bars show standard deviation. P-values of Student's t-test are shown to represent the significance of the relative change within each sample group across each weathering stage (ns: not significant).*

8.3.2 P-wave velocities

Figure 8.6 illustrates the interquartile ranges (IQR) of p-wave velocities (m/s) measured for all samples within each group across the experimental weathering phases. In general, independent of weathering history, data reflect the influence of cleavage orientation, with higher p-wave velocities measured parallel to the cleavage, for both v groups (~ 4500-5800 m/s) (Figure 8.6a-b), and lower velocities measured perpendicular to the cleavage, for both h groups (~ 1200-2700m/s) (Figure 8.6c-d).

Relative changes (%) with respect to baseline conditions are displayed in Figure 8.7. After Phase A (thermal cycling), a significant trend of decreasing p-wave velocity is evident for samples cut with horizontal cleavage (Figure 8.d). In contrast, samples with vertical cleavage (group ABv) showed no change (Figure 8.6b), nor did the pristine blocks (Bv, Bh), which were not exposed to Phase A (Figure 8.6a, c). After the 50th FTC, p-wave velocities of samples with vertical cleavage, both pre-stressed and pristine (ABv, Bv in Figure 8.6a-b), decreased by about 4.5% (solid and dotted blue lines in Figure 8.7). A much more pronounced decrease of 28-40% was evident for samples with horizontal cleavage after the same period (Figure 8.6c-d), even more so for the pre-stressed group (solid green line in Figure 8.7).

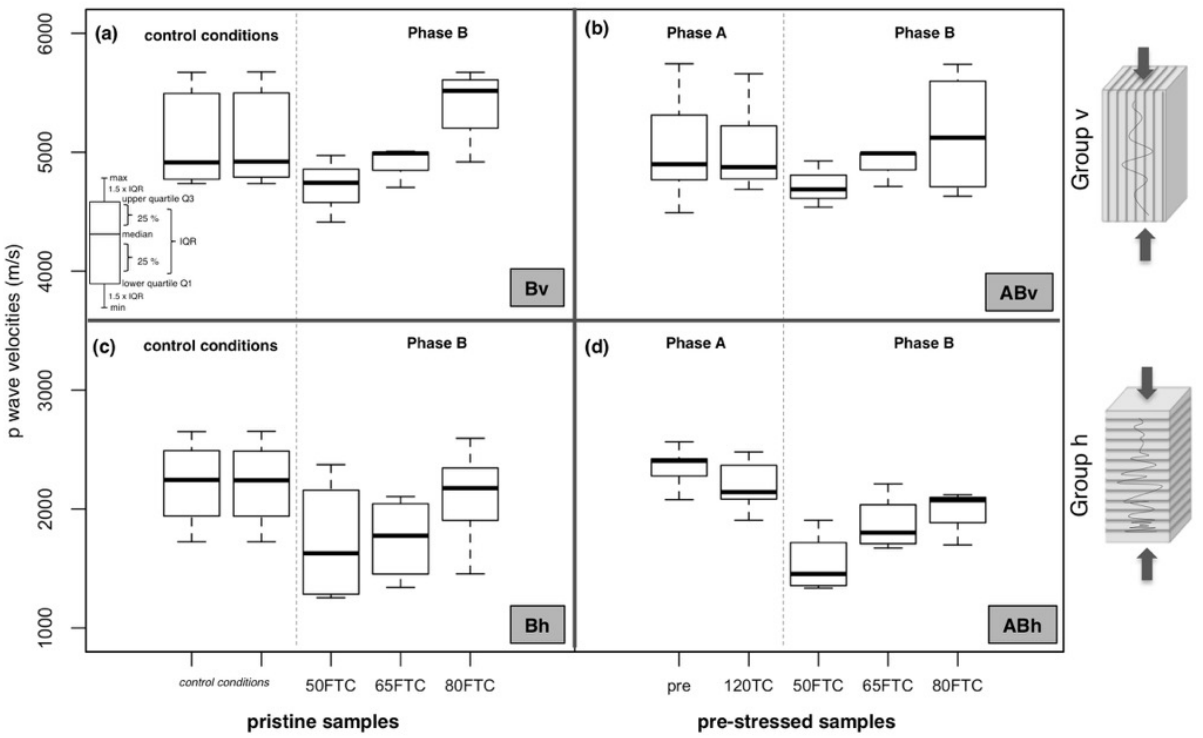

Figure 8.6: *P-wave velocities (m/s) measured for all seven samples within each group across 120 thermal cycles (TC) and 50, 65 and 80 freeze-thaw cycles (FTC). Boxplots show the interquartile ranges (IQR) with median values, minimum and maximum of each measured data set per sample group.*

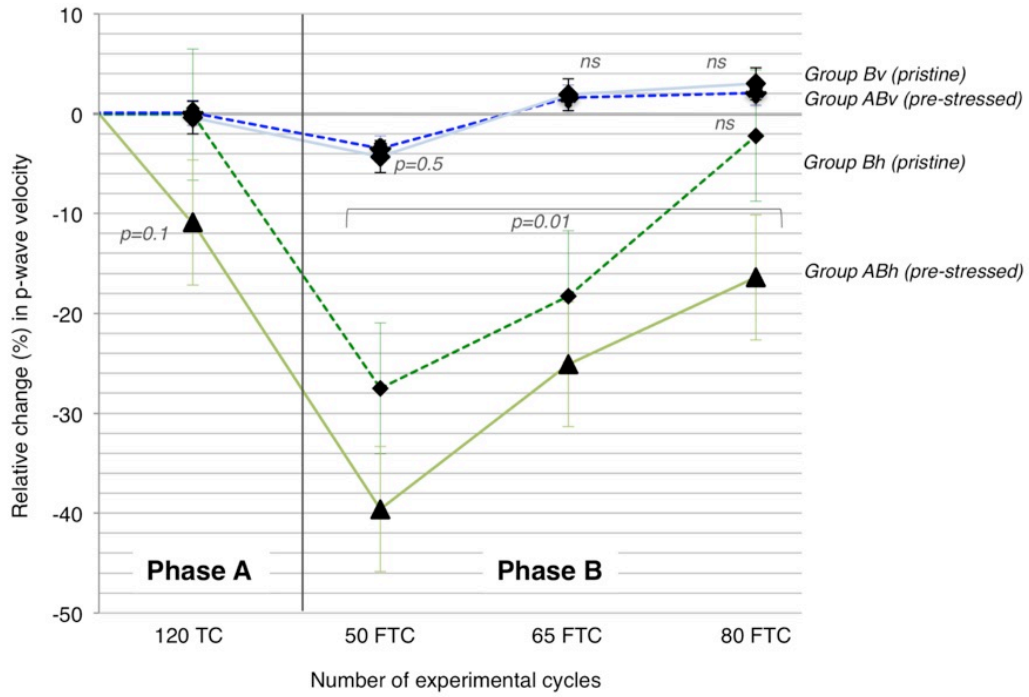

Figure 8.7: *Relative change (%) in p-wave velocity (median value) relative to baseline conditions across Phase A after 120 thermal cycles (TC) and Phase B after 50, 65 and 80 freeze-thaw cycles (FTC). Error bars show standard deviation. P-values of Student's t-test are shown to represent the significance of the relative change within each sample group across each weathering stage (ns: not significant).*

After the 65th FTC, p-wave velocities of all samples had increased, irrespective of cleavage orientation, and this trend continued to the end of the experiment to the 85th FTC (Figure 8.6a-d). While p-wave velocities of both groups with vertical cleavage finished close to their baseline conditions, those with horizontal cleavage showed a total relative change of -5% (Bv) and -16% (ABv) at the end of Phase B (Figure 8.7).

8.3.3 Surface hardness

The change in surface hardness of the four sample groups across the two-phase weathering experiment is shown in Figure 8.8. An overall trend is evident dependent on the cleavage direction; rocks with vertical/out-facing cleavage (relative to the Equotip reading, as shown in Figure 8.8a-b) had relatively hard surfaces with a relatively small IQR (430-700 HL) across all the weathering phases. In comparison, rocks with horizontal foliation (Figure 8.8c-d) were generally weaker and more heterogeneous, with values ranging from 230 to 670 HL.

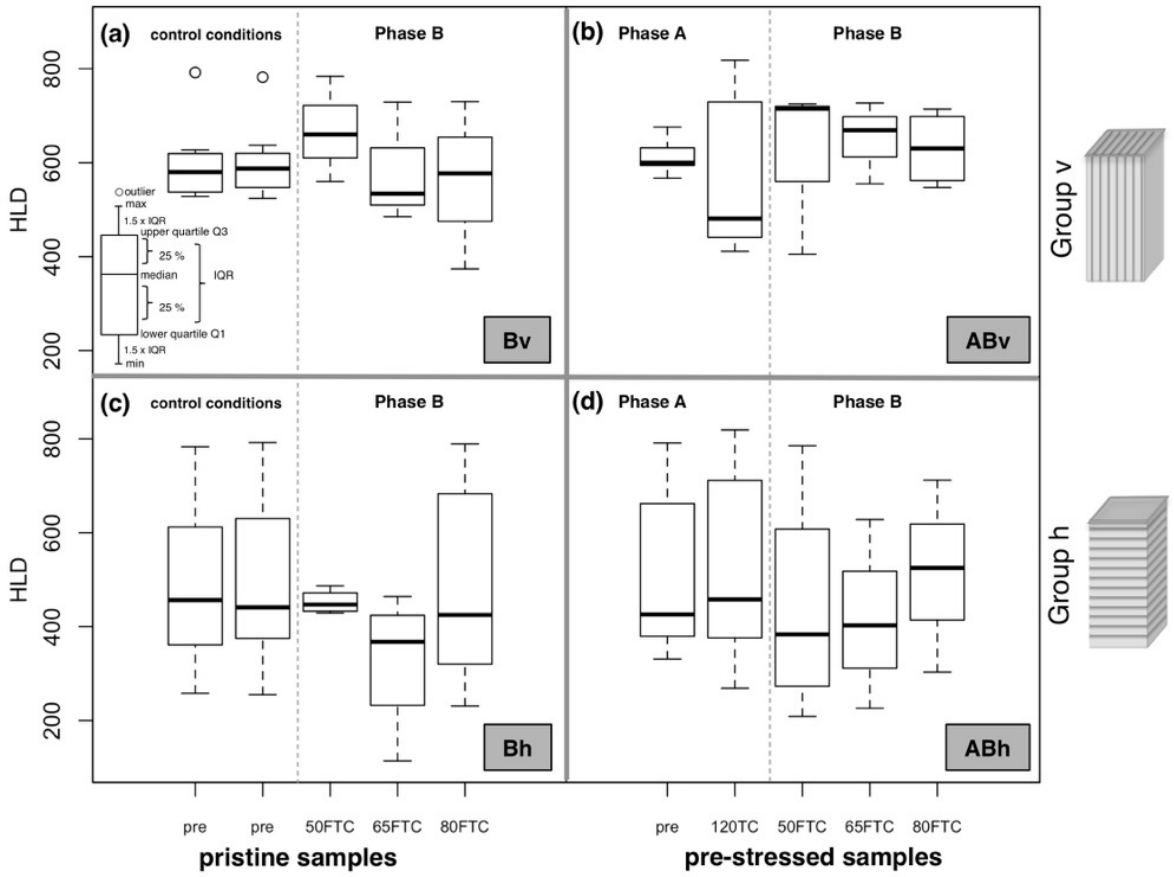

Figure 8.8: Surface hardness (expressed as Leeb Hardness 'HL, 'D' denotes the Equotip device, n = 10) over phases A and B.

For the two groups exposed to Phase A (thermal cycling), changes were evident for group ABv after 120 TC, which became significantly weaker and more heterogeneous (median and IQR in Figure 8.8b). Contrarily, hardness of group ABh (Figure 8.8d) showed no significant change, similar to the two 'pristine' groups Av and Bv that were not exposed to thermal cycling (Figure 8.8a, c). During Phase B (freeze-thaw cycling), diverging behaviour was evident between each sample group. Both pristine and pre-weathered rocks with vertical foliation (Figure 8.8a-b) became, first, significantly harder after 50 frost cycles, but progressively re-approached baseline conditions towards the end of Phase B. Independent of pre-weathering, the IQR of hardness values increased in comparison to the start of Phase A. In both h groups, hardness remained relatively constant across Phase B (Figure 8.8c,d). In comparison, the IQR of pristine blocks slightly increased towards the end, and the surface hardness of pre-weathered blocks became slightly higer and more homogenous (indicated by the smaller IQR in Figure 8.8d).

8.4 Interpretation of findings and discussion of methodology

8.4.1 Evaluation of methodology

Laboratory simulations with well-controlled conditions cannot reproduce the complex thermal regimes occurring in the field. Noted limitations in this study are the short-duration weathering simulation of compressed and extreme temperature cycles, the small sample dimensions as well as the limited frequency of intermediate monitoring measurements i.e. across Phase A and the limited set of applied measurements without additional information of deformational stresses.

Nevertheless, the experiment phases A and B were designed to simulate key characteristics of natural rock slope weathering and to approximate, as close as possible, thermal cycling and diurnal ice crystallisation in the bedrock near-surface (<10 cm). First, by using low-porosity mica schist samples taken from the surface of de-glaciated and rockfall-affected rock slopes in the Swiss Alps, rock properties contain a natural history/ legacy of several (de-)glaciation cycles, permafrost and long-term weathering. To exclude the possible effect of weathering rinds, centimetre-sized specimens were cut from only interior parts of the original boulder-sized field samples. Whilst the relatively small dimensions (9 x 3 x 3 cm, Figure 8.9) permit to investigate nano- to micro-scale weathering effects, the use of larger (i.e. decimetre-sized) specimens is recommended for future experiments as they allow a better simulation of the large thermal gradient in the near-surface of intact rock slopes.

A relatively realistic thermal cycling regime was designed based on field rock temperature records from 10 cm deep boreholes in rock slopes, where samples were taken from. Nevertheless it must be stressed that both experiment phases cycled according extreme minimum and maximum temperatures recorded during summer and winter. Thus, an idealised weathering regime has been designed to reflect the full range of temperature conditions that have been recorded in the field.

During the cabinet cycling, rock temperature monitoring at 1.5 cm inside rock specimens indicates that both positive temperature fluctuations (Phase A) as well as freezing (Phase B) penetrated into the rock centre

in good accordance to the programmed air regime (Figure 8.4b, c). The direct heating in Phase A by the 40Watt lamp (as recommended by Warke and Smith, 1998) therefore produced field-typical rock temperatures. Likewise, the plastic foil sealing in Phase B (designed to limiting drying of the rock) did not modify the thermal signal. Despite the compression of the real-time diurnal temperate cycles, the recorded temperature rates exclude the potential influence of sudden thermal shocks (Hall and Thorn, 2014) and suggest effective ice crystallisation that is fast enough to avoid ice extrusion inside the rocks (Jia et al., 2015). As no evidence of extruding ice was detected during Phase B, freezing is assumed to have taken place primarily within internal rock pores. Furthermore, by using only dry samples during Phase A (Figure 8.3), potential effects caused e.g. by hydration or salt crystallisation were minimized. Similarly, those influences may have been secondary in Phase B, given the small clay content and low solubility of the schists (Krautblatter, 2009). Therefore, it can be assumed that the observed mechanical changes derived from the individual and synergistic action of repeated thermal loading (thermal fatigue) and 9% volumetric expansion of crystallising ice.

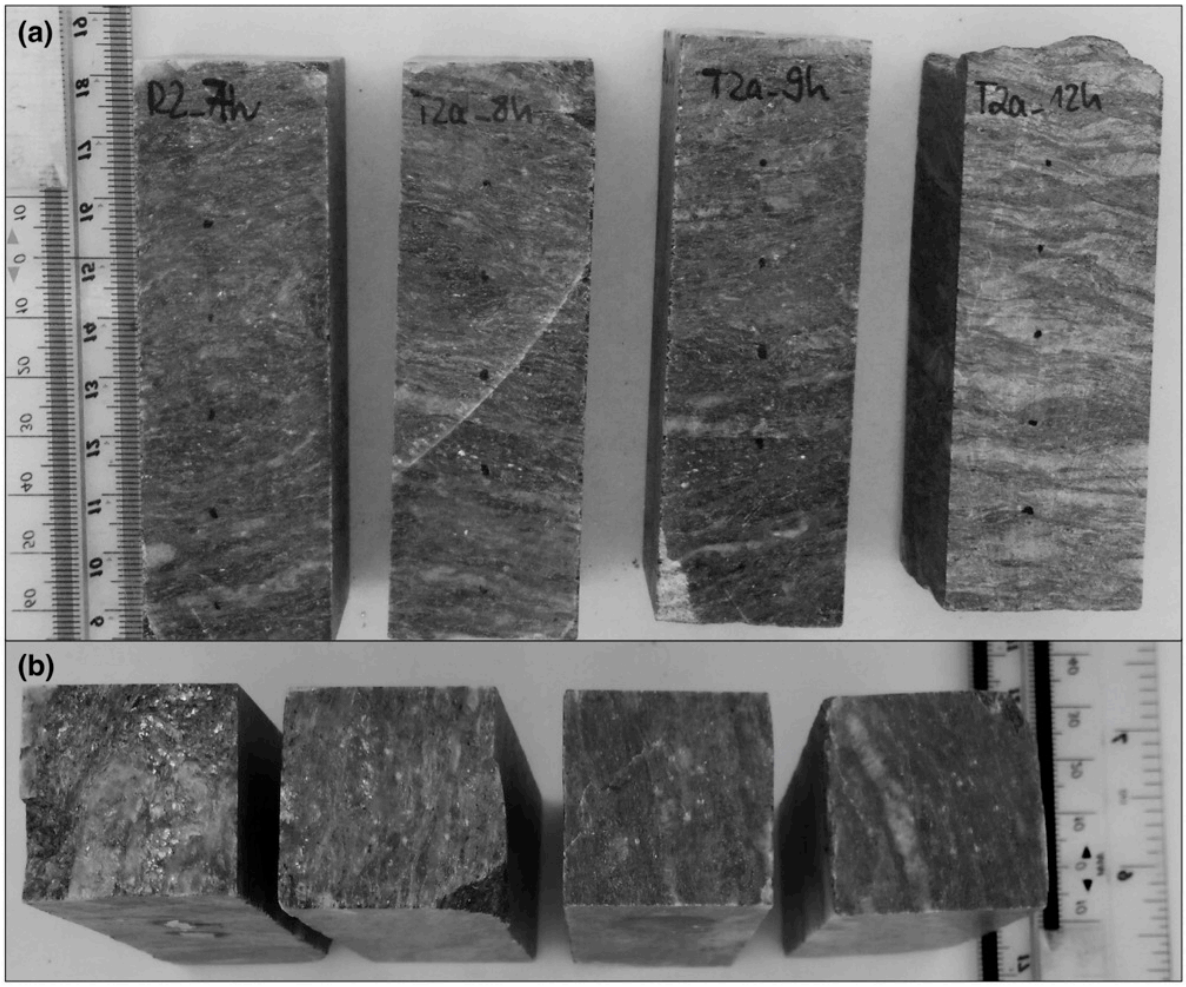

Figure 8.9: *Photographs of rock samples from (a) group h with distinct surface-parallel (horizontal) cleavage and (b) from top surfaces of group v with distinct surface-facing (vertical) cleavage perpendicular to the surface. In all samples, a variable composition of quartz and silicates is visible.*

However, given the heterogeneous mineralogical composition of the mica schist (Figure 8.2b, Figure 8.9), all micro-scale findings must be interpreted with caution. Although care was taken to select relatively comparable specimens (from same field boulders), all samples differed in their (internal) mineral components. Accordingly, the thermal response of each sample depends on the thermal expansion coefficients of its mineralogical components. Particularly in rocks with high quartz content, additional complexity occurs due to thermal anisotropy in different crystallographic directions (Luque et al., 2011). Moreover, where quartz dominates the exposed rock surface, as e.g. as is visible in Figure 8.9b, the heat transmission to depth and the steepness of the thermal gradient can be overestimated (Hall et al., 2008; Walsh and Lomov, 2013).

Neither after Phase A, nor after Phase B had ultimate rock breakdown or local damage in form of visible cracking been detected, despite the full saturation during the frost weathering experiment. Previous laboratory studies demonstrated that the likelihood of rock damage through repeated ice crystallisation increases with increasing saturation degree (Matsuoka, 1990, Prick, 1997). Although dependent on the amount and form of micro-pores, expansion of ice and effective associated stresses typically develop in pore spaces with more 91% water saturation (Jia et al., 2015). Although the sample preparation for Phase B may contradict the variable moisture conditions at the near-surface of natural rock slopes as an open system, experiments of Jia et al. (2015) on similarly small sandstone samples indicate that the degree of saturation does not change the timing and qualitative pattern of deformation, but only the quantitative degree. Therefore, the lack of significant rock failure despite full saturation and extreme temperature cycles emphasises the general high resistance of low-porosity mica schists to relatively repeated thermal- and frost-induced fatigue. For future laboratory experiments, a longer simulation period, ideally with multiple repetitions of consecutive thermal and frost cycling, is needed to test the sensitivity to long-term stress accumulation. Ideally, those experiments should use rock samples of larger dimensions to reproduce more realistic (deeper) temperature gradients.

Nevertheless, the methodology allows interpretation of micro-scale mechanical changes in the context of consecutive near-surface rock weathering typical for high-alpine rock slopes. It is assumed that the accelerated thermal cycling during Phase A (120 x 8h cycles) is representative of a real-time 4-month summer period of diurnal warming and cooling (Figure 8.1a). Likewise, the 80 half-daily frost cycles in Phase B are likely to approach a winter period of diurnal freeze-thaw (Figure 8.1a). Therefore, acknowledging all methodological and systemic restrictions and limitations, the results of this study provides valuable insights into the individual and synergistic micro-scale (<10 cm) weathering effects of sun-induced thermal cycling and diurnal freeze-thaw in low-porosity metamorphic rocks.

8.4.2 Can repeated thermal cycling affect mechanical properties of low porosity, foliated mica schist?

Sun-induced temperature changes can lead to cyclic loads within bedrock with creates sub-critical stresses often far below the actual strength of the rock mass (Yatsu, 1988). Where those internal stresses are constantly repeated and exceed, through accumulation, the capacity of rock to adjust, mechanical properties progressively change and irreversible damage occurs through thermal fatigue (Wang and Liaw, 2008). While the importance

of this nano- or micro-scale rock weathering process is long accepted and studied in detail in the context of building stone (Sobott, 2004; Luque et al., 2011; Akentuna et al., 2016) and hot deserts on Earth or Mars (Eppes et al., 2015; Molaro et al., 2015; Viles et al., in review), comparatively little emphasis is given to cold environments and even less to high-alpine rock slopes. However, most knowledge derives from exfoliated granite, e.g. in the form of boulder fields in Antarctica (Hall, 1999; Hall and André, 2001; Hall et al., 2008; Viles et al., 2010) or, most recently, steep rock slopes in the Yosemite National Park (Collins and Stock, 2016). To address this knowledge gap and to return to the original question posed in the introduction, Phase A of this study explored whether repeated thermal cycling alone can be sufficient to cause mechanical changes in low-porosity, foliated metamorphic rocks.

The observed changes in open porosity after Phase A (Table 8.1) demonstrate noticeable differences between rocks exposed to thermal cycling and those, which were kept under control, constant conditions. While the control group showed (as expected) no changes, 120 thermal cycles led to a significant increase in open porosity, particularly where the exposed surface had schistosity perpendicular to the external heat source (group v) (Figure 8.5b). The gain in effective porosity is interpreted as a nano-scale, cumulative effect of the differential crystal expansion and contraction in response to the simulated heating and cooling. When temperature rises, particularly quartz crystals of the mica schists show a distinct thermal anisotropy and directional dependence in their thermal expansion: whilst one axis expands, the other axis typically contracts (Janio de Castro Lima and Paraguassú, 2004; Weiss et al., 2004). Such anisotropic thermal expansion of quartz relative to the deformation of, for example, surrounding silicates, may have caused internal separation of crystals from their borders (Siegesmund et al., 2008; Luque et al., 2011) and increased pre-existing pores. However, it is important to state that the progressive crystal separation may not have necessarily resulted in more pores. Instead, it is rather the degree of inter-pore connectivity with the surface that is changed, likely due to the enlargement of pre-existing pores (Weiss et al., 2004).

The cleavage-dependent change in open porosity in Figure 8.5 suggests furthermore that the thermally induced enlargement and coalescence of pores operates along the pre-existing cleavage. Such preferential nano-scale structural damage is comparable to the propagation of pre-existing micro-cracks along bedding planes of igneous rocks (Eppes et al., 2015; Eppes and Keanini, 2017). These results therefore reveal that out-facing cleavage generally favours enhanced pore connectivity with the exposed surface compared to horizontal bedding. In latter conditions, structural modifications due to thermal fatigue may remain 'hidden' in the near sub-surface parallel to the cleavage.

P-wave velocity measurements also show significant changes for specific samples exposed to 120 thermal cycles (Figure 8.6b,d) compared to control blocks, which remained constant (Figure 8.6a,c). The 10% decrease found for group h after Phase A indicates a higher amount of air-filled voids (e.g. in form of pores and/or micro-cracks) in the sub-surface compared to their baseline conditions. Similar findings have been reported in previous of both frost and thermal weathering (Spencer and Nur, 1976; Hall, 1988; Yavuz et al., 2006; Draebing and Krautblatter, 2012; Jia et al., 2015). In most of these studies, p-wave velocities were found to correlate with a loss of elastic rock strength as a result of thermal, often cumulative stress accumulation. It is therefore assumed that the repeated heating and cooling led to efficient tensile stresses, which were sufficient

to cause micro-scale structural dilatation (McFadden et al., 2005). However, Figure 8.6d suggests that mica schists with horizontal bedding are, in particular, most sensitive to those sub-surface rock changes.

Interestingly, p-wave velocities of sample group v did not significantly change after exposure to 120 thermal cycles, despite this group showing the greatest increase in open porosity (Figure. 8.5). Although this seems contradictory, previous studies emphasised that (open) porosity is not the only determining control on p-wave velocities, particularly in metamorphic rocks (Matsuoka, 1990; Draebing and Krautblatter, 2012). Further important influences are, for example, the individual pore form and the direction of interlinked pores or (micro-)cracks relative to the p-wave travel path. Therefore, the opposite trends in Figure 8.5 and 8.6 demonstrate three key points: (a) an open porosity increase must not automatically be detectable in the ultrasonic travel time, particularly where p-waves follow parallel to cleavage and likely parallel to newly developed inter-linked pores. As a consequence, (b) a better inter-pore connectivity (such as in group v after thermal cycling) is a micro- or nano-scale phenomenon and is spatially restricted to the outer few mm of bedrock. And in turn, (c) thermally induced pores and micro-cracks, which develop 'hidden' in the subsurface along surface-parallel cleavages (as was likely in group h), do not automatically affect the open porosity. Rather, they can significantly decrease the internal structural competence, which is detectable by p-wave velocity changes.

Using rock hardness as a proxy for the surface weathering degree, Figure 8.8 evidences that 120 thermal cycles also modified the exposed rock surface (Figure 8.8). In comparison to control blocks, the surfaces of samples exposed to weathering Phase A became more heterogeneous with respect to hardness (Figure 8.8b,d) and, in addition, distinctly weaker where cleavage was outfacing (Figure 8.8b). This cleavage-dependent weakening of group ABv fits well with the measured increase in open porosity (ABv in Figure 8.5) demonstrating that thermal cycling caused pore-scale surface deterioration and weakening along crystal (or grain) boundaries (Mol and Viles, 2012). Aoki and Matsukura (2008) showed that Equotip hardness declines often correlate with decreasing elasticity and compressive strength at the surface. The results therefore imply that rocks with out-facing schistocity and distinct micro-scale surface roughness (Figure 8.2c) are particularly sensitive to thermal modification of surface hardness compared to horizontally bedded and 'smoother' rock surfaces.

Whether micro-cracks have developed in response to the simulated cycling loading is unclear. Thin sections of the top rock surfaces (Figure 8.10) reveal no clear evidences for new, thermally induced micro-cracks in pre-weathered rocks. Although the crystal orientation parallel to the cleavage (i.e. where schistosity is out-facing as in Figure 8.10a) provides favourable pre-existing weakness zones for sub-critical thermal fatigue (McFadden et al., 2005), the p-wave and porosity measurements suggest that structural damage of mica schists mainly occur at a pore-scale in form of enlarging and coalescing pre-existing pores

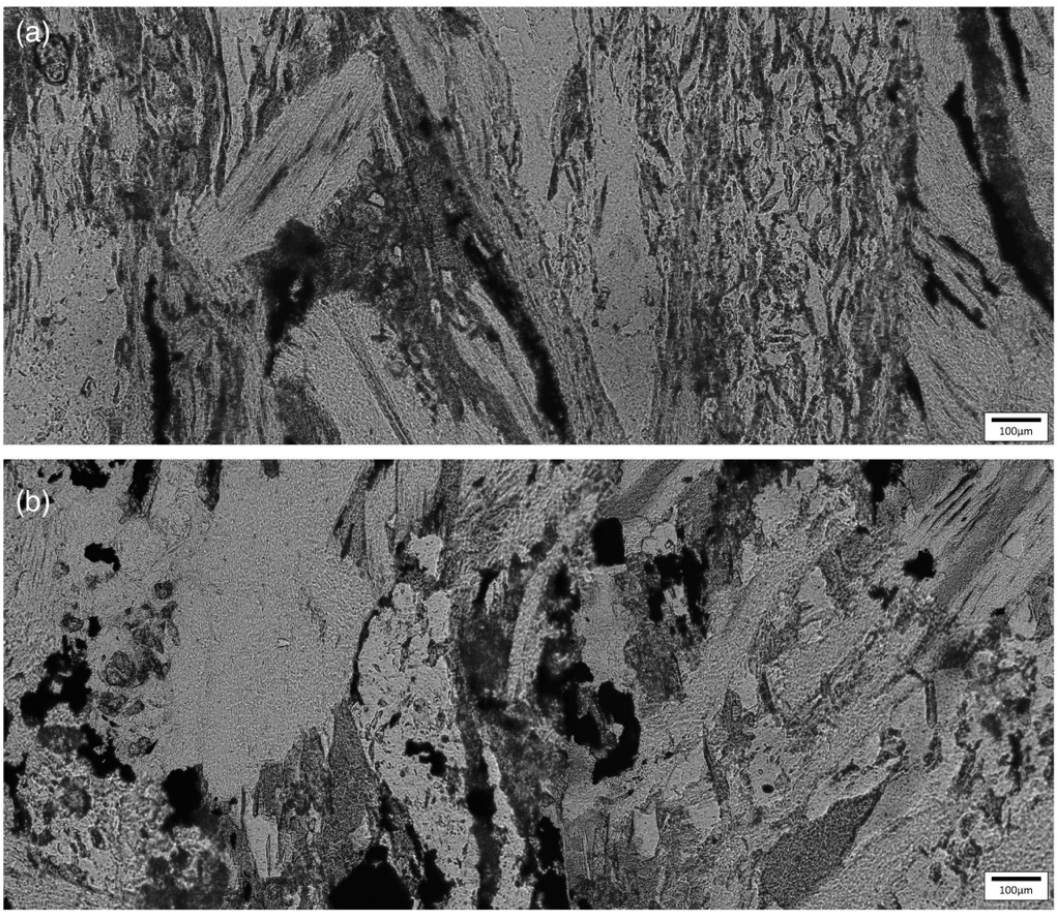

Figure 8.10: *Thin sections (10 × magnification) of pre-weathered (120 thermal cycles) and frost-exposed (80 frost cycles) rock samples at the end of the experiment. Photographs taken from exposed rock surfaces of (a) group v with surface-facing cleavage perpendicular to the surface and (b) group h with surface-parallel (horizontal) cleavage.*

8.4.3 Does repeated diurnal freeze-thaw action become (more) efficient due to its synergy with thermal pre-stressing?

The significance of diurnal freeze-thaw cycles and the role of volumetric ice expansion as a potential cause for rock weathering on high-alpine rock slopes is highly-debated amongst researchers and often critically rejected. Although the 9% volume expansion during water-to-ice phase change is not a matter of doubt, the theoretically assumed maximum pressure of 207 MPa required to cause tensile rock deformation is rarely reached under natural conditions. As well as variable moisture content in the first 10 cm of bedrock (Rohde et al., 2016), the permeability of natural rock slopes is discussed as clear evidence that seasonal and the slow segregation of ice is more realistic than diurnal ice crystallisation (Walder and Hallet, 1985; Hallet, 2006; Murton et al., 2016). However, although each individual event of volumetric expansion is subcritical, the recent laboratory experiment by Jia et al. (2015) demonstrates that a high frequency of frost events can systematically cause rock fatigue due to the long-term damage accumulation. While these results of Jia et al. (2015) are based on high-porosity sandstone, other laboratory studies give reason to assume that volumetric ice expansion is inefficient, by contrast, in low-porosity rocks (Lautridou and Ozouf, 1982; Matsuoka, 1990). Therefore the question arises whether the weathering efficiency of repeated diurnal frost can be enhanced in low-porosity metamorphic

rocks by previous near-surface rock damage caused by long-term thermal cycling. To address this, a similar temperature regime as used by Jia et al. (2015) was been applied in the freeze-thaw experimental Phase B.

The surface hardness measurements across Phase B (Figure 8.8) revealed no clear trend that could be explained by previous thermal cycling, nor by pre-existing cleavage. Although top surfaces of the pre-weathered group v were comparatively weakened after Phase A (Figure 8.8b), their median values re-approached baseline conditions at the end of Phase B, similar to the samples without pre-stressing. However, almost all frost-exposed samples became progressively more heterogeneous in their surface hardness and elasticity as indicated by their wider hardness IQR at the end of Phase B (Figure 8.8). Following Nicholson (2008), it is likely that repeated ice crystallisation in near-surface pores is less efficient where quartz minerals dominate, whereas mica and amphibole may have favoured efficient rock weakening, not least due to their higher micro-scale roughness (Figure 8.2c-d). These results suggest that frequent volumetric ice expansion can generally modify structural surface properties of rocks and can efficiently erase pore-scale surface signatures of previous weathering history, but this effect is strongly controlled by the pre-existing mineral composition.

Likewise, open porosity of all samples significantly increased by 10-50% following frost exposure (Figure 8.5). While Jia et al. (2015) found an increase of more than 100% in sandstone samples after only 17 cycles, experimental Phase B reveals that a longer repetition of more than 50 diurnal freeze-thaw events is necessary to cause cumulative rock fatigue for this lithology, but that change is possible even for low-porosity mica schists. This assumption is also supported by the detected trend in Figure 8.6, showing a p-wave increase of up to 40% until the 50th frost cycle in all samples exposed to experimental weathering.

However, in comparison to rocks without pre-stressing, the data provide evidence that the previous exposure to 120 thermal cycles increased the sensitivity of the rock near-surface zone to subsequent frost action. For example, the greater increases in open porosity of both pre-weathered sample groups suggest that their better inter-pore connectivity immediately after Phase A (i.e. group ABv in Figure 8.5) provided more pathways for water penetration (during thawing periods) and more confined space for ice crystallisation (during freezing) (Davidson and Nye, 1985; Nicholson, 2001; Sass, 2005a). A similar rock response is reflected by the p-wave velocity evolution in Figure 8.7, where the greatest changes are linked to those samples that reacted most to pre-stressing in Phase A (group h in Figure 8.6d). Interestingly, whilst the large open porosity increase of the pre-weathered group v after Phase A was not mirrored by change in p-wave velocity, it was associated with a sudden, although small (4%), decline in p-waves after the 50th cycle (Figure 8.7). Although a general correlation with open porosity is difficult to establish (Draebing and Krautblatter, 2012), lower p-wave velocities could result from newly connected, air-filled pores that reached a critical size and rock depth, favoured by the vertical cleavage (Hall, 1988); or, untypical for thermal fatigue (Hall and Thorn, 2014), developed independently from the pre-existing cleavage in a horizontal direction, so that they become detectable in the ultrasonic measurements.

Additionally, both p-wave velocities and open porosity reflect a cleavage-dependent rock response that overlays, in parts, the pre-weathering pattern (as in Figure 8.7). In both measurements, sample groups with surface-parallel schistosity recorded the steepest rates of change until the 50th frost cycle. Similar observations were made by Matsuoka (1990), who identified intense p-wave changes particularly for rocks with initially low

values (similar to group h in Figure 8.6a, c). Therefore, also in good agreement to Draebing and Krautblatter (2012), the findings of Phase B emphasise that rocks with schistosity perpendicular to freezing and thawing are generally most sensitive to freeze-thaw; although the propensity for internal damage is increased for pre-weathered (thermally fatigued) rocks.

Interestingly, after the 50th frost cycle (or at the latest after the 65th), initial increases in open porosity (Figure 8.5) and decreases in p-wave velocities (Figure 8.7) revert to relatively constant values (within error range) for the remainder of the simulation. As the cleavage-dependent trend is still visible, the potential influence of technical measurement errors is excluded. Instead, similar patterns have been reported in previous frost weathering experiments (Nicholson, 2001; Jia et al., 2015). While Nicholson (2001) proposes nano-scale compaction and pore collapse as a plausible cause for decreasing pore-inter-linkage after repeated frost action, it is also likely that after a certain cycling threshold (e.g. after 50 cycles based on Figure 8.5) a negative feedback occurred. Given the deformation measurements by Jia et al. (2015), for example, it must be assumed that increasing pore connectivity due to frost action led to a decreasing damage efficiency as pores became too large to avoid ice extrusion and increased instead the overall rock elasticity.

Therefore, with respect to the second research question posed at the beginning, the two-stage pattern found across Phase B of the experiment highlights that: (i) repeated sub-critical ice crystallisation can cause pore-scale structural damage at the surface, and in the upper sub-surface, even in low-porosity mica schists, and (ii) previous stresses and structural changes induced by thermal cycling (Phase A) enhanced the rock response to subsequent frost action. Both of these effects were strongly contingent upon the orientation of the cleavage relative to exposed rock surface.

8.5 Summary and outlook

In this study, a two-phase weathering experiment using low-porosity, strongly foliated mica schist was used to investigate the individual and synergistic rock weathering effects of repeated thermal cycling (Phase A) and high-frequency diurnal ice crystallisation (Phase B). Each of the experimental phases addresses a major research question prevailing on the efficacy of near-surface, low-magnitude weathering events at high-alpine, metamorphic rock. The laboratory findings can be summarised as follows:

Can repeated thermal cycling induce (trigger) mechanical damage in low-porosity metamorphic rocks?

(i) Whilst the significance of thermal fatigue in cold environments has been shown primarily for granite rocks, repeated sun-induced thermal cycles during Phase A generated significant structural damage of mica schists, despite their low-porosity. Although cumulative stressing was inefficient to cause larger crack patterns or ultimate failure, it led to detectable pore-scale signs of deterioration at the exposed surface and within the near-surface.

(i) Open porosity of all samples exposed to 120 thermal cycles significantly increased by up to 16%. It is assumed that long-term differential and anisotropic crystal expansion and contraction led to crystal separation along their borders.

(ii) P-wave velocity declined by up to 10% in rocks where schistosity was parallel to external heating and cooling. The p-wave decrease is interpreted as evidence for pore-scale structural dilatation (i.e. more voids) in the rock interior through progressive stress accumulation.

(iii) Rocks with out-facing schistosity primarily responded surficially in the form of surface weakening and better pore connectivity. In contrast, structural modifications remained 'hidden' in the rock interior, where cleavage was parallel to the surface. This cleavage-dependent trend indicates that thermal deformation of pre-existing pores operates parallel to the cleavage.

Is the efficiency of repeated diurnal ice crystallisation enhanced (prepared) due to its synergy with previous thermal cycling?

(ii) Although the stresses produced during one single diurnal cycle of ice crystallisation is postulated to be insignificant for rock weathering, long-term repetition of experimental frost cycles produced clear micro-scale structural damage in the (sub-)surface of all mica schist samples. Rock responses distinctly varied dependent on the pre-weathering history, which demonstrates that previous sun-induced thermal fatigue can enhance the efficiency of low-magnitude frost action.

(iii) Greatest open porosity increases (up to 50%) and strongest declines in p-wave velocity (up to 40%) caused by freeze-thaw were recorded for samples that had reacted most to previous thermal cycling. In comparison to un-weathered rocks, these findings are interpreted as clear signs that the previous history of (fine-scale) structural damage and (i.e. enhanced inter-pore connectivity) provided more pathways for moisture and more confined space for ice crystallisation upon subsequent freezing.

(iv) Both p-wave and porosity data indicate a two-stage rock response to freeze-thaw cycling, with an initial peak after the $50^{th}/65^{th}$ frost cycle and decelerating behaviour until the end of the experiment. It is assumed that a certain number of frost events can initiate negative feedbacks, where either nano-scale pore collapse leads to pore compaction or progressive pore size increase counteracts the formation of efficient ice pressures.

(v) The findings also reveal that frost-induced mechanical changes are independent of any nano-scale weathering history, but vary according to the cleavage orientation and the minerals present. Rocks with schistosity perpendicular to the exposed surface and with low quartz/ high mica content were generally found to be most sensitive to freeze-thaw.

This study emphasises that sun- and frost-induced fatigue of the near-surface of rock should receive more attention in periglacial research, especially when studying unstable rock slopes affected by small-sized rockfall events. This is particularly true with respect to on-going temperature rises in alpine environments, where diurnal temperature variations will likely span greater minima and maxima during summer, and will become more dominant during winter. To build on these insights, more sophisticated laboratory experiments are

needed in the future that ideally address. The final step, however, must be to transfer the laboratory findings to natural rock slopes with complex thermal and mechanical regimes. Rock weathering has been simulated here under well-controlled experimental conditions, yet this study documents significant rock responses that have important implications for the near-surface destabilisation of rock slopes (i) that experience a history and synergistic influence of combined thermal cycling and freeze-thaw cycling, and (ii) with either slope-facing or slope-parallel schistosity. It is argued that the cleavage orientation dependent trends found in this study are the key to scale-up the micro-scale weathering experiments of intact mica schist samples to metamorphic rock slopes with distinct discontinuities.

Acknowledgements

This study derives from a research stay at the Rock Breakdown Laboratory of Oxford University Laboratory, funded by the German Exchange Service (DAAD) (03/16-03/17) and the German German Academic Scholarship Foundation (Studienstiftung) (04/17-09/17). Rock samples used in this study were collected during the field campaign in August 2016, funded by the Dr. Hohmann-Förderung of the Gesellschaft für Erdkunde zu Köln e.V. Many thanks go Renate and Richard Dikau for driving 50 kg rock material through Switzerland to Bonn, as well as to the strong Geomorph Chicks Katharina Eibisch and Luise Martin, who organised the dispatch of those rocks to Oxford. Laboratory assistance during the weathering experiment by Mona Edwards and Hong Zhang (University of Oxford) is highly appreciated. Likewise, Owen Green (Oxford Earth Science Institute) is thanked for assistance with thin section analyses. Cutting of rock samples was conducted by William Revie (Construction Materials Consultants, Stirling). Special thanks go to Lucie Fusade and Martin Michette for fruitful discussions and for providing the final 'clue'.

PART C

Meidhorn and Bella Tola

----- BLANK -----

Chapter 9

SYNOPTIC DISCUSSION

We do not improve our theories or models by admiring them, or by proclaiming how well they seem to fit our observations. The only way to improve them, and therefore to make progress, is actively to seek conflict between our models and the real world. Hypothesis testing is just one way to seek this conflict. However, the aim should not be the wholly negative 'refutation' of the theory that is proposed by my admittedly strawman view of critical rationalism, but the constant revision and improvement of theory. (McCarroll, 1997, p.1)

Chapter 9 provides a synoptic discussion of findings and observations made in study I-V (Chapter 4-8) with respect to the major objectives and hypotheses of this thesis. Section 9.1 comes back to the question of key destabilising factors (***Objective 1***) and summarises key controls and processes identified in this study within a new conceptual scale-model of rock slope systems. Section 9.2 discusses the findings from different time scales of rockfall activity with respect to key paraglacial and non-paraglacial factors and weathering processes (***Objective 2***) and presents different scenarios. Section 9.3 discusses the geomorphic role of rock slope instability in alpine cascading systems (***Objective 3***) and provides evidence for the major significance of small- to medium-sized rockfalls for rockwall-talus coupling, talus evolution and catchment sediment flux. Section 9.4 finally discusses the methodological consequences of the scale-dependency of rock slope instability by showing 'ten ways to be wrong' (***Objective 4***). Section 9.5 concludes with five practical and philosophical recommendations for future research.

9.1 Relative importance of rock slope destabilising factors – a question of scale

Many diverse key controls of rock slope instability and rockfall initiation have been recognised in previous research studies in alpine systems (Chapter 2). However, which factors and processes are most dominant and relevant is intensively, albeit controversially debated. Most disagreement is about whether rock slope instability is driven by external topoclimatic or internal thermomechanical controls and/or by factors related to glacier retreat and atmospheric warming. While there seems to be general agreement between researchers about which small-scale variables to explore in laboratory studies, interestingly, as temporal and spatial dimensions of investigation increase, the spectrum of different variables used also increases. Faced with this debate, ***Objective 1*** of this dissertation was to evaluate the relative importance of key rock slope destabilising and rockfall initiating factors in alpine systems. It was argued that a multi-scale perspective is needed to bring further light into the present-day debate. In particular, it was hypothesised that the relative importance of rock slope destabilising factors is scale-dependent (***Hypothesis 1***) and a result of scale linkages (***Hypothesis 2***) (Section 3.2).

Figure 9.1 presents a conceptual three-scale model of key controls involved in rock slope instability based on the factors and processes identified in research studies I-V (Chapter 4-8). The three spatial scales span from the lowest level of intact rock of about < 1 m^2, over the rockwall scale of about 1 m^2 to 1 km^2 to the largest level of alpine valleys of > 1 km^2. Each spatial level is associated with a time span ranging from seconds to years (intact rock scale), from present to decades (rockwall scale) and to the last glacial maximum (LGM). Definition of 'graded' and 'cyclic' times is based on the concept of Schumm and Lichty (1965). Although

Schumm and Lichty's focus was on landform evolution in fluvial systems, application of their time definition has great value for this study in context of paraglacial rock slope instability, as will be later discussed in Section 9.2. Importantly, the spatial and temporal dimensions should be considered as being flexible, depending on the object of interest. For instance, while Schumm and Lichty (1965) investigated as longest time span a 'geological scale' beginning 1.000.000 years ago, in this thesis, focus was primarily on processes and conditions since LGM. Similarly, the spatial dimensions must be understood as approximate ranges as the size of intact (unjointed) rock, the rockwall length/width and the catchment size of alpine valleys can highly vary. Thus, definition of scale borders/transitions should be always flexible and adjustable, ideally according to the system properties observed. The next three sections summarise the findings for each scale.

9.1.1 Valley scale

At the valley scale, observations made in this thesis emphasised that rock slope instability is essentially governed by two externally and internally acting factor groups (Figure 9.1): External topoclimatic parameters and internal paraglacial forcing by permafrost thawing and warming. Particularly, valley position (i.e. distance to glacier) and hillslope profile (i.e. slope angle) were identified as the two first-order topographic controls that, in turn, determine the annual sum and variability of incoming solar radiation depending on the large-scale geographic setting (i.e. latitude, altitude). Due to long-term changes in solar energy e.g. atmospheric warming during the Holocene, glacier retreat exposes near-vertical and initally frozen bedrock. Evidence was provided that valley-scale permafrost degradation after LGM is the first-order paraglacial driver (Figure 4.6), consistent with pervious studies from the European Alps (Sass, 2005b; Ravanel and Deline, 2011; Fischer et al., 2012). While glacier retreat usually leads to positive feedback effects (permafrost thaw, redistribution of the large-scale in-situ stress pattern), findings of this thesis additionally suggested that paraglacial adjustment may be associated with negative valley-scale system feedbacks, due to lower amounts of solar energy of glacially steepened valley flanks (Figure 4.5) and retarded permafrost degradation (Chapter 4). Observations furthermore emphasised that sensitivity for paraglacial failure is significantly conditioned by non-paraglacial large-scale factors.

For instance, pre-existing tectonic structures in metamorphic settings can delay paraglacial rockfall release, at sites where bedding planes dip into the slope, and lead to a temporary higher stability of steep valley flanks (Chapter 4, 6). Contrary, paraglacial bedrock adjustment appears to be reinforced by out-dipping (cataclinal) tectonic layers due to fast activation of shear planes (Figure 4.9). These observations support notions made by Bell (1976) and Cruden and Hu (1993). Moreover, as highlighted by Schumm (1991), they underline that history matters, because tectonic processes can provide systems trajectories for post-LGM and present-day rock slope instability and mediate influences of valley-scale topoclimatic and paraglacial controls.

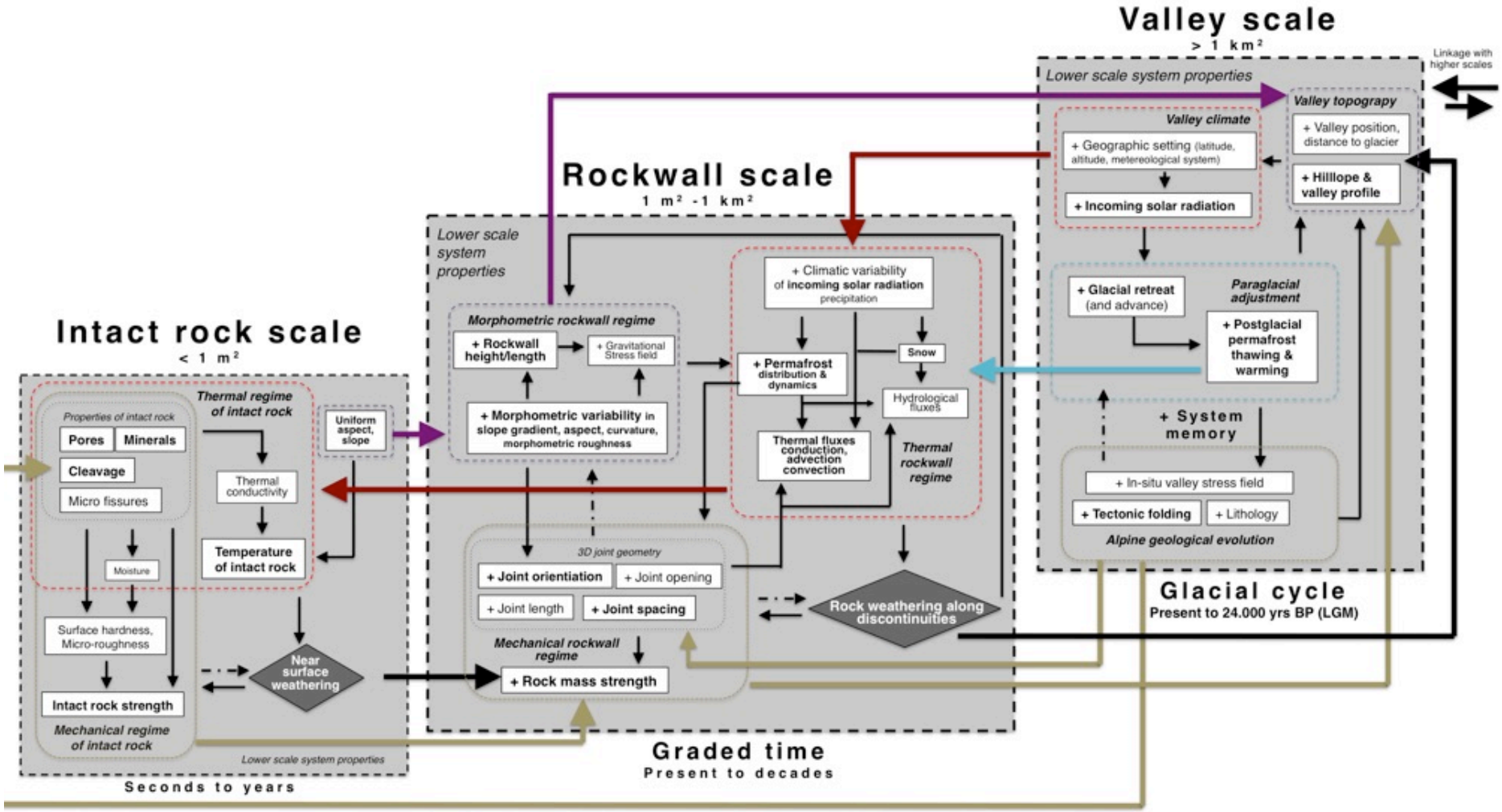

Figure 9.1: *Conceptual scale model of key controls and processes acting at different spatial and temporal scales of rock slope systems. At each scale, new system properties are dominant and interact leading to emergent and non-linear complex behaviour. Additionally, scale linkages between scales can cascade upwards and downwards through scales. (See text for further description).*

9.1.2 Rockwall scale

One spatial and temporal scale lower, observation of this study highlighted that instability of individual rockwalls is predominated by three interdependent variables (Figure 9.1): Rockwall morphometry, mechanical rockwall regime and thermal rockwall regime. The high morphometric variability is associated with high internal thresholds for failure, with highest sensitivity at steep (> 60°) slopes with long profiles (> 180 m) due to high gravitational stresses (Chapter 6). In turn, feedbacks arise with the thermal regime. For instance, rockwall roughness determines whether and how high a rockwall snow cover can accumulate (Chapter 7), while changes in convexity in combination with steepness lead to complex heat transfer into depth (Chapter 4). The role of slope aspect is twofold with effects on both the mechanical and thermal regime. While variations in slope aspect determine different orientations of joints and thus, different failure mechanisms (Figure 7.7). At the same time, aspect-controlled variability in incoming short- and long-wave radiation leads to a heterogeneous spatial permafrost distribution over short distances (Chapter 4,6). Importantly, frozen bedrock with ice-filled joints can also positivity influence the morphometric and mechanical regime by increasing the rock mass strength (RMS) despite steep slope gradients (see also Krautblatter, 2009). At sites with seasonal active layer dynamics, however, the temporal interplay between convective, advective and conductive thermal fluxes through the underground can lead to complex mechanical responses, particularly where snowmelt occurs, as discussed in Chapter 7. It is obvious that thermal and hydrological fluxes can only arise due to discontinuities in the rock mass, which provide effective pathways between the atmosphere and the rock depth. In turn, field observation and numerical modelling demonstrated that the anisotropy of rock mass results in complex frost weathering regimes with depth-, intensity- and time-varying rockfall efficiency from years to decades (Chapter 6,7). However, while rock weathering usually enhances the risk for failure (positive feedback), it is also reasonable that rock weathering activity and fracturing intensity can diminish as a result of negative feedbacks e.g. when progressively widening of joint or 'zero-conditions' after rockfall detachment (see e.g. Phillips, 2005, Viles, 2013b).

9.1.3 Intact rock scale

At the smallest scale investigated in this thesis, two first-order controls on the instability of intact rock became evident (Figure 9.1): micro-scale rock properties and rock temperature. Particularly pores, minerals and cleavage (direction) cause a distinct micro-scale anisotropy (Chapter 8), which in turn determines the intact rock strength, as quantified in the field (Chapter 6, 7). At the same time, thermal conductivity linked to micro-scale properties significantly dictates conductive heat fluxes into depth. This was evident both in field measurements, where MART and NSRT of investigated intact rock varied by several degrees despite comparable aspects, slope inclinations and higher-scale topoclimatic, simply due to small-scale rock properties (Chapter 6, 7); and in the laboratory experiment, where cleavage-dependent thermal rock responses were recorded albeit the same external temperature forcing (Chapter 8). Given enough repetition of temperature variations, sub-critical stresses through thermal cycling or ice volumetric expansion (if bedrock is saturated) are likely to cause effective near-surface/pore-scale rock weathering, as observed in laboratory experiments (Chapter 8). However, laboratory findings also highlighted that rock damage (output) is not necessarily

proportional to rates of thermal and mechanical stresses (input), in particular where different types of weathering processes act in competition and synergy (see also Phillips, 2001). Thus, pre-existing intact rock strength (Chapter 6, 7), cleavage, surface micro-roughness and anisotropic thermal behaviour of minerals such as quartz (Chapter 8) must be considered as important sources for non-linear rock responses.

9.1.4 Scale-dependency and scale inter-linkages of rock slope systems

The crucial point made in Figure 9.1 is that rock slope instability is scale-dependent. At each spatial and temporal scale, different first-order (bold in Figure 9.1) and second-order system variables act together and their mutual organisation causes new system properties and laws. Referring to Harrison (2003), this quantitative organisation of causes/variables leads to emergent rock slope behaviour with scale-dependent effects on rock slope instability. Importantly, such emergent behaviour can be qualitative, as later discussed in Section 9.4. Emergence can arise due to complex feedback effects between variables associated with non-linear responses that can either reinforce or buffer rock slope instability in alpine valleys. Therefore, observations of this study provide support for ***Hypothesis 1*** and emphasise that, as size and time change, the relative importance of rock slope destabilising factors changes too. At each scale, different variables become dominant and causative, while other factors become secondary or even irrelevant (Figure 9.1). An extreme example are micro-scale rock properties such as cleavage, which are of major importance at the lowest scale, but become secondary at the rock slope scale and irrelevant for valley-scale/long-term rock instability. A similar perspective on causal and non-causal or, 'independent' and 'dependent' variables was early proposed by Schumm and Lichty (1965) for fluvial landform evolution. They suggested that river morphology during cyclic (geological) time scales is dependent on climate, geology and relief, while during short time spans (graded) lower-scale runoff and sediment yield dominate and initial relief is irrelevant.

While the question of scale is little explored in the context of rock slope instability, it has been frequently discussed from a broader philosophical perspective (see e.g. Anderson, 1972; Phillips, 1988; De Boer, 1992; Deutsch, 1998; Phillips, 1999; Harrison, 2001; Phillips, 2003b; Murray et al., 2009). Specifically in fluvial, aeolian and coastal systems (see e.g. Schumm and Lichty, 1965; Lane and Richards, 1997; Murray et al., 2014), it is controversially discussed whether scales can be linked. Likely as a consequence of the rise of process geomorphology (see also Rhoads and Thorn, 1993), several researchers postulated that scales are significantly decoupled and act independently from lower- or higher-scale system behaviour (Werner, 1995; Lazarus et al., 2011). However, observations made in this thesis show the opposite and that scale decoupling is not valid for rock slope systems. In support for ***Hypothesis 2***, the findings evidence that scales are indeed interlinked by both bottom-up and top-down interactions (Figure 9.1).

At least, five upward interactions are evident. For instance, as suggested by Kugler (1964) and Dikau (1992), morphometric characteristics of each level are the sum of lower-scale (land)form elements including form facets (intact rock), relief forms (rockwall) and relief form association (valley) (see Table 2.1). Likewise, rock mass strength at rockwall-scale is not solely controlled by joint properties, but is to a large extent dependent on lower-scale strength of intact rock (Chapter 6 and 7, see also Selby, 1980). In turn, rock mass strength of rock

slopes significantly governs higher scale hillslope profiles of alpine valleys (see also Augustinus, 1992) and can mediate the valley-scale significance of paraglacial permafrost thaw (Chapter 4,6). Likewise, pore enlargement and micro cracking e.g. through micro-scale thermal fatigue (Chapter 8), can influence the higher scale 3D joint geometry with consequences for the thermal regime of jointed rock slopes. The same scale-linking effect accounts for rock weathering along discontinuities, as shown by Hales and Roering (2009), which may – over long temporal time scales – act as large-scale 'frost buzzsaw' limiting the relief of mountain ranges.

At the same time, Figure 9.1 highlights at least three downward interactions between scales. For example, energy input in form of solar energy results from higher scale climatic forcing, which is evident up to the lowest scale. Similarly, as discussed in Chapter 4, valley scale glacier retreat after LGM may still determine the thermal signal of individual rock slopes and may cause rock failure, albeit permafrost is not longer present (see also Verleysdonk et al., 2011). Alpine tectonic folding represents another large-scale and historical process that still conditions the sensitivity of both lower scale rockwalls due to main joint sets parallel to the metamorphic nappes and of intact rock due to tectonically-derived cleavage/schistosity.

From an epistemological perspective, this scale interaction is of crucial importance when it comes to understanding and predicting rock slope failure. It shows that each scale does not only need its own explanation and causation, but moreover, cause and effect relationships can obviously also cascade up and down through scales, as described by Murray et al. (2014) for coastal and aeolian systems. In this way, scale decoupling could lead to erroneous conclusions on e.g. mechanisms and timing of rock failure. Particularly, the path-dependency on tectonic bedding observed in this study highlights that each scale "is more than only the sum of its parts", as stated by Jensen (1998 p. 59) and requires "higher-level theories to understand them", as argued by Harrison (2003, p. 332). A more in-depth discussion of the methodological consequences of scale dependency follows in Section 9.4.

Therefore, returning to the general debate about which factor and process is most important or relevant for rock slope instability, it becomes clear that this debate is a question of scale. As temporal and spatial scales change, explanations and causation also change. Accordingly, rather than attempting to extrapolate from a detailed set of small-scale variables obtained in the laboratory, or, in turn, using general laws from large-scale modelling, it is believed that thinking widely across spatial and temporal scales will be a valuable way to understand and predict causes, effects and mechanisms of rock slope instability in alpine systems.

9.2 Spatiotemporal rockfall activity on deglaciated rockwalls

The previous section (9.1) emphasised that rock slope instability is a condition that varies over different spatial and temporal scales due to different scale-dependent and interlinked controls. Consequently, the intensity and magnitude of rockfall release from unstable rock slopes is highly complex over time, particularly in valleys affected by glacier retreat. *Objective 2* of this thesis was to estimate potential paraglacial scenarios of rock slope instability with respect to their paraglacial and non-paraglacial controls and to quantify the frequency-magnitude pattern of rockfall events on deglaciated rock slopes.

9.2.1 Valley scale paraglacial rockfall activity after LGM

Both study sites of this thesis show a characteristic spatial clustering of active talus slopes with a distinct overrepresentation in upper basins and on north-exposed slopes in close distance to the glacier cirque, as is typical for alpine valleys (Figure 4.2, Figure 5.7). Many researchers interpreted such spatial patterns as evidence for paraglacial forcing (Bovis, 1990; Cossart et al., 2015; Ostermann and Sanders, 2016). Regional-scale modelling in Chapter 4 provided support that paraglacial rock slope adjustment *is* a major control on spatial rockfall activity in the Turtmann Valley. With increasing time following deglaciation, rockfall activity can significantly increase (Equation 4.3), depending on site-specific characteristics of the source rockwall (Table 4.3). It was shown that rockfall probability is highest at recently deglaciated rock slopes (< 100 years) in upper basins (Figure 4.5J), whilst rockfall source areas are largely inactive at the trough shoulders, where deglaciation started earlier ca. 18-12 kyrs ago. Likewise in Val Müschauns, the legacy of former glaciation and, in particular, the importance of glacial valley morphology, is mirrored in a present-day rockfall dominance in and close to the upper cirque. Likewise here, activity abruptly diminishes from the mid to the lower basin (Figure 5.7). Using ergodic reasoning, these findings suggested that paraglacial rock slope adjustment (after LGM) evolves in an exhaustion mode, as proposed by Cruden and Hu (1993), with the strongest rockfall peak immediately after deglaciation and a fast decline towards the end of the paraglacial period (Chapter 4, Figure 4.9). A conceptual model of valley-scale and post-LGM rockfall activity (cyclic time scale in Figure 9.1) is shown as curve A in Figure 9.2.

9.2.2 Structurally controlled paraglacial adjustment – rapid response vs. linear decline

At the rock slope scale, two different scenarios of paraglacial rockfall activity were identified dependent on site-specific geological settings and tectonically-derived dip direction of joints (Chapter 4, Figure 4.9). A combination of a 'rapid response model' (Evans and Clague, 1994; Allen et al., 2011) and Cruden and Hu's (1993) 'exhaustion model' is suggested for cataclinal rock slopes (curve B in Figure 9.2). Here, out-facing joints parallel to the tectonic bedding may favour a very intense, but rapidly declining paraglacial response due to the prompt initial of pre-existing shear planes (Chapter 4). A similar notion was made by Augustinus (1992, 1995) on cataclinal rock slopes in Southern New Zealand Alps. With removal of most weathered material, rockfall activity may diminish to a minimum, as reflected by local geotechnical observations and talus slope surveys on cataclinal rock slopes (Chapter 6). In contrast, a more linear decline must be assumed for anaclinal rock slopes (curve C in Figure 9.2), confirming the 'steady state decline model' of Ballantyne and Stone (2013). Despite glacially steepened slope inclination, slope-indipping joint orientations may favour first a temporary high rock stability after deglaciation, as described by Selby (1982). Consequently, rockfall activity may have a rather delayed and less intense peak after glacier retreat, but in turn might be enhanced for several decades or millennia, as observed at anaclinal sites in relatively great distance from the glacier in Chapter 6.

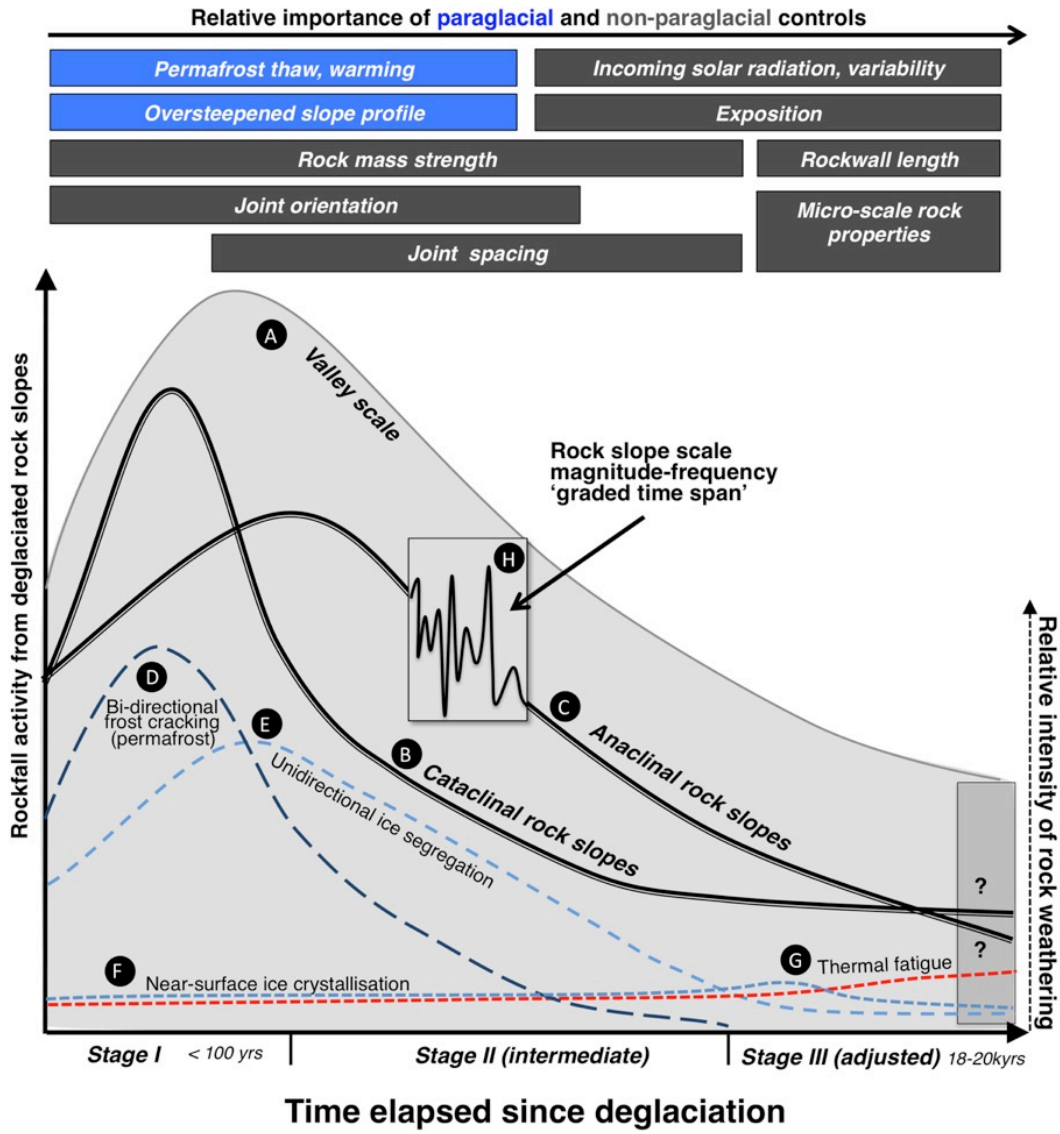

Figure 9.2: *Conceptual model of paraglacial rockfall activity on different spatial and temporal scales with respect to key synergetic weathering mechanisms and different paraglacial and non-paraglacial controls.*

9.2.3 Short-term rockfall frequency and magnitude – fluctuations about the 'mean'

Research of this study emphasised that long-term and valley-scale rockfall activity after glacier retreat is overlain by a local and seasonal-to-decadal rockfall pattern (H in Figure 9.2). Rockfall activity of rock slopes on the north-exposed Hungerli Peak, classified by an intermediate paraglacial stage II (Chapter 6), spanned from (i) boulder-sized (14-61 m^3) planar slides with return periods of 250 years, (ii) high-frequency (~every 17-50 years) debris falls (<14 m^3) in form of wedge and toppling failures to (iii) seasonal release of flake-like clasts (3-6 events/year) (Chapter 7). Following Schumm and Lichty (1965), this short-term rockfall variability on individual rock slopes can be interpreted as a 'graded time' signal that causes fluctuation about the mean paraglacial rate. In the context of fluvial drainage basins, Schumm and Lichty (1965) described this state as dynamic equilibrium. They suggest that continual adjustment between system variables cause negative feedbacks (self-regulations), which approach the system to steady state conditions (see Figure 9.2). During

those graded conditions, Schumm and Lichty (1965) assumed that time and initial relief become irrelevant as controlling factors, but vegetation, for example, becomes one of the key (independent) system variables. The same seems to be true for alpine rock slopes, as shown in this research. Observations in Chapter 6 highlighted that paraglacial forcing is secondary for short-term rockfall fluctuation or frequency-magnitude pattern, while 3D joint geometry and thermal regime become major controls. In this way, the post-glacial or 'cyclic' rockfall rate after LGM (Figure 9.2) can be seen as a series or sum of rock thermo-mechanically controlled fluctuations approaching to a non-glacial (dynamic) strength equilibrium.

9.2.4 A conceptual model of paraglacial rock weathering

All research studies (study I-V) of this thesis emphasised that rockfall timing and intensity during paraglacial periods are closely linked to successively and synergistically operating rock weathering agents. Figure 9.2 (curves D-G) further presents a conceptualisation of rock weathering during the paraglacial period. The model is based on data presented in this thesis and is a further development of the concept proposed by Viles (2013a), earlier shown in Figure 2.22.

In ***stage I*** (< 100 yrs), deep-seated bi-direction freezing and thawing over the active permafrost layer is one of the key causes for bedrock destabilisation and rockfall peak immediately after deglaciation (D in Figure 9.2). Evidence was provided in Chapter 4, where highest rockfall activity was identified at bedrock areas at 2900-3300 m, in close distance to the hanging glaciers, and with a permafrost probability of more than 90%. This agrees with previous observations in (formerly) glaciated alpine areas (e.g. Wegmann et al., 1998; Fischer et al., 2006; Gruber and Haeberli, 2007, Ballantyne et al., 2014, Ravanel and Deline, 2015).

With increasing permafrost out-melt, the relative role of bi-directional ice segregation decreases (Figure 9.2), as reflected by positive MARTs recorded at rock slopes in a later paraglacial state in the Turtmann Valley (Chapters 6,7). Instead, unidirectional freezing becomes more dominant at those formerly affected permafrost sites leading to frost cracking within the upper meters of bedrock (Figure 6.9, Figure 7.10). This transition from deep-seated bi-directional freezing to near-surface bedrock cracking via seasonal ice segregation towards the end of ***stage I*** could explain the decreasing rockfall intensity after the first initial peak (E in Figure 9.2).

During ***stage II***, the optimal location for segregation ice formation (frost cracking window) continues to rise in altitude in response to further atmospheric warming, as shown by Hales and Roering (2009) for the New Zealand Alps. Consequently, the relative destabilising role of both bi-directional and unidirectional freeze-thaw may diminish (Figure 9.2). In three hanging valleys of the Turtmann Valley, it was shown that this can be associated with an inverse trend between frost cracking intensity and time since LGM deglaciation (Chapter 6).

In ***stage III,*** micro-scale weathering agents such as ice crystallisation and thermal fatigue become relatively more dominant, albeit their rate may remain constant (F, G in Figure 9.2). Frequent rock temperature oscillations around the freezing point, as recorded between autumn and spring at northern rock slopes in the Pipji and Brändji Valley (Figure 6.7), favour optimal condition for diurnal ice crystallisation. Long-tem repetition of ice volumetric pressures may cause pore-scale rock damage, particularly in synergy with sun-induces thermal fatigue (Chapter 8, peak G in Figure 9.2). Such subcritical rock fatigue of synergetic micro-

scale weathering agents could explain the lowest rock failure rates at the end of the paraglacial period (***stage III***). Flake-like rockfall supply, as described by André (1907) in Svalbard and as observed at all adjusted rock slopes in the Turtmann Valley (Chapter 6) appear to dominate. Although there is still little evidence about the efficiency of sun-induced thermal cycles in low-porosity alpine rocks ("*?*" in Figure 9.2), laboratory weathering experiments (Chapter 8) and recent investigations by Collins and Stock (2016) give reason to assume that thermal fatigue represents an important destabilising, if not key rockfall trigger after paraglacial adjustment.

9.2.5 Spatiotemporal interplay of paraglacial and non-paraglacial controls

"As glacial cycles evolve, the factors influencing slope stability change" (McColl 2012, p. 2). In his review paper about paraglacial rock slope instability, McColl (2012) postulates that this involves both paraglacial and non-paraglacial controls. As a consequence, rock slope instability after glacier retreat gains in complexity. In this thesis, different key influences on paraglacial rockfall activity have been identified at different temporal stages (upper part of Figure 9.2):

In ***stage I***, permafrost in freshly deglaciated rock slopes and its subsequent thawing and warming represents a first-order paraglacial rockfall control (Chapter 4). Permafrost degradation can therefore explain the first intense peak of low- and high-magnitude rockfalls, as illustrated in Figure 2.15 (Krautblatter et al, 2012; Krautblatter and Leith, 2015), due to decreasing shear strength of ice-bonded joints (Davis et al. 2001), increase in hydrostatic pressures (Krautblatter and Hauck, 2007) and intensified frost cracking (Murton et al., 2016). Additionally, rockfall susceptibility in this early stage is crucially enhanced by glacially steepened slope profiles (Chapter 4, 5, 6) and high horizontal shear stresses (e.g. Bovis, 1990, Holm et al. 2004).

With increasing time since deglaciation, when permafrost becomes patchy or absent (Figure 6.1B) and MARTs become positive (Figure 6.8), increasing solar radiation sums (Chapter 3) and the specific slope exposition (Chapter 6) gain in significance towards the end of the paraglacial ***stage III*** (Figure 9.2). Likewise, slope gradients and effective rockwall heights may decrease (Chapter 6), due to long-term rockfall erosion and growing talus thickness/length (see e.g. Kirkby and Statham, 1975) and become the limiting rockfall controls during ***stage III*** (Chapter 6). Therefore, the importance of paraglacial controls decreases with time since deglaciation, while topoclimatic factors and specifically the efficient rockwall area become most decisive.

In agreement with McColl (2012), research of this thesis emphasised that paraglacial bedrock instability is significantly conditioned – at various spatial scales - by rock mechanical properties. Major controls identified in this study include (i) rock mass strength, (ii) joint spacing, (iii) joint orientation, and, at a later temporal stage, (iii) micro-scale rock properties. Joint orientation relative to slope surface is most significant in the first half of paraglacial period (Chapter 3), being the prime controls on whether rockfall activity evolves either exponentially or more linearly during the paraglacial period (B and C in Figure 9.2). Joint spacing (or density) is a major control on both rockfall size and activity (Chapter 6) consistent with previous studies in Svalbard (André, 1997) and Southern New Zealand Alps (Augustinus, 1992, 1995).

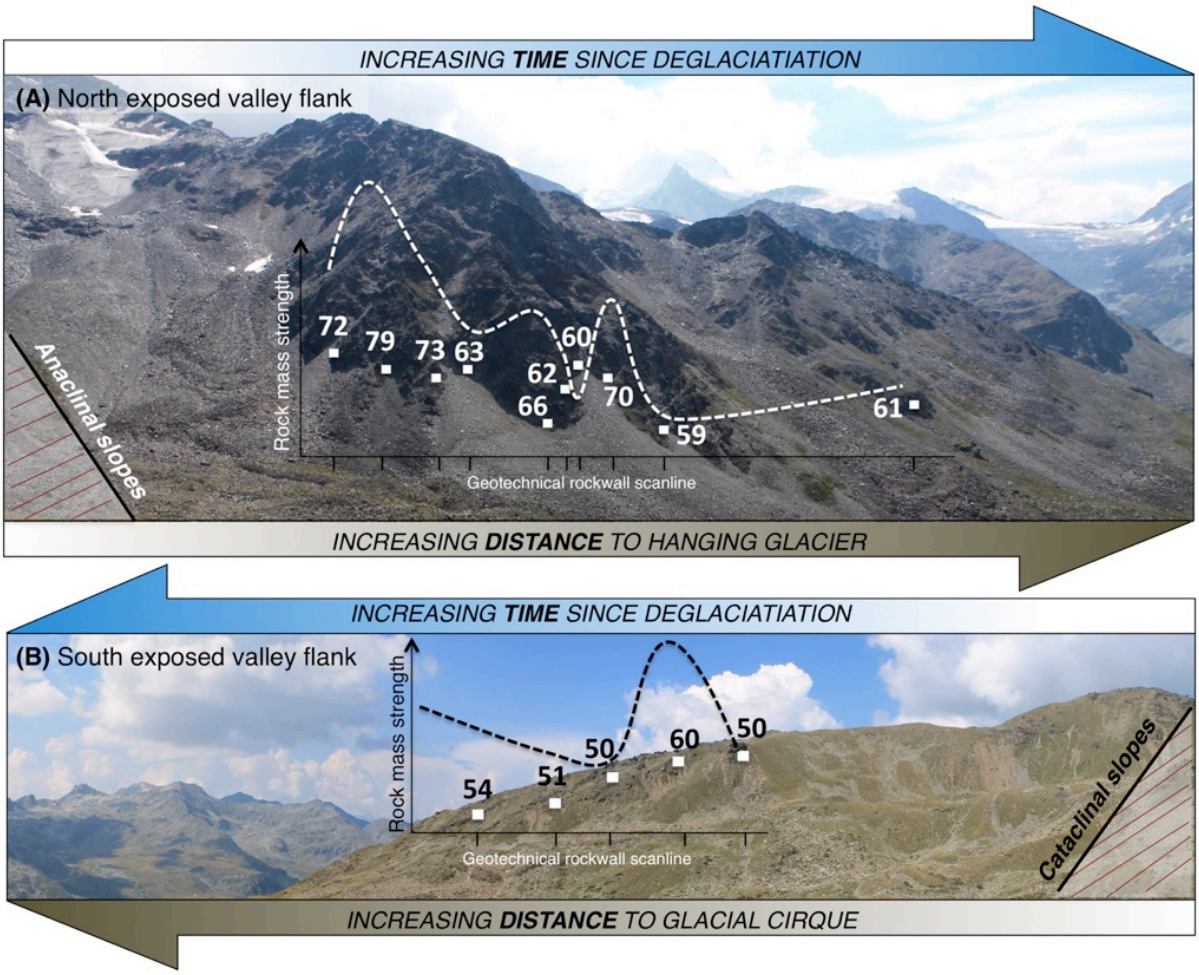

Figure 9.3: *Ergodic principle exemplified based on spatial variability of Rock mass strength (RMS values detected along north-exposed anaclinal and south-exposed cataclinal rock slopes in the Hungerli Valley (Chapter 6 and Chapter 7).*

Contrarily to Moore et al. (2009), no statistically significant evidence for a paraglacial trend between rockfall activity and RMS was found in this thesis (Figure 6.10). Nevertheless, RMS results summarised in Figure 9.3 imply a slightly increasing trend with decreasing distance to hanging glacier and/or decreasing time since deglaciation, and a second peak of high RMS values near the trough shoulder. Therefore, from a rock mechanical perspective, RMS must still be considered as a key influence on paraglacial rock slope failure, as its combination with thermal drivers causes small-scale variability in bedrock instability that overlays the higher-scale paraglacial pattern (Chapter 6,7).

Finally, after paraglacial adjustment to non-glacial strength conditions (***stage III***), when rock weathering primarily occurs within the near-surface, 3D joint properties are likely to become secondary, while micro-scale rock properties gain in relative importance (Figure 9.2). In metamorphic settings, cleavage orientation represent a prime control for different rock responses to thermal fatigue and ice crystallisation (Chapter 8). Transferring laboratory experiments in Chapter 8 to the slope scale, it appears that rock slopes with surface-parallel cleavage (as on cataclinal slopes) are most sensitive for micro-scale thermal fatigue and frost weathering at the end of the paraglacial period.

In summary, it became clear that timing and intensity of paraglacial rock slope instability is scale-dependent, because of different paraglacial and non-paraglacial variables that change in relative importance as the paraglacial cycle proceeds. It has been shown that paraglacial rockfall activity evolves at a valley scale and long temporal scale (e.g. since LGM) according to an exhaustion model, as postulated by Cruden and Hu (1993). Mainly dictated by permafrost degradation and associated frost weathering, highest rockfall peaks occur immediately after deglaciation, followed by a subsequent exponential decline towards a permafrost-free, near-surface weathering regime. These findings provide therefore only in part support for ***Hypothesis 3***. In fact, while an exhaustion model is plausible at the valley scale, ***Hypothesis 3*** applies not for smaller spatial scales. On individual rock slopes, paraglacial activity can evolve either rapidly declining or more linearly, primarily depending on the joint orientation parallel to the tectonic bedding. Moreover, rockwall scale trend is additionally overlain by a site-specific and short-term (seasonal to years) rockfall frequency-magnitude pattern, which is largely independent from paraglacial forcing, but predefined by rock mass characteristics. These findings give support for ***Hypothesis 4*** and are reason to rework ***Hypothesis 3*** by future research.

9.3 Geomorphic significance of rock slope instability in alpine cascading systems

Although geomorphologists have largely recognised rock slope instability as the initial source for alpine sediment cascades, Krautblatter et al. (2012), amongst others, emphasise that the qualitative and quantitative significance of rock slopes e.g. for talus slope evolution or valley-scale sediment fluxes is poorly addressed in previous research. Section 6.1 highlighted that this is largely linked to the strong scientific focus on sediment storages and budgets in geomorphic research, as it is most evident in the context of the paraglacial concept. ***Objective 3*** of this thesis was to provide quantitative and qualitative evidence for the significance of rock slope instability for alpine sediment cascading systems at different spatial scales. Based on key findings from the Turtmann Valley and Swiss National Park, Figure 9.4 presents a revision of our traditional framework of alpine sediment cascades (e.g. previously proposed by Schrott et al., 2002).

9.3.1 Small- and medium-sized rockfalls events matter!

Frequency-magnitude estimates at the Hungerli Peak (Chapter 7) suggested a dominance of debris falls (< 14 m^3) and boulder falls (14-61 m^3) (Figure 9.4). Similarly, in the Brändji and Pipji Valley (Table 6.1), potential rockfall sizes estimated at twelve source rockwalls spanned from small-sized to medium-sized (Chapter 6). Smallest potential block sizes were identified at permafrost-affected limestone cliffs in the Pipji Valley linked to small joint spacing. This overall size spectrum of rockwall source areas was well mirrored by corresponding talus slope deposits (Figure 6.4, Figure 7.4). Similar qualitative observations have been made in the Swiss National Park (Chapter 5), where one third of hillslope sediment routes from calcareous rockwalls to the stream of Val Müschauns are currently driven by low-magnitude rockfall events (Figure 5.7, Table 5.2).

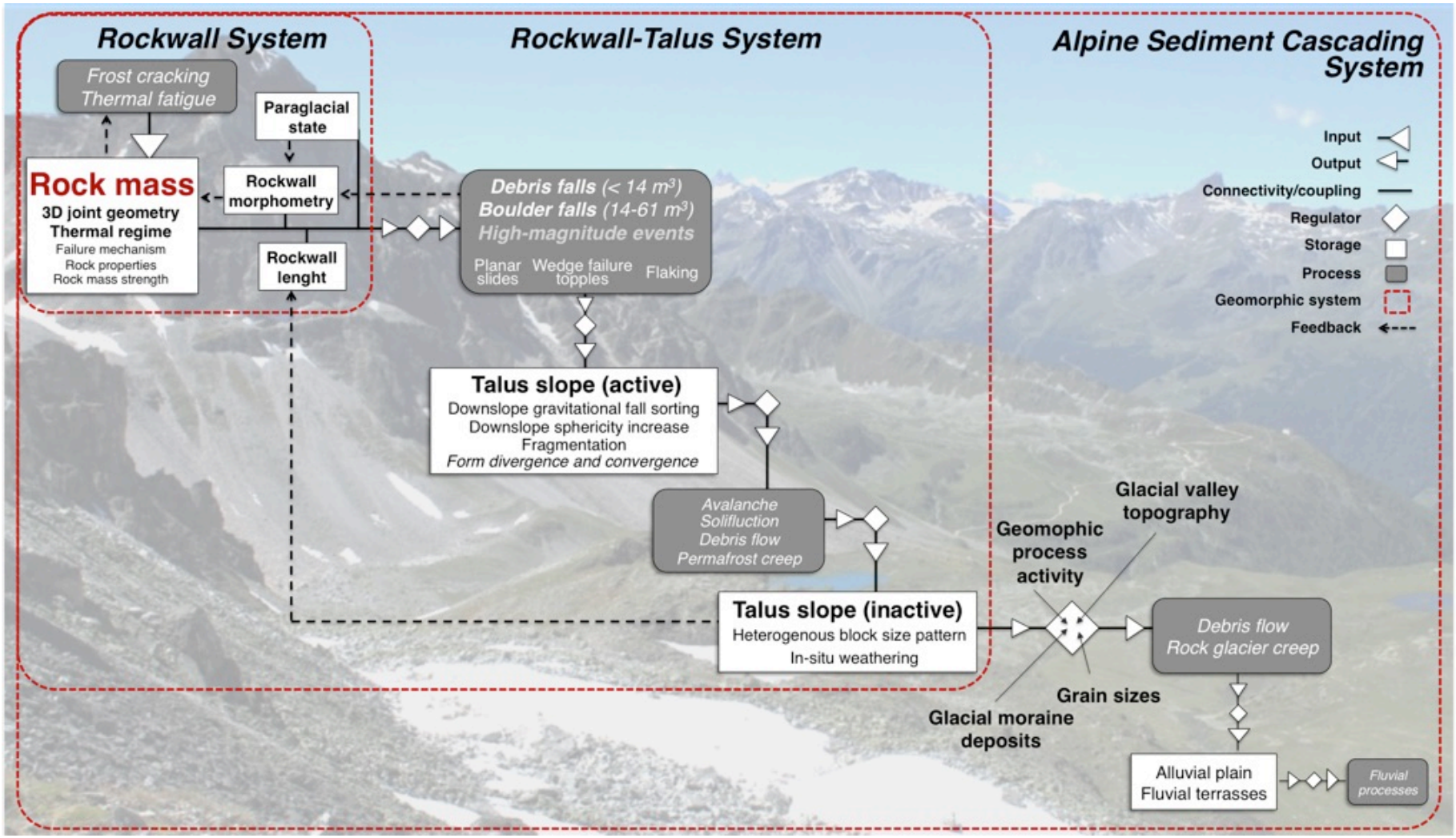

Figure 9.4: *Conceptual of rockfall sediment cascades in alpine valleys based on key findings from rockfall-dominated sediment cascades in the Turtmann Valley and Swiss National Park.*

Consequently, observations from both study sites provide support for ***Hypothesis 5*** and emphasise the significance of small- to medium-sized rockfalls for sediment production, release and transfer at different scales (hillslope, catchment), in different paraglacial contexts and lithological settings. However, it is important to state that high-magnitude rock failures cannot be ruled out, due to the lack of direct rockfall observations such as repeated laser scanning or due to the small sample set of only twelve rockwall-talus systems (Chapter 6). Therefore, much more future research is needed to extend the data set presented in this thesis. Nevertheless, on a seasonal to decadal scale, the findings of this study are consistent with previous rockfall estimates from formerly or still glaciated areas including magmatic settings (Douglas, 1980), banked limestone cliffs (Sass, 1998; Krautblatter and Moser, 2009) and low-porosity metamorphic rockwalls (Jäckli, 1957; Rapp, 1960, André, 1997). Contrarily, the observations made in both study sites contrast, amongst others, with findings from carbonate rocks in the Bavarian Alps by Krautblatter et al. 2012), where > 60% of rockfalls typically occur as high-magnitude Bergsturz events and cliff falls. It is therefore argued that the debate whether small-sized rockfalls or high-magnitude rock slope failures dominate in alpine valleys (Wolman and Miller, 1960; Jäckli, 1957; Heim, 1932; Krautblatter et al., 2012) cannot be solved at a valley-scale, but must rather be set into a smaller-scale rock slope context, where thermomechanical properties of source rockwalls emerge.

9.3.2 Rock slope instability as driver for rockwall-talus coupling

The widespread occurrence of talus slopes in alpine valleys such as in the Turtmann Valley and Swiss National Park (Figure 5.7, Figure 6.1) highlight the major significance of rock slope instability for rockfall sediment cascades (Chapter 6). Quantitative support has been provided in Val Münschauns, where one third of the basin's overall geomorphic coupling results from active rockwall-talus coupling via rockfalls (Figure 5.9). However, at the same time, rock slopes and bedrock outcrops can also decouple and interrupt significant portions (20%) of alpine sediment fluxes (Chapter 5). Such transport-limited conditions are particularly true at less-inclined and concave glacial valley flanks e.g. of glacier cirques (Figure 5.9) and paraglacially adjusted and dissected bedrock (Figure 6.3D-E). These observations emphasise that rock slope instability dictates geomorphic coupling of rockwall-talus systems (Figure 9.4), which is crucial for the performance of the downslope sediment cascade (Chorley et al., 1984; Caine, 1986).

9.3.3 On the significance of rock slope instability for talus slope evolution

Research of this thesis emphasised that the source rock mass significantly controls landform and material characteristics within rockwall-talus systems (Figure 9.4). For instance, it has been shown that longitudinal depositional patterns of talus slopes vary with paraglacial bedrock activity (Chapter 6 and 7). Talus slopes beneath paraglacially active rockwalls typically have pronounced downslope gravitational fall sorting in common with cm-sized and platy debris at the apex and large, spherical boulders at the foot (Figure 6.4, Figure 7.4). These observations are consistent to findings of Caine (1967) and Gardner (1972) in the Southern Alps of New Zealand and Canadian Rocky Mountains. By contrast, fall sorting is typically missing at adjusted and inactive rockwalls, (Chapter 6). Instead in-situ weathering and secondary reworking (debris flows, solifluction)

lead to heterogeneous patterns. According to Ballantyne and Benn (1994), these material characteristics are typical for the final state of paraglacial talus slope evolution. Interestingly, with decreasing time since rockwall deglaciation (and towards the glacier), average talus block sizes were found to generally decrease (Figure 6.9c). Following e.g. Krautblatter and Leith (2015), this spatial pattern was assumed to indicate that large rockfall magnitudes are released with a time-delay after glacier retreat.

While previous studies postulated that talus morphometry reflects a temporal evolution (Caine, 1967, 1969; Pérez, 1989; Jomelli and Francou, 2000), in this study no clear trend was found amongst investigated talus slope profile. Independent of slope aspect or rockfall activity, some talus slopes (e.g T1 in Chapter 7 and Bt5 in Chapter 6) were distinctly rectilinear and steep (~34°) at their upper and mid slope segments (with smaller-scale convexities) and flattened first at their toes (20-5°), whilst others showed the typically postulated bi-segmented slope profile (T2 in Chapter 7). Therefore, in contrast to the model proposed by Francou and Manté (1990), talus morphometry analysed in this thesis cannot be linked to talus maturity after glacier retreat, and cannot used as a proxy for temporal rockfall activity.

Furthermore, it became clear that 3D joint geometry dictate form and shape characteristics of talus sediments. While, wedge and toppling failures from densely jointed rockwalls were associated with homogeneous talus block size spectrum (Chapter 7, Figure 7.6b), talus deposits were generally more heterogeneous beneath rockwalls with sliding conditions and large erosional size-spectrum (Chapter 6, Figure 7.6a). Importantly, this relationship between kinematic failure mechanism and talus material was detected independent from topo-climatic and morphometric rockwall characteristics (Chapter 6). Similar observations as made here on paragneiss rockwalls (Hungerli Peak) were previously reported from both crystalline (Matasci et al., 2015, Loye et al., 2012) and granodiorite settings (Santana et al., 2012). It appears therefore that lithology type plays a secondary role for form-material characteristics of talus slopes, whilst site-specific 3D joint geometry (Chapter 7) and particularly joint spacing are key controls on median block sizes of talus slopes (Chapter 6).

In combination with rockwall morphometry and bedrock thermal regime, 3D joint geometry can explain a large proportion (78%, see Chapter 6) of the factors involved in talus slope evolution within alpine valleys. Due to the interplay of slope gradients and aspect (Chapter 6), curvature (Chapter 4), rockwall snow cover (Chapter 7) and incoming solar radiation (Chapter 4, 6), near surface rock temperatures can highly vary across short distances, as previously shown by Gubler et al. (2011). MART difference of 2.34 °C (Figure 6.7), within an elevation belt of 2600-2800 m asl and an area of 12 x 10^6 m^2 can lead to varying bedrock depths and intensities of segregation ice (Figure 6.9, Figure 7.10). Dependent on site-specific 3D joint geometry, those different frost cracking depths and intensities can be mirrored in contrasting talus block size spectra (Chapter 7). However, in agreement to Hall (2006), sediments in alpine areas and in particular, small and platy clasts at upper talus segments, need not exclusively derive from frost events. Instead, it must be assumed that repetition of sun-induced thermal cycles, as typical for both southern and northern rock slopes during summer (Figure 6.8, Figure 7.9), can cause thermal fatigue in the outermost bedrock and promote detachments of small flakes, particularly at paragneiss with surface-parallel cleavage (Chapter 8).

Ultimate size of talus material is furthermore influenced by rockwall height and length and associated kinetic energy gained during fall and subsequent block disintegration (Figure 6.4). The probability of fragmentation and small-sized talus material additionally increases on densely banked limestone, as on metamorphic rocks with schistosity (Chapter 7). Block breakage along those pre-existing joints and parallel-arranged minerals after first ground impact can significantly reduce the original block size, as estimated for the Hungerli Peak (Chapter 8).

These findings highlight that, even though rockfalls are the dominant process of sediment delivery on alpine rock slopes, morphology and material of associated talus slopes can vary considerably due to morphometry, rock mechanical conditions, (micro-)climate and weathering activity of source rockwalls. It is therefore argued that source rockwalls must be considered in a more meaningful way when studying rockfall sediment cascades (Figure 9.3). As will be discussed in Section 9.4, our cause-effect reasoning of rockfall sediment fluxes is highly complicated due to the complex and nonlinear variable interplay in rock slope systems Consequently, caution is necessary using specific talus forms and material characteristics as a proxy for rock slope instability and rockfall activity.

9.3.4 The importance of rock slope instability and emergent sediment connectivity in alpine cascading system

A unique landform characteristic of steep, high-alpine terrain is the high proportion of bedrock without significant soil and sediment coverage, as was evident in both study sites of this thesis. Whilst 66% of the land surface in Val Müschauns is made of calcareous bedrock (Table 5.1), paragneiss and limestone rock slopes in the Turtmann Valley account for a quarter of the hanging valley surface (Figure 6.1b). The larger bedrock proportion in Val Müschauns is mainly linked to the two upper, bedrock-dominated hanging valleys (with glacial cirques), representing one third of the total catchment area (Figure 5.7). Contrarily, the Turtmann Valley hosts a significant amount of moraine deposits (Otto and Dikau, 2004). Otto (2009) calculated a postglacial rockwall erosion rate of 0.7-2.2 mm/a for the Turtmann Valley. Long-term rock slope instability and rockfall release resulted in more than 220 talus slopes covering today the lower rock slopes within the hanging valleys accounting for 8.7-12.3% of the tributaries' total sediment volume. Local field mapping in the Hungerli, Brändji and Pipji Valley suggested a talus slope cover of 16% (Figure 6.1a). These observations are consistent with results obtained in Val Münschauns, where talus slopes cover 16% of the total valley area and even 48% of the sediment storage surface (Table 5.1).

These significant proportions of both bedrock and surface coverage of rockfall material in the form of talus slopes highlight that rock slope instability is a prime driver for sediment production and storage of one of the key sediment bodies in high alpine cascading systems. Importantly, this is independent from lithology, geographic and topoclimatic setting given the comparable findings in both contrasting study sites. Moreover, it must be assumed that the percentage of talus coverage estimated in both study sites is likely still underestimated. A significant amount of rockfall material, particularly from small-sized bedrock instability,

might be deposited inside rockwall couloirs, as favoured by the horizontal bedding of the dolomitic rocks in Val Müschauns (Figure 5.2B).

Further downslope, the dominance of rockfall material in alpine valleys influences the overall mode and connectivity of catchment sediment flux. Evidence was provided by toposequence analyses in Val Müschauns, where more than 42% of the potential sediment pathways between rock slopes and stream initiate on talus bodies (Figure 5.5). Similarly, Otto (2006, Table 5.4) estimated that 67% of toposequences in the hanging valleys derive from rockwall-talus systems. In lower basins with high sediment connectivity (Figure 5.8), talus slopes can be a source area for debris flows (Chapter 5) and rock glaciers (Chapter 6), that deliver rockfall material to the fluvial system. However, high connectivity between rockwalls and the fluvial system (or lower valley floor) is mostly the exception rather the rule, in both the Turtmann Valley and Val Müschauns. Most talus slopes are currently disconnected from the overall catchment flux system, e.g. by moraine deposits (Figure 6.1a) or bedrock outcrops (Table 5.2). In Val Müschauns, for example, one third of the basin's sediment trajectories, which includes 68% of talus slopes, do not enter the channel stream. As similar observations were reported in other studies, it appears that in many alpine valleys most of the material detached from unstable rock slopes since LGM and stored in form of talus slopes is still stored within the upper part of alpine sediment cascades. Thus, albeit rock slope instability is one of the most active and erosional processes in alpine settings (Walling and Webb, 1996; Hinderer, 2001), present hillslope-channel connectivity of coarse rockfall material (Chapter 6) can be remarkably limited due to distinct glacial valley morphology (Chapter 5) and low geomorphic process activity (Chapter 3).

Therefore, in support for Hypothesis 5, this thesis provides several examples for the major significance of rock slope instability for alpine sediment cascades, particularly for geomorphic coupling, sediment production and deposition in rockwall-talus systems. However, ***Hypothesis 6*** can be supported only in part. Due to the lack of sediment connectivity between most talus slopes and the fluvial system, it became clear, that the influence of the rock mass is largely restricted to rockwall-talus systems and does often not directly dictate catchment sediment flux at a higher scale. This in turn highlights that the local hillslope-channel connectivity is presently the limiting factor. How long this state of disconnectivity will proceed and how long rock slope instability will lead to gradual filling of alpine basins is uncertain. Yet, it is likely that in response to atmospheric warming both connectivity between rock slopes and the lower basins may increase due to a higher process activity in alpine systems.

9.4 A note on methodology

9.4.1 Evaluation of multi-scale systems approach

Previous research on rock slope instability in alpine environments has been conducted on a wide range of spatial and temporal scales. Equally comprehensive is the range of scientific methods and techniques, by which conditions, causes and effects of rock slope instability are assessed to describe past developments and to predict future evolution. Studies span from GIS modelling using high resolution DTMs of entire alpine valleys or mountain ranges, local field investigations of unstable rockwalls or more commonly, of depositional landforms, over numerical rock stability modelling to laboratory experiments. However, as Chorley et al. (1985, p. 14) pointed out, in most work "*scale* is implicit, rather than explicit". Although Chorley, Schumm and Sudgen originally referred, in general, to geomorphic studies until the late 1980s, this statement applies just as much to rock slope instability research today. Far too often, emphasis is given to the *method* or *technique* to investigate unstable rock slopes, whilst at the same time the scientific justification for the specific choice of investigated scale and the derived cause-effect relationships remains vague. To the author's knowledge, only a few geomorphologists (e.g. Krautblatter, McColl, Fischer, Hartmeyer, Dräbing) have made attempts to study alpine rock slope instability, quantitatively or qualitatively, using an explicit *multi-scale systems approach*.

In Section 3.1 of this thesis, it was hypothesised that investigating rock slope instabilities is both a systemic and methodological question of scale, which can be addressed by hierarchical systems approaches and ergodic reasoning. To test this ***Hypothesis 7***, ***Objective 4*** of this thesis was to (re)develop and apply a hierarchical and holistic methodology that is able to address emergent and non-linear rock slope systems. The previous discussion provides support for ***Hypothesis 7.*** Figure 9.1 demonstrates that different scientific problems of rock slope instability arise depending on the scale of consideration and require different types of scientific explanation. At each spatial and temporal level of rock slope systems, different scientific approaches, different explanatory variables and types of generalisation were needed to explain e.g. controlling factors (Chapter 9.1), destabilising processes and weathering agents (Figure 9.3), rockfall activity after glacier retreat (Section 9.2) and alpine sediment cascades (Section 9.3). Progress has been made to address this scale-dependency and non-linear complexity of rock slope instability in this thesis by means of the multi-scale approach proposed in Section 3.2 and by using ergodic reasoning at different levels of investigations (Chapter 4-7).

To demonstrate more precisely why hierarchical approaches are important and why ergodic reasoning is helpful, it is useful to discuss 'ten ways to be wrong' that a researcher may face when studying rock slopes (Table 9.1). Obviously, the author thereby refers to the thought-provoking book of Stanley Schumm one of the key works for geomorphologists and Earth scientists. In his book, Schumm (1991) explores ten scientific problems associated with reasoning about scale and place (1 to 3), cause-effect relationships (4 and 5) and system responses (6 to 10) of Earth phenomena in order to stress the need of systems approaches rather than an 'accumulation' of scientific methods. Although Schumm did not directly speak about 'multi-scale' research, his ten examples ideally highlight ten reasons why multi-scale systems approaches are needed to study rock slopes. The following section is an attempt to apply Schumm's concept to rock slope systems, as shown in

Table 9.1, by revisiting practical and philosophical problems identified in this work and providing five solutions based on the methodology developed and used in this thesis.

Table 9.1: *Ten ways to be wrong after Schumm (1991) applied to rock slope systems using examples of this thesis. Five practical and philosophical solutions are proposed (see text for further details).*

	Ten ways to be wrong after Schumm (1991)	Examples from rock slope systems	Five practical and philosophical solutions
Space and time	1) Time	• Short data records and measurement periods • Temporal discrepancy between long-term/postglacial rock slope instability and short-term magnitude-frequency pattern • Temporal reversals of short-term depositional talus pattern due to external disturbances such as release of secondary rockfalls	1) Hierarchical spatial ordering
	2) Space	• With increasing space and size, different variables become causal and non-causal, new system properties emerge leading to complex behaviour • While short-term frequency-magnitude pattern of individual rckwalls is controlled by joint spacing and frost cracking depth, these variables become secondary at the valley scale where tectonic layering and glacier retreat dominate large-scale rockfall pattern	2) Scale linkage
	3) Location	• Rock slope instability and sediment flux can highly differ amongst valleys, between neighbouring rock slopes, across one rock slope due to contrasting glaciation history, joint patterns or weathering regimes • Geographic and personal determinism of research findings and measurements	4) Ergodic reasoning
Cause-effect	4) Convergence	• Near-surface frost weathering and sun-induced thermal cycling can both result in shallow bedrock instability and small-sized, flake-line sediment deposits	3) Multiple explanation approaches (abductiv +deductive +inductive reasoning
	5) Divergence	• Deglaciation of rock slopes may rapidly activate shear failure at rock slopes with out-dipping joints, but can have delayed effects at anaclinal slopes with high rock mass strength	
System response	6) Efficiency	• The relative amount of work done during different rockfall events does not automatically represent the relative importance of these events • Although small-scale volumetric ice expansion is insignificant by its own, the efficiency can be enhanced if following a preceding history of rock damage caused by e.g. thermal fatigue (event ordering)	
	7) Multiplicity	• Permafrost degradation and glacial slope steepening can only partially explain timing and magnitude of postglacial rockfall activity. Instead, in combination with morphometric and mechanical rockwall properties, different parts of rock slope are effected.	1) Hierarchical spatial ordering 2) Scale linkage
	8) Singularity	• Each rock slope displays distinct landform, material and process characteristics • Laboratory rock sample can respond slightly differently to weathering simulations and causes 'unwelcomed' scatting in the data set • 3D joint geometry and rock temperatures can highly vary within one alpine valley despite similar tectonic and lithological settings, between neighbouring rockwalls and even across the same rockwall	4) Ergodic reasoning
	9) Sensitivity	• Glacier retreat in response to atmospheric warming (extrinsic threshold) can lead to unbalance between resisting and driving forces and to a sensible and persistent response of rock slopes • Long-term rock weathering under constant conditions (intrinsic threshold) can increase porosity, widen joints and reduce the strength of joints and the rock mass • Path-dependency on tectonic (pre-existing joint pattern) control present-day response of rockwalls	1) Hierarchical spatial ordering
	10) Complexity	• Rock slope systems are inherently complex and behave non-linear due to source of non-linearity such as temporary storage effects (rockfall material within rockwalls), self-reinforcing and self-limiting feedbacks between competitive processes (synergistic weathering agents) or self-organisation (rockfall downslope travel and deposition). • Chaotic and complex mechanical and thermal rock behaviour due to cleavage-dominated anisotropy, joint-dominated anisotropy and valley scale tectonically caused anisotropy.	2)Scale linkage
			5) Field observation

9.4.2 'Ten ways to be wrong' when studying rock slope instability

1) Time

The problem of time is twofold. First, the period of observation is usually too short to get a full record of alpine rock slope instability. Although quantification of present-day variables such as rock temperature or joint pattern appears to be unproblematic, we are typically challenged by inherited and path-dependent variables related to rock slopes' geological, climatic and glacial history (Chapter 4-5, see also Verleysdonk et al., 2011).

Thus, *without* adequate scientific reasoning on time, seasonal field research can yield erroneous conclusions, weathering experiments remain despite accelerated conditions restricted to the laboratory time-scale and DTM-based modelling can display solely a snapshot of alpine valleys.

Another important point stressed by Schumm (1991, p. 37), which became evident in Section 9.2, is that "we deal with physical systems that operate over varying time spans", thus "results obtained during short-time-span studies must be applied with care to the solution of long-time-span problems" – and vice versa. This is particularly true in valleys undergoing deglaciation, where present-day rockfall significantly differ in timing and magnitude (Chapter 6) from long-term rockfall activity after LGM (Chapter 4). While the latter can diminish in various modes after the first peak after glacier retreat, short-term rockfall activity can highly fluctuate around this mean paraglacial rate (Section 9.2). Although it appears therefore easier to focus just on short time spans of rock slope failure, temporary reversals of cause and effect due to external disturbances can lead to methodological dilemma. For example, depletion of internal rockwall storages, as observed in Val Müschauns (Chapter 5), due to secondary rockfalls after intensive rainfalls can modify the 'normal' depositional pattern of talus slopes. Those modifications are usually insignificant on a longer time scale (Krautblatter and Dikau, 2007), but they can be a scientific dilemma if talus material is mapped quantitatively to infer rockfall frequency-magnitude *without* reference to other locations and *without* knowledge about the source rockwall.

2) Space (and emergence)

As with time, rock slope instability varies with spatial scale. It is useful to expand the spatial scale problem by 'emergence', according to Harrison (2001), because as size increases new system properties emerge leading to complex (problem 10) system behaviour of alpine rock slopes. The findings of this thesis (Figure 9.1) highlighted that at different spatial scales, new (and often unknown) combinations of variables become causal or non-causal (see also Schumm and Lichty, 1965). As appropriately commented by Chorley et al. (1985, p.14) this "gives a particular flavour to geomorphic work". For example, although valley-scale rockfall activity is dictated by regional tectonic layering of Alpine nappes and valley climate (Chapter 4), those variables must not provide explanations for magnitude-frequency-pattern on individual rock slopes (Chapter 7). Similarly, although key variables that were determined in full detail in the laboratory (Chapter 8) may work well in a frost cracking modelling for intact rock, their explanation may fail at a higher scale, where the emergence of new system properties lead to complex thermal fluxes and weathering processes (Chapter 6,7). It becomes clear that *without* explicit reasoning on spatial scale, bottom-up or bottom-down approaches are not valid to explain rock slope instability.

3) Location

The problem of location involves the difficulty of extrapolation from one alpine valley or one rock slope to another site. Although alpine areas have typical topo-climatic similarities in common (Barsch and Caine, 1984), rock slope instability and associated sediment flux can differ between two locations due to site-specific glaciation history (Chapter 4,5), contrasting rock mass properties and joint patterns, and different thermal

(weathering) regimes (Chapter 6,7). Schumm (1991) goes even further emphasising the geographic determinism of scientific outcomes. Similarly to Blue and Brierley (2016), who critically note that the researchers' training, knowledge and existing theory, as well as the prevailing social, political and scientific climate determine to a large extent the attributes we finally measure (see also Rhoads and Thorns, 1996).

4) Convergence

As earlier discussed in section 9.3, the problem of convergence is most evident when talus slopes are used as a proxy for rock slope instability. For example, a variety of different rock weathering processes can lead to same shapes and sizes of talus material (convergence). Particularly platy, cm-sized clasts at the talus apex may derive from near-surface frost weathering (Chapter 7), but also thermal fatigue (Chapter 6,8, see also Hall et al., 2002). Similarly, two talus slopes can be dominantly small-sized, although one source rock slope is already adjusted to paraglacial conditions, while postglacial permafrost thaw is the major driver for large-scale failure on the other side (Figure 6.4). However, in the latter case, high-magnitude failures may become 'erased' due to near-vertical slope profiles and intense rockfall fragmentation (Chapter 6).

5) Divergence

At the same time, when similar causes and processes generate different effects, the problem of divergence arises. A snow-rich winter as in 2015 in the Swiss Alps, for instance, can cause constant sub-zero rock temperatures (e.g. Figure 7.9a) and reduced depth of active layer thaw (Luetschg and Haeberli, 2005) due to a thick rockwall snow cover. A thin or lacking snow cover, on the other hand, allows buoyancy-driven convective air ventilation into depth and enhances progressive cooling of the underground (e.g. Figure 7.9b). Likewise, deglaciation of rock slopes may rapidly activate shear failure at rock slopes with out-dipping joints, but the same glacier retreat can have delayed effects at anaclinal slopes with high rock mass strength (Figure 4.9). Thus, conclusion on rockfall activity from talus slopes can be erroneous *without* knowledge about the source rockwall.

6) Efficiency

As the relative amount of work done during different events of rock slope failures does not automatically represent the relative importance of these events, the problem of efficiency arises. Schumm refers here particularly to Wolman and Miller's (1960) magnitude-frequency concept (Chapter 7). The problem of efficiency also accounts for controls and processes on rock slope instability, which can vary significantly in efficiency. For example, although small-scale rock weathering agents such as volumetric ice expansion appear insignificant, the efficiency can be enhanced if following a preceding history of rock damage caused by e.g. thermal fatigue (Chapter 8). Schumm describes this as 'event-ordering' that dictates the efficiency of processes. At the same time, the efficiency of weathering agents can decrease despite constant stresses, for example, due to changing rock porosity (Chapter 8) or joint width, or when rockfall detachment set rockwall systems to 'zero conditions' (see Figure 3b in Viles, 2013b). Similarly, even on presumably efficient slopes with steep slope angles, frozen bedrock condition and high rock mass strength can significantly reduce rockfall efficiency (e.g

Pr1 in Chapter 6). These examples show that without explicit consideration of temporal and configurational context, predictions of magnitude and frequency of rock slope instability can be flawed.

7) Multiplicity

Figure 9.1 demonstrates that rock slope instability results from of a multiplicity of causes and processes that act simultaneously and in combination. Particularly when it comes to understanding paraglacial slope adjustment (Figure 9.2), each individual factor such as permafrost degradation or glacial slope steepening can only partially explain timing and magnitude of postglacial rockfall activity (Chapter 4, see also McColl, 2012). Instead of a *single* key control, different interplays of variables affect different parts of rock slope systems such as rock morphometry, rock mechanics and permafrost degradation (Table 4.3, Table 6.2). Thus, *single* explanations and application of *only one* approach provide only partial answers about causality in non-linear and complex rock slope systems (see problem 10).

8) Singularity

It became clear in Chapter 2 that each rock slope displays distinct landform, material and process characteristics, wherefore the study of rock slope instability is faced with the problem of singularity (Schumm 1991) or 'indeterminacy' (Leopold and Langbein, 1963). This problem arises not just in laboratory experiments, where each rock sample can respond slightly differently to weathering simulations and causes 'unwelcomed' scatter in the entire data set (Chapter 8). Likewise, 3D joint geometry and rock temperatures can highly vary within one alpine valley despite similar tectonic and lithological settings (Chapter 6), between two neighbouring rockwalls (Chapter 7), and even across the same rockwall (Figure 7.6). Singularity does not mean that generalisation of e.g. geotechnical and thermal findings from one rock slope or alpine valley are not valid at other sites. However, *without* explanatory framework of cause-effect relationship, it is difficult to say whether an outlier in a dataset or the specific discontinuity pattern of individual rockwalls is of *general* relevance for rock slope instability.

9) Sensitivity (and path-dependency)

The problem of sensitivity, as described by the concept of Brunsden and Thornes (1979), is evident when rock slopes fail due to internal and external system changes. Any minor change in controls as shown in Figure 9.1 can lead to a crossing of a threshold, so that rock slopes react with 'a sensible, recognisable, sustained but complex response' (Brunsden, 2001, p. 99). In this way, within alpine valleys there are sensitive and insensitive rock slopes depending on extrinsic thresholds such as glacier retreat in response to atmospheric warming (Chapter 4) or intrinsic thresholds. A good example for the latter is long-term rock weathering under constant conditions that can increase porosity (Chapter 8), widen joints and reduce the strength of joints and the rock mass (see also Phillips, 2005). Importantly, rock slope sensitivity can be path-dependent on the system's historicity including past climatic, topographic and tectonic processes (Chapter 4-5, see also Verleysdonk et al., 2011). Therefore, in order to extrapolate past or predict future system responses a consideration of the rock slope system's sensitivity and historical configuration states is necessary (see also Lane and Richards, 1997).

10) Complexity (and non-linearity)

Rock slope systems represent inherently non-linear dynamical systems that are prone to chaotic and complex behaviour (see Viles, 2013b and Phillips, 2005). It makes therefore sense to extend Schumm's problem of complexity by the problem of non-linearity sensu Phillips (2003). Non-linear complexity means that outputs or system responses of rock slopes must not change proportionally to changes in input. Particularly, the anisotropy of rock material causes complex and often chaotic mechanical and thermal behaviour at all scales including the intact rock scale (cleavage-dominated anisotropy in Chapter 8), rockwall scale (joint-dominated anisotropy in Chapter 6, 7) and valley scale (tectonically caused anisotropy in Chapter 4). Further sources of non-linearity are, for example, temporary storage effects of rockfall material within rockwalls (Chapter 4), self-reinforcing and self-limiting feedbacks due to synergistic and competitive weathering agents (Chapter 9), self-organisation of rockfall downslope travel and deposition (Chapter 7). Thus, without acknowledging complex response of rock slope systems to external and internal changes, confident extrapolation and prediction is difficult.

9.5 Practical and philosophical recommendation for future research of unstable rock slopes - five ways to be less wrong

For a more in-depth description of the above-presented problems, the author encourages to read the book of Schumm (1991) and also refers to Rhoads and Thorn (1996). In addition to examples given from this work, there are certainly many more 'pitfalls' of 'how to be wrong' sensu Schumm. Therefore, the research community is called upon to extend this list by further examples from different study sites and scales. However, the brief discussion above already demonstrates that studying rock slope instability implies specific philosophical, theoretical and practical problems that can neither be addressed by a single method or technique, nor by one exclusive explanatory approach. Moreover, Schumm's ten problems are powerful arguments against purely deterministic and reductionist causal laws. "The experiments with which geological history confronts us are not reversible or repeatable", as put in a nutshell by Schumm (1991, p. 4). No matter how detailed a set of variables is used for modelling, laboratory and field studies is, it cannot fully display "the outcome of unsupervised natural experiment of often immense duration", as stressed by Kennedy (2006 p. 5). However, if reductionist approaches are consequently unable to unravel emergent and often contingent rock slope behaviour (see also Gleick, 1997), what alternative research approaches do exist? In fact, there is no universal 'secret recipe' or step-by-step approach to study rock slope instability, but in agreement with Schumm (1991), the awareness for the existence of those scientific barriers in our reasoning is already a significant step forward on the path to better system and process understanding. Nevertheless, to be more specific concerning potential solutions, the methodology of this thesis reveals at least five practical and philosophical ways that helps to improve our understanding of rock slopes instability (Table 9.1):

1) Order your system and think across scales!

First, it became clear that it is inevitable to develop a spatial ordering of rock slope systems. The three-level hierarchical division into intact rock, rockwall (or rockwall-talus scale) and valley, as proposed in Chapter 3 (see also Figure 2.1), can be *one* valuable way. But importantly, its spatiotemporal dimension must be always flexible and adjustable to its entities under study, as discussed in Section 9.1. It is argued that such a hierarchical view, as in Figure 9.1, will help us to *think* across scales. Albeit our object of interest comprises only one particular scale, multi-scale theories and explanations enable us to deal not only with the problem of space and time, but also with the scale-varying multiplicity of controls, complexity and sensitivity of rock slope systems (Table 9.1).

When it comes to investigating each scale, the scientific method itself is less important than the characteristics of the methodology (cf. Schumm, 1991, p. 96). This is not to be understood as an argument against modelling, field and laboratory techniques in general. Both traditional methods and new technological developments with high resolution are of huge value to increase our long-term measurements (see also Viles, 2016), particularly in steep alpine terrain where data are often scarce. In this thesis, for example, the novel model combination of DTM-based multivariate regression and machine learning was a successful tool to decipher regional-scale rockfall susceptibility (Chapter 4). Similarly, rock temperature monitoring over two years by means of miniature data loggers provided high-resolution data, which could further processed in numerical frost cracking modelling (Chapter 6, 7). Likewise, the accelerated two-phase laboratory experiment provided important insights in small-scale rock behaviour under controlled set of variables (Chapter 8). However, the pure application of novel techniques can neither overcome the question of scale, nor the problem of sensitivity, complexity and multiplicity. Although quantification of rock slope instability is essential, it can also 'act to obscure the contextual nature of geomorphic knowledge' as pointed out by Blue and Brierley (2016).

Therefore, we must accept our inability to isolate and capture all potentially relevant factors and, in agreement with Harrison (2001) and Church (1996), and acknowledge qualitative and narrative models in addition to process-based studies. This may particularly encourage low-budget research, but the point made is even stronger. It underlines that we must recognise the importance of scale and emergence. In this research study, each hierarchical and temporal level of rock slope systems required its own scientific explanation on causes, effects and process activity (Section 9.1-9.3). This scale-dependent causality means that we cannot proceed with using bedrock scale findings e.g. from laboratory weathering experiments to extrapolate valley-scale modelling, nor can we apply valley-scale knowledge from e.g. GIS-modelling to predict individual rock slope instability. However, if we acknowledge the epistemological consequences of this scale-dependency, succeed to avoid mixing causalities and system variables from different scales and if we accept a covariance of qualitative and quantitative explanations, than our measurements and observations at different hierarchical scales will highly contribute to better process and system understanding of rock slopes instability.

2) Crack the nut and find one scale link!

Studying rock slope instability is even more challenging when it comes to finding the *link* between temporal and spatial scales. The right question was asked by Sugden et al. (1997, p. 193): "How best does one link small-scale process studies, carried out over time-scales of weeks or a few years, to the larger-scale components of the landscape that have evolved over thousands to millions of years? If geomorphology is to say something useful about the links between short-term processes and large-scale forms, then this is a nut that must be cracked".

Although this nut is still not fully cracked in this thesis, discontinuities of rock slopes have been identified as *one* key link between all scales. In support to ***Hypothesis 8***, particularly in metamorphic bedrock, the orientation of the dominating joint set of individual rockwalls was mirrored (Chapter 6, 7) in a parallel cleavage orientation of intact rock (Chapter 8) and, at a valley scale, in a parallel tectonic bedding orientation (Chapter 4). By using mica schist samples with surface-parallel and -perpendicular cleavage for accelerated weathering simulation it was possible to apply observed small-scale rock damage to natural rock slopes with in- and out-dipping schistosity (Figure 8.1). Although it still remains an observation of a well-controlled laboratory setting with a reductionist set of variables, information about the cleavage orientation allowed more confident conclusions on near-surface rock weathering agents acting in the field (Section 9.1-9.2). The same accounts for large-scale modelling. Using tectonic bedding orientation as a higher-scale modelling parameter of joint orientation (Chapter 4), valley-scale extrapolation and prediction of paraglacial rockfall activity was achieved, which accounts for lower-scale structural pre-defining in alpine valleys (Figure 4.9, Figure 9.1).

The question asked by Sugden et al. (1997) is of major importance in all Earth Science studies and should be equally addressed in rock slope instability research. Admittedly, the scale linkage will be the biggest 'nut to crack' when dealing with scale-dependent rock slope systems. However, researchers are encouraged to find at least *one* key scale link in their specific object of interest. Such a scale linkage will not only help us to approach the problem of spatial and temporal variability of rock failures (Table 9.1). Moreover, it provides a type of semantics that helps us to theoretically and practically bridge the gap between small-scale laboratory, large-scale modelling and natural rock slope systems.

3) Integrate multiple explanations!

The problem of multiplicity demonstrates that there is no exclusive or universal explanation to describe and predict alpine rock slope instability (see also Mosley and Zimpfer, 1976). Instead, a multiple explanation approach is needed (cf. Schumm, 1999). Holistic and integrative rockwall-talus approaches, as proposed in this thesis, have great potential to improve our system understanding of both local rock slope instability (Section 7.3) and valley scale rockfall activity (Section 4.3). Using geomorphometric and material characteristics of talus slopes as proxies for retrospective estimation of potential causes, process responses and efficiencies of rock slopes (Baker, 1996), requires to argue actualistically and to select a range of often narrative hypotheses. Therefore, knowledge on source rockwalls is inevitable for dealing with the problem of 'lucky guessing' associated to convergence and divergence and for minimising the problem of uniformitarism (see Inkpen and Wilson, 2013). Integration of deductive rockwall surveys such as geotechnical joint mapping or rock

temperature monitoring allows for testing the diverse hypotheses derived from talus slopes. Then, talus slopes and regional scale inventory are indeed valuable proxies for rock slope instability. Moreover, abductive talus approaches are of major significance to decrease the degree of reductionism of most process-based rockwall measurements by providing a multiplicity of hypotheses. Instead of favouring one ultimate type of scientific reasoning and rejecting all others, we should proceed to a combination of abductive, deductive and ideally inductive approaches in rock slope instability research (see also Engelhardt and Zimmermann, 1988). It is believed that such a holistic and integrative research design will increase the confidence of our measurements on multiple interacting controls involved in rock slope instability and moreover, allows us to deal with the problem of convergence, divergence and efficiency (Table 9.1).

4) Substitute space for time

Historical information is obviously needed to solve the problem of time. Similarly, the problem of location, sensitivity and complexity can be addressed by following conditions of rock slope instability through time (Schumm 1991, p. 100). However, in most alpine valleys, long time-series and historical data are typically limited. Research of this thesis demonstrated that ergodic reasoning or space-for-time substitution represents a key solution (Peine, 1985). In particular to deal with the lack of information on deglaciation history, spatial sequences of rock slopes between glacier cirque and valley outlet allow interpretation of time sequences of glacier retreat e.g. since the LGM (Chapter 4). If applying those chronosequences with the awareness for historical contingency (Gleick, 1997), they provide valuable means for postdiction of long-time rock slope instability and the changing controls over time (Chapter 4, 6). Ergodic reasoning also indirectly addresses the problem of singularity (Table 9.1), as it involves comparative measurements of a variety of different rock slopes with respect to present conditions. It provides a valuable basis to infer generalised scenarios, as in Figure 9.2, from which not only past, but most importantly, potential future system trajectories can be estimated as in course of on-going atmospheric warming and glacier retreat. Yet, one of its key benefits is certainly that ergodic reasoning allows us to see the 'big picture' of rock slope instability.

5) Come back to the human scale and observe!

It became clear that future research on rock slope instability must involve working at all spatial and temporal scales. Depending upon what problem of rock slope systems is under consideration, laboratory, field and large-scale modelling approaches can each contribute one piece of the puzzle of our knowledge on complex and emergent rock slope systems – or at least, will provide new questions. Due to the scale inter-linkages (Figure 9.1) we *do* need large- and small-scale studies on rock slope instability, but at the end, we need to ask for the *most relevant* scale today. It is argued here that we always need to come back to the 'human scale', where the issue of rock slope instability raises most relevant challenges for society particularly considering on-going climate change (Table 9.1). Moreover, Figure 9.1 emphasises that this is the scale, where most positive and negative feedback can occurs and where the highest degree of non-linearity and complexity is dominant. This is important to state, as, in agreement with Schumm (1991, p. 38), it often appears that geomorphologists work at the wrong spatial and temporal scale for the problem that they want to solve. Inkpen and Wilson (2013, p. 24)

also critically raise the question how large-scale findings of long duration (they specifically refer to Davis' peneplain) can help us to solve landform-related issues such as rock slope stability. As appropriate scale, Schumm (1999, p. 47f) proposes a scale from 1/10 of millimetres to a few kilometres in size and from 1/10 of seconds to a few decades in time.

This thesis provided several examples, where direct field observations were of major significance e.g. to select potential input parameter for multivariate modelling (Chapter 4), to improve DTM-based connectivity modelling by theories about sediment cascades (Chapter 5), to compare rock slopes and exclude singularity (Chapter 6), to decide whether numerical frost cracking is plausible in anisotropic rock slopes (Chapter 6, 7), and to critically interpret laboratory findings (Chapter 8). It is important to emphasise that all findings of this thesis were dependent to large degree on heuristic knowledge obtained during fieldwork and field observations. This highlights again that the data we collect depend not only on measurable variables, but they also reflect our questions, pre-existing theories as well as our knowledge and experience (see also Phillips, 2012a; Blue and Brierley, 2016). Conversely, this means, that we may not need increasingly more detailed parameterization and more sophisticated techniques (cf. Harrison, 2001, p. 333) to ask questions, to decide what we should measure and to train our view for the big picture. Instead, our natural laboratory and the primary source of ideas should be the earth's surface (cf. Phillips 2003, p. 20).

----- BLANK -----

Chapter 10

CONCLUSION AND OUTLOOK

Die Wirklichkeit von der wir sprechen können, ist nie die Wirklichkeit an sich, sondern […] eine von uns gestaltete Wirklichkeit. (Heisenberg, 1989, p. 59)

Faced with the hazard potential and geomorphic importance of rock slopes adjusting to glacier retreat and current climate warming, the motivation of this dissertation was to increase our systemic and process understanding of rock slope instability in alpine geomorphic systems. It was hypothesised that a deeper understanding of rock slope instability can be achieved by thinking across scales and accounting for the emergence of non-linear, complex rock slope systems. For this reason, a novel hierarchical methodological approach has been developed. The methodology integrates multivariate modelling and geomorphic field mapping at the valley-scale, rockwall-scale geotechnical, geomorphological and sedimentological field surveys in the Turtmann Valley and Swiss National Park as well as numerical frost cracking modelling and laboratory weathering simulations at the intact rock scale. By means of this multi-method and, most importantly, multi-scale systems approach, some progress was made towards current research debates about (i) the key controls of rock slope instability in areas affected by glacier retreat, (ii) associated paraglacial and short-term rockfall activity and (iii) their geomorphic consequences for alpine sediment cascade systems. To return to questions posed at the beginning, the research of this thesis emphasises that the questions of:

…*why* rock slopes become instable is a matter of scale and scale interaction. Valley-scale permafrost degradation in the course of glacier retreat after LGM, the path-dependency of historical Alpine tectonic and glacial processes, rockwall-scale properties including rock mass strength, joint spacing, joint orientation and depth-varying frost cracking intensities as well as micro-scale effects of cleavage orientation and rock porosity have been identified as the *key interplay* of scale-dependent controls. Importantly, this work highlighted that a scale-decoupling is not acceptable and can lead to erroneous interpretation. Both, bottom-up and top-down interactions were identified. Thus, scales of rock slope systems *are* interlinked, amongst others, by discontinuities of the rock mass, which in turn results in non-linear and emergent behaviour. While recognising that the set of factors identified here is not all-inclusive, the new hierarchical concept presented in this thesis can assist other scientists in studying rock slope instability as a scale- and time-varying condition in response to complex and non-linear feedbacks between multiple variables *within* and *in-between* scales.

…*when* rock slopes fail after ice removal is a matter of the time-evolving interplay between paraglacial and non-paraglacial or independent and dependent factors. An exhaustion model, as proposed by Cruden and Hu (1993) and Ballantyne (2002), was found to be valid to describe the valley-scale paraglacial rockfall rate. This is associated with the transition from post-LGM permafrost degradation and frost cracking to a non-paraglacial, near-surface rock weathering regime. However, the observations in this thesis also highlighted that the prevailing theory of an exhaustion model needs revision when it comes to accounting for different tectonic and structural conditions of alpine valleys. Different trajectories of paraglacial adjustment were identified, in which post-glacial rockfall activity can evolve either rapidly declining or more linearly dependent on joint orientation and rock mass strength. It was furthermore demonstrated that seasonal to decadal rockfall frequency-magnitude patterns generate fluctuations around the mean postglacial rate, which are largely independent from

paraglacial forcing, but dependent on small-scale thermo-mechanical rockwall properties. The different temporal scenarios of rockfall activity proposed in this thesis can yield direct scientific benefits, as they offer not only an alternative view on our traditional paraglacial framework of sediment fluxes, but can help to evaluate the time-dependent cause-effect relationships of hazardous rockfall events.

…*which role* rock slope instability plays further downslope for alpine sediment cascades requires a refreshed holistic upslope perspective. This thesis provides quantitative and qualitative evidence for the major significance of rock slope instability - particularly in form of small- to medium-sized rockfall events - for sediment production, flux and storage in different lithological, paraglacial and topoclimatic settings. Rockfall deposits originating from rock slope instability account for up to 48% of the sediment storage surface in the studied alpine valleys and currently lead to a gradual filling of upper glacially-shaped basins. Thus, the lack of hillslope-channel connectivity is the present-day limiting, but likely a main future control on the catchment-scale efficiency of sediment fluxes from unstable rock slopes to fluvial systems. As there is a general danger that geomorphic studies place too much attention on sediment storages, rather on their initial source, a revised conceptual framework of alpine sediment cascades is proposed. The framework can be of value for future geomorphic research as it enables to consider the influence of rock slope systems on rockfall size and shape, geomorphic coupling of rockwall-talus systems, talus slopes evolution as well as hillslope-channel connectivity in a more meaningful way, whilst underlining typical scientific pitfalls such as convergence and divergence.

The findings of this thesis, the newly derived and revised concepts as well as the proposed multi-scale methodology are of relevance for geomorphic research in general, and research of alpine rock slope instability in particular. They provide a fresh perspective on cause-effect relationships and temporal dynamics of rock slope instability, which in turn can offer new possibilities to understand and predict downslope consequences for alpine sediment systems. Surely, this work provides just one further piece to the whole puzzle of rock slope instability, whilst still having its own methodological and systemic limitations. This work leaves a lot of new questions. Questions, for instance, about the past occurrence of large-magnitude rock failures in the Turtmann Valley, about the thermal signal stored in jointed rock slopes after permafrost thaw, about inherent small-scale mechanical stresses resulting from past regional glaciation cycles, about the role of sun-induced thermal cycling as rockfall preparatory and triggering factor, about the thermal and mechanical influence of vegetation in jointed rock mass, the role of vegetation for hillslope-channel connectivity of rockfall material and certainly, questions about future trajectories of deglaciated and permafrost-affected rockwalls in course of on-going atmospheric warming.

Therefore, much more work is needed that expands the findings presented in this thesis in different directions. It is believed that Geomorphology as Earth Science discipline has much to offer to current questions about rock slope instability and can significantly contribute to tackle present-day challenges linked to climate warming, glacier retreat and human activity. For that, however, it is more important than ever to raise our eyes up from the low-lying sediments to their source areas and to proceed to increase our research activities on deglaciated and highly sensitive alpine rock slopes. Particularly in populated alpine valleys adjusting to glacier retreat and permafrost degradation, realistic future scenarios for often hazardous catchment sediment fluxes are strongly needed that explicitly recognise the multiplicity and nonlinear interaction of factors and

processes acting on unstable rock slopes. It is encouraging to see that both traditional and novel methods and techniques have an immense potential to help us on this scientific way. They help us to test our hypotheses, to improve our theories and to ask more questions. However, no matter how novel, expensive or detailed the method is that we use, our most valuable gain of knowledge should derive from direct observations, ideally at a 'human scale' relevant for present-day challenges. In this way, it is fundamental to observe and make use of all knowledge, while accepting an unknowability at the same time. It therefore is of utmost importance to address the philosophical and methodological consequences associated with the scale-dependency of geomorphic phenomena such as rock slope instability. Multi-scale approaches with scale-specific causations, ergodic field observations as well as an accepted coexistence of narrative approaches next to process-based studies can be first valuable steps towards a future research agenda.

> *Creating a new theory is not like destroying an old barn and erecting a skyscraper in its place. It is rather like climbing a mountain, gaining new and wider views, discovering unexpected connections between our starting points and its rich environment. But the point from which we started out still exists and can be seen, although it appears smaller and forms a tiny part of our broad view gained by the mastery of the obstacles on our adventurous way up.*
>
> (Einstein and Leopold, 1938, p. 159)

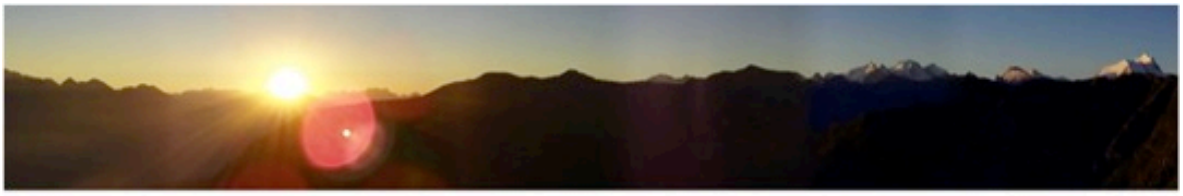

11 REFERENCES

Abele, G., 1972. Kinematik und Morphologie spät- und postglazialer Bergstürze in den Alpen. Zeitschrift für Geomorphologie NF, 14, 138–149.

Abellán, A., Oppikofer, T., Jaboyedoff, M., Rosser, N.J., Lim, M., Lato, M.J., 2014. Terrestrial laser scanning of rock slope instabilities. Earth Surf Proc Land, 39(1), 80–97.

Adhikary, D.P., Dyskin, A.V., Jewell, R.J., Stewart, D.P., 1997. A study of the mechanism of flexural toppling failure of rock slopes. Rock Mech Rock Eng, 30(2), 75-93.

Agliardi, F., Crosta, G.B., 2003. High resolution three-dimensional numerical modelling of rockfalls. International Journal of Rock Mechanics and Mining Sciences, 40(4), 455–471.

Aguilera, A.M., Escabias, M., Valderrama, M.J., 2006. Using principal components for estimating logistic regression with high-dimensional multicollinear data. Computational Statistics & Data Analysis, 50(8), 1905–1924.

Akentuna, M., Kim, S.S., Nazzal, M., Abbas, A.R., Arefin, M.S., 2016. Study of the thermal stress development of asphalt mixtures using the Asphalt Concrete Cracking Device (ACCD). Construction and Building Materials, 114, 416-422.

Åkerman, H., 1984. Notes on Talus Morphology and Processes in Spitsbergen. Geografiska Annaler. Series A, Physical Geography, 66(4), 267-284.

Albjär, G., Rehn, J., Strömquist, L., 1979. Notes on Talus Formation in Different Climates. Geografiska Annaler. Series A, Physical Geography, 61(3/4), 179-185.

Alejano, L.R., Gómez-Márquez, I., Martínez-Alegría, R., 2010. Analysis of a complex toppling-circular slope failure. Eng Geol, 114(1–2), 93-104.

Allen, S., Huggel, C., 2013. Extremely warm temperatures as a potential cause of recent high mountain rockfall. Global and Planetary Change, 107, 59–69.

Allen, S.K., Cox, S.C., Owens, I.F., 2011. Rock avalanches and other landslides in the central Southern Alps of New Zealand: a regional study considering possible climate change impacts. Landslides, 8(1), 33-48.

Allen, S.K., Gruber, S., Owens, I.F., 2009. Exploring steep bedrock permafrost and its relationship with recent slope failures in the Southern Alps of New Zealand. Permafrost and Periglacial Processes, 20(4), 345-356.

Allison, P.D., 2001. Logistic Regression Using the SAS System: Theory and Application. SAS Publishing.

Allison, R.J., Goudie, A.S., 1990. The form of rock slopes in tropical limestone and their association with rock mass strength. Z Geomorphol, 34(2), 129-148.

Amitrano, D., Gruber, S., Girard, L., 2012. Evidence of frost-cracking inferred from acoustic emissions in a high-alpine rock-wall. Earth and Planetary Science Letters., 341–344, 86–93.

Andersen, J.L., Egholm, D.L., Knudsen, M.F., Jansen, J.D., Nielsen, S.B., 2015. The periglacial engine of mountain erosion - Part 1: Rates of frost cracking and frost creep. Earth Surface Dynamics, 3(4), 447–462.

Anderson, P.W., 1972. More Is Different. Science, 177(4047), 393.

Anderson, R.S., 1998. Near-Surface Thermal Profiles in Alpine Bedrock: Implications for the Frost Weathering of Rock. Arctic and Alpine Research, 30(4), 362–372.

Anderson, R.S., Anderson, S.P., 2012. Geomorphology: The Mechanics and Chemistry of Landscapes. Cambridge University Press, Cambridge.

André, M.-F., 1997. Holocene rockwall retreat in Svalbard: A triple-rate evolution. Earth Surf Proc Land, 22(5), 423–440.

André, M.F., 2002. Rates of postglacial rock weathering on glacially scoured outcrops (Abisko–Riksgränsen area, 68°N). Geografiska Annaler: Series A, Physical Geography, 84(3-4), 139-150.

Aoki, H., Matsukura, Y., 2007. A new technique for non-destructive field measurement of rock-surface strength: an application of the Equotip hardness tester to weathering studies. Earth Surf Proc Land, 32(12), 1759-1769.

Aoki, H., Matsukura, Y., 2008. Estimating the unconfined compressive strength of intact rocks from Equotip hardness. Bull Eng Geol Environ, 67(1), 23-29.

Apostolou, E., Agioutantis, Z., Steiakakis, C., 2015. Integrated Evaluation of Rockfall Triggering Mechanism for Road Monitoring. In: G. Lollino, D. Giordan, G.B. Crosta, J. Corominas, R. Azzam, J. Wasowski, N.

Sciarra (Eds.), Engineering Geology for Society and Territory - Volume 2: Landslide Processes. Springer International Publishing, Cham, pp. 1975-1978.

Asteriou, P., Saroglou, H., Tsiambaos, G., 2012. Geotechnical and kinematic parameters affecting the coefficients of restitution for rock fall analysis. International Journal of Rock Mechanics and Mining Sciences, 54, 103-113.

Atkinson, B.K., 1982. Subcritical crack propagation in rocks: theory, experimental results and applications. Journal of Structural Geology, 4(1), 41-56.

Atkinson, P., Jiskoot, H., Massari, R., Murray, T., 1998. Generalized linear modelling in geomorphology. Earth Surface Processes and Landforms, 23(13), 1185-1195.

Augustinus, P.C., 1992. The influence of rock mass strength on glacial valley cross-profile morphometry: A case study from the Southern Alps, New Zealand. Earth Surf Proc Land, 17(1), 39–51.

Augustinus, P.C., 1995. Rock mass strength and the stability of some glacial valley slopes. Z Geomorphol, 39(1), 55-68.

Aydin, A., 2015. ISRM Suggested Method for Determination of the Schmidt Hammer Rebound Hardness: Revised Version. In: R. Ulusay (Ed.), The ISRM Suggested Methods for Rock Characterization, Testing and Monitoring: 2007-2014. Springer International Publishing, Cham, pp. 25–33.

Azzoni, A., La Barbera, G., Zaninetti, A., 1995. Analysis and prediction of rockfalls using a mathematical model. International Journal of Rock Mechanics and Mining Sciences & Geomechanics Abstracts, 32(7), 709-724.

BAFU, 2005. Permafrost map of Switzerland. http://www.bafu.admin.ch/naturgefahren/14186/14801/15607/index.html?lang=de.

Bahr, H.-A., Fischer, G., Weiss, H.-J., 1986. Thermal-shock crack patterns explained by single and multiple crack propagation. Journal of Materials Science, 21, 136–140.

Bai, S.-B., Wang, J., Lü, G.-N., Zhou, P.-G., Hou, S.-S., Xu, S.-N., 2010. GIS-based logistic regression for landslide susceptibility mapping of the Zhongxian segment in the Three Gorges area, China. Geomorphology, 115(1–2), 23-31.

Baker, V.R., 1996. Hypotheses and geomorphological reasoning. In: B.L. Rhoads, C.E. Thorn (Eds.), The scientific Nature of Geomorphology. Wiley, New York, pp. 57–85.

Bakker, J.P., Le Heux, J.W.N., 1947. Theory on central rectilinear recession of slopes, I and II. Koninklijke Nederlandsche Akademie van Wetenschapen, Series B(50), 959–966, 1154–1162.

Bakker, J.P., LeHeux, W.N., 1952. A remarkable new geomorphological law. I. Physical Geography, Series B, 55(4), 399-410.

Balk, R., 1939. Disintegration of glacial cliffs. Journal of Geomorphology, 2, 305–334.

Ballantyne, C.K., 1986. Landslides and slope failures in Scotland: A review. Scot Geogr Mag, 102(3), 134-150.

Ballantyne, C.K., 2002a. A general model of paraglacial landscape response. Holocene, 12(3), 371-376.

Ballantyne, C.K., 2002b. Paraglacial geomorphology. Quaternary Science Reviews, 21(18), 1935-2017.

Ballantyne, C.K., 2003. Paraglacial landform succession and sediment storage in deglaciated mountain valleys: theory and approaches to calibration. Zeitschrift für Geomorphologie Supplement Volumes, 132, 1-18.

Ballantyne, C.K., Benn, D.I., 1994. Paraglacial Slope Adjustment and Resedimentation Following Recent Glacier Retreat, Fabergstolsdalen, Norway. Arctic and Alpine Research, 26(3), 255-269.

Ballantyne, C.K., Harris, C., 1994. The Periglaciation of Great Britain. Cambridge University Press, Cambridge.

Ballantyne, C.K., Stone, J.O., 2013. Timing and periodicity of paraglacial rock-slope failures in the Scottish Highlands. Geomorphology, 186(0), 150-161.

Ballantyne, C.K., Wilson, P., Gheorghiu, D., Rodés, À., 2014. Enhanced rock-slope failure following ice-sheet deglaciation: timing and causes. Earth Surf Proc Land, 39(7), 900–913.

Barlow, J., Lim, M., Rosser, N., Petley, D., Brain, M., Norman, E., Geer, M., 2012. Modeling cliff erosion using negative power law scaling of rockfalls. Geomorphology, 139–140, 416–424.

Barry, R.G., Chorley, R.J., 2010. Atmosphere, weather, and climate. 10th edition. Routledge, New York.

Barsch, D., 1992. Permafrost creep and rockglaciers. Permafrost and Periglacial Processes, 3, 175–188.

Barsch, D., Caine, N., 1984. The nature of mountain geomorphology. Mountain Research and Development, 4(4), 287-298.

Barsch, D., Fierz, H., Haeberli, W., 1979. Shallow core drilling and bore-hole measurements in the permafrost of an active rock glacier near the Grubengletscher, Wallis, Swiss Alps. Arctic and Alpine Research, 215-228.

Barton, N., 1990. Scale effects or sampling bias?, Proc. Int. Workshop Scale Effects in Rock Masses. Balkema Publ., Rotterdam, pp. 31-55.

Barton, N., 2006. Rock quality, seismic velocity, attenuation and anisotropy. Taylor & Francis, UK & Netherlands.

Barton, N., 2013. Shear strength criteria for rock, rock joints, rockfill and rock masses: Problems and some solutions. Journal of Rock Mechanics and Geotechnical Engineering, 5(4), 249-261.

Barton, N., Choubey, V., 1977. The shear strength of rock joints in theory and practice. Rock Mechanics, 10, 1-54.

Bearth, P., 1980. Geologischer Atlas Schweiz 1:25000. Blatt: 1308 St. Niklaus. Erläuterungen, Bern.

Beel, C.R., Orwin, J.F., Holland, P.G., 2011. Controls on slope-to-channel fine sediment connectivity in a largely ice-free valley, Hoophorn Stream, Southern Alps, New Zealand. Earth Surf Proc Land, 36(7), 981-994.

Bell, D.H., 1976. Slope evolution and slope stability, Kawarau valley, Central Otago, New Zealand. Bull Eng Geol Environ, 13, 5-16.

Benda, L., Dunne, T., 1997. Stochastic forcing of sediment supply to channel networks from landsliding and debris flow. Water Resources Research, 33(12), 2849-2863.

Benn, D.I., Evans , D.J.A., 2010. Glaciers and glaciation. Hodder Education, London.

Bennett, G.L., Molnar, P., McArdell, B.W., Burlando, P., 2014. A probabilistic sediment cascade model of sediment transfer in the Illgraben. Water Resources Research, 50(2), 1225-1244.

Bennett, G.L., Molnar, P., McArdell, B.W., Schlunegger, F., Burlando, P., 2013. Patterns and controls of sediment production, transfer and yield in the Illgraben. Geomorphology, 188, 68-82.

Bieniawski, Z.T., 1987. Engineering Rock Mass Classsifications. Wiley & Sons, New York.

Bierman, P.R., Montgomery, D.R., 2013. Key Concepts in Geomorphology. WH Freeman.

Bishop, M.P., James, L.A., Shroder Jr, J.F., Walsh, S.J., 2012. Geospatial technologies and digital geomorphological mapping: Concepts, issues and research. Geomorphology, 137(1), 5-26.

Blackwelder, E., 1933. The insolation hypothesis of rock weathering. American Journal of Science, 26, 97–113

Blikra, L.H., Christiansen, H.H., 2014. A field-based model of permafrost-controlled rockslide deformation in northern Norway. Geomorphology, 208, 34–49.

Blue, B., Brierley, G., 2016. 'But what do you measure?' Prospects for a constructive critical physical geography. Area, 48(2), 190-197.

Böhme, M., Derron, M.H., Jaboyedoff, M., 2014. Quantitative spatial analysis of rockfalls from road inventories: a combined statistical and physical susceptibility model. Nat. Hazards Earth Syst. Sci. Discuss., 2(1), 81-121.

Borgomeo, E., Hebditch, K.V., Whittaker, A.C., Lonergan, L., 2014. Characterising the spatial distribution, frequency and geomorphic controls on landslide occurrence, Molise, Italy. Geomorphology, 226, 148-161.

Borselli, L., Cassi, P., Torri, D., 2008. Prolegomena to sediment and flow connectivity in the landscape: A GIS and field numerical assessment. Catena, 75(3), 268-277.

Bovis, M.J., 1990. Rock-slope deformation at Affliction Creek, southern Coast Mountains, British Columbia. Canadian Journal of Earth Sciences, 27(2), 243-254.

Bozzolo, D., Pamini, R., 1986. Simulation of rock falls down a valley side. Acta Mechanica, 63(1), 113-130.

Brardinoni, F., Hassan, M.A., 2006. Glacial erosion, evolution of river long profiles, and the organization of process domains in mountain drainage basins of coastal British Columbia. Journal of Geophysical Research: Earth Surface, 111(F1), F01013.

Breiman, L., 2001. Random Forests. Machine Learning, 45(1), 5-32.

Brenning, A., 2005. Spatial prediction models for landslide hazards: review, comparison and evaluation. Natural Hazards and Earth System Sciences, 5(6), 853-862.

Brideau, M.-A., Stead, D., 2010. Controls on Block Toppling Using a Three-Dimensional Distinct Element Approach. Rock Mech Rock Eng, 43(3), 241-260.

Brierley, G., Fryirs, K., Jain, V., 2006. Landscape connectivity: the geographic basis of geomorphic applications. Area, 38(2), 165-174.

Brierley, G.J., Hickin, E.J., 1985. The downstream gradation of particle sizes in the Squamish river, British Columbia. Earth Surf Proc Land, 10(6), 597-606.

Broili, L., 1974. Ein Felssturz in Großversuch. Rock Mechanics Suppl., 3.

Brook, M.S., Hutchinson, E., 2008. Application of rock mass classification techniques to weak rock masses: A case study from the Ruahine Range, North Island, New Zealand. Canadian Geotechnical Journal, 45(6), 800-811.

Brown, W.S., Jacobs, H.R., Thompson, R.E., 1972. Thermal Fatigue in Teeth. Journal of Dental Research, 51(2), 461-467.

Brunner, F.K., Scheidegger, A.E., 1973. Exfoliation. Rock Mechanics, 5(1), 43-62.

Brunsden, D., 1996. Geomorphological events and landform change. Zeitschrift für Geomorphologie N.F., 40(3), 273-288.

Brunsden, D., 2001. A critical assessment of the sensitivity concept in geomorphology. Catena, 42(2–4), 99-123.

Brunsden, D., 2004. Relaxation time. In: A. Goudie (Ed.), Encyclopedia of Geomorphology. Routledge, London, pp. 838–840.

Brunsden, D., Kesel, R.H., 1973. Slope development on a Mississippi River Bluff in historic time. The Journal of Geology, 81(5), 576-598.

Brunsden, D., Prior, D.B., 1984. Slope instability. Wiley (John) & Sons, Limited, Chichester.

Brunsden, D., Thornes, J.B., 1979. Landscape sensitivity and change. Transactions of the Institute of British Geographers, 4(4), 463-484.

Büdel, J. (Ed.), 1977. Climatic Geomorphology. Princeton University Press, Princeton, N.J.

Burt, T.P., Allison, R.J., 2010. Sediment cascades an integrated approach. Wiley, Chichester, West Sussex; Hoboken, NJ.

Caine, N., 1967. Texture of talus in Tasmania. Journal of Sedimentary Petrology, 37(3), 796–803.

Caine, N., 1969. The analysis of surface fabrics on talus by means of ground photography. Arctic and Alpine Research, 1(2), 127–134.

Caine, N., 1974. The geomorphic processes of the alpine environment. In: J.D. Ives, R.G. Barry (Eds.), Arctic and Alpine Environments. Methuen, London, pp. 721–748.

Caine, N., 1976. A uniform measure of subaerial erosion. Geological Society of America Bulletin, 87(1), 137–140.

Caine, N., 1982. Toppling failures from alpine cliffs on ben Lomond, Tasmania. Earth Surf Proc Land, 7(2), 133-152.

Caine, N., 1986. Sediment movement and storage on alpine slopes in the Colorado Rocky Mountains. In: A.D. Abrahams (Ed.), Hillslope processes. Allan & Unwin, London, pp. 115–137.

Caine, N., 2001. Geomorphic systems of Green Lakes Valley. In: W.D. Bowman, T.R. Seastedt (Eds.), Structure and Function of an Alpine Ecosystem: Niwot Ridge, Colorado. Oxford University Press, Oxford, pp. 45-74.

Caine, N., Swanson, F.J., 1989. Geomorphic coupling of hillslope and channel systems in two small mountain basins. Z Geomorphol, 33(2), 189–203.

Calcaterra, D., Parise, M., 2010. Weathering as a predisposing factor to slope movements: an introduction. Geological Society, London, Engineering Geology Special Publications, 23(1), 1-4.

Cammeraat, E., van Beek, R., Kooijman, A., 2005. Vegetation succession and its consequences for slope stability in SE Spain. Plant Soil, 278(1-2), 135-147.

Cardozo, N., Allmendinger, R.W., 2013. Spherical projections with OSXStereonet. Computers & Geosciences, 51, 193–205.

Carlsson, A., Olsson, T., 1982. High rock stresses as a consequence of glaciation. Nature, 298(5876), 739-742

Carniel, P., Scheidegger, A.E., 1974. Morphometry of an Alpine scree slope. Revista Italiana di Geografica, 23, 95-100.

Carrara, A., Guzzetti, F., Cardinali, M., Reichenbach, P., 1999. Use of GIS technology in the prediction and monitoring of landslide hazard. Nat Hazards, 20(2-3), 117–135.

Carrea, D., Abellan, A., Derron, M.-H., Jaboyedoff, M., 2015. Automatic Rockfalls Volume Estimation Based on Terrestrial Laser Scanning Data. In: G. Lollino, D. Giordan, B.G. Crosta, J. Corominas, R. Azzam, J. Wasowski, N. Sciarra (Eds.), Engineering Geology for Society and Territory - Volume 2: Landslide Processes. Springer International Publishing, Cham, pp. 425–428.

Carrivick, J.L., Geilhausen, M., Warburton, J., Dickson, N.E., Carver, S.J., Evans, A.J., Brown, L.E., 2013. Contemporary geomorphological activity throughout the proglacial area of an alpine catchment. Geomorphology, 188(0), 83-95.

Carslaw, H.S., Jaeger, J.C., 1986. Conduction of Heat in Solids. Oxford University Press, Oxford.

Carson, M.A., 1977. Angles of repose, angles of shearing resistance and angles of talus slopes. Earth Surface Processes, 2(4), 363-380.

Carson, M.A., Petley, D.J., 1970. The existence of threshold hillslopes in the denudation of the landscape. Transactions of the Institute of British Geographers(49), 71-95.

Catani, F., Lagomarsino, D., Segoni, S., Tofani, V., 2013. Landslide susceptibility estimation by random forests technique: sensitivity and scaling issues. Natural Hazards and Earth System Sciences, 13(11), 2815-2831.

Cavalli, M., Marchi, L., 2008. Characterisation of the surface morphology of an alpine alluvial fan using airborne LiDAR. Natural Hazards and Earth System Sciences, 8(2), 323-333.

Cavalli, M., Trevisani, S., Comiti, F., Marchi, L., 2013. Geomorphometric assessment of spatial sediment connectivity in small Alpine catchments. Geomorphology, 188, 31-41.

Chandler, R.J., 1973. The Inclination of Talus, Arctic Talus Terraces, and Other Slopes Composed of Granular Materials. The Journal of Geology, 81(1), 1-14.

Chau, K.T., Wu, S.Z., Zhu, W.C., Tang, C.A., Yu, T.X., 2003a. Dynamic fracture and fragmentation of spheres, 16th ASCE Engineering Mechanics Conference, University of Washington, Seattle.

Chau, T.K., Wong, C.R.H., Liu, J., Lee, F.C., 2003b. Rockfall Hazard Analysis for Hong Kong Based on Rockfall Inventory. Rock Mech Rock Eng, 36(5), 383–408.

Chen, J., Blume, H.-P., Beyer, L., 2000. Weathering of rocks induced by lichen colonization — a review. Catena, 39(2), 121-146.

Chiverrell, R.C., Foster, G.C., Marshall, P., Harvey, A.M., Thomas, G.S.P., 2009. Coupling relationships: Hillslope–fluvial linkages in the Hodder catchment, NW England. Geomorphology, 109(3–4), 222-235.

Chorley, R., Kennedy, B., 1971. Physical Geography: A Systems Approach. Prentice-Hall, London.

Chorley, R.J., Schumm, S.A., Sudgen, S.E., 1984. Geomorphology. Routledge, London, New York.

Church, M., 1996. Space, time and the mountain: how do we order what we see? In: B.L. Rhoads, C.E. Thorn (Eds.), The Scientific Nature of Geomorphology. Wiley, pp. 147-170.

Church, M., 2010. Mountains and Montane Channels, Sediment Cascades. John Wiley & Sons, Ltd, pp. 17-53.

Church, M., Ryder, J.M., 1972. Paraglacial sedimentation - a consideration of fluvial processes conditioned by glaciation. Geological Society of America Bulletin, 83(10), 3059-3072.

Church, M., Slaymaker, O., 1989. Disequilibrium of Holocene sediment yield in glaciated British Columbia. Nature, 337(6206), 452-454.

Church, M., Stock, R.F., Ryder, J.M., 1979. Contemporary Sedimentary Environments on Baffin Island, N.W.T., Canada: Debris Slope Accumulations. Arctic and Alpine Research, 11(4), 371-401.

Clague, J.J., 1986. The Quaternary stratigraphic record of British Columbia—evidence for episodic sedimentation and erosion controlled by glaciation. Canadian Journal of Earth Sciences, 23(6), 885-894.

Clauser, C., Huenges, E., 2013. Thermal Conductivity of Rocks and Minerals, Rock Physics & Phase Relations. American Geophysical Union, pp. 105-126.

Coe, J.A., Harp, E.L., 2007. Influence of tectonic folding on rockfall susceptibility, American Fork Canyon, Utah, USA. Natural Hazards and Earth System Sciences, 7(1), 1–14.

Collins, B.D., Stock, G.M., 2016. Rockfall triggering by cyclic thermal stressing of exfoliation fractures. Nature Geosci, 9(5), 395-400.

Conacher, A.J., Dalrymple, J.B., 1977. The nine-unit landsurface model: An approach to pedogeomorphic research. Geoderma, 18(1-2), 1-154.

Coombes, M.A., Viles, H.A., Naylor, L.A., La Marca, E.C., 2017. Cool barnacles: Do common biogenic structures enhance or retard rates of deterioration of intertidal rocks and concrete? Science of The Total Environment, 580, 1034-1045.

Copons, R., Vilaplana, J.M., Linares, R., 2009. Rockfall travel distance analysis by using empirical models (Solà d'Andorra la Vella, Central Pyrenees). Nat. Hazards Earth Syst. Sci., 9(6), 2107-2118.

Corenblit, D., Baas, A.C.W., Bornette, G., Darrozes, J., Delmotte, S., Francis, R.A., Gurnell, A.M., Julien, F., Naiman, R.J., Steiger, J., 2011. Feedbacks between geomorphology and biota controlling Earth surface processes and landforms: A review of foundation concepts and current understandings. Earth-Science Reviews, 106(3–4), 307-331.

Corominas, J., 1996. The angle of reach as a mobility index for small and large landslides. Canadian Geotechnical Journal, 33(2), 260-271.

Corominas, J., Copons, R., Moya, J., Vilaplana, J.M., Altimir, J., Amigó, J., 2005. Quantitative assessment of the residual risk in a rockfall protected area. Landslides, 2(4), 343-357.

Corominas, J., Moya, J., 2010. Contribution of dendrochronology to the determination of magnitude–frequency relationships for landslides. Geomorphology, 124(3–4), 137–149.

Cossart, E., 2008. Landform connectivity and waves of negative feedbacks during the paraglacial period, a case study: the Tabuc subcatchment since the end of the Little Ice Age (massif des Ecrins, France). Géomorphologie: relief, processus, environnement(4), 249-260.

Cossart, E., Braucher, R., Fort, M., Bourlès, D.L., Carcaillet, J., 2008. Slope instability in relation to glacial debuttressing in alpine areas (Upper Durance catchment, southeastern France): Evidence from field data and 10Be cosmic ray exposure ages. Geomorphology, 95(1–2), 3-26.

Cossart, E., Mercier, D., Decaulne, A., Feuillet, T., Jónsson, H.P., Sæmundsson, Þ., 2014. Impacts of post-glacial rebound on landslide spatial distribution at a regional scale in northern Iceland (Skagafjörður). Earth Surface Processes and Landforms, 39(3), 336-350.

Coutard, J.P., Francou, B., 1989. Rock temperature measurements in two alpine environments: Implications for frost shattering. Arctic and Alpine Research, 21(4), 399-416.

Crosta, G.B., Agliardi, F., 2004. Parametric evaluation of 3D dispersion of rockfall trajectories. Nat. Hazards Earth Syst. Sci., 4(4), 583-598.

Crozier, M.J. (Ed.), 1989. Landslides: Causes, consequences and environment. Routledge.

Crozier, M.J., Glade, T., 1999. Frequency and magnitude of landsliding. Zeitschrift für Geomorphologie Supplement Volumes, 115, 141–155.

Cruden, D.M., Hu, X.Q., 1993. Exhaustion and steady-state models for predicting landslide hazards in the Canadian Rocky Mountains. Geomorphology, 8, 279–285.

Cruden, D.M., Hu, X.Q., 1994. Topples on underdip slopes in the Highwood-Pass, Alberta, Canada. Q J Eng Geol Hydroge, 27, 57–68.

Cruden, D.M., Hu, X.Q., 1998. Landslides in the Rocky Mountains of Canada. In: J. Kalvoda, C. Rosenfeld (Eds.), Geomorphological Hazards in High Mountain Areas. The GeoJournal Library. Springer Netherlands, pp. 133–148.

Cruden, D.M., Varnes, D.J., 1996. Landslide types and processes, Transportation Research Board, National Research Council, Washington DC.

Curry, A.M., Black, R., 2003. Structure, sedimentology and evolution of rockfall talus, Mynydd Du, south Wales. Proceedings of the Geologists' Association, 114(1), 49-64.

Curry, A.M., Morris, C.J., 2004. Lateglacial and Holocene talus slope development and rockwall retreat on Mynydd Du, UK. Geomorphology, 58(1–4), 85–106.

Cutler, D.R., Edwards, T.C., Beard, K.H., Cutler, A., Hess, K.T., Gibson, J., Lawler, J.J., 2007. Random forests for classification in ecology. Ecology, 88(11), 2783-2792.

D'Amato, J., Hantz, D., Guerin, A., Jaboyedoff, M., Baillet, L., Mariscal, A., 2016. Influence of meteorological factors on rockfall occurrence in a middle mountain limestone cliff. Natural Hazards Earth System Science, 16(3), 719-735.

Dalrymple, J.B., Blong, R.J., Conacher, A.J., 1968. An hypothetical nine unit landsurface model. Zeitschrift für Geomorphologie N.F., 12, 60-76.

Darwin, C.R., 1842. The structure and distribution of coral reefs. Being the first part of the geology of the voyage of the Beagle, under the command of Capt. Fitzroy, R.N. during the years 1832 to 1836. . Smith Elder and Co, London.

Davidson, G.P., Nye, J.F., 1985. A photoelastic study of ice pressure in rock cracks. Cold Regions Science and Technology 11(2), 143–153.

Davies, M.C.R., Hamza, O., Harris, C., 2001. The effect of rise in mean annual temperature on the stability of rock slopes containing ice-filled discontinuities. Permafrost and Periglacial Processes, 12(1), 137-144.

Davies, M.C.R., Hamza, O., Lumsden, B.W., Harris, C., 2000. Laboratory measurement of the shear strength of ice-filled rock joints. Ann Glaciol, 31, 463-467.

Davies, T.R.H., Korup, O., 2010. Sediment Cascades in Active Landscapes, Sediment Cascades. John Wiley & Sons, Ltd, pp. 89-115.

Davis, W.M., 1899. The geographical cycle. Geograph. J., 4, 481–504.

De Blasio, F.V., Sæter, M.-B., 2009. Small-scale experimental simulation of talus evolution. Earth Surf Proc Land, 34(12), 1685–1692.

De Boer, D.H., 1992. Hierarchies and spatial scale in process geomorphology: a review. Geomorphology, 4(5), 303–318.

Dearman, W.R., 1991. Engineering geological mapping. Butterworth - Heinemann Ltd., Oxford.

Deere, D.U., Miller, R.P., 1966. Engineering classification and index properties of rock, Albuquerque.

Delaloye, R., Lambiel, C., 2005. Evidence of winter ascending air circulation throughout talus slopes and rock glaciers situated in the lower belt of alpine discontinuous permafrost (Swiss Alps). Norsk Geografisk Tidsskrift - Norwegian Journal of Geography, 59(2), 194-203.

Delonca, A., Gunzburger, Y., Verdel, T., 2014. Statistical correlation between meteorological and rockfall databases. Natural Hazards and Earth System Sciences, 14(8), 1953–1964.

Derron, M.H., Jaboyedoff, M., Blikra, L.H., 2005. Preliminary assessment of rockslide and rockfall hazards using a DEM (Oppstadhornet, Norway). Nat. Hazards Earth Syst. Sci., 5(2), 285-292.

Deutsch, 1998. The fabric of reality. Penguin, London.

Dietrich, W.E., Dunne, T., 1978. Sediment budget for a small catchment in mountainous terrain. Z Geomorphol, Suppl.-Bd. 29, 191–206.

Dikau, R., 1989. The application of a digital relief model to landform analysis in geomorphology. In: J. Raper (Ed.), Three Dimensional Application of Geographic Information Systems. CRS Press, London, pp. 51–77.

Dikau, R., 1992. Computergestützte Geomorphographie. Habilitationsschrift, University of Heidelberg, Heidelberg, Germany.

Dikau, R., 1993. Geographical information systems as tools in geomorphology. Zeitschrift für Geomorphologie N.F., Suppl.-Bd. 92, 231–239.

Dikau, R., 1994. Computergestützte Geomorphographie und ihre Anwendung in der Regionalisierung des Reliefs. Petermanns Geographische Mitteilungen, 138, 99-114.

Dikau, R., 1996. Geomorphologische Reliefklassifikation und -analyse. Heidelberger Geographische Arbeiten, 104, 15–36.

Dikau, R., 2006. Oberflächenprozesse - ein altes oder ein neues Thema? Geographica Helvetica, 3, 170–180.

Dikau, R., Brunsden, D., Schrott, L., Ibsen, M.-L., 1996a. Landslide Recognition. Identification, Movement and Causes. Wily & Sons, Chichester.

Dikau, R., Schrott, L., Dehn, M., 1996b. Topple. In: R. Dikau, D. Brunsden, L. Schrott, M.-L. Ibsen (Eds.), Landslide Recognition. Identification, Movement and Causes. Wiley & Sons, Chichester, pp. 29-41.

Dixon, J.C., Thorn, C.E., 2005. Chemical weathering and landscape development in mid-latitude alpine environments. Geomorphology, 67(1–2), 127-145.

Domaas, U., 1994. Geometrical methods of calculating rockfall range, Norwegian Geotechnical Institute, Norwegian Geotechnical Institute.

Dorren, L.K.A., 2003. A review of rockfall mechanics and modelling approaches. Prog Phys Geog, 27(1), 69-87.

Dorren, L.K.A., Berger, F., Putters, U.S., 2006. Real-size experiments and 3-D simulation of rockfall on forested and non-forested slopes. Nat. Hazards Earth Syst. Sci., 6(1), 145-153.

Dorren, L.K.A., Seijmonsbergen, A.C., 2003. Comparison of three GIS-based models for predicting rockfall runout zones at a regional scale. Geomorphology, 56(1-2), 49-64.

Douglas, G.R., 1980. Magnitude frequency study of rockfall in Co. Antrim, N. Ireland. Earth Surface Processes, 5(2), 123–129.

Draebing, D., 2014. Influences of snow cover on thermal and mechanical processes in steep permafrost rock walls. PhD thesis, University of Bonn.

Draebing, D., Krautblatter, M., 2012. P-wave velocity changes in freezing hard low-porosity rocks: a laboratory-based time-average model. The Cryosphere, 6(5), 1163–1174.

Draebing, D., Krautblatter, M., Dikau, R., 2014. Interaction of thermal and mechanical processes in steep permafrost rock walls: A conceptual approach. Geomorphology, 226(0), 226–235.

Dramis, F., Govi, M., Guglielmin, M., Mortara, G., 1995. Mountain permafrost and slope instability in the Italian Alps: The Val Pola Landslide. Permafrost and Periglacial Processes, 6(1), 73-81.

Duarte, R.M., Marquinez, J., 2002. The influence of environmental and lithologic factors on rockfall at a regional scale: an evaluation using GIS. Geomorphology, 43(1-2), 117-136.

Duhnforth, M., Anderson, R.S., Ward, D., Stock, G.M., 2010. Bedrock fracture control of glacial erosion processes and rates. Geology, 38(5), 423-426.

Dussauge, C., Grasso, J.-R., Helmstetter, A., 2003. Statistical analysis of rockfall volume distributions: implications for rockfall dynamics. Journal of Geophysical Research B, 108 (B6), 2286.

Dwivedi, R., Singh, P., Singh, T., Singh, D., 1998. Compressive strength and tensile strength of rocks at sub-zero temperature. Indian Journal of Engineering & Materials Sciences, 5, 43–48.

Eberhardt, E., Stead, D., Coggan, J.S., 2004. Numerical analysis of initiation and progressive failure in natural rock slopes—the 1991 Randa rockslide. International Journal of Rock Mechanics and Mining Sciences, 41(1), 69-87.

Eck, H., 1994. Graubünden und Tessin. Von den Gipfeln Rätiens bis in die Sonnenstube der Schweiz. Kohlhammer, Stuttgart.

Edelbro, C., 2003. Rock Mass Strength - A Review. Technical Report, Lulea University of Technology.

EEA, 2009. Regional climate change and adaptation: the Alps facing the challenge of changing water resources., Copenhagen.

Eichel, J., 2016. Biogeomorphic dynamics in the Turtmann glacier forefield, Switzerland. PhD thesis, University of Bonn.

Einstein, A., Leopold, I., 1938. The Evolution of Physics. Cambridge University Press„ Cambridge.

Einstein, H.H., Veneziano, D., Baecher, G.B., O'Reilly, K.J., 1983. The effect of discontinuity persistence on rock slope stability. International Journal of Rock Mechanics and Mining Sciences & Geomechanics Abstracts, 20(5), 227-236.

Eppes, M.-C., Keanini, R., 2017. Mechanical weathering and rock erosion by climate-dependent subcritical cracking. Reviews of Geophysics, 55(2), 470-508.

Eppes, M.-C., Willis, A., Molaro, J., Abernathy, S., Zhou, B., 2015. Cracks in Martian boulders exhibit preferred orientations that point to solar-induced thermal stress. Nature Communications, 6, 6712.

Eppes, M.C., Griffing, D., 2010. Granular disintegration of marble in nature: A thermal-mechanical origin for a grus and corestone landscape. Geomorphology, 117(1–2), 170-180.

Eppes, M.C., Magi, B., Hallet, B., Delmelle, E., Mackenzie-Helnwein, P., Warren, K., Swami, S., 2016. Deciphering the role of solar-induced thermal stresses in rock weathering. Geol Soc Am Bull, 128(9-10), 1315-1338.

Erismann, T.H., Abele, G., 2001. Dynamics of Rockslides and Rockfalls. Springer Berlin Heidelberg, Berlin, Heidelberg.

Escabias, M., Aguilera, A.M., Valderrama, M.J., 2005. Modeling environmental data by functional principal component logistic regression. Environmetrics, 16(1), 95-107.

Escher, H., 1970. Bestimmung der klimatischen Schneegrenze in den Schweizer Alpen. Gegraphica Helvetica, 25, 35-43.

ESRI, 2006. ArcGIS 10.1. Environmental System Research Institute, Inc., Redlands, CA.

Evans, I.S., 2012. Geomorphometry and landform mapping: What is a landform? Geomorphology, 137(1), 94-106.

Evans, R.S., 1981. An analysis of secondary toppling rock failures—the stress redistribution method. Q J Eng Geol Hydroge, 14(2), 77-86.

Evans, S.G., Clague, J.J., 1994. Recent climatic change and catastrophic geomorphic processes in mountain environments. Geomorphology, 10(1-4), 107-128.

Evans, S.G., Clague, J.J., Woodsworth, G.J., Hungr, O., 1989. The Pandemonium Creek rock avalanche, British Columbia. Can Geotech J, 26, 427–446.

Evans, S.G., Hungr, O., 1993. The assessment of rockfall hazard at the base of talus slopes. Can Geotech J, 30(4), 620–636.

Everett, D.H., 1961. The thermodynamics of frost damage to porous solids. Transactions of the Faraday Society, 57(0), 1541–1551.

Fahey, B.D., 1983. Frost action and hydration as rock weathering mechanisms on schist: A laboratory study. Earth Surf Proc Land, 8(6), 535-545.

Fahey, B.D., Dagesse, D.F., 1984. An experimental study of the effect of humidity and temperature variations on the granular disintegration of argillaceous carbonate rocks in cold climates. Arctic and Alpine Research, 16(3), 291–298.

Faulkner, H., 2008. Connectivity as a crucial determinant of badland morphology and evolution. Geomorphology, 100(1–2), 91-103.

Ferrari, F., Thoeni, K., Giacomini, A., Lambert, C., 2016. A rapid approach to estimate the rockfall energies and distances at the base of rock cliffs. Georisk: Assessment and Management of Risk for Engineered Systems and Geohazards, 10(3), 179-199.

Ferri, F., Di Toro, G., Hirose, T., Han, R., Noda, H., Shimamoto, T., Quaresimin, M., de Rossi, N., 2011. Low- to high-velocity frictional properties of the clay-rich gouges from the slipping zone of the 1963 Vaiont slide, northern Italy. Journal of Geophysical Research: Solid Earth, 116(B9), 1-17.

Feuillet, T., Coquin, J., Mercier, D., Cossart, E., Decaulne, A., Jonsson, H.P., Saemundsson, P., 2014. Focusing on the spatial non-stationarity of landslide predisposing factors in northern Iceland: Do paraglacial factors vary over space? Prog Phys Geog, 38(3), 354-377.

Fischer, L., 2010. Slope instabilities on perennially frozen and glacierized rock walls: multi-scale observations, analysis and modelling. PhD thesis, University of Zürich, Zürich, Switzerland.

Fischer, L., Amann, F., Moore, J.R., Huggel, C., 2010. Assessment of periglacial slope stability for the 1988 Tschierva rock avalanche (Piz Morteratsch, Switzerland). Eng Geol, 116(1–2), 32-43.

Fischer, L., Huggel, C., 2008. Methodical design for stability assessments of permafrost affected high-mountain rock walls, Proceedings of the 9th International Conference on Permafrost, Fairbanks, pp. 439-444.

Fischer, L., Kääb, A., Huggel, C., Noetzli, J., 2006. Geology, glacier retreat and permafrost degradation as controlling factors of slope instabilities in a high-mountain rock wall: the Monte Rosa east face. Natural Hazards and Earth System Sciences, 6(5), 761-772.

Fischer, L., Purves, R.S., Huggel, C., Noetzli, J., Haeberli, W., 2012. On the influence of topographic, geological and cryospheric factors on rock avalanches and rockfalls in high-mountain areas. Nat. Hazards Earth Syst. Sci., 12(1), 241-254.

Flageollet, J.-C., Weber, D., 1996. Fall. In: R. Dikau, D. Brunsden, L. Schrott, M.-L. Ibsen (Eds.), Landslide Recognition. Identification, Movement and Causes. Wiley & Sons, Chichester, pp. 13-28.

Folk, R.L., Ward, W.C., 1957. Brazos River bar: a study in the significance of grain size parameters. Journal of Sedimentary Research, 27, 3–26.

Francke, T., Güntner, A., Mamede, G., Müller, E.N., Bronstert, A., 2008. Automated catena-based discretization of landscapes for the derivation of hydrological modelling units. International Journal of Geographical Information Science 22(2), 111-132.

Francou, B., Manté, C., 1990. Analysis of the segmentation in the profile of alpine talus slopes. Permafrost and Periglacial Processes, 1(1), 53-60.

Frattini, P., Crosta, G., Carrara, A., Agliardi, F., 2008. Assessment of rockfall susceptibility by integrating statistical and physically-based approaches. Geomorphology, 94(3–4), 419-437.

Frattini, P., Crosta, G.B., Agliardi, F., 2012. Rockfall characterization and modeling. In: J.J. Clague, D. Stead (Eds.), Landslides: Types, Mechanisms and Modeling. Cambridge University Press, Cambridge, pp. 266-282.

Frayssines, M., Hantz, D., 2006. Failure mechanisms and triggering factors in calcareous cliffs of the Subalpine Ranges (French Alps). Eng Geol, 86(4), 256-270.

Freitas, M.H.d., Watters, R.J., 1973. Some field examples of toppling failure. Géotechnique, 23(4), 495-513.

Fryirs, K., 2013. (Dis)Connectivity in catchment sediment cascades: a fresh look at the sediment delivery problem. Earth Surf Proc Land, 38(1), 30-46.

Fryirs, K., Brierley, G.J., Erskine, W.D., 2012. Use of ergodic reasoning to reconstruct the historical range of variability and evolutionary trajectory of rivers. Earth Surf Proc Land, 37(7), 763-773.

Fryirs, K.A., Brierley, G.J., Preston, N.J., Kasai, M., 2007. Buffers, barriers and blankets: The (dis)connectivity of catchment-scale sediment cascades. Catena, 70(1), 49-67.

Fu, P., Rich, P.M., 2002. A geometric solar radiation model with applications in agriculture and forestry. Computers and Electronics in Agriculture, 37(1–3), 25-35.

García-Ruiz, J.M., Valero-Garcés, B., González-Sampériz, P., Lorente, A., Martí-Bono, C., Beguería, S., Edwards, L., 2001. Stratified scree in the Central Spanish Pyrenees: palaeoenvironmental implications. Permafrost and Periglacial Processes, 12(3), 233-242.

Gardiner, V., Dackombe, R., 1983. Geomorphological Field Manual. Allen & Unwin, London.

Gardner, J., 1970. Rockfall, a geomorphic process in high mountain terrain. Albertan Geogapher, 6, 15–20.

Gardner, J., 1980. Frequency, magnitude, and spatial distribution of mountain rockfalls and rockslides in the Highwood Pass area, Alberta, Canada. In: D.R. Coates, J.D. Vitek (Eds.), Thresholds in geomorphology. Allen and Unwin, London, pp. 267–295.

Gardner, J., 1983. Rockfall frequency and distribution in the Highwood Pass Area, Canadian Rocky Mountains. Z Geomorphol, 27(3), 311–324.

Gardner, J.S., 1972. Morphology and sediment characteristics of mountain debris slopes in the Lake Louise district. Zeitschrift für Geomorphologie, 15, 390-402.

Gärtner-Roer, I., Heinrich, I., Gärtner, H., 2013. Wood anatomical analysis of Swiss willow (Salix helvetica) shrubs growing on creeping mountain permafrost. Dendrochronologia, 31(2), 97–104.

Gerber, E., 1974. Klassifikation von Schutthalden. Geogr. Helv., 29(2-3), 73-82.

Gerber, E., Scheidegger, A.E., 1969. Stress-induced weathering of rock masses. Eclogae geologicae Helvetiae, 62, 401–416.

Giacomini, A., Buzzi, O., Renard, B., Giani, G.P., 2009. Experimental studies on fragmentation of rock falls on impact with rock surfaces. International Journal of Rock Mechanics and Mining Sciences, 46(4), 708–715.

Gilbert, G.K., 1877. Land sculpture. Report on the Geology of the Henry Mountains: Geographical and Geological Survey of the Rocky Mountain Region. U.S. Gov. Print. Office, Washington, D. C.

Gili, J.A., Ruiz, R., Matas, G., Corominas, J., Lantada, N., Nunez, M.A., Mavrouli, O., Buill, F., Moya, J., Prades, A., Moreno, S., 2016. Experimental study on rockfall fragmentation: In situ test design and first results, Landslides and Engineered Slopes. Experience, Theory and Practice. CRC Press, pp. 983–990.

Giordan, D., Manconi, A., Facello, A., Baldo, M., dell'Anese, F., Allasia, P., Dutto, F., 2015. Brief Communication: The use of an unmanned aerial vehicle in a rockfall emergency scenario. Natural Hazards Earth System Science, 15(1), 163–169.

Girard, L., Gruber, S., Weber, S., Beutel, J., 2013. Environmental controls of frost cracking revealed through in situ acoustic emission measurements in steep bedrock. Geophys Res Lett, 40(9), 1748-1753.

Gischig, V.S., Moore, J.R., Evans, K.F., Amann, F., Loew, S., 2011a. Thermomechanical forcing of deep rock slope deformation: 1. Conceptual study of a simplified slope. Journal of Geophysical Research: Earth Surface, 116(F4), 1–17.

Gischig, V.S., Moore, J.R., Evans, K.F., Amann, F., Loew, S., 2011b. Thermomechanical forcing of deep rock slope deformation: 2. The Randa rock slope instability. Journal of Geophysical Research: Earth Surface, 116(F4), 1–17.

Glade, T., Crozier, M.J., 2005. The Nature of Landslide Hazard Impact, Landslide Hazard and Risk. John Wiley & Sons, Ltd, pp. 41-74.

Gleick, J., 1997. Chaos: Making a New Science. Vintage; New Ed edition, London.

Glover, J., Bartelt, P., Christen, M., Gerber, W., 2015. Rockfall-Simulation with Irregular Rock Blocks. In: G. Lollino, D. Giordan, G.B. Crosta, J. Corominas, R. Azzam, J. Wasowski, N. Sciarra (Eds.), Engineering Geology for Society and Territory - Volume 2: Landslide Processes. Springer International Publishing, Cham, pp. 1729-1733.

Gobiet, A., Kotlarski, S., Beniston, M., Heinrich, G., Rajczak, J., Stoffel, M., 2014. 21st century climate change in the European Alps—A review. Science of The Total Environment, 493, 1138-1151.

Godard, A., 1965. Recherches en géomorphologie en Écosse du Nord-Ouest. Thèse d'État, 701 pp.

Gokceoglu, C., Sonmez, H., Ercanoglu, M., 2000. Discontinuity controlled probabilistic slope failure risk maps of the Altindag (settlement) region in Turkey. Eng Geol, 55(4), 277-296.

Gold, L.W., Lachenbruch, A.H., 1973. Thermal conditions in permafrost: A Review of North American literature. 3-25.

Gómez-Heras, M., Smith, B.J., Fort, R., 2006. Surface temperature differences between minerals in crystalline rocks: Implications for granular disaggregation of granites through thermal fatigue. Geomorphology, 78(3–4), 236-249.

Gómez-Heras, M., Smith, B.J., Fort, R., 2008. Influence of surface heterogeneities of building granite on its thermal response and its potential for the generation of thermoclasty. Environmental Geology, 56(3), 547-560.

Goodman, R.E., 1964. The resolution of stresses in rock using stereographic projection. International Journal of Rock Mechanics and Mining Sciences & Geomechanics Abstracts, 1(1), 93-103.

Goodman, R.E., 1989. Introduction to Rock Mechanics, Second edition. Willey & Sons.

Goodman, R.E., Bray, J.W., 1976. Toppling of Rock Slopes, Proc. Specialty Conference on Rock Engineering for Foundations and Slopes. ASCE, Boulder, Colorado, pp. 201-234.

Goodrich, L.E., 1982. The influence of snow cover on the ground thermal regime. Canadian Geotechnical Journal, 19(4), 421–432.

Götz, J., Krisai, R., Schrott, L., 2013. Postglacial sediment storage and rockwall retreat in a semi-closed inner-Alpine sedimentary basin (Gradenmoos, Hohe Tauern, Austria). Geografia Fisica e Dinamica Quaternaria, 36, 63-80.

Goudie, A., 1981. Geomorphological Techniques. Allen & Unwin, London.

Goudie, A.S. (Ed.), 2004. Encyclopedia of Geomorphology, Volume 1, A–I. Routledge.

Graham, M.H., 2003. Confronting multicollinearity in ecological muliple regression. Ecology, 84(11), 2809-2815.

Grämiger, L.M., Moore, J.R., Gischig, V.S., Ivy-Ochs, S., Loew, S., 2017. Beyond debuttressing: Mechanics of paraglacial rock slope damage during repeat glacial cycles. Journal of Geophysical Research: Earth Surface, n/a-n/a.

Griggs, D.T., 1936. The Factor of Fatigue in Rock Exfoliation. The Journal of Geology, 44(7), 783-796.

Gruber, S., 2005. Mountain Permafrost: Transient Spatial Modelling, Model Verification and the Use of Remote Sensing. PhD, University of Zurich, Zürich.

Gruber, S., Haeberli, W., 2007. Permafrost in steep bedrock slopes and its temperature-related destabilization following climate change. Journal of Geophysical Research-Earth Surface, 112(F2).

Gruber, S., Hoelzle, M., Haeberli, W., 2004a. Permafrost thaw and destabilization of Alpine rock walls in the hot summer of 2003. Geophys Res Lett, 31(13), n/a-n/a.

Gruber, S., Hoelzle, M., Haeberli, W., 2004b. Rock-wall temperatures in the Alps: modelling their topographic distribution and regional differences. Permafrost and Periglacial Processes, 15(3), 299–307.

Gruber, S., Peter, M., Hoelzle, M., Woodhatch, I., Haeberli, W., 2003. Surface temperatures in steep alpine rock faces – A strategy for regional-scale measurement and modelling. In: M. Phillips, M.S. Springman, L.U. Arenson (Eds.), Permafrost. Proceedings 8th International Conference on Permafrost, 21-25 July, Zurich, Switzerland, pp. 325-330.

Gubler, S., Fiddes, J., Keller, M., Gruber, S., 2011. Scale-dependent measurement and analysis of ground surface temperature variability in alpine terrain. The Cryosphere, 5(2), 431–443.

Gudmundsson, G.H., 1994. An order-of-magnitude estimate of the current uplift-rates in Switzerland caused by the Würm alpine deglaciation. Eclogae geologicae Helvetiae, 87(2), 545-557.

Guerin, A., Rossetti, J.-P., Hantz, D., Jaboyedoff, M., 2013. Estimating rock fall frequency in a limestone cliff using LIDAR measurements, First International Conference on Landslides Risk, Tabarka, Tunisia, pp. 293–301.

Günther, A., Wienhöfer, J., Konietzky, H., 2012. Automated mapping of rock slope geometry, kinematics and stability with RSS-GIS. Nat Hazards, 61(1), 29–49.

Gunzburger, Y., Merrien-Soukatchoff, V., 2011. Near-surface temperatures and heat balance of bare outcrops exposed to solar radiation. Earth Surf. Process. Landf., 36, 1577–1589.

Gunzburger, Y., Merrien-Soukatchoff, V., Guglielmi, Y., 2005. Influence of daily surface temperature fluctuations on rock slope stability: case study of the Rochers de Valabres slope (France). International Journal of Rock Mechanics and Mining Sciences, 42(3), 331-349.

Günzel, F., 2008. Shear strength of ice-filled rock joints, Proceedings of the 9th international conference on permafrost, 29 Jun - 03 Jul 2008, Fairbanks, Alaska, USA, pp. 581–586.

Guthrie, R.H., Evans, S.G., 2004. Magnitude and frequency of landslides triggered by a storm event, Loughborough Inlet, British Columbia. Natural Hazards Earth System Science, 4(3), 475–483.

Guthrie, R.H., Evans, S.G., 2007. Work, persistence, and formative events: The geomorphic impact of landslides. Geomorphology, 88(3–4), 266–275.

Guzzetti, F., Carrara, A., Cardinali, M., Reichenbach, P., 1999. Landslide hazard evaluation: a review of current techniques and their application in a multi-scale study, Central Italy. Geomorphology, 31(1-4), 181–216.

Guzzetti, F., Reichenbach, P., Wieczorek, G.F., 2003. Rockfall hazard and risk assessment in the Yosemite Valley, California, USA. Nat. Hazards Earth Syst. Sci., 3(6), 491-503.

Haberkorn, A., Hoelzle, M., Phillips, M., Kenner, R., 2015a. Snow as a driving factor of rock surface temperatures in steep rough rock walls. Cold Regions Science and Technology, 118, 64–75.

Haberkorn, A., Phillips, M., Kenner, R., Rhyner, H., Bavay, M., Galos, S.P., Hoelzle, M., 2015b. Thermal Regime of Rock and its Relation to Snow Cover in Steep Alpine Rock Walls: Gemsstock, Central Swiss Alps. Geografiska Annaler: Series A, Physical Geography, 97(3), 579-597.

Haeberli, W., 1992. Construction, environmental problems and natural hazards in periglacial mountain belts. Permafrost and Periglacial Processes, 3(2), 111-124.

Haeberli, W., Beniston, M., 1998. Climate Change and Its Impacts on Glaciers and Permafrost in the Alps. Ambio, 27(4), 258-265.

Haeberli, W., Hallet, B., Arenson, L., Elconin, R., Humlum, O., Kääb, A., Kaufmann, V., Ladanyi, B., Matsuoka, N., Springman, S., 2006. Permafrost creep and rock glacier dynamics. Permafrost and periglacial processes, 17(3), 189-214.

Haeberli, W., Rickenmann, D., Zimmermann, M., Rösli, U., 1990. Investigation of 1987 debris flows in the Swiss Alps: general concept and geophysical soundings. IAHS Publication, 194, 303-310.

Haeberli, W., Wegmann, M., Vonder Muhll, D., 1997. Slope stability problems related to glacier shrinkage and permafrost degradation in the Alps. Eclogae Geologicae Helvetiae, 90(3), 407-414.

Hales, T.C., Roering, J.J., 2005. Climate-controlled variations in scree production, Southern Alps, New Zealand. Geology, 33(9), 701–704.

Hales, T.C., Roering, J.J., 2007. Climatic controls on frost cracking and implications for the evolution of bedrock landscapes. Journal of Geophysical Research: Earth Surface, 112(F2), F02033.

Hales, T.C., Roering, J.J., 2009. A frost "buzzsaw" mechanism for erosion of the eastern Southern Alps, New Zealand. Geomorphology, 107(3-4), 241–253.

Hall, K., 1988. A laboratory simulation of rock breakdown due to freeze-thaw in a maritime Antarctic environment. Earth Surf Proc Land, 13(4), 369-382.

Hall, K., 1997. Rock Temperatures and Implications for Cold Region Weathering. I: New Data from Viking Valley, Alexander Island, Antarctica. Permafrost and Periglacial Processes, 8(1), 69-90.

Hall, K., 1999. The role of thermal stress fatigue in the breakdown of rock in cold regions. Geomorphology, 31(1–4), 47-63.

Hall, K., 2006. Perceptions of rock weathering in cold regions: a discussion on space and time attributes of scale. Geomorphologie(3), 187-196.

Hall, K., André, M.-F., 2001. New insights into rock weathering from high-frequency rock temperature data: an Antarctic study of weathering by thermal stress. Geomorphology, 41(1), 23-35.

Hall, K., André, M.-F., 2003. Rock thermal data at the grain scale: applicability to granular disintegration in cold environments. . Earth Surf. Process. Landf., 28, 823–836.

Hall, K., Guglielmin, M., Strini, A., 2008. Weathering of granite in Antarctica: I. Light penetration into rock and implications for rock weathering and endolithic communities. Earth Surf Proc Land, 33(2), 295-307.

Hall, K., Hall, A., 1996. Weathering by wetting and drying: Some experimental results. Earth Surf Proc Land, 21, 365–376.

Hall, K., Hall, J., Arocena, J., Boelhouwers, Z., Liping, 2005. The influence of aspect on the biological weathering of granites: observations from the Kunlun Mountains, China. Geomorphology, 67(1), 171-188.

Hall, K., Otte, W., 1990. Observations regarding biological weathering on nunataks of the Juneau Icefield, Alaska. Permafrost and Periglacial Processes, 1, 189–196.

Hall, K., Thorn, C., 2011. The historical legacy of spatial scales in freeze–thaw weathering: Misrepresentation and resulting misdirection. Geomorphology, 130(1–2), 83-90.

Hall, K., Thorn, C., Sumner, P., 2012. On the persistence of 'weathering'. Geomorphology, 149, 1-10.

Hall, K., Thorn, C.E., 2014. Thermal fatigue and thermal shock in bedrock: An attempt to unravel the geomorphic processes and products. Geomorphology, 206, 1-13.

Hall, K., Thorn, C.E., Matsuoka, N., Prick, A., 2002. Weathering in cold regions: some thoughts and perspectives. Prog Phys Geog, 26(4), 577-603.

Hallet, B., 2006. Why Do Freezing Rocks Break? Science, 314(5802), 1092–1093.

Hallet, B., Walder, J.S., Stubbs, C.W., 1991. Weathering by segregation ice growth in microcracks at sustained subzero temperatures: Verification from an experimental study using acoustic emissions. Permafrost and Periglacial Processes, 2(4), 283-300.

Halliday, G.S., 2010. Large-scale toppling of schist in North-west Otago, Southern Alps, NZ; a precursor to rockslides and rock avalanches. , Geologically Active - 11th Congress of the International Association for Engineering geology and the Environment, Auckland, New Zealand.

Hamés, V., Lautridou, J.P., Ozer, A., Pissart, A., 1987. Variations dilatométriques de roches soumises à des cycles 'humidification – séchage'. Géographie physique et quaternaire XLI, 345–354.

Han, J.C., 2007. Thermal shock resistance of ceramic coatings. Acta Materialia, 55(10), 3573-3581.

Harbor, J.M., 1992. Numerical modeling of the development of U-shaped valleys by glacial erosion. Geological Society of America Bulletin, 104(10), 1364-1375.

Harker, A., 1904. The Tertiary Igneous Rocks of Skye. Memoirs of the Geological survey of the United Kingdom, 560. H. M. Stationery off., by J. Hedderwick & sons, Glasgow.

Harker, A., 1905. Ice erosion in the Cuillin Hills, Skye Transactions of the Royal Society of Edinburgh, 40(2), 221-252.

Harris, C., 2005. Climate Change, Mountain Permafrost Degradation and Geotechnical Hazard. In: U. Huber, H.M. Bugmann, M. Reasoner (Eds.), Global Change and Mountain Regions. Advances in Global Change Research. Springer Netherlands, pp. 215-224.

Harris, C., Arenson, L.U., Christiansen, H.H., Etzelmüller, B., Frauenfelder, R., Gruber, S., Haeberli, W., Hauck, C., Hölzle, M., Humlum, O., Isaksen, K., Kääb, A., Kern-Lütschg, M.A., Lehning, M., Matsuoka, N., Murton, J.B., Nötzli, J., Phillips, M., Ross, N., Seppälä, M., Springman, S.M., Vonder Mühll, D., 2009. Permafrost and climate in Europe: Monitoring and modelling thermal, geomorphological and geotechnical responses. Earth-Science Reviews, 92(3–4), 117-171.

Harris, C., Haeberli, W., Vonder Mühll, D., King, L., 2001. Permafrost monitoring in the high mountains of Europe: the PACE Project in its global context. Permafrost and Periglacial Processes, 12(1), 3-11.

Harris, C., Vonder Mühll, C., Isaksen, K., Haeberli, W., Sollid, J.L., King, L., Holmlund, P., Dramis, F., Gugliemin, M., Palacios, D., 2003. Warming permafrost in European mountains. Global and Planetary Change, 39, 215–225.

Harrison, S., 2001. On reductionism and emergence in geomorphology. Transactions of the Institute of British Geographers, 26(3), 327–339.

Harshberger, J.W., 1929. The Vegetation of the Screes, or Talus Slopes of Western North America. Proceedings of the American Philosophical Society, 68(1), 13–25.

Hartmann-Brenner, D.C., 1974. Ein Beitrag zum Problem der Schutthaldenentwicklung an Beispielen des Schweizerischen Nationalparks und Spitzbergens PhD thesis, University of Zürich, 134 pp.

Hartmeyer, I., Keuschnig, M., Schrott, L., 2012. A scale-oriented approach for the long-term monitoring of ground thermal conditions in permafrost-affected rock faces, Kitzsteinhorn, Hohe Tauern Range, Austria. Austrian Journal of Earth Science, 105(2), 128-139.

Harvey, A.M., 2001. Coupling between hillslopes and channels in upland fluvial systems: implications for landscape sensitivity, illustrated from the Howgill Fells, northwest England. Catena, 42(2–4), 225-250.

Harvey, A.M., 2002. Effective timescales of coupling within fluvial systems. Geomorphology, 44(3–4), 175-201.

Harvey, A.M., 2010. Local Buffers to the Sediment Cascade: Debris Cones and Alluvial Fans, Sediment Cascades. John Wiley & Sons, Ltd, pp. 153-180.

Harvey, A.M., 2012. The coupling status of alluvial fans and debris cones: a review and synthesis. Earth Surf Proc Land, 37(1), 64-76.

Hasler, A., Geertsema, M., Foord, V., Gruber, S., Noetzli, J., 2015. The influence of surface characteristics, topography and continentality on mountain permafrost in British Columbia. The Cryosphere, 9(3), 1025-1038.

Hasler, A., Gruber, S., Font, M., Dubois, A., 2011a. Advective heat transport in frozen rock clefts: Conceptual model, laboratory experiments and numerical simulation. Permafrost and Periglacial Processes, 22(4), 378–389.

Hasler, A., Gruber, S., Haeberli, W., 2011b. Temperature variability and offset in steep alpine rock and ice faces. The Cryosphere, 5(4), 977-988.

Hasselman, D.P.H., 1969. Unified Theory of Thermal Shock Fracture Initiation and Crack Propagation in Brittle Ceramics. Journal of the American Ceramic Society, 52(11), 600-604.

Heckmann, T., Hilger, L., Meßenzehl, K., Hoffmann, T., Schwanghart, W., Götz, J., Buckel, J., 2014. Network analysis of sediment cascades derived from digital geomorphological maps – a comparative study of three catchments in the Austrian and Swiss Alps. Geophysical Research Abstracts, 16(EGU2014-11452, 2014).

Heckmann, T., Hilger, L., Vehling, L., Becht, M., 2016. Integrating field measurements, a geomorphological map and stochastic modelling to estimate the spatially distributed rockfall sediment budget of the Upper Kaunertal, Austrian Central Alps. Geomorphology, 260, 16-31.

Heckmann, T., Schwanghart, W., 2013. Geomorphic coupling and sediment connectivity in an alpine catchment — Exploring sediment cascades using graph theory. Geomorphology, 182(0), 89-103.

Heim, A., 1932. Bergsturz und Menschenleben. Beiblatt zur Viertelsjahrschrift der Naturforschenden Gesellschaft Zürich(77), 1–218.

Heisenberg, W., 1989. Ordnung der Wirklichkeit. Piper Verlag, München.

Hencher, S.R., Lee, S.G., Carter, T.G., Richards, L.R., 2011. Sheeting joints: Characterisation, shear strength and engineering. Rock Mech Rock Eng, 44(1), 1-22.

Hengl, T., Reuter, H.I., 2009. Geomorphometry: Concepts, Software, Applications. Developments in Soil Science, 33. Elsevier, Amsterdam.

Hétu, B., 1995. Le litage des Éboulis Stratifiés Cryonivaux en Gaspésie (Québec, Canada): Rŏle de la Sédimentation Nivéo-Éolienne et des Transits Supranivaux. Permafrost and Periglacial Processes, 6(2), 147-171.

Hétu, B., Gray, J.T., 2000. Effects of environmental change on scree slope development throughout the postglacial period in the Chic-Choc Mountains in the northern Gaspé Peninsula, Québec. Geomorphology, 32(3–4), 335-355.

Hewitt, K., Clague, J.J., Orwin, J.F., 2008. Legacies of catastrophic rock slope failures in mountain landscapes. Earth-Science Reviews, 87(1), 1-38.

Hinchliffe, S., 1999. Timing and significance of talus slope reworking, Trotternish, Skye, northwest Scotland. The Holocene, 9(4), 483-494.

Hinchliffe, S., Ballantyne, C.K., 1999. Talus accumulation and rockwall retreat, Trotternish, Isle of Skye, Scotland. Scottish Geographical Journal, 115(1), 53-70.

Hinderer, M., 2001. Late Quaternary denudation of the Alps, valley and lake fillings and modern river loads. Geodin. Acta, 14(4), 231-263.

Hipp, T., Etzelmüller, B., Westermann, S., 2014. Permafrost in Alpine Rock Faces from Jotunheimen and Hurrungane, Southern Norway. Permafrost and Periglacial Processes, 25(1), 1-13.

Hoek, E., Bray, J.W., 1981. Rock Slope Engineering, Revised 3rd edition. The Institution of Mining and Metallurgy, London.

Hoek, E., Brown, E.T., 1997. Practical estimates of rock mass strength. International Journal of Rock Mechanics and Mining Sciences, 34(8), 1165-1186.

Hoffmann, T., Müller, T., Johnson, E.A., Martin, Y., 2014a. Impact of glaciations on the Interglacial sediment fluxes. Journal of Geophysical Research F: Earth Surface.

Hoffmann, T., Müller, T., Johnson, E.A., Martin, Y.E., 2013. Postglacial adjustment of steep, low-order drainage basins, Canadian Rocky Mountains. Journal of Geophysical Research: Earth Surface, 118(4), 2013JF002846.

Hoffmann, T., Schrott, L., 2002. Modelling sediment thickness and rockwall retreat in an Alpine valley using 2D-seismic refraction (Reintal, Bavarian Alps). Zeitschrift für Geomorphologie N.F., Suppl.-Bd. 127, 153-173.

Hoffmann, U., Hoffmann, T., Johnson, E.A., Kuhn, N.J., 2014b. Assessment of variability and uncertainty of soil organic carbon in a mountainous boreal forest (Canadian Rocky Mountains, Alberta). Catena, 113(0), 107-121.

Höllermann, P., 1983. Verbreitung und Typisierung der Glatthänge. In: H. Poser, E. Schunke (Eds.), Mesoformen des Reliefs im heutigen Periglazialraum. Abhandlungen der Akademie der Wissenschaften zu Göttingen, Göttingen, pp. 241-260.

Holm, K., Bovis, M., Jakob, M., 2004. The landslide response of alpine basins to post-Little Ice Age glacial thinning and retreat in southwestern British Columbia. Geomorphology, 57(3–4), 201-216.

Holm, K., Jakob, M., 2009. Long rockfall runout, Pascua Lama, Chile. Canadian Geotechnical Journal, 46(2), 225-230.

Hooke, J., 2003. Coarse sediment connectivity in river channel systems: a conceptual framework and methodology. Geomorphology, 56(1–2), 79-94.

Hörsch, B., 2002. Zusammenhang zwischen Vegetation und Relief in alpinen Einzugsgebieten des Wallis (Schweiz). Ein multiskaliger GIS- und Fernerkundungsansatz. Ph.D. Thesis, Rheinische Friedrich-Wilhelms-Universität, Bonn.

Hosmer, D.W., Lemeshow, S., 2005. Multiple Logistic Regression. Applied Logistic Regression. John Wiley & Sons, Inc.

Hsü, K.J., 1975. Catastrophic Debris Streams (Sturzstroms) Generated by Rockfalls. Geological Society of America Bulletin, 86(1), 29-140.

Huggel, C., Clague, J.J., Korup, O., 2012. Is climate change responsible for changing landslide activity in high mountains? Earth Surf Proc Land, 37(1), 77-91.

Hungr, O., Evans, S.G. (Eds.), 1988. Engineering Evaluation of Fragmental Rockfall Hazards. Proceedings of the 5th International Symposium on Landslides, 1. Balkema.

Hungr, O., Evans, S.G., Harzard, J., 1999. Magnitude and frequency of rock falls and rock slides along the main transportation corridors of southwestern British Columbia. Can Geotech J, 36(2), 224-238.

Hungr, O., Leroueil, S., Picarelli, L., 2014. The Varnes classification of landslide types, an update. Landslides, 11(2), 167-194.

Inkpen, R., Wilson, W., 2013. Science, philosophy and physical geography. Routledge, United Kingdom.

IPCC, 2014. Climate Change 2014: Synthesis Report. Contribution of Working Groups I, II and III to the Fifth Assessment Report of the Intergovernmental Panel on Climate Change [Core Writing Team, R.K. Pachauri and L.A. Meyer (eds.)]. Geneva, Switzerland.

Ishikawa, M., Kurashige, Y., Hirakawa, K., 2004. Analysis of crack movements observed in an alpine bedrock cliff. Earth Surf Process Landforms, 29, 883–891.

ISRM, 1978. International Society of Rock Mechanics, Commission on Standardisation of Laboratory and Field Tests: Suggested methods for the quantitative description of discontinuities in rock mass. . International Journal of Rock Mechanics and Mining Sciences and Geomechanical Abstracts, 15(6), 319–368.

Iverson, R.M., 1997. The physics of debris flows. Reviews of Geophysics, 35(3), 245-296.

Ivy-Ochs, S., Kerschner, H., Maisch, M., Christl, M., Kubik, P.W., Schlüchter, C., 2009. Latest Pleistocene and Holocene glacier variations in the European Alps. Quaternary Science Reviews, 28(21–22), 2137–2149.

Jaboyedoff, M., Couture, R., Locat, P., 2009. Structural analysis of Turtle Mountain (Alberta) using digital elevation model: Toward a progressive failure. Geomorphology, 103(1), 5-16.

Jaboyedoff, M., Labiouse, V., 2011. Technical Note: Preliminary estimation of rockfall runout zones. Nat. Hazards Earth Syst. Sci., 11(3), 819-828.

Jaboyedoff, M., Metzger, R., Oppikofer, T., Couture, R., Derron, M.H., Locat, J., Turmel, D., 2007. New insight techniques to analyze rock-slope relief using DEM and 3D-imaging cloud points, Rock Mechanics: Meeting Society's Challenges and Demands, Two Volume Set. Taylor & Francis, pp. 61-68.

Jäckli, H., 1957. Gegenwartsgeologie des bündnerischen Rheingebietes: Ein Beitrag zur exogenen Dynamik alpiner Gebirgslandschaften (Exogene dynamics of an Alpine landscape). Beiträge zur Geologie der Schweiz, Geotechnische Serie. Kümmerly u. Frey, Bern.

Jaeger, J.C., Cook, N.G.W., Zimmerman, R.W., 2007. Fundamentals of Rock Mechanics. Wiley-Blackwell.

Jain, V., Tandon, S.K., 2010. Conceptual assessment of (dis)connectivity and its application to the Ganga River dispersal system. Geomorphology, 118(3–4), 349-358.

Janio de Castro Lima, J., Paraguassú, A.B., 2004. Linear thermal expansion of granitic rocks: influence of apparent porosity, grain size and quartz content. Bulletin of Engineering Geology and the Environment, 63(3), 215-220.

Janke, J.R., 2005. Modeling past and future alpine permafrost distribution in the Colorado Front Range. Earth Surf Proc Land, 30(12), 1495-1508.

Jarman, D., 2006. Large rock slope failures in the Highlands of Scotland: Characterisation, causes and spatial distribution. Eng Geol, 83(1–3), 161-182.

Jensen, P., 1998. Particle Physics and Our Everyday World. Phys.Today, 58-59.

Jia, H., Xiang, W., Krautblatter, M., 2015. Quantifying rock fatigue and decreasing compressive and tensile strength after repeated freeze-thaw cycles. Permafrost and Periglacial Processes, 26, 368-377.

John, K.W., 1970. Engineering analysis of three- dimensional stability problems utilizing the reference hemisphere, Proc. 2nd Int. Cong. International Society for Rock Mechanics, Belgrade, pp. 314-321.

Johnson, P.G., 1984. Paraglacial conditions of instability and mass movement: a discussion. Z Geomorphol, 28, 235–250.

Jomelli, V., Francou, B., 2000. Comparing the characteristics of rockfall talus and snow avalanche landforms in an Alpine environment using a new methodological approach: Massif des Ecrins, French Alps. Geomorphology, 35(3–4), 181-192.

Kaiser, H., 1958. The varimax criterion for analytic rotation in factor analysis. Psychometrika, 23(3), 187-200.

Keller, F., Gubler, H., 1993. Interaction between snow cover and high mountain permafrost, Murtèl/Corvatsch, Swiss Alps, Proceedings of the 6th International Conference on Permafrost, Beijjin, pp. 332–337.

Keller, M., Hungerbuehler, G., Knecht, O., Sheikh, S., Beutel, J., Gubler, S., Fiddes, J., Gruber, S., 2010. iAssist: rapid deployment and maintenance of tiny sensing systems, Proceedings of the 8th ACM Conference on Embedded Networked Sensor Systems. ACM, Zürich, Switzerland, pp. 401–402.

Kelly, M.A., Buoncristiani, J.-F., Schlüchter, C., 2004a. A reconstruction of the last glacial maximum (LGM) ice-surface geometry in the western Swiss Alps and contiguous Alpine regions in Italy and France. Eclogae Geologicae Helvetiae, 97(1), 57-75.

Kelly, M.A., Kubik, P.W., Von Blanckenburg, F., Schlüchter, C., 2004b. Surface exposure dating of the Great Aletsch Glacier Egesen moraine system, western Swiss Alps, using the cosmogenic nuclide 10Be. Journal of Quaternary Science, 19(5), 431–441.

Kennedy, B., 2006. Inventing the Earth: Ideas on Landscape Development Since 1740. Blackwall Publishing, Oxford.

Kershaw, L.J., Gardner, J.S., 1986. Vascular plants of mountain talus slopes, Mt. Rae area, Alberta, Canada. Phys Geogr, 7(3), 218-230.

Keuschnig, M., Hartmeyer, I., Otto, J.C., Schrott, L., 2011. A new permafrost and mass movement monitoring test site in the Eastern Alps – Concept and first results of the MOREXPERT project. Managing Alpine Future II - Inspire and drive sustainable mountain regions, Innsbruck Conference, November 21-23, 2011. Verlag der Österreichischen Akademie der Wissenschaften, Wien.

Keusen, H., Haeberli, W., 1983. Site investigation and foundation design aspects of cable car construction in Alpine permafrost at the "Chli Matterhorn," Wallis, Swiss Alps, Permafrost: Proceedings of the 4th International Conference. Natl. Acad. Press, Washington, D. C., pp. 601-605.

King, L., 1996. Dauerfrostboden im Gebiet Zermatt-Gornergrat-Stockhorn: Verbreitung und permafrostbezogene Erschliessungsarbeiten. Z. Geomorph. N. F., 104, 73–93.

Kirkby, M.J., Statham, I., 1975. Surface stone movement and scree formation. The Journal of Geology, 83(3), 349–362.

Kleinbaum, D.G., Kupper, L.L., Muller, K.E., Nizam, A., 1998. Applied regression analysis and other multivariable methods. Duxbury Press.

Kohl, T., 1999. Transient thermal effects below complex topographies. Tectonophysics, 306(3–4), 311-324.

Kohl, T., Gruber, S., 2003. Evidence of paleaotemperature signals in mountain permafrost areas, 8th International Conference on Permafrost, Extended Abstracts, Zürich, pp. 83-84.

Koppes, M., Hallet, B., 2006. Erosion rates during rapid deglaciation in Icy Bay, Alaska. Journal of Geophysical Research: Earth Surface, 111(F2), F02023.

Korup, O., 2005. Geomorphic imprint of landslides on alpine river systems, southwest New Zealand. Earth Surf Proc Land, 30(7), 783-800.

Korup, O., 2012. Chapter 1: Landslides in the Earth system. In: J.J. Clague, D. Stead (Eds.), Landslides - Types, Mechanisms and Modeling. Cambridge University Press, Cambridge, pp. 10-24.

Korup, O., Densmore, A.L., Schlunegger, F., 2010. The role of landslides in mountain range evolution. Geomorphology, 120(1), 77-90.

Krautblatter, M., 2009. Detection and quantification of permafrost change in alpine rock walls and implications for rock instability. PhD thesis, Universitiy of Bonn, Bonn.

Krautblatter, M., Dikau, R., 2007. Towards a uniform concept for the comparison and extrapolation of rockwall retreat and rockfall supply. Geografiska Annaler: Series A, Physical Geography, 89(1), 21–40.

Krautblatter, M., Draebing, D., 2014. Pseudo 3-D P wave refraction seismic monitoring of permafrost in steep unstable bedrock. Journal of Geophysical Research: Earth Surface, 119(2), 287-299.

Krautblatter, M., Funk, D., Gunzel, F.K., 2013. Why permafrost rocks become unstable: a rock-ice-mechanical model in time and space. Earth Surf Proc Land, 38(8), 876–887.

Krautblatter, M., Hauck, C., 2007. Electrical resistivity tomography monitoring of permafrost in solid rock walls. Journal of Geophysical Research: Earth Surface, 112(F2S20), 1-14.

Krautblatter, M., Leith, K., 2015. Glacier- and permafrost-related slope instabilities. In: C. Huggel, M. Carey, J.J. Clague, A. Kääb (Eds.), The High-Mountain Cryosphere. Cambridge University Press, Cambridge, pp. 147-165.

Krautblatter, M., Moore, J.R., 2014. Rock slope instability and erosion: toward improved process understanding. Earth Surf Proc Land, 39(9), 1273–1278.

Krautblatter, M., Moser, M., 2009. A nonlinear model coupling rockfall and rainfall intensity based on a four year measurement in a high Alpine rock wall (Reintal, German Alps). Natural Hazards and Earth System Sciences, 9(4), 1425–1432.

Krautblatter, M., Moser, M., Schrott, L., Wolf, J., Morche, D., 2012. Significance of rockfall magnitude and carbonate dissolution for rock slope erosion and geomorphic work on Alpine limestone cliffs (Reintal, German Alps). Geomorphology, 167–168(0), 21–34.

Krautblatter, M., Verleysdonk, S., Flores-Orozco, A., Kemna, A., 2010. Temperature-calibrated imaging of seasonal changes in permafrost rock walls by quantitative electrical resistivity tomography (Zugspitze, German/Austrian Alps). Journal of Geophysical Research: Earth Surface, 115(F2), 1-15.

Kugler, H., 1964. Großmaßstäbige geomorphologische Kartierung und geomorphologische Reliefanalyse. Dissertation, University of Leipzig, Leipzig, Germany.

Kuhn, M., Johnson, K. (Eds.), 2013. Applied Predictive Modeling. Springer.

Kuhn, T., 1962. The Structure of Scientific Revolutions. Chicago University Press, Chicago.

Kühnlein, M., Appelhans, T., Thies, B., Nauß, T., 2014. Precipitation Estimates from MSG SEVIRI Daytime, Nighttime, and Twilight Data with Random Forests. Journal of Applied Meteorology and Climatology, 53(11), 2457-2480.

Kuo, C.-W., Brierley, G.J., 2013. The influence of landscape configuration upon patterns of sediment storage in a highly connected river system. Geomorphology, 180–181(0), 255-266.

Labhart, T.P., 2009. Geologie der Schweiz. Ott Verlag, Thun.

Lamp, J.L., Marchant, D.R., Mackay, S.L., Head, J.W., 2017. Thermal stress weathering and the spalling of Antarctic rocks. Journal of Geophysical Research: Earth Surface, 122(1), 3-24.

Lane, S.N., Richards, K.S., 1997. Linking River Channel Form and Process: Time, Space and Causality Revisited. Earth Surf Proc Land, 22(3), 249-260.

Lanin, A., Fedik, I., 2008. Thermal Stress Resistance of Materials. Springer, Berlin.

Laphart, T.P., 1992. Geologie der Schweiz. Ott Verlag, Thun.

Lautridou, J.P., Ozouf, J.C., 1982. Experimental frost shattering. Prog Phys Geog, 6(2), 215-232.

Lazarus, E., Ashton, A., Murray, A.B., Tebbens, S., Burroughs, S., 2011. Cumulative versus transient shoreline change: Dependencies on temporal and spatial scale. Journal of Geophysical Research: Earth Surface, 116(F2).

Leemann, A., Niessen, F., 1994. Holocene glacial activity and climatic variations in the Swiss Alps: reconstructing a continuous record from proglacial lake sediments. The Holocene, 4(3), 259-268.

Lehmann, O., 1933. Morphologische Therorie der Verwitterung von Steinschlagwänden Vierteljahresschrift der Naturforschunden Gesellschaft Zürich, 78, 83-126.

Leine, R.I., Schweizer, A., Christen, M., Glover, J., Bartelt, P., Gerber, W., 2014. Simulation of rockfall trajectories with consideration of rock shape. Multibody System Dynamics, 32(2), 241-271.

Leith, K., Amann, F., Moore, J.R., Kos, A., Loew, S., 2010a. Conceptual modelling of nearsurface extensional fracture in the Matter and Saas Valleys, Switzerland, Delegate Papers, Geologically Active, 11th Congress of the International Association for Engineering Geology and the Environment, Auckland, Aotearoa, New Zealand, pp. 363–371.

Leith, K., Moore, J., Amann, F., Loew, S., Slope failure induced by post-glacial extensional fracturing in the Matter and Saas Valleys, S., 2010b. Slope failure induced by post-glacial extensional

fracturing in the Matter and Saas Valleys, Switzerland. Geophysical Research Abstracts, 12(EGU2010-4599).

Leith, K., Moore, J.R., Amann, F., Loew, S., 2014a. In situ stress control on microcrack generation and macroscopic extensional fracture in exhuming bedrock. Journal of Geophysical Research-Solid Earth, 119(1), 594–615.

Leith, K., Moore, J.R., Amann, F., Loew, S., 2014b. Subglacial extensional fracture development and implications for Alpine Valley evolution. Journal of Geophysical Research: Earth Surface, 119(1), 2012JF002691.

Levy, J.S., Head, J.W., Marchant, D.R., 2011. Gullies, polygons and mantles in Martian permafrost environments: cold desert landforms and sedimentary processes during recent Martian geological history. Special Publications, Geological Society, London, 354, 167–182.

Levy, J.S., Marchant, D.R., Head, J.W., 2010. Thermal contraction crack polygons on Mars: A synthesis from HiRISE, Phoenix, and terrestrial analog studies. Icarus, 206(1), 229-252.

Lewis, W.V., 1954. Pressure Release and Glacial Erosion. Journal of Glaciology, 2(16), 417-422.

Lewkowicz, A.G., 2001. Temperature regime of a small sandstone tor, latitude 80 °N, Ellesmere Island, Nunavut, Canada. Permafrost and Periglacial Processes, 12(4), 351-366.

Lexartza-Artza, I., Wainwright, J., 2009. Hydrological connectivity: Linking concepts with practical implications. Catena, 79(2), 146-152.

Li, L.-p., Sun, S.-q., Li, S.-c., Zhang, Q.-q., Hu, C., Shi, S.-s., 2016. Coefficient of restitution and kinetic energy loss of rockfall impacts. KSCE Journal of Civil Engineering, 20(6), 2297-2307.

Li, N., Zhang, P., Chen, Y., Swoboda, G., 2003. Fatigue properties of cracked, saturated and frozen sandstone samples under cyclic loading. International Journal of Rock Mechanics & Mining Sciences, 40, 145–150.

Liaw, A., Wiener, M., 2002. Classification and Regression by randomForest. R News, 2(3), 18-22.

Lim, M., Rosser, N.J., Allison, R.J., Petley, D.N., 2010. Erosional processes in the hard rock coastal cliffs at Staithes, North Yorkshire. Geomorphology, 114(1–2), 12–21.

Londe, P., 1965. Une méthode d'analyse à trois dimensions de la stabilité d'une rive rocheuse, Annales des Ponts et Chaussées, Paris, pp. 37–60.

López-Vicente, M., Poesen, J., Navas, A., Gaspar, L., 2013. Predicting runoff and sediment connectivity and soil erosion by water for different land use scenarios in the Spanish Pre-Pyrenees. Catena, 102, 62-73.

Loye, A., Jaboyedoff, M., Pedrazzini, A., 2009. Identification of potential rockfall source areas at a regional scale using a DEM-based geomorphometric analysis. Nat. Hazards Earth Syst. Sci., 9(5), 1643–1653.

Loye, A., Pedrazzini, A., Theule, J.I., Jaboyedoff, M., Liébault, F., Metzger, R., 2012. Influence of bedrock structures on the spatial pattern of erosional landforms in small alpine catchments. Earth Surf Proc Land, 37(13), 1407-1423.

Lozinski, W.M., 1909. Über die mechanische Verwitterung der Sandsteine im gemäßigten Klima. Bulletin International de l'Académie des Sciences de Cracovie, série des Sciences Mathématiques et Naturelles, 1, 1-25.

Lubbock, J., 1895. The Use of Life. Bernhard Tauchnitz, Leipzig.

Luckman, B.H., 1976. Rockfalls and rockfall inventory data: Some observations from surprise valley, Jasper National Park, Canada. Earth Surface Processes, 1(3), 287–298.

Luckman, B.H., 1988. Debris accumulation patterns on talus slopes in Surprise Valley, Alberta. Géographie physique et Quaternaire, 42(3), 247–278.

Luckman, B.H., 2013. Talus slopes. In: E. S.A. (Ed.), The Encyclopedia of Quaternary Science. Elsevier, Amsterdam, pp. 566-573.

Luckman, B.H., Fiske, C.J., 1995. Estimating long-term rockfall accretion rates by lichenometry. In: O. Slaymaker (Ed.), Steepland Geomorphology. Wiley, Chichester, pp. 233–255.

Luetschg, M., 2005. A model and field analysis of the interaction processes between snow cover and Alpine permafrost, University of Zurich, Zürich, Switzerland.

Luetschg, M., Haeberli, W., 2005. Permafrost evolution in the Swiss Alps in a changing climate and the role of the snow cover. Norsk Geografisk Tidsskrift - Norwegian Journal of Geography, 59(2), 78-83.

Luetschg, M., Lehning, M., Haeberli, W., 2008. A sensitivity study of factors influencing warm/thin permafrost in the Swiss Alps. Journal of Glaciology, 54(187), 696–704.

Luoto, M., Hjort, J., 2005. Evaluation of current statistical approaches for predictive geomorphological mapping. Geomorphology, 67(3-4), 299-315.

Luque, A., Ruiz-Agudo, E., Cultrone, G., Sebastián, E., Siegesmund, S., 2011. Direct observation of microcrack development in marble caused by thermal weathering. Environmental Earth Sciences, 62(7), 1375-1386.

Lüthi, M., Funk, M., 1997. Wie stabil ist der Hängegletscher am Eiger? Spektrum Wissenschaft 95(5), 21–24.

MacMillan, R.A., Shary, P.A., 2009. Chapter 9 Landforms and Landform Elements in Geomorphometry. In: T. Hengl, H.I. Reuter (Eds.), Developments in Soil Science. Elsevier, pp. 227-254.

Magnin, F., Deline, P., Ravanel, L., Noetzli, J., Pogliotti, P., 2015a. Thermal characteristics of permafrost in the steep alpine rock walls of the Aiguille du Midi (Mont Blanc Massif, 3842 m a.s.l). The Cryosphere, 9(1), 109-121.

Magnin, F., Krautblatter, M., Deline, P., Ravanel, L., Malet, E., Bevington, A., 2015b. Determination of warm, sensitive permafrost areas in near-vertical rockwalls and evaluation of distributed models by electrical resistivity tomography. Journal of Geophysical Research: Earth Surface, 1-18.

Mair, V., Zischg, A., Lang, K., Tonidandel, D., Krainer, K., Kellerer-Pirklbauer, A., Deline, P., Schoeneich, P., Cremonese, E., Pogliotti, P., Gruber, S., Böckli, L., 2011. PermaNET - Permafrost Long-term Monitoring Network. Synthesis report., Klagenfurt.

Marchenko, S., Etzelmüller, B., 2013. Permafrost: formation and distribution, thermal and mechanical properties. . In: J.F. Shroder, R. Giardino, J. Harbor (Eds.), Treatise on Geomorphology. Academic Press, San Diego, CA, pp. 202-222.

Marquínez, J., Menéndez Duarte, R., Farias, P., JiméNez Sánchez, M., 2003. Predictive GIS-Based Model of Rockfall Activity in Mountain Cliffs. Nat Hazards, 30(3), 341-360.

Martz, L.W., Garbrecht, J., 1992. Numerical definition of drainage network and subcatchment areas from Digital Elevation Models. Computers & Geosciences, 18(6), 747-761.

Matasci, B., Jaboyedoff, M., Loye, A., Pedrazzini, A., Derron, M.H., Pedrozzi, G., 2015. Impacts of fracturing patterns on the rockfall susceptibility and erosion rate of stratified limestone. Geomorphology, 241, 83-97.

Matsuoka, N., 1990. Mechanisms of rock breakdown by frost action: An experimental approach. Cold Regions Science and Technology, 17(3), 253-270.

Matsuoka, N., 1994. Diurnal freeze–thaw depth in rockwalls: Field measurements and theoretical considerations. Earth Surf Proc Land, 19(5), 423–435.

Matsuoka, N., 2001a. Direct observation of frost wedging in alpine bedrock. Earth Surf Proc Land, 26(6), 601-614.

Matsuoka, N., 2001b. Microgelivation versus macrogelivation: towards bridging the gap between laboratory and field frost weathering. Permafrost and Periglacial Processes, 12(3), 299–313.

Matsuoka, N., 2001c. Solifluction rates, processes and landforms: a global review. Earth-Science Reviews, 55(1–2), 107-134.

Matsuoka, N., 2008. Frost weathering and rockwall erosion in the southeastern Swiss Alps: Long-term (1994–2006) observations. Geomorphology, 99(1–4), 353-368.

Matsuoka, N., Hirakawa, K., Watanabe, T., Haeberli, W., Keller, F., 1998. The role of diurnal, annual and millenial freeze-thaw cycles in controlling alpine slope stability, 7th International Conference on Permafrost, Yellowknife, Canada, pp. 711-717.

Matsuoka, N., Hirakawa, K., Watanabe, T., Moriwaki, K., 1997. Monitoring of periglacial slope processes in the Swiss Alps: the first two years of frost shattering, heave and creep. Permafrost and Periglacial Processes, 8(2), 157-179.

Matsuoka, N., Murton, J., 2008. Frost weathering: recent advances and future directions. Permafrost and Periglacial Processes, 19(2), 195-210.

Matsuoka, N., Sakai, H., 1999. Rockfall activity from an alpine cliff during thawing periods. Geomorphology, 28(3–4), 309–328.

Matznetter, K., 1956. Der Vorgang der Massenbewegungen an Beispielen des Klostertales in Vorarlberg.

Mavrouli, O., Corominas, J., 2016. Comparing rockfall scar volumes and kinematically detachable rock masses. Eng Geol, in press.

McCarroll, D., 1997. Editorial - 'Really critical' geomorphology. Earth Surf Proc Land, 22(1), 1-2.

McCarroll, D., Shakesby, R.A., Matthews, J.A., 1998. Spatial and temporal patterns of Late Holocene rockfall activity on a Norwegian talus slope: A lichenometric and simulation-modeling approach. Arctic and Alpine Research, 30(1), 51–60.

McColl, S.T., 2012. Paraglacial rock-slope stability. Geomorphology, 153–154, 1–16.

McColl, S.T., Davies, T.R.H., 2013. Large ice-contact slope movements: glacial buttressing, deformation and erosion. Earth Surf Proc Land, 38(10), 1102-1115.

McColl, S.T., Davies, T.R.H., McSaveney, M.J., 2010. Glacier retreat and rock-slope stability: debunking debuttressing, Delegate Papers, Geologically Active, 11th Congress of the International Association for Engineering Geology and the Environment, Auckland, Aotearoa, 5–10 September 2010. Auckland, New Zealand, pp. 467–474.

McFadden, L.D., Eppes, M.C., Gillespie, A.R., Hallet, B., 2005. Physical weathering in arid landscapes due to diurnal variation in the direction of solar heating. GSA Bulletin, 117(1-2), 161-173.

McGreevy, J.P., 1985. Thermal properties as controls on rock surface temperature maxima, and possible implications for rock weathering. Earth Surf Proc Land, 10(2), 125-136.

McGreevy, J.P., Whalley, W.B., 1985. Rock Moisture Content and Frost Weathering under Natural and Experimental Conditions:A Comparative Discussion. Arctic and Alpine Research, 17(3), 337-346.

McGuire, B., 2010. Potential for a hazardous geospheric response to projected future climate changes. Philosophical Transactions of the Royal Society A: Mathematical, Physical and Engineering Sciences, 368(1919), 317–2345.

Meigs, A., Krugh, W.C., Davis, K., Bank, G., 2006. Ultra-rapid landscape response and sediment yield following glacier retreat, Icy Bay, southern Alaska. Geomorphology, 78(3–4), 207-221.

Mellor, M., 1973. Mechanical properties of rocks at low temperatures, 2nd International Conference on Permafrost. Northamerican Contribution 1973, Yakutsk, USSR, pp. 334-344.

Mercier, D., 2008. Paraglacial and paraperiglacial landsystems: concepts, temporal scales and spatial distribution. Géomorphologie: relief, processus, environnement, 14(4), 223-233.

Messenzehl, K., 2013. Alpine sediment cascades in the Swiss National Park, Graubünden. M.Sc., Rheinische Friedrich-Wilhelms-Universität, Bonn.

Messenzehl, K., Dikau, R., 2017. Structural and thermal controls of rockfall frequency and magnitude within rockwall–talus systems (Swiss Alps). Earth Surf Proc Land, DOI: 10.1002/esp.4155.

Messenzehl, K., Draebing, D., 2015. Multidisciplinary investigations on coupled rockwall-talus-systems (Turtmann valley, Swiss Alps). Geophysical Research Abstracts, 17, EGU2015-1935, 2015.

Messenzehl, K., Hoffmann, T., Dikau, R., 2014. Sediment connectivity in the high-alpine valley of Val Müschauns, Swiss National Park — linking geomorphic field mapping with geomorphometric modelling. Geomorphology, 221, 215–229.

Messenzehl, K., Meyer, H., Otto, J.-C., Hoffmann, T., Dikau, R., 2017. Regional-scale controls on the spatial activity of rockfalls (Turtmann valley, Swiss Alps) - A multivariate modelling approach. Geomorphology, 287, 29-45.

Messenzehl, K., Viles, H., Otto, J.-C., Ewald, A., Dikau, R., in review. Linking rock weathering, rockwall instability and rockfall sediment cascades in glaciated hanging valleys (Swiss Alps). Permafrost and Periglacial Processes

MeteoSwiss, 2013. Homepage of the Federal Office of Meteorology and Climatology MeteoSwiss.

MeteoSwiss, 2015. Klimareport 2014. In: B.f.M.u.K. MeteoSchweiz (Ed.), Zürich.

MeteoSwiss, 2016. Klimabulletin Jahr 2015. In: B.f.M.u.K. MeteoSchweiz (Ed.), Zürich.

Meyer, H., Kühnlein, M., Appelhans, T., Nauss, T., Comparison of four machine learning algorithms for their applicability in satellite-based optical rainfall retrievals. Atmospheric research, 169, 424-433.

Micheletti, N., Lambiel, C., Lane, S.N., 2015. Investigating decadal-scale geomorphic dynamics in an alpine mountain setting. Journal of Geophysical Research: Earth Surface, 120(10), 2155-2175.

Michoud, C., Derron, M.H., Horton, P., Jaboyedoff, M., Baillifard, F.J., Loye, A., Nicolet, P., Pedrazzini, A., Queyrel, A., 2012. Rockfall hazard and risk assessments along roads at a regional scale: example in Swiss Alps. Natural Hazards and Earth System Sciences, 12(3), 615–629.

Milanovic, P., 2004. Water Resources Engineering in Karst. CRC Press, Florida.

Milliman, J.D., Syvitski, J.P.M., 1992. Geomorphic/tectonic control of sediment discharge to the ocean: The importance of small mountainous rivers. The Journal of Geology, 100(5), 525-544.

Milne, G., 1935. Some suggested units of classification and mapping particularly for East African soils. Soil Research, 4, 183-198.

Mol, L., Viles, H.A., 2012. The role of rock surface hardness and internal moisture in tafoni development in sandstone. Earth Surf Proc Land, 37(3), 301-314.

Molaro, J.L., Byrne, S., Langer, S.A., 2015. Grain-scale thermoelastic stresses and spatiotemporal temperature gradients on airless bodies, implications for rock breakdown. Journal of Geophysical Research: Planets, 120(2), 255-277.

Montgomery, D.R., 2002. Valley formation by fluvial and glacial erosion. Geology, 30, 1047-1050.

Montgomery, D.R., Buffington, J.M., 1997. Channel-reach morphology in mountain drainage basins. Geological Society of America Bulletin, 109(5), 596-611.

Moon, B.P., 1984. Refinement of a technique for determining rock mass strength for geomorphological purposes. Earth Surf Proc Land, 9(2), 189-193.

Moon, B.P., Selby, M.J., 1983. Rock Mass Strength and Scarp Forms in Southern Africa. Geografiska Annaler. Series A, Physical Geography, 65(1/2), 135-145.

Moore, J.R., Gischig, V., Katterbach, M., Loew, S., 2011. Air circulation in deep fractures and the temperature field of an alpine rock slope. Earth Surf Proc Land, 36(15), 1985–1996.

Moore, J.R., Sanders, J.W., Dietrich, W.E., Glaser, S.D., 2009. Influence of rock mass strength on the erosion rate of alpine cliffs. Earth Surf Proc Land, 34(10), 1339–1352.

Morche, D., Schmidt, K.-H., Sahling, I., Herkommer, M., Kutschera, J., 2008. Volume changes of Alpine sediment stores in a state of post-event disequilibrium and the implications for downstream hydrology and bed load transport. Norsk Geografisk Tidsskrift - Norwegian Journal of Geography, 62(2), 89-101.

Moses, C., Robinson, D., Barlow, J., 2014. Methods for measuring rock surface weathering and erosion: A critical review. Earth-Science Reviews, 135, 141-161.

Müller, L., 1968. New considerations on the Vaiont Slide. Rock Mechanics and Engineering Geology, 6, 1-91.

Murray, A.B., Coco, G., Goldstein, E.B., 2014. Cause and effect in geomorphic systems: Complex systems perspectives. Geomorphology, 214(Supplement C), 1-9.

Murray, A.B., Lazarus, E., Ashton, A., Baas, A., Coco, G., Coulthard, T., Fonstad, M., Haff, P., McNamara, D., Paola, C., Pelletier, J., Reinhardt, L., 2009. Geomorphology, complexity, and the emerging science of the Earth's surface. Geomorphology, 103(3), 496–505.

Murton, J.B., Coutard, J.P., Lautridou, J.P., Ozouf, J.C., Robinson, D.A., Williams, R.B.G., 2001. Physical modelling of bedrock brecciation by ice segregation in permafrost. Permafrost and Periglacial Processes, 12(3), 255–266.

Murton, J.B., Kuras, O., Krautblatter, M., Cane, T., Tschofen, D., Uhlemann, S., Schober, S., Watson, P., 2016. Monitoring rock freezing and thawing by novel geoelectrical and acoustic techniques. Journal of Geophysical Research: Earth Surface, 121(12), 2309-2332.

Murton, J.B., Peterson, R., Ozouf, J.C., 2006. Bedrock fracture by ice segregation in cold regions. Science, 314(5802), 1127–1129.

Nardi, L., Rinaldi, M., Solari, L., 2012. An experimental investigation on mass failures occurring in a riverbank composed of sandy gravel. Geomorphology, 163–164, 56-69.

Nichols, T.C., 1980. Rebound, its nature and effect on engineering works. Quarterly Journal of Engineering Geology & Hydrogeology, 13, 133–115.

Nicholson, D.T., 2001. Pore properties as indicators of breakdown mechanisms in experimentally weathered limestones. Earth Surf Proc Land, 26(8), 819-838.

Nicholson, D.T., 2008. Rock control on microweathering of bedrock surfaces in a periglacial environment. Geomorphology, 101(4), 655-665.

Nicholson, D.T., Nicholson, F.H., 2000. Physical deterioration of sedimentary rocks subjected to experimental freeze-thaw weathering. Earth Surf Proc Land, 25, 1295-1397.

Noetzli, J., Gruber, S., 2009. Transient thermal effects in Alpine permafrost. The Cryosphere, 3(1), 85-99.

Noetzli, J., Gruber, S., Kohl, T., Salzmann, N., Haeberli, W., 2007. Three-dimensional distribution and evolution of permafrost temperatures in idealized high-mountain topography. Journal of Geophysical Research: Earth Surface, 112(F2), 1-14.

Noetzli, J., Hoelzle, M., Haeberli, W., 2003. Mountain permafrost and recent Alpine rock-fall events: a GIS-based approach to determine critical factors. In: M. Phillips, S. Springman, L. Arenson (Eds.), Proceedings of the 8th International Conference on Permafrost, Zürich, pp. 827-832.

Nogués-Bravo, D., Araújo, M.B., Errea, M.P., Martínez-Rica, J.P., 2007. Exposure of global mountain systems to climate warming during the 21st Century. Global Environmental Change, 17(3–4), 420-428.

Norrish, N.I., Wyllie, D.C., 1996. Rock slope stability analysis. Landslides: Investigation and Mitigation: Transportation Research Board Special Report, 247, 391-425.

NRC-Permafrost-Subcommitee, 1988. Glossary of permafrost and related ground-ice terms. In: N.T. Memorandum (Ed.), pp. 1-156.

Nyenhuis, M., 2005. Permafrost und Sedimenthaushalt in einem alpinen Geosystem. PhD-Thesis, University of Bonn, Bonn.

Nyenhuis, M., Hoelzle, M., Dikau, R., 2005. Rock glacier mapping and permafrost distribution modelling in the Turtmanntal, Valais, Switzerland. Zeitschrift für Geomorphologie, NF, 49(3), 275-292.

Obanawa, H., Hayakawa, Y.S., Matsukura, Y., 2009. Rates of slope decline, talus growth and cliff retreat along the Shomyo river in Central Japan: a space-time substitution approach. Geografiska Annaler: Series A, Physical Geography, 91(4), 269-278.

OECD, 2007. Klimawandel in den Alpen. OECD Publishing.

Ohlmacher, G.C., Davis, J.C., 2003. Using multiple logistic regression and GIS technology to predict landslide hazard in northeast Kansas, USA. Eng Geol, 69(3-4), 331-343.

Oke, T.R., 1987. Boundary layer climates. Cambridge University Press, Cambridge.

Olyphant, G.A., 1983. Analysis of the factors controlling cliff burial by talus within Blanca Massif, Southern Colorado. Arctic Alpine Research, 15, 65–75.

Oppikofer, T., Jaboyedoff, M., Keusen, H.-R., 2008. Collapse at the eastern Eiger flank in the Swiss Alps. Nature Geosci, 1(8), 531-535.

Ostermann, M., Sanders, D., 2016. The Benner pass rock avalanche cluster suggests a close relation between long-term slope deformation (DSGSDs and translational rock slides) and catastrophic failure. Geomorphology.

Otto, J.-C., 2006. Paraglacial sediment storage quantification in the Turtmann Valley, Swiss Alps. Ph.D. theses, Rheinische Friedrich-Wilhelms-Universität, Bonn.

Otto, J.-C., Dikau, R., 2004. Geomorphologic system analysis of a high mountain valley in the Swiss Alps. Z Geomorphol, 48(3), 323-341.

Otto, J.-C., Dikau, R. (Eds.), 2010. Landform - Structure, Evolution, Process Control - Proceedings of the International Symposium on Landform organised by the Research Training Group 437. Lecture Notes in Earth Sciences. Springer-Verlag Berlin Heidelberg.

Otto, J.-C., Kleinod, K., Konig, O., Krautblatter, M., Nyenhuis, M., Roer, I., Schneider, M., Schreiner, B., Dikau, R., 2007. HRSC-A data: a new high-resolution data set with multipurpose applications in physical geography. Prog Phys Geog, 31(2), 179-197.

Otto, J.-C., Sass, O., 2006. Comparing geophysical methods for talus slope investigations in the Turtmann valley (Swiss Alps). Geomorphology, 76(3–4), 257-272.

Otto, J.-C., Schrott, L., Jaboyedoff, M., Dikau, R., 2009. Quantifying sediment storage in a high alpine valley (Turtmanntal, Switzerland). Earth Surf Proc Land, 34(13), 1726-1742.

Owens, P.N., Slaymaker, O., 2004. An introduction to mountain geomorphology. In: P.N. Owens, O. Slaymaker (Eds.), Mountain Geomorphology. Arnold, London, pp. 3-33.

Paine, A.D.M., 1985. 'Ergodic' reasoning in geomorphology: time for a review of the term? Prog Phys Geog, 9(1), 1-15.

Palmstrom, A., 1982. The volumetric joint count - A useful and simple measure of the degree of rock mass jointing, IAEG Congress, New Delhi, New Delhi, pp. V.221–V.228.

Palmstrom, A., 2005. Measurements of and correlations between block size and rock quality designation (RQD). Tunnelling and Underground Space Technology, 20(4), 362–377.

Panizza, M., 1973. Glacio pressure implications in the production of landslides in the Dolomitic area. Geologia Applicata e Idrogeologia, 8, 289–297.

Patton, F.D., 1966. Multiple modes of shear failure in rock, 1st Congress of the International Society for Rock Mechanics, Laboratory of Civil Engineering, Lisbon, pp. 509–513.

Peirce, C.S., 1902. Verification. In: J.M. Baldwin (Ed.), Dictionary of Philosophy and Psychology. Macmillan, New York, pp. 761-762.

Penck, A., 1896. Die Geomorphologie als genetische Wissenschaft - Eine Einleitung zur Diskussion über geomorphologische Nomenklatur, Comptes Rendas, 6. Int. Geogr. Kongress, Sektion C, pp. 735–752.

Peng, G.-F., Bian, S.-H., Guo, Z.-Q., Zhao, J., Peng, X.-L., Jiang, Y.-C., 2008. Effect of thermal shock due to rapid cooling on residual mechanical properties of fiber concrete exposed to high temperatures. Construction and Building Materials, 22(5), 948-955.

Pennock, D.J., Zebarth, B.J., De Jong, E., 1987. Landform classification and soil distribution in hummocky terrain, Saskatchewan, Canada. Geoderma, 40, 297-315.

Pérez, F.L., 1985. Surficial Talus Movement in an Andean Paramo of Venezuela. Geografiska Annaler. Series A, Physical Geography, 67(3/4), 221-237.

Pérez, F.L., 1989. Talus fabric and particle morphology on Lassen Peak, California. Geografiska Annaler. Series A, Physical Geography, 71(1/2), 43–57.

Pérez, F.L., 1993. Talus movement in the high equatorial andes: A synthesis of ten years of data. Permafrost and Periglacial Processes, 4(3), 199–215.

Pérez, F.L., 1998. Talus fabric, clast morphology, and botanical indicators of slope processes on the Chaos Crags (California Cascades), USA. Geographie Physique et Quaternaire, 52(1), 47-68.

PERMOS, 2016. Permafrost in Switzerland 2010/2011 to 2013/2014.

Petley, D., 2012. Global patterns of loss of life from landslides. Geology, 40(10), 927-930.

Petley, D.N., Petley, D.J., 2005. On the initiation of large rockslides: perspectives from a new analysis of the Vajont movement record. In: S. Evans (Ed.), Large Rock Slope Failures. Kluwer (Nato Science Series), Rotterdam, pp. 77–84.

Pfeiffer, T.J., Bowen, T.D., 1989. Computer Simulation of Rockfalls. Bulletin of the Association of Engineering Geologists, XXVI(1), 135-146.

Phillips, J.D., 1988. The role of spatial scale in geomorphic systems. Geographical Analysis, 20(4), 308–317.

Phillips, J.D., 1999. Earth Surface Systems: complexity, order and scale. Blackwell Publishers, Oxford.

Phillips, J.D., 2003a. Alluvial storage and the long-term stability of sediment yields. Basin Res., 15(2), 153-163.

Phillips, J.D., 2003b. Sources of nonlinearity and complexity in geomorphic systems. Prog Phys Geog, 27(1), 1–23.

Phillips, J.D., 2005. Weathering instability and landscape evolution. Geomorphology, 67(1), 255-272.

Phillips, J.D., 2012a. Storytelling in Earth sciences: The eight basic plots. Earth-Science Reviews, 115(3), 153-162.

Phillips, J.D., 2012b. Synchronization and scale in geomorphic systems. Geomorphology, 137(1), 150-158.

Phillips, M., Haberkorn, A., Draebing, D., Krautblatter, M., Rhyner, H., Kenner, R., 2016. Seasonally intermittent water flow through deep fractures in an Alpine Rock Ridge: Gemsstock, Central Swiss Alps. Cold Regions Science and Technology, 125, 117–127.

Pichler, B., Hellmich, C., Mang, H.A., 2005. Impact of rocks onto gravel Design and evaluation of experiments. International Journal of Impact Engineering, 31(5), 559-578.

Pickett, S.A., 1989. Space-for-time substitution as an alternative to long-term studies. In: G. Likens (Ed.), Long-Term Studies in Ecology. Springer New York, pp. 110-135.

Piwowar, A., 1902. Über Maximalböschungen trockener Schuttkegel und Schutthalden. Vierteljahrsschrift der Naturforschenden Gesellschaft in Zürich, 48, 43-56.

Pogliotti, P., 2001. Influence of snow cover on MAGST over complex morphologies in mountain permafrost regions. PhD thesis, Università degli Studio di Torino, UTurin, Italy.

Prager, C., Zangerl, C., Patzelt, G., Brandner, R., 2008. Age distribution of fossil landslides in the Tyrol (Austria) and its surrounding areas. Nat. Hazards Earth Syst. Sci., 8(2), 377-407.

Price, M.F., Byers, A.C., Friend, D.A., Kohler, T., Price, L.W., 2013. Mountain Geography. Physical and Human Dimensions. University of California Press.

Prick, A., 1997. Critical Degree of Saturation as a Threshold Moisture Level in Frost Weathering of Limestones. Permafrost and Periglacial Processes, 8(1), 91-99.

Prick, A., 1999. Etude dilatométrique de la cryoclastie et de l'haloclastie. Académie Royale des Sciences de Belgique.

Prick, A., 2003. Frost weathering and rock fall in an arctic environment, Longyearbyen, Svalbard. In: M. Phillips (Ed.), Proceedings of the Eighth International Conference on Permafrost, Balkema, Lisse, pp. 907-912.

Priest, S.D., 1993. Discontinuity Analysis for Rock Engineering. Chapman&Hall, London.

Prinz, H., Strauß, R., 2011. Ingenieurgeologie. Spektrum Akademischer Verlag, Heidelberg.

Prisco, C.d., Vecchiotti, M., 2006. A rheological model for the description of boulder impacts on granular strata. Géotechnique, 56(7), 469-482.

Rapp, A., 1960a. Recent development of mountain slopes in Kaerkevagge and surroundings, Northern Scandinavia. Geografiska Annaler A, 42(2-3), 71–200.

Rapp, A., 1960b. Talus Slopes and Mountain "alls at Tempelfjorden, Spitsbergen. A geomorphological Study of the Denudation of Slopes in an Arctic Locality. Oslo University Press, Oslo.

Rasemann, S., 2004. Geomorphometrische Sturktur eines mesoskaligen alpinen Geosystems. Bonner Geographische Abhandlungen, 111. Asgard-Verlag, Sankt Augustin.

Ravanel, L., Deline, P., 2011. Climate influence on rockfalls in high-Alpine steep rockwalls: The north side of the Aiguilles de Chamonix (Mont Blanc massif) since the end of the 'Little Ice Age'. The Holocene, 21(2), 357-365.

Ravanel, L., Deline, P., 2015. Rockfall Hazard in the Mont Blanc Massif Increased by the Current Atmospheric Warming. In: G. Lollino, A. Manconi, J. Clague, W. Shan, M. Chiarle (Eds.), Engineering Geology for Society and Territory - Volume 1. Springer International Publishing, pp. 425-428.

Ravanel, L., Magnin, F., Deline, P., 2017. Impacts of the 2003 and 2015 summer heatwaves on permafrost-affected rock-walls in the Mont Blanc massif. Science of The Total Environment, 609, 132-143.

Rhoads, B.L., Thorn, C.E., 1993. Geomorphology as science: the role of theory. Geomorphology, 6(4), 287-307.

Rhoads, B.L., Thorn, C.E., 1996. The scientific Nature of Geomorphology. Wiley, New York.

Richter, D., Simmons, G., 1974. Thermal expansion behavior of igneous rocks. Int. J. Min. Sci. Geomech. Abstr. , 11, 403–411.

Richter, E., 1901. Geomorphologische Untersuchungen in den Hochalpen. Petermanns Geographische Mitteilungen, 24: 1-103., 24(1-103).

Rickenmann, D., Zimmermann, M., 1993. The 1987 debris flows in Switzerland: documentation and analysis. Geomorphology, 8(2-3), 175-189.

Ritchie, A.M., 1963. Evaluation of rockfall and its control. Highway Research Board, Washington DC.

Ritter, G., 1852. Einleitung zur allgemeinen vergleichenden Geographie und Abhandlungen zur Begründung einer mehr wissenschaftlichen Behandlung der Erdkunde. G. Reimer, Berlin.

Robinson, D.A., Williams, R.B.G., 1994. Rock Weathering and Landform Evolution. Wiley, Chichester.

Rochet, L., 1987. Application des modles numériques de progataion a l'etude des éboulements rocheux. Bulletin Liaison Pont Chaussée(150/151), 84-95.

Rode, M., Schnepfleitner, H., Sass, O., 2016. Simulation of moisture content in alpine rockwalls during freeze–thaw events. Earth Surf Proc Land, 41, 1937-1950.

Roer, I., 2005. Rock glacier Kinematics in a High Mountain Geosystem. PhD thesis, University of Bonn.

Ruhe, R.V., Walker, P.H., 1986. Hillslope models and soil formation. I. Open systems. Transactions of the 9th international congress of soil science, 4, 551-560.

Ruiz-Carulla, R., Corominas, J., Mavrouli, O., 2015. A methodology to obtain the block size distribution of fragmental rockfall deposits. Landslides, 12(4), 815-825.

Ruiz-Carulla, R., Corominas, J., Mavrouli, O., 2016. Comparison of block size distribution in rockfalls, Landslides and Engineered Slopes. Experience, Theory and Practice. CRC Press, pp. 1767-1774.

Ryder, J.M., 1971. Stratigraphy and morphology of para-glacial alluvial fans in South-Central British-Columbia. Canadian Journal of Earth Sciences, 8(2), 279-298.

Sandercock, P.J., Hooke, J.M., 2011. Vegetation effects on sediment connectivity and processes in an ephemeral channel in SE Spain. Journal of Arid Environments, 75(3), 239-254.

Sanderon, T., 1988. Ice Mechanics and Risks to Offshore Structures. Springer, Amsterdam.

Santana, D., Corominas, J., Mavrouli, O., Garcia-Sellés, D., 2012. Magnitude–frequency relation for rockfall scars using a Terrestrial Laser Scanner. Engineering Geology, 145–146, 50-64.

Sass, O., 1998. Die Steuerung von Steinschlagmenge durch Mikroklima, Gesteinsfeuchte und Gesteinseigenschaften im westlichen Karwendelgebirge (Bayerische Alpen). Münchner Geographische Abhandlungen Reihe B.

Sass, O., 2004. Rock Moisture Fluctuations During Freeze-thaw Cycles: Preliminary Results from Electrical Resistivity Measurements. Polar Geography, 28(1), 13-31.

Sass, O., 2005a. Rock moisture measurements: techniques, results, and implications for weathering. Earth Surf Proc Land, 30(3), 359-374.

Sass, O., 2005b. Spatial patterns of rockfall intensity in the northern Alps Zeitschrift für Geomorphologie N.F., Suppl.-Bd., 138, 51–65.

Sass, O., 2005c. Temporal variability of rockfall in the Bavarian Alps, Germany. Arct Antarct Alp Res, 37(4), 564–573.

Sass, O., 2007. Bedrock detection and talus thickness assessment in the European Alps using geophysical methods. Journal of Applied Geophysics, 62(3), 254-269.

Sass, O., 2010. Spatial and temporal patterns of talus activity - a lichenometric approach in the Stubaier Alps, Austria. Geografiska Annaler: Series A, Physical Geography, 92(3), 375–391.

Sass, O., Krautblatter, M., 2007. Debris flow-dominated and rockfall-dominated talus slopes: Genetic models derived from GPR measurements. Geomorphology, 86(1–2), 176–192.

Sass, O., Wollny, K., 2001. Investigations regarding Alpine talus slopes using ground-penetrating radar (GPR) in the Bavarian Alps, Germany. Earth Surf Proc Land, 26(10), 1071-1086.

Savi, S., Schneuwly-Bollschweiler, M., Bommer-Denns, B., Stoffel, M., Schlunegger, F., 2013. Geomorphic coupling between hillslopes and channels in the Swiss Alps. Earth Surf Proc Land, 38(9), 959-969.

Scapozza, C., Lambiel, C., Baron, L., Marescot, L., Reynard, E., 2011. Internal structure and permafrost distribution in two alpine periglacial talus slopes, Valais, Swiss Alps. Geomorphology, 132(3–4), 208-221.

Schär, C., Vidale, P.L., Luthi, D., Frei, C., Haberli, C., Liniger, M.A., Appenzeller, C., 2004. The role of increasing temperature variability in European summer heatwaves. Nature, 427(6972), 332-336.

Scheidegger, A.E., 1973. On the prediction of the reach and velocity of catastrophic landslides. Rock mechanics, 5(4), 231-236.

Schellenberg, K., Volkwein, A., Denk, M., Vogel, T., 2008. Falling weight tests on rock fall galleries with cushion layers, Interdisciplinary Workshop on Rockfall Protection,, Morschach, Switzerland, 23–25 June 2008, pp. 23–25.

Schlüchter, C., 2004. The Swiss glacial record - A schematic summary. In: J. Ehlers, P.L. Gibbard (Eds.), Developments in Quaternary Sciences. Elsevier, pp. 413–418.

Schlunegger, F., Badoux, A., McArdell, B.W., Gwerder, C., Schnydrig, D., Rieke-Zapp, D., Molnar, P., 2009. Limits of sediment transfer in an alpine debris-flow catchment, Illgraben, Switzerland. Quaternary Science Reviews, 28(11–12), 1097-1105.

Schlunegger, F., Hinderer, M., 2001. Crustal uplift in the Alps: why the drainage pattern matters. Terra Nova, 13(6), 425-432.

Schmid, M.O., Gubler, S., Fiddes, J., Gruber, S., 2012. Inferring snowpack ripening and melt-out from distributed measurements of near-surface ground temperatures. The Cryosphere, 6(5), 1127-1139.

Schmidt, J., Dikau, R., 1999. Extracting geomorphic attributes and objects form digital elevation models - Semantics, methods, future needs. In: R. Dikau, H. Saurer (Eds.), GIS for Earth Surface Systems. Borntraeger, Berlin, pp. 153-174.

Schmidt, J., Hewitt, A., 2004. Fuzzy land element classification from DTMs based on geometry and terrain position. Geoderma, 121(3–4), 243-256.

Schoch, A., 2013. Influences of hillslope-channel-coupling on two mountain headwater streams, Swiss National Park. (in German). Diploma thesis, University of Bonn.

Schrott, L., Götz, J., Geilhausen, M., Morche, D., 1999. Spatial and temporal variability of sediment transfer and storage in an Alpine basin (Reintal valley, Bavarian Alps, Gemany). Geogr. Helv., 61(3), 191-200.

Schrott, L., Götz, J., Geilhausen, M., Morche, D., 2006. Spatial and temporal variability of sediment transfer and storage in an Alpine basin (Reintal valley, Bavarian Alps, Gemany). Geographica Helvetica 3, 61(3), 191-200.

Schrott, L., Hoffmann, T., 2003. Determing sediment thickness of talus slopes and valley fill deposits using seismic refraction - a comparision of 2D interpretation tools. Zeitschrift für Geomorphologie N.F., Suppl.-Bd. 132, 71-87.

Schrott, L., Hufschmidt, G., Hankammer, M., Hoffmann, T., Dikau, R., 2003. Spatial distribution of sediment storage types and quantification of valley fill deposits in an alpine basin, Reintal, Bavarian Alps, Germany. Geomorphology, 55(1–4), 45-63.

Schrott, L., Niederheide, A., Hankammer, M., Hufschmidt, G., Dikau, R., 2002. Sediment storage in a mountain catchment: geomorphic coupling and temporal variability (Reintal, Bavarian Alps, Germany). Z Geomorphol, 127, 175-196.

Schrott, L., Sass, O., 2008. Application of field geophysics in geomorphology: Advances and limitations exemplified by case studies. Geomorphology, 93(1–2), 55-73.

Schumm, S.A., 1991. To Interpret the Earth – Ten Ways to be Wrong. Cambridge University Press, Cambridge.

Schumm, S.A., Lichty, R.W., 1965. Time, space, and causality in geomorphology. American Journal of Science, 263(2), 110-119.

Selby, M.J., 1980. A rock mass strength classification for geomorphic purposes: with test from Antarctica and New Zealand. Zeitschrift für Geomorphologie N.F., 24, 31–51.

Selby, M.J., 1982a. Controls on the stability and inclinations of hillslopes formed on hard rock. Earth Surf Proc Land, 7(5), 449–467.

Selby, M.J. (Ed.), 1982b. Hillslope Materials and Processes. Oxford University Press.

Selby, M.J. (Ed.), 1993. Hillslope Materials and Processes. Oxford University Press.

Sellmeier, B., Krautblatter, M., Thuro, K., 2015. Failure and Mobilization Analysis of Mid-Magnitude Rockfalls on a Steep Limestone Slope in the Bavarian Alps. In: G. Lollino, D. Giordan, G.B. Crosta, J. Corominas, R. Azzam, J. Wasowski, N. Sciarra (Eds.), Engineering Geology for Society and Territory - Volume 2: Landslide Processes. Springer International Publishing, Cham, pp. 817-820.

Siegesmund, S., Mosch, S., Scheffzük, C., Nikolayev, D.I., 2008. The bowing potential of granitic rocks: rock fabrics, thermal properties and residual strain. Environmental Geology, 55(7), 1437-1448.

Siegesmund, S., Ullemeyer, K., Weiss, T., Tschegg, E.K., 2000. Physical weathering of marbles caused by anisotropic thermal expansion. International Journal of Earth Sciences, 89(1), 170-182.

Siewert, M.B., Krautblatter, M., Christiansen, H.H., Eckerstorfer, M., 2012. Arctic rockwall retreat rates estimated using laboratory-calibrated ERT measurements of talus cones in Longyeardalen, Svalbard. Earth Surface Processes and Landforms, 37(14), 1542-1555.

Singh, B., Goel, R.K., 2011. Chapter 3 - Rock Material, Engineering Rock Mass Classification. Butterworth-Heinemann, Boston, pp. 13-19.

Slaymaker, O., 2003. The sediment budget as conceptual framework and management tool. Hydrobiologia, 494(1), 71-82.

Slaymaker, O., 2009. Proglacial, periglacial or paraglacial? Geological Society, London, Special Publications, 320(1), 71-84.

Smith, H.G., Dragovich, D., 2008. Sediment budget analysis of slope–channel coupling and in-channel sediment storage in an upland catchment, southeastern Australia. Geomorphology, 101(4), 643-654.

Sobott, R.J.G., 2004. Assessment of building stone degradation by ultrasonic measurements. In: R. Prikryl (Ed.), Dimension Stone. Taylor and Francis, London, pp. 219-222.

Sonklar, C., 1873. Allgemeine Orographie. Die Lehre von den Relief-Formen der Erdoberfläche. Wilhelm Braumüller, Wien.

Sougnez, N., van Wesemael, B., Vanacker, V., 2011. Low erosion rates measured for steep, sparsely vegetated catchments in southeast Spain. Catena, 84(1-2), 1-11.

Speight, J.G., 1974. A parametric approach to landform regions. Progress in Geomorphology, Institute of the British Geographers Special Publication, 7, 213-230.

Speight, J.G., 1990. Landform. In: R.C. McDonald, R.F. Isbell, J.G. Speight, J. Walaker, M.S. Hop (Eds.), Australian Soil and Land Survey Field Handbook. Inkata Press, Melbourne, pp. 9-57.

Spencer, J.W., Nur, A.M., 1976. The effects of pressure, temperature, and pore water on velocities in westerly granite. Journal of Geophysical Research, 81(5), 899-904.

Stark, C.P., Hovius, N., 2001. The characterization of landslide size distributions. Geophys Res Lett, 28(6), 1091–1094.

Statham, I., 1973. Scree Slope Development under Conditions of Surface Particle Movement. Transactions of the Institute of British Geographers(59), 41-53.

Statham, I., 1976. A scree slope rockfall model. Earth Surface Processes, 1(1), 43-62.

Stead, D., Wolter, A., 2015. A critical review of rock slope failure mechanisms: The importance of structural geology. Journal of Structural Geology, 74, 1-23.

Stock, G.M., Luco, N., Collins, B.D., Harp, E.L., Reichenbach, P., Frankel, K.L., 2014. Quantitative rock-fall hazard and risk assessment for Yosemite Valley, Yosemite National Park, California.

Stock, G.M., Martel, S.J., Collins, B.D., Harp, E.L., 2012. Progressive failure of sheeted rock slopes: the 2009–2010 Rhombus Wall rock falls in Yosemite Valley, California, USA. Earth Surf Proc Land, 37(5), 546–561.

Stoffel, M., 2006. A review of studies dealing with tree rings and rockfall activity: The role of dendrogeomorphology in natural hazard research. Nat Hazards, 39(1), 51-70.

Stolz, A., Huggel, C., 2008. Debris flows in the Swiss National Park: the influence of different flow models and varying DEM grid size on modeling results. Landslides, 5(3), 311-319.

Stott, T., Mount, N., 2007. Alpine proglacial suspended sediment dynamics in warm and cool ablation seasons: Implications for global warming. J Hydrol, 332(3-4), 259-270.

Strasser, M., Monecke, K., Schnellmann, M., Anselmetti, F.S., 2013. Lake sediments as natural seismographs: A compiled record of Late Quaternary earthquakes in Central Switzerland and its implication for Alpine deformation. Sedimentology, 60(1), 319-341.

Straumann, R.K., Korup, O., 2009. Quantifying postglacial sediment storage at the mountain-belt scale. Geology, 37(12), 1079-1082.

Strunden, J., Ehlers, T.A., Brehm, D., Nettesheim, M., 2015. Spatial and temporal variations in rockfall determined from TLS measurements in a deglaciated valley, Switzerland. Journal of Geophysical Research: Earth Surface, 120(7), 1251–1273.

Stumpf, A., Kerle, N., 2011. Object-oriented mapping of landslides using Random Forests. Remote Sensing of Environment, 115(10), 2564-2577.

Sugden, D.E., Summerfield, M.A., Burt, T.P., 1997. Editorial: Linking Short-term Geomorphic Processes to Landscape Evolution. Earth Surf Proc Land, 22(3), 193-194.

Swets, J., 1988. Measuring the accuracy of diagnostic systems. Science, 240(4857), 1285-1293.

Taber, S., 1929. Frost heaving. J. Geol., 37(5), 428– 461.

Tanarro, L.M., Muñoz, J., 2012. Rockfalls in the Duratón canyon, central Spain: Inventory and statistical analysis. Geomorphology, 169–170(0), 17-29.

Tarboton, D.G., 1997. A new method for the determination of flow directions and upslope areas in grid digital elevation models. Water Resources Research, 33(2), 309-319.

Tarboton, D.G., 2012. TauDEM 5.0, Terrain Analysis Using Digital Elevation Models, Utah State University, USA.

Terzaghi, K., 1946. Rock defects and loads on tunnel supports. Harvard University, Graduate School of Engineering, Cambridge.

Terzaghi, K., 1962. Stability of steep slopes on hard unweathered rock. Geotechnique, 12, 285–318.

Theler, D., Reynard, E., Lambiel, C., Bardou, E., 2010. The contribution of geomorphological mapping to sediment transfer evaluation in small alpine catchments. Geomorphology, 124(3–4), 113-123.

Thiel, M., Heckmann, T., Haas, F., Becht, M., 2011. Quantification of coarse sediment connectivity in alpine geosystems. . Geophysical research abstracts, 13(EGU2011-10449, 2011).

Thorn, C.E., 1992. Periglacial geomorphology: What, Where, When?, Periglacial geomorphology, Proceedings of the 22nd Annual Binghampton Syposium in Geomorphology. John Wiley and Sons, Chichester, UK.

Thorn, C.E., 2003. Making the most of new instrumentation. Permafrost and Periglacial Processes, 14(4), 411-419.

Tiranti, D., Cavalli, M., Crema, S., Zerbato, M., Graziadei, M., Barbero, S., Cremonini, R., Silvestro, C., Bodrato, G., Tresso, F., 2016. Semi-quantitative method for the assessment of debris supply from slopes to river in ungauged catchments. Science of The Total Environment, 554–555, 337-348.

Toppe, R., 1987. Terrain models: a tool for natural hazard mapping. In: B. Salm, H. Gubler (Eds.), Avalanche formation, movement and effects,. International Association of Hydrological Sciences, Wallingford, UK, pp. 629–638.

Tricart, J., 1956. Étude éxperimentale du problème de la gélivation. Biuletyn Peryglacjalny, 4(4), 285–318.

Tricart, J., 1970. Geomorphology of Cold Environments. (Trans. E. Watson), Macmillan, London.

Tricart, J., Cailleux, A. (Eds.), 1972. Introduction to Climatic Geomorphology. Longman.

Trümpy, B., Schmid, S.M., Conti, P., Froitzheim, N., 1997. Erläuterungen zur Geologischen Karte 1:50000 des Schweizerischen Nationalparks. (Geologische Spezialkarte Nr. 122), Zernez.

Tunnicliffe, J.F., Church, M., 2011. Scale variation of post-glacial sediment yield in Chilliwack Valley, British Columbia. Earth Surf Proc Land, 36(2), 229-243.

Tvergaard, V., Hutchinson, J.W., 1988. Microcracking in Ceramics Induced by Thermal Expansion or Elastic Anisotropy. Journal of the American Ceramic Society, 71(3), 157-166.

Twidale, C.R., 1973. On the origin of sheet jointing. Rock Mechanics, 5, 163-187.

UNESCO, 1993. International Geotechnical Societies UNESCO Working Party on World Landslide Inventory: A suggested method for describing the activity of a landslide, Bulletin of the International Association of Engineering Geology No. 47, pp. 53-57.

Usher, M.B., 2001. Landscape sensitivity: from theory to practice. Catena, 42(2-4), 375-383.

Van Asselen, S., Seijmonsbergen, A.C., 2006. Expert-driven semi-automated geomorphological mapping for a mountainous area using a laser DTM. Geomorphology, 78(3-4), 309-320.

Van Gasselt, S., Reiss, D., Thorpe, A.K., Neukum, G., 2005. Seasonal variations of polygonal thermal contraction crack patterns in a south polar trough, Mars. Journal of Geophysical Research: Planets, 110(E8), 1-15.

Van Steijn, H., Bertran, P., Francou, B., Texier, J.-P., Hétu, B., 1995. Models for the genetic and environmental interpretation of stratified slope deposits: Review. Permafrost and Periglacial Processes, 6(2), 125-146.

Van Steijn, H., Boelhouwers, J., Harris, S., Hétu, B., 2002. Recent research on the nature, origin and climatic relations of blocky and stratified slope deposits. Prog Phys Geog, 26(4), 551-575.

Van Tatenhove, F., Dikau, R., 1990. Past and Present Permafrost Distribution in the Turtmanntal, Wallis, Swiss Alps. Arctic and Alpine Research, 22(3), 302-316.

Vanacker, V., Vanderschaeghe, M., Govers, G., Willems, E., Poesen, J., Deckers, J., De Bievre, B., 2003. Linking hydrological, infinite slope stability and land-use change models through GIS for assessing the impact of deforestation on slope stability in high Andean watersheds. Geomorphology, 52(3-4), 299-315.

Vanwalleghem, T., Van Den Eeckhaut, M., Poesen, J., Govers, G., Deckers, J., 2008. Spatial analysis of factors controlling the presence of closed depressions and gullies under forest: Application of rare event logistic regression. Geomorphology, 95(3–4), 504-517.

Varnes, D.J., 1958. Landslide Types and Processes. In: E.B. Eckel (Ed.), Landslides and Engineering Practice. HRB.

Varnes, D.J., 1978. Slope movements: types and processes, Washington D.C.

Varnes, D.J. (Ed.), 1984. Landslide Hazard Zonation: A Review of Principles and Practice.

Vehling, L., Rohn, J., Moser, M., 2015. Quantification of rock fall processes in a proglacial high mountain areas. Austria. Z. Geomorphol., 60(1), 93–108.

Vehling, L., Rohn, J., Moser, M., 2016. Quantification of small magnitude rockfall processes at a proglacial high mountain site, Gepatsch glacier (Tyrol, Austria). Zeitschrift f. Geomorphologie, Supplementary Issues, 60(1), 93-108.

Ventura, S.J., Irvin, B.J., 2000. Automated landform classification methods for soil-landscape studies. In: J.P. Wilson, J.C. Gallant (Eds.), Terrain Analysis: Principles and Applications. Wiley and Sons, New York, pp. 267-294.

Verleysdonk, S., Krautblatter, M., Dikau, R., 2011. Sensitivity and path dependence of mountain permafrost systems. Geografiska Annaler Series A, Physical Geography, 93A(2), 113–135.

Veveakis, E., Vardoulakis, I., Di Toro, G., 2007. Thermoporomechanics of creeping landslides: The 1963 Vaiont slide, northern Italy. Journal of Geophysical Research: Earth Surface, 112(F3), 1-21.

Vilajosana, I., Suriñach, E., Abellán, A., Khazaradze, G., Garcia, D., Llosa, J., 2008. Rockfall induced seismic signals: case study in Montserrat, Catalonia. Nat. Hazards Earth Syst. Sci., 8(4), 805-812.

Viles, H., 2016. Technology and geomorphology: Are improvements in data collection techniques transforming geomorphic science? Geomorphology, 270(Supplement C), 121-133.

Viles, H., Ehlmann, B., Wilson, C.F., Cebula, T., Page, M., Bourke, M., 2010. Simulating weathering of basalt on Mars and Earth by thermal cycling. Geophysical Research Letters,, 37(18).

Viles, H., Goudie, A., Grab, S., Lalley, J., 2011. The use of the Schmidt Hammer and Equotip for rock hardness assessment in geomorphology and heritage science: a comparative analysis. Earth Surf Proc Land, 36(3), 320-333.

Viles, H., Messenzehl, K., Mayaud, J., Coombes, M., Bourke, M., in review. Stress histories control rock breakdown trajectories in arid environments. Geology.

Viles, H.A., 2013a. 4.2 Synergistic Weathering Processes A2 - Shroder, John F, Treatise on Geomorphology. Academic Press, San Diego, pp. 12-26.

Viles, H.A., 2013b. Linking weathering and rock slope instability: non-linear perspectives. Earth Surf Proc Land, 38(1), 62–70.

Volkwein, A., Schellenberg, K., Labiouse, V., Agliardi, F., Berger, F., Bourrier, F., Dorren, L.K.A., Gerber, W., Jaboyedoff, M., 2011. Rockfall characterisation and structural protection – a review. Nat. Hazards Earth Syst. Sci., 11(9), 2617-2651.

von Blanckenburg, F., 2006. The control mechanisms of erosion and weathering at basin scale from cosmogenic nuclides in river sediment. Earth and Planetary Science Letters, 242(3–4), 224-239.

von Engelhardt, W., Zimmermann, J., 1988. Theory of Earth Science. Cambridge University Press, Cambridge.

von Humboldt, A., 1814. Sur l'élévation des montagnes de l'Inde, Paris: de Feugueray.

Vorpahl, P., Elsenbeer, H., Märker, M., Schröder, B., 2012. How can statistical models help to determine driving factors of landslides? Ecological Modelling, 239(0), 27-39.

Vosteen, H.-D., Schellschmidt, R., 2003. Influence of temperature on thermal conductivity, thermal capacity and thermal diffusivity for different types of rock. Physics and Chemistry of the Earth, Parts A/B/C, 28(9–11), 499-509.

Wainwright, J., Turnbull, L., Ibrahim, T.G., Lexartza-Artza, I., Thornton, S.F., Brazier, R.E., 2011. Linking environmental régimes, space and time: Interpretations of structural and functional connectivity. Geomorphology, 126(3–4), 387-404.

Walder, J., Hallet, B., 1985. A theoretical model of the fracture of rock during freezing. Geological Society of America Bulletin, 96(3), 336–346.

Walling, D.E., 1983. The sediment delivery problem. J Hydrol, 65(1-3), 209-237.

Walling, D.E., Webb, B.W., 1996. Erosion and sediment yield: A global overview. In: D.E. Walling, B.W. Webb (Eds.), Erosion and Sediment Yield: Global and Regional Perspectives, (Proc. Exeter Symposium, July, 1996). IAHS Press, Wallingford, UK, pp. 3-19.

Walsh, S.D.C., Lomov, I.N., 2013. Micromechanical modeling of thermal spallation in granitic rock. International Journal of Heat and Mass Transfer, 65, 366-373.

Wang, G., Liaw, P., 2008. Fatigue And Fracture Behavior. In: M. Miller, P. Liaw (Eds.), Bulk Metallic Glasses. Springer US, Boston, MA, pp. 169-203.

Wang, Y., Tonon, F., 2011. Discrete Element Modeling of Rock Fragmentation upon Impact in Rock Fall Analysis. Rock Mechanics and Rock Engineering, 44(1), 23-35.

Warburton, J., 2010. Sediment transfer in steep upland catchments (Northern England, UK): Landform and sediment source coupling. In: J. Otto, R. Dikau (Eds.), Landform - Structure, Evolution, Process Control: Proceeding of the International Symposium on Landform oganised by the Research Training Group 437. Springer, Berlin, Heidelberg.

Warke, P.A., McKinley, J., Smith, B.J., 2006. Variable weathering response in sandstone: factors controlling decay sequences. Earth Surf Proc Land, 31(6), 715-735.

Warke, P.A., Smith, B.J., 1998. Effects of direct and indirect heating on the validity of rock weathering simulation studies and durability tests. Geomorphology, 22(3), 347-357.

Warke, P.A., Smith, B.J., Magee, R.W., 1996. Thermal response characteristics of stone: Implications for weathering of soiled surfaces in urban environments. Earth Surf Proc Land, 21(3), 295-306.

Watanabe, T., Matsuoka, N., Christiansen, H.H., Cable, S., 2017. Soil Physical and Environmental Conditions Controlling Patterned-Ground Variability at a Continuous Permafrost Site, Svalbard. Permafrost and Periglacial Processes, 28(2), 433-445.

Wegmann, M., 1998. Frostdynamik in hochalpinen Felswänden am Beispiel der Region Jungfraujoch - Aletsch, Zürich.

Wegmann, M., Gudmundsson, G.H., Haeberli, W., 1998. Permafrost changes in rock walls and the retreat of alpine glaciers: A thermal modelling approach. Permafrost and Periglacial Processes, 9(1), 23-33.

Weiss, T., Siegesmund, S., Kirchner, D., Sippel, J., 2004. Insolation weathering and hygric dilatation: two competitive factors in stone degradation. Environmental Geology, 46(3), 402-413.

Werner, B.T., 1995. Eolian dunes: Computer simulations and attractor interpretation. Geology, 23(12), 1107-1110.

Whalley, W.B., 1974. The mechanics of high-magnitude low-frequency rock failure. Reading Geographical Papers(27).

Whalley, W.B., 1984. Rockfalls. In: D. Brunsden, D.B. Prior (Eds.), Slope Instability. Wiley, Chichester, pp. 217-256.

Whitehouse, I.E., McSaveney, M.J., 1983. Diachronous Talus Surfaces in the Southern Alps, New Zealand, and Their Implications to Talus Accumulation. Arctic and Alpine Research, 15(1), 53–64.

Whittington, A.G., Hofmeister, A.M., Nabelek, P.I., 2009. Temperature-dependent thermal diffusivity of the Earth/'s crust and implications for magmatism. Nature, 458(7236), 319-321.

Wichmann, V., Heckmann, T., Haas, F., Becht, M., 2009. A new modelling approach to delineate the spatial extent of alpine sediment cascades. Geomorphology, 111(1–2), 70-78.

Wieczorek, G.F., Nishenko, S.P., Varnes, D.J., 1995. Analysis of rock falls in the Yosemite Valley. American Rock Mechanics Association, Reno, Nevada pp. 85–89.

Williams, P.J., Smith, M.W., 1989. The Frozen Earth. Fundamentals of geocryology. Cambridge University Press, Cambridge,.

Wilson, P., 2009. Rockfall talus slopes and associated talus-foot features in the glaciated uplands of Great Britain and Ireland: periglacial, paraglacial or composite landforms? Geological Society, London, Special Publications, 320(1), 133-144.

Wirz, V., Schirmer, M., Gruber, S., Lehning, M., 2011. Spatio-temporal measurements and analysis of snow depth in a rock face. The Cryosphere, 5(4), 893-905.

Wolman, M.G., Miller, J.P., 1960. Magnitude and frequency of forces in geomorphic processes. The Journal of Geology, 68(1), 54–74.

Worster, M.G., Wettlaufer, J.S., 1999. The fluid mechanics of premelted liquid films. In: W. Shyy, R. Narayanan (Eds.), Fluid Dynamics at Interfaces. Cambridge Univ. Press, Cambridge, pp. 339–351.

Wyllie, D.C., Mah, C.W. (Eds.), 2004. Rock slope engineering: civil and mining. Spon Press.

Wyrwoll, K.H., 1977. Causes of rock-slope failure in a cold area: Labrador-Ungava. Reviews in Engineering Geology, 3, 57-68.

Yatsu, E., 1988. The Nature of Weathering: An Introduction. Sozosha, Tokyo.

Yavuz, H., Altindag, R., Sarac, S., Ugur, I., Sengun, N., 2006. Estimating the index properties of deteriorated carbonate rocks due to freeze–thaw and thermal shock weathering. International Journal of Rock Mechanics and Mining Sciences, 43(5), 767-775.

Yin, Y., Wang, F., Sun, P., 2009. Landslide hazards triggered by the 2008 Wenchuan earthquake, Sichuan, China. Landslides, 6(2), 139-152.

Zepp, H., 2008. Geomorphologie: Grundriß Allgemeine Geographie. UTB, Stuttgart.

Zhang, T., 2005. Influence of the seasonal snow cover on the ground thermal regime: An overview. Reviews of Geophysics, 43(4), 1-23.

Zhang, Z.-P., Shao, Y.-F., Song, F., 2010. Characteristics of crack patterns controlling the retained strength of ceramics after thermal shock. Frontiers of Materials Science in China, 4(3), 251-254.